A CONTRIBUTION TO THE STUDY OF AXIALLY LOADED PILE FOUNDATIONS

A Thesis submitted for the degree of DOCTOR of PHILOSOPHY in the Faculty of Engineering and Applied Science, University of Southampton

P. K. Banerjee

December 1969

ABSTRACT

Faculty of Engineering and Applied Science

Prasanta Kumar Banerjee

Doctor of Philosophy

A study of some of the major parameters governing behaviour of pile foundations is described. The problems of:

(a) the load-displacement characteristics of single piles

(b) the load-displacement characteristics of free-standing pile groups with any arbitrary spacing,

(c) the interaction between a pile cap and its group,

(d) the stresses and pore water pressure around a driven pile,

are analysed by assuming an elastic ideally plastic model behaviour for soils. The elastic analysis is made by developing an integral equation method based on the theory of multidimensional singular integral equations. An algorithm for the solution of the singular integral equations is described. The computational work involved has been greatly reduced by choosing for singular solution of the integral equation, the kernel function due to a point load within an elastic half space.

Numerical solutions of the closely related topic of static response of buried rigid discs of arbitrary shape within a finite elastic layer are also obtained.

The behaviour of a driven pile is analysed and an equation is developed for predicting the changes in the pore water pressures due to the driven pile. The time dependent response of the pile resulting from the dissipation of these pore water pressures is then examined.

The theoretical solutions have been compared with published laboratory and field data with reasonable agreement obtained.

The results of dynamic penetration tests of model probes and blades at various rates of penetration are reported together with preliminary results of an investigation of the effects of an applied D.C. potential on the penetration resistance of model probes and blades.

ACKNOWLEDGEMENTS

The author acknowledges his indebtedness to many who have assisted directly or indirectly throughout the research programme and during the preparation of the thesis. Any omissions in the following direct acknowledgements do not indicate a lack of appreciation for the assistance afforded.

To all research students I express my gratitude for their help and cheerful company and specially to Messrs. K. Z. Andrawes, J. O. Watson, R. Beale, M. C. Edwards for their valuable suggestions and criticism throughout the research programme.

I extend my gratitude to the Director and staff of Computation Department, Southampton University for providing the necessary computer time and showing tolerance throughout the duration of the research project.

The financial support of the Military Engineering Experimental Establishment, Christchurch, is thankfully acknowledged.

I thank Mrs. J. Wells for her neat typing of the thesis and Mr. D. Orchard, Chief Technician for assistance in constructing the pile driving rig.

Lastly but certainly foremost I must express my gratitude to Mr. R. Butterfield for his interest and keen supervision of the project and helpful criticism in the preparation of the final manuscript.

CORRECTIONS

Page no:	Line no:	Error:	Correction
(v)	6	disc or arbitrary	disc of arbitrary
(xvi)	6	electric	elastic
(xvii)	13	N	N_γ
"	18	Total for	Total load for
4	1	1 ft per second	2 ft per second
11	25	shaft of the pile	shaft surface area of the pile
12	caption	piles London clay	piles in (London clay)
17	14	based	base
"	25	being	bearing
21	22	same	equivalent
23	26-27	effect of the depth	presence of
29	9	prlblems	problems
39	12	(iii) Have the...solution	omit
40	15	$p_i(A)$	$-p_i(A)$
41	20	$f_i(A_o)$	$-f_i(A_o)$
"	21	D_i	D_e
"	23	D_e	D_i
43	13	$\frac{1}{2}$ for the	$-\frac{1}{2}$ and $\frac{1}{2}$ for the
"	14	(2.16) and (2.17),	(2.16) and (2.17) respectively,
44	21	N × i	N × i_d
45	1 to 10	Read all i as	i_d
"	9	{F}	{f}
"	25	to regular	regular
63	1	z = C	z = c
111	3	n × n matrices	n × m matrices
157	14	the surface	the surface (see Chapter 3)
172	12	plasticity and	plasticity and Low
175	28	1966) assuming	1966) and assuming
201	25	Q_c, P_s	Q_c, P_c
222	23	is used.	is used).
224	1	boundary,	boundary respectively,
"	11	$\partial\sigma_{zz}/z = \gamma$	$\partial\sigma_{zz}/\partial z = \gamma$
231	24	Δu	ΔU
236	1	(7.27) and	(7.27) with respect to r and
"	2	(7.27) and	(7.27) by r and
248	Figure 7.7 & 7.8	$T = 0.15/a^2$	T = 0.00417
255	16	electric current	electro-osmotic flow
257	16	$\{\alpha\}[\bar{C}]\{\nabla\}E$	$\{\nabla\}^*[\bar{C}]\{\nabla\}E$
259	8	$\delta\sigma$	$\delta\sigma'$
260	6	temperature (t)	temperature(t) (Netoushil, 1953)
260	13	. Thus equation	equation

Page no:	Line no:	Error:	Correction
260	20	Casagrande	(Casagrande
265	1	Physucal	physical
267	22	This	Thus
273	19	Assuming that P can	Let P
"	24	$(B/m)x + (g - A/m)$	$(B/m)x = (g - A/m)$
281	17	pile face	pile face
286	14	R =	P =
316	8	the ultimate	that the ultimate
331	6	$\int_0^{2\pi}$	$\int_0^{\pi}$
"	8	"	"

CONTENTS

LIST OF FIGURES

LIST OF PLATES

NOTATION

The following symbols have been used throughout the text. Any deviations or additions are defined locally.

A	Cross-sectional area
A_b	Base area
A_m, B_n	The N number of points on the surface S
A_p	Cross-sectional area of pile
A_s	Area of pile-soil interface
A_o	A point on the surface S
B	Width of base
C	Apparent cohesion of soil
C_b	Cohesion at the pile base
C_u	Undrained cohesion of soil
C_v	Coefficient of consolidation in radial direction
C'	Mean C over the pile length
$[C]$	Conductivity matrix
D, D_s	Shaft diameter
D_B	Diameter of base
D_e	Outside domain
D_i	Inside domain
D_e^+, D_i^+	Defined in Figure 2.1
D_o	Dilectric constant
$\{DU\}$	Change in pore water pressures
$\{D\sigma'_{rr}\}$	Change in the effective radial stress at the pile face
E	Voltage and also defined as a region of exclusion
E_p	Young's modulus of the pile material
E_{im}	Error term
$[E]$	A matrix of finite difference coefficients

F_j	Forces acting at a point
F_s	Factor of safety
G, G'	Shear modulus with respect to the total stresses and effective stresses respectively
G_n	Weighting functions, n=1,2...etc
H	Thickness of the electric layer and also defined as hydraulic potential
H_e	Equivalent hydraulic potential
I_x, I_y, I_z	Current in X, Y and Z directions respectively
I_D, I_p	The values of the integrals given by equations (2.26), (2.29) and (2.30)
$\{I\}$	Current vector
$[I]$	Unit matrix
K'	The bulk modulus with respect to the effective stresses
KC, KR	The kernel functions of the first and second integral of equation (3.8)
K_o	A non-dimensional parameters
K_e, K_h	Electro-osmotic and hydraulic permeabilities respectively
K(c,r,z)	Kernel functions at the point designated by the bracketted coordinates
$(KCC_{ij})_{mn}$, $(KRC_{ij})_{pq}$	Defined by equation (3.27)
$K_{ij}(A,B)$	Kernel functions given by Mindlin's Solution
$(KCR_{ij})_{mn}$, $(KRR_{ij})_{pq}$	Defined by equation (3.28)
$[K_h]$, $[K_e]$	Hydraulic and electro-osmotic permeability matrix respectively
$KW_1(\ )$, $KU_1(\ )$ etc	The kernel functions given by Mindlin's Solution
$(KSS)_{ij}$, $(KRS)_{ij}$, $(KBS)_{ij}$	The coefficients obtained from the integrals listed in Appendix I

$[KSS]$, $[KRS]$ etc	Matrix representations of $(KSS)_{ij}$, $(KRS)_{ij}$ etc
$[K]$, $[KS]$	Matrix of coefficients for the displacement of single pile-soil interface
L	Length of pile
$[M]$	The $(N \times i)^2$ matrix defined by equation (2.27)
$[MC]$, $[MS]$	The matrix representations for the continuous and the singular kernels respectively
$M_{ij}(A_o,B)$	Functions given by equations (2.16) to (2.19)
$MC_{ij}(A,B)$, $MS_{ij}(A,B)$	Continuous and singular part of the kernel functions respectively
N	Number of piles and also number of divisions over the surface S
N_c, N_q and N	Bearing capacity factors
P	Load
P_c	Total load for a compressible pile
P_D, P_S	The static and dynamic load respectively
P_E	Base load and also the load under electro-osmosis
P_R	Total for a rigid pile
P_S	Shaft resistance
P_u	Ultimate bearing capacity
P_x, P_y and P_z	Forces in X, Y and Z directions respectively
P_{EC}, P_{ER}	The end loads for compressible and rigid piles respectively
Q_{e_1}	Flow through a capillary
R	A plane region and also defined as the radial distance between the electrodes
R_1, R_2	Radii
R_x, R_y	
S	Arbitrary surface and also defined as the pile spacings

S_e, S_I	Auxiliary surfaces defined by Figure 2.1
$(S_t)_i$	The limiting stress at the pile-soil interface
T	Surface tension
TC, TR	The kernel functions given by equation (3.9)
$T_{ijK}(A,B)$	Kernel functions for the stress integral representations
U	Pore water pressures
$\{U_s\}$	The radial displacement of the shaft elements
$\{U\}$	The pore water pressures at the nodal points
V_{hx}, V_{hy}, V_{hz}	The hydraulic velocities in X, Y and Z directions respectively
V_{ex}, V_{ey}, V_{ez}	The electro-osmotic velocities in X, Y and Z directions respectively
$\{V\}$	Velocity vector
W	Vertical displacement
$\{W\}$	The vertical displacement of the pile-soil surface
$(WC)_{ij}$	Defined by equation (3.13)
$(WC)_i$,$(WR)_i$	The vertical displacement of disc elements and the elements of the rigid layer respectively
$\{W_s\}$	The vertical displacement of the shaft elements
X, Y, Z	Cartesian coordinate system
a	Radius of the disc and the pile and half the width of the rectangular disc
a', b'	Semi-axes of elliptical disc
b	Radius of the pile base and half the length of the rectangular disc
c	The depth of the point of application of the load
(c,ξ,η)	Coordinates of the load position with respect to global axes
d	Shaft diameter
d_1, d_2, d_3	Defined in Figure (8.1)
dS_I, dS_e, dS, dS_o	Elements of S_I, S_e, S and S_o respectively

$d\xi$, $d\eta$	Elements of length in ξ and η directions
e	Volumetric strain
$f_i(A)$	Boundary conditions
g	Acceleration due to gravity
h	Height of fall
h_1, h_2	The thickness of annular rings on the disc area and the rigid layer surface respectively
i, j, k, p, q, m, n	Suffices
I_e, i_h	Electro-osmotic and hydraulic gradients respectively
ℓ	Length of the capillary
n_p	Components of the outward normal in the direction of the coordinate axes
p_o, q	Overburden pressure and ultimate pressure at the base respectively
r_{AB}	The radial distance between the points A and B
r_1, r_2	The radial distance between the load point and the field point
r, θ_r, z	Defined in Figure (3.2)
t	Temperature
u	Radial displacements
$u_i(A)$	Displacements at A in terms of a cartesian coordinate system
u_x, u_y, u_z	Displacements in X, Y and Z directions respectively
u_o	Initial velocity
$u_1(r,\theta,z)$, $u_2(r,\theta,z)$ etc	Radial displacements at a point designated by bracketted coordinates
$w_1(r,\theta,z)$, $w_2(r,\theta,z)$ etc	The vertical displacements at a point designated by the bracketted coordinates
x,y,z	Position of the field point
$\alpha, \alpha_o, \alpha_E$	Nondimensional factors

α_1, α_2	Angles defined in Figures (4.1) and (4.2) respectively
β	The ratio G/C_u
γ	Bulk density of soil
$\{\nabla\}$	Grad, operator
$\{\nabla\}^*$	Transpose of $\{\nabla\}$
$\Delta U, \Delta\sigma_{rr}, \Delta\sigma_{\theta\theta}, \Delta\sigma_{zz}$	Increase in pore water pressure and the total stresses
$\Delta\sigma_{mean}$	Increase in the mean total stresses
$\Delta\sigma_{oct}$	Increase in the octahedral shear stresses
δ	Angle of friction
$\delta S, \delta u_i(A)$	Elements of S and elemental displacements
ε	Radial distance of the load point from the origin
$\varepsilon_{rr}, \varepsilon_{\theta\theta}, \varepsilon_{zz}$	Radial, circumferential and vertical strains respectively
ϕ	Coulomb's friction angle
ϕ_j, ψ_j	Fictitious intensities
$\{\phi\}, \{\psi\}$	Column vectors for the unknown fictitious intensities
$\phi_i(A_m), \phi_j(B_n)$	The values of the vector ϕ_i at discrete set of points A_m and B_n, on the surface
ϕ_s, ϕ_b, ϕ_r	Unknown stress intensities
μ, μ_p	Poisson's ratio of the soil and the pile respectively
λ	The ratio of the Young's modulus of the pile material to the shear modulus of the soil
λ_o	A parameter of the integral equation
ρ_x, ρ_y, ρ_z	Resistivities in X, Y and Z directions respectively
$\sigma_{ip}(A)$	Components of the stresses at A
$\sigma_\varepsilon, \sigma_{\varepsilon\varepsilon}, \psi_{\varepsilon\theta}, \psi_\varepsilon$	The resultant normal stresses over the base area and the fictitious vertical stresses over the surface of the rigid layer
σ_n, ψ_p	The resultant vertical stress on the discretised base area and the fictitious vertical stress over the surface of the rigid layer respectively

$\sigma_{\xi\eta}, \psi_{\xi\eta}$	The resultant vertical stress over the surface of the disc and the fictitious vertical intensity on the surface of the rigid layer
$\sigma_{rr}, \sigma_{\theta\theta}, \sigma_{zz}, \sigma_{rz}$	The radial circumferential, vertical and shear stresses in r, θ, z coordinate system
$\sigma_{zz}(B)$	Vertical stress at the point B
τ, τ_S	Shear stresses
$\tau_{ij}(A,B)$	Defined by equation (2.7)
ω	A nondimensional parameter

Chapter 1

Introduction

1.1 Summary

A summary and review of the previously published theoretical and experimental work on pile foundations is described in this Chapter and the present state of knowledge of the behaviour of pile foundations examined. A brief historical background of the present research is also given and the scope of the investigation defined.

1.2 Background of the present research

The research project began in December 1966 and originally related to a programme concerning the investigation of high speed earth-cutting techniques. One of the major problems of earth-cutting is the 'sticking' of soil to the blades. It was suggested that any artificial method of reducing the adhesion would increase the efficiency of the earth-cutting tool. From a preliminary study of the mechanism of adhesion it became apparent that this may be achieved by a thin film of water between the blade and the soil. In this context, it was suggested that an application of an electric potential between the blade and the soil may well produce the required film of water.

As a part of the preliminary investigation it was decided to investigate the effects of applying an electric potential on the variation of the penetration resistance of model probes and blades driven into saturated clay. It was found that the application of an electric potential to a pile driven at rates of 0.16 inches per minute and 0.36 inches per minute altered the penetration resistance by up to 50 per cent. The actual amount depended on the moisture content of the clay, the geometry and polarity of the model probes and blades and the voltage gradient etc. Penetration resistance was found to increase for an anodic pile and decrease for a cathodic pile.

In order to explore the applicability of such a technique to high speed earth-cutting a research programme to investigate the effect of the rate of penetration on the variation of the penetration resistance was then planned. An apparatus capable of driving probes and blades at different speeds was constructed and a large number of dynamic penetration tests carried out. However, it was found that virtually no change in penetration resistance occurred when the rate of penetration exceeded

1 ft per second. Furthermore, it was decided that before any reasonable analysis could be attempted of the complex effects of electric potentials on the penetration of probes and blades the basic mechanics of probe-soil interaction needed to be studied. Thereafter the research programme was directed towards a theoretical investigation of the basic mechanics of pile soil interaction.

1.3 General

In foundation engineering a pile is a construction element - a column of wood, steel or concrete - either driven into or bored in the ground to transmit foundation loads into a layer of firm soil below the ground surface at an economical and practical depth, in such a way that these layers of soil or rock can sustain the loads. Piles may be classified into three major categories based on the manner in which they function (Terzaghi and Peck, 1948):

(i) Friction piles in coarse grained soil: These piles transfer most of the loads to the soil by skin friction. These are normally driven into the soil. Sometimes a large number of such piles are driven close together to reduce the porosity and compressibility of the soil around them, whence they are sometimes called compaction piles.

(ii) Friction piles in fine grained soil: These piles also transfer their loads to the soil by skin friction, but the soil is not compacted appreciably. Foundations supported on piles are called "floating" pile foundations.

(iii) End bearing piles: These piles transfer their loads on to a firm stratum located at a considerable depth below the base of the structure and are normally driven through overlying soft strata.

Piles have been used for well over a thousand years of human history (e.g. Caesar built a bridge on piles across the Rhine). Whenever bearing strata were thought to be incapable of supporting the load of continuous footings, piles have been considered as an alternative solution. Before the seventeenth century since there was abundant supply of timber and cheap labour, as many piles were driven as ground would take. Settlement caused no concern, because the prevalent type of structure could withstand considerable amount of differential settlement without

any damage (Terzaghi and Peck, 1948).

The industrial revolution created a demand for heavy but inexpensive structures, which made the cost of pile foundations an item of consequence. The engineers tried various ways of forecasting the minimum number of piles necessary to support a given load. This led to various empirical pile driving formulae which were summarised by Chellis (1951). The inherent short comings of these formulae were realised (Cummings, 1940), and consequently load tests were subsequently favoured (Terzaghi, 1943).

The majority of the pre-1950 research on pile foundations was associated with piling systems, construction methods and load tests and was still oriented towards the establishment of empirical design formulae. A very comprehensive bibliography of these works has been prepared by Nishida (1960). An obvious need for an understanding of the mechanics of pile-soil interaction has led to a great increase in research on pile foundations since this time.

A review of this more recent research into the mechanics of pile-soil interaction is given below. Reviews of published research work relating to the problems of:

(a) stress distribution under a rigid disc of arbitrary shape buried within an elastic half space and within a finite elastic layer underlain by a rigid base and

(b) the effects of applied electrical potentials on the dynamic penetration resistance of piles

are given in the introductions to Chapters 3 and 8 respectively, containing the present contributions on these subjects.

1.4 A review of the previous researches on single piles

Many attempts have been made to solve the basic problem of describing the behaviour of a single pile under the action of an axial

load; the majority of which were semi-empirical studies. Mayerhof (1951) summarised and reviewed these works and developed an approximate theory for the ultimate bearing capacity of deep and shallow foundations. His analysis was based on a solution of the equilibrium equations together with the Mohr-Coulomb failure criterion under the following assumptions:

(i) The failure surface is a logarithmic spiral

(ii) The effect of body forces can be linearly superimposed on the solution obtained without the body forces.

The theoretical results thus obtained were written in the same form as the equations for ultimate bearing capacity for shallow footings:

$$q = C\,N_c + p_o\,N_q + \gamma \cdot \frac{B}{2} \cdot N_\gamma \,. \qquad (1.1)$$

where q = ultimate normal pressure at the base

C = apparent cohesion of the soil

p_o = overburden pressure at the base level

γ = density of the soil

B = width of the base.

N_c, N_q, N_γ were defined as bearing capacity factors which depend on the depth of embedment, shape and roughness of the base as well as the apparent angle of friction of the soil. Various tables and charts were presented to show the effects of the different parameters on these factors. The theoretical results were compared with laboratory test results which were generally within ±15 per cent of the theoretical predictions. A series of laboratory tests on the ultimate bearing capacity of driven piles were also described. Whereas the ultimate bearing capacity of a pile driven in cohesive soil was found to increase with time the contribution by end bearing remained essentially constant.

For a purely cohesive soil ($\phi = 0$, hence $N_q = 1$, $N_\gamma = 0$), equation (1.1) simplifies to :

$$q = C.\ N_c + p_o \qquad (1.2)$$

A different method based on the analysis by Bishop, Hill and Mott (1945) of the deep punch problem in metals, was proposed by Gibson (1950). He obtained the pressure q required to expand a horizontal cylinder radially in an infinite mass of weightless cohesive soil and assumed it to be equal to the ultimate bearing capacity of a deep strip foundation. Thus:

$$q = C.\ (\mathrm{Log}_e\ E/_{3C} + 1) \qquad (1.3)$$

where E is the modulus of elasticity of the soil, based on an initial tangent to the stress-strain curve under appropriate stress conditions. Meyerhof (1951) obtained an equation analogous to (1.3) for deep circular footings in weightless cohesive soil. He obtained the pressure q required to expand a spherical cavity in an infinite mass of weightless cohesive soil as:

$$q = 4/_3\ .\ C\ (\mathrm{Log}\ E/_{3C} + 1). \qquad (1.4)$$

The term in the parenthesis is equivalent to N_c in equation (1.2). Thus the stress deformation characteristics were accounted for through the use of E as well as C. Using this method Mayerhof found N_c for a deep circular footing in an elastic ideally plastic material varies from 7.0 to 9.0 compared to 9.3 for his approximate rigid-plastic analysis. An equation analogous to (1.4) was deduced by Skempton, Yassin and Gibson (1953) for purely granular soil (C = 0) assuming the mode of failure under a pile base to be identical to the expansion of a spherical cavity in an infinite medium.

In establishing equations (1.3) and (1.4) the assumption is made that the shaft skin friction has no effect on the ultimate base resistance. Although it is conceivable that the ultimate end bearing capacity

would be affected by the shear stress distribution at the shaft-soil interface, no solution has been attempted which takes this into account. In spite of these drawbacks, the model and full scale field tests described by Meyerhof and Murdock (1953), Golder and Leonard (1954), Skempton (1959), Whitaker and Cooke (1966) and Cook and Whitaker (1961) showed the values of the ultimate end bearing within ±20% of the theoretical predictions based on equations (1.1), (1.2), and (1.4).

In summarising all the methods of determining the ultimate end load resistance, at the time, Skempton (1959) concluded that for saturated clay the value of $N_c = 9$ in equation (1.2) was about the average of the theoretical and experimental results for saturated clay and this was probably sufficiently accurate for practical purposes. This has subsequently been generally accepted by designers (Whitaker and Cooke, 1966).

Full scale experiments conducted by Whitaker and Cooke (1966) on piles embedded in fissured clay showed a value of N_c less than 9. This led to the introduction of an additional parameter in equation (1.2):

$$q = \omega . N_c . C_b \qquad (1.5)$$

where C_b is the cohesion at the pile base and ω is a non-dimensional factor which can be chosen to modify C_b to give the equivalent fissured strength.

The total ultimate bearing capacity of a pile (P_u) can be represented by:

$$P_u = P_S + P_E \qquad (1.6)$$

P_S = ultimate shaft resistance,

P_E = ultimate end bearing which is calculated from the formulae previously described.

To evaluate P_S one needs to know the condition of soil around the pile shaft. Clay around a pile either softens as a result of boring (and also concreting) or becomes remoulded due to pile driving and the lateral stresses at the pile face are time dependent due to reconsolidation of the soil mass around the pile. Meyerhof and Murdock (1953) found that the softened zone extended about 2 inches from the shaft face of bored cast-in-situ piles in London clay. The strength of clay in this zone was reduced by the initial increase in moisture content which occurred during construction. Little is known of the way the effective stresses are likely to be affected by this process, particularly in relation to the softened layer of clay immediately around a bored pile and the remoulded clay around a driven pile in saturated clay. It is therefore necessary to carry out an effective stress analysis. Pile tests are inevitably carried out at an early stage in the life of the pile at which time the lateral stresses are not fully effective. This results in an underestimation of the ultimate bearing capacity of driven or bored piles in saturated clay. It has been customary to express the ultimate shaft resistance of a pile in saturated clay as:

$$P_S = A_S \cdot \alpha \cdot C' \qquad (1.7)$$

Where A_S is the area of the pile soil interface,

α is a nondimensional factor,

C' is the mean C over the length of the pile.

Therefore the evaluation of α in equation (1.7) is of prime importance in the determination of the contribution made by the shaft. For bored piles in London clay the value of α was reported to be between 0.4 to 0.6 (Skempton, 1959, 1966; Whitaker and Cooke, 1961, 1966; Burland et al, 1966). For driven piles in saturated clay the value

of α was found to vary from 0.6 to 2.5 (Tomlinson, 1957). The magnitude was found to depend on various factors, the major ones being type of pile, length to diameter ratio of the pile, plasticity index of soil (Tomlinson, 1957), time after driving (Seed and Reese, 1955; Soderberg, 1963; Airhart, 1967; Chandler, 1968), and the sensitivity of the clay (Orrje and Broms, 1967).

Figure (1.1) shows a comparison between the calculated bearing capacity of single piles by the use of equations (1.6) and (1.7) assuming $N_c = 9$, $\alpha = 0.45$ and $\omega = 0.75$, and observed full scale field results of cast-in-situ bored piles in London clay. The agreement between the calculated and the observed ultimate bearing capacity indicates that the ultimate bearing capacity of a bored pile can be predicted within ±20 per cent. The prediction of the ultimate bearing capacity of a driven pile however, needs more attention.

Broms (1966) expressed the ultimate bearing capacity of piles embedded in granular soil as:

$$P_u = q \cdot A_b + \frac{1}{2} \cdot K_o L \gamma \tan \delta \cdot A_S \qquad (1.8)$$

where

P_u = ultimate bearing capacity,

q = ultimate end bearing pressure given by equation (1.1)

K_o = a non dimensional factor

L = length of the pile

γ = density of soil

δ = angle of friction between the pile and the surrounding soil.

A_b, A_s = area of the base of the pile and the shaft of the pile respectively.

Previous work showed that the value of K_o depended on the change in

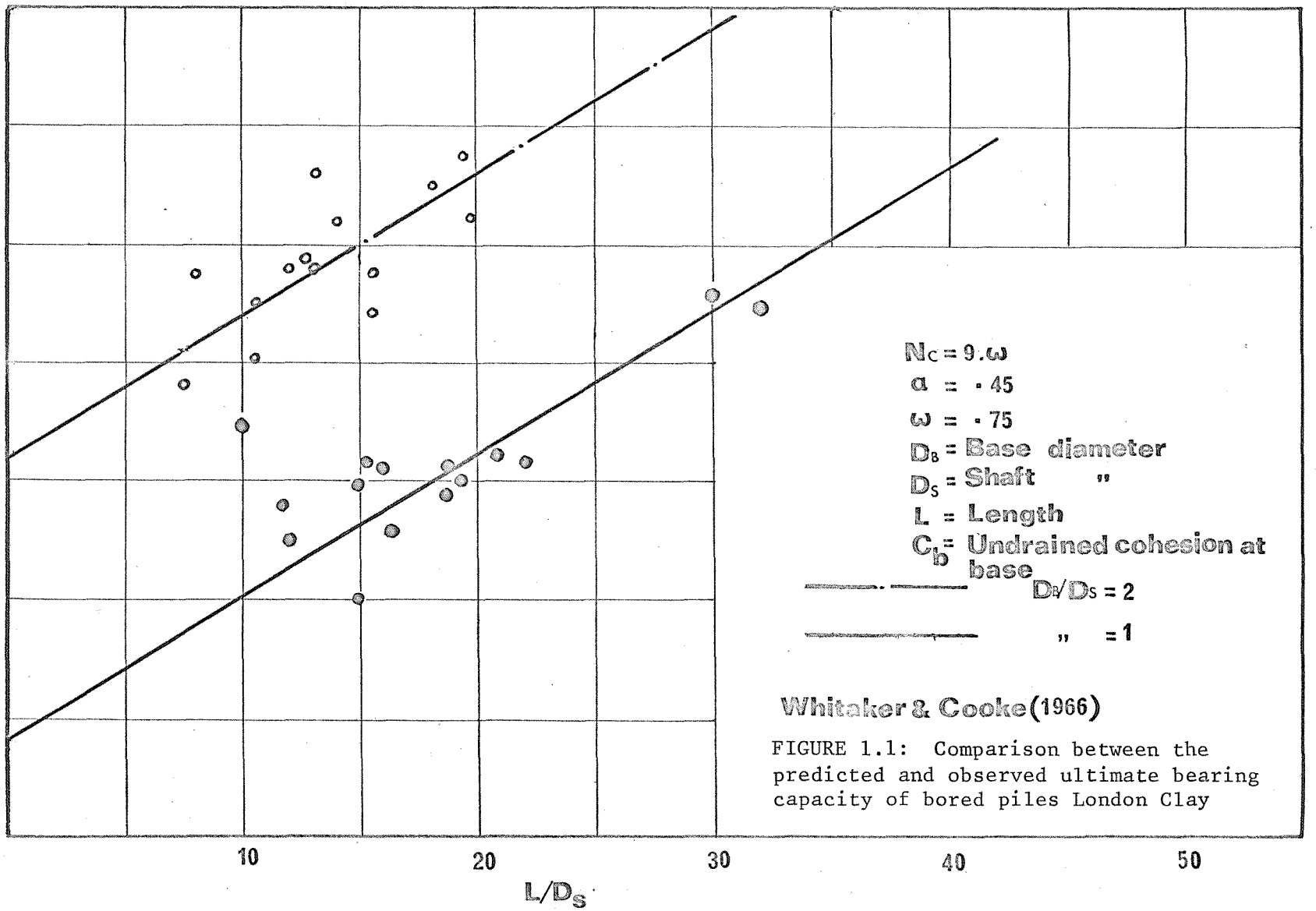

FIGURE 1.1: Comparison between the predicted and observed ultimate bearing capacity of bored piles London Clay

relative density caused by the placement of the pile (Meyerhof, 1959; Kezdi, 1960; Nishida, 1961; Robinsky and Morrison, 1964; de Beer, 1963; Feda, 1967) and found to be independent of the length to diameter ratio and surface roughness (Broms, 1966). The value of δ on the other hand has been observed to be dependent on the surface roughness and density of soil (Butterfield and Andrawes, 1968).

However, the evaluation of the ultimate bearing capacity is only the first step. The selection of the factor of safety in calculating the working load is usually governed by settlement considerations. Whitaker and Cooke (1966) observed that the consolidation settlement of a single axially loaded pile is usually negligible when compared with the immediate settlement and an approximate theoretical solution by Poulos and Davis (1968) confirmed this observation. The settlement of a foundation under working loads is almost always estimated by applications of the theory of elasticity. Although soil is not an elastic material, it was observed by Turnbull et al (1961) that at least for saturated clay the agreement between assumed elastic behaviour and the actual behaviour of foundations was generally good for loads less than half of the ultimate load.

Terzaghi (1943) suggested a method for calculating the displacement of a single pile, whereby an equivalent stress distribution at its tip was obtained by assuming the load to be concentrated at the mid-length of the pile and then applying Mindlin's solution (Mindlin, 1936) for a point load within a semi infinite solid. The consolidation settlement was then estimated by simple one dimensional consolidation theory. Subsequently various analytical approaches have been employed in an attempt to obtain an estimate of the settlement of a single pile. Assumptions on the manner in which the piles transmit their loads along

the shaft and the pile base to the surrounding soil are fundamental to all these studies. Seed and Reese (1955) attempted the problem of relating the stress deformation curves of soil to the displacement of a friction pile. If a point on the pile is assumed to move downwards by a certain distance, this downward movement must be related to the shear deformation of soil at that point in order to determine corresponding shear stresses which will develop the resisting forces along the pile. They suggested the use of a vane test adjacent to the pile face, to determine the relationship between the shear stress and shear strain curve for the soil. A field test pile fitted with strain gauges was installed and the load at different sections of the pile was recorded. The agreement between the calculate loads and the measured loads was within ±10%. A similar method based on shaft shear stress plotted against pile displacement curves obtained from simulated laboratory model tests was described by Coyle and Reese (1966). The load displacement behaviour of an end bearing pile was reported by D'Appolonia and Romualdi (1963) in which the action of a pile was assumed to be equivalent to a number of concentrated loads acting at the pile axis. The displacement of an element i (Figure, 1.2) due to an unit force acting at the centre of the j^{th} element was calculated using Mindlin's solution for a point load within an infinite solid (Mindlin, 1936). An allowance for an underlying rigid layer was made by placing a mirror image of the unit force on the other side of the rigid boundary (Figure, 1.2).

An identical analysis for a step-tapered pile was described by D'Appolonia and Hribar (1963), Salas and Belzunce (1965) adopted the same method of analysis for evaluating the effects of a consolidating soil mass on the behaviour of an end bearing pile. The load displacement characteristics of single axially loaded compressible pile was

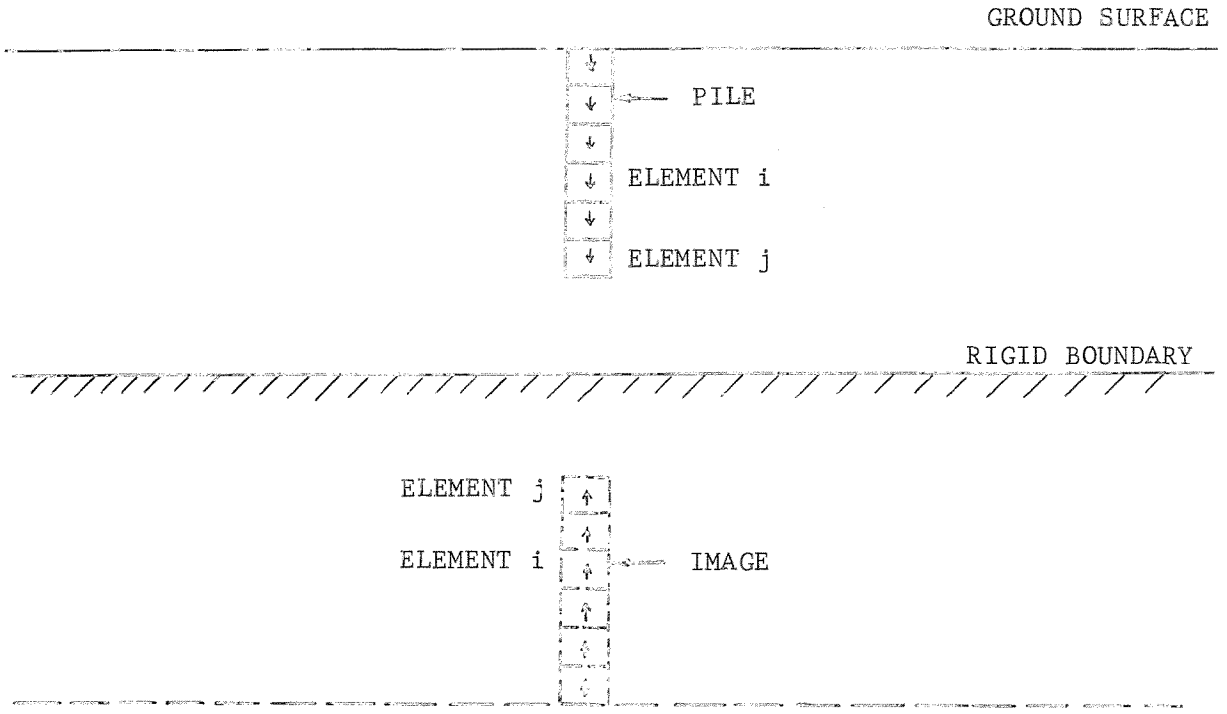

FIGURE 1.2

SINGLE PILE WITHIN A FINITE LAYER

analysed by Nair (1963), Thurman (1964) and Thurman and D'Appolonia (1965) using the approximate analysis described above.

Thurman (1964) also described an identical approximate elastic analysis for a single compressible pile in a layered soil, in which Westergaard's solution (Westergaard, 1938) for the point load in the interior of an elastic half space, which is elastic vertically but infinitely stiff horizontally, was used. Local slip between the pile and the surrounding soil was also taken into consideration.

The method of analysis adopted by the foregoing writers was based on the assumption that the pile is reduced to a line, which is only a

reasonable assumption for slender piles. Therefore any effect of the length to diameter ratio of the pile cannot appear in the results. Moreover, the research described above did not cover the effects of other variables, e.g. base diameter to shaft diameter, modulus of elasticity of the pile to that of the soil etc.

An approximate general study of the settlement behaviour of single axially loaded piles and piers was described by Poulos and Davis (1968), Mattes and Poulos (1969a, 1969b) under the following assumptions in addition to those of ideally elastic soil:

(i) The action of the pile may be represented by a number of uniformly loaded rings acting along the shaft face together with a uniformly loaded smooth disc at the base of the pile

(ii) The disturbance of the continuity of the elastic half space due to the presence of the pile may be ignored.

The displacement at the mid-length of an element j (Figure, 1.2) was obtained by integration of Mindlin's solution over the shaft surface of the element i and over the base. The effects of the ratios of the length to diameter, base diameter to shaft diameter, compressibility of pile to that of the soil, length of the pile to the depth of the elastic layer were studied and the effects of the depth of the elastic layer were evaluated by using the Steinbrenner approximation (Steinbrenner, 1934) for vertical displacements. An analysis of an end bearing pile was also presented (Mattes and Poulos, 1969b) using the mirror image technique (D'Appolonia and Romualdi, 1963). These authors also studied the effects of local slip between the pile and the soil medium by assuming the limiting shear stress at the pile soil interface to be the same as that described by Thurman and D'Appolonia (1965) and Salas (1965).

Time dependent settlement of a single pile due to dissipation of excess pore water pressure was analysed by Poulos and Davis (1968).

This analysis was analytically approximate in that it did not allow for the variation of mean stress throughout the medium with time. It was found that the magnitude of the time dependent settlement is very small compared with the immediate settlement which agrees with Whitaker and Cooke's experimental observations (Whitaker and Cooke, 1966).

The above research on a single pile is related to free-standing piles (i.e. piles with cap not bearing on the ground) only. It was always suspected that the behaviour of a piles with cap bearing on the ground may well be different from that of a free-standing pile. Kishida and Meyerhof (1965) carried out laboratory tests to find the effect of a cap on the ultimate bearing capacity of a single pile. They found that the ultimate bearing capacity of a capped pile was higher than that of a free-standing pile. Poulos (1968a) analysed the settlement behaviour of a pile with a circular based on the assumption that the cap is rigid, smooth and may be represented by a number of uniformly loaded annular rings, together with the assumptions made in his earlier paper (Poulos and Davis, 1968). It was found that for the pile cap and pile geometries commonly encountered in practice the effect of the pile cap on the load displacement characteristics is negligible. The shear stress distribution at the pile-soil interface, however, changes drastically due to the presence of the cap.

1.5 A summary and review of previous researches on pile groups

Most of the published work has been concerned with single piles which usually in practice form only one unit within a large group. In the great majority of cases the being capacity is calculated or measured for a single pile and the group behaviour is extrapolated by empirical means by use of so called "efficiency formulae" or "rules of thumb"

(Terzaghi and Peck, 1948). For such foundations one should be able to express the load-displacement characteristics in terms of various physical quantities in order to arrive at a safe, economically feasible design. Field experience have shown that dynamic driving formulae do not give satisfactory results (Cummings, 1940).

It has been known for nearly three decades that the ultimate bearing capacity of a pile group is not a simple multiple of the ultimate bearing capacity of a single isolated pile and various rules have been designed to allow for this (Terzaghi and Peck, 1948). Terzaghi and Peck (1948) considered the use of "efficiency formulae" to be contrary to good design since these formulae do not take into account the various parameters which are known to influence the group behaviour. They suggested that in the design, the behaviour of the block composed of the soil and the piles within the perimeter of the outer piles (which will be called a block subsequently) should be examined. Peck, Hanson and Thornburn (1953) described a simple method of design in which the failure of this block is determined using the same method as for a single pile. Skempton (1952, 1953) discussed the settlement ratio (defined as the ratio of the settlement of a group of N piles under a load of N•P to the settlement of a single pile under a load P) of pile groups in sand, taking a series of examples from practice for which data were available. He found that the general trend of the group behaviour is identical with that of plates of same sizes as the width of the groups. Whitaker (1957) examined two major aspects of the group behaviour, namely:

(i) The evaluation of the efficiency and the settlement ratio of groups in relation to the number of piles, spacings, lengths and diameters.

(ii) The distribution of load between the piles in a group.

He presented results from an extensive series of model tests on free-standing pile groups in soft remoulded clay, which covered a wide range of spacings to diameter ratios, length to diameter ratios and group sizes. In his tests failure took place by the group either behaving as a single unit (i.e. as a block) or as individual piles. The mode of failure was found to be dependent on the pile spacing and group size. A mechanism of failure was suggested which showed the progressive failure of the piles starting with the exterior ones spreading into the centre of the group as the load was increased.

Meyerhof (1959, 1960) discussed the practical significance of sand compaction caused by driving piles. Based on a series laboratory and field tests he presented design curves relating to pile group and single pile settlement to foundation width, pile spacing and factor of safety (F) on a single pile. The case of free-standing pile groups was not considered and his results referred to capped groups with the pile cap bearing on the sand surface. Modifications to his curves were suggested to allow for eccentricity and inclination of the loading. These publications are extremely useful especially his analysis of sand compaction which was done semiempirically. He observed that, in general, compaction of loose sand and loosening of dense sand took place in the vicinity of piles during placing but the original density of sand had an important influence on the degree of compaction or loosening occurring. It was conclusively shown that the extent of compaction or loosening was dependent on the relative density.

Model tests were carried out by Fleming (1958) and Kezdi (1960) in sand and further work has been reported by Whitaker (1960) and Saffery and Tate (1961) for capped groups and Sowers et al (1961) for free standing pile groups in clays. Fleming worked with square groups in

dry sand and his findings confirmed the general trend reported by Kezdi (1957). Using smaller scale models than his previous tests Kezdi (1960) found that the ultimate load depended on the group shape as well as pile spacing and that a single row of piles showed little increase in ultimate efficiency over unity. The ultimate efficiency was defined as the ratio of the ultimate group load to the product of the ultimate load of a single pile at the same depth, in the same soil condition as the group and the number of piles in the group.

Whitaker (1960) extended his previous investigations in clays to cover the influence of the cap bearing on the clay surface. The main influence of the cap was to cause 'blocking' (i.e. the piles with the cap behaving as a single block) even at spacings up to 4 pile diameters compared to about 2 diameters for free-standing pile groups. The settlement ratios (defined by Whitaker as the ratio of settlement of a group to that of a comparable single pile when both carry the same fraction of their failure load) for 3 square capped pile groups were found to be nearly the same as that for 3 square free-standing pile groups. However, for larger groups, the settlement ratios for capped groups were found to be up to 50 per cent higher than the corresponding free-standing groups, the actual increase being dependent on the pile spacing and the size of the group. Whitaker confined his studies to piles with length to diameter ratio of 48 and the effect of the variation of the length to diameter ratio on the response of a capped group was not studied. The results of Saffery and Tate and Sowers et al were in agreement with those presented by Whitaker (1957). Saffery and Tate also investigated the effects of an eccentric loading on the load displacement behaviour of a free-standing pile group in clay. They found difference of up to 30% in settlement behaviour and no noticeable difference in the ultimate

load due to eccentricity of loading up to 2/3 pile spacings.

Konder (1962) developed a non-dimensional technique based on the methods of dimensional analysis to develop analytical expressions for the load displacement characteristics of axially loaded friction pile groups in cohesive soils based on an assumed hyperbolic stress-strain response of cohesive soils. The variables included were, the settlement of the group, the pile diameter, the pile spacing, the number of piles in the group, the depth of embedment, the geometric arrangement of the piles and the shear strength of the cohesive soil penetrated by the piles. The analytical expressions were compared with the field and laboratory test results with agreement of 15 per cent. Kishida and Mayerhof (1965) conducted a series of model tests with pile groups in sand with the cap resting on the surface and the effects of eccentricity of loading on the group behaviour were studied. The ultimate bearing capacity was found to decrease with the increase in the eccentricity of loading. Hanna (1963) described the results of a large number of laboratory loading tests on model pile groups in dry sand. It was found that the ultimate bearing capacity of a group of piles may be greater or less than the ultimate bearing capacity of a single pile multiplied by the number of piles in the group, due to compaction or loosening caused by driving the piles. Settlement of a group was however found to be several times greater than the settlement of a single pile under the equivalent load, so that usually a large factor of safety would be necessary to control group settlement. An extensive comparison between model test results and the full scale field test results indicated the presence of an additional scale factor which made extrapolation of the results of the model tests to field practice difficult.

The test results described by Kezdi (1957, 1960), Schiff (1961) were on groups of piles between 1/5th and 1/20th of field scale, while Skempton (1953) and Meyerhof (1959, 1960) Berezantzev et al (1961) gave records of full scale foundations. Comparisons between the results of the model tests described by Hanna (1963) and these other model tests revealed (Hanna, 1963) that:

(i) The ultimate group efficiencies in the field tests are greater than the laboratory model tests.

(ii) The settlement ratios of the full scale field tests and the laboratory model tests are greater than the intermediate model test values.

(iii) The individual pile driving ratios (defined as the penetration resistance of the successive piles to the penetration resistance of the first pile) are greater in field tests than in the laboratory tests.

Thus it would appear that more full scale tests data are needed to formulate design rules for pile groups. Full scale field tests are expensive, however, a theoretical analysis of pile groups could be usefully developed.

Attempts to establish approximate theoretical solutions based on the theory of elasticity were made by Nishida (1961, 1964). To simplify the mathematical complexity of the problem Nishida assumed an empirical pattern of shear stress distribution at the pile soil interface. This therefore cannot be regarded as a satisfactory solution, because the distribution of the shear stress at the pile-soil interface is not known before the analysis. Moreover, his analysis was based on the assumption that the 'zone of influence" of a single pile in a group was limited to a radius of half the pile spacings. This assumption led to the calculated

efficiency curve being independent of the geometric configuration of the group and dependent on the length to diameter ratios only. A comparison with the model test results of Whitaker (1957) revealed that except for 9 x 9 pile groups the theoretical results underestimated the efficiency of a group by as much as 100%. Doroshkevich and Bartolomey (1965) obtained an approximate analysis of single piles, single rows of piles, and pile groups with square and rectangular arrangements assuming the pile group to behave as a single 'block' (Terzaghi, 1943). They used Melan's solution (Melan, 1932) in the calculation of the settlement of single row pile foundations and Mindlin's solution (Mindlin, 1936) for the pile groups with square and rectangular arrangements. The analysis is in no way different from the one suggested by Terzaghi (1943) and does not take into account of the variation of load distribution within the pile group. A very comprehensive analysis of pile groups was described by Poulos (1968b) in which he used Mindlin's solution to calculate the interaction factors between two piles. The load displacement relationships of rigid pile groups and the load distribution within the pile group were analysed using the interaction factors derived for a two pile group. The interaction factor for two rigid piles was found to be a function of the spacing to diameter ratios, and length to diameter ratios. It is however, conceivable that other factors such as position of the pile in a group, and the compressibility of the piles are likely to influence the values of these interaction factors. No allowance for these was made in his analysis. He also attempted an approximate evaluation of the effect of the depth of the elastic layer on the load displacement response of a pile group using the Steinbrenner approximation. The effect of the depth of the elastic layer was found to influence the group behaviour more than it did to single pile.

The problem of the interaction between a pile cap and its group still remains to be solved.

1.6 Definition of the problem and scope of the present research

It can be seen from the previous sections that the design of pile foundations ideally requires detailed knowledge of the subsoil properties before and after placing the pile in addition to the basic mechanics of pile-soil interaction. Thus neither a wholly theoretical nor a completely experimental study of pile foundations is likely to give an adequate basis of design. To develop a rational design theory one must be able to assess the relative importance of the different variables on the behaviour of pile foundations. This is what is examined in the major part of the work presented below in which the following aspects of pile foundations and the associated problems are described:

(i) A theoretical investigation into the load displacement characteristics of axially loaded plain and under-reamed piles and deep foundations.

(ii) A theoretical analysis of load displacement characteristics of free-standing pile groups of arbitrary spacing.

(iii) The interaction between a pile cap and its group.

(iv) The analysis of the ultimate bearing capacity of a driven pile.

(v) An experimental investigation of the effects of an applied electric potential and rate of penetration on the penetration resistance of model probes and blades.

Chapter 2

Integral equations in three-dimensional elasticity

2.1 Summary

An integral method which can be used in principle to obtain a numerical solution of any problem in classical elasticity is described in this Chapter. The method is compared with some widely used differential methods. Earlier applications of integral equation methods to the problems of elasticity are also reviewed and compared with the method described in this Chapter. A scheme of numerical calculations suitable for digital computers is outlined which has been used successfully for the solutions displayed in the subsequent Chapters.

2.2 Introduction

With the advent of computers, numerical methods are being used more often and the days of solution of differential equations by suitably chosen series polynomials are virtually gone. Numerical methods may be classified under two major categories:

(i) Differential methods,

(ii) Integral methods.

Differential methods, such as the finite difference, finite element, collocation and Rayleigh-Ritz methods are primarily designed to satisfy the governing equations approximately. In finite difference method the basic differential equation of the problem is replaced by difference equations over a set of points in the domain (Allen, 1955). The finite element method, originally developed by Turner et al (1956) and subsequently by Clough (1960) and Zienkiewicz (1967) has proved to be a very useful tool for the solution of many complicated problems. The body or region in which the solution is required, is divided into a suitable number of triangular, tetrahedral, cubic or rectangular parallelopiped elements, for each of which a suitable compatible elemental displacement field is chosen (in the stiffness method). A set of equations is then derived by satisfying equilibrium (in the stiffness formulation) at the element nodes. In the collocation method, or point matching technique as it is sometimes called, a functional representation containing a number of arbitrary constants is chosen. These are substituted in the basic differential equations of the problem. A set of simultaneous equations is then obtained by evaluating the function at a number of points equal to the number of unknown constants. The Rayleigh-Ritz method entails the selection of a series of functions with unknown constants, each of which satisfies the geometric boundary conditions. The chosen series of functions are then substituted into the energy conservation equations corresponding

to the given field equations and minimised with respect to the unknown constants. A set of simultaneous equations for the unknown constants is thus obtained. A comprehensive treatment of these variational methods is given in Mikhlin (1964).

Differential methods, finite element in particular, have the advantage of being very general and therefore theoretically able to cope with complex constitutive laws for the materials involved. The major disadvantage of these methods is that the resulting system of equation is large and may be ill-conditioned (Massonnet, 1965).

Integral equation methods often give accurate results more economically. A particular solution which satisfies the differential equation of the given problem is chosen. By distributing these particular solutions over the surface of the given domain (i.e. by the principle of superposition) a general solution in terms of an arbitrary function is developed. For the general solution to satisfy the boundary condition, the arbitrary function must satisfy an integral equation over the boundary. There are generally fewer unknowns and the error of discretisation is usually confined to the boundaries, because in this method the boundaries are only discretised whereas differential methods need the whole domain to be discretised. The use of principle of superposition restricts the application of such a method to problems involving non linear constitutive laws for the materials.

The first rigorous investigation of an integral equation was made by Fredholm as late as 1903. There has been a considerable development, particularly in connection with field theory, since then. The method has been applied to solutions of problems of elasticity, notably by Soviet writers. The works of Muskhelishvili (1953) and Mikhlin (1957) are well known.

Muskhelishvili's method of solution, being based on complex variable

theory, cannot easily be extended to three dimensional problems of elasticity. Mikhlin's work on multidimensional singular integral equations is much more useful in this respect. Vectors, such as stress components can be written directly in a vectorial integral equation, which is effectively a system of simultaneous scalar integral equations.

None of the above mentioned writers considered the translation of such a method into a suitable algorithm for the numerical solution of engineering prlblems. Massonnet (1965) described a numerical solution of the stress boundary value problem formulated in terms of a vectorial singular integral equation of the second kind. His formulation was based on the use of Boussinesq's point load solution (Boussinesq, 1885) for a half space. Since Boussinesq's solution has a line of doublets extending from zero to infinity on the negative side of the half space, his formulation is not valid for some concave domains where the outward normal to the surface cuts the domain more than once. His method is valid for smooth surfaces hence would produce good results for bodies without sharp edges and corners. Difficulties caused by sharp edges and corners were partially overcome by a method described by Oliveira (1968), in which the elementary singular solution is distributed over an auxiliary boundary adjacent to the actual boundary. The fictitious intensities (the arbitrary functions) are distributed over the auxiliary boundary in such a manner that the given boundary conditions on the actual boundary are reproduced. Such a method has an advantage over Massonnet's for bodies with sharp edges and corners. The major deficiency is that it has to be possible to analytically continue the functions representing the displacement field into the region between the auxiliary boundary and the actual boundary, without the occurrence of a singularity. Oliveira assumes without the proof that this is

possible.

Oliveira restricted his formulation to plane stress problems only. The particular solution chosen is an intensity, defined by two parameters, distributed linearly from a maximum to zero over two adjacent elements of the auxiliary boundary. Such an approach would appear to be better than Massonnet's method of uniform variation of intensity across each element. In general, if the auxiliary boundary sufficiently far away from the actual boundary the resulting system of equations may be ill-conditioned. Even if a double precision technique of numerical solution is adopted, the variation of the unknown fictitious intensities over the boundary would be very rapid. If, however, the auxiliary boundary is taken indefinitely close to the actual boundary the method suggested by Oliveira would produce good results, provided the kernel functions (at least the nearly singular part of it) are evaluated analytically (see Article,2.9).

Kupradze (1964) described an integral formulation for the displacement of an elastic body subjected to periodic body forces and boundary conditions considering the static problem as a particular case. He has given the proof of the existence of the proposed integral representation and investigated its uniqueness using Mikhlin's work on multidimensional singular integral equations (Mikhlin, 1957, 1965).

The method described below is both an improvement and generalisation of Oliveira's and Massonnet's methods for the three-dimensional problems. Some of Kupradze's results have been used in the derivation of the integral equations. A method of numerical solution of the integral equation is suggested which can deal with any regular variation of the unknown functions over the boundary. Body forces have been assumed to be zero and small strain theory has been used throughout.

2.3 Statement of the problem

We consider a body of arbitrary shape enclosed within a surface, S. The region outside S is denoted by D_e and the interior region by D_i. The surface S is assumed to satisfy a smoothness condition, such as that of Lyapunov (see Smirnov, 1964). The condition is, however, not too restrictive. In future, we specify this requirement by stating that the surface is sufficiently smooth. The boundary conditions on S are given by (in Cartesian Coordinates):

(i) $u_i(A) = f_i(A)$

(ii) $\sigma_{ip}(A).n_p = p_i(A) = f_i(A)$

(iii) $\sigma_{ip}(A).n_p + u_i(A) = p_i(A) + u_i(A) = f_i(A)$

where $A \in S$

$u_i(A)$ denotes the displacement vector on S,

n_p is the unit normal to S (+ ve for outward normals and - ve for inward normals),

$f_i(A)$ are the given boundary conditions which are assumed to satisfy a Lipschitz condition (Mikhlin, 1957), which we may interpret in engineering sense as reasonably well behaved functions

$\sigma_{ip}(A)$ denotes the stress tensor at a point on S, and $p_i(A)$ the stress resultants at a point on S,

i,p = 3,2 for 3-dimensional and two-dimensional problems respectively and summation is implied over repeated suffixes.

Alternatively in matrix notation (with respect to X, Y, Z axes, Figure 2.2):

$$\sigma_{ip}.n_p \equiv \begin{bmatrix} \sigma_{xx} & \sigma_{xy} & \sigma_{xz} \\ \sigma_{yx} & \sigma_{yy} & \sigma_{yz} \\ \sigma_{zx} & \sigma_{zy} & \sigma_{zz} \end{bmatrix} \begin{Bmatrix} n_x \\ n_y \\ n_z \end{Bmatrix} = \begin{Bmatrix} p_x \\ p_y \\ p_z \end{Bmatrix} \equiv p_i$$

where $\sigma_{ip} = \sigma_{pi}$, i.e. $[\sigma]$ is symmetrical; (2.1)

and,

$$u_i = \begin{Bmatrix} u_x \\ u_y \\ u_z \end{Bmatrix}, \qquad f_i = \begin{Bmatrix} f_x \\ f_y \\ f_z \end{Bmatrix} .$$

2.4 Some definitions

Figure 2.1 defines some regions by symbols which are used in subsequent articles. The surfaces S_e and S_I are two surfaces in the immediate neighbourhood of S.

D_e^+ = Domain outside S_I and contains D_e,

D_e = Domain outside S,

D_i^+ = Domain inside S_e and contains D_i,

D_i = Domain inside S.

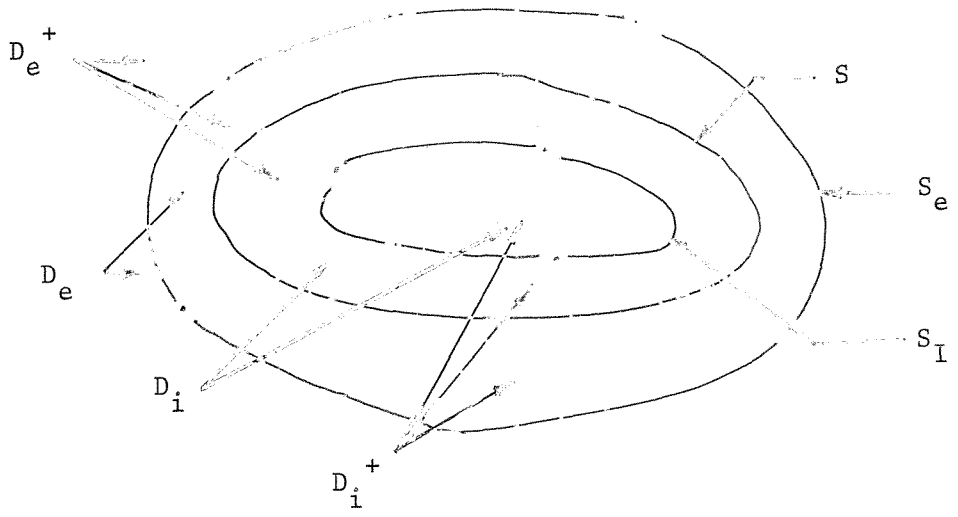

FIGURE 2.1

SOME DEFINITIONS OF SURFACES AND REGIONS

2.5 A basic elementary solution

Before we can make any kind of mathematical formulation of the problem we need to select an elementary solution which satisfies the basic equation of equilibrium and compatibility everywhere in the domain of interest. The following elementary singular solution have been used by previous investigators:

(i) Flamant's two-dimensional simple radial stress distribution (Massonnet, 1965),

(ii) Boussinesq's solution for a concentrated load on the surface of a half space (Massonnet, 1965),

(iii) Kelvin's solution for a point load within an infinite space (Kupradze, 1964; Watson, 1968).

In the present work the singular solution of a point load in the interior of a half space (Mindlin, 1936) will be used. There is a distinct advantage in using Mindlin's solution for many foundation engineering problems because the singular solution satisfies the zero stress boundary condition on the surface of the half space. The singular part of solution (iii) has the same singularity at the point of application of the load as has Mindlin's solution. Thus for the purpose of the analytical formulation of the singular integral equation they can be regarded as identical.

As shown in Figure (2.2) forces P_x, P_y, P_z are acting at $B(\xi, \eta, \zeta)$ in the X, Y and Z directions respectively. The displacements and stresses due to these forces can be obtained everywhere in the half space (defined as the materials filling $Z \geq 0$ region) from Mindlin's solution (Mindlin, 1936) given below:

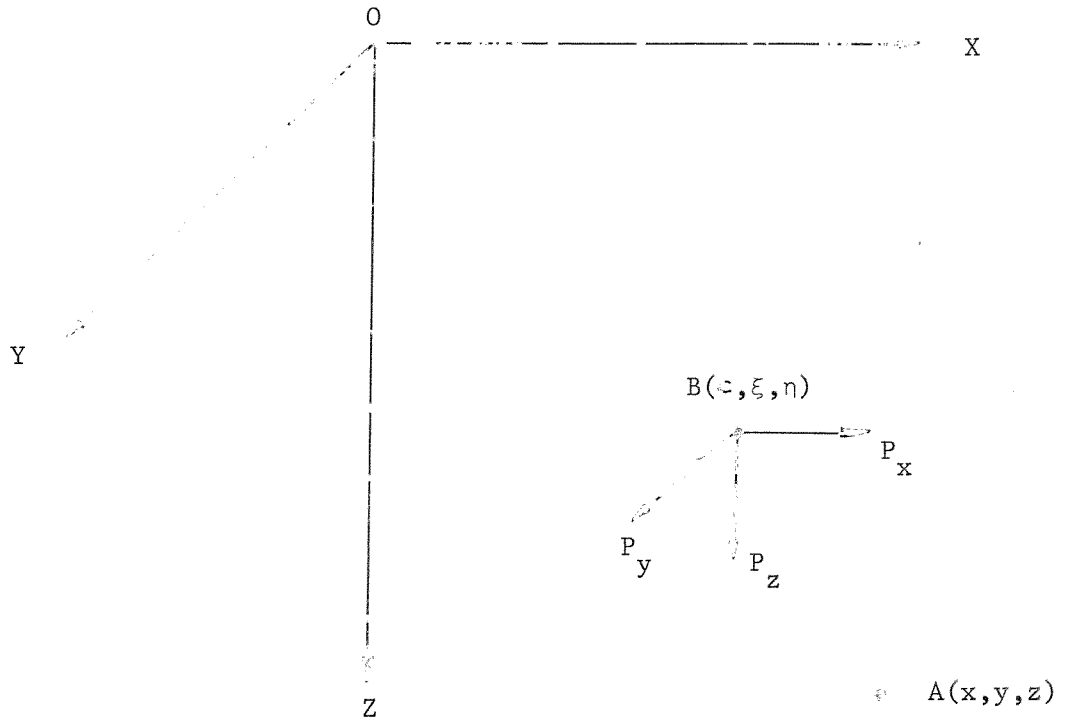

MINDLIN'S PROBLEM

FIGURE 2.2

The displacements and stresses at A due to the force P_x acting at B are given by:

$$u_x = \frac{P_x}{16\pi G(1-\mu)}\left[\frac{3-4\mu}{R_1}+\frac{1}{R_2}+\frac{x_o^2}{R_1^3}+\frac{(3-4\mu)x_o^2}{R_2^3}+\frac{2cz}{R_2^3}\left(1-\frac{3x_o^2}{R_2^2}\right)+\frac{4(1-\mu)(1-2\mu)}{R_2+z+c}\left(1-\frac{x_o^2}{R_2(R_2+z+c)}\right)\right]$$

$$u_y = \frac{P_x x_o y_o}{16\pi G(1-\mu)}\left[\frac{1}{R_1^3}+\frac{3-4\mu}{R_2^3}-\frac{6cz}{R_2^5}-\frac{4(1-\mu)(1-2\mu)}{R_2(R_2+z+c)^2}\right],$$

$$u_z = \frac{P_x x_o}{16\pi G(1-\mu)}\left[\frac{z-c}{R_1^3}+\frac{(3-4\mu)(z-c)}{R_2^3}-\frac{6cz(z+c)}{R_2^5}+\frac{4(1-\mu)(1-2\mu)}{R_2(R_2+z+c)}\right],$$

$$\sigma_{xx} = \frac{P_x x_o}{8\pi(1-\mu)}\left[-\frac{(1-2\mu)}{R_1^3}+\frac{(1-2\mu)(5-4\mu)}{R_2^3}-\frac{3x_o^2}{R_1^5}-\frac{3(3-4\mu)x_o^2}{R_2^5}\right.$$
$$\left.-\frac{4(1-\mu)(1-2\mu)}{R_2(R_2+z+c)^2}\left(3-\frac{x_o^2(3R_2+z+c)}{R_2^2(R_2+z+c)}\right)+\frac{6c}{R_2^5}\left(3c-(3-2\mu)(z+c)+\frac{5x_o^2z}{R_2^2}\right)\right],$$

$$\sigma_{yy} = \frac{P_x x_o}{8\pi(1-\mu)}\left[\frac{(1-2\mu)}{R_1^3}+\frac{(1-2\mu)(3-4\mu)}{R_2^3}-\frac{3y_o^2}{R_1^5}-\frac{3(3-4\mu)y_o^2}{R_2^5}\right.$$
$$\left.-\frac{4(1-\mu)(1-2\mu)}{R_2(R_2+z+c)^2}\left(1-\frac{y_o^2(3R_2+z+c)}{R_2^2(R_2+z+c)}\right)+\frac{6c}{R_2^5}\left(c-(1-2\mu)(z+c)+\frac{5y_o^2z}{R_2^2}\right)\right],$$

$$\sigma_{zz} = \frac{P_x x_o}{8\pi(1-\mu)}\left[\frac{(1-2\mu)}{R_1^3}-\frac{(1-2\mu)}{R_2^3}-\frac{3(z-c)^2}{R_1^5}-\frac{3(3-4\mu)(z+c)^2}{R_2^5}+\frac{6c}{R_2^5}\left(c+(1-2\mu)(z+c)+\frac{5z(z+c)^2}{R_2^2}\right)\right],$$

$$\sigma_{yz} = \frac{P_x x_o y_o}{8\pi(1-\mu)}\left[-\frac{3(z-c)}{R_1^5}-\frac{3(3-4\mu)(z+c)}{R_2^5}+\frac{6c}{R_2^5}\left(1-2\mu+\frac{5z(z+c)}{R_2^2}\right)\right],$$

$$\sigma_{zx} = \frac{P_x}{8\pi(1-\mu)}\left[-\frac{(1-2\mu)(z-c)}{R_1^3}+\frac{(1-2\mu)(z-c)}{R_2^3}-\frac{3x_o^2(z-c)}{R_1^5}-\frac{3(3-4\mu)x_o^2(z+c)}{R_2^5}\right.$$
$$\left.-\frac{6c}{R_2^5}\left(z(z+c)-(1-2\mu)x_o^2-\frac{5x_o^2z(z+c)}{R_2^2}\right)\right], \qquad (2.2)$$

$$\sigma_{xy} = \frac{P_x y_o}{8\pi(1-\mu)}\left[-\frac{(1-2\mu)}{R_1^3}+\frac{(1-2\mu)}{R_2^3}-\frac{3x_o^2}{R_1^5}-\frac{3(3-4\mu)x_o^2}{R_2^5}\right.$$
$$\left.-\frac{4(1-\mu)(1-2\mu)}{R_2(R_2+z+c)^2}\left(1-\frac{x_o^2(3R_2+z+c)}{R_2^2(R_2+z+c)}\right)-\frac{6cz}{R_2^5}\left(1-\frac{5x_o^2}{R_2^2}\right)\right].$$

where G and μ are elastic constants, modulus of rigidity and Poisson's ratio respectively.

$$R_1 = \left[(x-\xi)^2 + (y-\eta)^2 + (z-c)^2\right]^{\frac{1}{2}},$$

$$R_2 = \left[(x-\xi)^2 + (y-\eta)^2 + (z+c)^2\right]^{\frac{1}{2}},$$

$x_o = [x-\xi]$, $y_o = [y-\eta]$, u_x, u_y, u_z are displacements in X, Y, Z directions respectively.

The displacements and stresses at A due to the force P_y acting at B can be obtained from:

$$u_x = \frac{P_y}{16\pi G(1-\mu)}\left[\frac{3-4\mu}{R_1}+\frac{1}{R_2}+\frac{x_1^2}{R_1^3}+\frac{(3-4\mu)x_1^2}{R_2^3}+\frac{2cz}{R_2^3}\left(1-\frac{3x_1^2}{R_2^2}\right)+\frac{4(1-\mu)(1-2\mu)}{R_2+z+c}\left(1-\frac{x_1^2}{R_2(R_2+z+c)}\right)\right]$$

$$u_y = \frac{P_y x_1 y_1}{16\pi G(1-\mu)}\left[\frac{1}{R_1^3}+\frac{3-4\mu}{R_2^3}-\frac{6cz}{R_2^5}-\frac{4(1-\mu)(1-2\mu)}{R_2(R_2+z+c)^2}\right],$$

$$u_z = \frac{P_y x_1}{16\pi G(1-\mu)}\left[\frac{z-c}{R_1^3}+\frac{(3-4\mu)(z-c)}{R_2^3}-\frac{6cz(z+c)}{R_2^5}+\frac{4(1-\mu)(1-2\mu)}{R_2(R_2+z+c)}\right],$$

$$\sigma_{xx} = \frac{P_y x_1}{8\pi(1-\mu)}\left[-\frac{(1-2\mu)}{R_1^3}+\frac{(1-2\mu)(5-4\mu)}{R_2^3}-\frac{3x_1^2}{R_1^5}-\frac{3(3-4\mu)x_1^2}{R_2^5}\right.$$
$$\left.-\frac{4(1-\mu)(1-2\mu)}{R_2(R_2+z+c)^2}\left(3-\frac{x_1^2(3R_2+z+c)}{R_2^2(R_2+z+c)}\right)+\frac{6c}{R_2^5}\left(3c-(3-2\mu)(z+c)+\frac{5x_1^2 z}{R_2^2}\right)\right],$$

$$\sigma_{yy} = \frac{P_y x_1}{8\pi(1-\mu)}\left[\frac{(1-2\mu)}{R_1^3}+\frac{(1-2\mu)(3-4\mu)}{R_2^3}-\frac{3y_1^2}{R_1^5}-\frac{3(3-4\mu)y_1^2}{R_2^5}\right.$$
$$\left.-\frac{4(1-\mu)(1-2\mu)}{R_2(R_2+z+c)^2}\left(1-\frac{y_1^2(3R_2+z+c)}{R_2^2(R_2+z+c)}\right)+\frac{6c}{R_2^5}\left(c-(1-2\mu)(z+c)+\frac{5y_1^2 z}{R_2^2}\right)\right],$$

$$\sigma_{zz} = \frac{P_y x_1}{8\pi(1-\mu)}\left[\frac{(1-2\mu)}{R_1^3}-\frac{(1-2\mu)}{R_2^3}-\frac{3(z-c)^2}{R_1^5}-\frac{3(3-4\mu)(z+c)^2}{R_2^5}+\frac{6c}{R_2^5}\left(c+(1-2\mu)(z+c)+\frac{5z(z+c)^2}{R_2^2}\right)\right],$$

$$\sigma_{yz} = \frac{P_y x_1 y_1}{8\pi(1-\mu)}\left[-\frac{3(z-c)}{R_1^5}-\frac{3(3-4\mu)(z+c)}{R_2^5}+\frac{6c}{R_2^5}\left(1-2\mu+\frac{5z(z+c)}{R_2^2}\right)\right],$$

$$\sigma_{zx} = \frac{P_y}{8\pi(1-\mu)}\left[-\frac{(1-2\mu)(z-c)}{R_1^3}+\frac{(1-2\mu)(z-c)}{R_2^3}-\frac{3x_1^2(z-c)}{R_1^5}-\frac{3(3-4\mu)x_1^2(z+c)}{R_2^5}\right.$$
$$\left.-\frac{6c}{R_2^5}\left(z(z+c)-(1-2\mu)x_1^2-\frac{5x_1^2 z(z+c)}{R_2^2}\right)\right], \qquad (2.3)$$

$$\sigma_{xy} = \frac{P_y y_1}{8\pi(1-\mu)}\left[-\frac{(1-2\mu)}{R_1^3}+\frac{(1-2\mu)}{R_2^3}-\frac{3x_1^2}{R_1^5}-\frac{3(3-4\mu)x_1^2}{R_2^5}\right.$$
$$\left.-\frac{4(1-\mu)(1-2\mu)}{R_2(R_2+z+c)^2}\left(1-\frac{x_1^2(3R_2+z+c)}{R_2^2(R_2+z+c)}\right)-\frac{6cz}{R_2^5}\left(1-\frac{5x_1^2}{R_2^2}\right)\right].$$

where G, μ, R_1, R_2 are quantities defined previously.

$$x_1 = [y-\eta] ,$$

$$y_1 = [\xi-x] ,$$

The stresses and displacements at A due to the force P_z are given by:

$$u = \frac{P_z \gamma}{16\pi G(1-\mu)}\left[\frac{z-c}{R_1^3}+\frac{(3-4\mu)(z-c)}{R_2^3}-\frac{4(1-\mu)(1-2\mu)}{R_2(R_2+z+c)}+\frac{6cz(z+c)}{R_2^5}\right],$$

$$u_z = \frac{P_z}{16\pi G(1-\mu)}\left[\frac{3-4\mu}{R_1}+\frac{8(1-\mu)^2-(3-4\mu)}{R_2}+\frac{(z-c)^2}{R_1^3}+\frac{(3-4\mu)(z+c)^2-2cz}{R_2^3}+\frac{6cz(z+c)^2}{R_2^5}\right],$$

$$\sigma_{xx} = \frac{P_z}{8\pi(1-\mu)}\left[\frac{(1-2\mu)(z-c)}{R_1^3} - \frac{3x_o^2(z-c)}{R_1^5} + \frac{(1-2\mu)[3(z-c)-4\mu(z+c)]}{R_2^3}\right.$$
$$\left. - \frac{3(3-4\mu)x_o^2(z-c) - 6c(z+c)[(1-2\mu)z - 2\mu c]}{R_2^5} - \frac{30cx_o^2z(z+c)}{R_2^7}\right.$$
$$\left. - \frac{4(1-\mu)(1-2\mu)}{R_2(R_2+z+c)}\left(1 - \frac{x_o^2}{R_2(R_2+z+c)} - \frac{x_o^2}{R_2^2}\right)\right],$$

$$\sigma_{xy} = \frac{P_z}{8\pi(1-\mu)}\left[\frac{(1-2\mu)(z-c)}{R_1^3} - \frac{3y_o^2(z-c)}{R_1^5} + \frac{(1-2\mu)[3(z-c)-4\mu(z+c)]}{R_2^3}\right.$$
$$\left. - \frac{3(3-4\mu)y_o^2(z-c) - 6c(z+c)[(1-2\mu)z - 2\mu c]}{R_2^5} - \frac{30cy_o^2z(z+c)}{R_2^7}\right.$$
$$\left. - \frac{4(1-\mu)(1-2\mu)}{R_2(R_2+z+c)}\left(1 - \frac{y_o^2}{R_2(R_2+z+c)} - \frac{y_o^2}{R_2^2}\right)\right],$$

$$\sigma_{zz} = \frac{P_z}{8\pi(1-\mu)}\left[-\frac{(1-2\mu)(z-c)}{R_1^3} + \frac{(1-2\mu)(z-c)}{R_2^3} - \frac{3(z-c)^3}{R_1^5}\right. \qquad (2.4)$$
$$\left. - \frac{3(3-4\mu)z(z+c)^2 - 3c(z+c)(5z-c)}{R_2^5} - \frac{30cz(z+c)^3}{R_2^7}\right],$$

$$\sigma_{yz} = \frac{P_z y_o}{8\pi(1-\mu)}\left[-\frac{(1-2\mu)}{R_1^3} + \frac{(1-2\mu)}{R_2^3} - \frac{3(z-c)^2}{R_1^5} - \frac{3(3-4\mu)z(z+c) - 3c(3z+c)}{R_2^5} - \frac{30cz(z+c)^2}{R_2^7}\right],$$

$$\sigma_{zx} = \frac{P_z x_o}{8\pi(1-\mu)}\left[-\frac{(1-2\mu)}{R_1^3} + \frac{(1-2\mu)}{R_2^3} - \frac{3(z-c)^2}{R_1^5} - \frac{3(3-4\mu)z(z+c) - 3c(3z+c)}{R_2^5} - \frac{30cz(z+c)^2}{R_2^7}\right],$$

$$\sigma_{xy} = \frac{P_z x_o y_o}{8\pi(1-\mu)}\left[-\frac{3(z-c)}{R_1^5} - \frac{3(3-4\mu)(z-c)}{R_2^5} + \frac{4(1-\mu)(1-2\mu)}{R_2^2(R_2+z+c)}\left(\frac{1}{R_2+z+c} + \frac{1}{R_2}\right) - \frac{30cz(z+c)}{R_2^7}\right].$$

$$u_x = u_o \left\{(x-\xi)/\left[(x-\xi)^2 + (y-\eta)^2\right]^{\frac{1}{2}}\right\},$$

$$u_y = u_o \left\{(y-\eta)/\left[(x-\xi)^2 + (y-\eta)^2\right]^{\frac{1}{2}}\right\},$$

where u is the radial displacement (because the last case is an axisymmetric one) and $r = \left[(x-\xi)^2 + (y-\eta)^2\right]^{\frac{1}{2}}$.

It can be seen from equations (2.2), (2.3) and (2.4) that as A approaches B indefinitely the terms containing R_1 in the denominator become infinite whereas the terms containing R_2 in the denominator remain finite, and also by letting $R_2 \to \infty$ the solutions for point loads (P_x, P_y, P_z) in an

infinite space can be derived (Love, 1953; Mindlin, 1936).

Equations (2.2), (2.3) and (2.4) can be combined and written as:

$$u_i(A) = P_j \, K_{ij}(A,B) \tag{2.5}$$

$$\sigma_{ij}(A) = P_k \, T_{ijk}(A,B) \tag{2.6}$$

where $u_i(A)$ are displacements at A

$\sigma_{ij}(A)$ are the stress components at A

P_j are the forces at B

$K_{ij}(A,B)$, $T_{ijk}(A,B)$ are known functions which can be obtained from equations (2.2), (2.3) and (2.4).

Equation (2.6) may be reduced, with the help of equation (2.1), to

$$p_i(A) = P_j \, \tau_{ij}(A,B) \tag{2.7}$$

where $p_i(A)$ are the stress resultants on a surface at A and

$$\tau_{ij}(A,B) = T_{ijk}(A,B) \cdot n_k .$$

2.6 Formulation of the integrals for the stress resultants and displacements in D_e and D_i

If we now distribute fictitious surface stress intensities ϕ_j over the surface S, and let δS be an element of the surface S, then for the elemental loads the elemental displacements are given by

$$\delta u_i(A) = \phi_j(B) \, K_{ij}(A,B) \quad \delta S \tag{2.8}$$

The displacements $u_i(A)$ at a point A due to all such elemental surface intensities given by

$$u_i(A) = \int_S \phi_j(B) \, K_{ij}(A,B) \quad dS \tag{2.9}$$

Similarly the stress resultants at a point on a surface through A due to all elemental surface intensities acting over S can be obtained from

$$p_i(A) = \int_S \phi_j(B) \quad \tau_{ij}(A,B) \quad dS \qquad (2.10)$$

The kernel functions of the integrals (2.9) and (2.10) have a singularity when A and B coincide. The order of the singularity for the displacement integrals is $1/r_{AB}$ and that for the stress integrals $1/r_{AB}^2$, where

$$r_{AB} = \left|(z-c)^2 + (x-\xi)^2 + (y-\eta)^2\right|^{\frac{1}{2}}.$$

Before we can proceed any further we need to investigate the following:

(i) Does the integral representation satisfy the equations of equilibrium and compatibility everywhere?

(ii) Do the integrals exist everywhere on D_e, D_i and on S?

(iii) Have the integral equations got a unique solution?

The functions (2.9) and (2.10) satisfy the equations of equilibrium and compatibility in D_e and D_i, because the elementary solution is chosen to satisfy these conditions. The integrals (2.9) and (2.10) exist in D_e and D_i since they are proper integrals of continuous functions (the kernel functions are continuous and bounded in D_e and D_i). The integrals for the displacements satisfy the regularity condition at infinity. But the existence of the integral representation as A approaches S from D_e and D_i needs to be established.

2.7 Behaviour on S

We consider the integral (2.9)

$$u_i(A) = \int_S \phi_j(B) \; K_{ij}(A,B) \; dS$$

Let A_o be a point on S. For the point A tending to S from either side (i.e. either from D_e or from D_i), the above can be written as

$$\lim_{A \to A_o} u_i(A) = \lim_{A \to A_o} \int_S \phi_j(B)\, K_{ij}(A,B)\, dS$$

$$= \lim_{A \to A_o} \left[\int_S [\phi_j(B) - \phi_j(A_o)]\, K_{ij}(A,B)\, dS \right.$$

$$\left. + \int_S \phi_j(A_o)\, K_{ij}(A,B)\, dS \right] \qquad (2.11)$$

where $\phi_j(A_o)$ is the value of $\phi(B)$ at $A_o \in S$.

It has been shown by Kupradze (1964) that for Lt $A \to A_o$ equation (2.11) can be written as

$$u_i(A) = \int_S \phi_j(B)\, K_{ij}(A_o,B)\, dS \qquad (2.12)$$

Similarly, the integral for stress resultants is

$$p_i(A) = \int_S \phi_j(B)\, \tau_{ij}(A,B)\, dS$$

As Lt $A \to A_o$, $A_o \in S$ from D_i

$$p_i(A) = \frac{1}{2}\, \phi_i(A_o) + \int_S \phi_j(B)\, \tau_{ij}(A_o,B)\, dS \qquad (2.13)$$

and also Lt $A \to A_o$, $A_o \in S$ from D_e

$$p_i(A) = \frac{1}{2}\, \phi_i(A_o) - \int_S \phi_j(B)\, \tau_{ij}(A_o,B)\, dS \qquad (2.14)$$

subject to the conditions that the surface is smooth and functions ϕ_j are well behaved. The proofs of these results are rather lengthy, and are not

reproduced here (See Kupradze, 1964).

Thus we know that the integrals for displacements exist in the normal sense over S as S is approached from D_i or D_e, but the integrals for the stress resultants are discontinuous, as can be seen from equations (2.13) and (2.14).

The generality and uniqueness of the integral representations (2.13) and (2.14) for the stress resultants has been established by Kupradze (1964).

2.8 Derivation of the integral equations

For the displacement boundary value problem (i) the integral equation in terms of the given boundary displacements $f_i(A_o)$ is, by equation (2.12),

$$f_i(A_o) = \int_S \phi_j(B)\, K_{ij}(A_o,B)\, dS \qquad (2.15)$$

where

$f_i(A_o)$ are the given displacements on the boundary S,

$\phi_j(B)$ are the unknown fictitious intensities distributed on S.

The integral equation (2.15) is applicable to the boundary value problem in terms of displacements in both domains D_e and D_i.

Similarly, the equation of stress resultant boundary value problem is:

$$f_i(A_o) = \frac{1}{2}\,\phi_i(A_o) - \int_S \phi_j(B)\, \tau_{ij}(A_o,B)\, dS \qquad (2.16)$$

for D_i and

$$f_i(A_o) = \frac{1}{2}\,\phi_i(A_o) + \int_S \phi_j(B)\, \tau_{ij}(A_o,B)\, dS \qquad (2.17)$$

for D_e.

In the foregoing derivation of the integral equations the fictitious intensities are distributed on S. If however the fictitious intensities are distributed over an auxiliary boundary (Oliveira, 1968), the integral equations become:

$$f_i(A_o) = \int_{S_I} \phi_j(B_I)\, K_{ij}(A_o,B_I)\, dS_I$$

$$f_i(A_o) = \int_{S_I} \phi_j(B_I)\, \tau_{ij}(A_o B_I)\, dS_I \qquad (2.18)$$

$$A_o \in S,\ B_I \in S_I,$$

for boundary value problems in the domain D_e and:

$$f_i(A_o) = \int_{S_e} \phi_j(B_e)\, K_{ij}(A_o,B_e)\, dS_e$$

$$f_i(A_o) = \int_{S_e} \phi_j(B_e)\, \tau_{ij}(A_o,B_e)\, dS_e \qquad (2.19)$$

$$A_o \in S,\ B_e \in S_e\ ,$$

for boundary value problems in the domain D_i:

where dS_I and dS_e are the elemental surfaces of S_I and S_e respectively. The functions $K_{ij}(A_o,B_I)$, $K_{ij}(A_o,B_e)$, $\tau_{ij}(A_o,B_I)$ and $\tau_{ij}(A_o,B_e)$ are wholly continuous for D_e and D_i and exist in the normal sense. These integrals are proper integrals of continuous functions. Oliveira (1968) adopted the equivalent representations of (2.18) and (2.19) for two-dimensional problems. He claimed to have established the necessary and sufficient conditions for the existence and uniqueness of representations (2.18) and (2.19) (it has not been possible for the author to obtain the publications cited in the above mentioned paper). If the auxiliary boundaries S_I and S_e do not coincide with the boundary S the representations

(2.18) and (2.19) become integral equations of the first kind with continuous kernels. The resulting system of equations for such integral equations may be unstable (Baker et al, 1966) and produce oscillations in the values of $\phi_j(B_e)$ and $\phi_j(B_I)$. For the purpose of an approximate engineering analysis it is possible to choose the boundaries S_I and S_e sufficiently near S so that the kernel functions become nearly singular and the resulting system of equations is stable (see Art 2.9).

Equations (2.15), (2.16), (2.17), (2.18) and (2.19) can all be represented by:

$$f_i(A_o) = \alpha . \phi_i(A_o) + \lambda_o \int_{S_o} \phi_j(B) M_{ij}(A_o,B) \, dS_o \qquad (2.20)$$

where $f_i(A_o)$ are the given boundary conditions on S.

$\alpha \phi_i(A_o)$ is the term for the discontinuity, $\alpha = o$ for the integrals which exist in the normal sense and $\frac{1}{2}$ for the equations (2.16) and (2.17),

$M_{ij}(A_o,B)$ are functions given by equations (2.16), (2.17), (2.18) and (2.19),

A_o is a point on the boundary S,

B is the moving point on the chosen boundary S_o (which may either be S or S_I or S_e) on which the fictitious stress intensities are distributed,

λ_o is a parameter which can be obtained by comparing equation (2.20) with the parent equations,

dS_o is an element of S_o.

2.9 Solution of the integral equations

The method of solution is kept sufficiently general by illustrating the solution of equation (2.20). The kernel $M_{ij}(A_o,B)$ is divided into a continuous part $MC_{ij}(A_o,B)$ and a part $MS_{ij}(A_o,B)$ containing singularity when $(A_o = B)$. The equation (2.20) then becomes:

$$f_i(A_o) = \alpha\ \phi_i(A_o) + \lambda_o \int_{S_o} \phi_j(B)\ MC_{ij}(A_o,B)\ dS_o$$

$$+ \lambda_o \int_{S_o} \phi_j(B)\ MS_{ij}(A_o,B)\ dS_o \qquad (2.21)$$

Using Saint Venant's principle that for points sufficiently far from the point of application of the load the stresses and displacements at these points are independent of the manner in which the load is applied, it is possible to apply a simple linear quadrature formula to (2.21) to all regions except those near to $A_o = B$. Equation (2.21) can therefore be written in a discrete linear form as:

$$\alpha.\ \phi_i(A_m) + \lambda_o \sum_{n=1}^{N} G_n\ MC_{ij}(A_m,B_n)\ \phi_j(B_n)$$

$$+ \lambda_o \sum_{n=1}^{N} G_n\ MS_{ij}(A_m,B_n)\ \phi_j(B_n) + E_{im} = f_i(A_m) \qquad (2.22)$$

where E_{im} are the error terms (which will be neglected),

G_n are weighting functions (constants for a given interval of integration),

$A_m = A_1, A_2, A_3, \ldots A_N$ are the N values of A_o corresponding to N intervals of integration on the surface S_o.

Equation (2.22) therefore represents a system of N × i linear algebraic

equations for the N × i unknown values of ϕ. This system of equation can then be written in matrix notation as:

$$\alpha \left|I\right| + \left[MC\right] \{\phi\} + \left|MS\right| \{\phi\} = \{f\} \qquad (2.23)$$

where

$\left|I\right|$ = (N × i) × (N × i) unity matrix,

$\left|MC\right|$ and $\left|MS\right|$ = (N × i) × (N × i) matrices and are, in general, fully populated,

$\{\phi\}$= (N × i) × 1 vector for the unknowns,

$\{F\}$= (N × i) × 1 vector for the boundary conditions,

i = 2, 3 depending depending on number of space dimensions.

The accuracy of the solution of equation (2.21) depends upon the accuracy with which the integral equation is replaced by the quadrature formulae. For the problems solved in the present work very simple quadrature formulae (e.g. Simpson's rule or the trapezoidal rules) were used for evaluating the coefficients of the matrix $\left|MC\right|$ and the off diagonal elements (i.e. $A_o \neq B$) of the matrix $\left|MS\right|$.

Since Saint Venant's principle does not apply for points near to the application of the unknown intensity, the diagonal elements of the matrix $\left|MS\right|$ were evaluated by the method given below. These diagonal elements involve the evaluation of the integrals of the type

$$I_D = \int_{S_{-1}}^{S_{+1}} MS(A_o,B)\ \phi(B)\ dS_o \qquad (2.24)$$

where S_{-1} and S_{+1} denote the limits of an element of the discretised surface S_o,

The kernel function $MS(A_o,B)$ is singular at $A_o = B$.

Since the unknown function is assumed to regular it can be expanded in the form of a Taylor series about A_o, hence

$$\phi(B) = \phi(A_o) + (B-A_o)\ \phi'(A_o) + \frac{(B-A_o)^2}{2!}\ \phi''(A_o) + \ldots \qquad (2.25)$$

where

$\phi'(A_o)$, $\phi''(A_o)$ denotes differention with respect to the independent variable on the surface S_o. $\phi'(A_o)$, $\phi''(A_o)$ can be represented by their finite difference approximation over the surface.

Substituting (2.25) in (2.24) leads to:

$$I_D = \phi(A_o) \int_{S_{-1}}^{S_{+1}} MS(A_o,B)\ dS_o + \phi'(A_o) \int_{S_{-1}}^{S_{+1}} (B-A_o).MS(A_o,B)\ dS_o$$

$$+ \phi''(A_o) \int_{S_{-1}}^{S_{+1}} \frac{(B-A_o)}{2!}\ MS(A_o,B)\ dS_o + \ldots \qquad (2.26)$$

Equation (2.26) only involve known functions under the integral sign. It is seen that this method deals with virtually any rapidly varying distribution of ϕ. In most problems, good results have been obtained by simply taking the first term of the series. However, the integrals in (2.26) still have to be evaluated. If the method of the auxiliary boundary is used (i.e. when the boundary S_o is not the same as S) the integrals in (2.26) exist in the normal sense and may be evaluated analytically or numerically by a fine mesh quadrature over the element. If the fictitious intensities are distributed on the boundary S the integrals (the first or the first two, depending on the order of singularity) are singular integrals which only exist as Cauchy principal values. The method of evaluation of these integrals is given in the following section. When this has been accomplished equations (2.23) can be combined and written as:

$$[M]\ \{\phi\} = \{f\} \tag{2.27}$$

where

$[M]$ is a fully populated $(N \times i)^2$ matrix.

The formal solution of (2.27) which provides $(N \times i)$ discrete, approximate values of ϕ as:

$$\{\phi\} = [M]^{-1}\ \{f\} \tag{2.28}$$

2.10 Evaluation of the principal value of the singular integrals

Let us consider a plane region R, sufficiently small, to represent an element of the surface S, enclosed by a curve C_1 (Figure 2.3) at a distance of $a.\rho_1(\theta)$ from A_o and containing a small region E which is within a curve C_2 at a distance $\varepsilon\ \rho_o(\theta)$ from A_o, ε being an arbitrarily small constant. The curve C_1 is of some convenient geometric configuration to fit the scheme of surface discretisation. The present problem is to evaluate the integrals in equation (2.26) over the region R. It is convenient to perform the integration with respect to local axes through A_o.

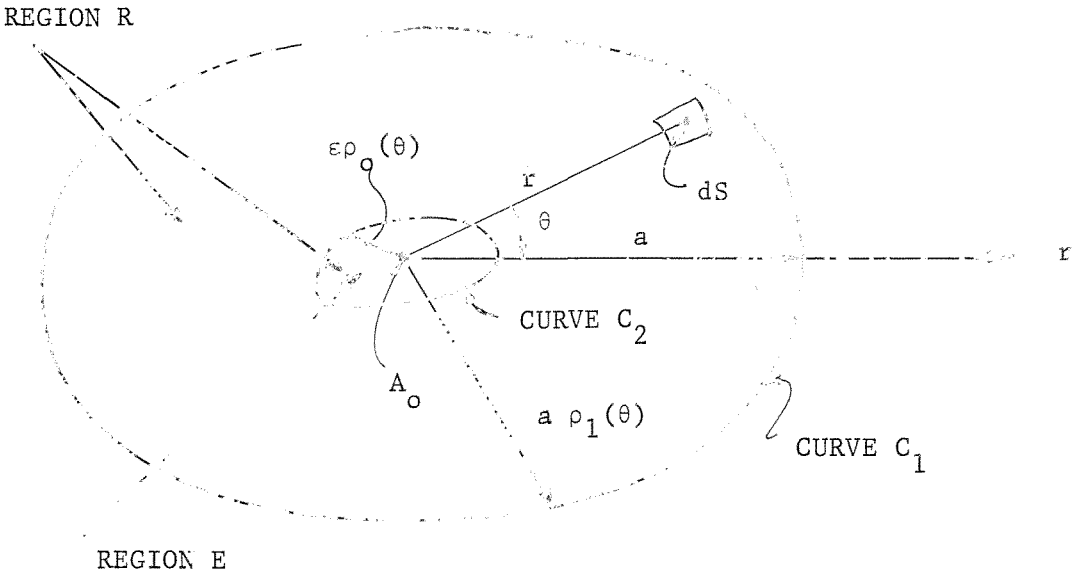

FIGURE 2.3

A SYMMETRICAL REGION OF EXCLUSION AROUND THE SINGULARITY

In terms of the local variable r and θ the displacement integrals are reduced to the form:

$$I_p = \int_R \frac{\cos\theta}{r}\, dS$$

$$= \lim_{\varepsilon \to o} \int_o^{2\pi} \int_{\varepsilon\, \rho_o(\theta)}^{a\rho_1(\theta)} \frac{\cos\theta}{r} .r.dr.d\theta$$

$$= \lim_{\varepsilon \to o} \int_o^{2\pi} \int_{\varepsilon\, \rho_o(\theta)}^{a\rho_1(\theta)} \cos\theta.dr.d\theta = \int_o^{2\pi} a\rho_1(\theta)\, \cos\theta\, d\theta \qquad (2.29)$$

where I_p denotes the principal value of the integral.
Equation (2.29) shows that the displacement integrals exist in the normal sense over S. They are evaluated by a fine mesh quadrature over the region. The mesh size is reduced until I_p becomes independent of the mesh size.

In terms of the local variable r and θ the integrals for the stress resultants are reduced to the form:

$$I_p = \int_R \frac{\cos^\theta}{r^2}\, dS = \lim_{\varepsilon \to o} \int_o^{2\pi} \int_{\varepsilon\rho_o(\theta)}^{a\rho_1(\theta)} \frac{\cos\theta}{r^2}.\ r.dr.d\theta$$

$$= \lim_{\varepsilon \to o} \int_o^{2\pi} \left|\log\{a\rho_1(\theta)\} - \mathrm{Log}\{\varepsilon\, \rho_o(\theta)\}\right| \cos\theta\, d\theta$$

$$= \lim_{\varepsilon \to o} \int_o^{2\pi} \mathrm{Log}\{a\rho_1(\theta)\}\cos\theta\, d\theta - \lim_{\varepsilon \to o} \int_o^{2\pi} \cos\theta\, \mathrm{Log}\{\varepsilon\, \rho_o(\theta)\}\, d\theta$$

$$= \int_o^{2\pi} \mathrm{Log}\{a\rho_1(\theta)\}\, \cos\theta\, d\theta - \int_o^{2\pi} \mathrm{Log}\, \rho_o(\theta)\, \cos\theta\, d\theta$$

$$- \lim_{\varepsilon \to 0} \text{Log}\varepsilon \int_0^{2\pi} \text{Cos}\theta \, d\theta$$

$$= \int_0^{2\pi} \text{Log}\{a\rho_1(\theta)\} \text{Cos}\theta \, d\theta - \int_0^{2\pi} \text{Log}\, \rho_o(\theta) \text{Cos}\theta \, d\theta \qquad (2.30)$$

The integrals in (2.30) can now be evaluated either analytically or numerically. For the results described in the present work, these integrals have been evaluated by Simpson's rule.

2.11 Discussion

The method of numerical analysis developed in this Chapter can be used to solve any problem of classical elastostatics. The formulation is sufficiently general to be able to deal with bodies of arbitrary shape if Kelvin's solution is used (i.e. R_2 is put equal to infinity in equations (2.2), (2.3) and (2.4)). Since the present work is exclusively concerned with the problems with a plane horizontal unloaded ground surface, the formulation based on Mindlin's solution is used which ensures that the integral representations (2.15), (2.16), (2.17), (2.18), (2.19) satisfy this boundary condition for the stress resultants on the surface.

The singularity of the kernel function is very important in the present analysis because this leads to a very stable system of algebraic equations with dominant diagonal elements.

Chapter 3

The load displacement characteristics of an embedded rigid disc of arbitrary shape

3.1 Summary

In this chapter the load displacement characteristics of a rigid disc embedded within an elastic half space and also within a finite elastic layer underlain by a smooth rigid base are examined. The solution is developed using the integral equation method described in Chapter 2. Numerical solutions for a rigid circular disc and a rigid rectangular disc are presented.

Specific results, for a range of burial depths and ratios of the dimensions of the disc to the depth of the elastic layer are illustrated in various graphs. These results agree closely with the analytical solutions available for comparable surface discs.

3.2 Introduction

The stresses and displacements within a homogeneous soil mass due to an imposed load are directly influenced by, amongst other factors, the flexibility of the loading surface, the shape of the loaded area, the depth of burial and thickness of the elastic layer. A perfectly flexible loading may be considered to allow a direct transmission of applied pressure over the loaded area.

Following Boussinesq's solution (Boussinesq, 1885) many problems of uniformly loaded foundations at the surface of an elastic solid have been solved. Newmark (1935) and Love (1929) calculated stresses and displacements due to uniformly loaded rectangular areas while Deresiewicz (1959) has calculated the stresses due to a load uniformly distributed over an ellipse and Harr (1966) obtained the stresses and displacements under any axi-symmetric loading on the surface of an elastic half space.

Though the condition of full rigidity of footing is more likely to occur in practice, very few attempts have been made at the solution of the problems of rigid discs. The above mentioned solutions are not really applicable to most foundation situation where the footing is relatively rigid. In these situations the stresses and displacements need to be computed on the basis of a specified displacement of the loaded area. The available solutions of rigid footings exclusively deal with the cases of surface loadings. Boussinesq (1885) obtained the stress distribution under a rigid circular disc, Sadowski (1928) that under a rigid strip, more recently Schiffman and Aggarwala (1961) analysed the problem of a rigid elliptical disc and Cheung and Zienkiewicz (1965) that of square plates of various stiffnesses resting on the surface.

The most widely used foundation geometry is that of a rigid rectangular footing. It is common practice to use Boussinesq's solution for a rigid

circular disc to approximate the stresses under a rectangular footing by matching the contact areas. This approximation seems to be reasonable for square footings but it is natural to believe that this approximation becomes less accurate as the side ratio of the footing departs from unity. A better approximation can be achieved if the rectangular footing is approximated by an ellipse with the ratio of the semi-axes and the contact area of the ellipse the same as the ratio and contact area of the rectangular footing (Schiffman and Aggarwala, 1961).

In many situations footings are placed on or within soil which is underlain by a rigid layer. In such cases the foregoing solutions are of little relevance. The problems of uniformly loaded circular and rectangular footings on the surface of an elastic layer were analysed by Burmister (1956). An earlier approximate solution of the problem of an uniformly loaded circular disc was given by Steinbrenner (1934). His results and approximations were discussed by Terzaghi (1943). Poulos (1968c) analysed the problem of a rigid circular disc on the surface of an elastic layer using Steinbrenner's approximation. Since Steinbrenner's approximation becomes increasingly inaccurate for depth of layer less than two times the diameter of the footing, the solution cannot be regarded as a satisfactory one.

None of the foregoing writers have considered the effect of burial depth on the stresses and displacements under a loaded area. Mackey and Khafagy (1968) obtained numerical results for the vertical stress under an uniformly loaded circular disc embedded within a half space.

In the following the problem of a rigid disc of arbitrary shape either buried within or resting on the surface of (a) a half space and (b) a finite elastic layer underlain by a smooth rigid base is considered. The embedded discs are analysed on the basis of following assumptions:

(i) The disc is smooth and bonded with the medium,

(ii) The underlying rigid layer is smooth.

The assumption (i) implies that the shear stresses at the disc-medium interfaces are zero but tensile stresses can exist on the top surface of the disc. The effect of smoothness of a circular disc resting on the surface of a half space was considered by Lee (1963), who found that the solutions to the problems of a smooth disc and a rough disc are identical for Poisson's ratio $= \frac{1}{2}$ and differ by negligible amount for other values of Poisson's ratio. The assumption of a bonded disc is likely to give inaccurate results for shallow foundations but seems to be adequate for deep footings as long as the weight of the soil above the footing level produce a net compressive stress on the top surface of the disc. The effect of the assumption (ii) was investigated by Biot (1935), who considered the problems of a point load on the surface of an elastic layer underlain by rigid smooth and rigid rough base. It was found that smoothness of the surface of the rigid layer did not produce any noticeable difference in the computed vertical stresses even on the surface of the rigid layer. It seems, therefore quite reasonable to assume the same assumption is valid for an embedded disc.

3.3 Development of the analysis

The vertical stress $\sigma_{zz}(r_1,z)$ and displacement $w(r_1,z)$ at a point $Q(r_1,z)$ due to a vertical point load P acting within an elastic half space occupying a part of the region $z \geq o$ (Figure,3.1) are given by (see Chapter 2):

$$w(r_1,z) = P.\ K(c,r_1,z) \tag{3.1}$$

$$\sigma_{zz}(r_1,z) = P.\ T(c,r_1,z) \tag{3.2}$$

where $K(c,r_1,z)$ and $T(c,r_1,z)$ are known functions given by Mindlin (1936) at the points designated by the bracketed coordinates. Equations (3.1) and (3.2) may be expressed in a cartesian coordinate system as:

$$w(\overset{o}{x},\overset{o}{y},z) = P.\ K(\overset{o}{x},\overset{o}{y},z,c) \tag{3.3}$$

$$\sigma_{zz}(\overset{o}{x},\overset{o}{y},z) = P.\ T(\overset{o}{x},\overset{o}{y},z,c) \tag{3.4}$$

where the z axis passes through the point of application of the load so that $\overset{o}{x}$ and $\overset{o}{y}$ are distances measured from the point of application of the load.

3.3.1 General formulation for a disc of arbitrary shape within an elastic layer

If a resultant vertical stress intensity $\sigma_{\varepsilon\theta}$ acts on an elemental area $\varepsilon.\delta\theta.\delta\varepsilon$ on a horizontal place at $z = c$ (point A, Figure 3.2), the vertical displacement at $Q(r,\theta_r,z)$ due to the load $(\sigma_{\varepsilon\theta}.\varepsilon.\delta\theta.\delta\varepsilon)$ acting at A is given by equation (3.1) as:

$$\delta w\ (r,\theta_r,z) = (\sigma_{\varepsilon\theta}.\varepsilon.\delta\theta.\delta\varepsilon).\ K(c,r_1,z) \tag{3.5}$$

where $r_1 = \left[r^2 + \varepsilon^2 - 2r\varepsilon\cos(\theta_r - \theta_\varepsilon)\right]^{\frac{1}{2}}$ and δw denotes the vertical displacement due to elemental load. The total vertical displacement at $Q(r,\theta_r,z)$ due to all elemental loads over the disc area (S) bounded by F is given by:

$$w_1(r,\theta_r,z) = \iint_S \sigma_{\varepsilon\theta}.\varepsilon.\ K(c,r_1,z)\ d\varepsilon\ d\theta \tag{3.6}$$

Equation (3.6) therefore represents the solution for vertical displacement at a point Q within an elastic half space due to $\sigma_{\varepsilon\theta}$ distributed over the disc area bounded by F. If the disc is flexible $\sigma_{\varepsilon\theta}$ will be equal to the applied loading and equation (3.6) becomes a definite integral

which can be evaluated directly for the point Q everywhere in the half space.

However, if the disc is rigid $\sigma_{\varepsilon\theta}$ is unknown and the integral (3.6) cannot be evaluated until $\sigma_{\varepsilon\theta}$ is obtained from the boundary conditions.

To include the effect of a smooth rigid layer at a depth H below the surface we apply a "fictitious" vertical intensity $\psi_{\varepsilon\theta}$ at c = H. The vertical displacement at the point Q due to $\psi_{\varepsilon\theta}$ acting over the surface of the rigid layer can be obtained by analogy with (3.6) as:

$$w_2(r,\theta_r,z) = \int_0^{2\pi}\int_0^{\infty} \psi_{\varepsilon\theta}.\varepsilon.\ K(H,r_1,z)\ d\varepsilon\ d\theta \qquad (3.7)$$

Thus the total vertical displacement at Q due to a disc of arbitrary shape embedded within an elastic layer is given by:

$$w(r,\theta_r,z) = \iint_S \sigma_{\varepsilon\theta}.\varepsilon.\ K(c,r_1,z)\ d\varepsilon\ d\theta + \int_0^{2\pi}\int_0^{\infty} \psi_{\varepsilon\theta}.\varepsilon.\ K(H,r_1,z)\ d\varepsilon\ d\theta \qquad (3.8)$$

Similarly the vertical stress at a point Q due to the loaded disc can be obtained from:

$$\sigma_{zz}(r,\theta_r,z) = \iint_S \sigma_{\varepsilon\theta}.\varepsilon.\ T(c,r_1,z)\ d\varepsilon\ d\theta + \int_0^{2\pi}\int_0^{\infty} \psi_{\varepsilon\theta}.\varepsilon.\ T(H,r_1,z)\ d\varepsilon\ d\theta \qquad (3.9)$$

By virtue of the choice of Mindlin's solution the boundary conditions:

$$\sigma_{zz} = o, \ \sigma_{rz} = \sigma_{\theta z} = o \text{ at } z = o ,$$

$$\sigma_{rz} = \sigma_{\theta z} = o \text{ at } z = c \text{ over the disc area}, \qquad (3.10)$$

$$\sigma_{rz} = \sigma_{\theta z} = o \text{ at } z = H$$

have already been satisfied. The boundary conditions for the vertical displacement of the disc can be satisfied by considering the points B within F and substituting z = c in equation (3.8) which then becomes:

$$w(r,\theta_r,c) = \iint_S \sigma_{\varepsilon\theta}.\varepsilon. \ K(c,r_1) \ d\varepsilon \ d\theta$$

$$+ \int_o^{2\pi} \int_o^{\infty} \psi_{\varepsilon\theta}.\varepsilon. \ K(H,r_1 c) \ d\varepsilon \ d\theta \qquad (3.11)$$

Similarly the vertical displacement of the rigid base can be satisfied by considering the points on the surface of the rigid base and substituting z = H in equation (3.8) which then becomes:

$$w(r,\theta_r,H) = \iint_S \sigma_{\varepsilon\theta}.\varepsilon. \ K(c,r_1,H) \ d\varepsilon \ d\theta$$

$$+ \int_o^{2\pi} \int_o^{\infty} \psi_{\varepsilon\theta}.\varepsilon. \ K(H,r_1) \ d\varepsilon \ d\theta \qquad (3.12)$$

Equations (3.11) and (3.12) can be represented over the disc area and over a finite area of the rigid base surface in a discrete linear form (see Chapter 2) by application of quadrature formulae. Thus the vertical displacement of the elements (i,j) of the disc can be obtained from (see Figure 3.3):

$$(WC)_{ij} = \sum_{n=1}^{n} \sum_{m=1}^{m} \sigma_{mn} \, (KCC_{ij} \, \Delta A)_{mn}$$

$$+ \sum_{p=1}^{p} \sum_{q=1}^{q} \psi_{pq} \, (KRC_{ij} \, \Delta B)_{pq} \qquad (3.13)$$

where $(WC)_{ij}$ are the vertical displacements of disc elements (i,j).

σ_{mn}, ψ_{pq} are the resultant vertical stress intensity on the disc elements and the 'fictitious' normal stress intensities on the elements on the surface of the rigid base,

$(KCC_{ij} \, \Delta A)_{mn}$ are the values of the kernel function of the first integral of equation (3.11), ΔA being the constant weighting function,

$(KRC_{ij} \, \Delta B)_{pq}$ are the values of the kernel function of the second integral of equation (3.11), ΔB being the constant weighting function,

m,n are the arbitrary number of elemental divisions within the disc area in r,ε and θ_r,θ_ε directions (Figure 3.3)

p,q are the arbitrary number of elemental divisions within a finite surface of the rigid base in r,ε and θ_r, θ_ε directions.

i = 1,2,3 ..... n, j = 1,2,3 ..... m.

Similarly by application of numerical quadrature formulae to equation (3.12) the vertical displacements of the elements (i,j) on the surface of the rigid base can be written in analogy with equation (3.13) as:

$$(WR)_{ij} = \sum_{n=1}^{n} \sum_{m=1}^{m} \sigma_{mn} \, (KCR_{ij} \cdot \Delta A)_{mn}$$

$$+ \sum_{p=1}^{p} \sum_{q=1}^{q} \sigma_{pq} \, (KRR_{ij} \, \Delta B)_{pq} \cdot \qquad (3.14)$$

where

$(WR)_{ij}$ are the vertical displacements of elements on the surface of the rigid base,

$(KCR_{ij}.\Delta A)_{mn}$ are the values of the kernel function of the first integral of equation (3.12),

$(KRR_{ij}.\Delta B)_{pq}$ are the values of the kernel function of the second integral of equation (3.12).

$i = 1,2,3.....p, \quad j = 1,2,.....p.$

If now unit vertical displacement of the rigid disc and zero vertical displacement of the rigid base is specified, $(WC)_{ij} = 1$ and $(WR)_{ij} = 0$, then from (3.13) and (3.14) we obtain

$$\sum_{n=1}^{n}\sum_{m=1}^{m} \sigma_{mn} (KCC_{ij}\ \Delta A)_{mn} + \sum_{p=1}^{p}\sum_{q=1}^{q} \psi_{pq} (KRC_{ij}.\Delta B)_{pq} = 1$$

$$\sum_{n=1}^{n}\sum_{m=1}^{m} \sigma_{mn} (KCR_{ij}\ \Delta A)_{mn} + \sum_{p=1}^{p}\sum_{q=1}^{q} \psi_{pq} (KRR_{ij}.\Delta B)_{pq} = 0 \qquad (3.15)$$

Equation (3.15) represents $(m.n + p.q)$ linear equations for the $(m.n)$ unknown σ_{mn} and $(p.q)$ unknown ψ_{pq}. Having obtained the solution for σ_{mn} and ψ_{pq} the vertical displacements and vertical stresses at a point B, by analogy with equation (3.8) and (3.9), are:

$$w(B) = \sum_{n=1}^{n}\sum_{m=1}^{m} \sigma_{mn} (KC.\Delta A)_{mn} + \sum_{p=1}^{p}\sum_{q=1}^{q} \psi_{pq} (KR.\Delta B)_{pq}$$

$$\sigma_{zz}(B) = \sum_{n=1}^{n}\sum_{m=1}^{m} \sigma_{mn} (TC.\Delta A)_{mn} + \sum_{p=1}^{p}\sum_{q=1}^{q} \psi_{pq} (TR.\Delta B)_{pq} \qquad (3.16)$$

respectively.

where, the functions KC, KR, TC and TR are obtained from the the equations (3.8) and (3.9).

The second equation of (3.16) is undefined for points on the disc and rigid base surface. The vertical stress on the surface of the rigid base and the disc can be obtained by calculating the limiting value as the surfaces are approached uniformly from either side (see Chapter 2).

The total load P carried by the rigid disc can be evaluated as:

$$P = \sum_{n=1}^{n} \sum_{m=1}^{m} \sigma_{mn} \cdot \Delta A. \qquad (3.17)$$

The solution for a rigid disc embedded within a half space (Butterfield and Banerjee, 1969a) can be obtained from the formulation described above by substituting $\psi_{pq} = 0$ and considering equation (3.13) only.

3.3.2 Solution for a rigid circular disc

Because of the axial symmetry of this problem we can use $\theta_r = 0$ throughout (Figure 3.4) the quantities σ and ψ are functions of ε only. The stresses and displacements are functions of r and z. Hence from equations (3.11) and (3.12) we have

$$w(r,c) = \int_0^a \sigma_\varepsilon \cdot \varepsilon \int_0^{2\pi} K(c,r_1)\, d\theta\, d\varepsilon + \int_0^{\infty} \psi_\varepsilon \cdot \varepsilon \int_0^{2\pi} K(H,r_1,c)\, d\theta\, d\varepsilon \qquad (3.18)$$

and

$$w(r,H) = \int_0^a \sigma_\varepsilon \cdot \varepsilon \int_0^{2\pi} K(c,r_1,H)\, d\theta\, d\varepsilon + \int_0^{\infty} \psi_\varepsilon \cdot \varepsilon \int_0^{2\pi} K(H,r_1)\, d\theta\, d\varepsilon$$

in which now a direct integration with respect to θ can be carried out.

Thus for n number of annular rings for the disc and p number of annular rings of the finite rigid base surface we have

$$(WC)_i = \sum_{n=1}^{n} \sigma_n . (KCC_i . h_1)_n + \sum_{p=1}^{p} \psi_p . (KRC_i . h_2)_p \qquad (3.19)$$

where $i = 1,2...n$ and

$$(WR)_i = \sum_{n=1}^{n} \sigma_n (KCR_i . h_1)_n + \sum_{p=1}^{p} \psi_p . (KRR_i . h_2)_p \qquad (3.20)$$

where $i = 1,2..,p$, h_1 and h_2 are the thickness of the annular rings for the disc and the rigid base respectively.

If again for a rigid disc $(WC)_i = 1$ and for the rigid base $(WR)_i = 0$, then

$$\sum_{n=1}^{n} \sigma_n . (KCC_i . h_1)_n + \sum_{p=1}^{p} \psi_p (KRC_i . h_2)_p = 1$$

$$\sum_{n=1}^{n} \sigma_n . (KCR_i . h_1)_n + \sum_{p=1}^{p} \psi_p (KRR_i . h_2)_p = 0 \qquad (3.21)$$

and σ_n and ψ_p can be obtained from the solution of these (n+p) linear algebraic equations. Having obtained σ_n and ψ_p the vertical displacements and vertical stresses elsewhere (except at the disc surface and the surface of the rigid base) can be obtained from,

$$w(B) = \sum_{n=1}^{n} \sigma_n . (KC . h_1)_n + \sum_{p=1}^{p} \psi_p . (KR . h_2)_p$$

$$\sigma_{zz}(B) = \sum_{n=1}^{n} \sigma_n . (TC . h_1)_n + \sum_{p=1}^{p} \psi_p . (TR . h_2)_p \qquad (3.22)$$

which are analogous to (3.16).

3.3.3 Solution for a rigid rectangular disc

As before a resultant vertical stress $\sigma_{\xi\eta}$ is assumed to act on an elemental area $\delta_{\xi\eta}$ of a horizontal plane at a depth $z = c$ (Point $A(\xi,\eta)$, Figure 3.5). The vertical displacement at $Q(x,y,z)$ due to a load $(\sigma_{\xi\eta}.\delta\xi.\delta\eta)$ acting at A is given by (3.3) as:

$$\delta w\ (x,y,z) = \sigma_{\xi\eta}.\delta\xi.\delta\eta.\ K(\overset{o}{x},\overset{o}{y},z,c) \tag{3.23}$$

where

$$\overset{o}{x} = \lfloor x - \xi \rfloor^{\frac{1}{2}},\quad \overset{o}{y} = \lceil y - \eta \rceil^{\frac{1}{2}}.$$

If as before, we considered all such intensities on the surface of the disc the vertical displacement at $Q(x,y,z)$ due to the rigid disc can be obtained from:

$$w_1(x,y,z) = \int_{-b}^{b} \int_{-a}^{a} \sigma_{\xi\eta}.\ K(\overset{o}{x},\overset{o}{y},z,c)\ d\xi.\ d\eta. \tag{3.24}$$

We distribute a 'fictitious' intensity $\psi_{\xi\eta}$ over the surface of the rigid base, the vertical displacement at $Q(x,y,z)$ due to this fictitious intensity can be obtained from:

$$w_2(x,y,z) = \int_{-\alpha}^{\alpha} \int_{-\alpha}^{\alpha} \psi_{\xi\eta}.\ K(\overset{o}{x},\overset{o}{y},z,H)\ d\xi\ d\eta. \tag{3.25}$$

Thus the total vertical displacement at a point $Q(x,y,z)$ due to a rigid rectangular disc can be obtained from:

$$w(x,y,z) = \int_{-b}^{b} \int_{-a}^{a} \sigma_{\xi\eta}.\ K(\overset{o}{x},\overset{o}{y},z,c)\ d\xi\ d\eta$$

$$+ \int_{-\alpha}^{\alpha} \int_{-\alpha}^{\alpha} \psi_{\xi\eta}.\ K(\overset{o}{x},\overset{o}{y},z,H)\ d\xi\ d\eta \tag{3.26}$$

If as before, points B on the plane $z = C$ and at $z = H$ are considered and the boundary condition for the vertical displacements of finite numbers of elements of the rigid rectangular disc and rigid base surface are considered we obtain:

$$\sum_{n=1}^{n}\sum_{m=1}^{m} \sigma_{mn} \left(KCC_{ij} \cdot \Delta A\right)_{mn} + \sum_{p=1}^{p}\sum_{q=1}^{q} \psi_{pq} \left(KRC_{ij} \cdot \Delta B\right)_{pq} = 1 \qquad (3.27)$$

where $i = 1,2....n$, $j = 1,2....m$ and

$$\sum_{n=1}^{n}\sum_{m=1}^{m} \sigma_{mn} \left(KCR_{ij} \cdot \Delta A\right)_{mn} + \sum_{p=1}^{p}\sum_{q=1}^{q} \psi_{pq} \left(KRR_{ij} \cdot \Delta B\right)_{pq} = 0 \qquad (3.28)$$

where $i = 1,2....p$, $j = 1,2....q$, n and p denotes the numbers of elemental dimensions chosen in ξ directions and m and q denotes the number of dimensions chosen in η directions respectively. The order of the unknowns in equations (3.27) and (3.28) can be reduced by the quadrantal symmetry of the problem. For elements having the same σ and ψ values a direct summation can be carried over them. Having obtained the values of σ_{mn} and ψ_{pq} the displacements and stresses can be obtained from equations similar to (3.16) in terms of the variables in the Cartesian coordinate system.

3.3.4 Notes on computer programme for the solution for vertical stress and displacement under a rigid disc within a finite layer

The computer programme discussed has been developed for the solution of the problems described in the preceeding sections. The listing of the programme is given in Banerjee (1969).

The main features of the computer programme are the procedures (an ALGOL word, used for a set of algorithms to carry out some specific operations in the computer). The following paragraphs are devoted to brief descriptions of the procedures used (see also Banerjee, 1969):

(i) procedure 'Simpson'

This procedure evaluates a multidimensional definite integral by Simpson's rule of quadrature.

(ii) procedure 'Circ Disc Array'

This procedure evaluates the vertical displacements at the centre of a number of annular rings (field points) of a circular disc at a depth ζ due to the vertical loading intensities acting on a number of annular rings (load points) of another circular disc placed at a depth H. Thus by adjusting the values of ζ and H all the integrals of equation (3.18) can be evaluated by this procedure. Special provisions are made within this procedure to evaluate a singular integral. These singularities occur when the load point and the field point coincide.

(iii) procedure 'Rect Disc Array'

This procedure evaluates the vertical displacements at the centre of a number of rectangular elements of a rectangular disc at a depth ζ due to vertical loading intensities acting on a number of rectangular elements of another rectangular disc placed at a depth H. Hence, as before, by adjusting the values of ζ and H all the coefficients of equations (3.27) and (3.28) can be obtained. There is a special provision for evaluating a singular integral over a local rectangular region.

(iv) procedure 'Inp'

(v) procedure 'Crout 2'

(vi) procedure 'Solve'

The procedures (iv), (v) and (vi) are used to solve a set of linear algebraic equations by Gaussian elimination.

(vii) procedure 'Print Array'

This procedure prints an array of quantities in a pre-set format

of floating point arithmatic.

The main body of the programme calls the above procedure to solve a particular problem, depending on the type of input. The following problems have been solved using this programme:

(i) A circular disc at any depth within an elastic half space.

(ii) A circular disc at any depth within a finite layer.

(iii) A rectangular disc at any depth within an elastic half space.

(iv) A rectangular disc at any depth within a finite layer.

The remainder of the main body of the programme is devoted to the calculation of the total load carried by the disc and also the vertical stresses under the centre and under the edge or corner of the disc.

3.3.5 The stability and accuracy of the solution

The accuracy of the results of the numerical analysis would depend on how accurately the integrals are replaced by the quadrature formulae. Simpson's rule and trapezoidal rules are adopted in the present analysis, mainly for their simplicity. For the circular disc a direct integration with respect to θ is carried out by choosing 50 dimensions to represent 180^{o} in the θ direction. The disc is divided into n number of annular rings. The calculated load for n = 5 is found to be about 5% higher than that obtained for n = 10 and about 6% higher than that obtained for n = 20. Hence for all the results described in this chapter the disc is divided into 10 annular rings. The resulting system of equations is characterised by predominant diagonal elements which suggest a good stability of the solution.

The problem of the circular disc within a finite layer is analysed by choosing 50 divisions to represent 180^{o} in the θ direction for direct integration. The disc is divided into 10 annular rings and the rigid

base area is assumed to be a finite area with a diameter = 10 times the diameter of the disc. The increase in area of the rigid layer beyond 10 times the diameter of the disc seemed to produce no noticeable change in the calculated load. The rigid base area is divided into 20 annular rings.

Figures (3.6) and (3.7) which are independent of Poisson's ratio show the results of the present analysis and the analytical solution for a circular disc on the surface of the half space (Boussinesq, 1885). The maximum difference is about 5% for the vertical stress immediately below the centre of the disc. The calculated load is about 1% higher than the corresponding analytical solution.

For the rectangular disc there is a quadrantal symmetry. For each quadrant 10 intervals in ξ, x direction and 10 intervals in η, y direction appears to be the optimum from the point of view of accuracy and computer store and time. This leads to 400 elements representing the rectangular disc surface. The local integration (i.e. integration over the elements on which the intensity is acting) was done by subdividing the element into a further 100 dimensions in both directions in such a manner that a symmetrical region of exclusion is left out (see Chapter 2).

The problem of the rectangular disc within a finite layer is analysed by choosing the same number of elements to represent the rigid base surface. The dimensions of the rigid base are assumed to be 10 times the dimensions of the rigid rectangular disc.

No analytical solution is available even for rigid rectangular or square disc on the surface of a half space. The numerical results are compared with solutions for equivalent circular and elliptical discs (Schiffman and Aggarwala, 1961). Figure (3.8), which is independent of Poisson's ratio, shows a comparison of calculated vertical centreline

stresses for an elliptical disc with semi-axes a' and b' chosen to give $a'/a = b'/b$ and $\pi a'b' = 4ab$. The agreement is sufficiently close to indicate the accuracy of the numerical solution.

3.4 The results of the analysis

The results of the analysis are presented in Figures (3.9) to (3.21) below. Figures (3.9) to (3.14) refer to rigid circular discs for which the following points are of interest.

Figures (3.9.1) and (3.9.2) show the effect on the vertical centre-line stresses of varying the burial depth (c), Poisson's ratio (μ) for a disc embedded within a half space. The effect of Poisson's ratio is shown to be negligible and for the depths of burial greater than four disc diameters the stress becomes essentially independent of burial depth also. Similar results are obtained for the vertical stress under the edge of the disc and these are shown in Figures (3.10.1) and (3.10.2). The vertical stresses under the edge of the disc are higher (theoretically infinite at the edge) than those under the centreline, near the disc surface but are considerably lower than those under the centreline beyond a depth of typically a/2.

The load displacement characteristics of the disc are presented in Figure (3.11.1) as a dimensionless stiffness ($P/2GaW$) related to the burial depth and Poisson's ratio. The stiffness is seen to be dependent on Poisson's ratio and show very little increase with the burial depth beyond about four diameters. Figure (3.11.2) shows the ratio of the stiffness of the buried disc to that of a surface disc. At burial depths greater than around four diameters this ratio is approximately two for typical values of Poisson's ratio.

It has been mentioned before that in the present analysis the disc

is assumed to be completely bonded vertically to the elastic medium and therefore, in general, tensile stresses will exist on the top surface of the disc. Whereas the unbonded solution will obviously give stress distribution different from those calculated here, it is thought that the stiffness of the bonded system will not be greatly in excess of that of the unbonded system.

Figures (3.12) to (3.14) refer to a rigid disc within an elastic layer. Figure (3.12.1) shows the contact pressure distribution for a surface disc. The contact pressure distribution is dependent on both the Poisson's ratio and the ratio of depth of the elastic layer to the radius of the disc. The contact pressure distribution approaches the distribution shown in Figure (3.6) for deeper layer. Figure (3.12.2) shows the vertical stress under the centre of a rigid circular disc founded on the surface of an elastic layer. The vertical stress distribution appear to be significantly different from those shown in Figures (3.9.1) and (3.9.2) for the discs on the surface ($c/2a = 0$), though there is a trend to approach the same distribution for a deeper layer. The vertical stresses seemed to be dependent on the Poisson's ratio which is different from what is observed for a disc on the surface of an elastic half space.

Figure (3.13) shows the vertical stress distribution under the centreline of an embedded disc within an elastic layer of a different depth to diameter of disc ratios. The stresses are higher than those found for the corresponding discs within a half space. Figure (3.14) shows that effect of $H/2a$ ratio and $c/2a$ on the nondimensional stiffness. The presence of a rigid layer increases the stiffness of the system, which approaches the half space solution for deeper layer.

Figures (3.15) to (3.21) refer to the solution for a ractangular disc. Figure (3.15) shows the contact pressure contours for two

different rectangular discs, which illustrate both their approximately elliptical form over a large portion of the disc area and rapid approach to two dimensional strip solution as a/b ratio decreases. The rectangular disc solution approximates to that for a strip for values of $a/b \leq 1/6$ (Figure 3.16.5). Calculated values of the vertical stresses under the centre for $a/b = 1/10$ shows a variation of less than 5% from that of $a/b = 1/6$ values.

Figures (3.16.1) to (3.16.5) give the vertical centreline stresses under rectangular discs at various depths of burial over the range $a/b = 1$ to $1/6$ (for $\mu = 0.5$). As for the circular discs the stresses are insensitive to the value of Poisson's ratio. Figures (3.17.1) to (3.17.5) give similar results for the vertical stress under the corners of the discs. It is interesting to note that the effect of increasing the burial depth dies out less rapidly as a/b values decreases. A comprehensive set of dimensionless stiffness curves are given in Figure (3.18) for a range of disc shapes, burial depths and μ values.

Figures (3.19) to (3.21) refer to the rectangular discs within a finite elastic layer. Figure (3.19) shows the vertical stress distribution under a rectangular disc ($a/b = 2/3$) for two depths of finite layer. The vertical stresses are higher and of different distribution to those of the half space solutions. The Poisson's ratio is shown to have small effect on the stress distribution. Figure (3.20) shows the vertical stresses under a buried disc. The results are shown for $\mu = 0.5$ and $\mu = 0$ cases only. Here again the vertical stresses are higher than those solutions for the discs buried within a half space. Figure (3.21) shows the non-dimensional stiffness of a rectangular disc ($a/b = 2/3$) plotted against H/a for a surface disc and an embedded disc ($c/a = 4$) for two values of Poisson's ratio. The effect of this is small beyond

$H/a = 16$ for $\mu = 0$ and 30 for $\mu = 0.5$.

3.5 Conclusions

(1) A general method of solution has been presented for the determination of the complete stress displacement fields due to the vertical displacement of a rigid bonded disc of arbitrary shape both within a half space and within a finite elastic layer.

(2) The results obtained have been compared with the earlier analytical solutions for surface discs, where possible and good agreement found.

(3) Graphs have been prepared illustrating values of vertical centre line and edge stresses and vertical stiffnesses for rigid circular discs at different depths.

(4) The stresses and stiffnesses remain essentially unchanged when the depth of burial is increased beyond about 4 diameters and stiffness at this depth is about twice the surface value for a disc embedded within a half space.

(5) The effect of layer thickness appear to have considerable influence on the vertical stress distribution as well as on the stiffness. The stiffness of a disc within a half space is less than the corresponding disc within a finite layer.

(6) The stiffness of a disc within a finite elastic layer converges to within 10% of the half space solution as the depth below the disc exceeds eight diameters.

(7) Similar curves are also presented for rigid rectangular discs. The limiting stiffness values in these cases are functions of disc geometry, depth of elastic layer and Poisson's ratios.

(8) The vertical stresses in the half space becomes essentially

independent of the resulting disc loading stress for disc geometries having $a/b \leq 1/6$, which therefore corresponds approximately to the two dimensional strip solution.

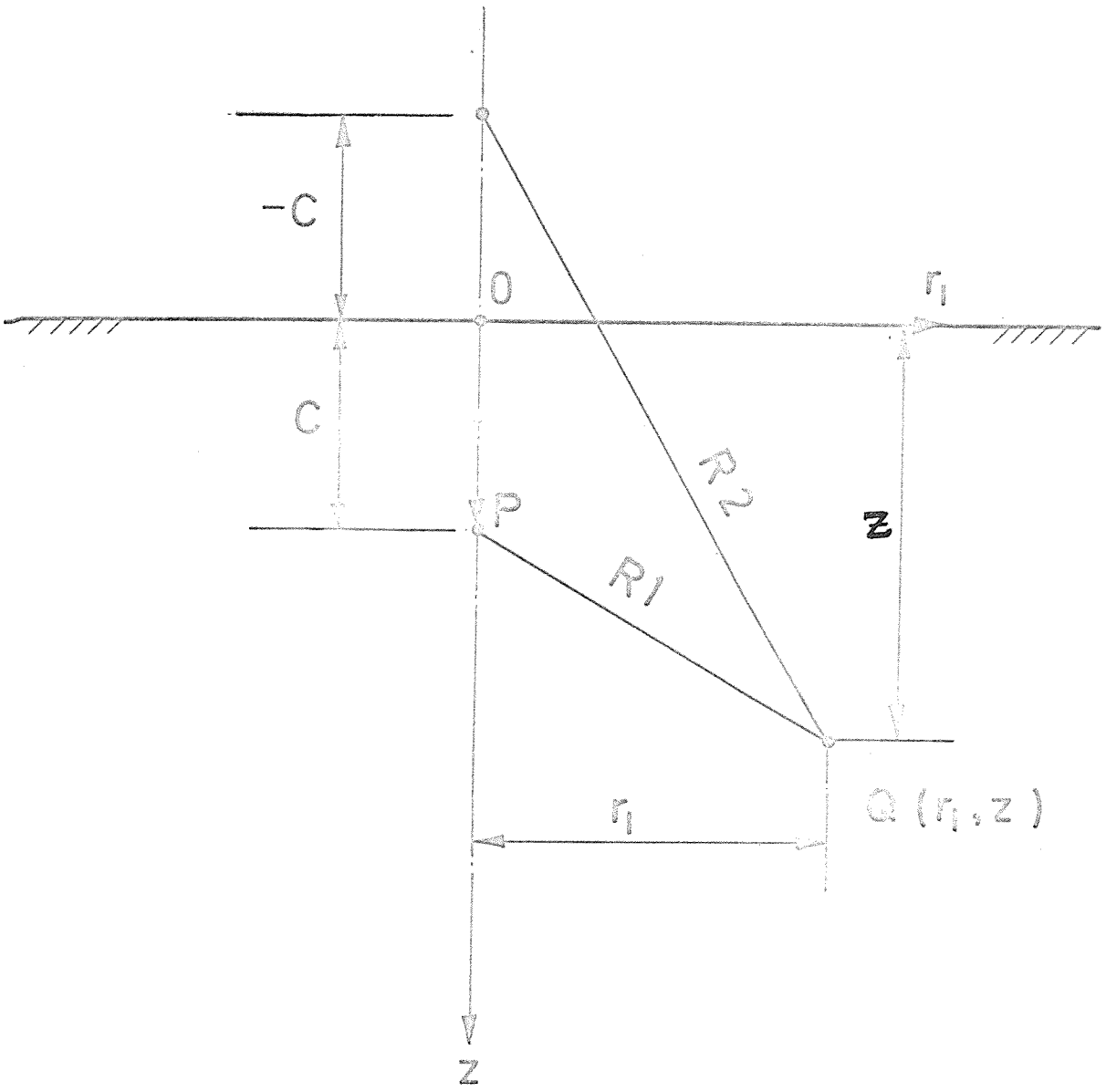

FIGURE 3.1

MINDLIN'S PROBLEM FOR A POINT LOAD WITHIN A HALF SPACE

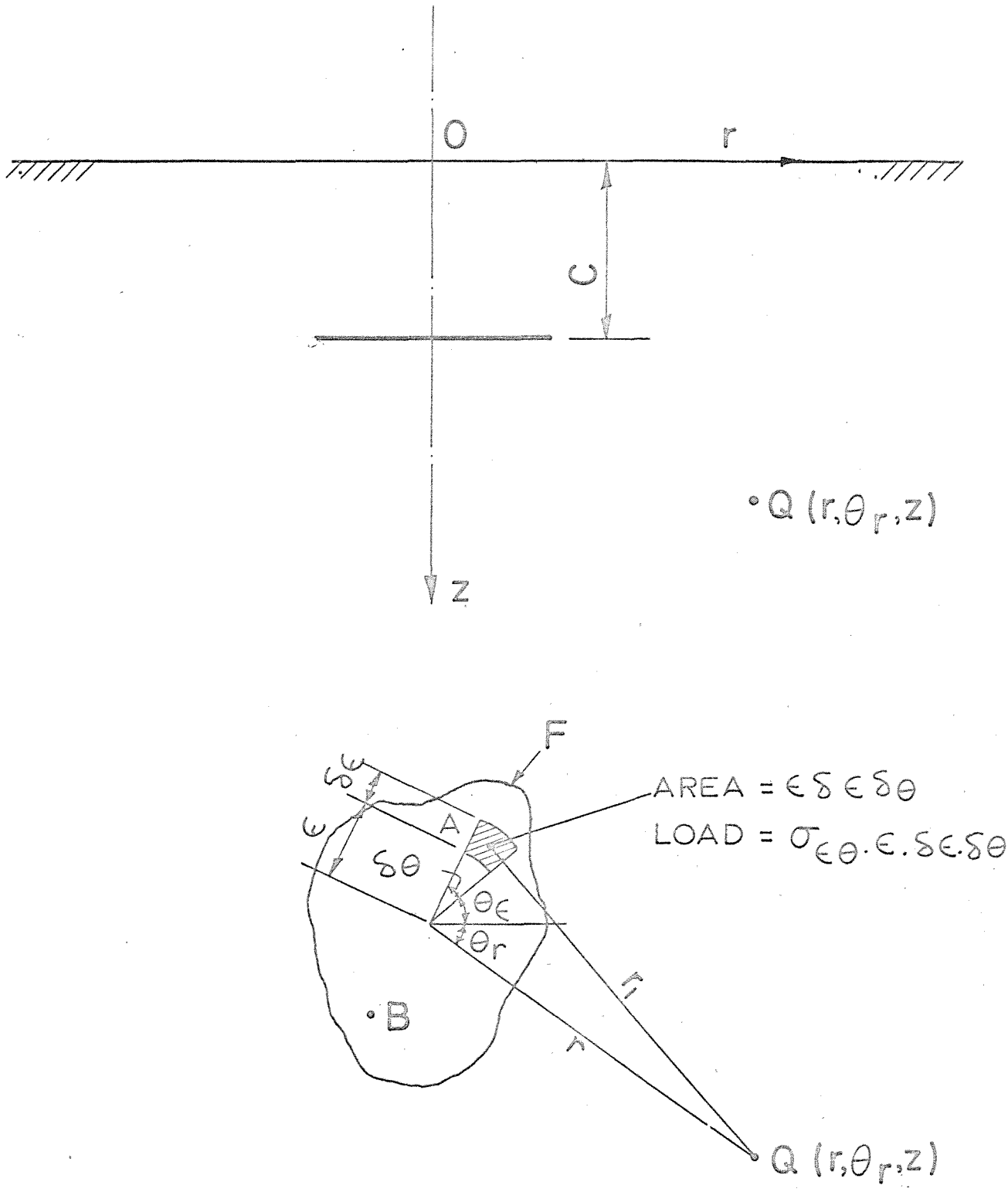

FIGURE 3.2

RIGID DISC OF ARBITRARY SHAPE

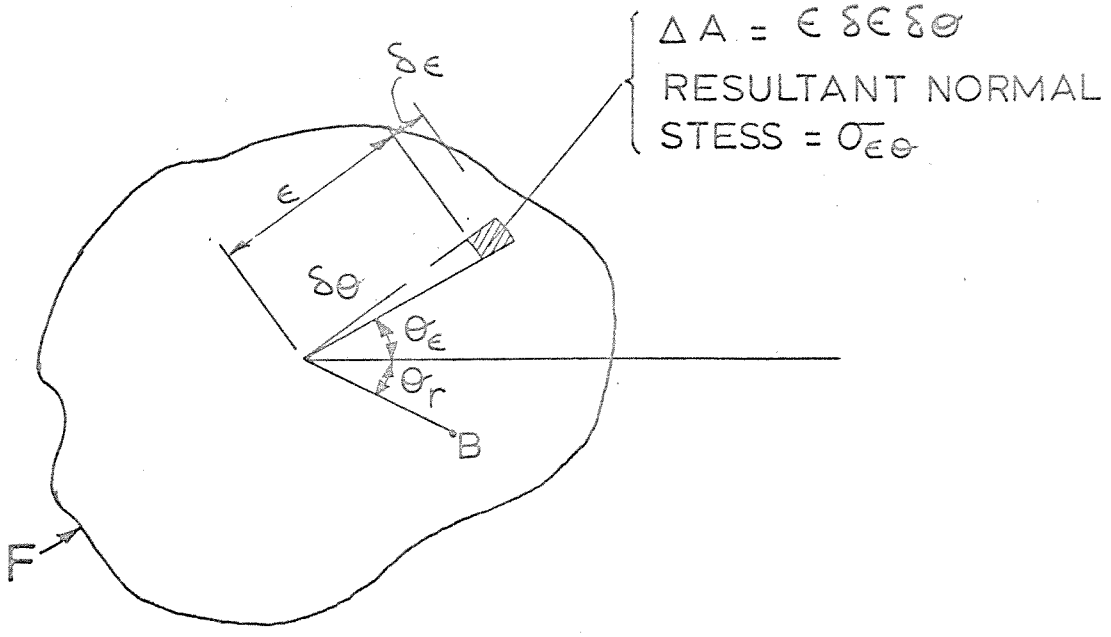

CONTINUOUS SYSTEM

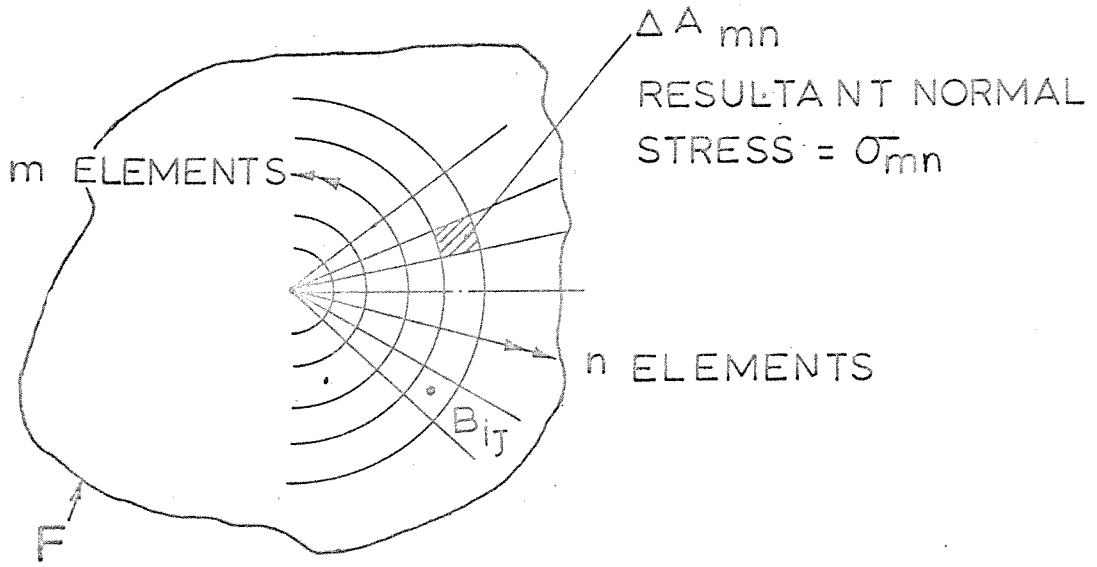

DISCRETE SYSTEM

FIGURE 3.3

DISCRETISATION OF THE CONTINUOUS SYSTEM

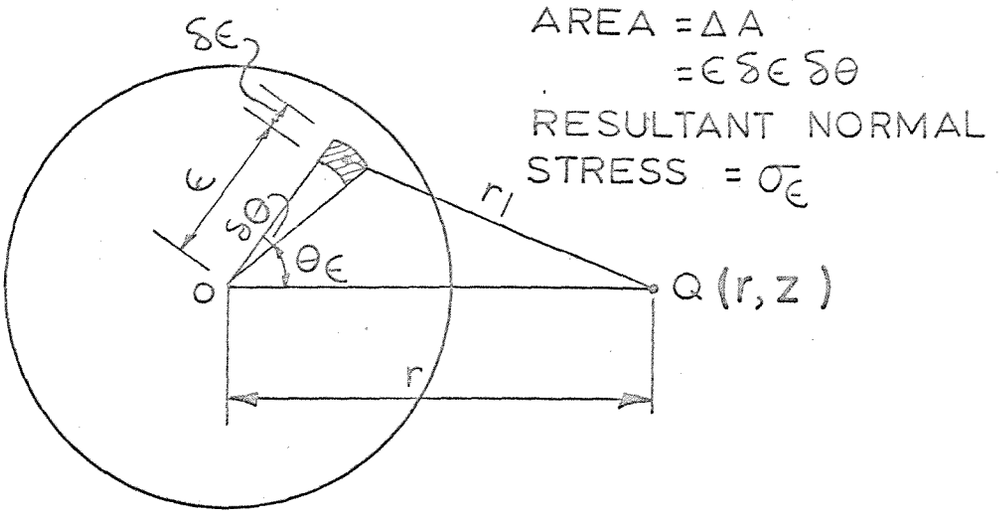

FIGURE 3.4

A CIRCULAR DISC

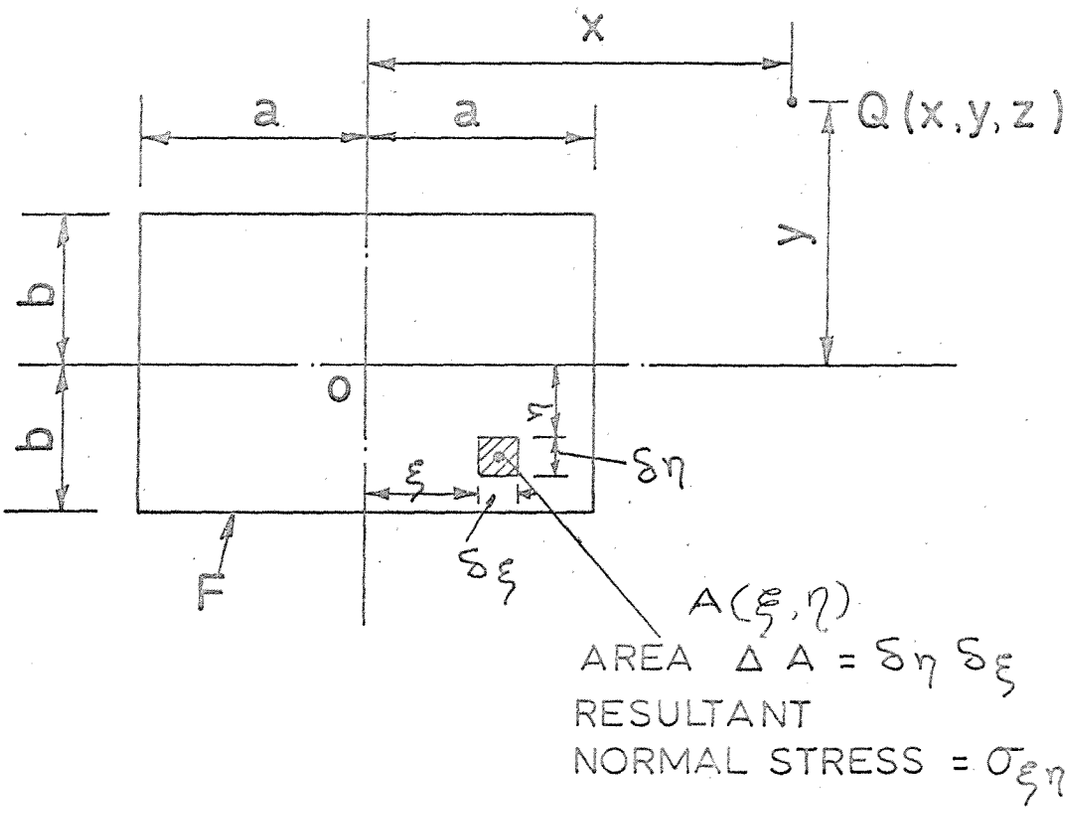

FIGURE 3.5

A RECTANGULAR DISC

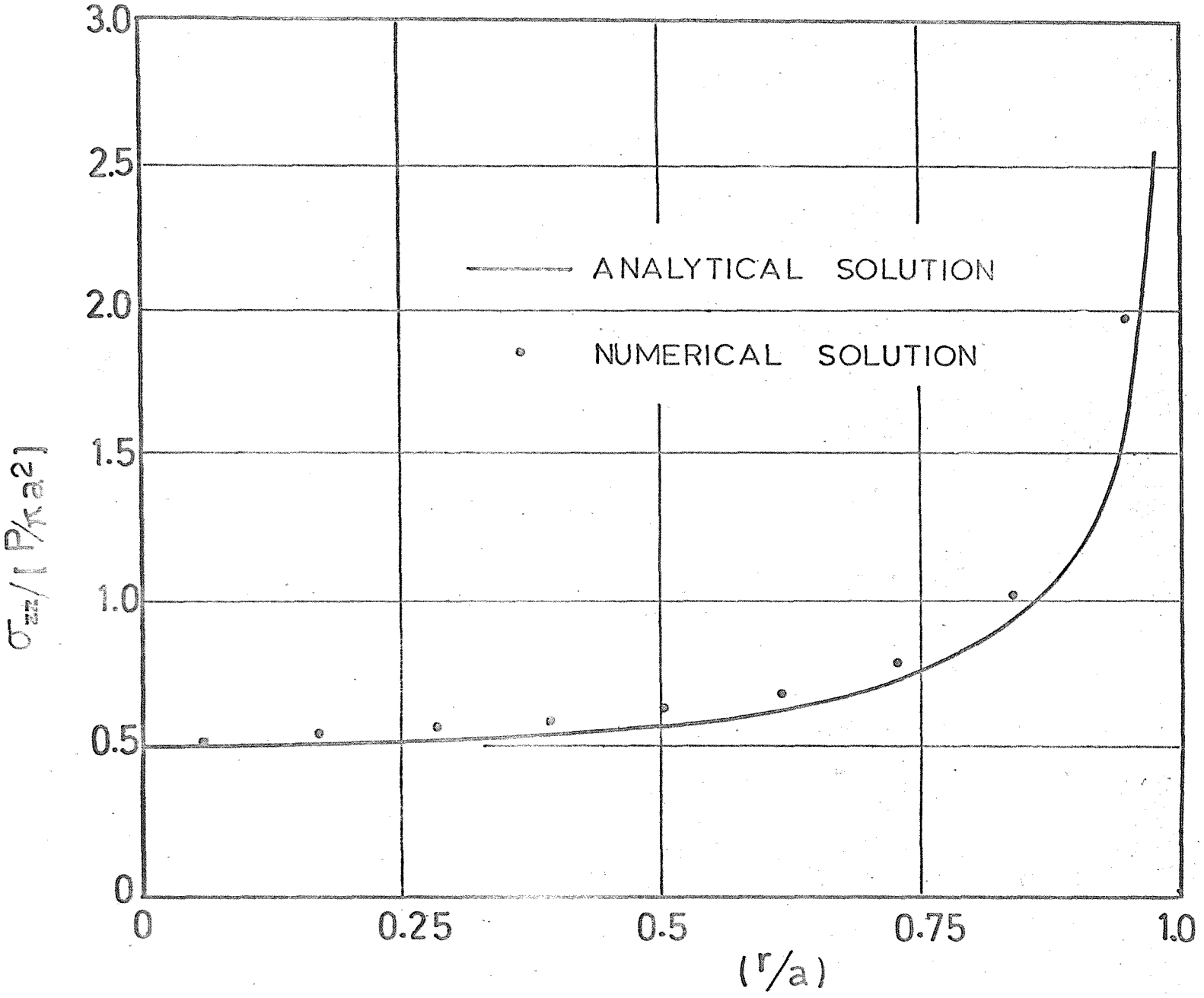

FIGURE 3.6: COMPARISON BETWEEN THE ANALYTICAL AND NUMERICAL SOLUTION FOR THE VERTICAL CONTACT PRESSURE UNDER A RIGID CIRCULAR DISC (c/a = 0, H/a = ∞)

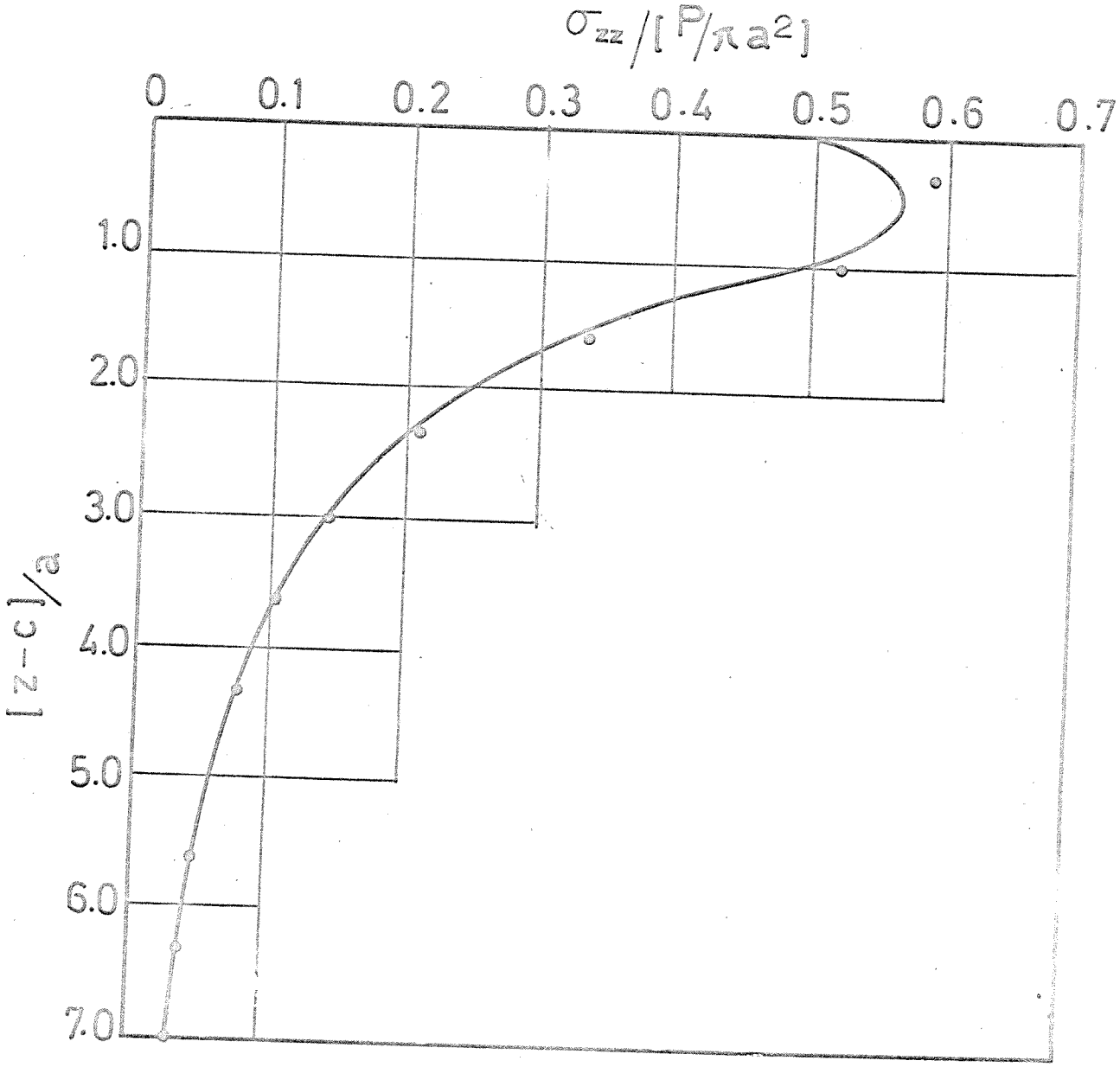

FIGURE 3.7: COMPARISON BETWEEN THE ANALYTICAL AND NUMERICAL SOLUTION FOR THE VERTICAL STRESSES UNDER THE CENTRE OF A RIGID DISC ($c/a = 0$, $E/a = \infty$)

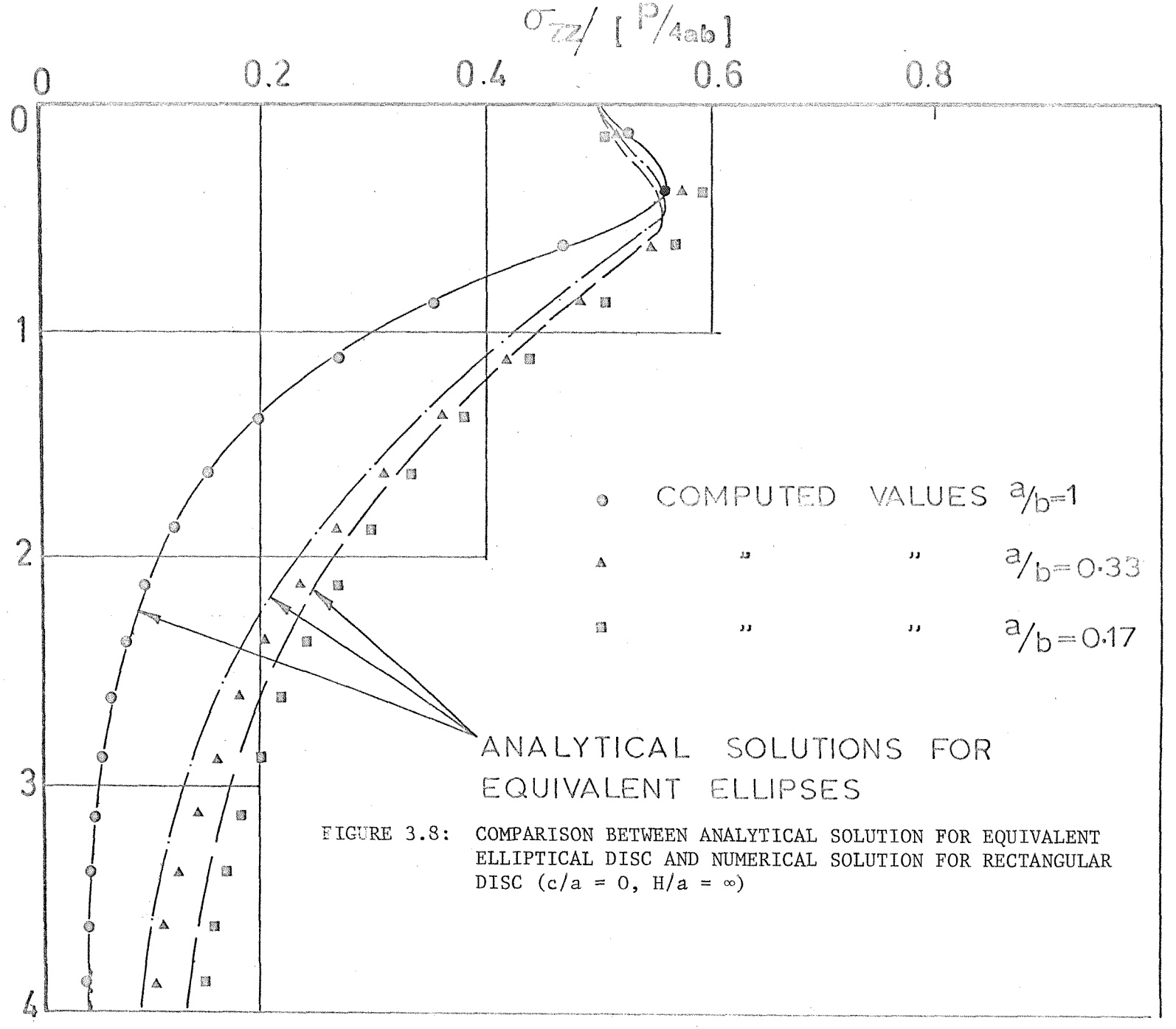

FIGURE 3.8: COMPARISON BETWEEN ANALYTICAL SOLUTION FOR EQUIVALENT ELLIPTICAL DISC AND NUMERICAL SOLUTION FOR RECTANGULAR DISC ($c/a = 0$, $H/a = \infty$)

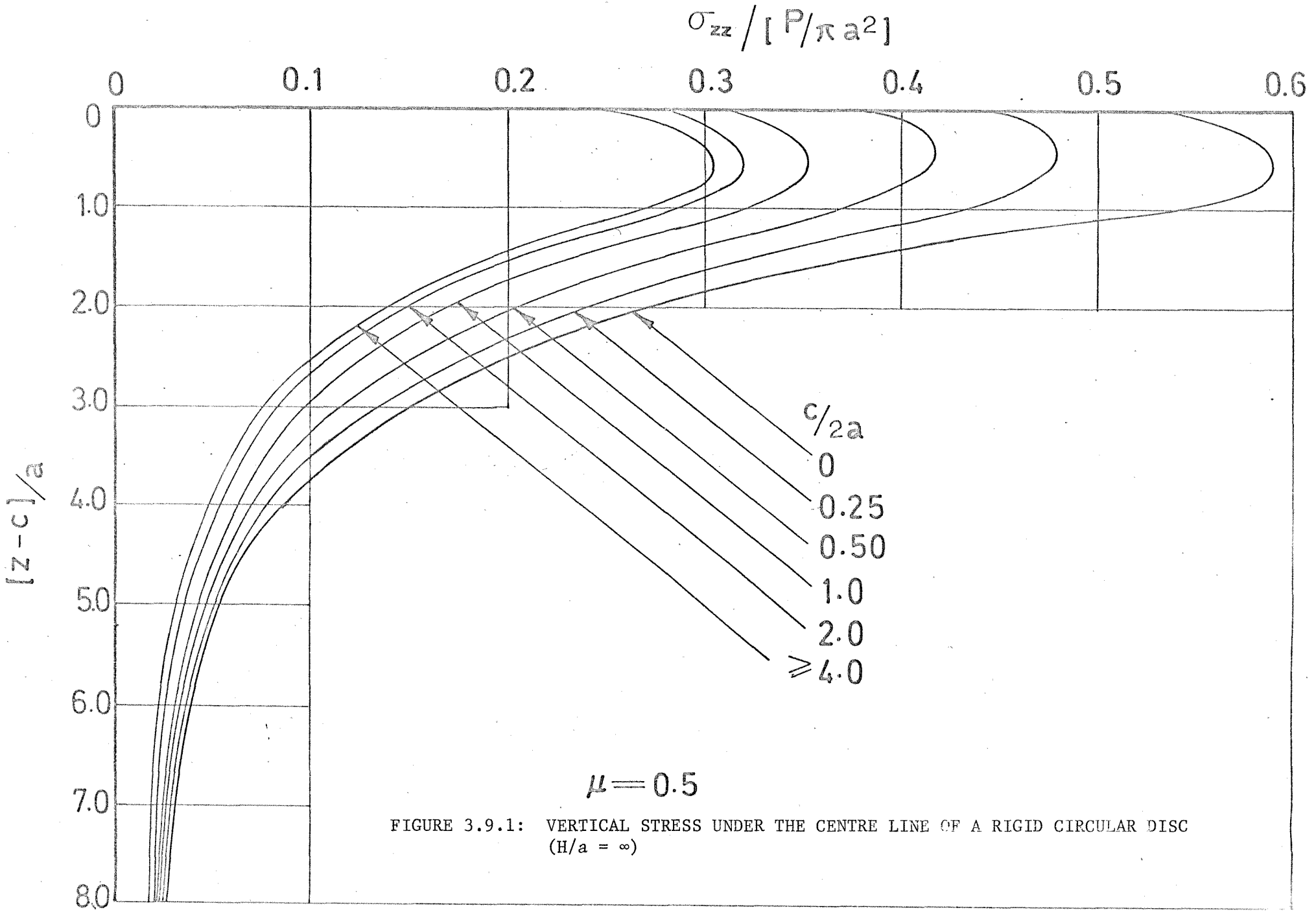

FIGURE 3.9.1: VERTICAL STRESS UNDER THE CENTRE LINE OF A RIGID CIRCULAR DISC ($H/a = \infty$)

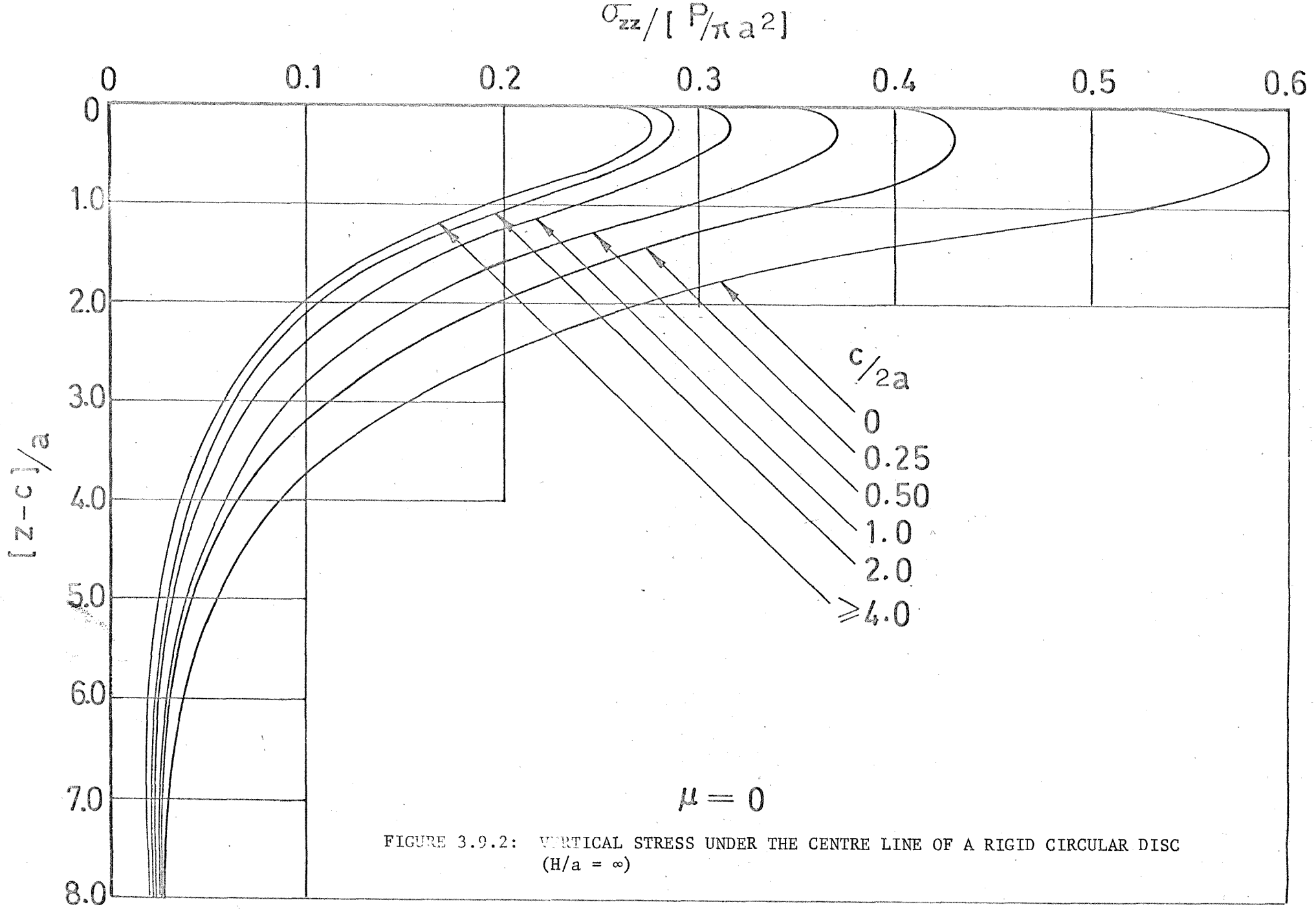

FIGURE 3.9.2: VERTICAL STRESS UNDER THE CENTRE LINE OF A RIGID CIRCULAR DISC ($H/a = \infty$)

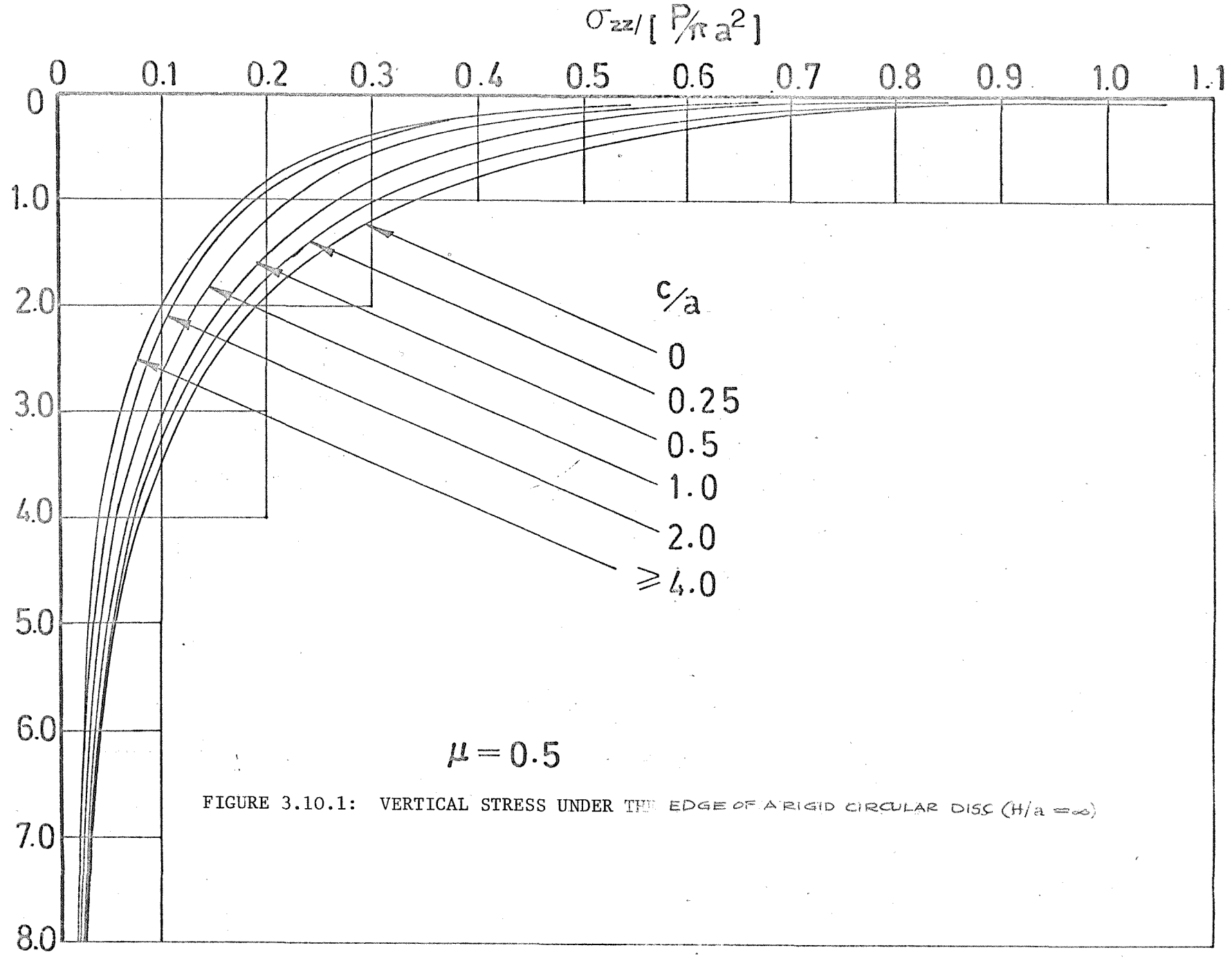

FIGURE 3.10.1: VERTICAL STRESS UNDER THE EDGE OF A RIGID CIRCULAR DISC ($H/a = \infty$)

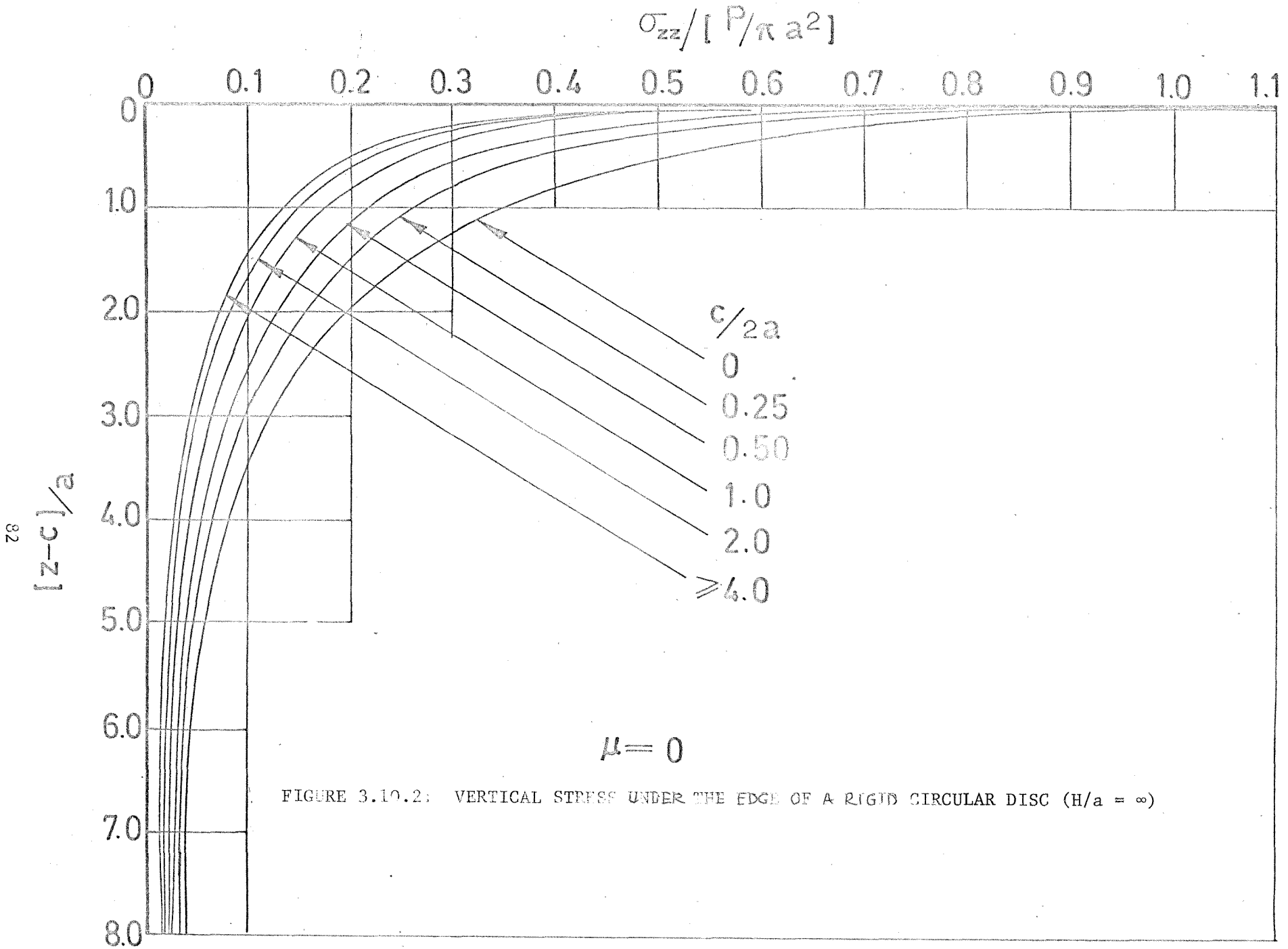

FIGURE 3.10.2: VERTICAL STRESS UNDER THE EDGE OF A RIGID CIRCULAR DISC (H/a = ∞)

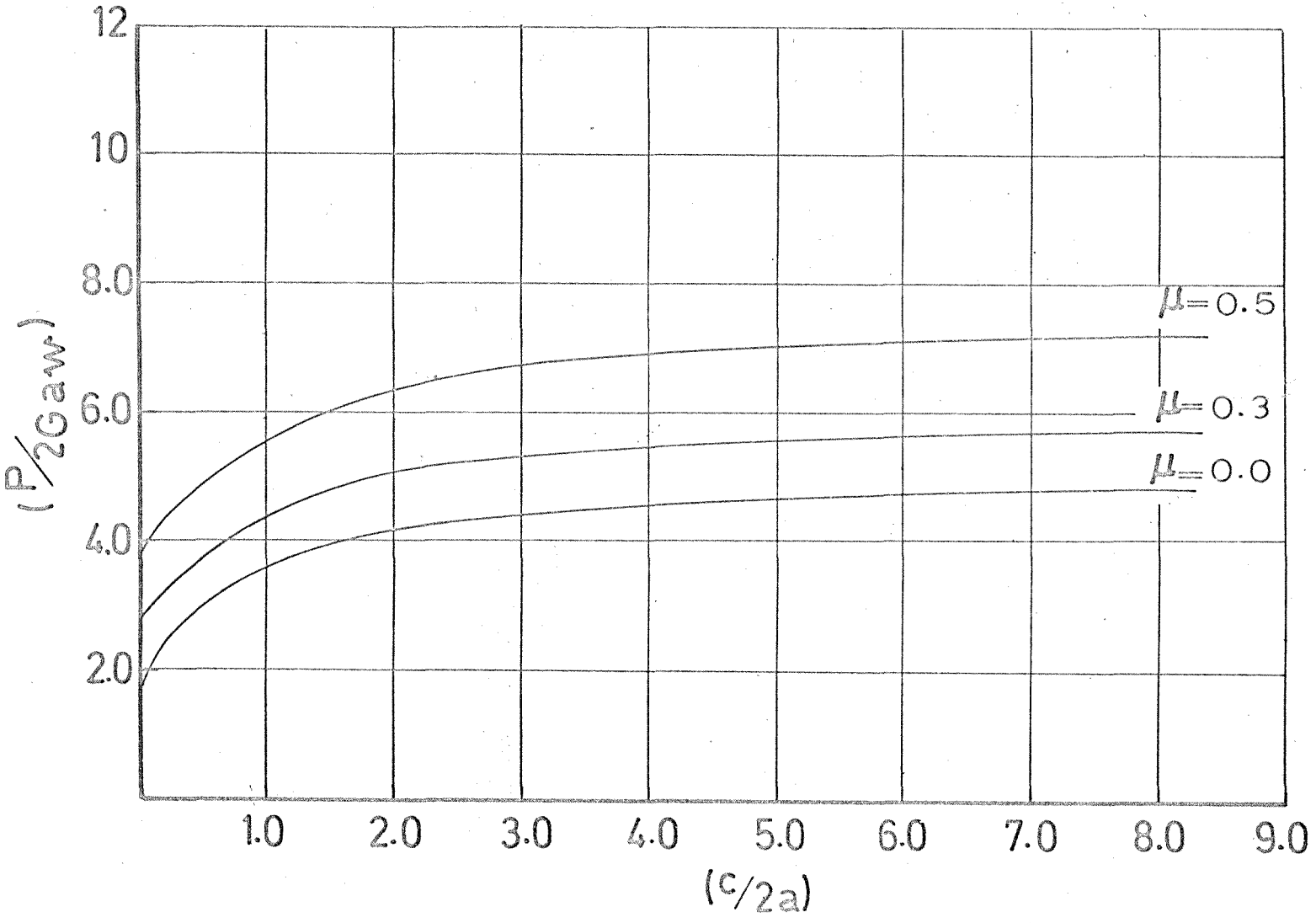

FIGURE 3.11.1: LOAD-DISPLACEMENT CHARACTERISTICS OF CIRCULAR DISC (H/a = ∞)

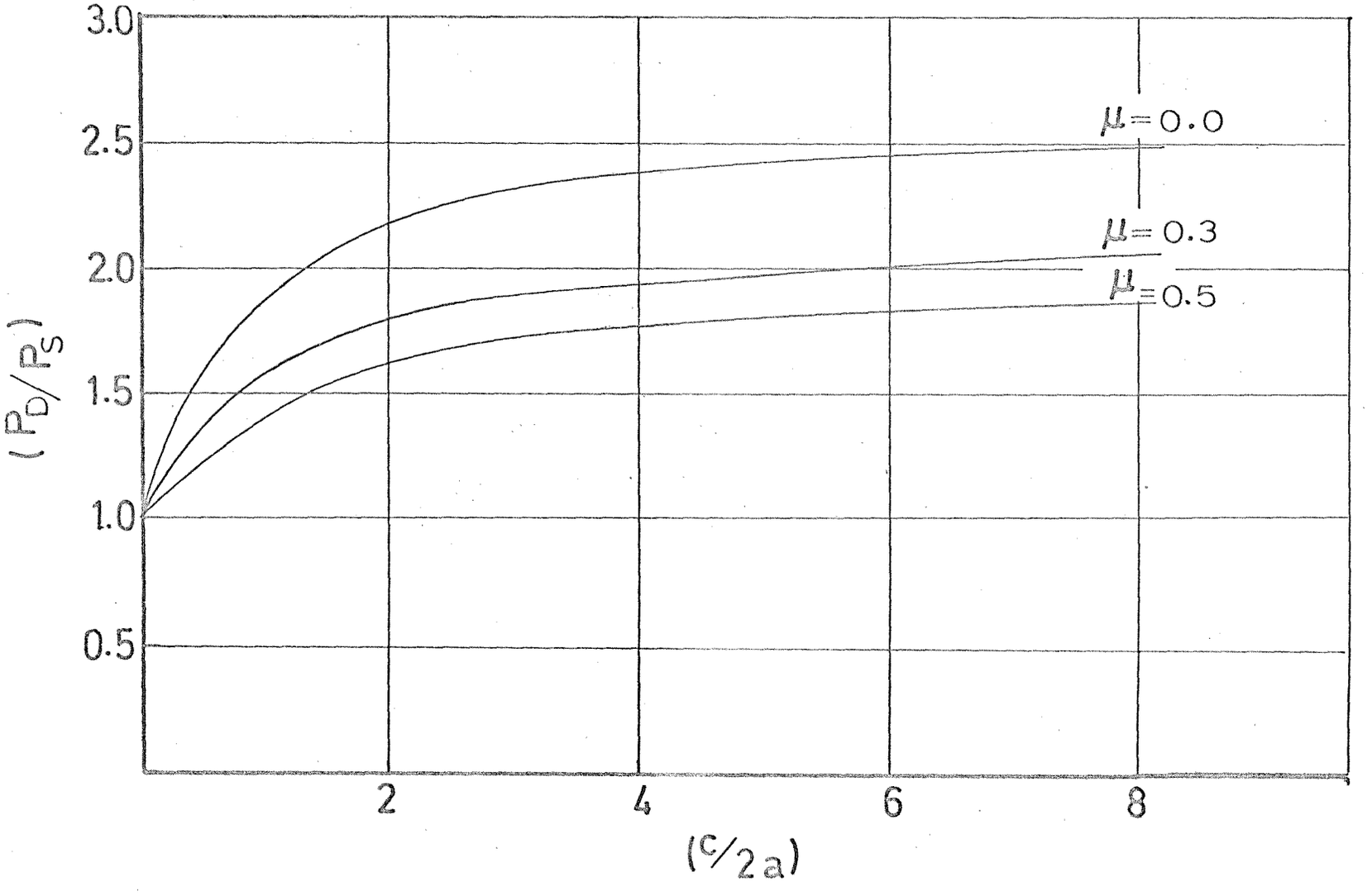

FIGURE 3.11.2: EFFECT OF DEPTH OF EMBEDMENT ON THE STIFFNESS OF A CIRCULAR DISC ($H/a = \infty$)

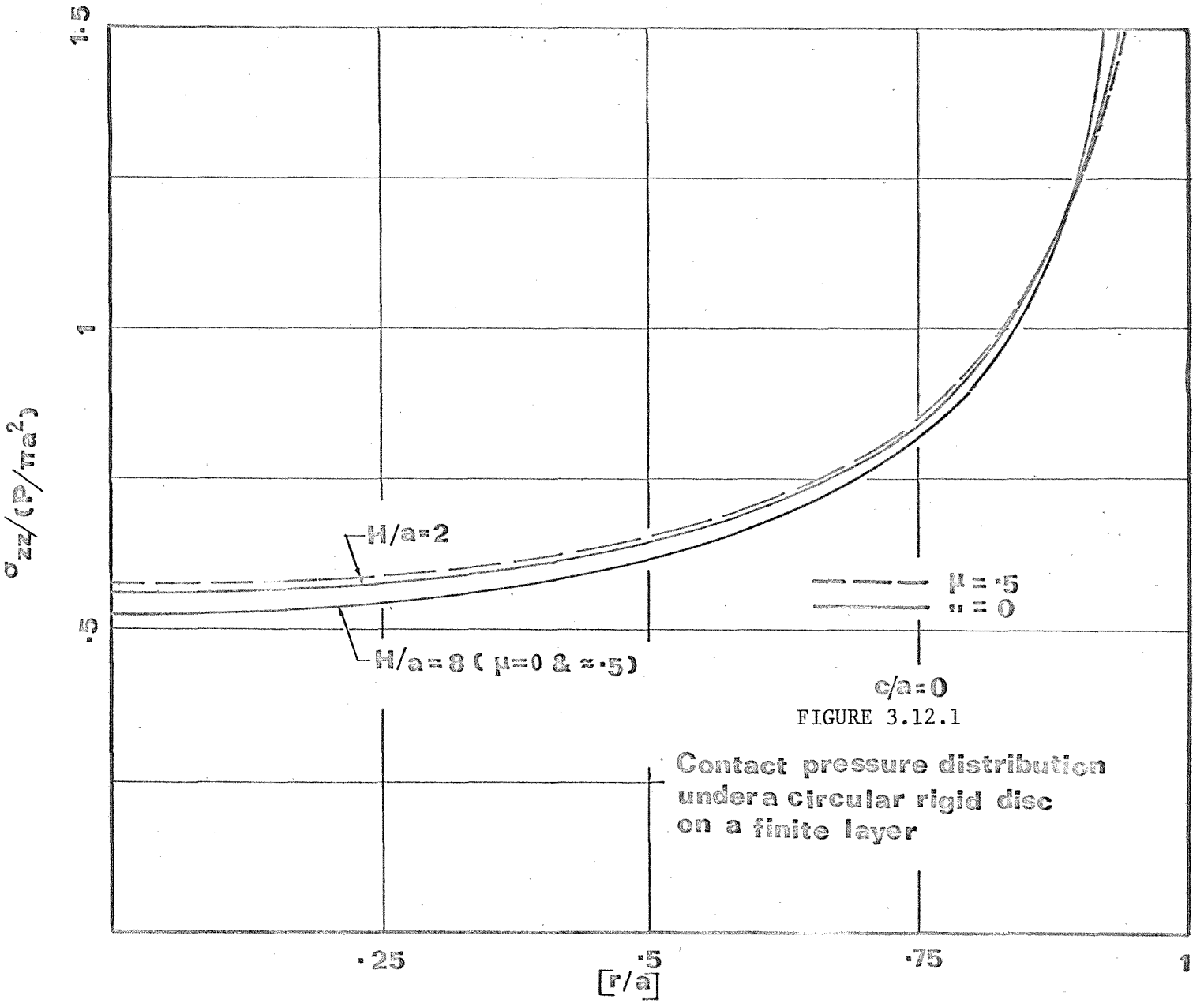

FIGURE 3.12.1

Contact pressure distribution under a circular rigid disc on a finite layer

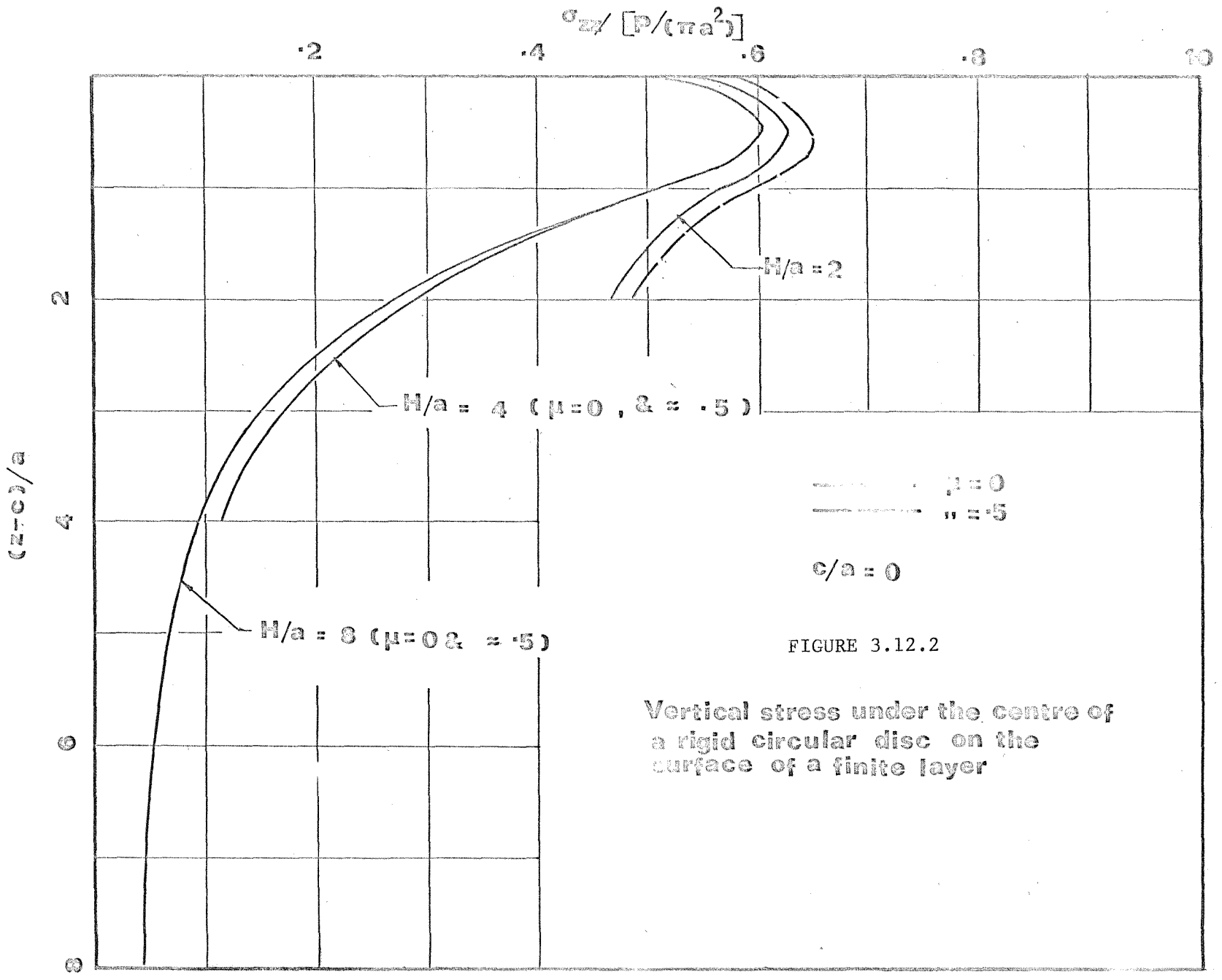

FIGURE 3.12.2

Vertical stress under the centre of a rigid circular disc on the surface of a finite layer

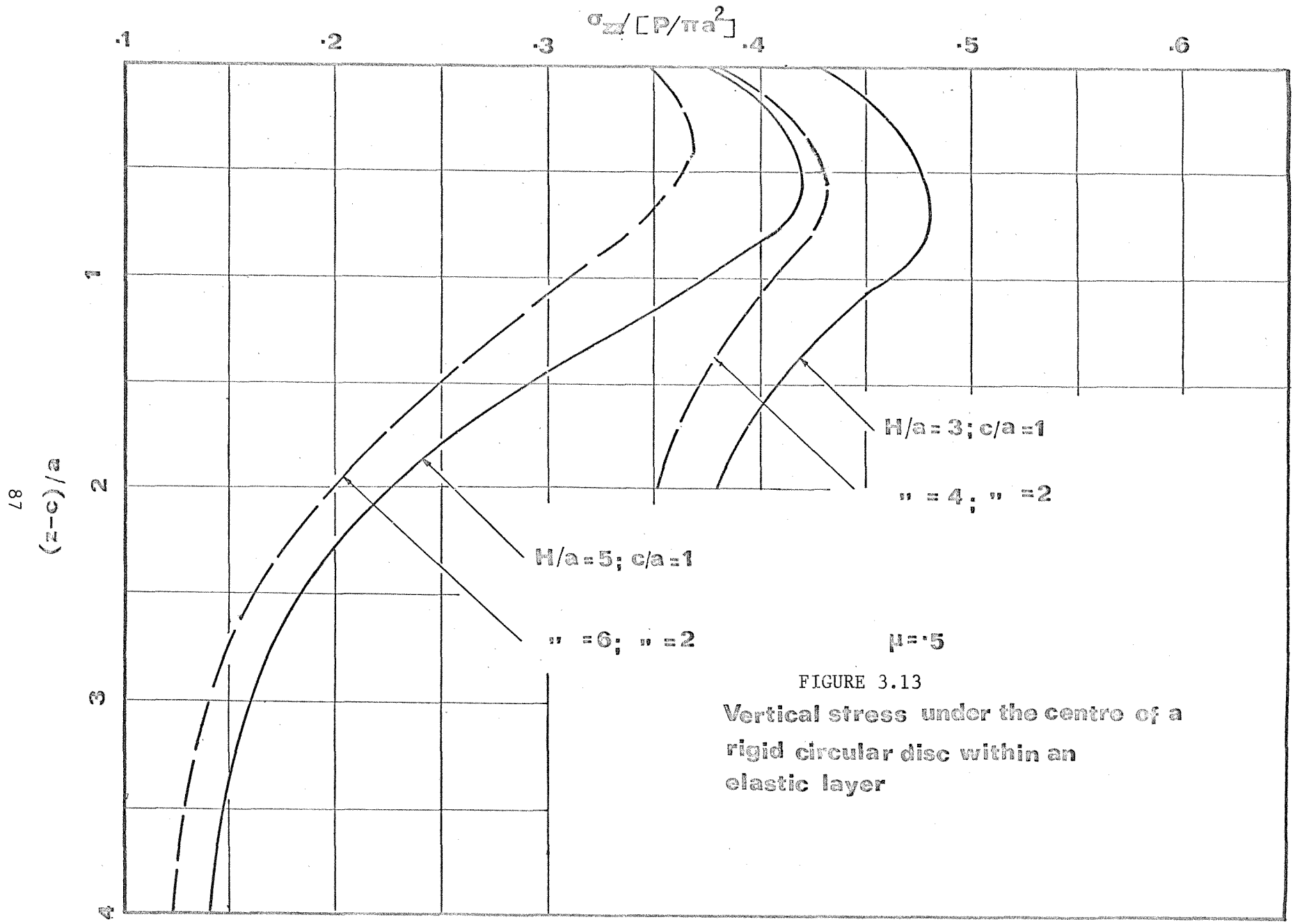

FIGURE 3.13

Vertical stress under the centre of a rigid circular disc within an elastic layer

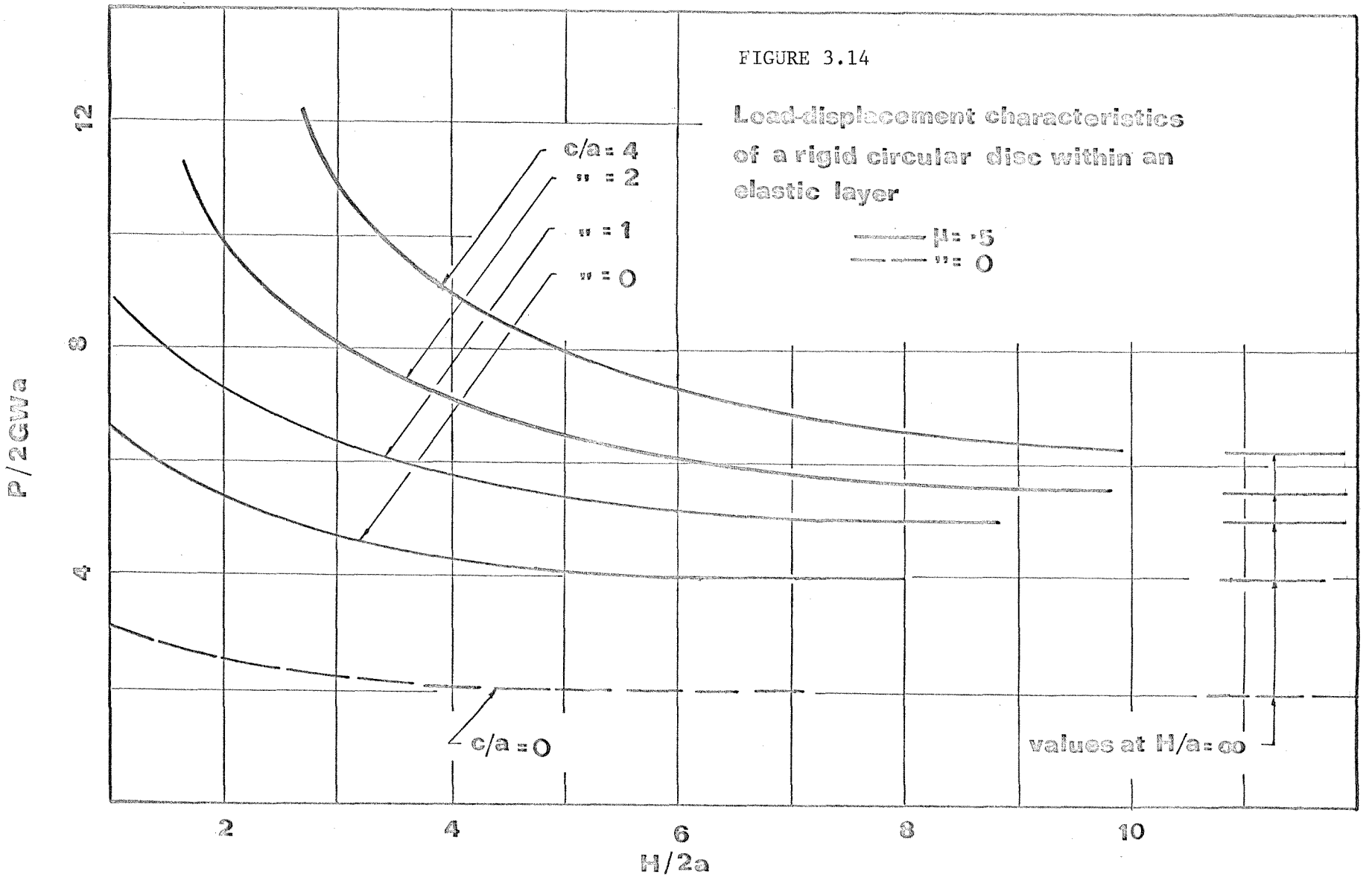
FIGURE 3.14
Load-displacement characteristics of a rigid circular disc within an elastic layer
μ = ·5
" = 0
c/a = 4
" = 2
" = 1
" = 0
c/a = 0
values at H/a = ∞
P/2GWa
H/2a
12
8
4
2
4
6
8
10

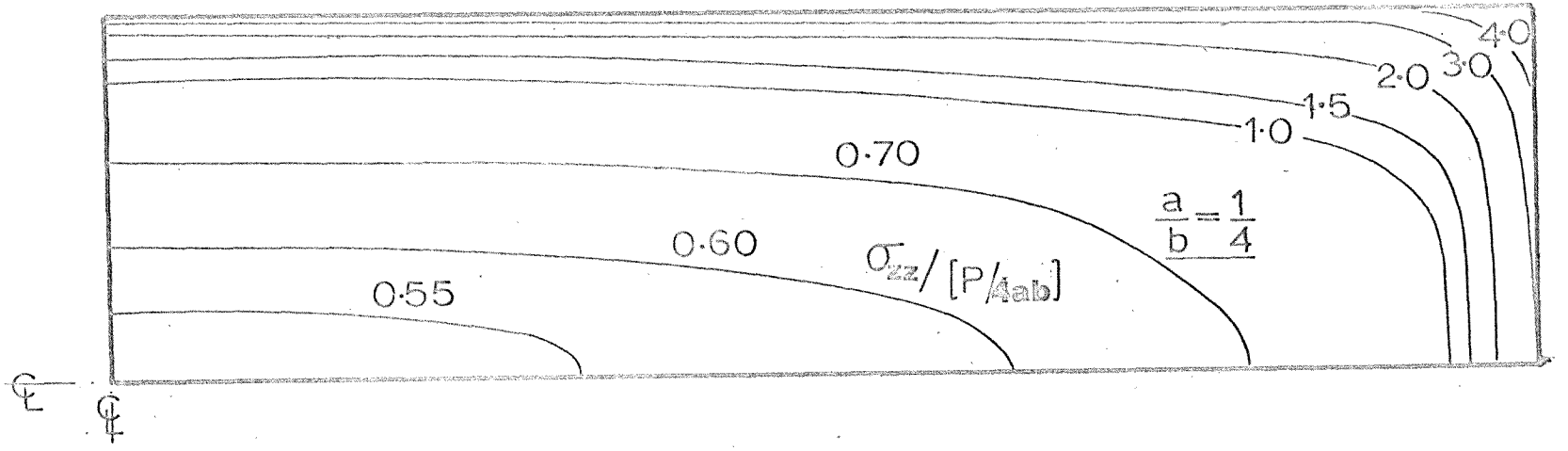

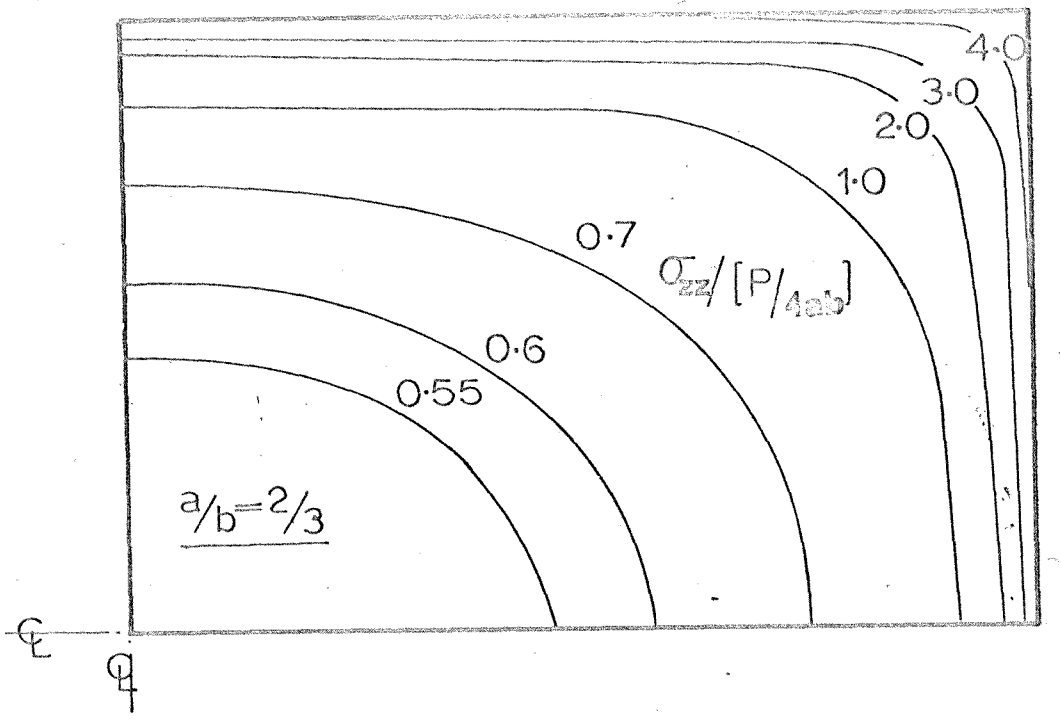

FIGURE 3.15: CONTACT PRESSURE DISTRIBUTION UNDER A RECTANGULAR DISC ($H/a = \infty$ $c/a = 0$)

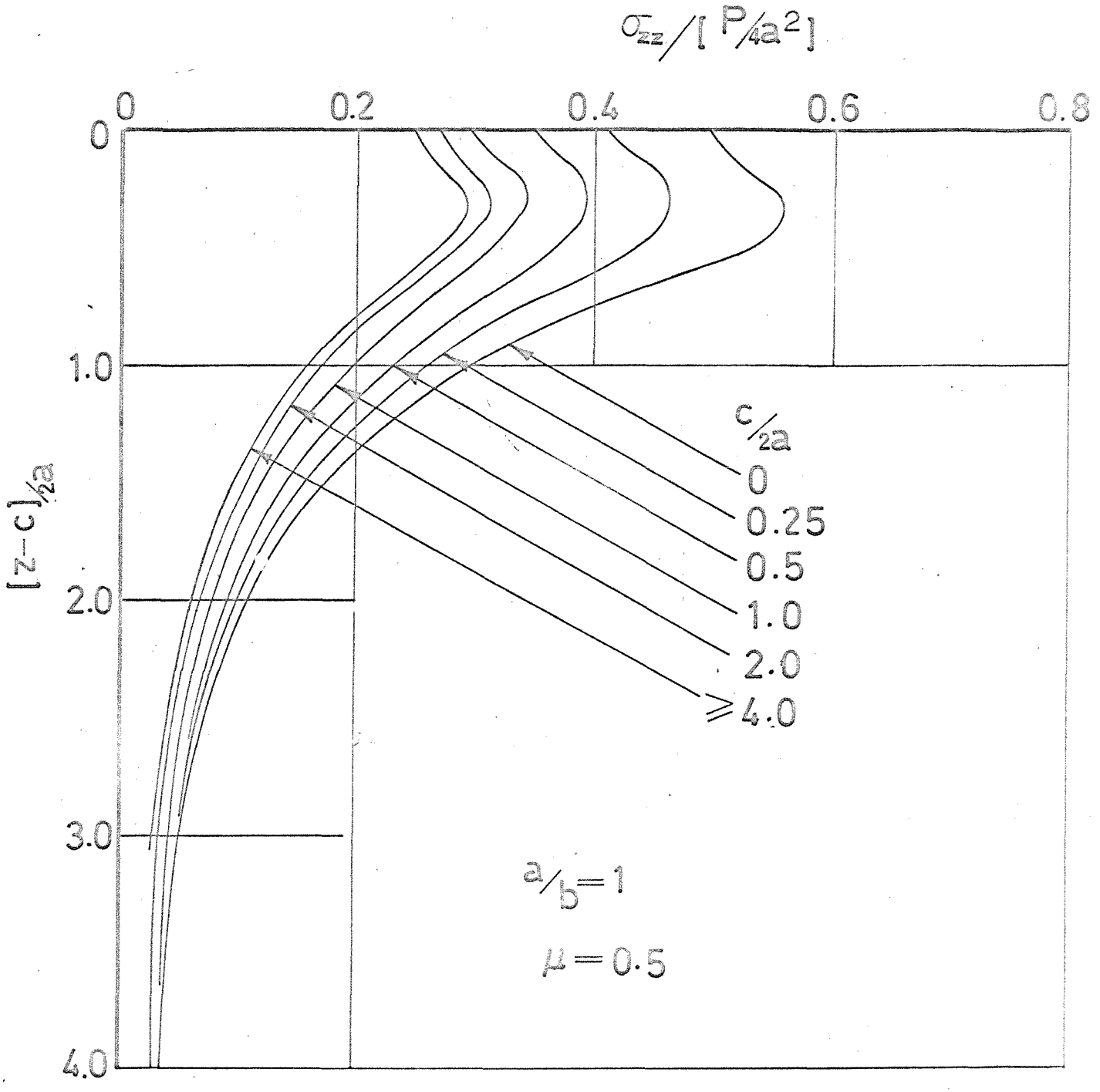

FIGURE 3.16.1: VERTICAL STRESS UNDER THE CENTRE OF A RECTANGULAR DISC ($H/a = \infty$)

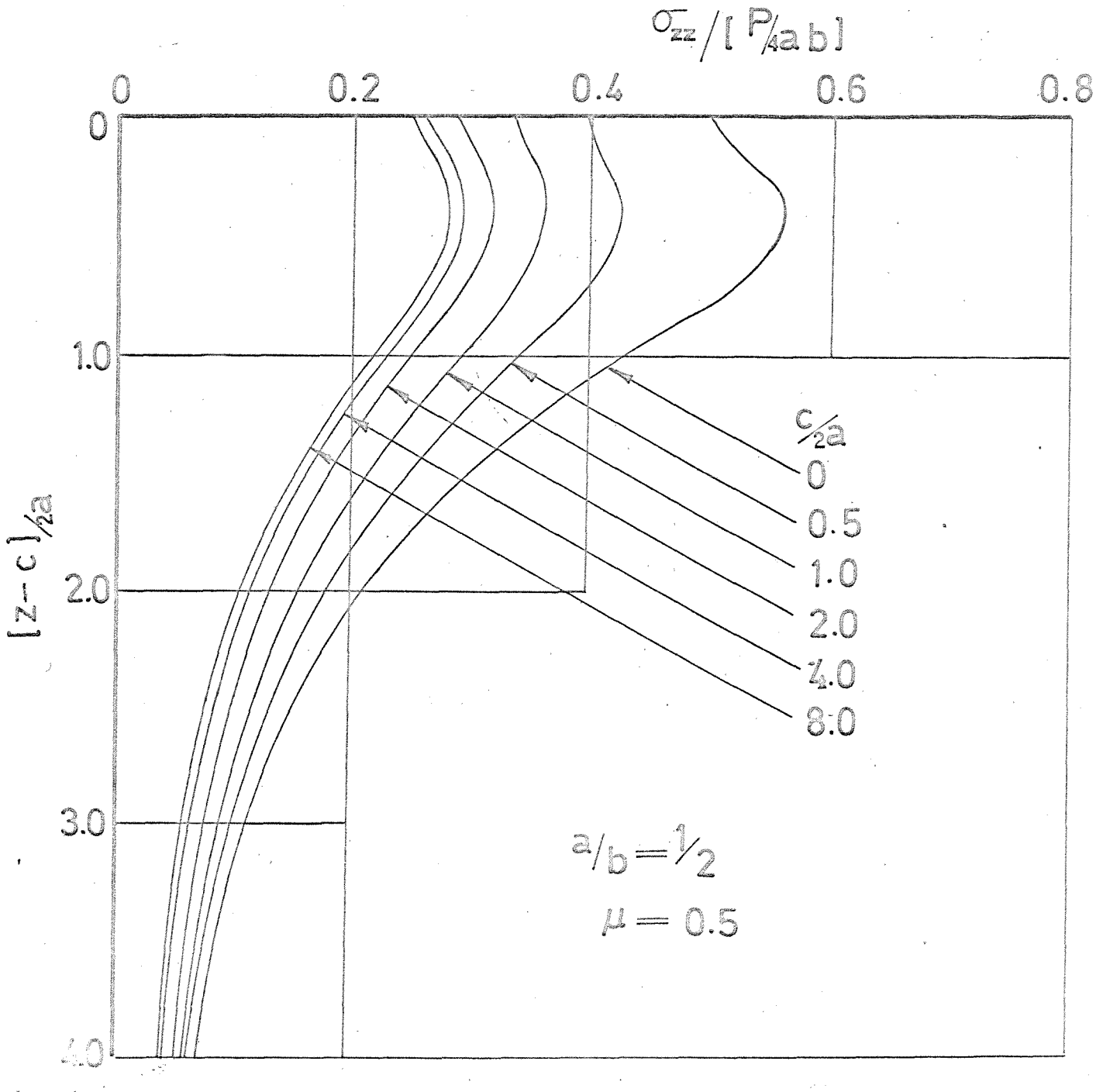

FIGURE 3.16.2: VERTICAL STRESS UNDER THE CENTRE OF A RECTANGULAR DISC ($H/a = \infty$)

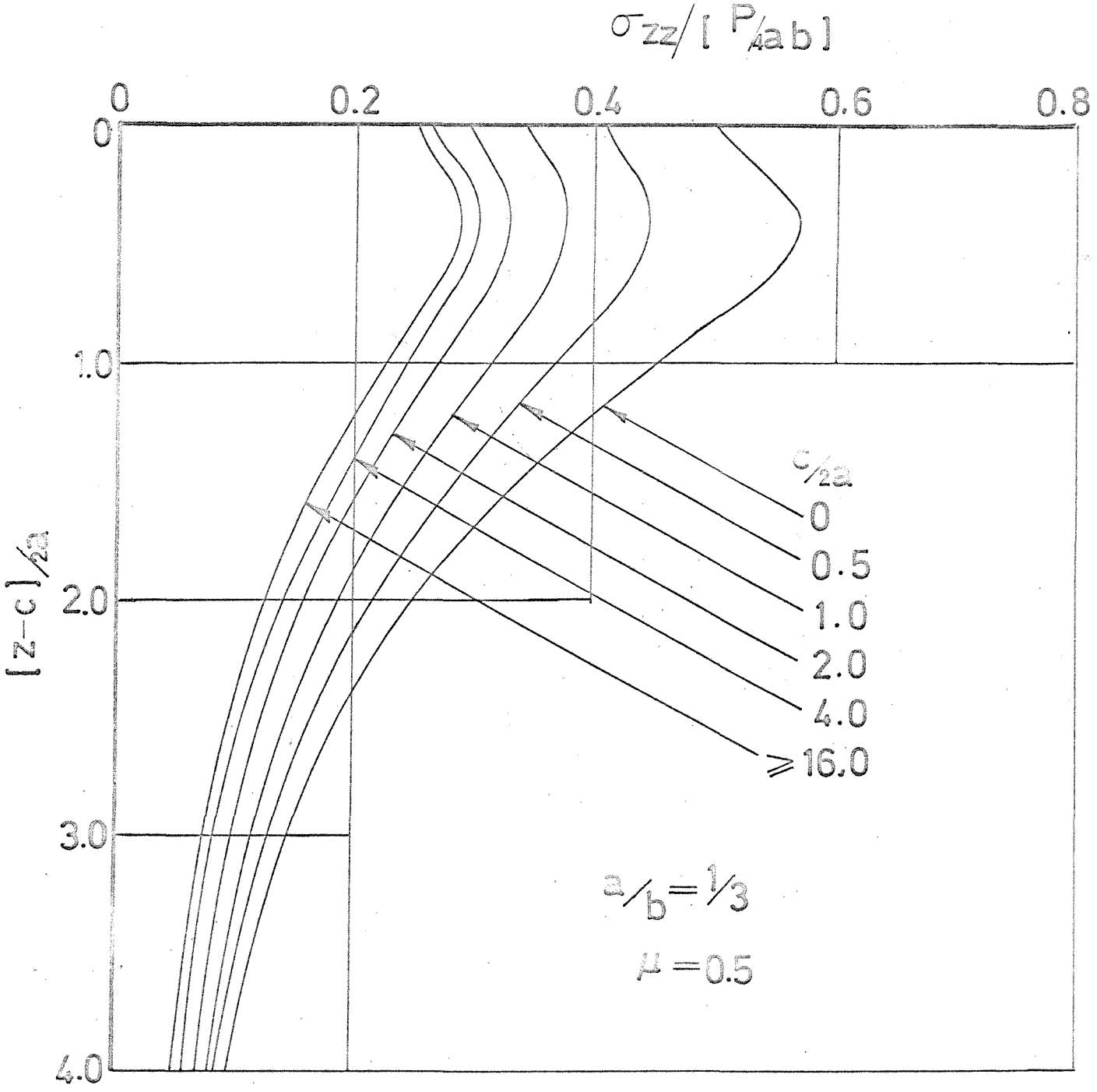

FIGURE 3.10.3: VERTICAL STRESS UNDER THE CENTRE OF A RECTANGULAR DISC (H/a = ∞)

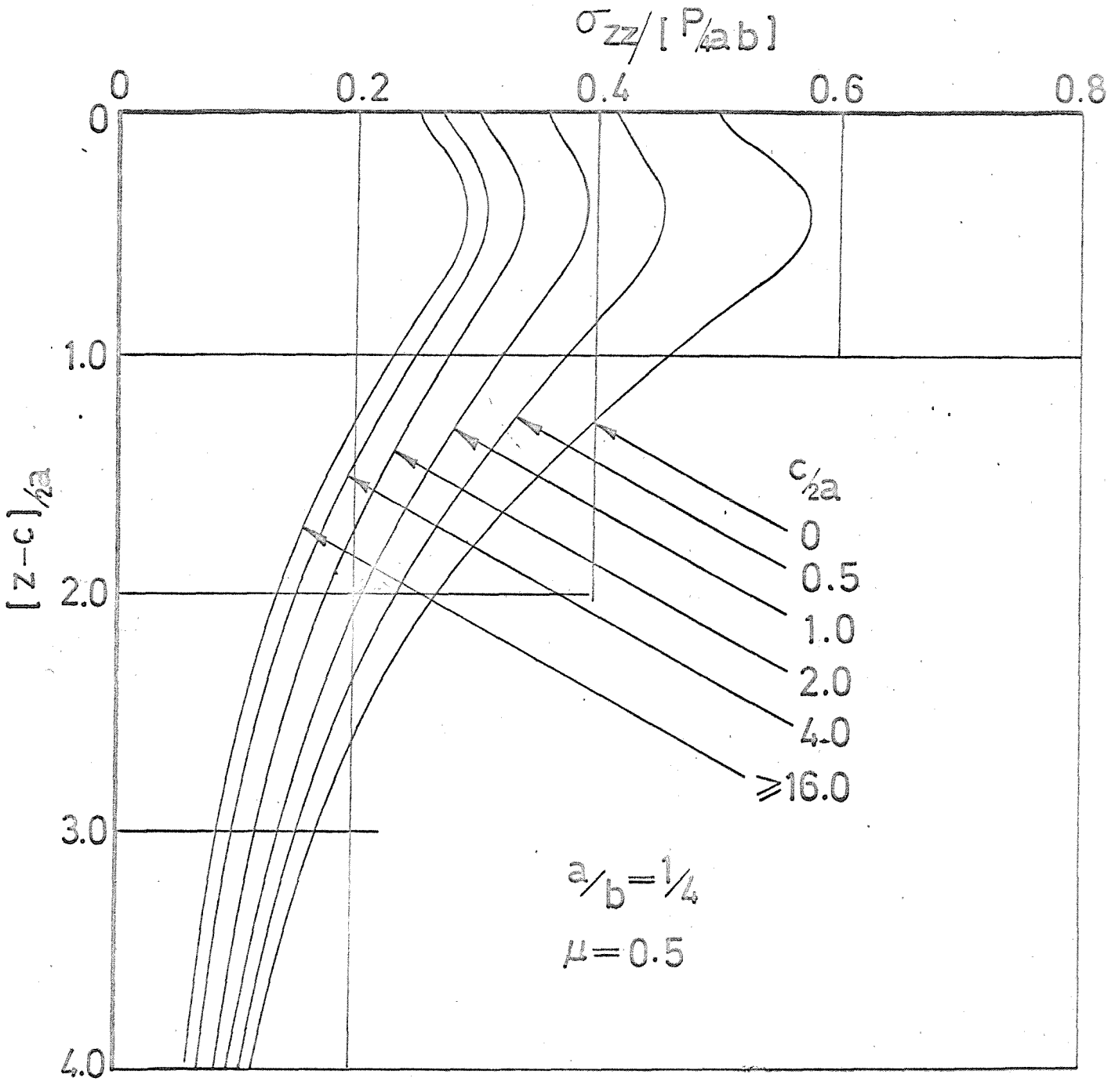

FIGURE 3.16.4: VERTICAL STRESS UNDER THE CENTRE OF A RECTANGULAR DISC ($H/a = \infty$)

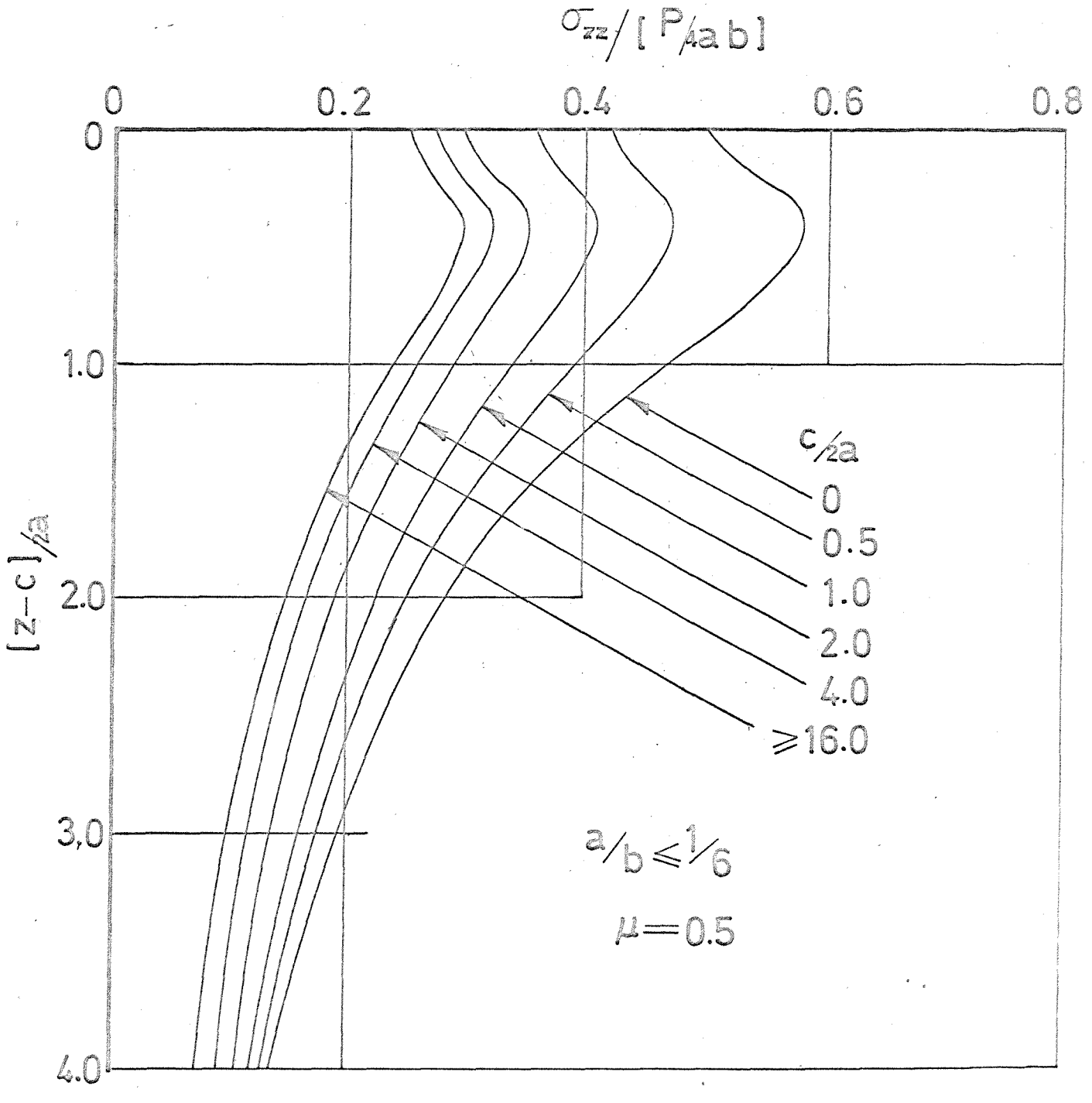

FIGURE 3.16.3: VERTICAL STRESSES UNDER THE CENTRE OF A RECTANGULAR DISC ($H/a = \infty$)

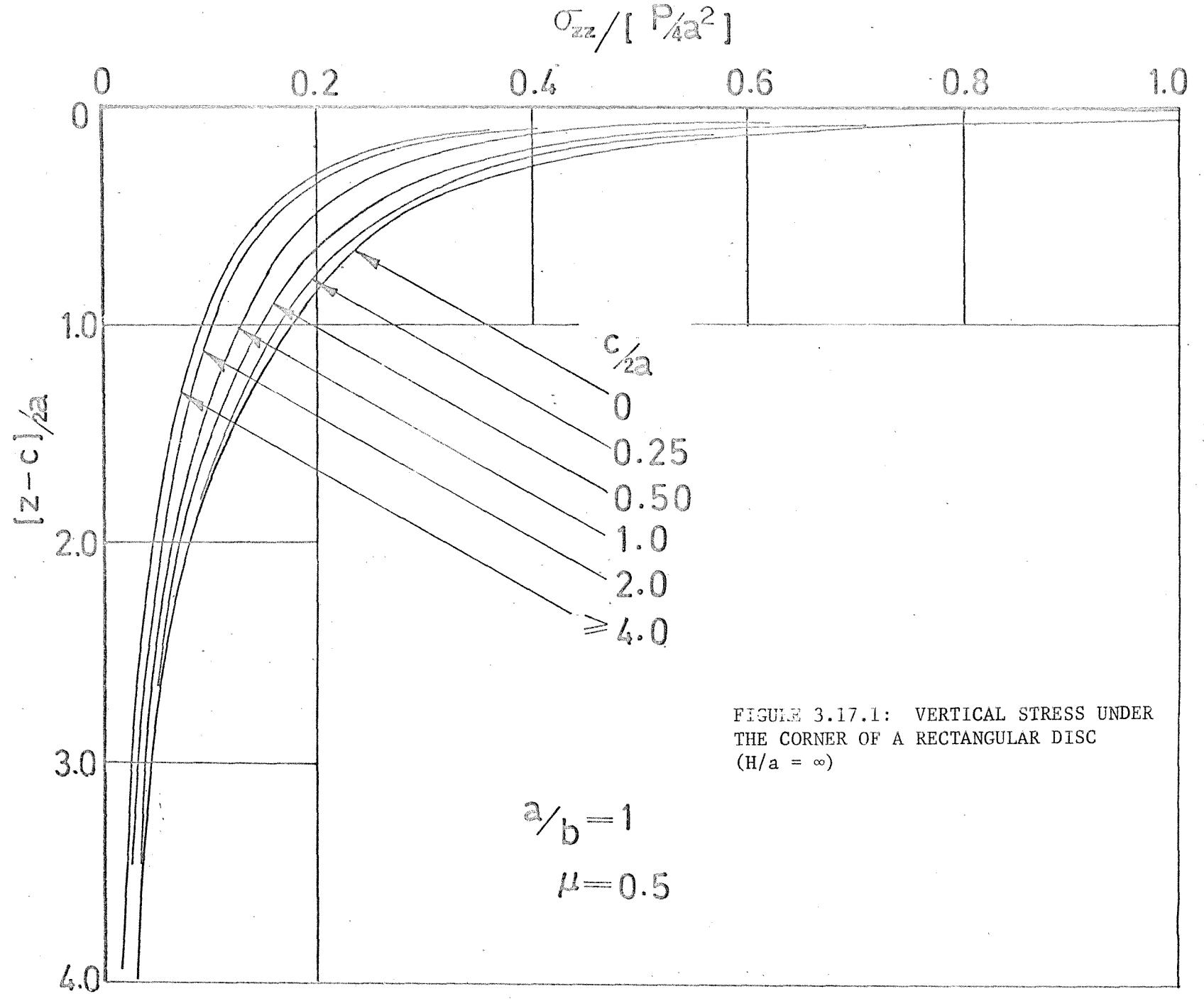

FIGURE 3.17.1: VERTICAL STRESS UNDER THE CORNER OF A RECTANGULAR DISC ($H/a = \infty$)

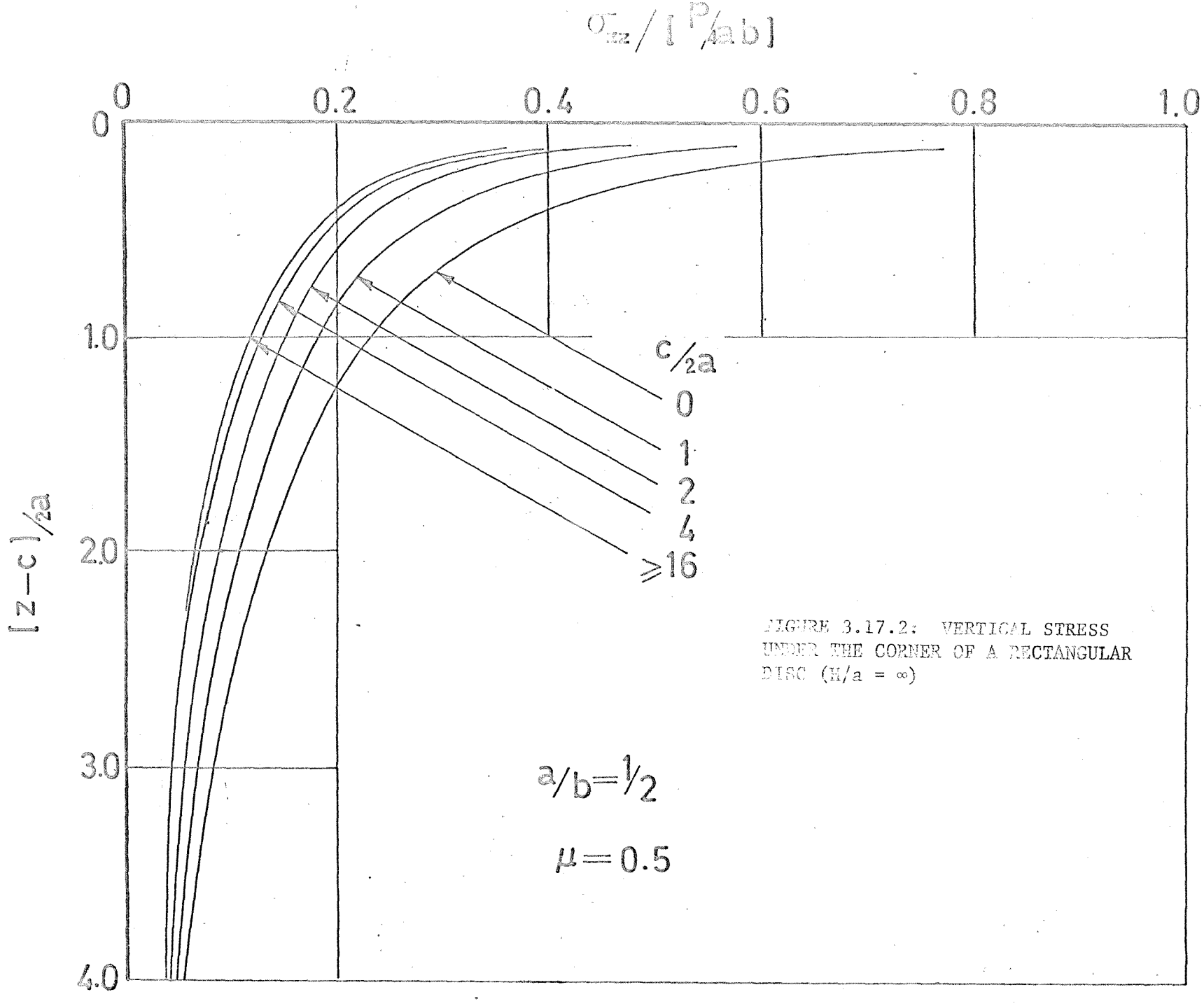

FIGURE 3.17.2: VERTICAL STRESS UNDER THE CORNER OF A RECTANGULAR DISC ($H/a = \infty$)

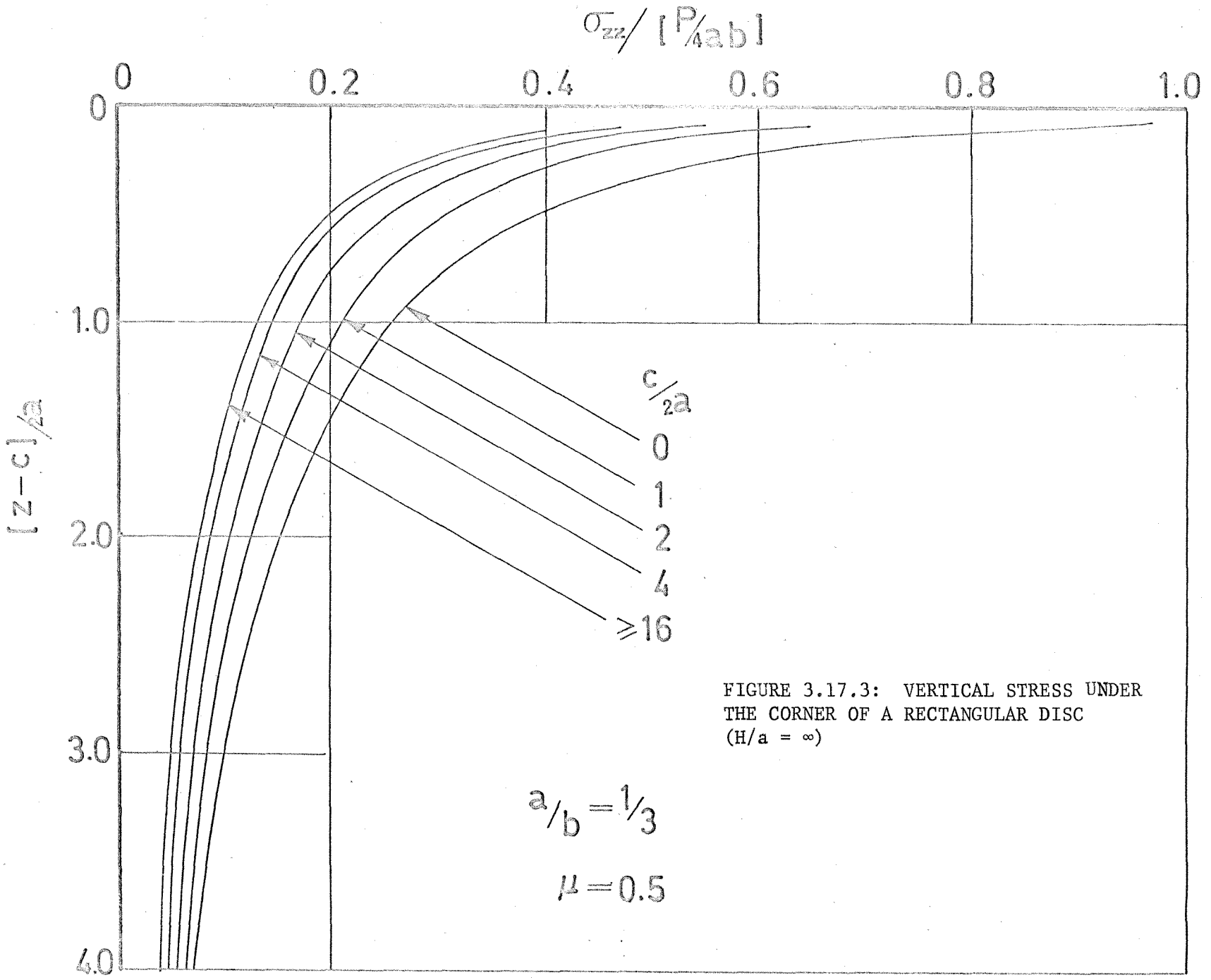

FIGURE 3.17.3: VERTICAL STRESS UNDER THE CORNER OF A RECTANGULAR DISC ($H/a = \infty$)

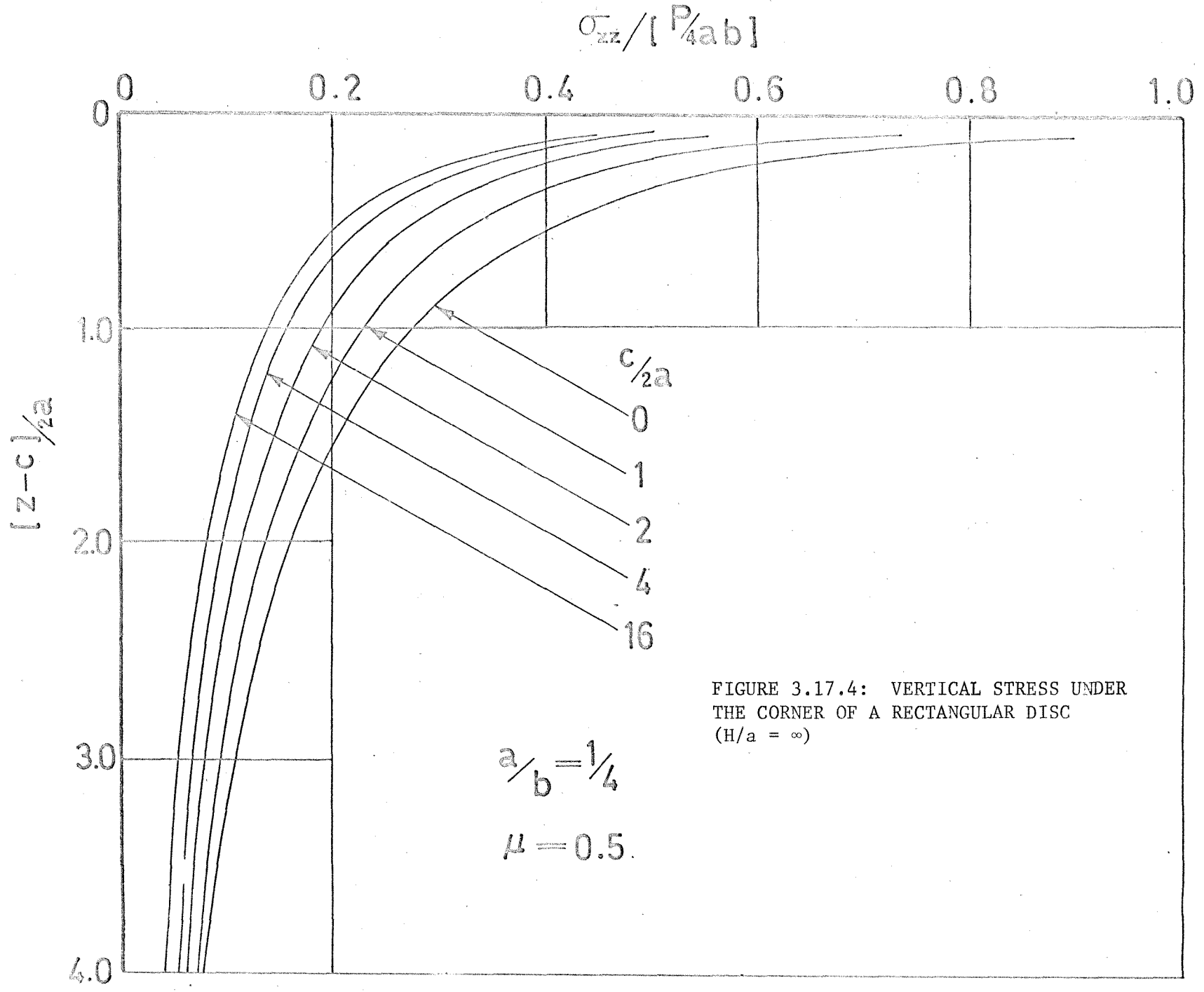

FIGURE 3.17.4: VERTICAL STRESS UNDER THE CORNER OF A RECTANGULAR DISC (H/a = ∞)

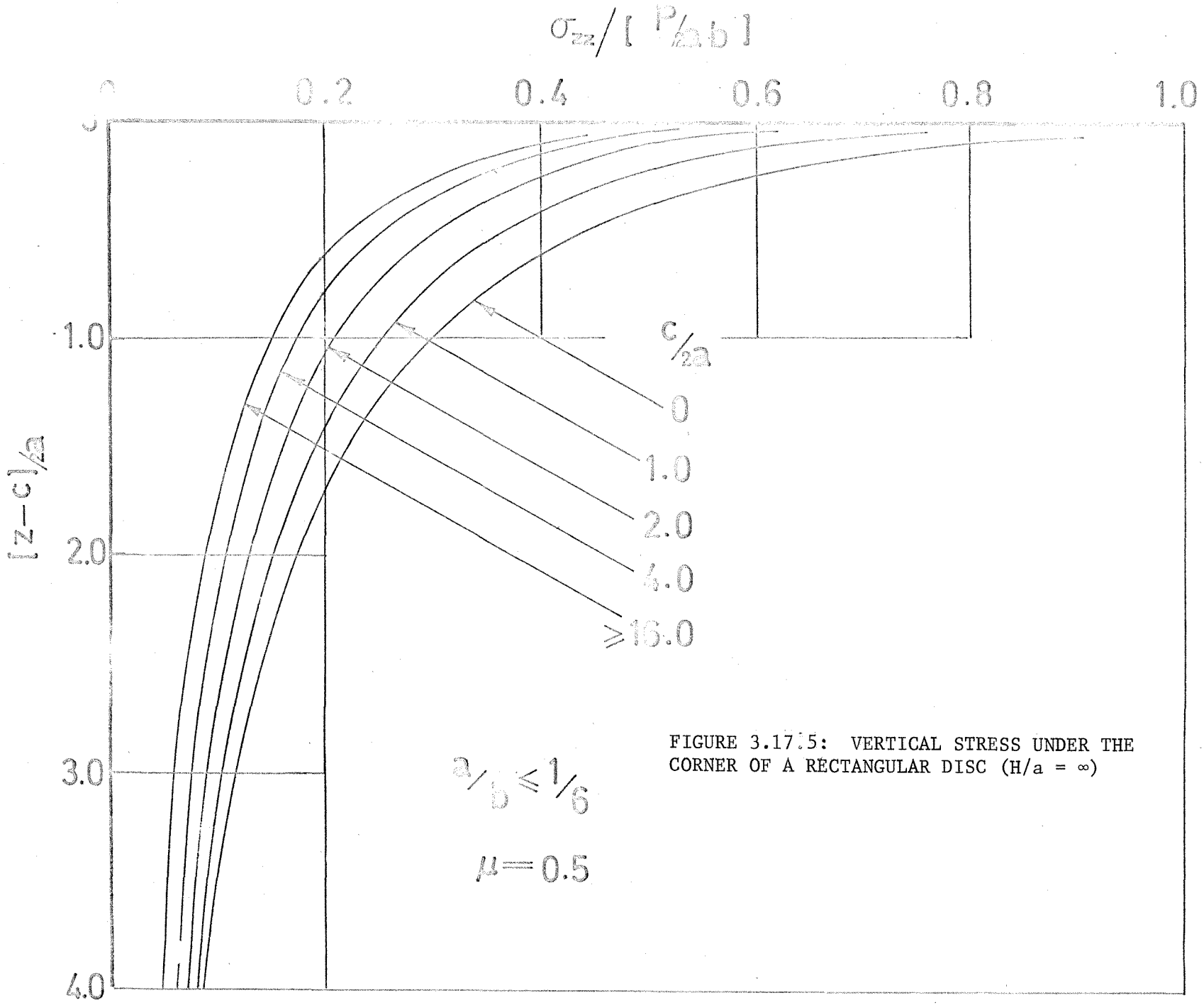

FIGURE 3.17.5: VERTICAL STRESS UNDER THE CORNER OF A RECTANGULAR DISC (H/a = ∞)

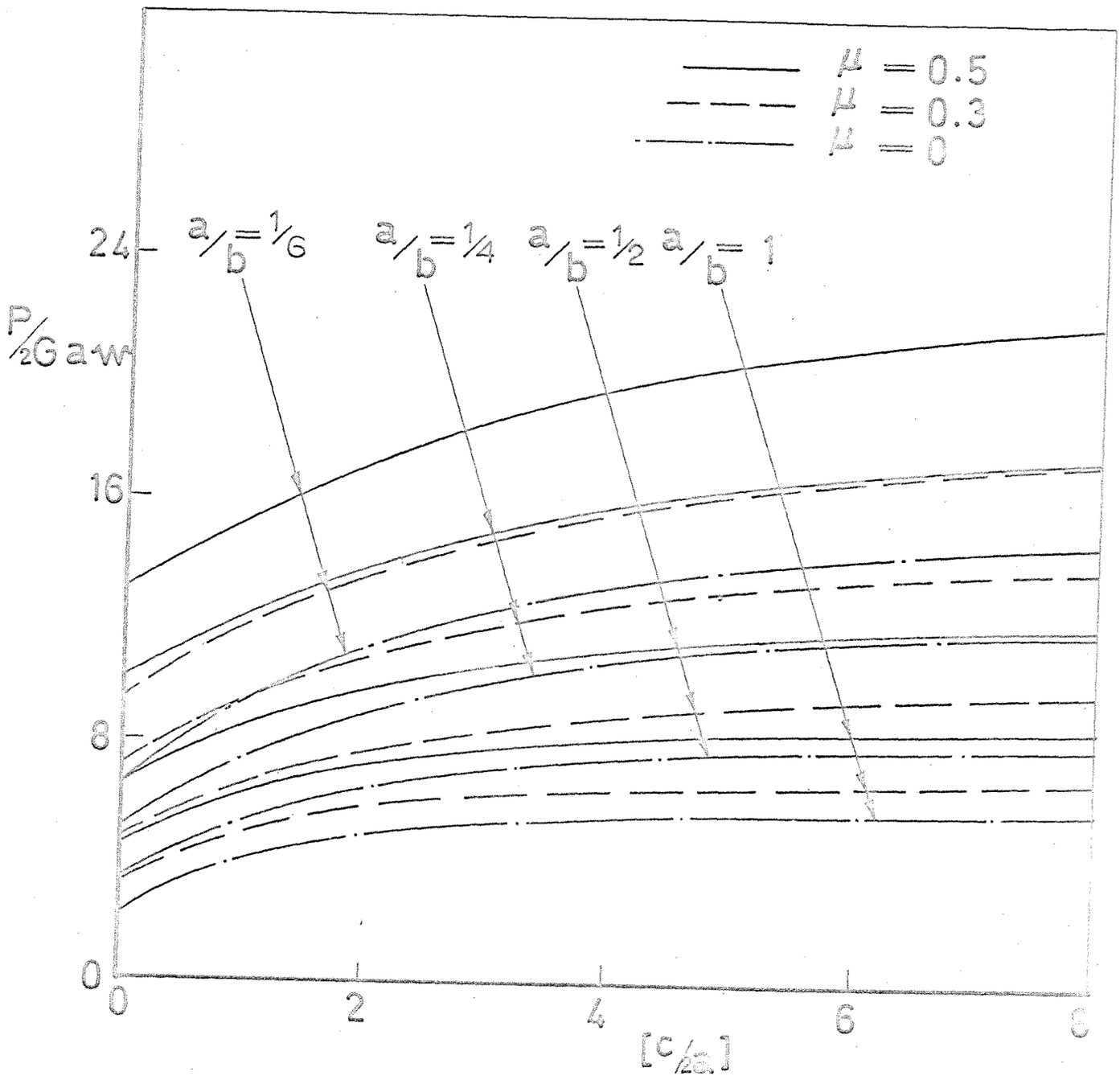

FIGURE 3.18: LOAD DISPLACEMENT CHARACTERISTICS OF RIGID RECTANGULAR DISCS ($H/a = \infty$)

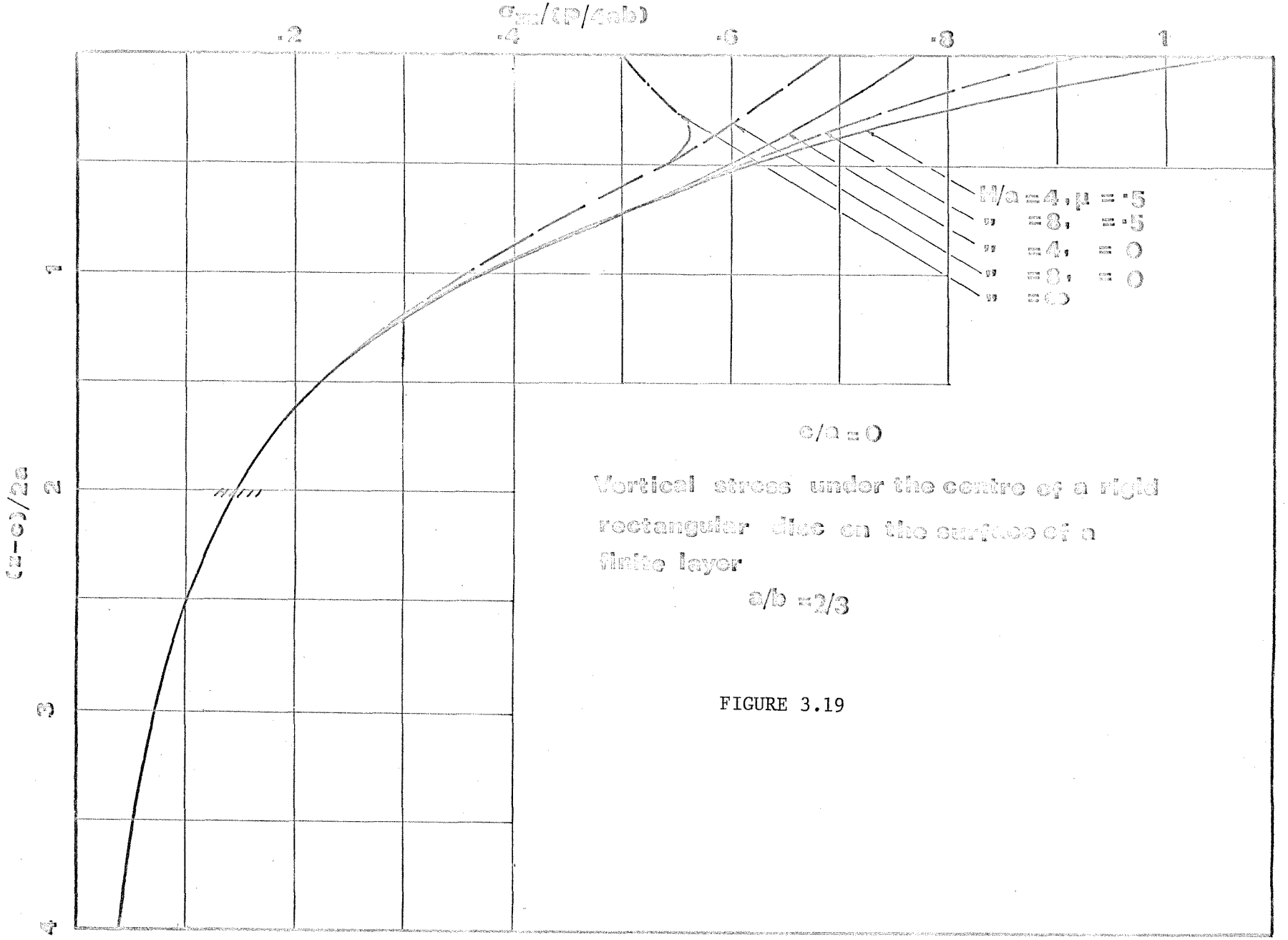

Vertical stress under the centre of a rigid rectangular slab on the surface of a finite layer

a/b = 2/3

FIGURE 3.19

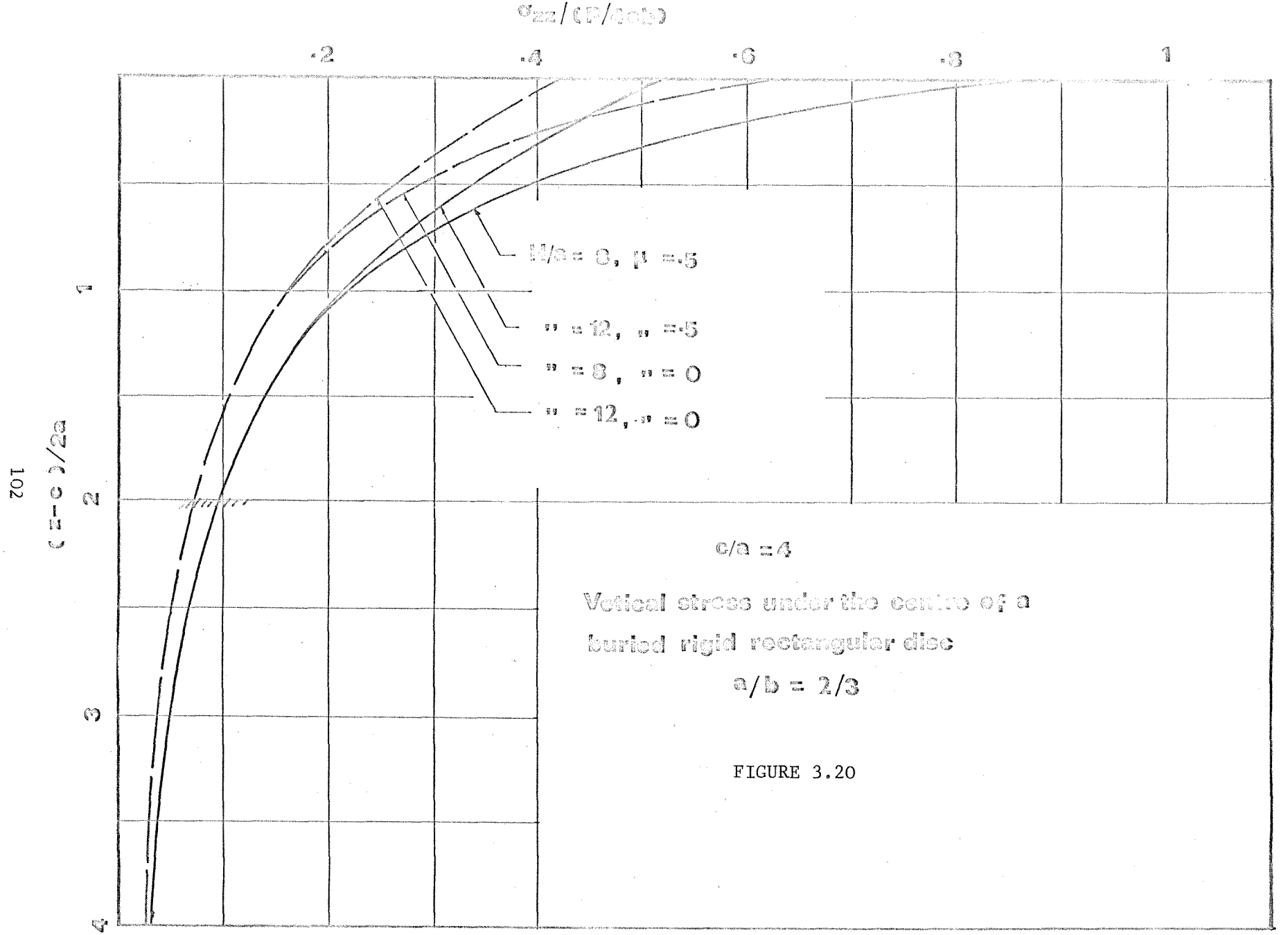
σzz/(P/4ab)
·2
·4
·6
·3
1
2
3
4
(z−c)/2a
H/a = 8, μ = .5
" = 12, " = .5
" = 8, " = 0
" = 12, " = 0
c/a = 4
Vertical stress under the centre of a
buried rigid rectangular disc
a/b = 2/3

FIGURE 3.20

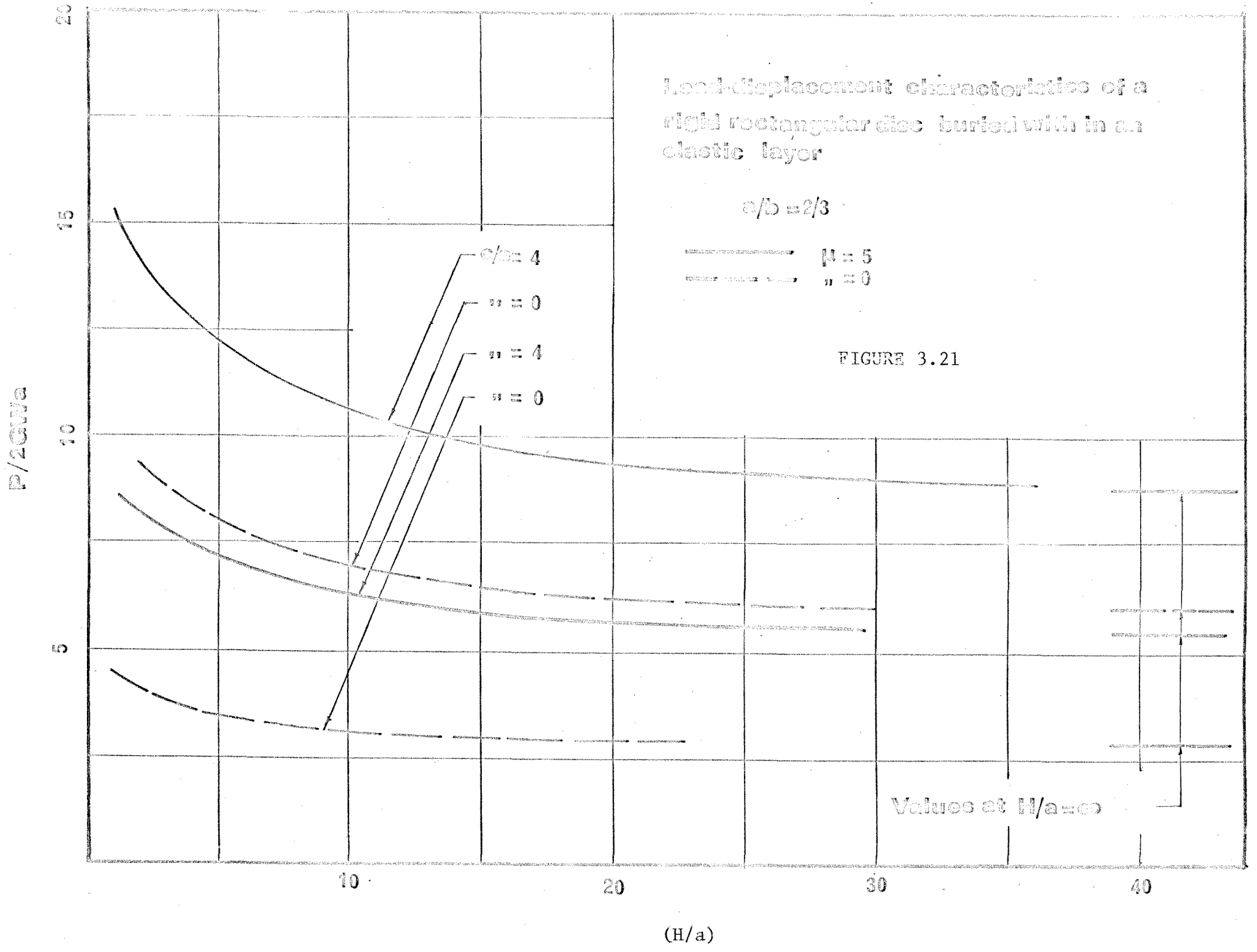
Load-displacement characteristics of a rigid rectangular disc buried with in an elastic layer
c/b = 2/3
μ = 5
" = 0
c/a = 4
" = 0
" = 4
" = 0
Values at H/a=∞
P/2GNa
(H/a)
5
10
15
20
10
20
30
40

FIGURE 3.21

Chapter 4

An analysis of single axially loaded plain and under-reamed piles

4.1 Summary

The load displacement characteristics of single axially loaded piles and piers are described in this chapter. The elastic response of both rigid and compressible piles embedded in a homogeneous isotropic elastic half space and a finite layer underlain by a rigid smooth base has been obtained by the use of an alogorithm based on integral equation method described in Chapter 2.

The method has been extended to analyse local slip between the pile and surrounding soil. The results of the analysis are compared with previously published experimental data and are presented as a series of graphs showing the effects of variation of the ratios of pile length to diameter, modulus of elasticity of piles to that of the soil, pile length to thickness of the elastic layer and the effects of the base enlargement on the load displacement characteristics.

4.2 General

The analysis of a single, compressible pile embedded within both an elastic half space and a finite elastic layer which is underlain by a rigid base, is presented below under the following assumptions:

(i) Both the soil and the pile material are elastic, isotropic homogeneous.

(ii) The pile is bonded with the medium at the pile medium interface.

(iii) The elastic soil layer is underlain by a rigid and smooth surfaced layer.

(iv) The base of the pile is assumed to be smooth.

Assumption (i) is an idealisation of stress-strain response of real soil. However, the results of a long series of experiments at the Waterways Experimental Station, summarised by Turnbul et al (1961) have shown that for saturated clays, quite close agreement between experimentally observed stresses under surface loads and the values computed from elastic solutions based on Bussinesq's analysis (Boussinesq, 1885). There is therefore some justification for attempting to obtain useful predictions of load displacement characteristics of piles based on elastic theory. Assumption (ii) implies no slip at the pile-soil interface. In practice, however, the shear stress at the pile - soil interface will have a maximum limit depending on various factors, such as, method of construction, roughness of the pile surface etc. (Tomlinson, 1957). The present analysis has been extended to take the local slip between the pile and the soil medium into considerations. The effects of assumptions (iii) and (iv) have been discussed already in Chapter 3.

4.3 Analytical formulation for an axially loaded single pile embedded within a half space

A cylindrical pile of length L and radius 'a' is embedded in an

elastic, isotropic half space defined by elastic constants G and μ as shown in Figure (4.1). If ϕ_s is the vertical shaft stress intensity at a depth c below the surface, the vertical and radial displacements

$$\delta w_1(r,z) = \int_0^{2\pi} a.\ \phi_s.\ \{KW_1(c,r_1,z)\ \delta c\}\ d\theta \qquad (4.1)$$

$$\delta u_1(r,z) = \int_0^{\pi} a.\ \phi_s\ \{KU_1(c,r_1,z)\ \delta c\}\ \cos\alpha_1\ d\theta \qquad (4.2)$$

Where $KW_1(c,r_1,z)$ and $KU_1(c,r_1,z)$ can be obtained from the first and the second equation respectively, of equations (2.4) by substituting $r_1^2 = r^2 + a^2 - 2ra\cos\theta_\varepsilon$ for r,

α_1 is the angle between r_1 and the outward normal to a surface at B (Figure, 4.1)

The total vertical and radial displacements at B(r,z) due to all such elemental shaft intensities is then obtained by integration, as:

$$w_1(r,z) = \int_0^{L} \int_0^{2\pi} \phi_s.\ a.\ KW_1(c,r_1,z)\ d\theta\ dc \qquad (4.3)$$

and

$$u_1(r,z) = \int_0^{L} \int_0^{2\pi} \phi_s.\ a.\ KU_1(c,r_1,z)\ \cos\alpha_1\ .\ d\theta.\ dc \qquad (4.4)$$

Similarly if we consider ϕ_b to be the resultant vertical stress (see Chapter 3) over the base area of the pile acting at a point $O'(\varepsilon,\theta_\varepsilon,L)$. Figure (4.2),the vertical and the radial displacements at B(r,z) due to the base intensity can be expressed by analogy with (4.3) and (4.4) as.

$$w_2(r,z) = \int_0^{b} \int_0^{2\pi} \phi_b.\ \varepsilon.\ KW_2(L,r_2,z)\ d\theta\ d\varepsilon \qquad (4.5)$$

$$u_2(r,z) = \int_0^{b} \int_0^{\pi} \phi_b.\ \varepsilon.\ KU_2(L,r_2,z)\ \cos\alpha_2\ d\theta\ d\varepsilon \qquad (4.6)$$

Where $KW_2(L,r_2,z)$ and $KU_2(L,r_2,z)$ can be obtained by substituting $c = L$ and $r_2^2 = r^2 + \varepsilon^2 - 2r\varepsilon \cos\theta_\varepsilon$ for r in the first and the second equation respectively, of equations (2.4),

α_2 is the angle between r_2 and the outward normal to surface at B (Figure, 4.2).

Now if we apply a 'fictitious radial stress' ϕ_r over the pile shaft, the vertical and radial displacements at $B(r,z)$ due to ϕ_r can be obtained by integrating over the pile shaft surface, Mindlin's solution for an embedded point load acting parallel to the surface of an elastic half space (equations, 2.2 and 2.3). The displacements are given by (Figure, 4.3):

$$w_3(r,z) = \int_0^L \int_0^{2\pi} a.\ \phi_r.\ KW_3(c,r,z)\ d\varepsilon\ dc \qquad (4.7)$$

$$u_3(r,z) = \int_0^L \int_0^{2\pi} a.\ \phi_r\ KU_3(c,r,z)\ d\theta\ dc \qquad (4.8)$$

Where

$KU_3(c,r,z) = K_u(c,r,z)\ \mathrm{Cos}\theta_\varepsilon + K_v(c,r,z)\ \mathrm{Sin}\theta_\varepsilon$,

$K_u(c,r,z)$, $K_v(c,r,z)$ and $KW_3(c,r,z)$ can be obtained from first three equations respectively, of equations (2.2) by substituting $x_o = r\ \mathrm{Cos}\theta_\varepsilon = a$ and $y_o = r\ \mathrm{Sin}\theta_\varepsilon$.

Thus the total vertical and radial displacements at a point $B(r,z)$ due to a pile loaded with an axial load are given by:

$$w(r,z) = \int_0^L \int_0^{2\pi} \phi_S.\ a.\ KW_1(c,r_1,z)\ d\theta\ dc$$

$$+ \int_0^L \int_0^{2\pi} \phi_r.\ a.\ KW_3(c,r,z)\ d\theta\ dc \qquad (4.9)$$

$$+ \int_0^b \int_0^{2\pi} \phi_b.\ \varepsilon.\ KW_2(L,r_2,z)\ d\theta\ d\varepsilon$$

$$U(r,z) = \int_0^L \int_0^{2\pi} \phi_S \cdot a \cdot KU_1(c,r_1,z)\, \cos\alpha_1\, d\theta\, dc$$

$$+ \int_0^L \int_0^{2\pi} \phi_r \cdot a \cdot KU_3(c,r,z)\, d\theta\, dc \qquad (4.10)$$

$$+ \int_0^b \int_0^{2\pi} \phi_b \cdot \varepsilon \cdot KU_2(L,r_2,z)\, d\theta\, d\varepsilon$$

Equations (4.9) and (4.10) are valid everywhere within the half space (see Chapter 2) and satisfy the boundary conditions:

$$B(r,o),\ \sigma_{zz} = \sigma_{rz} = o$$

$$B(r,L),\ \sigma_{rz} = o,\quad o \leq r \leq b. \qquad (4.11)$$

Equations (4.9) and (4.10) can now be used to calculate the displacement components at any point within the half space, if the distribution of ϕ_S, ϕ_r and ϕ_b are known from the prescribed displacement boundary conditions of the pile-soil interface.

4.4 Solution for an axially loaded plain and under-reamed pile

By bringing the field point B(r,z) onto the pile-soil interface we can obtain integral equations for displacements of the pile-soil interface. A simple numerical treatment of these integral equations has been outlined previously (Chapter 2), in which the pile shaft is divided into n similar segments of thickness G_1 and the base in 'm' rings each of annular radius G_2. The vertical and the radial displacements of any element (i) on the shaft can then be written in a discrete linear form (see Appendix 1) as:

$$(W_S)_i = \sum_{j=1}^{n} (\phi_S)_j\, (KSS)_{ij} + \sum_{j=1}^{n} (\phi_r)_j\, (KRS)_{ij} + \sum_{j=1}^{m} (\phi_b)_j\, (KBS)_{ij} \qquad (4.12)$$

$$(U_S)_i = \sum_{j=1}^{n} (\phi_S)_j (KSU)_{ij} + \sum_{j=1}^{n} (\phi_r)_j (KRU)_{ij} + \sum_{j=1}^{m} (\phi_b)_j (KBU)_{ij} \qquad (4.13)$$

where $i = 1, 2, 3 \ldots n$.

Similarly the vertical base displacements $(W_b)_i$ are given by:

$$(W_b)_i = \sum_{j=1}^{n} (\phi_S)_j (KSB)_{ij} + \sum_{j=1}^{n} (\phi_r)_j (KRB)_{ij} + \sum_{j=1}^{m} (\phi_b)_j (KBB)_{ij} \qquad (4.14)$$

where $i = 1, 2, \ldots m$.

The integrals involved in the calculation of the coefficients $(KSS)_{ij}$, $(KRS)_{ij}$ etc. (except $(KSS)_{ii}$, $(KRU)_{ii}$, $(KBB)_{ii}$) are proper integrals of continuous functions and are evaluated by Simpsons rule. The integrals involved in calculation of the coefficients $(KSS)_{ii}$, $(KRU)_{ii}$ and $(KBB)_{ii}$ are singular integrals and are evaluated by a fine mesh quadrature leaving a symmetric region of exclusion around the singularity (see Chapter 2). The mesh size was reduced until the coefficients became essentially independent of the mesh size.

Equations (4.12), (4.13) and (4.14) may be written in matrix notation as:

$$\begin{Bmatrix} [W_S] \\ [U_S] \\ [W_b] \end{Bmatrix} = \begin{bmatrix} [KSS] & [KRS] & [KBS] \\ [KSU] & [KRU] & [KBU] \\ [KSB] & [KRB] & [KBB] \end{bmatrix} \begin{Bmatrix} [\phi_S] \\ [\phi_r] \\ [\phi_b] \end{Bmatrix} \qquad (4.15)$$

where, $\{W_S\}$, $\{U_S\}$, $\{\phi_S\}$ and $\{\phi_r\}$ are n x 1 vectors for the given vertical displacements of the shaft elements, the radial displacements of the shaft elements, the unknown shear stress and the fictitious radial stress at the pile-soil interface respectively.

$\{W_b\}$, $\{\phi_b\}$ are m x 1 vectors for given vertical base displacements and the resultant stress normal to the base area of the pile respectively.

$[KSS]$, $[KRS]$, $[KSU]$, $[KRU]$ are n x n matrices,

$[KSB]$, $[KRB]$ are m x n matrices,

$[KBS]$, $[KBU]$ are n x n matrices,

$[KBB]$ is a m x m matrix of coefficients.

Equation (4.15) can be written more compactly as:

$$\begin{Bmatrix} \{W_S\} \\ \{U_S\} \\ \{W_b\} \end{Bmatrix} = [K] \begin{Bmatrix} \{\phi_S\} \\ \{\phi_r\} \\ \{\phi_b\} \end{Bmatrix} \tag{4.16}$$

where $[K] = \begin{bmatrix} [KSS] & [KRS] & [KBS] \\ [KSU] & [KRU] & [KBU] \\ [KSB] & [KRB] & [KBB] \end{bmatrix}$, a $(2n+m)^2$ matrix of coefficients.

This system of linear algebraic equation can be solved for the unknowns $\{\phi_S\}$, $\{\phi_r\}$, $\{\phi_b\}$ if the displacements $\{W_S\}$, $\{U_S\}$ and $\{W_b\}$ are obtained from the solution of the pile domain.

For a rigid pile, the vertical displacements of all points on the shaft and the base are equal to the displacement of the head of the pile. The radial shaft displacement is zero. Thus, if we apply a unit vertical displacement to the head of the pile, we have:

$$\{W_S\} = \{1\}, \ \{U_S\} = \{0\}, \ \{W_b\} = \{1\} \tag{4.17}$$

Substituting (4.17) in (4.16) we obtain a set of linear algebraic equations which can be solved for the unknown stress intensities at the pile-soil interface. Having obtained $\{\phi_S\}$, $\{\phi_r\}$ and $\{\phi_b\}$ the stresses and displacements anywhere in the soil media can be computed from the integrals similar to (2.9) and (2.10) (see Chapter 2). The stresses acting at the pile-soil interface can be obtained by essentially computing

the stresses at B(r,z) as the point B approaches vanishingly close to the pile-soil interface.

Thus when the distribution of ϕ_S and ϕ_b, over the pile shaft and pile base respectively, have been obtained for prescribed displacement boundary conditions for a rigid pile, the load P_Z carried by the pile at any depth below the surface is found from

$$P_Z = \int_L^Z 2\pi a.\ \phi_S.\ dc + \int_o^b 2\pi \varepsilon.\ \phi_b.\ d\varepsilon \qquad (4.18)$$

The total load P required to produce unit displacement of the head of the rigid pile is given by substituting Z = 0 in equation (4.18). The solution from equation (4.16) and (4.17) will, if applied to a compressible pile, lead to an underestimation of the displacement of the pile head for a given load.

If the pile is assumed to be perfectly bonded to the medium, the vertical displacement of a shaft element at a depth Z, will differ from that at a depth (Z + dZ) by an amount equal to the elastic compression of the pile length dZ (Figure, 4.4). Since for any pile section the vertical direct stress is much greater than other stresses, then to a good approximation we can write:

$$\frac{\partial W}{\partial Z} = -\frac{P_Z}{A_p.E_p}, \qquad U = -\mu_p.\ \frac{\partial W}{\partial Z}\ .\ a \qquad (4.19)$$

where

A_p = Cross-sectional area of the pile shaft,

E_p = Young's modulus of the pile material,

μ_p = Poisson's ratio of the pile material.

Equation (4.19) can be written in finite difference form and used in an iterative scheme for the solution for a compressible pile as follows:

(i) The rigid pile solution form (4.16) and (4.17) is obtained.

(ii) Values of P_Z are found from equation (4.18) and substituted in (4.19) as a first approximation, giving new $\{W_S^1\}$, $\{W_b^1\}$ and $\{U_S^1\}$ values, where $\{W_S^1\}$, $\{W_b^1\}$ and $\{U_S^1\}$ stand for the first approximation of $\{W_S\}$, $\{W_b\}$ and $\{U_S\}$ values for compressible pile respectively.

(iii) $\{W_S^1\}$, $\{W_b^1\}$ and $\{U_S^1\}$ are substituted in (4.16) as an approximation giving new $\{\phi_S^1\}$, $\{\phi_r^1\}$, $\{\phi_b^1\}$, where $\{\phi_S^1\}$, $\{\phi_r^1\}$, $\{\phi_b^1\}$ stand for the first approximation of $\{\phi_S\}$, $\{\phi_r\}$ and $\{\phi_b\}$ for compressible pile.

(iv) A new value of P_Z^1 is obtained for each section of the pile and the cycle (ii), (iii) and (iv) is repeated until the values of P_Z^n between two successive iterations differs by an acceptably small value.

In what follows, the foregoing method of solution will be described as a 'rigorous solution' since it allows for radial displacement compatibility at the pile-soil interface (i.e. the effect of the presence of the pile in disturbing the continuity of the half space). If, however, the presence of the pile within the half space is ignored, we need only to consider vertical displacement compatibility. The resulting system of equation to be solved thus reduces to:

$$\begin{Bmatrix} \{W_S\} \\ \{W_b\} \end{Bmatrix} = \begin{bmatrix} [KSS] & [KBS] \\ [KSB] & [KBB] \end{bmatrix} \begin{Bmatrix} \{\phi_S\} \\ \{\phi_b\} \end{Bmatrix}$$

$$\text{or} \quad \begin{Bmatrix} \{W_S\} \\ \{W_b\} \end{Bmatrix} = [KS] \begin{Bmatrix} \{\phi_S\} \\ \{\phi_b\} \end{Bmatrix} \qquad (4.20)$$

where $[KS] = \begin{bmatrix} [KSS] & [KBS] \\ [KSB] & [KBB] \end{bmatrix}$, $(n+m)^2$ matrix of coefficients.

Equation (4.20) provides n discrete approximate values of $\{\phi_s\}$ and m discrete approximate values of $\{\phi_b\}$ once the vertical displacement boundary conditions for rigid and compressible pile are incorporated as shown previously.

4.4.1 Some notes on the computer programme for solution of a single axially loaded pile within a half space

The computer programme discussed below has been developed to solve the problems described in the preceeding sections. The listing of the programme is given in Banerjee (1969). The programme is essentially designed to perform the following operations:

(i) Read data.

(ii) Calculate coefficients of the matrices $[K]$ and $[KS]$.

(iii) Solve for the unknowns $\{\phi_s\}$, $\{\phi_b\}$ and $\{\phi_r\}$.

(iv) Calculate the total load for a given head displacement.

(v) Calculate the stresses and displacements at a given radial distance from the pile surface.

The operations listed above have been carried out by a set of procedures described below (for listing of these procedures see Banerjee, 1969).

(i) Procedure 'Print array'

(ii) Procedure 'inp'

(iii) Procedure 'Crout 2'

(iv) Procedure 'Solve'

(v) Procedure 'Simpson'

The above mentioned procedures have been discussed in Chapter 3.

(vi) Procedure 'Mult'

This procedure multiplies a matrix A $[N_1 \times N_2]$ and a matrix B $[N_2 \times N_3]$ to give a matrix C $[N_1 \times N_3]$. The matrices A and B remain unaltered.

(vii) Procedure 'Invert'

This procedure uses procedures 'inp', 'Crout 2', and 'solve' to obtain in the inverse of matrix K. The original matrix K is destroyed and the results of the inversion are stored in K.

(viii) Procedure 'Direction'

This procedure calculates the value of $\text{Cos}\alpha_1$ and $\text{Cos}\alpha_2$ (see equations (4.4) and (4.6) respectively).

(ix) Procedure 'Elevert'

This procedure calculates the coefficients of ϕ_s and ϕ_b of the system of equations (4.16) and (4.20) and also similar integrals for the stresses which involve the evaluation of definite integrals (i.e. where the load point and the field point do not coincide). The integrals are evaluated by using procedure 'Simpson'.

(x) Procedure 'Elehorz'

This procedure performs operations that are identical to those of the procedure 'Elevert'. It calculates the coefficients of ϕ_r of the system of equations (4.16) and also similar integrals for the stresses.

(xi) Procedure 'Form array'

This procedure calls the procedures 'Elehorz' and 'Elevert' to calculate the coefficients of the matrices $[K]$ and $[KS]$. Provision is made in this procedure to calculate the principal value of the singular integrals that are necessary in evaluating the coefficients $(KSS)_{ii}$, $(KRU)_{ii}$ and $(KBB)_{ii}$.

The remainder of the programme is devoted to the solution of the system of linear algebraic equation, calculation of the total load carried by the pile for a given displacement, and calculation of the stresses at a radial distance ε from the surface of the pile.

4.4.2 Convergence of the solution

The accuracy of the solution would depend on the accurate evaluation of the integrals listed in Appendix (1). These integrals were evaluated by Simpson's rule and the trapezoidal rule. Because of the axial symmetry of the problem a direct integration with respect to θ was carried out using Simpson's rule, choosing 50 divisions to represent 180° in θ direction. The principal value of the singular integrals was evaluated by subdividing the individual segments of the pile surface intd 50 divisions. The integrals were then evaluated by leaving out a symmetric region of exclusion, small enough not to influence the results (see Chapter 2).

The pile shaft was divided into 10 segments and the base into 5 annular rings. Thus the total number of equations solved was 25 for a rigorous analysis and 15 for an approximate analysis. Pile displacements for a given load calculated by using 25 equations for a rigorous analysis were found to be about 5% higher than those using 13 equations (for 5 shaft-segments and 3 base-annular-rings) and 1% lower than those obtained by using 50 equations (for 20 shaft segments and 10 base-annular rings). An exactly similar trend was also observed for the approximate analysis.

4.4.3 Results of the analysis

The results of the elastic analysis of axially loaded plain and under-reamed piles are presented in Figures (4.5) to (4.11). It was found that the rigorous analysis gives essentially identical results to those obtained by approximate analyses (which ignores the radial displacement compatibility at the pile-soil interface) for the load displacement relationship of the pile. The difference being relatively less for piles with length to diameter ratio (L/d) greater than 10, and

Poisson's ratio of pile (μ_p) less than 0.2.

Various results for L/d = 10, and Poisson's ratio (μ) of soil = 0.5 are given in Figures (4.5.1) to (4.5.4). Figure (4.5.1) shows the radial displacement u(a,z) to be of the order of 5×10^{-3} times the displacement of the head of the pile (W_o) both near the surface (Z/L = 0) and at the bottom of the shaft (Z/L = 1) from the approximate analysis. That is, of course, identically zero for a rigid pile in the rigorous analysis (the negative sign indicates that the displacement is towards the pile face). Figure (4.5.2) shows the shear stress at the pile face for a rigid pile plotted in nondimensional form as $\tau / (P/\pi dL)$, where τ = the shear stress at the pile-soil interface, P = the total load acting on the pile, d = diameter of the pile = 2a; and L = length of the pile. The distribution of the shear stresses calculated by both the analyses are identical at the bottom of the pile but differ in the upper portion of the interface. Figure (4.5.3) shows the radial stresses calculated by both methods. The magnitude of the radial stresses are of the order of 1/2 the shear stress at the extremities of the shaft and are of the order of 1/50th of the shear stresses over the middle portion of the pile shaft (compressive stresses are indicated by a negative sign). Figure (4.5.4) shows the shear stress distribution for two values of pile material Poisson's ratio (μ_p = 0, 0.2) calculated by the rigorous analysis (in the approximate analysis the Poisson's ratio of the pile does not enter into calculation). The compressibility ratio λ (λ = the ratio of Young's modulus of the pile to the shear modulus of the soil) is chosen as 6000. The shear stress distribution differs noticeably although the calculated loads are within 6%. Thus for analysis of load displacement characteristics for practical uses the approximate analysis, which ignores the presence of the pile within the half space, appear to be adequate.

Whereas, if the pile-medium interface stresses are required then the rigorous analysis is needed.

The results presented in Figures (4.6) to (4.11) have been obtained from the approximate analysis. Figures (4.6) to (4.8) refer to single compressible plain piles and Figures (4.9) and (4.10) apply to compressible under-reamed piles. In all cases a range of $6000 \leq \lambda \leq \infty$ is considered which covers the range of macerial properties of practical interest.

Figures (4.6.1) and (4.6.2) show the effect of length to diameter ratio and λ on the shear stress distribution at the shaft face. For the shorter pile the effect of λ is seen to be negligible and the stress distribution agrees closely with that obtained by more approximate analysis (Poulos and Davis, 1968, Mattes and Poulos, 1969a). Figure (4.6.2) shows the shear stress distribution at the shaft face for slender piles ($L/D = 80$) in which $\lambda = 60{,}000$ and $\lambda = \infty$ results are almost identical and similar to the short pile results. However, the shear stress distribution is radically altered in the more compressible system ($\lambda = 6000$). Figure (4.7) shows the load displacement characteristics of plain piles for various values of λ. For piles with length to diameter ratios less than 20 the effect of λ is shown to be negligible. Figures (4.8.1) and (4.8.2) shows the effect of ignoring the compressibility on the ratio of (P_C/P_R) and (P_{EC}/P_{ER}), where P_C, P_{EC} are the total load and the end load respectively for a compressible pile and P_R, P_{ER} are the total load and the end load respectively for a rigid pile, for a given head displacement.

Comprehensive load displacement curves are presented in figures (4.9.1) to (4.9.5) for compressible underreamed piles over a range of base to shaft diameter ratios ($1 \leq D_B/D_S \leq 6$). Whereas, these curves enable absolute value of the pile head displacements to be estimated,

the relative influence of (D_B/D_S) and λ can be seen more clearly in Figure (4.10) where they are related to the ratio (R_o) of the settlement of an under-reamed pile to that of a plain pile under the same load. In all cases the effect of λ on R_o is seen to be very small ($6000 \leq \lambda \leq \infty$). The stiffening of the system (i.e. decrease in R_o) achieved by enlarging the base is also seen to be very small for longer piles ($L/D = 80$) and even for shorter piles ($L/D = 20$), R_o is only reduced to around 0.8 for $D_B/D_S = 4$. Figures (4.11.1) to (4.11.3) shows the percentage of load taken by the base for various base to shaft diameter ratios. It can be seen from these Figures that the advantages gained by under-reaming are limited to piles with length to diameter ratios less than 20 and Base to shaft diameter ratios less than 3, which agrees with current practice (Whitaker and Cooke, 1966; Burland et al, 1966).

4.5 Solution for an axially loaded pile within a finite elastic layer

The formulation described above can be easily extended to solve the problem of an axially loaded pile embedded within a finite elastic layer. The following assumptions have been made to reduce the computational work involved:

(i) Since the introduction of radial displacement compatitibility at the pile-soil interface does not produce any major alteration in the overall load displacement response, only vertical displacement compatibility of the pile-soil interface is considered in the subsequent analyses.

(ii) The surface of the rigid layer is assumed to be smooth.

Thus if we distribute a fictitious vertical stress intensity ψ on a horizontal surface at a depth H below the ground surface ($H > L$), the vertical displacement at $B(r,z)$ due to ψ can be obtained as:

$$\omega_4(r,z) = \int_0^{\infty} \int_0^{2\pi} \psi.\ \varepsilon.\ KW_4\ (H,r_2,z)\ d\theta\ d\varepsilon \qquad (4.21)$$

The integral (4.21) is obtained by substituting $b = \infty$, $\phi_b = \psi$ and $L = H$ in equation (4.5) and ia also identical to the integral on the right hand side of equation (3.11). Thus the total vertical displacement at B(r,z) due to an axially loaded pile can be written as:

$$W(r,z) = \int_0^{L} \int_0^{2\pi} \phi_S.\ a.\ KW_1\ (c,r_1,z)\ d\theta\ dc$$

$$\int_0^{b} \int_0^{2\pi} \phi_b.\ \varepsilon.\ KW_2(L,r_2,z)\ d\theta\ d\varepsilon \qquad (4.22)$$

$$+ \int_0^{\infty} \int_0^{2\pi} \psi.\ \varepsilon.\ KW_4(H,r_2,z)\ d\theta\ dc$$

The integral representation (4.22) exists in the ordinary sense everywhere within the finite elastic layer and satisfies the following boundary conditions:

$$B(r,o)\ ,\quad \sigma_{zz} = \sigma_{rz} = o;$$

$$B(r,L)\ ,\quad o \leq r \leq b,\ \sigma_{rz} = o;$$

$$B(r,H),\quad o \leq r \leq \infty,\ \sigma_{rz} = o.$$

As before if we replace the integrals in equation (4.22) in a discrete linear form over n segments of shaft surface, m annular rings over base surface and s annular rings to represent a large enough area over the surface of the rigid layer, we obtain (see Appendix 1):

$$(W_S)_i = \sum_{j=1}^{n} (\phi_S)_j (KSS)_{ij} + \sum_{j=1}^{m} (\phi_b)_j (KBS)_{ij} + \sum_{j=1}^{s} (\psi)_j (KLS)_{ij} \qquad (4.23)$$

where $(W_S)_i$ is the vertical displacement of an element i of the pile shaft, $i = 1, 2, \ldots n$.

Similarly the vertical base displacements $(W_b)_i$ are given by:

$$(W_b)_i = \sum_{j=1}^{n} (\phi_S)_j (KSB)_{ij} + \sum_{j=1}^{m} (\phi_b)_j (KBB)_{ij} + \sum_{j=1}^{s} (\psi)_j (KLB)_{ij} \qquad (4.24)$$

where $i = 1, 2, \ldots m$; and the vertical displacements $(W_\ell)_i$ are given by

$$(W_\ell)_i = \sum_{j=1}^{n} (\phi_S)_j (KSL)_{ij} + \sum_{j=1}^{m} (\phi_b)_j (KBL)_{ij} + \sum_{j=1}^{s} (\psi)_j (KLL)_{ij} \qquad (4.25)$$

where $i = 1, 2, \ldots s$.

The method of evaluation of the coefficients $(KSS)_{ij}$, $(KBS)_{ij}$, $(KSB)_{ij}$ and $(KBB)_{ij}$ have been described previously. The integrals involved in determining the coefficients $(KSL)_{ij}$, $(KBL)_{ij}$, $(KLS)_{ij}$ and $(KLB)_{ij}$ are definite integrals of continuous functions and they are evaluated directly by Simpson's rule. The integrals involved in determining the coefficients of $(KLL)_{ij}$ are singular for $i = j$ and they are evaluated by a fine mesh quadrature, leaving a symmetric region of exclusion around the singularity. Equations (4.23), (4.24) and (4.25) can be written in matrix notation as:

$$\begin{Bmatrix} \{W_S\} \\ \{W_b\} \\ \{W_\ell\} \end{Bmatrix} = \begin{bmatrix} |KSS| & |KBS| & |KLS| \\ |KSB| & |KBB| & |KLB| \\ |KSL| & |KBL| & |KLL| \end{bmatrix} \begin{Bmatrix} \{\phi_S\} \\ \{\phi_b\} \\ \{\psi\} \end{Bmatrix} \qquad (4.26)$$

Where

$\{W_\ell\}$, $\{\psi\}$ are s x 1 vectors for the given vertical displacements of the rigid layer ($\{W_\ell\} = 0$) and the fictitious vertical stress intensity on the surface of the rigid layer, respectively.

$[KLS]$, $[KLB]$, $[KSL]$, $[KBL]$ and $[KLL]$ are n x s, m x s, s x n, s x m, s x s matrices of coefficients respectively.

All other matrices have been defined previously.

Equation (4.26) represents (n + m + s) unknowns. Having obtained $\{\phi_S\}$, $\{\phi_b\}$, $\{\psi\}$ the total loads for the prescribed displacement boundary conditions for rigid pile and compressible pile, the total load is obtained from equation (4.18).

4.5.1 Numerical analysis and discussion of the results

The computer programme developed for the analysis of plain and under-reamed piles is discussed in Chapter 5 in connection with the analysis of free standing pile groups of arbitrary spacing in which the analysis of a single pile becomes a particular case. The results of the analysis of axially loaded single compressible plain and under-reamed piles are shown in Figures (4.12.1) and (4.12.2). These are calculated by using 10 segments over the pile shaft surface, 5 annular rings over the base area of the pile and 20 annular rings over a radius equal to the depth of the elastic layer, to represent the surface of the rigid layer. Solutions obtained from solution of these 35 equations were compared with those obtained by using 70 equations (i.e. by doubling the number of elements to represent the pile-soil interface and the surface of the rigid layer) and found to be within 5%.

Figure (4.12.1) shows the non-dimensional stiffness plotted against H/L for a plain pile. The shape of the curves is not significantly

different for piles with L/D = 20 and 40; $\lambda = \infty$, 6000. In all cases the stiffnesses appear to converge to the half space solutions beyond H/L = 5 and becomes asymtotic as H/L approaches 0. Figure (4.12.2) shows similar curves for under-reamed piles for $1 \leq {}^{D_B}/_{D_S} \leq 4$. The shape of the curves is also similar to those shown in Figure (4.12.1) for plain piles with very similar trends except that the piles with higher ${}^{D_B}/_{D_S}$ ratio becomes increasingly stiffer as H/L approches zero. In all cases the presence of a rigid layer reduces the displacement under a given load.

4.6 Analysis of local slip at the pile-soil interface

In the analysis described above assumption is made that the pile is bonded to the medium and the soil is capable of resisting any state of stress which may be developed around the loaded pile. However, real soils have a finite shear strength and the interface between the pile shaft and the surrounding soil has a finite ahdesive strength, depending on various factors, such as, method of construction, variation of the effective stresses and moisture content after the construction etc. When the shear strength at the shaft-soil interface reaches this limit slip occurs.

An approximate analysis of local slip may be carried out by a modification of the elastic analysis given above. When the shaft shear stress or base normal stress reaches a specified maximum, local yield will occur and the vertical displacement compatibility between the pile and the soil for that element will no longer hold. The load and displacement at which this occurs is readily calculated. Any further increase in load will cause a redistribution of the interface stresses amongst the remaining elements, where elastic conditions prevail. Such an analysis has been described by Salas (1965), Poulos and Davis (1968), Mattes and Poulos (1969a) for a pile in cohesive soil, Thurman and D'Appolonia (1965)

for a pile in sand and D'Appolonia and Romualdi (1963), Mattes and Poulos (1969b) for end bearing piles. The analysis presented by these writers was based on the assumption that purely elastic conditions prevail at the base of the pile until the base load of the pile attained the ultimate end bearing load. The analysis described below is essentially identical with the one described above with a step by step yielding of the rigid pile base included.

Equation (4.20) can be written for (n + m) elements of discrete pile-soil interface as

$$(W)_i = \sum_{j=1}^{(n+m)} (KS)_{ij} (\phi)_j , \quad i = 1, 2, \ldots (n+m); \tag{4.27}$$

where $(W)_i$ are the specified vertical displacements of n elements of discrete shaft-soil interface and m elements of discrete base-soil interface

$(\phi)_j$ are the n unknown shear stress intensities ϕ_s over the shaft-soil interface and m unknown vertical stresses ϕ_b over the base soil interface.

If we define the limiting stress at the pile-soil interface as $(S_t)_i$ for n elements of shaft-soil interface and m elements of base-soil interface; and if p^{th} element of pile-soil interface is brought to a state of limiting stress $(S_t)_i$ we can modify equation (4.27) to:

$$(W)_i = \sum_{j=1}^{(n+m)} (KS)_{ij} (\phi)_j - (KS)_{ip} \phi_p + (KS)_{ip} (S_t)_p \tag{4.28}$$

where $i = 1,2,\ldots.(p-1), (p+1), (p+2)\ldots.(n+m)$.

Equation (4.28) represents a set of (n+m-1) equations that can be solved for (n+m-1) unknowns. This process of modification of the elastic analysis is repeated until all the elements of the shaft-soil interface and base-soil interface have attained $(S_t)_i$ state of stress. The

limiting shaft-shear stresses and the base normal stresses are calculated from equations (1.4) and (1.6) respectively.

In this analysis the development of plastic zones within the soil has not been taken into consideration. Although such an analysis would be likely to involve little inaccuracy in the early stages of yielding, the load displacement relationship is likely to be inaccurate as the load approaches the ultimate load of the pile.

4.6.1 Numerical analysis and results

The results of the analysis were obtained by using 10 elements to represent the shaft-soil interface and 5 elements for the pile base. The computer programme developed for the present analysis is essentially the same as the one described for the elastic analysis with the following 'procedures' added:

(i) Procedure 'Limit stress'

Calculates the (n+m) elements of $(S_t)_i$ from equations (1.4) and (1.6).

(ii) Procedure 'Solve plastic'

Solves the system of equation (4.28) and (4.29) for the successive load increments up to failure.

Load displacement curves for axially loaded plain and under-reamed piles are given in Figures (4.13.1) and (4.13.2), the displacements being plotted in terms of a factor I_S. It was found the shape of the curves is independent of the ratio G/C_b where C_b is the cohesion at the pile base, although the magnitude of the settlement does depend on this ratio, which agrees with the solutions given by Poulos and Davis (1968) and Mattes and Poulos (1969a). Figure (4.13.1) shows the ratio (P/P_u) plotted against I_S for plain rigid and compressible piles. For a given (P/P_u) ratio the piles with L/D = 10 settles less than the pile with

L/D = 50. A trapezoidal distribution of shear strength as shown in Figure (4.13.1) is assumed for these results. It is interesting to note that the theoretical load displacement curves are linear up to $(P/P_u) \approx 0.7$. Figure (4.13.2) shows a similar curve for an under-reamed pile (L/D = 15, $^{D}B/D_S = 2$) for a triangular distribution of shear strength over the pile length. The result for a plain pile is also shown for comparison. The load displacement curve for a plain pile is linear up to $(P/P_u) \approx 0.7$ but that for the under-reamed pile is distinctly curved above $(P/P_u) \approx 0.4$. For a given (P/P_u) ratio the settlement of an under-reamed pile is more than that of a plain pile of the same L/D ratio, which agress with the test results of Whitaker and Cooke (1966).

4.7 Comparison with the laboratory and field test results

A series of full scale tests on bored piles with and without enlarged bases in stiff fissured overconsolidated London Clay were carried out by Whitaker and Cooke (1966). Figures (4.14.1) to (4.14.3) show the comparison between these test results and the theoretical predictions. For the purpose of comparison the following relevant parameters were assumed:

Mean L/D = 15, Mean $^{D}B/D_S$ for underreamed pile = 2

$\alpha = 0.45$, $q = \omega . N_c$, $\omega = 0.75$ and $N_c = 9$ (Whitaker and Cooke, 1966).

$\lambda = 1000$, $\mu = 0.45$, $G = 4000$ psi

uniform cohesion over the pile length.

Figure (4.14.1) shows the percentage of load taken by the base for plain and under-reamed piles plotted for $(P/P_u) = 0.5$. One test result given by Sowers (1961) for a plain pile under very similar conditions is also plotted in the same figure. The theoretical and experimental results are in good agreement. The theoretical load-displacement relationships for plain and under-reamed piles are compared with the mean experimental

curves in Figure (4.14.2), in which the theoretical results agree reasonably with the mean experimental values only up to $(P/P_u) \approx 0.4$. The comparison between the theoretical and mean experimental ratios of (P/P_u) values for an under-reamed pile to that of a plain pile for various settlement to diameter ratios is shown in Figure (4.14.3). The theoretical results and the mean observed field results sufficiently close to suggest that the behaviour of under-reamed piles is predictable provided the relevant elastic parameters are obtained from the load tests on single pile. The same figure also shows the theoretical and mean experimental average shaft stress plotted against mean shaft strain for both plain and under-reamed piles which are also in good agreement.

4.8 Conclusion

(i) A rigorous elastic analysis of bonded compressible plain and under-reamed piles has been presented. It has been shown that for the analysis of load-displacement characteristics for practical uses, the approximate analysis which ignores the presence of the pile within the half space, appears to be adequate. Whereas if the pile-soil interface stresses are required then the rigorous analysis is needed.

(ii) The amount of load taken by the base for a practical range of length to diameter ratios ($10 \leq L/D \leq 30$) for a plain pile is only about 10% of the total load.

(iii) Settlement of a compressible pile may be up to 50% higher than that of a rigid pile under the same load. Pile compressibility is of consequence only for piles with length to diameter ratios greater than 20.

(iv) The reduction in settlement gained by under-reaming are limited to piles with length to diameter ratios between 10 and 20 and $^{D}B/D_S < 3$.

(v) The presence of a rigid layer underneath the pile reduces the settlement but beyond H/L = 5 the presence of a rigid layer produces no noticeable change in the load displacement response.

(vi) The elastic analysis is modified to take local slip into consideration; it was found that for a given (P/P_u) ratio the settlement of an under-reamed pile ($^{D}B/D_S$ = 2, L/D = 15) is about 1½ to 2 times the settlement of a plain pile, which agrees well with the experimental results of Whitaker and Cooke (1966).

(vii) The results of the analysis have been compared with experimental results. It was found that theory not only gives qualitative description of the behaviour of an axially loaded pile, which agrees with the experiment, but also shows that it is possible to predict accurately the load displacement behaviour of an under-reamed pile provided the relevant elastic parameters are selected from the test results on single piles.

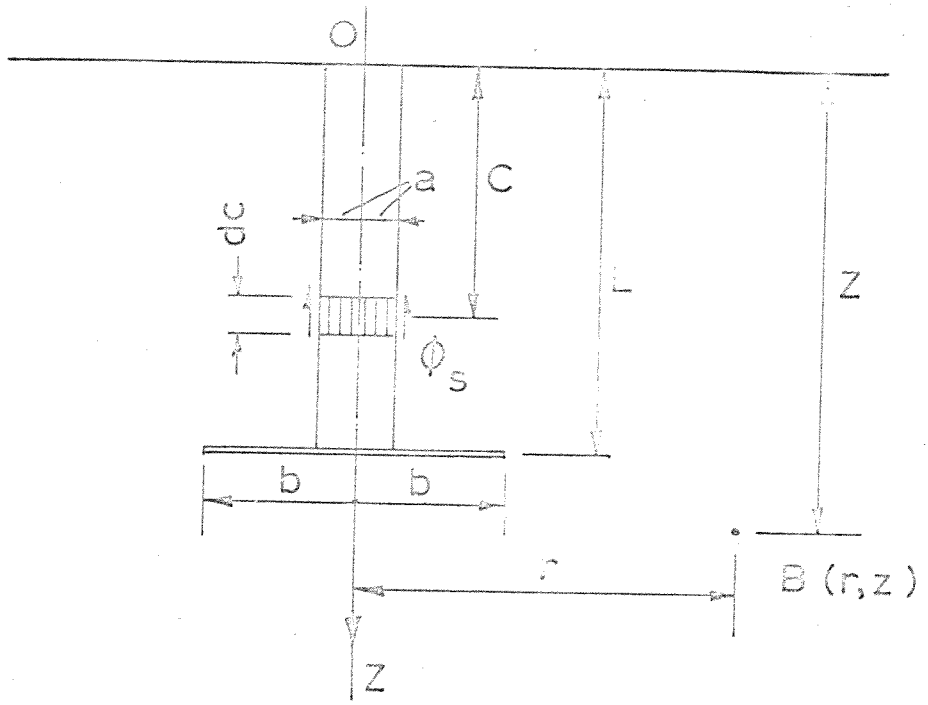

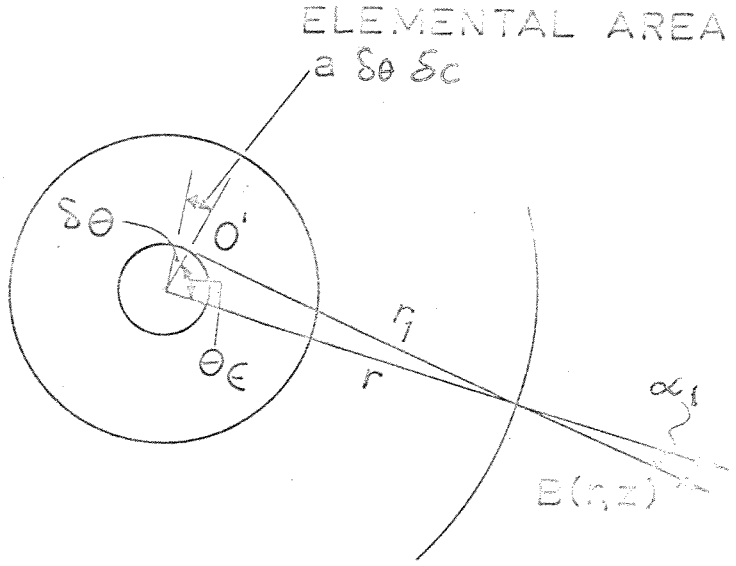

FIGURE - 4.1

INTEGRATION OVER THE PILE SHAFT FOR DISPLACEMENTS DUE TO φ_s

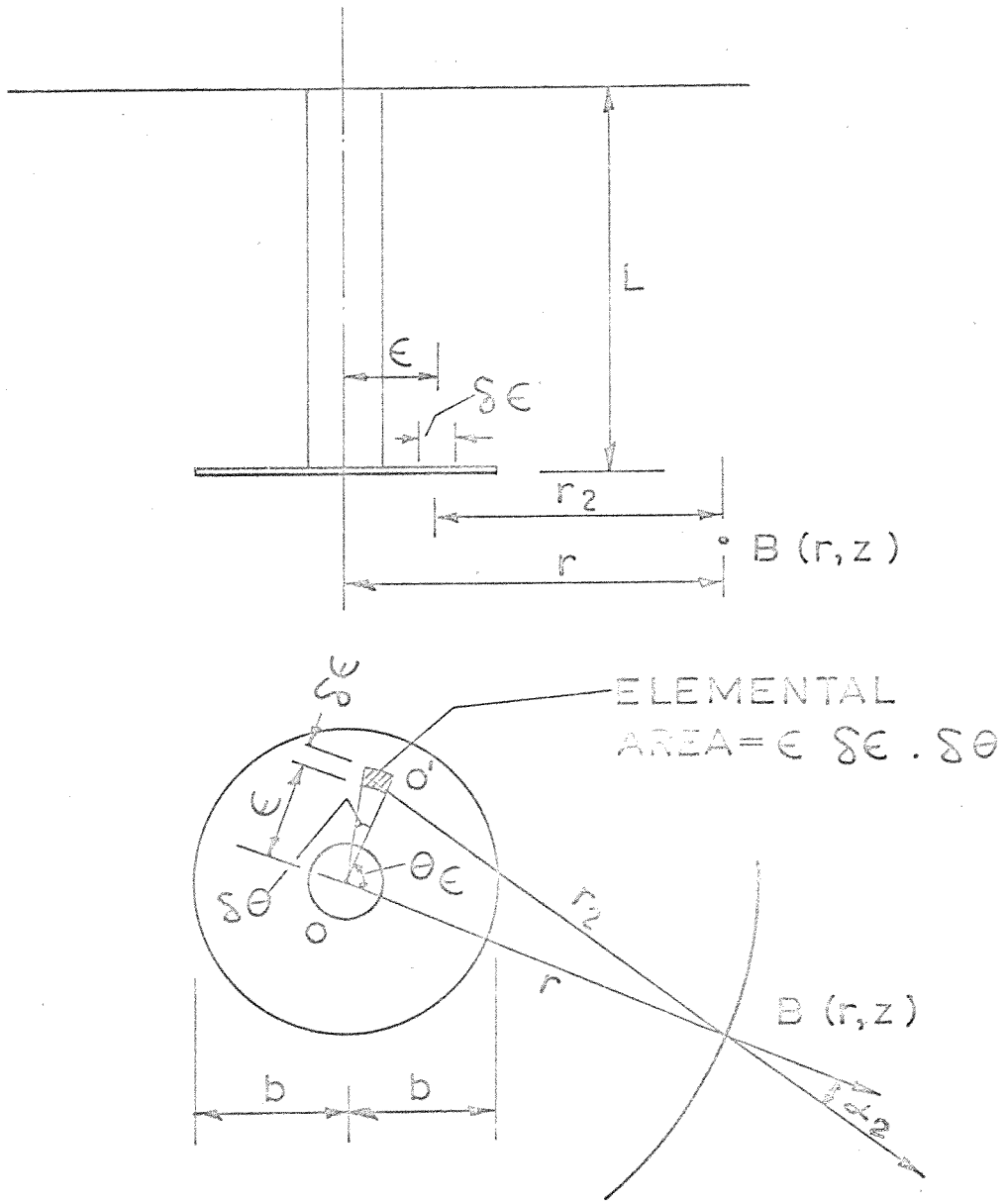

FIGURE - 4.2

INTEGRATION OVER THE BASE FOR DISPLACEMENTS DUE TO ϕ_b

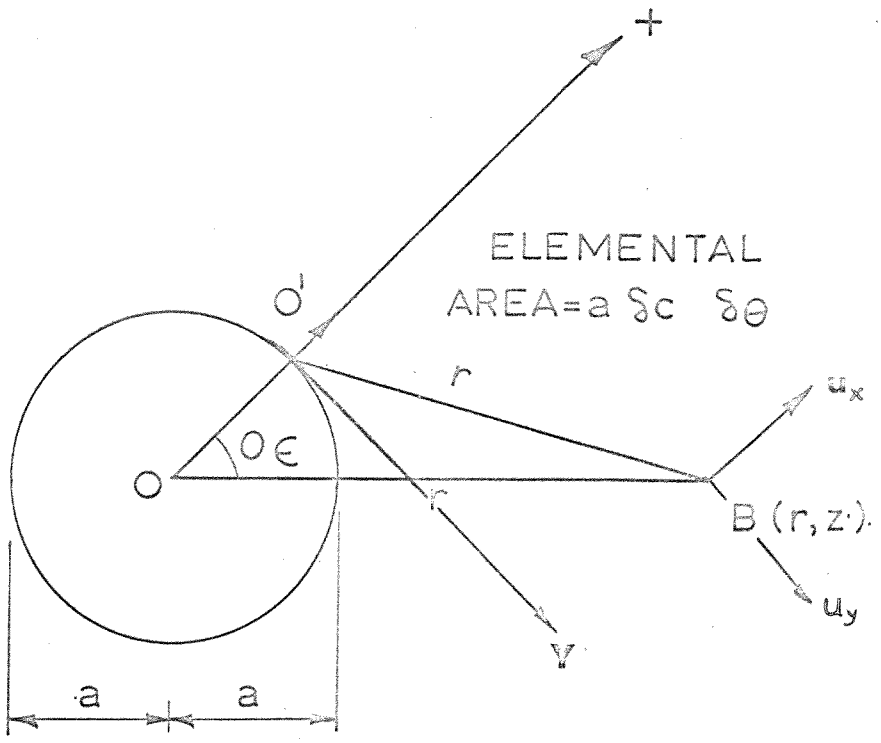

$$u = u_x \cos\theta_\epsilon - u_y \sin\theta_\epsilon$$

FIGURE - 4.3

INTEGRATION OVER THE SHAFT FOR DISPLACEMENTS DUE TO Φ_r

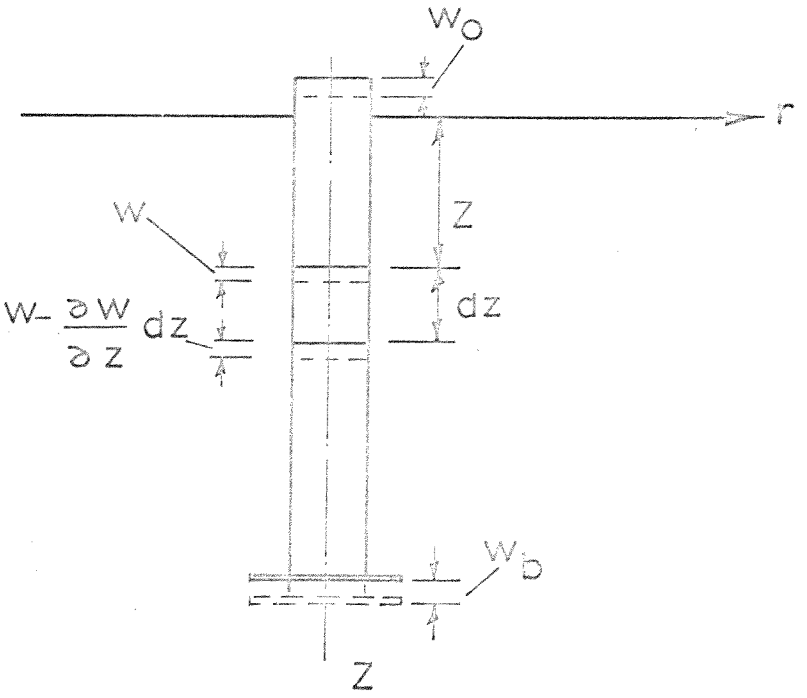

FIGURE - 4.4

VERTICAL DISPLACEMENT OF PILE DOMAIN

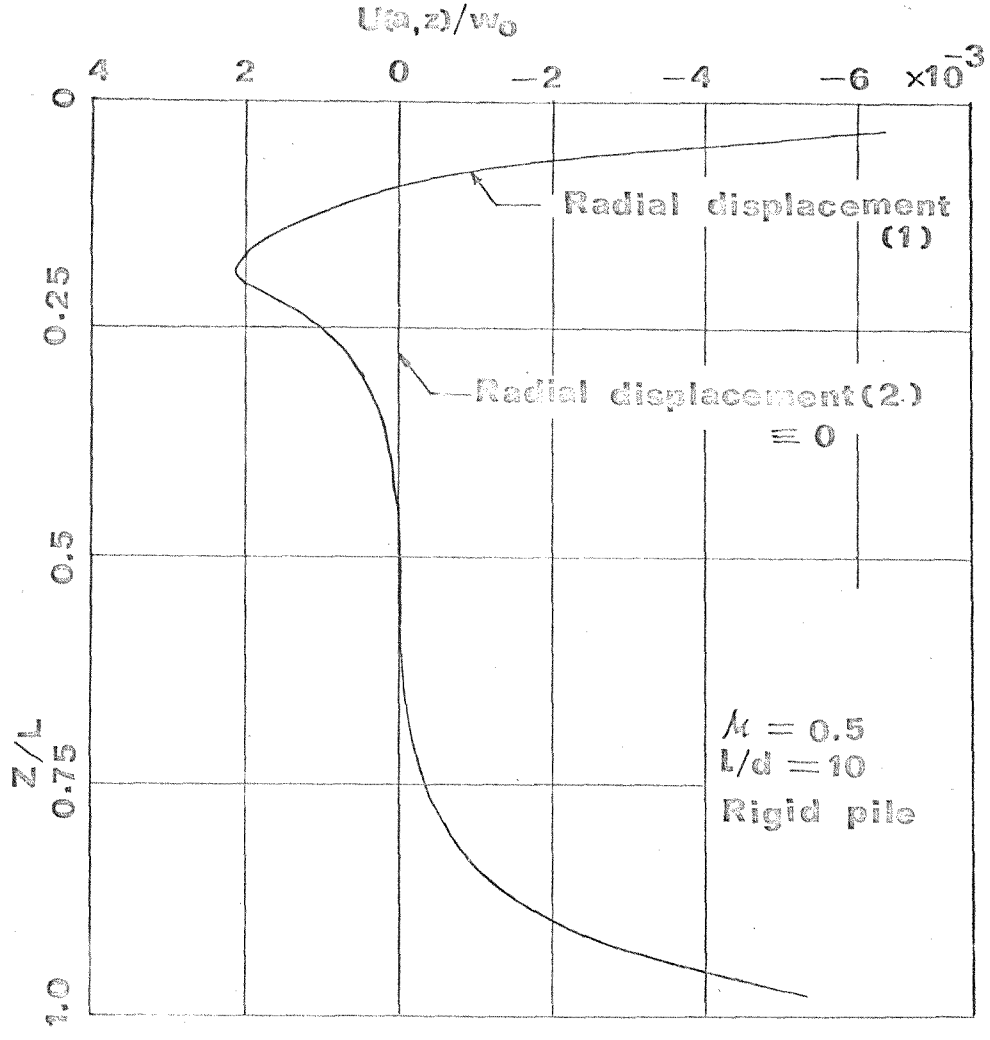

FIGURE 4.5.1.
RADIAL DISPLACEMENT OF PILE SOIL INTERFACE.

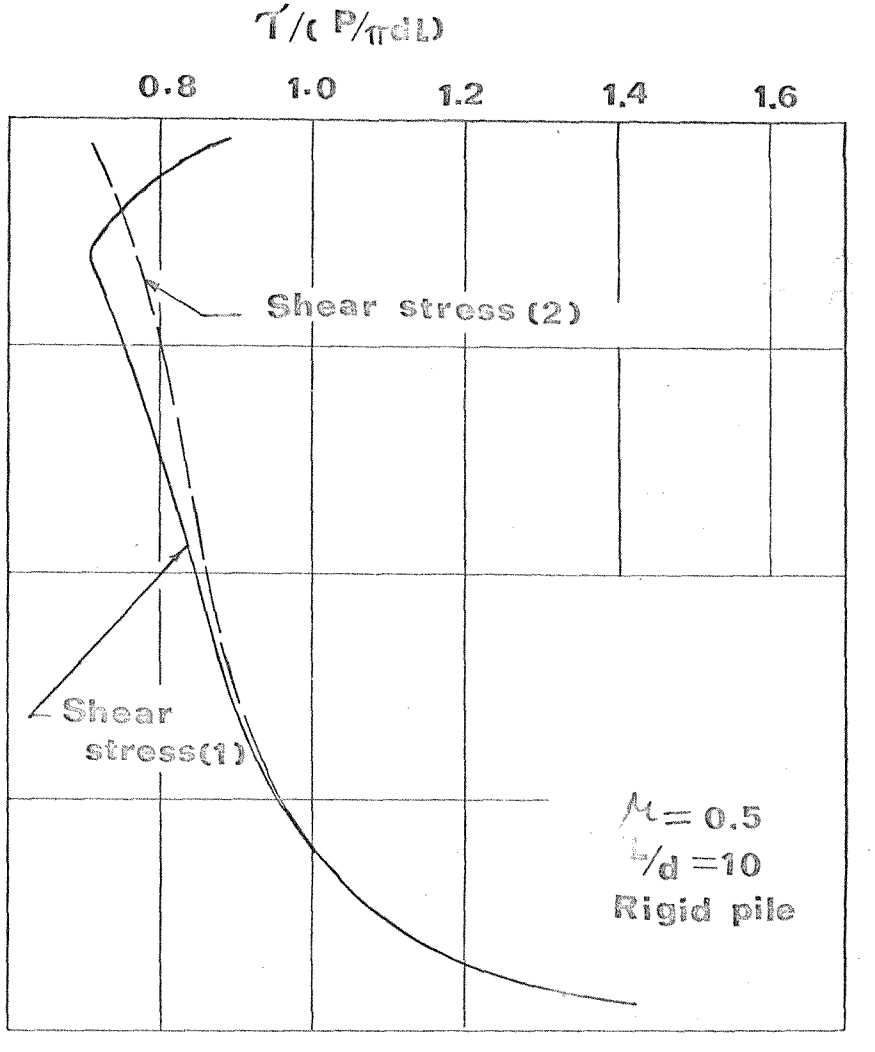

FIGURE 4.5.2.
SHEAR STRESS AT THE SHAFT FACE FOR A RIGID PILE.

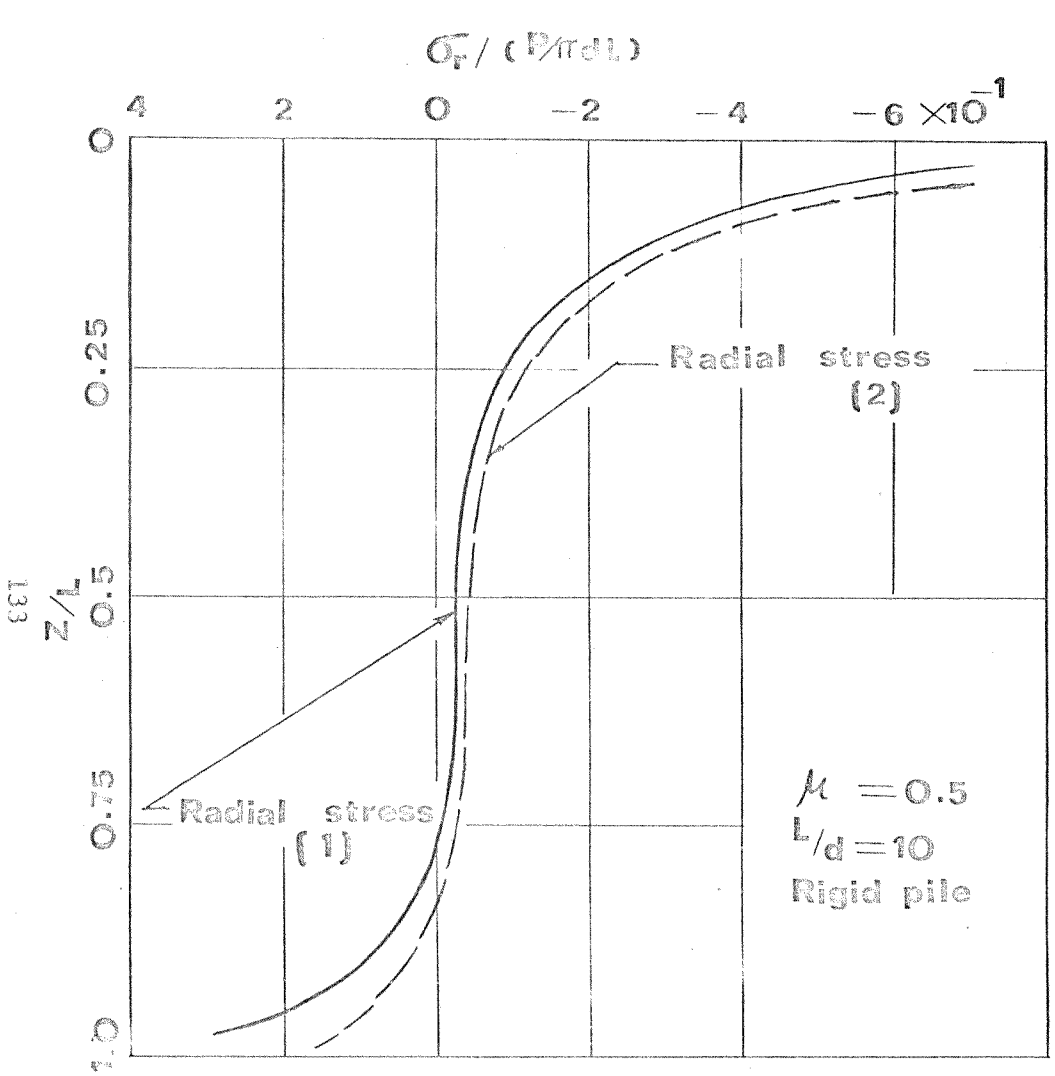

FIGURE - 4.5.3

RADIAL STRESS AT THE SHAFT FACE

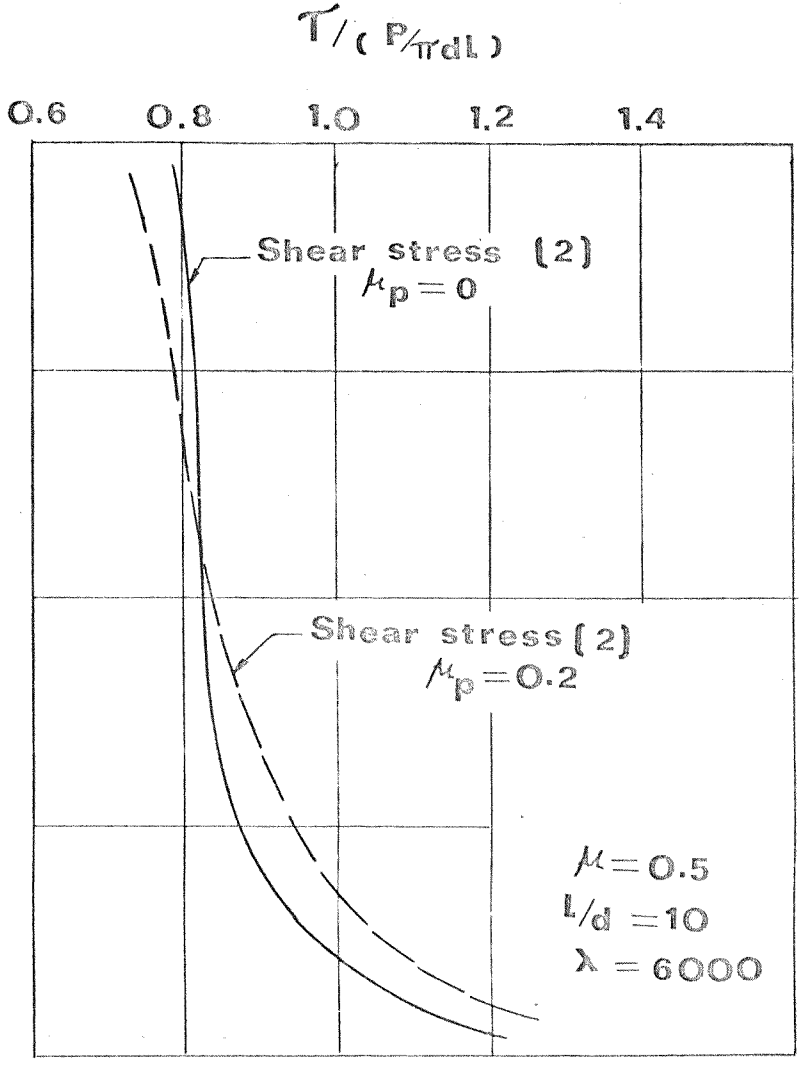

FIGURE - 4.5.4.

SHEAR STRESS AT THE SHAFT FACE FOR A COMPRESSIBLE PILE

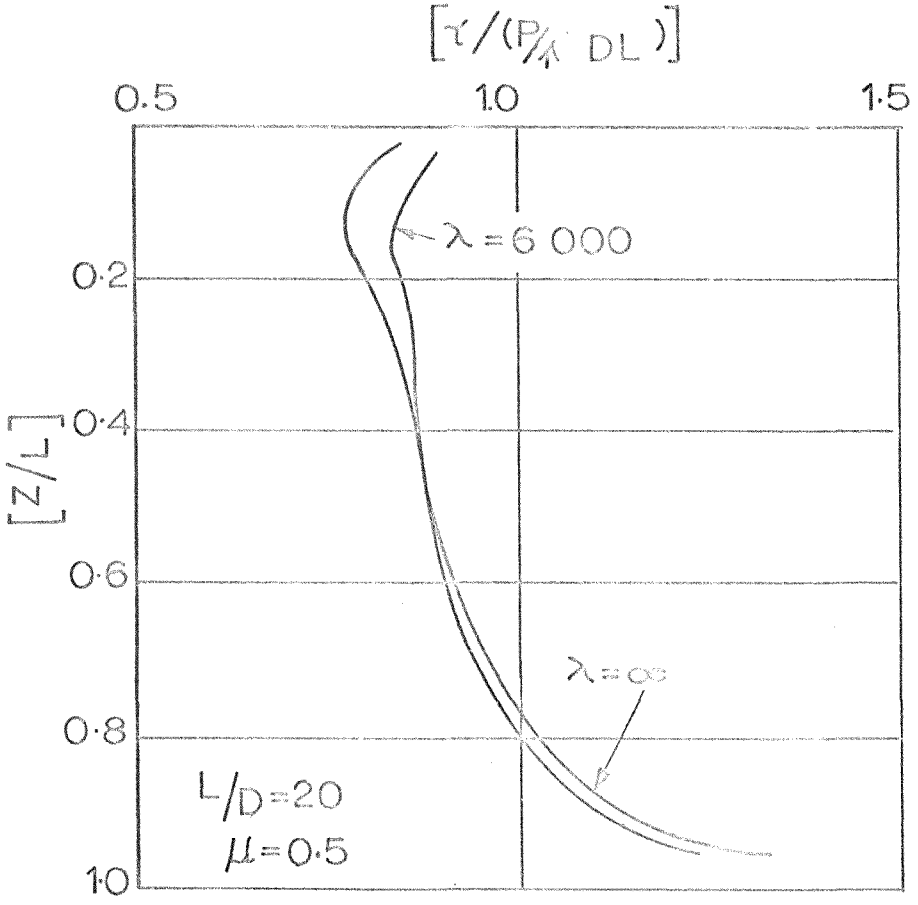

FIGURE - 4.6.1

SHEAR STRESS AT THE SHAFT FACE FOR A SHORT PILE

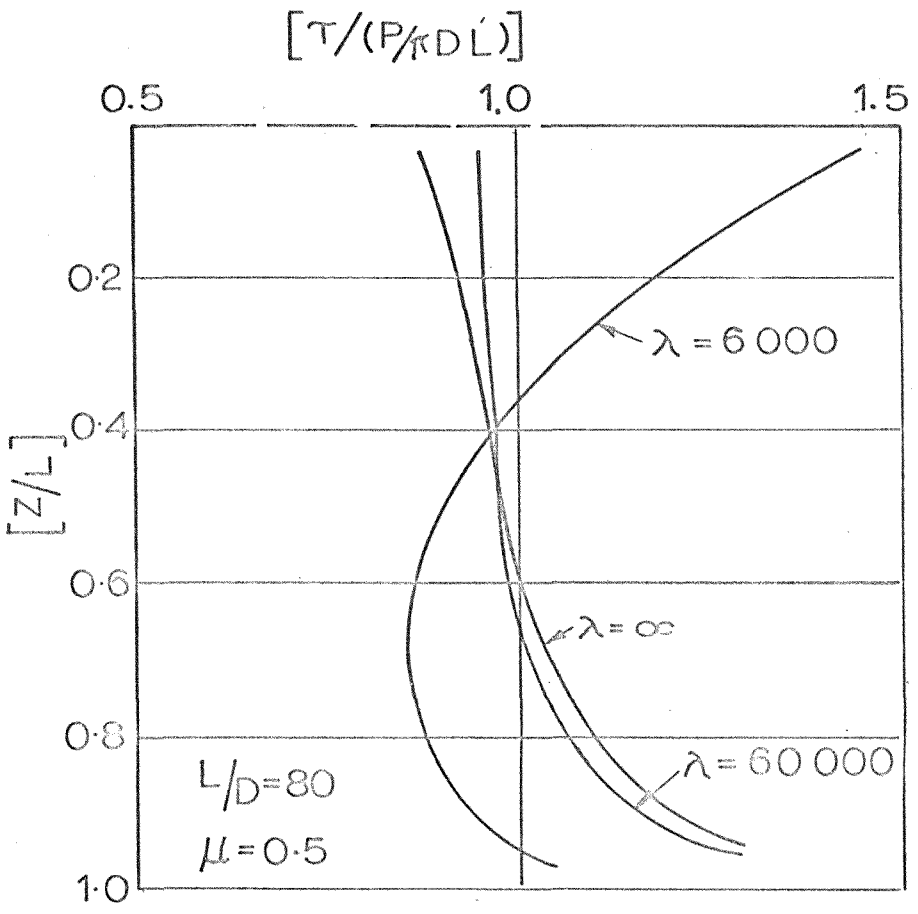

FIGURE - 4.6.2

SHEAR STRESS AT THE SHAFT FACE FOR A LONG PILE

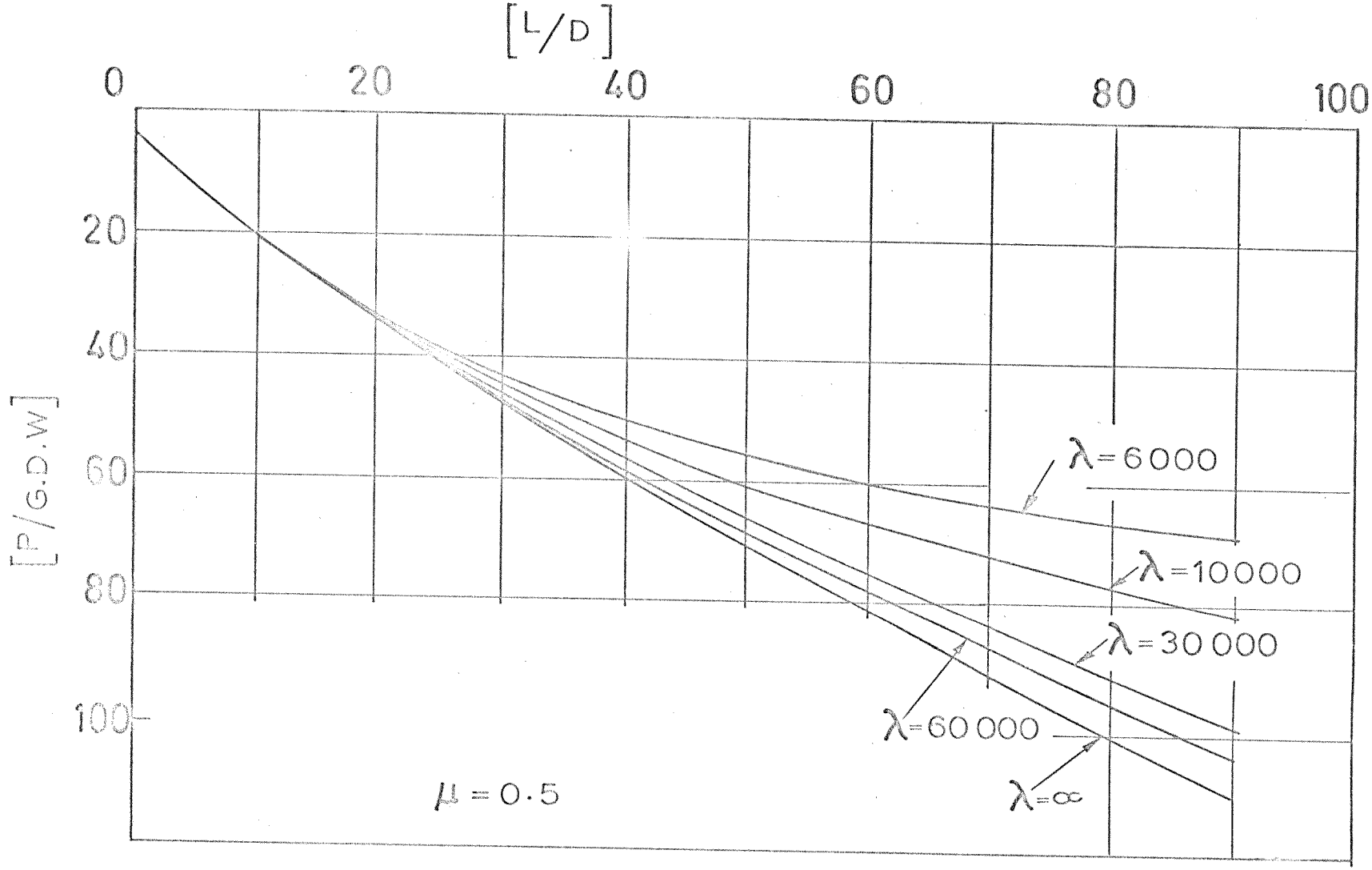

FIGURE - 4.7

LOAD DISPLACEMENT CHARACTERISTICS OF PLAIN PILES

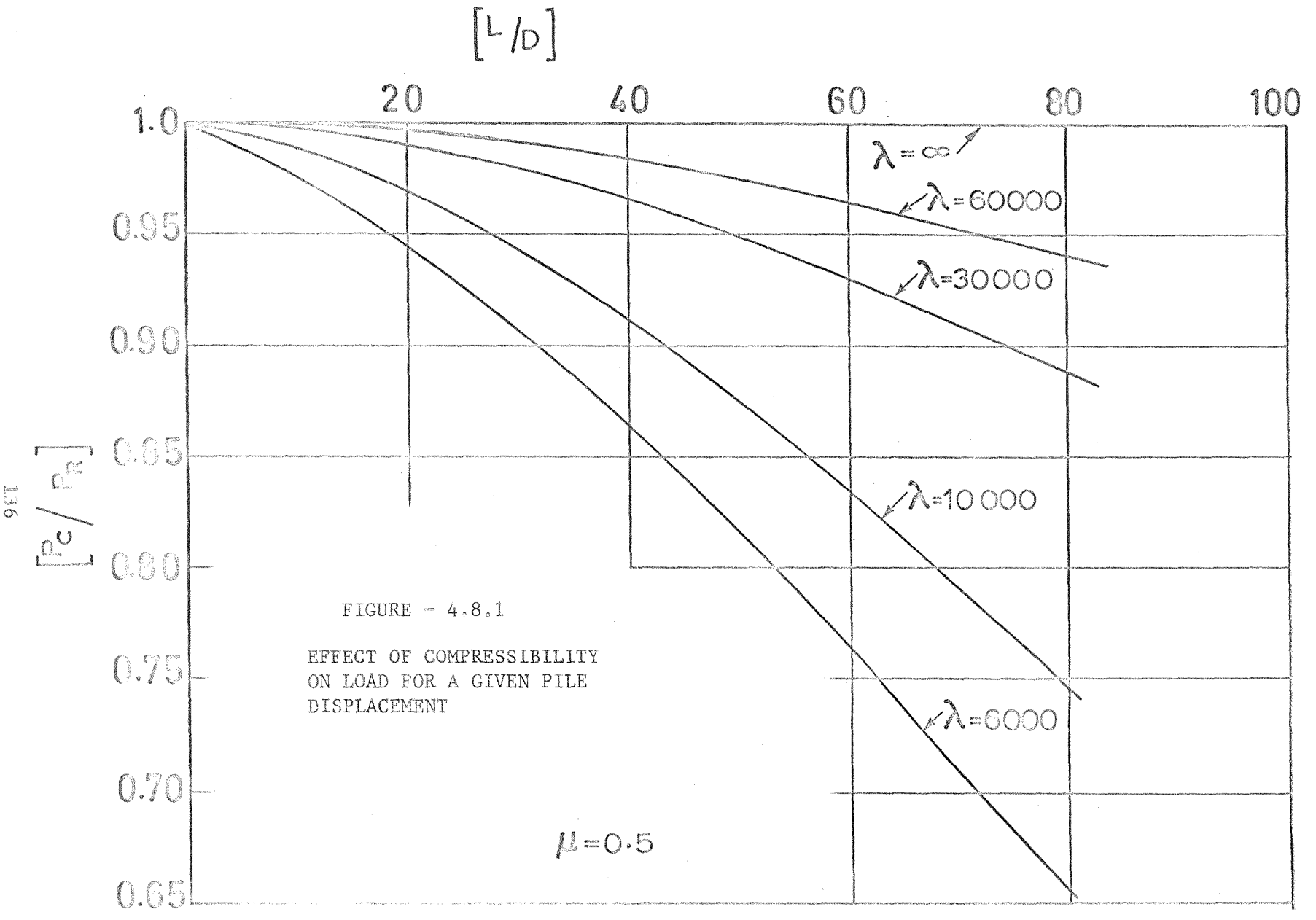

FIGURE - 4.8.1

EFFECT OF COMPRESSIBILITY ON LOAD FOR A GIVEN PILE DISPLACEMENT

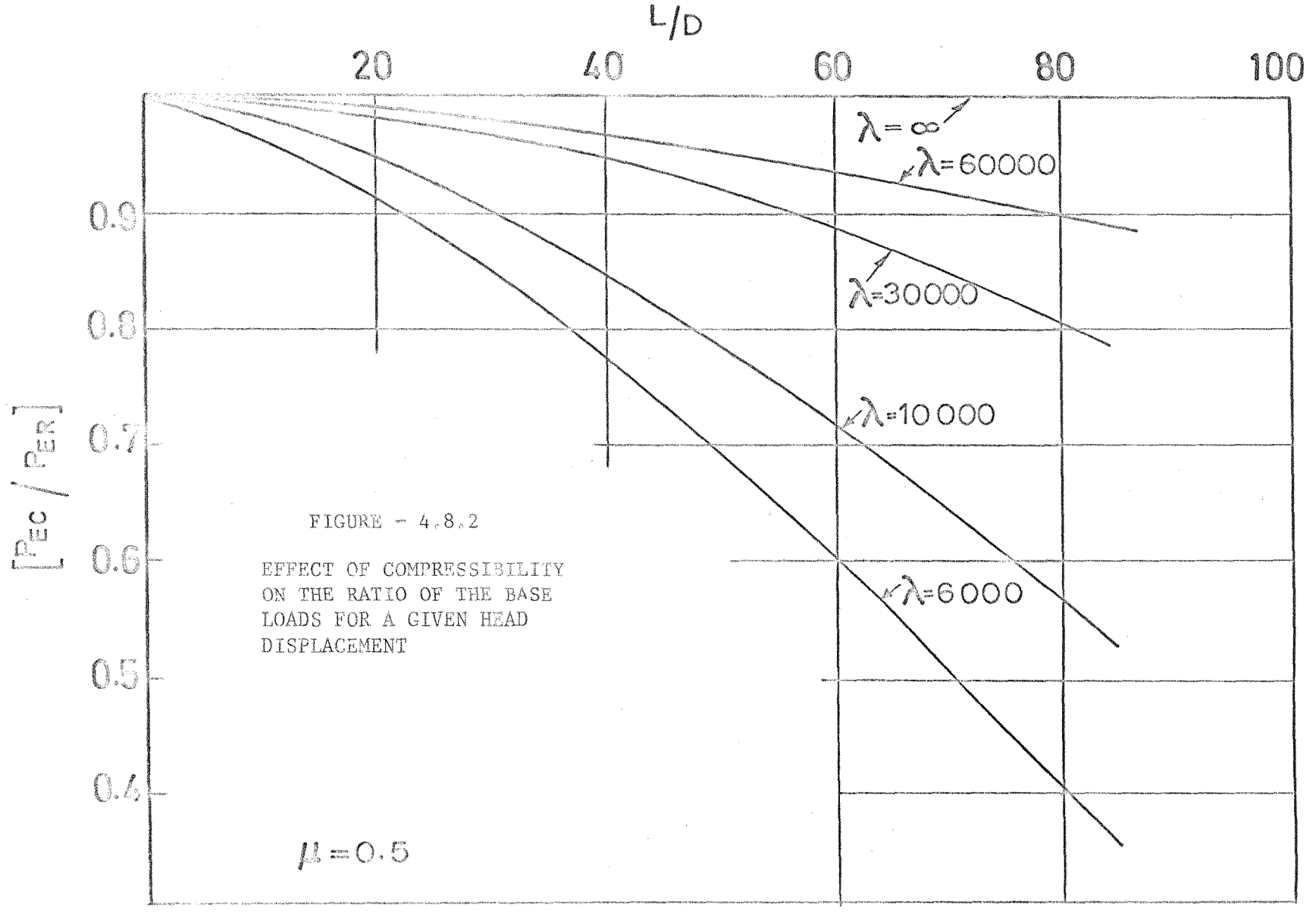

FIGURE - 4.8.2

EFFECT OF COMPRESSIBILITY ON THE RATIO OF THE BASE LOADS FOR A GIVEN HEAD DISPLACEMENT

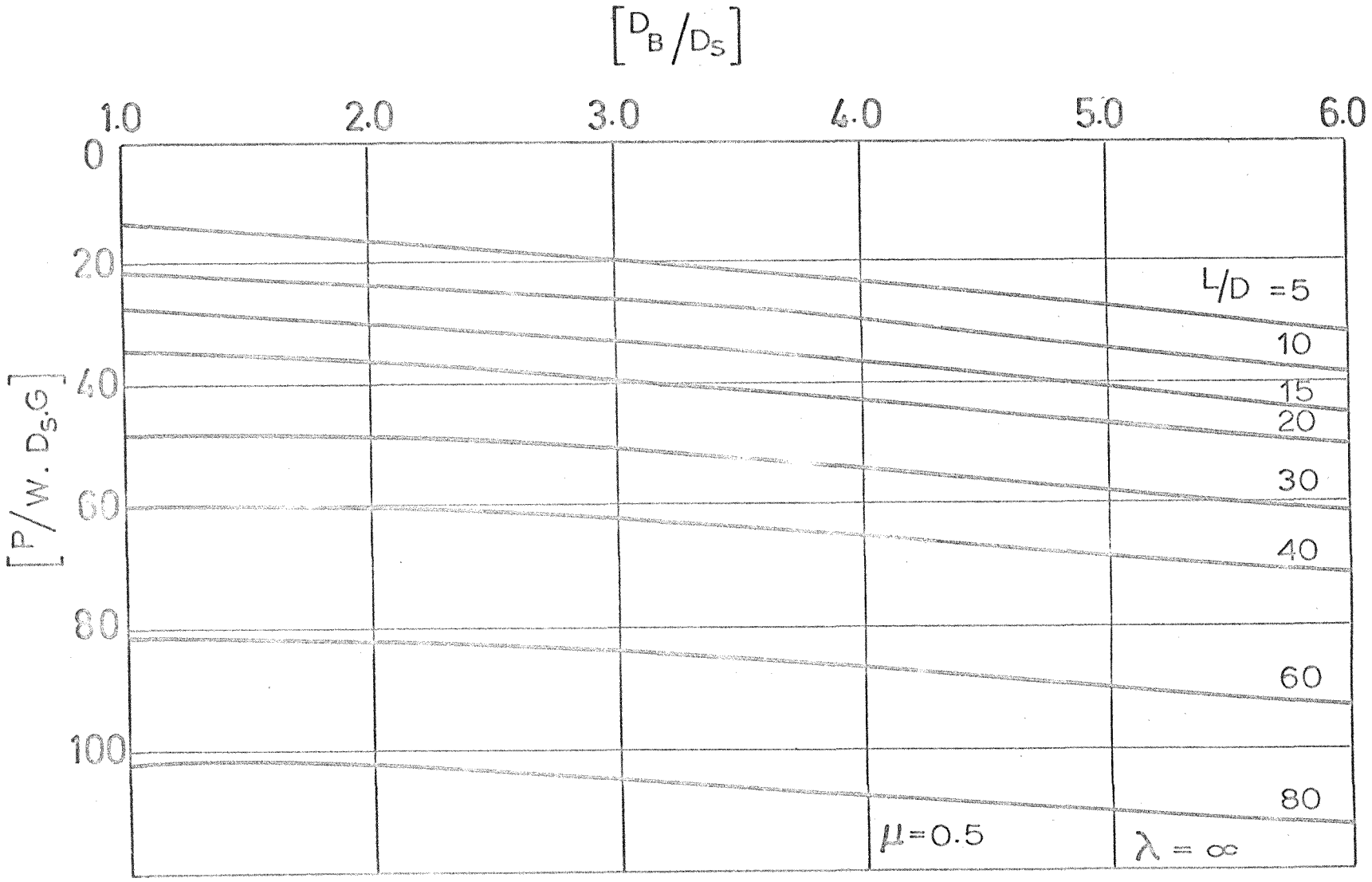

FIGURE - 4.9.1

LOAD DISPLACEMENT CHARACTERISTICS OF UNDER-REAMED PILES

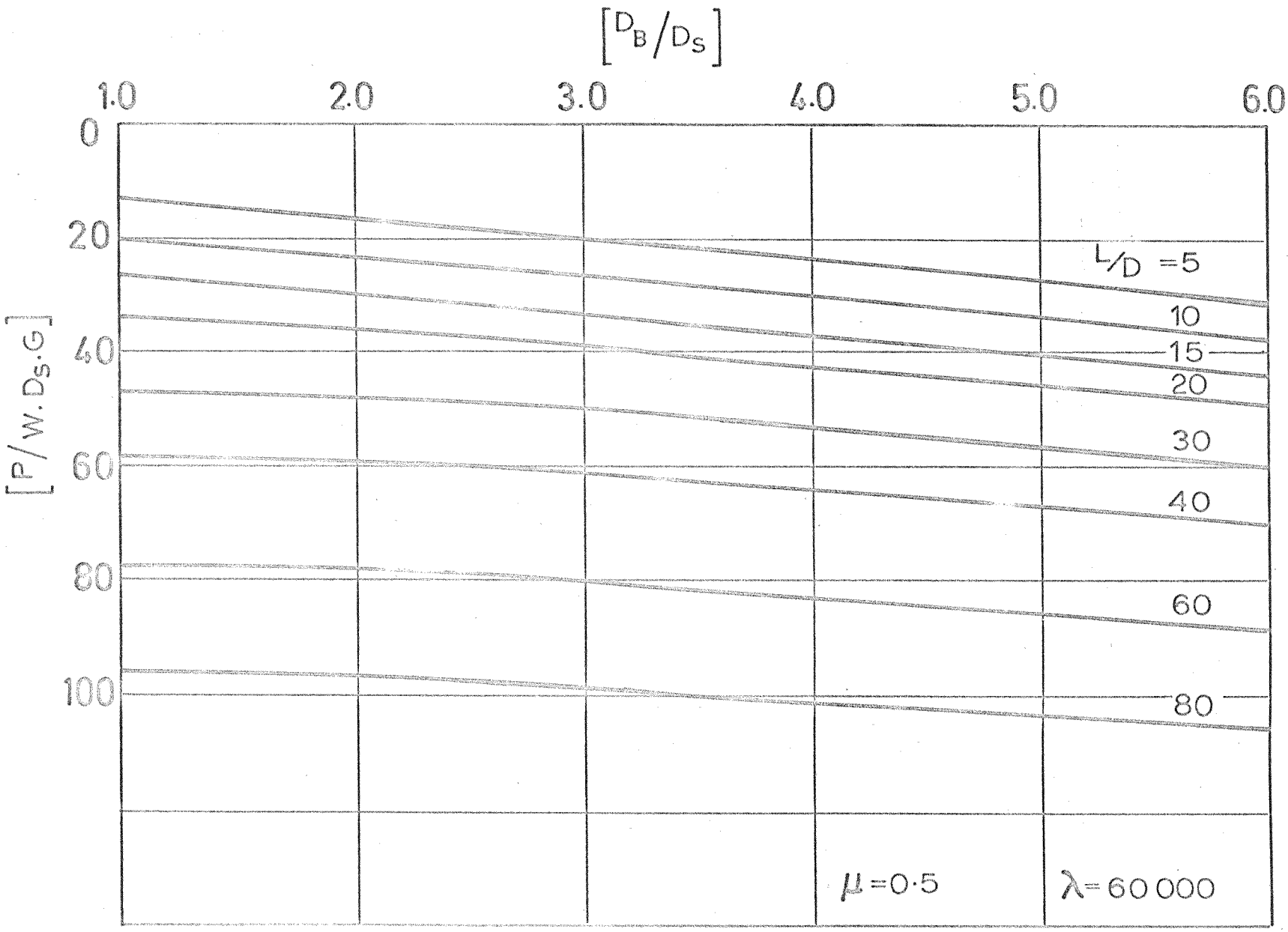

FIGURE 4.9.2

LOAD DISPLACEMENT CHARACTERISTICS OF UNDER-REAMED PILES

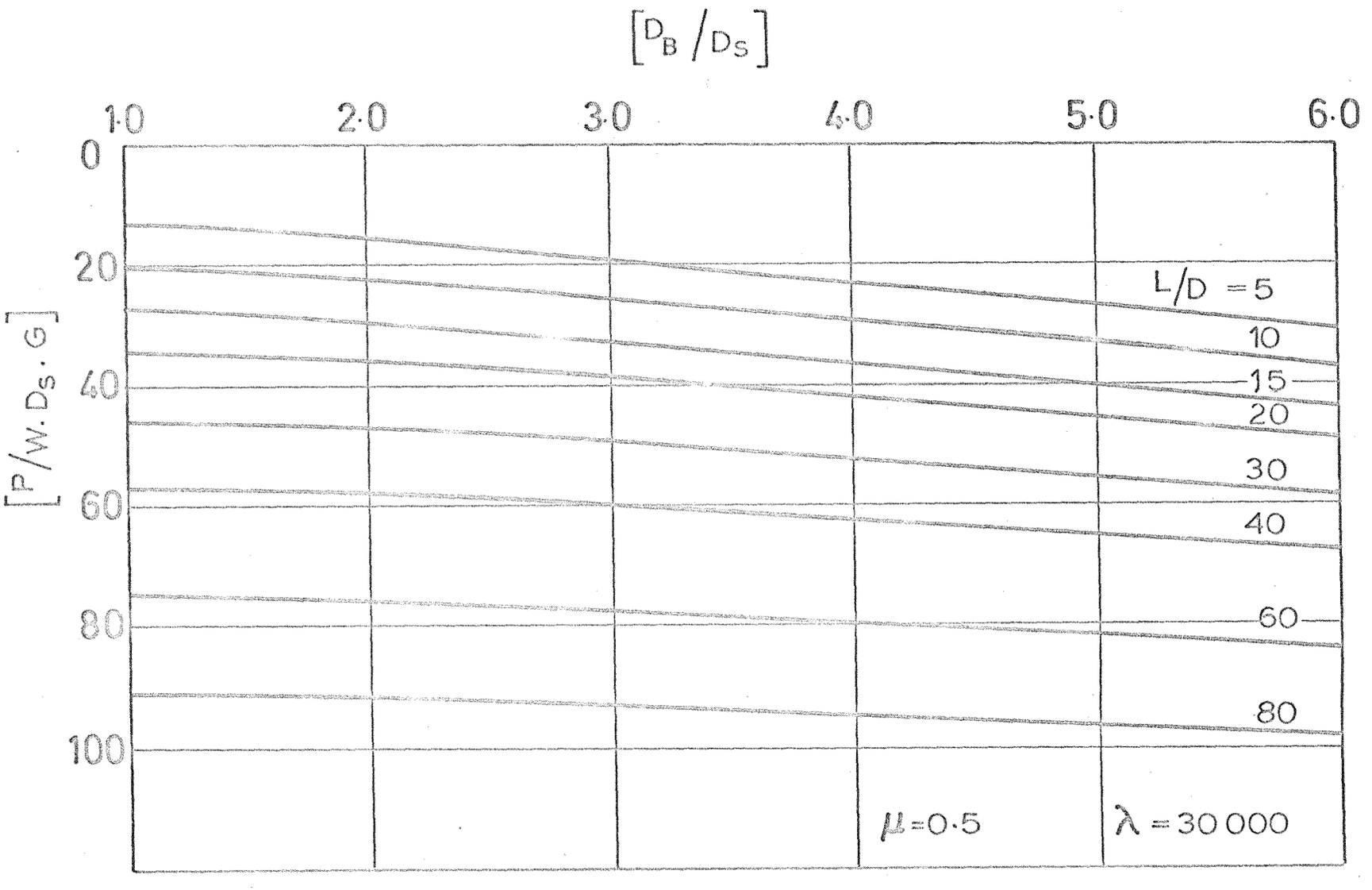

FIGURE - 4.9.3

LOAD DISPLACEMENT CHARACTERISTICS OF UNDER-REAMED PILES

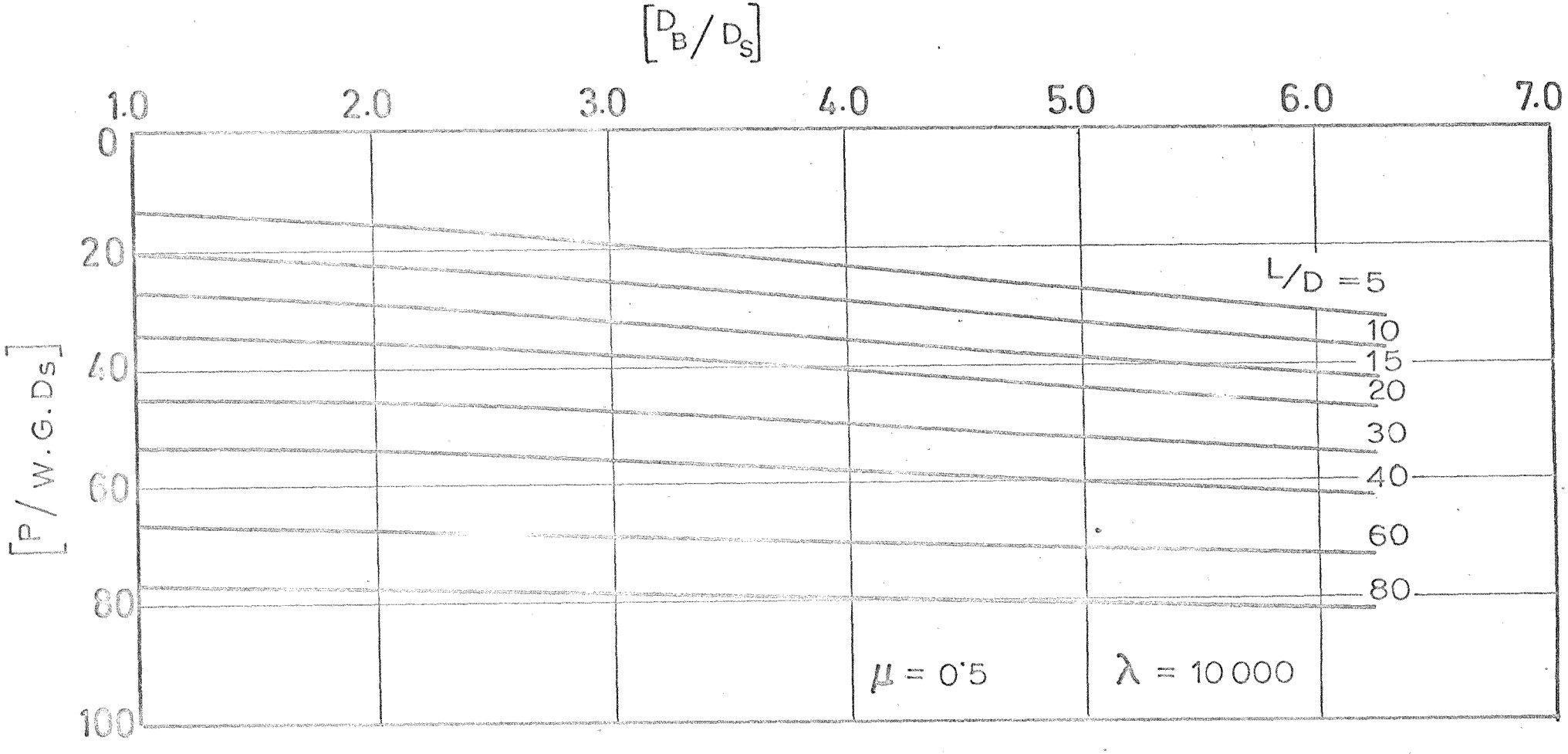

FIGURE - 4.9.4

LOAD DISPLACEMENT CHARACTERISTICS OF UNDER-REAMED PILES

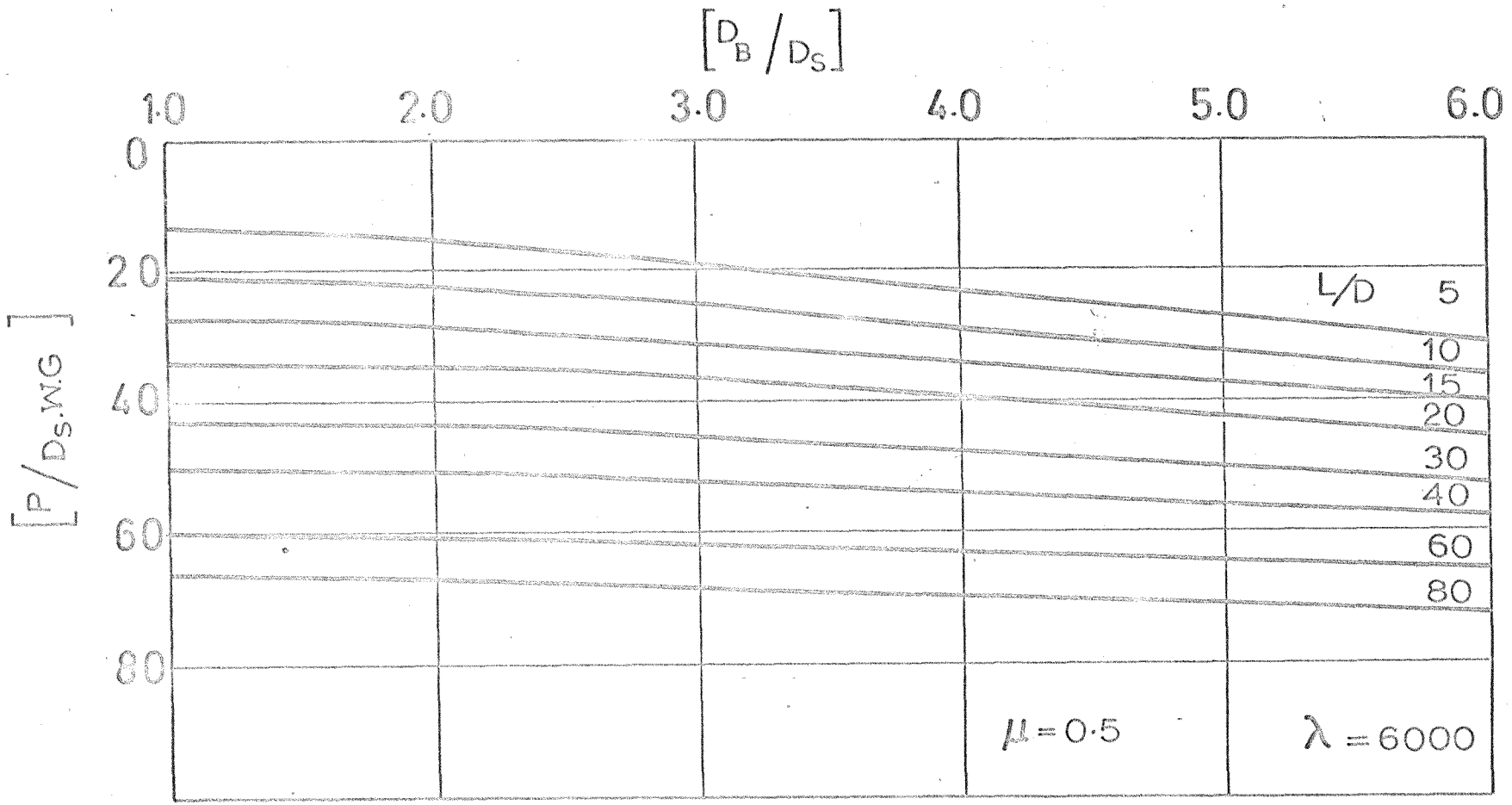

FIGURE - 4.9.5

LOAD-DISPLACEMENT CHARACTERISTICS OF UNDER-REAMED PILES

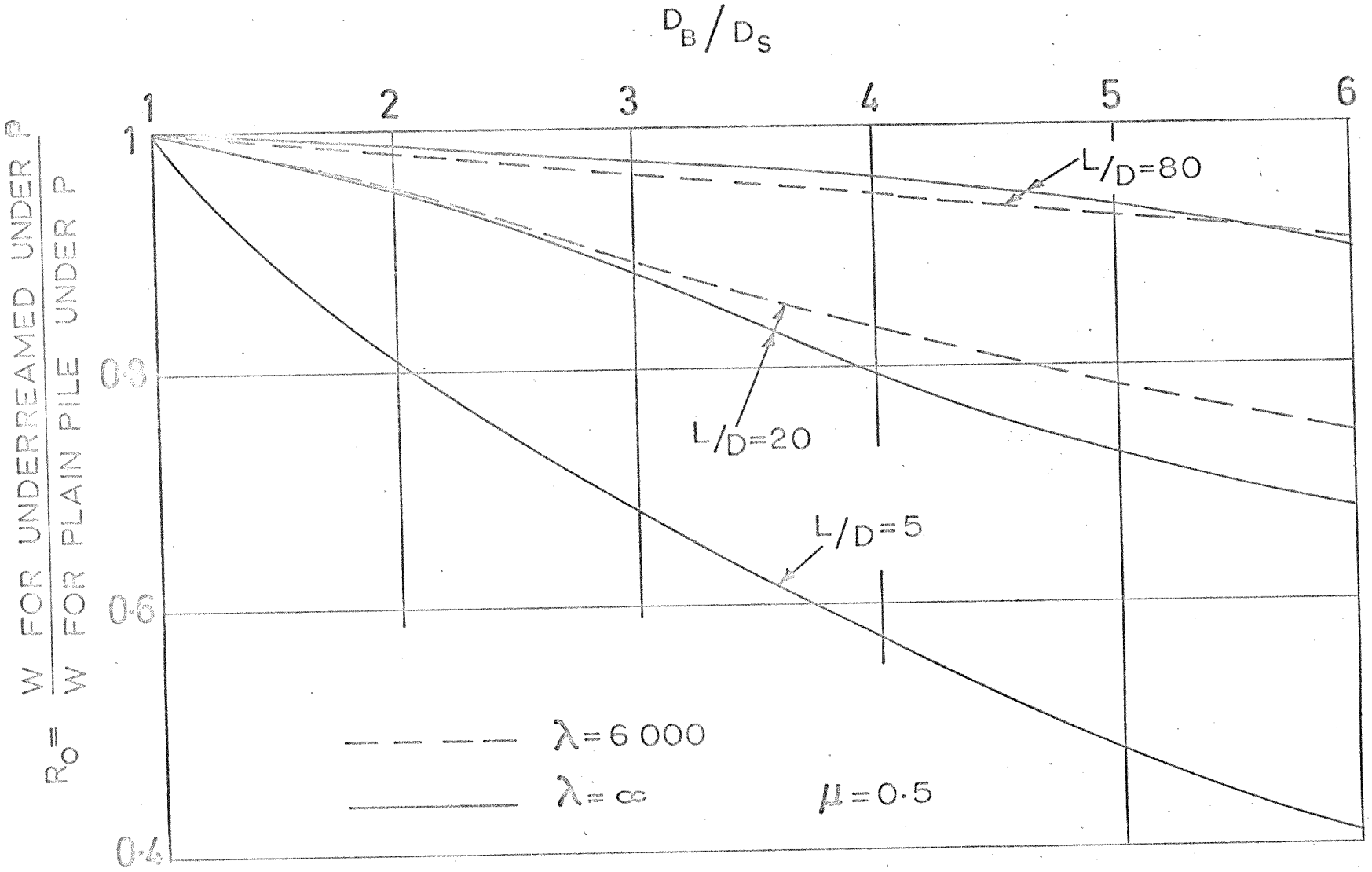

FIGURE - 4.10
THE EFFECTS OF UNDER-REAMING A PILE

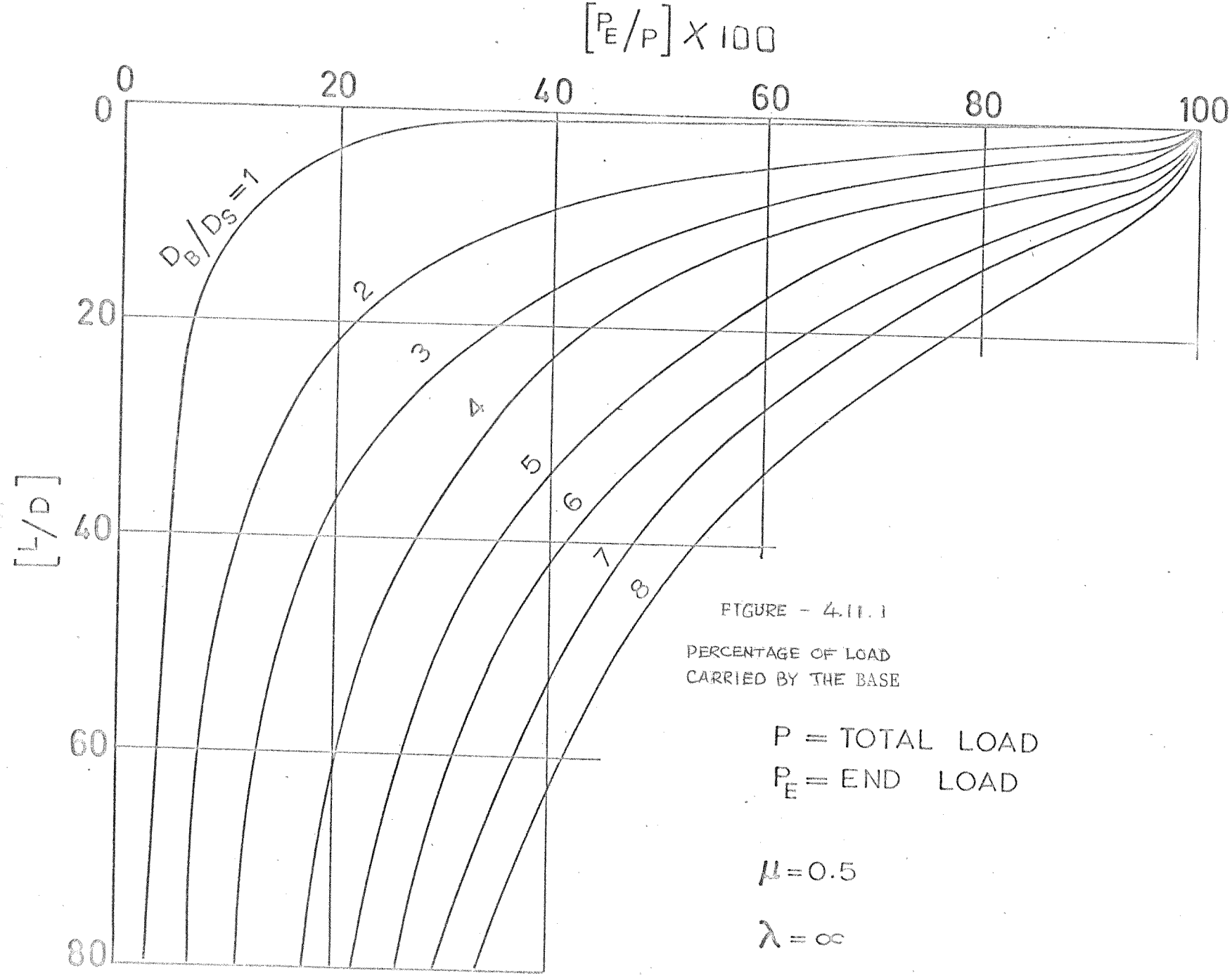

FIGURE - 4.11.1

PERCENTAGE OF LOAD CARRIED BY THE BASE

P = TOTAL LOAD

P_E = END LOAD

$\mu = 0.5$

$\lambda = \infty$

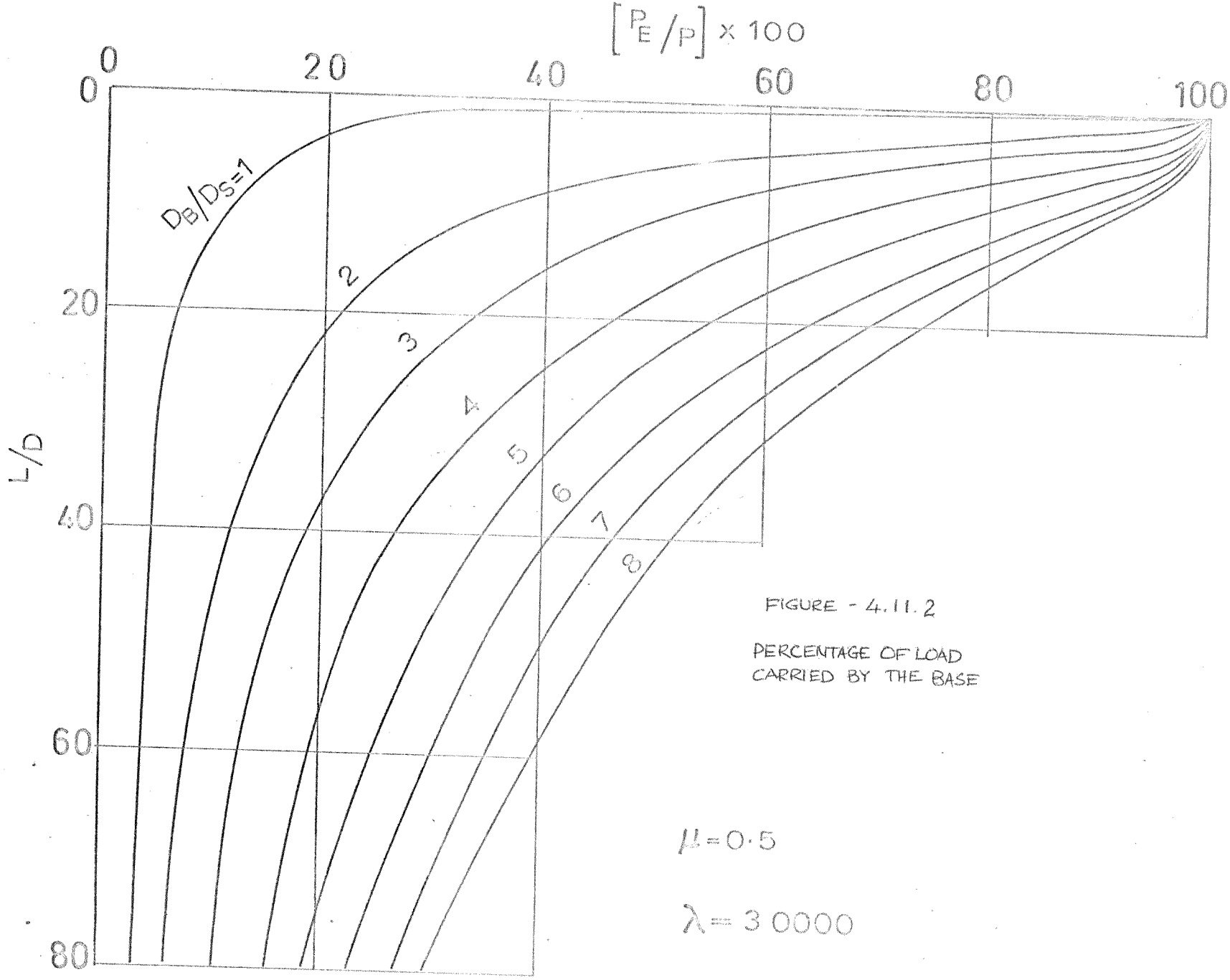

FIGURE - 4.11.2

PERCENTAGE OF LOAD CARRIED BY THE BASE

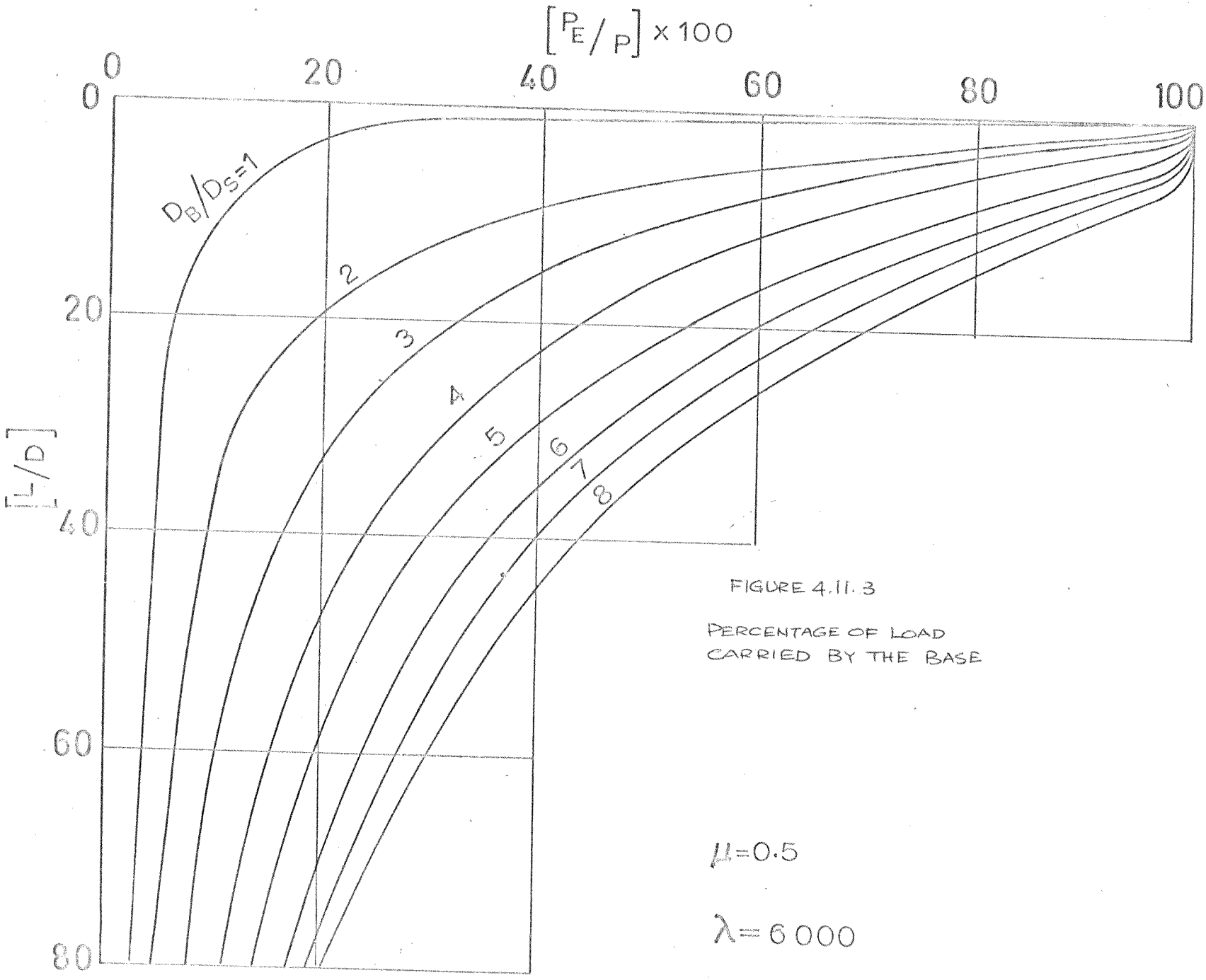

FIGURE 4.11.3

PERCENTAGE OF LOAD CARRIED BY THE BASE

$\mu = 0.5$

$\lambda = 6000$

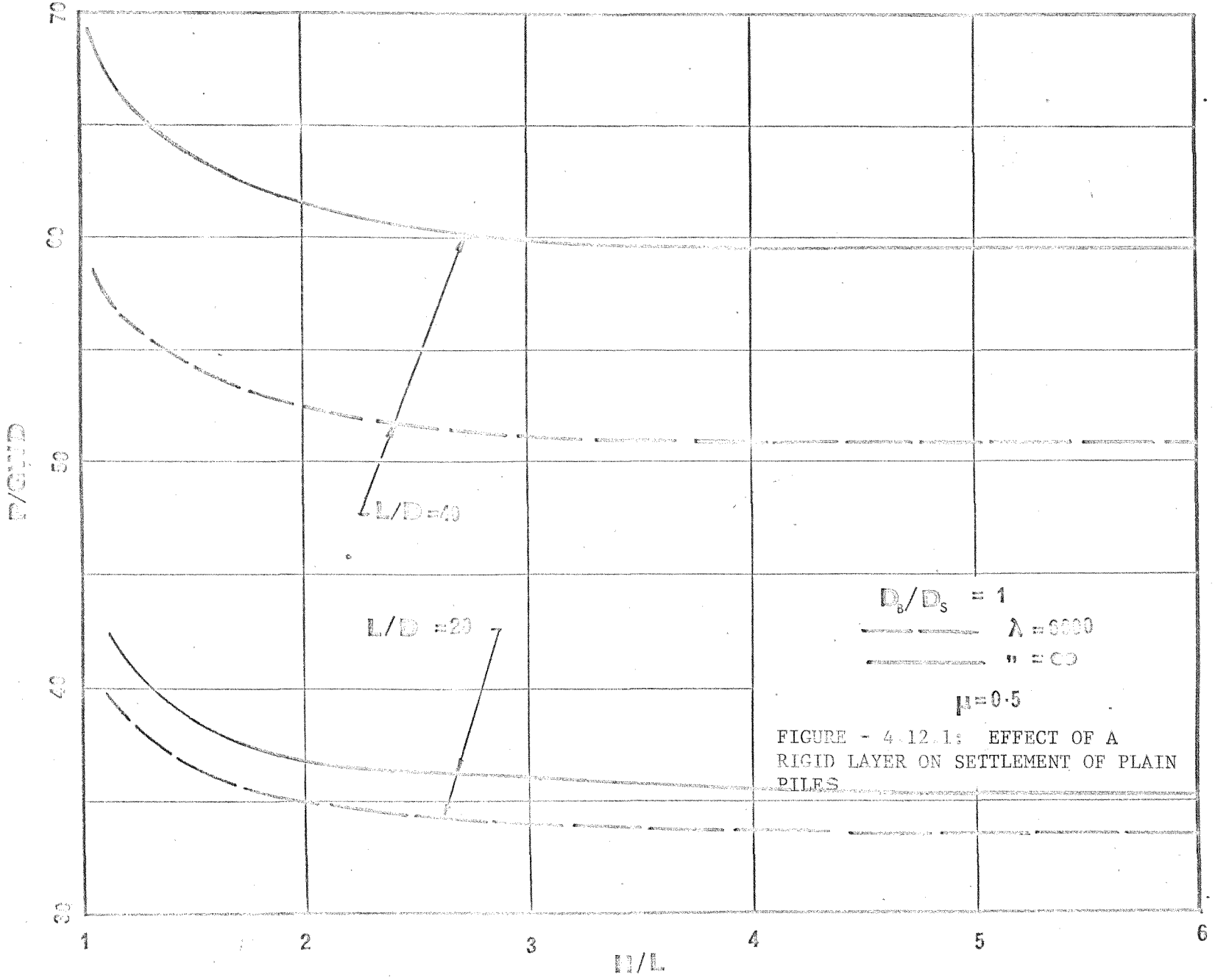

FIGURE - 4.12.1: EFFECT OF A RIGID LAYER ON SETTLEMENT OF PLAIN PILES

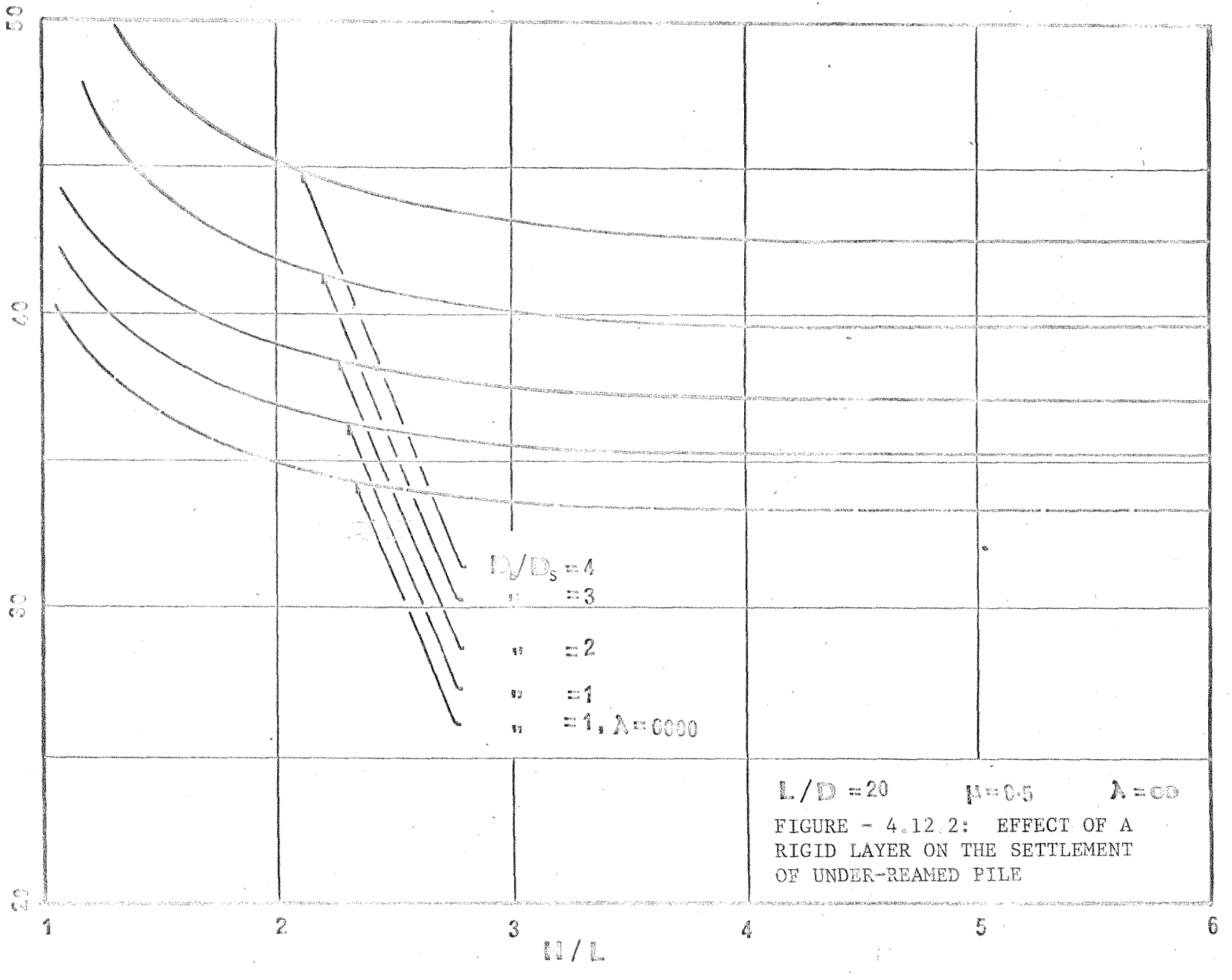

L/D = 20 μ = 0.5 λ = ∞

FIGURE - 4.12.2: EFFECT OF A RIGID LAYER ON THE SETTLEMENT OF UNDER-REAMED PILE

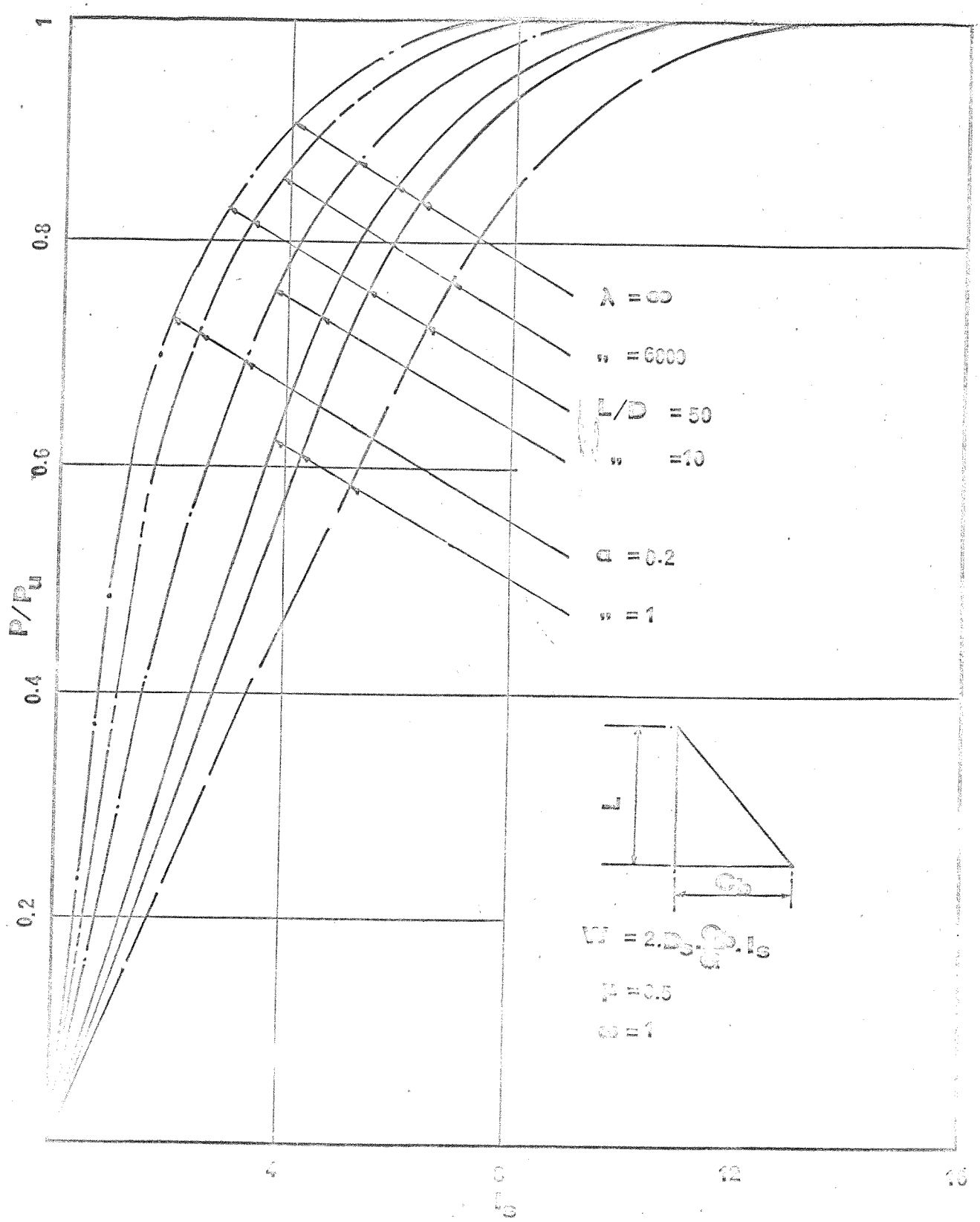

FIGURE - 4.13.1

LOAD-DISPLACEMENT CURVES FOR PLAIN PILE

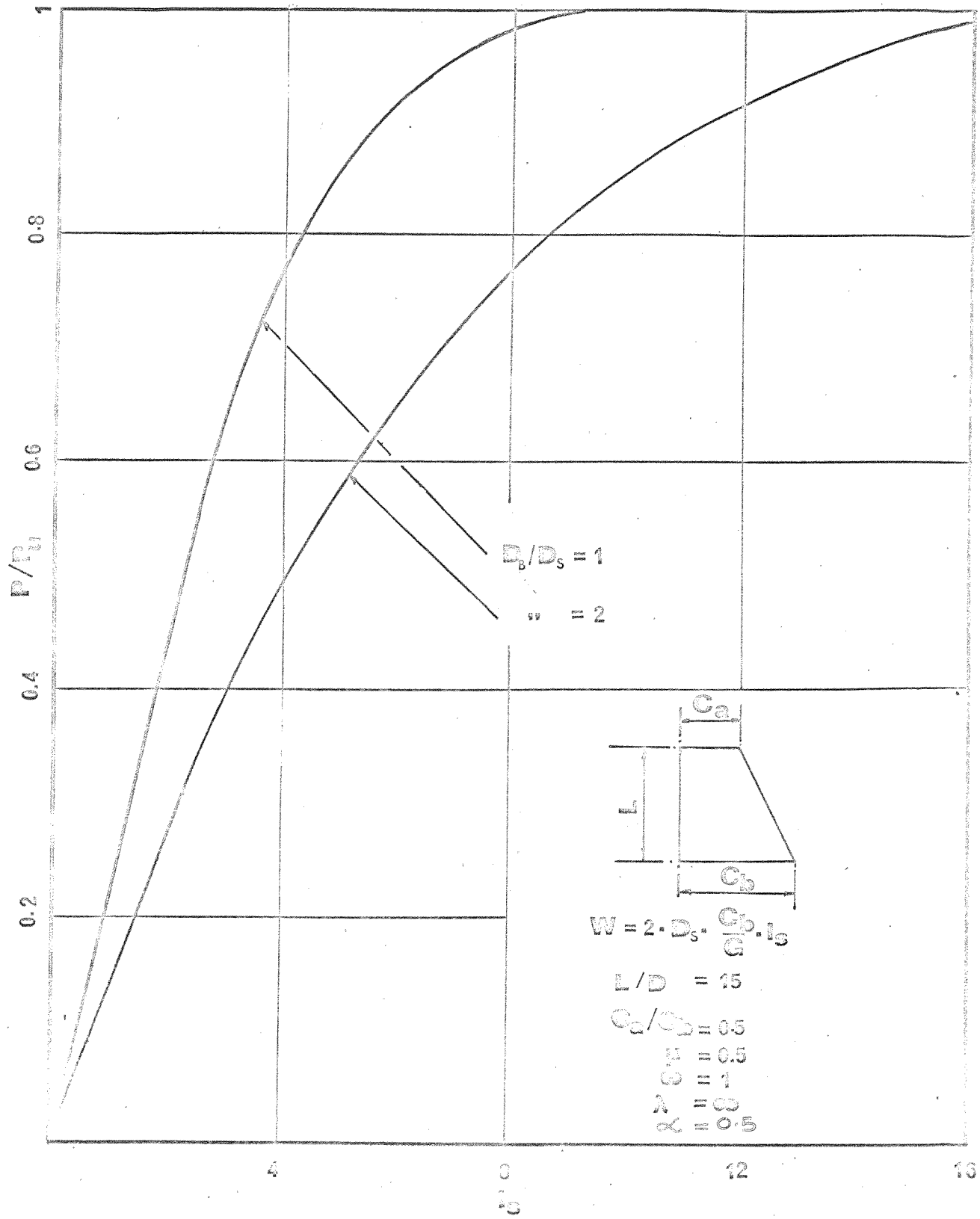

FIGURE - 4.10.2

LOAD-DISPLACEMENT CURVE FOR UNDER-REAMED PILE

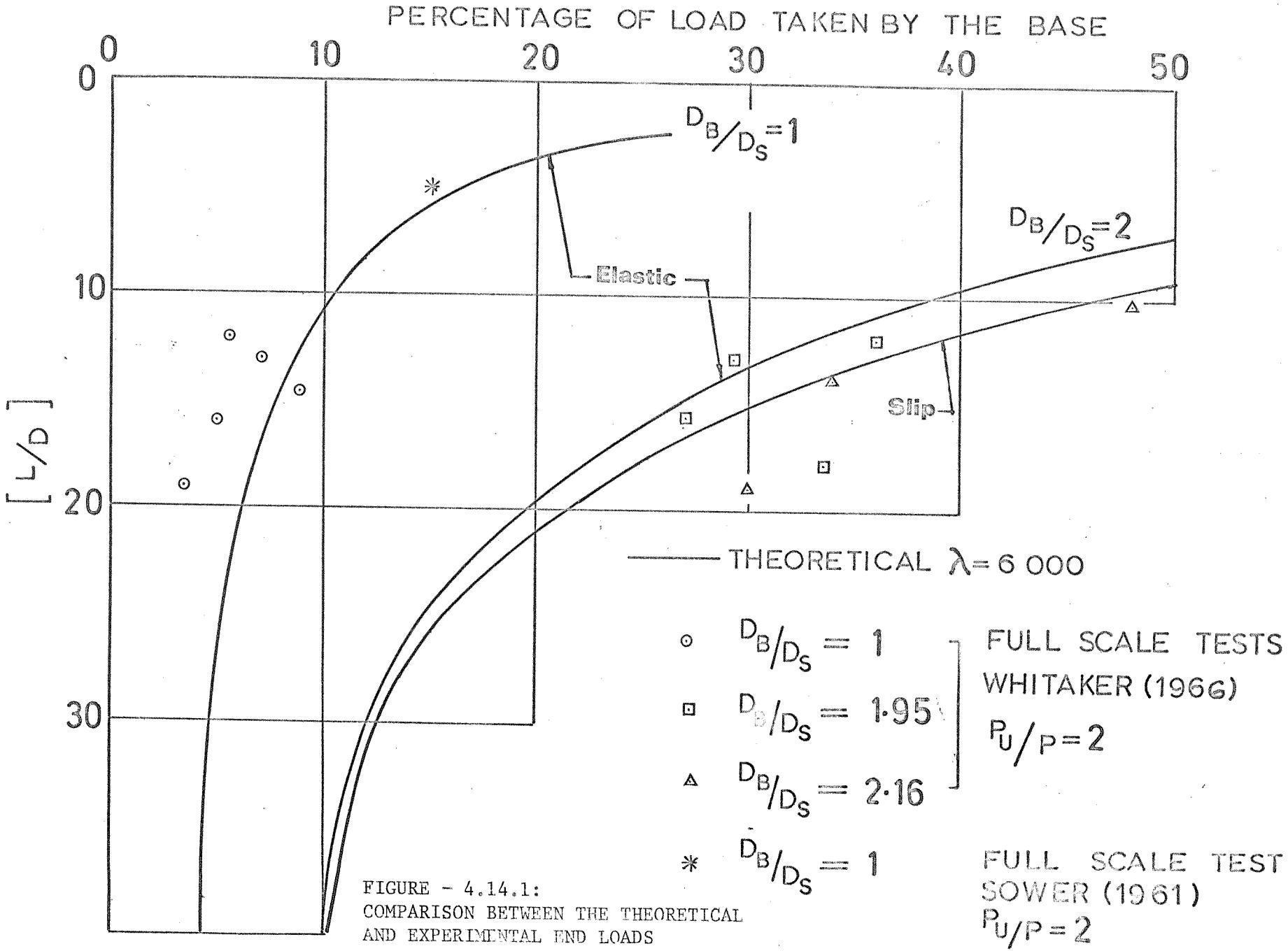

FIGURE - 4.14.1:
COMPARISON BETWEEN THE THEORETICAL AND EXPERIMENTAL END LOADS

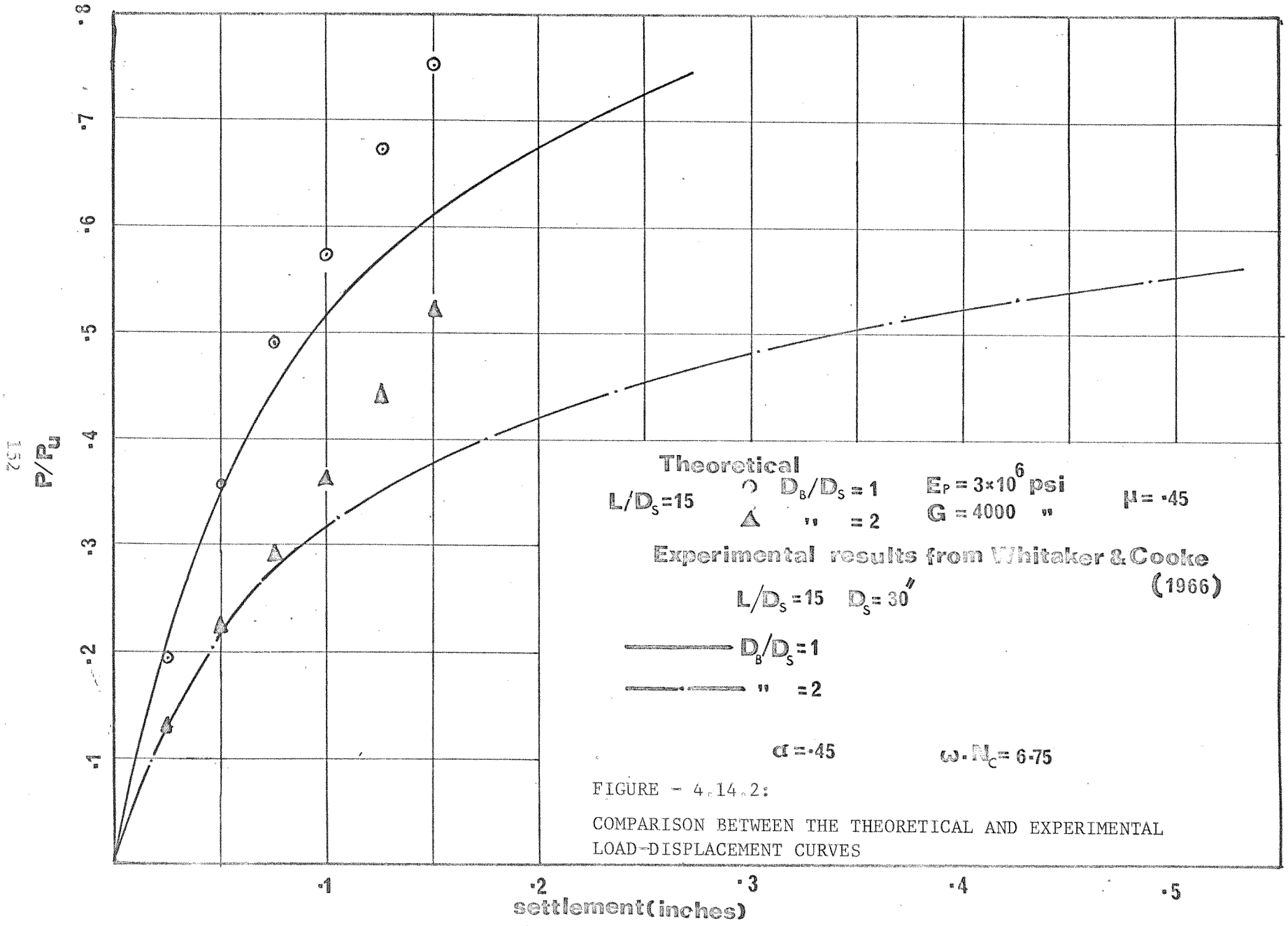

FIGURE - 4.14.2:

COMPARISON BETWEEN THE THEORETICAL AND EXPERIMENTAL LOAD-DISPLACEMENT CURVES

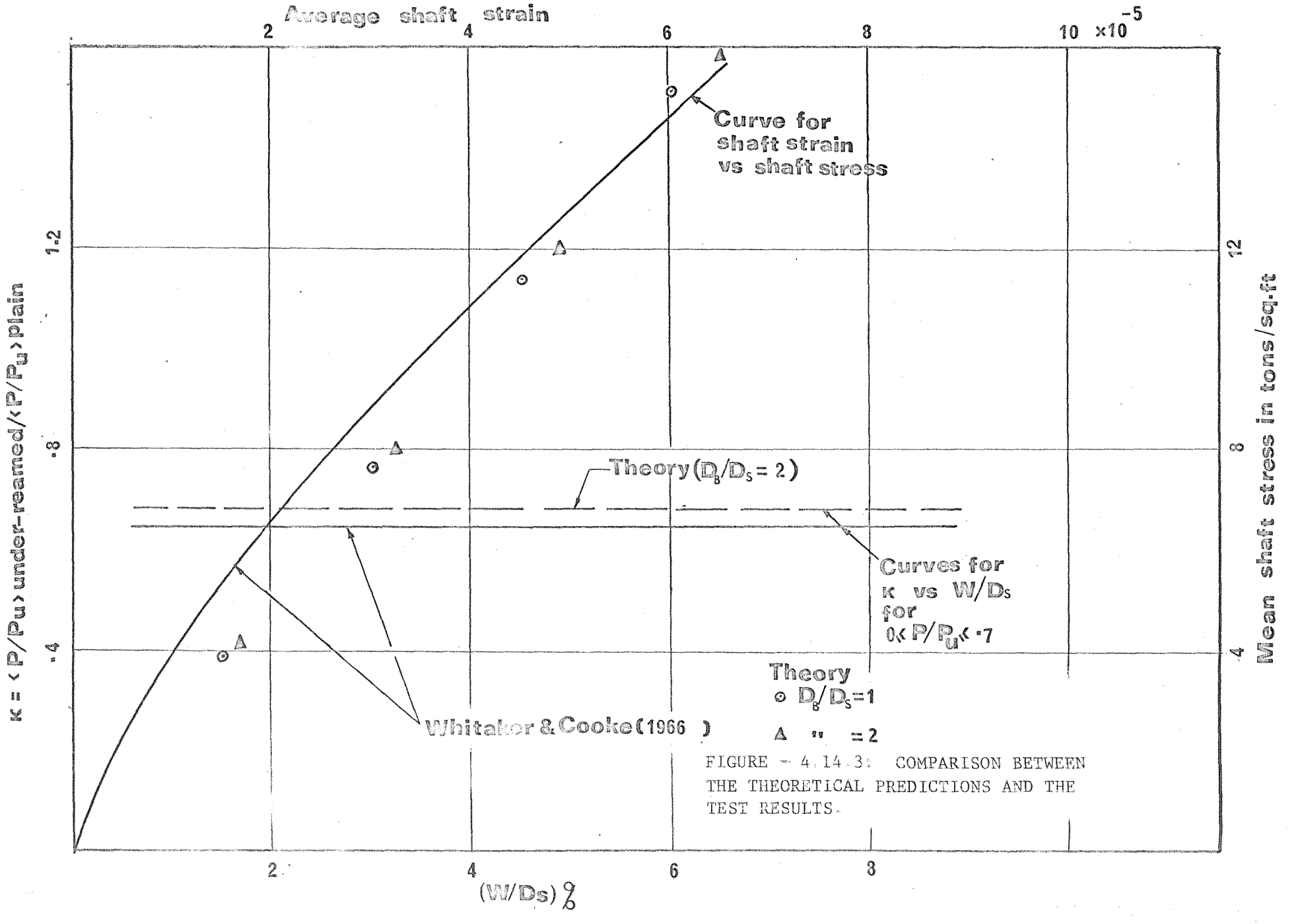

FIGURE - 4.14.3: COMPARISON BETWEEN THE THEORETICAL PREDICTIONS AND THE TEST RESULTS.

Chapter 5

An analysis of pile groups

5.1 Summary

This Chapter deals with an elastic analysis of pile groups obtained by an extension of the integral formulation described in Chapter 4 for single piles. The results of the analysis are presented graphically to show the relative effects of the ratios of length to diameter, spacing to diameter, length of the pile to the thickness of the elastic layer, compressibility of the pile to that of the soil and the geometry of the group.

The theoretical predictions are compared with laboratory model tests and full scale field tests, with reasonable agreement in most cases.

A method of predicting the load displacement behaviour of a pile group based on field test data for single piles is also presented.

5.2. General

It has been found from the analysis of a single axially loaded pile that the theoretical predictions are in general agreement with the observed behaviour. The theoretical analysis is also capable of giving satisfactory quantitative predictions of pile displacements under working loads. The success of the elastic theory in analysing the behaviour of a single pile therefore suggests that, it may also be useful in analysing the behaviour of pile groups.

The analysis for a single pile described in Chapter 4 can be extended directly to deal with general pile groups. The following approximations are introduced in order to reduce the number of simultaneous equations involved in the analysis

(i) Since the introduction of a fictitious radial intensity produces a negligible effect on the overall load displacement response horizontal displacement compatibilities of the pile-soil interfaces are ignored.

(ii) The bases of the piles and also the surface of the rigid layer are assumed to be smooth.

(iii) The piles are assumed to be bonded to the medium.

(iv) The pile cap is rigid and lies above the surface of the soil (i.e. the groups are free-standing).

Assumptions (i) and (ii) have been discussed in Chapter 4 and Chapter 3 respectively. Assumption (iii) implies no slip occurs between the pile and the adjacent soil and thus solutions presented herein are valid only while purely elastic conditions prevail. However, an examination of actual load-displacement curves (see Figures 4.13.1 and 4.13.2) reveals that these curves are linear up to 1/3 or 1/2 the ultimate load. Therefore at normal working loads the assumption of elastic behaviour appears

to be reasonable. Assumption (iv) implies that all piles in the group settle equally and the cap is not in contact with the ground surface. Though the condition of full rigidity is more likely to occur in practice, free-standing pile groups are much less common. If the cap rests on the soil the problem becomes more complex and the solution involves the consideration of displacement compatibility between the pile cap and the piles. This problem is analysed in the next Chapter.

5.3 Development of the analysis

We define two systems of coordinates, a local cylindrical co-ordinate system defined by $(c, \varepsilon_o, \theta_o)$ and the global cartesian co-ordinate system defined by (x,y,z); both systems have their origins at the ground surface (see Figure 5.1). If we distribute intensities $\phi_s(c, \theta_o)$ along the shaft-soil interface $\phi_b(\varepsilon_o, \theta_o)$ normal to the base-soil interface and $\psi(\xi, \eta)$ normal to the surface of the rigid layer at a depth H below the surface we can write an integral representation for the vertical displacement of a point B(x,y,z) within the finite elastic layer due to a number (N) of arbitrarily spaced piles (Figure 5.1), by analogy with equation (4.22) and (3.25), as:

$$w(x,y,z) = \sum_{p=1}^{N} \left[\int_o^L \int_o^{2\pi} \phi_s^p(c, \theta_o) \cdot a \cdot KW_1(c, r_1, z)\, d\theta_o\, dc \right.$$

$$\left. + \int_o^b \int_o^{2\pi} \phi_b^p(\varepsilon_o, \theta_o)\ \varepsilon_o\ KW_2(L, r_2, z)\, d\theta_o\, d\varepsilon_o \right] \qquad (5.1)$$

$$+ \int_{-\alpha}^{\alpha} \int_{-\alpha}^{\alpha} \psi(\xi, \eta)\ KW(x,y,z,\xi,\eta,H)\, d\xi\, d\eta$$

Where

$$r_1 = \left[r_p^2 + a^2 - 2r_p \cdot a\ Cos\theta_o \right]^{\frac{1}{2}}, \quad r_2 = \left[r_p + \varepsilon_o^2 - 2r_p \cdot \varepsilon_o\ Cos\theta_o \right]^{\frac{1}{2}}$$

$$r_p = \left[(x - x_p)^2 + (y - y_p)^2 \right]^{\frac{1}{2}}$$

x_p and y_p are the co-ordinates of the local origin with reference to the global axes.

The intensities ϕ_s^p and ϕ_b^p are functions of (c,θ_o) and (ε_o,θ_o) respectively and allowing for this would again increase the number of simultaneous equations to be solved, therefore ϕ_s^p and ϕ_b^p are approximated by equivalent rotationally symmetric distributions about the local axes. It is thought that these approximations will introduce negligible errors in the calculated displacements and loads for the pile spacings commonly encountered in practice ($S/D \geq 2.5$).

Thus we can write equation (5.1) as:

$$w(x,y,z) = \sum_{p=1}^{N} \left[\int_o^L \phi_s^p(c)a. \int_o^{2\pi} KW_1(c,r_1,z)\, d\theta_o\, dc + \int_o^b \phi_b^p(\varepsilon_o) \int_o^{2\pi} \varepsilon_o .\, KW_2(L,r_2,z)\, d\theta_o\, d\varepsilon_o \right] + \int_{-\infty}^{\infty} \int_{-\infty}^{\infty} \psi(\xi,\eta)\ KW(x,y,z,\xi,\eta,H)\, d\xi\, d\eta \qquad (5.2)$$

5.4 Analysis of a symmetrical pile group

A symmetrical pile group may be defined as a pile group in which the piles are spaced equally around the circumference of a circle, consequently each pile displaces equally and carries the same load. For such a case we can write equation (5.2) as:

$$w(x,y,z) = \int_o^L \phi_s^1 .a. \int_o^{2\pi} KW_1(c,r_1,z)\, d\theta_o\, dc + \int_o^b \phi_b^1 \int_o^{2\pi} \varepsilon_o\ KW_2(L,r_2,z)\, d\theta_o\, d\varepsilon_o + \sum_{p=2}^{N} \left[\int_o^L \phi_s^p\ a \int_o^{2\pi} KW_1(c,r_1,z)\, d\theta_o\, dc + \int_o^b \phi_b^p \int_o^{2\pi} \varepsilon_o\ KW_2(L,r_2,z)\, d\theta_o d\varepsilon_o \right] + \int_{-\infty}^{\infty} \int_{-\infty}^{\infty} \psi(\xi,\eta)\ KW(x,y,z,\xi,\eta,H)\, d\xi\, d\eta \qquad (5.3)$$

By bringing the field point B(x,y,z) onto the pile-soil interface of the first pile of the group we obtain an integral equation for the displacement of the pile-soil interface. The first two integrals of equation (5.3) are exactly analogous to the first two integrals of equation (4.22). As before, discretising the integrals over n segments of the shaft surface, m annular rings

over the base area and s rectangular or square elements to represent a large enough area over the surface of the rigid layer, we obtain:

$$(W_s^1)_i = \sum_{j=1}^{n} (\phi_s^1)_j \left[(KSS)^1_i + \sum_{p=2}^{NS} (KSS)^p_i \right]_j + \sum_{j=1}^{m} (\phi_b^1) \left[(KBS)^1_i + \sum_{p=2}^{NS} (KBS)^p_i \right]_j$$

$$+ \sum_{j=1}^{s} (\psi)_j \, (KLS)_{ij} \qquad (5.4)$$

where $i = 1,2,\ldots.n$.

Similarly

$$(W_b^1)_i = \sum_{j=1}^{n} (\phi_s^1)_j \left[(KSB)^1_i + \sum_{p=2}^{NS} (KSB)^p_i \right]_j + \sum_{j=1}^{m} (\phi_b^1) \left[(KBB)^1_i + \sum_{p=2}^{NS} (KBB)^p_i \right]_j$$

$$+ \sum_{j=1}^{s} (\psi)_j \, (KLB)_{ij} \qquad (5.5)$$

where $i = 1,2,\ldots.m$; and the vertical displacements $(W_\ell)_i$ are given by

$$(W_\ell)_i = \sum_{j=1}^{n} (\phi_s^1)_j \left[(KSL)^1_i + \sum_{p=1}^{NS} (KSL)^p_i \right]_j + \sum_{j=1}^{m} (\phi_b^1)_j \left[(KBL)^1_i + \sum_{p=2}^{NS} (KBL)^p_i \right]_j$$

$$+ \sum_{j=1}^{s} (\psi)_j \, (KLL)_{ij} \qquad (5.6)$$

where $i = 1,2,\ldots.s$.

In the above equations (W_s^1), (W_b^1), (W_ℓ) are the vertical displacements of the shaft, the base of pile no. 1 and the rigid layer respectively. (ϕ_s^1), (ϕ_b^1), (ψ) are the shaft shear stress, normal stress at the base of pile no. 1 and the fictitious vertical stress intensity on the surface of the rigid layer respectively.

$(KSS)^1$, $(KBS)^1$, $(KSB)^1$ etc. are the coefficients for displacements at pile no. 1 due to the stress intensities acting on its surface

$(KSS)^p$, $(KBS)^p$, $(KSB)^p$ etc. are the coefficients for displacements at the pile no. 1 due to the stress intensities acting on the surface of

the p^{th} pile.

NS = number of piles in the symmetrical group.

(KLS), (KLB), (KLL) are defined in Chapter 4.

The integrals involved in evaluation of the coefficients $(KSS)^1_{ij}$, $(KBS)^1_{ij}$, $(KSB)^1_{ij}$ and $(KBB)^1_{ij}$ are identical to those of equations (4.23) and (4.24). The integrals involved in evaluating the coefficients of $(KLL)_{ij}$ are identical to those of equation (3.25). The other coefficients in the above set of equations are calculated from integrals taken over non local regions (i.e. regions at some distance away from the points on the surface of pile no. 1 and the surface of the rigid layer). These integrals are evaluated by Simpson's rule for displacements at the centre-line of pile no. 1.

Equations (5.4), (5.5) and (5.6) may be combined and written as:

$$(W^1)_i = \sum_{j=1}^{n+m} (\phi^1)_j \, (KSP)^1_{ij} + \sum_{j=1}^{s} (\psi)_j \, (KLP)^1_{ij} \qquad (5.7)$$

where i = 1,2,3...(n+m); and

$$(W_\ell)_i = \sum_{j=1}^{n+m} (\phi^1)_j \, (KPL)^1_{ij} + \sum_{j=1}^{s} (\psi)_j \, (KLL)_{ij} \qquad (5.8)$$

where i = 1, 2, 3....s.

By incorporating the boundary conditions for the rigid pile and the rigid layer and writing equations (5.7) and (5.8) in matrix notation we arrive at:

$$\begin{Bmatrix} \{W^1\} \\ \{W_\ell\} \end{Bmatrix} = \begin{Bmatrix} \{1\} \\ \{0\} \end{Bmatrix} = \begin{bmatrix} [KSP]^1_1 & [KLP]^1 \\ [KPL] & [KLL] \end{bmatrix} \begin{Bmatrix} \{\phi^1\} \\ \{\psi\} \end{Bmatrix} \qquad (5.9)$$

where, $(W^1)_i$ are vertical displacements of (n+m) elements of pile-soil interface of pile no. 1 and $\{W^1\}$ the equivalent (n+m) x 1 matrix,

$(W_\ell)_i$ are vertical displacements of s elements of the finite rigid layer-soil interface and $\{W_\ell\}$ the equivalent s x 1 matrix,

$(\phi^1)_j$ are stress intensities acting over n elements of shaft and m elements of base of the pile no. 1, and $\{\phi^1\}$ is the equivalent (n+m) x 1 matrix,

$\{\psi\}$ is s x 1 values of fictitious vertical stress intensity on the surface of the rigid layer,

$(KSP)^1_{ij}$, $(KLP)^1_{ij}$, $(KPL)^1_{ij}$ are given by equations (5.4), (5.5) and (5.6) by comparison with equations (5.7) and (5.8);

$[KSP]^1$, $[KLP]^1$, $[KPL]^1$, $[KLL]$ are (n+m) x (n+m), (n+m) x s, s x (n+m) and s x s matrices of coefficients.

5.5 Analysis of arbitrarily spaced pile groups

A general pile group with arbitrarily spaced piles can be considered to be equivalent to a number (NP) of symmetrical pile groups where each symmetrical pile group carries different loads. Thus the partial symmetry of a general pile group may be utilised by carrying out a direct summation over the surfaces of the piles that carry equal loads. Therefore the integral representation (5.2) can be written in a discrete linear form via equation (5.7) as (writing the equations for one pile from each symmetrical group):

$$(W^p)_i = \sum_{q=1}^{NP} \sum_{j=1}^{n+m} (\phi^q)_j \, (KSP)^{pq}_{ij} + \sum_{j=1}^{s} (\psi)_j \, (KLP)^p_{ij} \qquad (5.10)$$

where p = 1, 2...NP, i = 1,2...(n+m); and

$$(W_\ell)_i = \sum_{q=1}^{NP} \sum_{j=1}^{n+m} (\phi^q)_j \, (KPL)^q_{ij} + \sum_{j=1}^{s} (\psi)_j \, (KLL)_{ij} \qquad (5.11)$$

where $i = 1,2....s$;

$(W^p)_i$ are the vertical displacements of the pile-soil interface of the p^{th} pile, $p = 1,2....NP$.

$(\phi^q)_j$ are the shaft and the base stress intensities over the pile surface of the q^{th} pile, $q = 1,2...NP$.

NP is the number of symmetrical pile groups within the general pile group, therefore $N = NS \times NP$.

$(KSP)^{pq}_{ij}$ are the coefficients $(KSP)_{ij}$ evaluated at the p^{th} pile due to q^{th} symmetrical group.

$(KLP)^p_{ij}$ are the coefficients $(KLP)_{ij}$ evaluated at the p^{th} pile.

$(KPL)^q_{ij}$ are the coefficients $(KPL)_{ij}$ evaluated over the elements on the surface of the rigid layer due to q^{th} symmetrical group.

Again equations (5.10) and (5.11) may be combined and written in matrix notation as:

$$\begin{Bmatrix} \{W^1\} \\ \vdots \\ \{W^{NP}\} \\ \{W_\ell\} \end{Bmatrix} = \begin{bmatrix} [KSP]^{11} & \cdots & [KSP]^{1\,NP} & [KLP]^1 \\ \vdots & & \vdots & \vdots \\ [KSP]^{NP\,1} & \cdots & [KSP]^{NP\,NP} & [KLP]^{NP} \\ [KPL]^1 & \cdots & [KPL]^{NP} & [KLL] \end{bmatrix} \begin{Bmatrix} \{\phi^1\} \\ \vdots \\ \{\phi^{NP}\} \\ \{\psi\} \end{Bmatrix} \qquad (5.12)$$

where $\{W^1\}.....\{W^{NP}\}$ denote (n+m) x 1 vectors for vertical displacements of pile no. 1, pile no. 2 etc., each representing a typical pile of different symmetrical groups.

$\{\phi^1\}....\{\phi^{NP}\}$ denote (n+m) x 1 vectors for the shaft stress and base stress intensities for pile no. 1, pile no. 2... etc., each representing a typical pile of different symmetrical groups.

$\{W_\ell\}$ and $\{\psi\}$ are s x 1 vectors for vertical displacements and the fictitious vertical stress on the surface of the rigid layer respectively.

$[KSP]^{11}$, $[KSP]^{1NP}$ etc. are (n+m) x (n+m) matrices.

$[KLP]^{1}$.... $[KLP]^{NP}$, $[KPL]^{1}$.... $[KPL]^{NP}$ are (n+m) x s and s x (n+m) matrices.

Equation (5.12) represents a set of NP x (n+m) + s linear algebraic equations which can be solved for rigid and compressible pile groups as shown earlier (Chapter 4). The solution for rigid or compressible pile groups embedded within an elastic half space (Butterfield and Banerjee, 1969b) can be obtained by substituting $\{\psi\} = 0$ in equation (5.12).

5.6 Notes on the computer programme for the analysis of pile groups

The computer programme and the associated 'procedures' developed for the theory in the preceding articles are described below. The listing of the computer programme and the procedures are given elsewhere (Banerjee, 1969).

'Procedures'

(i) Print array, Inp, Crout 2, Solve, Simpson, Mult, and Invert have been discussed in Chapters 3 and 4.

(ii) Issa: Calculates the coefficients $(KSS)^{p}_{ij}$ of equation (5.4).

(iii) Ibba: Evaluates the coefficients $(KBB)^{p}_{ij}$ of equation (5.5).

(iv) Isba: Calculates the coefficients $(KSB)^{p}_{ij}$ of equation (5.5).

(v) Ibsa: Calculates the coefficients $(KBS)^{p}_{ij}$ of equation (5.6).

The integrals involved in evaluating the various coefficients by using procedures (ii) to (v) listed above are proper integrals of continuous functions and are evaluated by using the procedure Simpson.

(vi) Copy: Copies a matrix A from a matrix B.

(vii) Cumadd: Adds a matrix A to a matrix B to form a new matrix A. This procedure is used to carry out a direct summation for coefficients for piles carrying the same load.

(viii) Single pile array: Calculates the matrix $[KS]$ (see Chapter 4).

(ix) Typical pile array: Calculates the coefficients $(KSP)^{1}_{ij}$ of equation (5.8) and $(KSP)^{pq}_{ij}$ (for $p = q$) of equation (5.10) by calling procedures Issa, Ibba, Isba, Ibsa, Copy and Cumadd.

(x) Inf another typ array: The coefficients $(KSP)^{pq}_{ij}$ (for $p \neq q$) of equation (5.10) are evaluated by the use of procedures Issa, Ibba, Isba, Ibsa, Copy and Cumadd.

(xi) Form Load array: Forms a (n+1) x NP load matrix for the group from the integration of the surface stress intensities. The loads are calculated at different section of the pile lengths for only one typical pile of each symmetrical group.

(xii) Displ array: Forms a (n+m). NP x 1 column matrix of pile displacements from the calculated loads at each pile section.

(xiii) Cap array: Calculates the coefficients $(KLL)_{ij}$ of equation (5.8) and (5.11), for a finite rectangular or square surface of the rigid layer.

(xiv) Inf on pile array: Calculates the coefficients $(KLP)^{1}_{ij}$ of equation (5.7) and $(KLP)^{p}_{ij}$ at the typical pile of p^{th} symmetrical group.

(xv) Inf on cap array: Evaluates the coefficients $(KPL)^{1}_{ij}$ of equation (5.8) and coefficients $(KPL)^{q}_{ij}$ due to the q^{th} symmetrical pile group.

(xvi) Form rigid layer: Assembles the sub-matrices $[KLP]^{1} \ldots [KLP]^{NP}$, $[KPL]^{1} \ldots [KPL]^{NP}$, $[KLL]$ to form a modified K-matrix for a pile group embedded with a finite elastic layer. For data input corresponding to a pile group embedded within an elastic half space this procedure and hence procedures cap array, Inf on pile array, Inf on cap array, is not used.

The main body of the programme calculates the various coefficients for a single pile (Chapter 4) and assembles the sub-matrixes $[KSP]^{1}$, $[KSP]^{pq}$ to form a K-matrix for a pile group within a half space. If a solution for a pile group within a finite elastic layer is desired it proceeds to modify the K-matrix using the procedures (xiii) to (xvi). The resulting system of simultaneous equation is then solved by Gaussian elimination.

5.7 Accuracy and convergence of the solution

The results described in this Chapter have been obtained by using 10 equal cylindrical segments over the pile-shaft surface and 5 annular rings over the base of the pile. The group analyses involve evaluation of the integrals for coefficients of the resulting system of equations, over the local and non local pile surfaces. The integrals over the local pile surfaces are identical to those involved in the analyses of axially loaded single pile and the numerical evaluation of these integrals has been discussed in Chapter 4. The intervals of integration necessary for accurate evaluation of the integrals over the non local pile surfaces are found to be dependent on the pile spacings. The Table 1 shows the minimum nonlocal intervals of integration required for the convergence of the solution by using 15 divisions of pile-soil interfaces of a four pile group (L/D = 20, H/L = ∞) at various spacings.

TABLE - 1

NO.	PILE SPACINGS S/D	INTERVALS OF INTEGRATION	
		FOR 180° IN θ_o-DIRECTION	SUB-INTERVALS IN α-DIRECTION
1	2.5	20	4
2	5	10	2
3	10	4	1

The use of the numerical quadrature No. 3 (Table, 1) to pile groups with S/D = 2.5 produced only 3% increase in the calculated load over that obtained

by using No. 1. Therefore the results described in this Chapter have been obtained by using this. Trial computations were carried out to test the stability of the system of simultaneous equations and the convergence of the results. It was observed that for a four-pile group (L/D = 20, S/D = 5) embedded within a half space the calculated loads for a given pile displacement by using 15 equations (10 for the shaft and 5 for the base) was about 2.6% lower than that obtained by 10 equations (8 for the shaft and 2 for the base) and 1% higher than that obtained by using 25 equations (20 for the shaft and 5 for the base). Hence the use of 10 equations for shaft surface and 5 for base area would appear to be a satisfactory compromise.

For the analysis of pile groups embedded within a finite elastic layer the selection of a finite surface area of the rigid layer is necessary. This area was found to be dependent on the width and breadth of the pile group as well as the depth of the layer. From a series of trial computations it was found that the width and breadth of the rigid layer surface may be approximated as the width of the pile group plus twice the depth of the layer and the breadth of the group plus twice the depth of the layer respectively. The results described in this Chapter were obtained by using 36 equations (i.e. 144 elements) to represent the finite rigid layer surface. A detailed discussion of the numerical evaluation of the integrals involved for the coefficients of these equations is given in Chapter 3.

5.8 Results of the analysis

The results of the analysis are presented in graphs showing the effects of the different parameters that may be considered to affect the load-displacement behaviour of axially loaded pile groups in an ideal elastic sub-soil are as follows:

(i) Number of piles and arrangement of the piles in the group

(ii) The length to diameter ratio of the piles in the group

(iii) The spacing to diameter ratio

(iv) The Poisson's ratio of the soil

(v) The compressibility of piles

(vi) The ratio of the thickness of the elastic layer to the length of the piles.

It is impracticable to undertake an exhaustive evaluation of the relative effects of all the variables listed above, therefore some typical cases of 2, 3, 5, 6 and 7 pile groups and square groups of 4, 9, 16, and 25 piles are considered below. The solutions are given for $\mu = 0.5$ cases which are thought to be appropriate for calculating the immediate settlement of pile groups in saturated clay.

The settlement ratio (R_S) is a commonly used parameter for describing the settlement of a pile group. It is best defined as the ratio of the settlement of a group to the settlement of a single pile carrying the same average load as a pile in the group.

Figures (5.2) to (5.11) refer to pile groups embedded within a half space. Figures (5.2) and (5.3) give the settlement ratio for groups of (N) compressible piles (N = 2, 3, 4) under a rigid cap for L/D ratios of 20 and 40 and λ values of 6000 and ∞ plotted against various S/D ratios. The curves for a rigid pile ($\lambda = \infty$, Figure, 5.2) are very similar to those given by Poulos (1968b). The settlement ratio of longer piles ($L/D \approx 80$) is about 50% higher than that for shorter piles ($L/D \approx 20$). Whereas R_S is strongly influenced by L/D and S/D ratios, the effect of λ is seen to be small for all groups with the exception of groups of longer piles. The settlement ratio for longer piles is influenced by both λ and (S/D) ratios, which makes the principle of superposition as used by Poulos (1968b), not applicable to compressible piles.

TABLE 2

$L/D = 25$, $\mu = 0.5$, $S/D = 2.5$, $H/L = \infty$

Type of group	2^2	3^2	4^2	5^2
R_S (Poulos, 1968b) $\lambda = \infty$	2.69	4.88	7.35	10.10
R_S (present analysis) $\lambda = \infty$	2.66	4.95	7.30	9.90
$\lambda = 6000$	2.48	4.50	6.72	9.28

TABLE 3

$S/D = 2.5$, $L/D = 25$, $\mu = 0.5$, $H/L = \infty$

Type of group	Pile no.	P/P_{av} (B) $\lambda = \infty$	P/P_{av} (A) $\lambda = \infty$	$\lambda = 6000$
3^2	1	1.520	1.510	1.380
	2	0.740	0.750	0.760
	3	0.050 (tension)	0.060 (tension)	0.120
4^2	1	2.020	2.020	1.840
	2	0.960	0.965	0.965
	3	0.050	0.044	0.180
5^2	1	2.580	2.520	2.300
	2	1.180	1.190	1.190
	3	1.160	1.160	1.141
	4	0.010	0.048	0.145
	5	0.010	0.106	0.119
	6	0.190	0.095	0.095

TABLE 4

Values of the settlement ratio (R_S)

$L/D = 25$, $\mu = 0.5$, $\lambda = \infty$

S/D \ H/L		∞	5	2.5	1.5	1.2
2.5	A	4.95	4.50	4.20	4.00	3.70
	B	4.88	4.45	4.30	3.48	2.54
5	A	3.82	3.70	2.90	2.60	2.05
	B	3.74	3.27	3.05	2.30	1.75
10	A	2.81	2.51	2.20	1.70	1.55
	B	2.73	2.20	1.98	1.48	1.27

Curves showing both the load-displacement behaviour and the individual pile load sharing of larger groups of compressible piles under a rigid pile cap are presented in Figures 5.4 to 5.10. A standard close spacing of S/D = 2.5 has been adopted throughout in order to indicate the likely worst case values of R_S.

Figure 5.4 shows the value of P/GWD plotted against L/D ratio for compressible symmetrical pile groups of 2, 3 and 4 piles. The effect of compressibility is negligible for piles with L/D $\approx$ 20 and also for piles with L/D = 40 has only a small effect on the overall load-displacement response. Figures (5.5) to (5.10) refer to the results of general pile groups. Variation of λ is seen to have considerable effect on the load distribution between the piles within the group but a much smaller effect on the load displacement behaviour. A reduction in λ from ∞ to 6000 produces about a 10% reduction in R_S (Table 2), whereas the individual pile load sharing pattern changes drastically. As λ decreases the load carried by the internal piles in a group (Figures, 5.5 to 5.10) increases although the contribution of these piles in 4^2 and 5^2 groups (Figures, 5.9 and 5.10; Table, 3) is still generally less than 10% of that of the outer piles.

Tables 2 and 3 show a comparison between the numerical results obtained from the present analysis (A) and the analysis (B) described by Poulos (1968b). It can be seen that while both methods give identical results for rigid pile, the settlement of compressible pile is over-estimated in Poulos's analysis.

The results of 3^2 and 5^2 groups embedded within a half space are summarised in Figure (5.11) in which the settlement ratios are plotted against S/D. The length to diameter ratio and the compressibility of longer piles appears to have strong influence on the settlement behaviour

of larger groups.

The effect of the presence of a rigid layer on the settlement ratio of a 3^2 pile group is shown in Table 4. As might be expected the effect of the rigid layer is to reduce the interaction between the piles, particularly at larger spacings. The results of the present analysis (4) are also compared with the approximate analysis (B) of Poulos (1968b) obtained by the use of Steinbrenner's approximation for vertical displacement (Steinbrenner, 1934). It can be seen that the both methods give results within 15% in all but thinner layers (H/L = 1.5, 1.2). While Poulos's analysis is likely to improve in accuracy for thicker layers but become increasingly inaccurate for shallower layers, the present analysis follows the opposite trend. It is, however, possible to increase the accuracy of the present analysis by considering more elements to represent larger areas of the rigid layer, at the expense of increased computer storage and computing time.

5.10 Comparison between the theoretical and model test results

The applicability of the foregoing theoretical analysis to the design of free standing pile groups can be investigated by comparing the theoretical results with the laboratory and full scale tests on such groups. Results of tests on laboratory models have been reported by Whitaker (1957, 1960), Sowers et al (1961), Saffery and Tate (1961), Hanna (1963), while Berezantzev et al (1961) described full scale tests on pile groups. Because the depth of the soil layer and the length to diameter ratio of piles varies in each case the test results have been compared with the theoretical results corresponding to appropriate H/L and L/D ratios. Unfortunately in most cases the authors (Whitaker 1957, 60; Sowers et al, 1961; Saffery and Tate, 1961) adopted a different and much less satisfactory definition of the settlement ratio, which causes considerable confusion in interpreting

their results. The Poisson's ratio has been assumed to be 0.5 throughout, as it has a negligible effect on the value of settlement ratio.

Comparison with Whitaker (1957, 1960)

Whitaker (1957, 1960) carried out a large number of small scale model tests on pile groups driven in remoulded London Clay of undrained cohesion of about 0.6 to 1.3 lbs/sq in. The model piles were 1/8 inches diameter brass rods with tips formed to 60^{o} cones, the top ends being plane. The pile caps were designed to permit the piles to be driven singly in any order to form a group by pushing them through a template. The cap was essentially rigid and remained above the soil surface throughout the test. The effects of variation of length to diameter ratio and spacing to diameter ratios on the settlement, ultimate bearing capacity were studied. These results are compared with the theoretical results in Figures 5.12 to 5.15. The depth of the soil layer was not specified by Whitaker but from the photograph of the general arrangement of the testing rig it would appear that the soil bin was probably 9 inches deep. Hence for L/D = 24 and 48, H/L is assumed to be 3 & 1.5 respectively. The brass piles may be considered to be rigid compared to the soft remoulded clay.

The experimental results show considerable scatter. The theoretical settlement ratios are in good agreement with the mean experimental results (Figures, 5.12 and 5.13) for L/D = 48 but the theoretical results for L/D = 24 are about 20% higher than the mean experimental results. The discrepancy is likely due to the definition of the settlement ratio which Whitaker defined as the settlement of a pile group to the settlement of single pile at half the ultimate load for each. Without the load-displacement curves of single piles it has not been possible to modify the experimental results according to the definition of settlement ratio

in the present analysis. Figures 5.14 and 5.15 show the load sharing between the piles within the pile group of half the ultimate load, compared with the theoretical results which are not very sensitive to small variations of L/D (between 16 and 24) and H/L (between 2 to 4). The theoretical results suggest that the corner piles may take about 2 to 3 times the average load per pile whereas the central pile takes negligible load at close spacing. The experimental results of Whitaker show a more uniform load distribution than that predicted by the theory.

Comparison with Sowers et al (1961)

Sowers et al (1961) described a series of model tests on groups of 1/2 in and 1.21 in diameter piles driven into a mixture of commercial bentonite clay and water of uniform composition, high plasticity and permeability. Before each test the soil was remoulded and then the group was forced into place. An isolated single pile was also pushed into the same soil to provide a standard for comparison. The group and the single pile were then tested after 7 days.

For the purpose of comparison with the theory the piles have been considered to be rigid. The theoretical settlement ratios are compared with the experimental values at half the ultimate loads in Figure (5.16). The ultimate bearing capacity of smaller groups of 2 and 4 piles were nearly equal to that of an isolated single pile. Hence the present definition of settlement ratio applies to these results for smaller groups. But for larger groups the average load per pile at half the ultimate group load is lower than half the ultimate load in the single pile. Hence the theoretical results are within 10% of the mean experimental results for smaller groups. However for larger groups of 9 and 16 piles the theoretical results are about 30% higher than the mean experimental results. The load-displacement curves for isolated single piles are not available,

therefore the results for larger groups cannot be modified to suit the present definition of settlement ratio. The load sharing between different piles within a 3^2 pile group is shown in Figure (5.14) in which the results from Whitaker (1957) are also presented. The results of Sowers et al appear to agree well with the theoretical results for pile no. 2, but for pile no. 1 the theoretical results are about 10% higher, and for pile no. 3 the theoretical results are about 20% lower. The results of load distribution obtained by Whitaker (1957) are considerably more uniform than both those obtained by Sowers et al and those predicted by the theory.

Comparison with Saffery and Tate (1961)

Saffery and Tate carried out a series of model tests on groups of 1/4 inch diameter stainless steel piles with toes formed to a 60° cone, driven into soft remoulded London Clay. They studied the effect of eccentricity on the ultimate bearing capacity and settlement of 3^2 pile groups. The remoulded clay bed was formed in a cylindrical container in four to five layers each three inches deep.

Figure (5.17) shows a comparison between the theoretical settlement ratio and the experimental values at half the ultimate loads. The theoretical results have been obtained by assuming $\lambda = \infty$, appropriate for rigid pile. The thickness of the layer probably lies between 12 inches to 15 inches, hence for a pile of L/D = 30, H/L has been chosen to be 1.8. The settlement ratios are in good agreement with the theoretical results for H/L = 1.8 but are about 10% lower than the theoretical values, which might have been again due to the difference in the definition of the settlement ratios. The theoretical result for $H/L = \infty$ is also shown in the same figure to emphasise the effect of the presence of the rigid layer on the interaction between the piles.

Comparison with Hanna (1963)

Hanna (1963) described a series of model tests on groups of 0.367 in diameter wooden piles driven into loose and dense sand. The load-displacement characteristics and ultimate bearing capacity of pile groups of square and rectangular arrangement were studied. The L/D and H/L ratios were about 30 and 3 respectively. The value of λ for wooden piles in sand has been assumed as 6000, the theoretical solutions, however, are not very sensitive to λ for the pile length under consideration.

The theoretical settlement ratios for S/D = 2.3 and 4.6 of square groups of 4, 9, 15 and 25 piles are compared with the corresponding experimental results for groups in dense sand and loose sand respectively (Figure 5.18) for a factor of safety (F_S) of 2 on single pile. The theoretical results are lower than the corresponding laboratory test results for dense sand and higher than the test results for groups in loose sand, but are within 15% of the mean experimental results for dense sand and loose sand for a given spacing of piles. The theoretical analysis, presented takes no account of the factors such as the order of driving the piles, layering of the soil profile, the difference in the changes in the soil properties caused by driving a single pile and a pile group. From Figure (5.18) it is apparent that there may have been more compaction or loosening due to driving a pile group than that due to driving a single isolated pile.

Comparison with Berezantzev et al (1961)

Berezantzev et al (1961) described a series of full scale tests on groups of 4, 5, 9, 16 and 25 piles. The piles were 28 cm diameter 5.6 metres long and driven into fine dense sand. His load-displacement curves are replotted in Figures (5.19) and (5.20). The piles are considered to be rigid.

The theoretical results for pile groups within a half space are compared with the settlement ratios calculated from the experimental load displacement curves for pile groups and isolated piles (see Figures, 5.19 and 5.20) in Figure (5.21). The experimental results are generally within 15% of the theoretical predictions and are higher, which follows the same trend as the comparison of theoretical results with Hanna (1963). This is obviously due to the fact that the volume expansion caused by driving a pile group is higher than that caused by an isolated pile, driven in dense sand.

From the foregoing comparison between the theoretical and the experimental results it may be concluded that the analysis described in this Chapter is not only capable of predicting the general trend of pile group behaviour but is also capable of predicting the group settlement, which is of primary importance in the design of pile groups. It should be emphasised that this analysis is only applicable to free-standing pile groups i.e. no allowance has been made for the action of a pile cap contacting the ground. This is examined in the next Chapter.

Application of the present analysis directly to pile groups in practice would involve the assessment of the three elastic parameters, G, μ and Ep, of which the determination of G and μ for appropriate field conditions is very difficult. Soils exhibit stress-strain relations which are often curved throughout their entire length. The variable and seemingly unpredictable stress-strain properties of soils preclude the selection of proper elastic moduli. However, these uncertainties can be overcome by calculating the value of G from the load-displacement curves of isolated single piles which are approximately linear upto the working loads (see the load-displacement curves of Whitaker and Cooke, 1966) assuming μ, since the values of the settlement ratio are insensitive to the value of μ. The settlement ratios plotted in Figure, (5.21) have been calculated using this method.

5.11 Conclusions

An elastic analysis of free-standing pile groups of arbitrary spacing is presented. Solutions have been obtained for the load distribution in a pile group under a rigid floating cap and also its settlement. The effects of the various parameters L/D, S/D, H/L and group size on the settlement and load distribution are studied. The major conclusions may be summarised as follows:

(i) The settlement ratios of pile groups are strongly influenced by the ratios of length to diameter, spacing to diameter, thickness of the elastic layer to the length of pile and the number of piles in a group and their arrangement.

(ii) The compressibility of piles has a relatively negligible effect on the settlement ratio of groups of short piles ($L/D \leq 20$), whereas for groups of longer piles ($L/D = 80$) the compressibility may reduce the settlement ratio by as much as 40%.

(iii) The corner piles of a group under a rigid floating cap carry 2 to 3 times the average load per pile in a group and the piles at the centre of a group carry virtually no load. The load distribution between the piles in a group is very strongly affected by the pile compressibility. With increase in pile compressibility the load distribution approaches a more uniform distribution, but with the corner piles still taking the maximum load.

(iv) The settlement ratio of a 25 pile group may be as high as 12 at $S/D = 3$, $L/D = 48$, $H/L = \infty$ and $\lambda = \infty$ which emphasises the importance of accurate evaluation of settlement in pile group design.

(v) The presence of a rigid layer reduces the interaction between the piles particularly at larger spacings, e.g. for 3^2 pile group ($L/D = 25$, $\lambda = \infty$) embedded within a half space the settlement ratio at $S/D = 10$ is 2.81 against the settlement ratio of 1.70 for the same pile within a finite layer ($H/L = 1.5$).

(vi) The presence of a rigid layer beyond $H/L = 5$ for a 3^2 pile group has only small ($< 10\%$) influence on the settlement ratio.

(vii) For a pile group of a given width and breadth the settlement ratio is almost independent of the number of piles in a group (for S/D between 3 and 10). Hence it is more economical to use less number of piles at large spacings than to use a large number of piles at close spacings.

(viii) Comparisons between the theoretical and experimental results reveal that theoretical method is capable of predicting the settlement of any pile group, using the elastic parameters obtained from field tests on an isolated single pile.

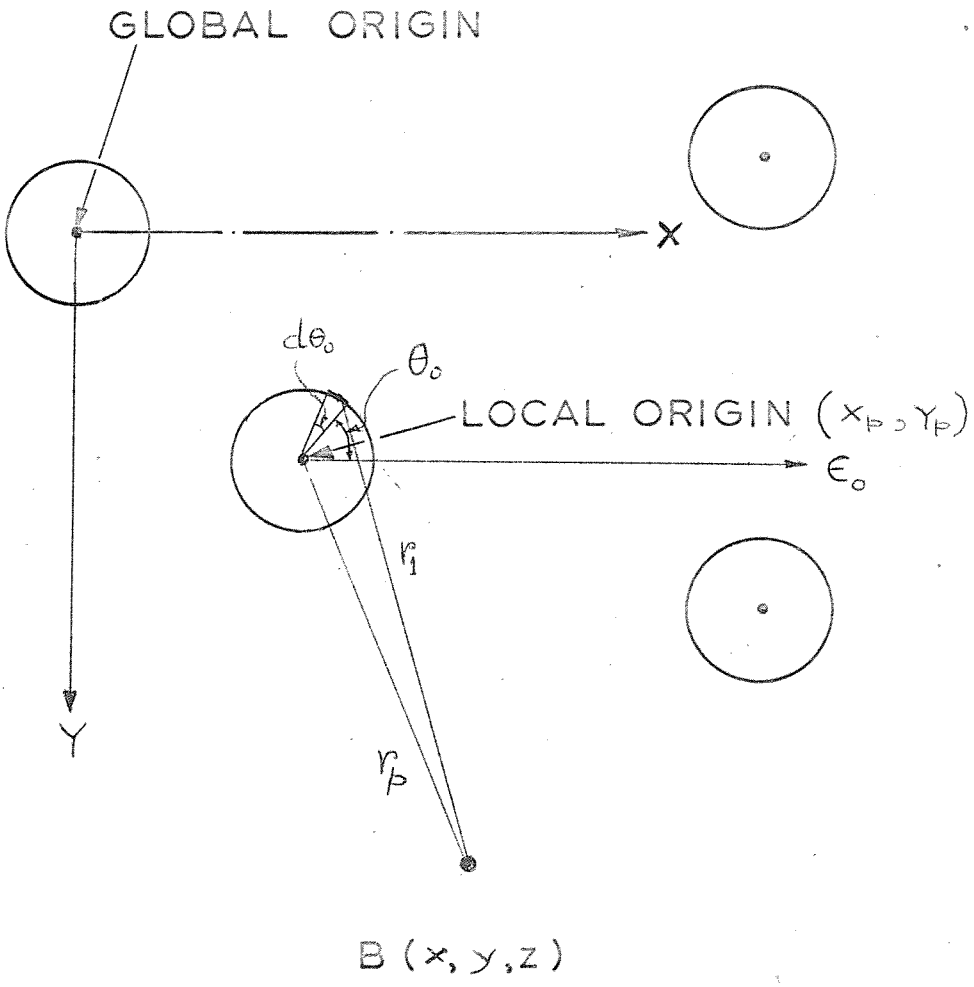

FIGURE - 5.1

PILE GROUP COORDINATE SYSTEMS

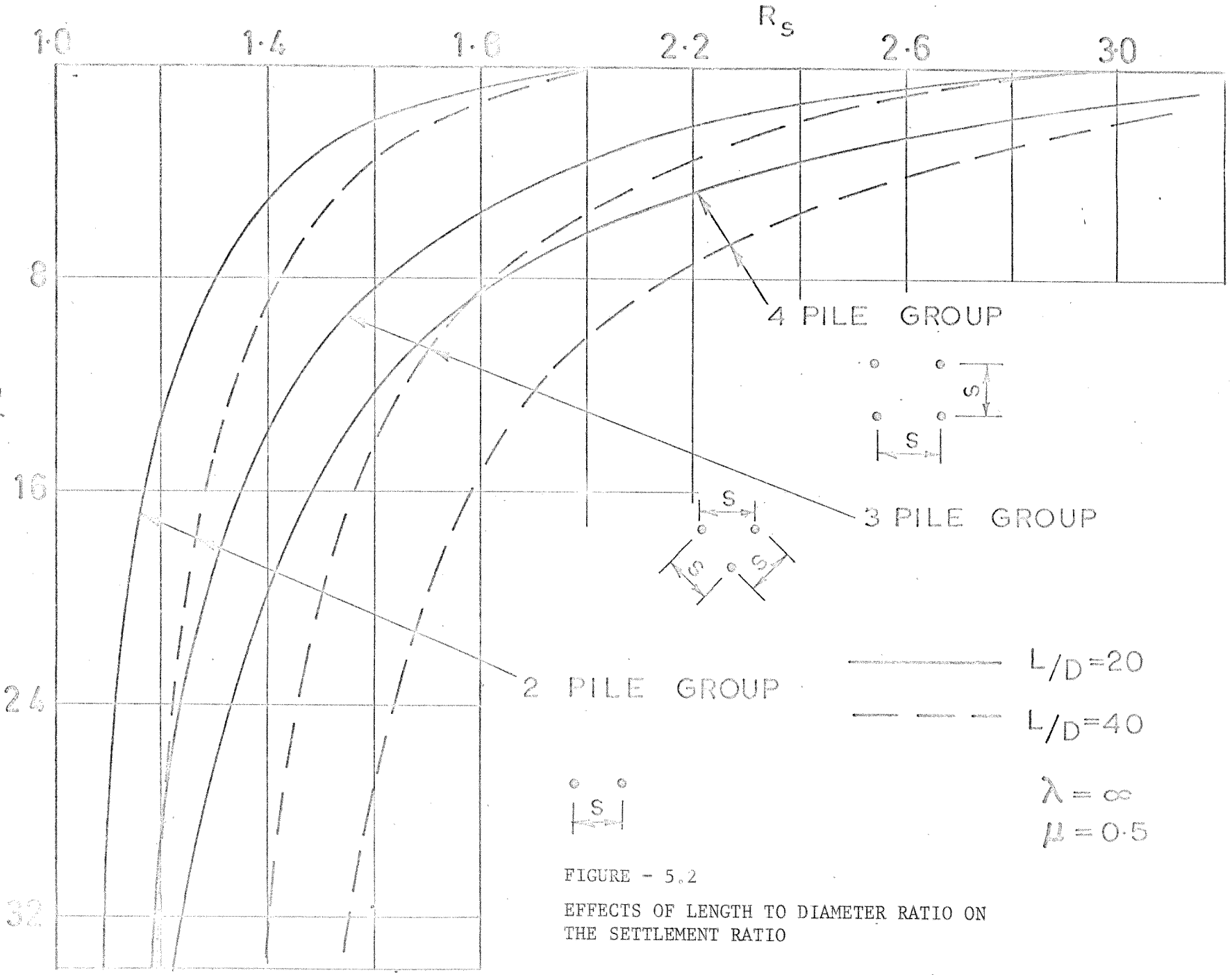

FIGURE - 5.2

EFFECTS OF LENGTH TO DIAMETER RATIO ON THE SETTLEMENT RATIO

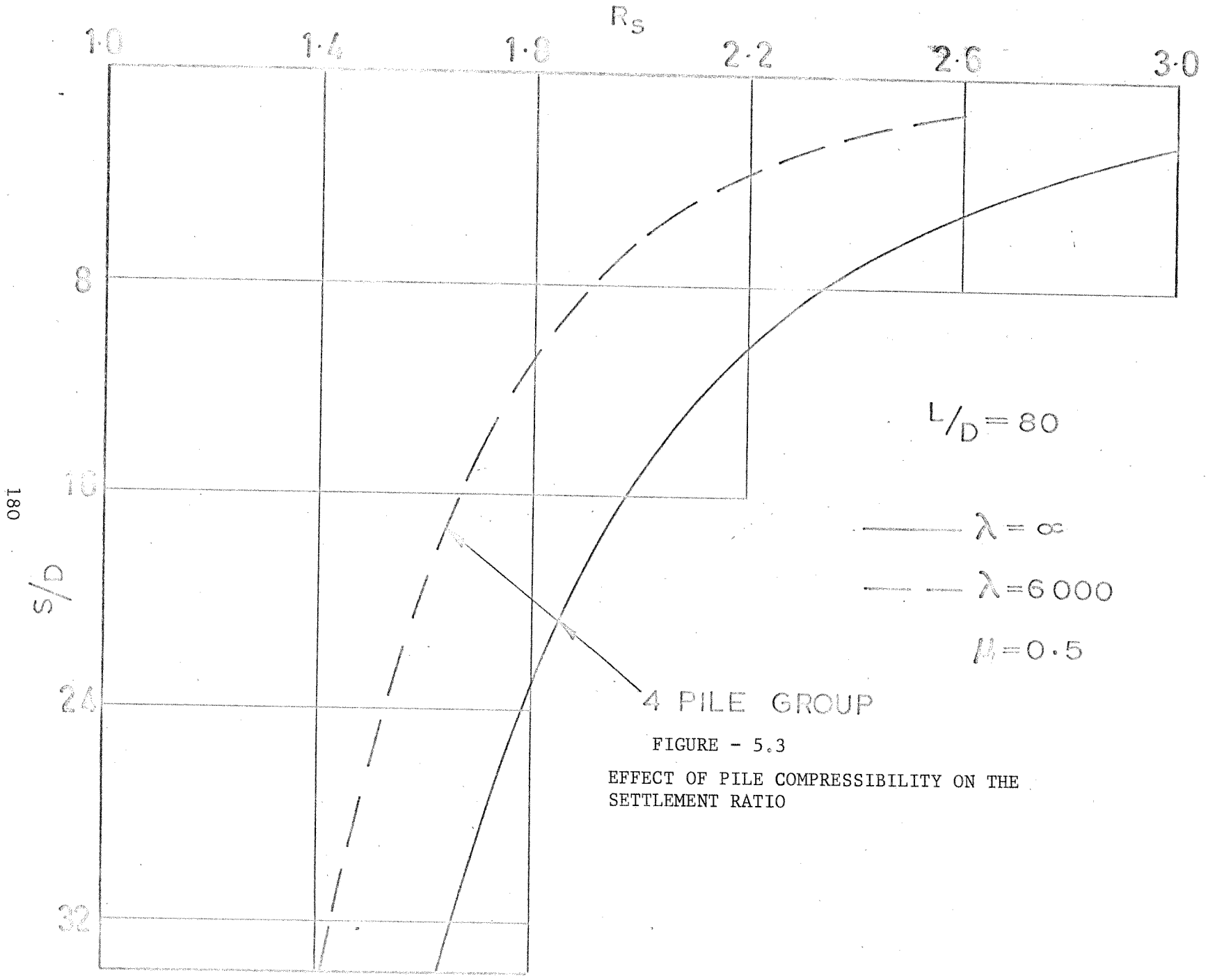

FIGURE - 5.3

EFFECT OF PILE COMPRESSIBILITY ON THE SETTLEMENT RATIO

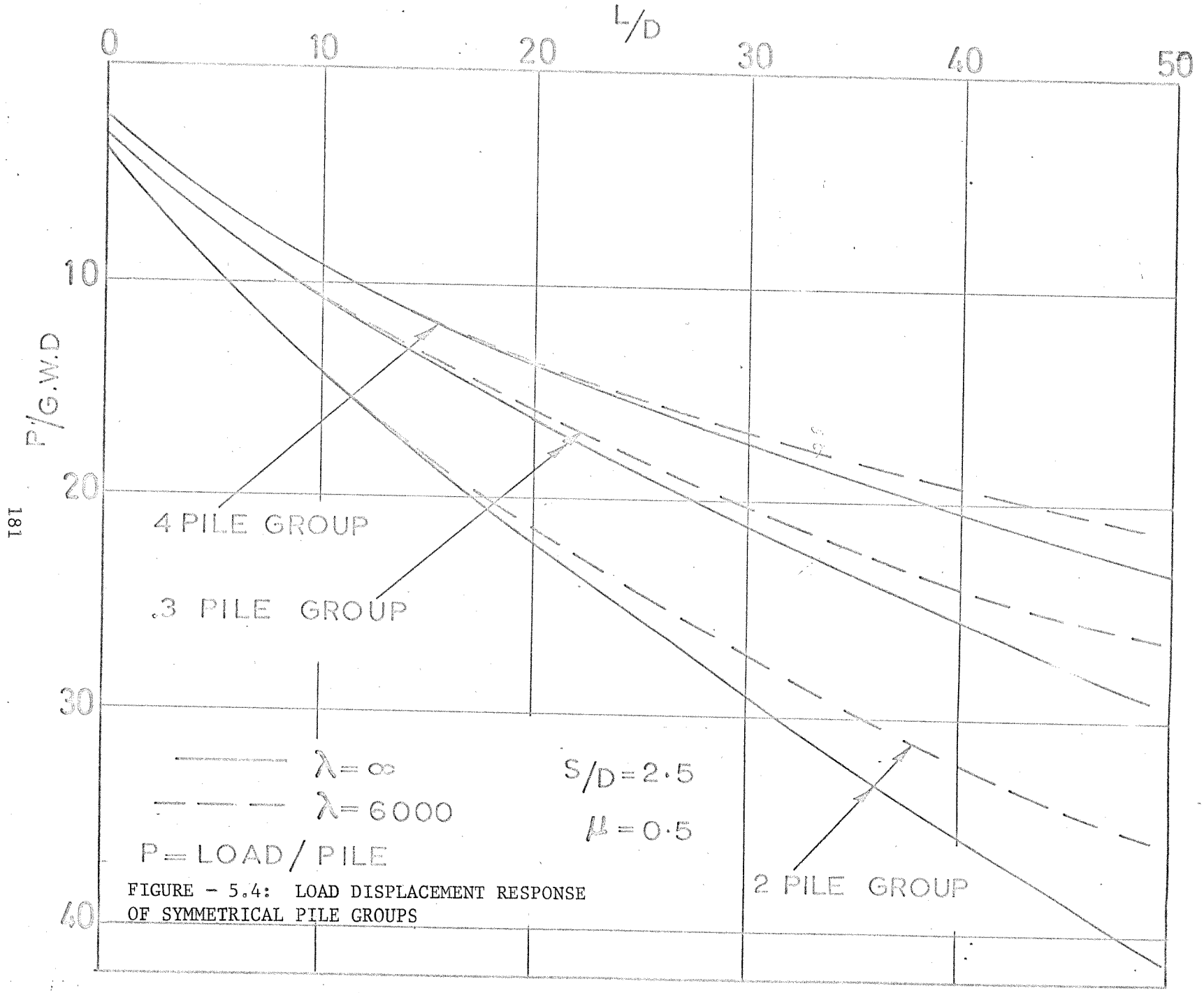

FIGURE - 5.4: LOAD DISPLACEMENT RESPONSE OF SYMMETRICAL PILE GROUPS

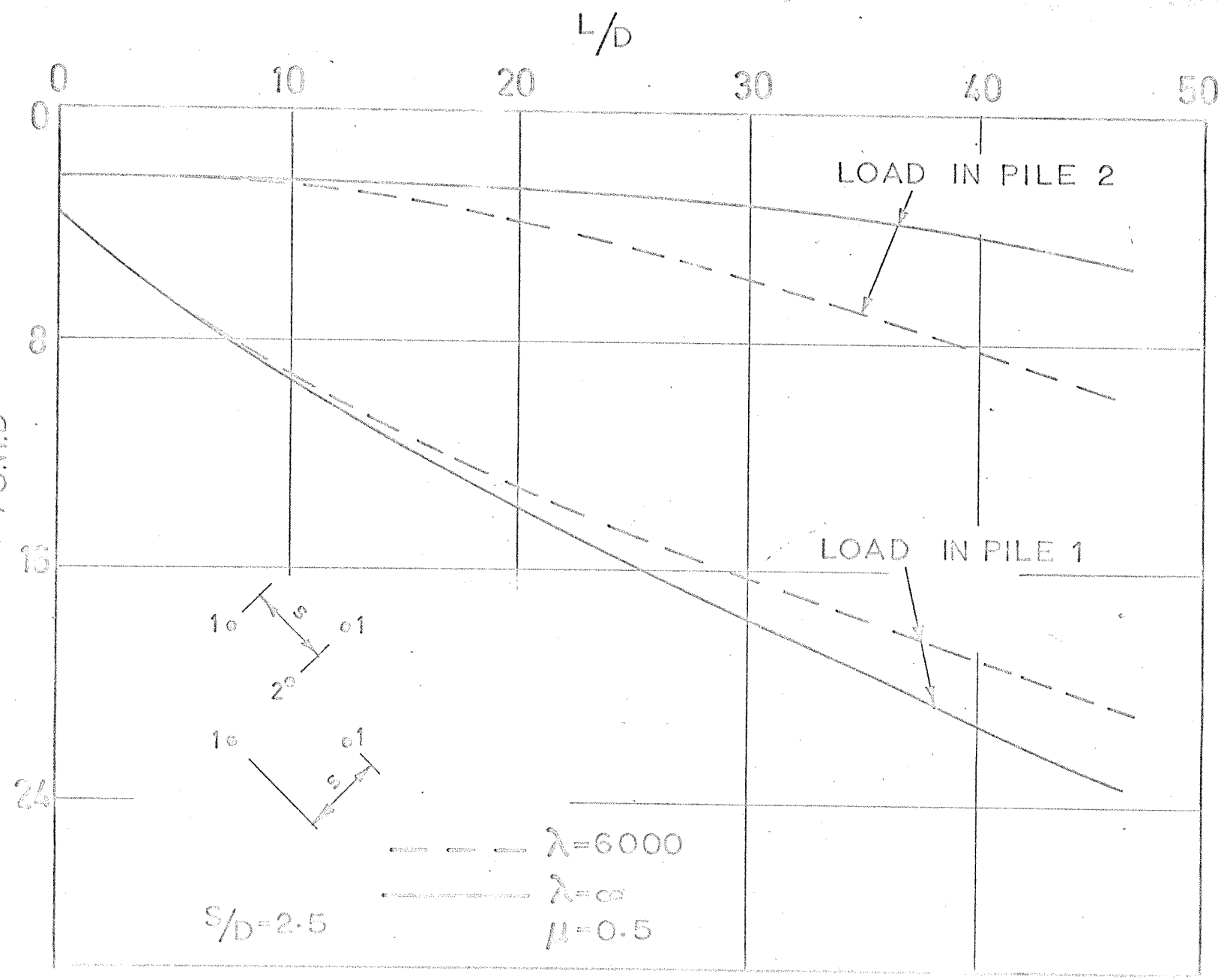

FIGURE - 5.5: DISTRIBUTION OF LOAD WITHIN A 5-PILE GROUP

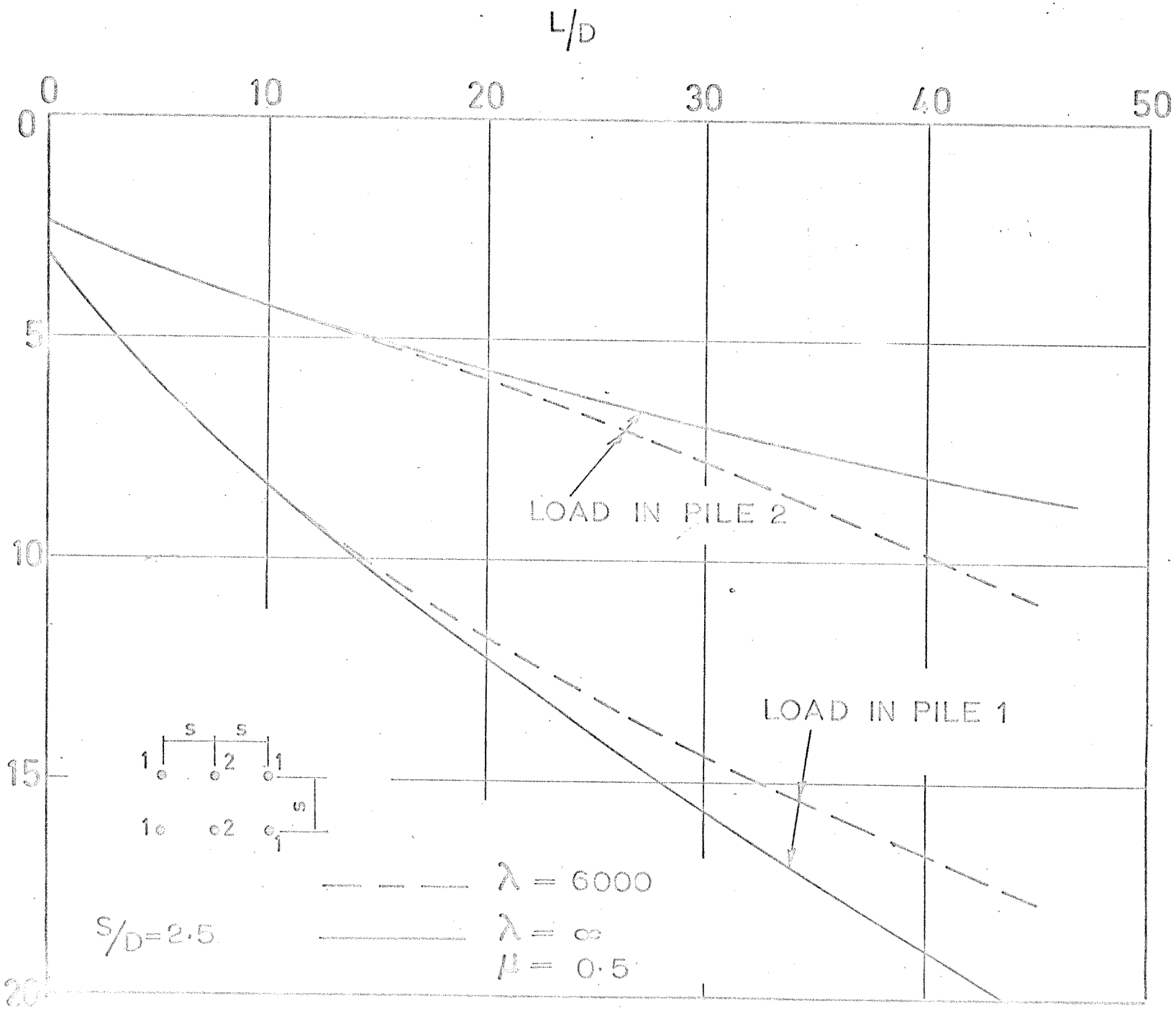

FIGURE - 5.6: DISTRIBUTION OF LOAD WITHIN A 6-PILE GROUP

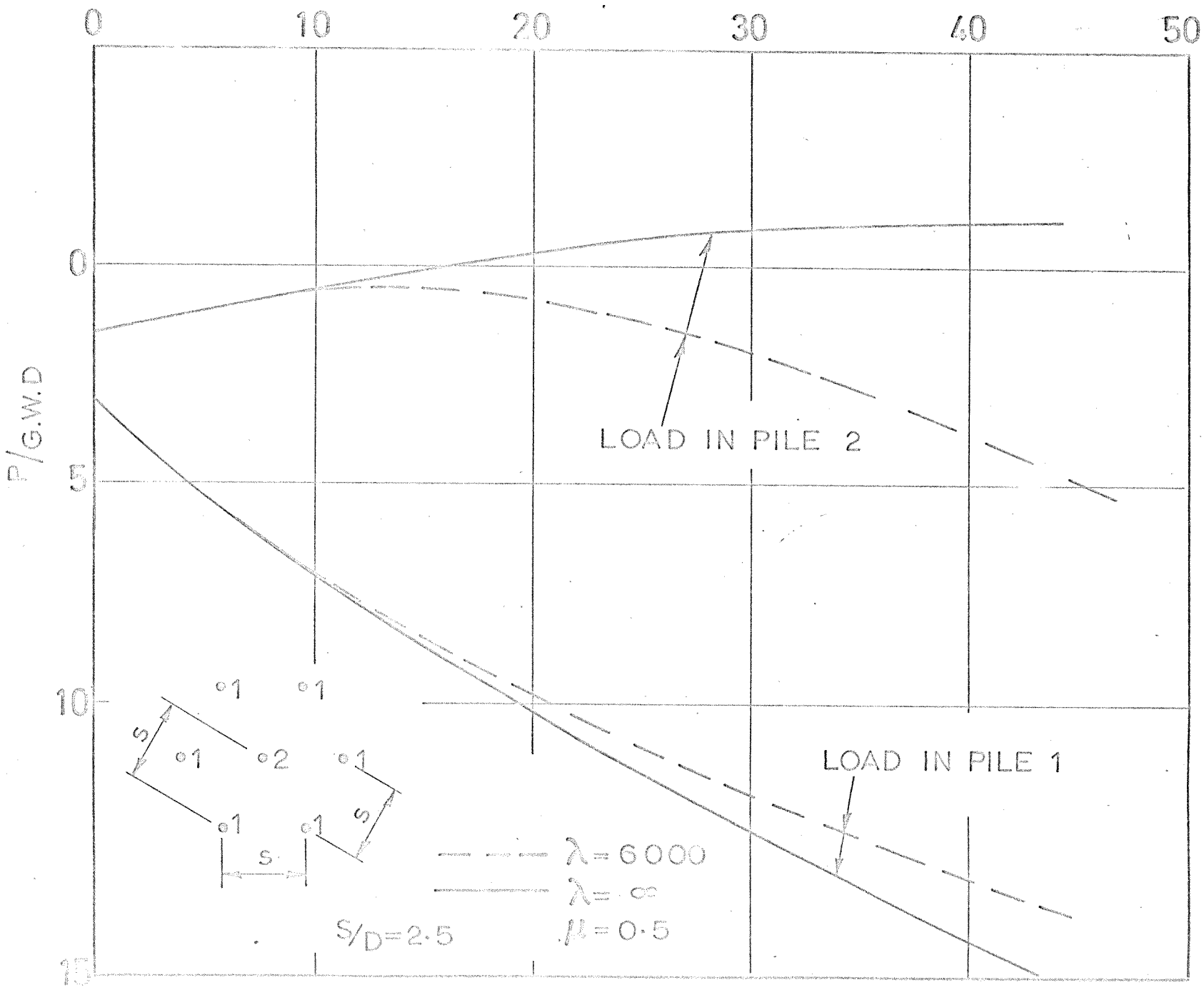

FIGURE - 5.7: DISTRIBUTION OF LOAD WITHIN A 7-PILE GROUP

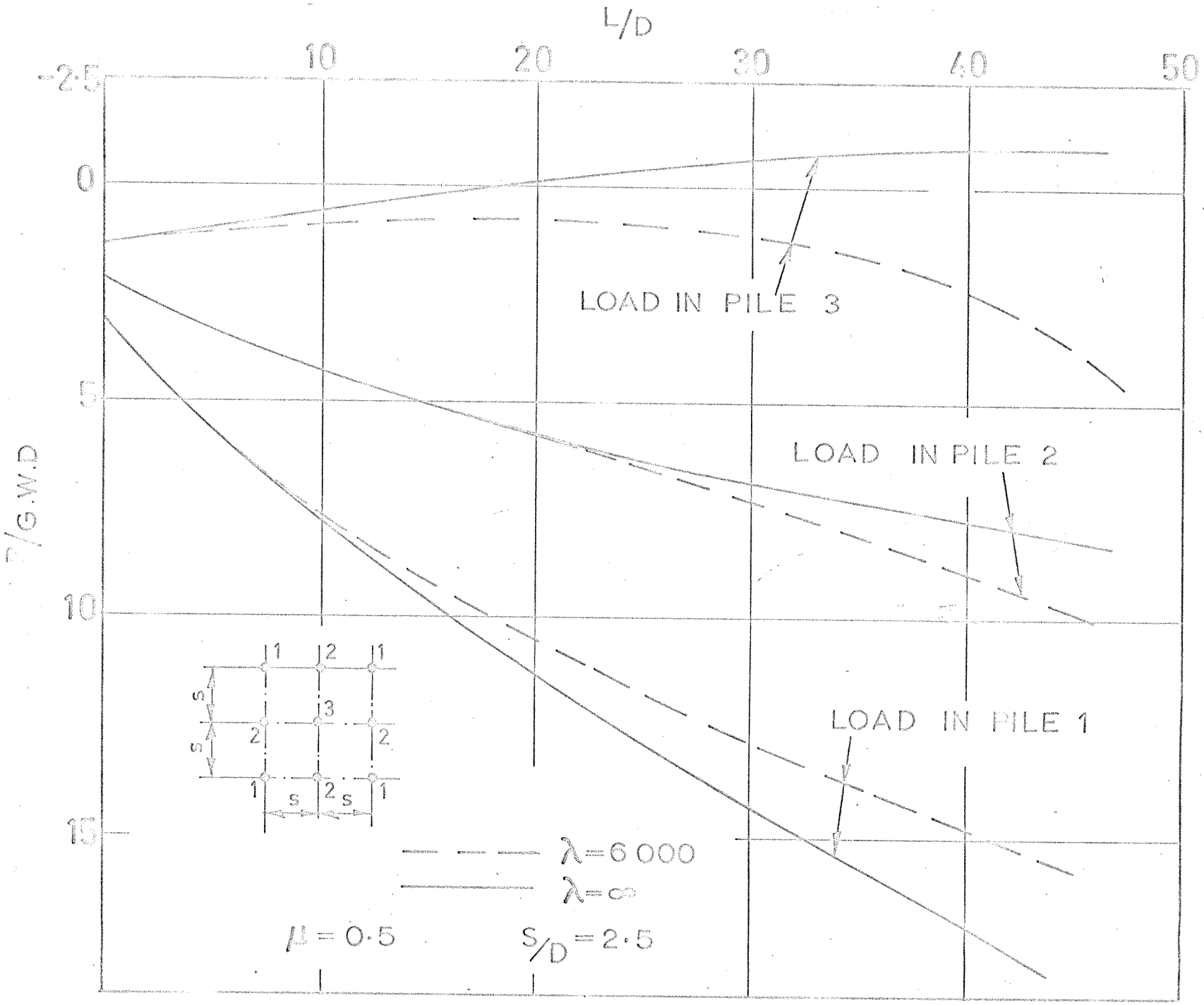

FIGURE - 5.8: DISTRIBUTION OF LOAD WITHIN A 3-SQ. PILE GROUP

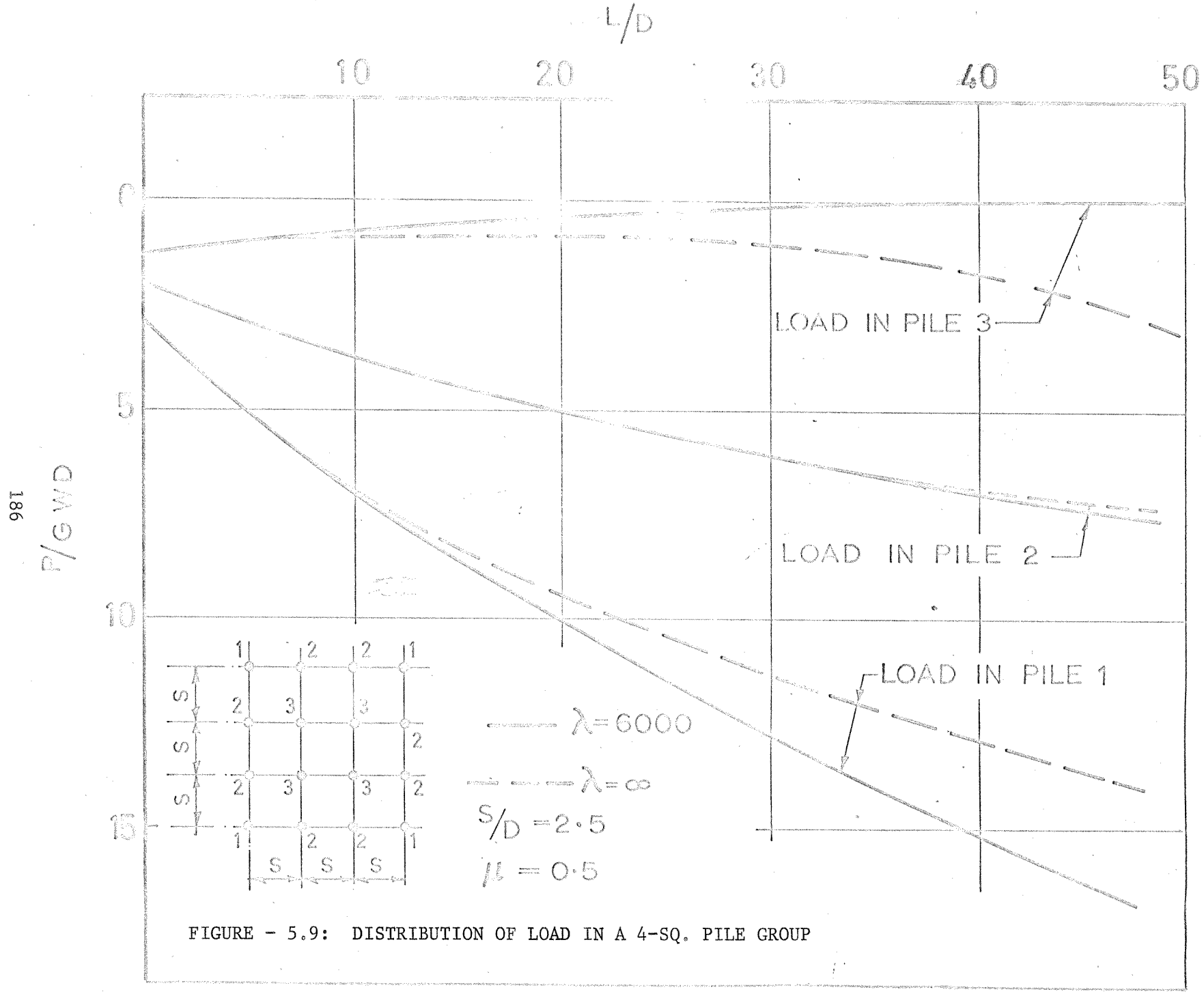

FIGURE - 5.9: DISTRIBUTION OF LOAD IN A 4-SQ. PILE GROUP

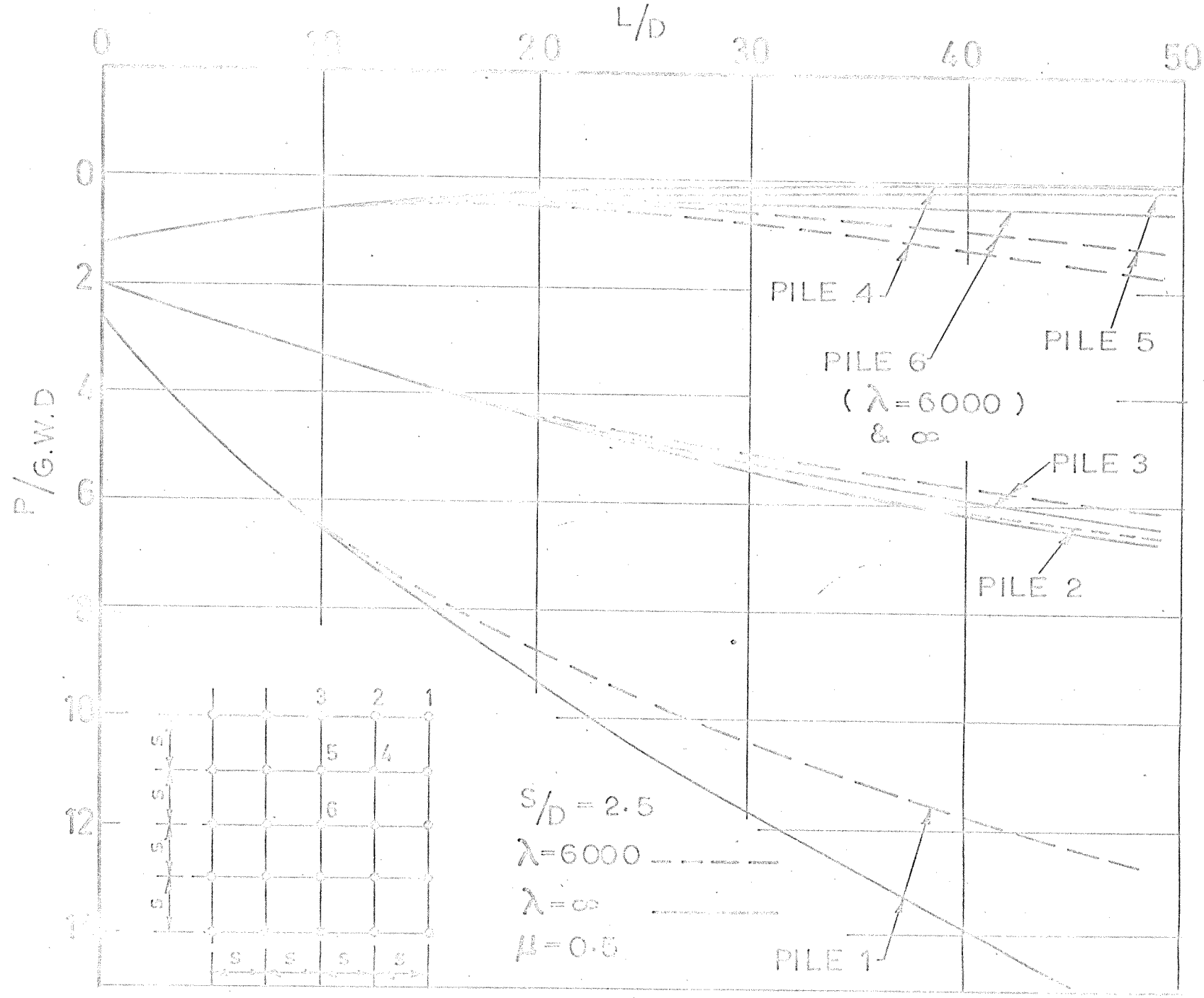

FIGURE - 5.10: DISTRIBUTION OF LOAD WITHIN A 5-SQ PILE GROUP

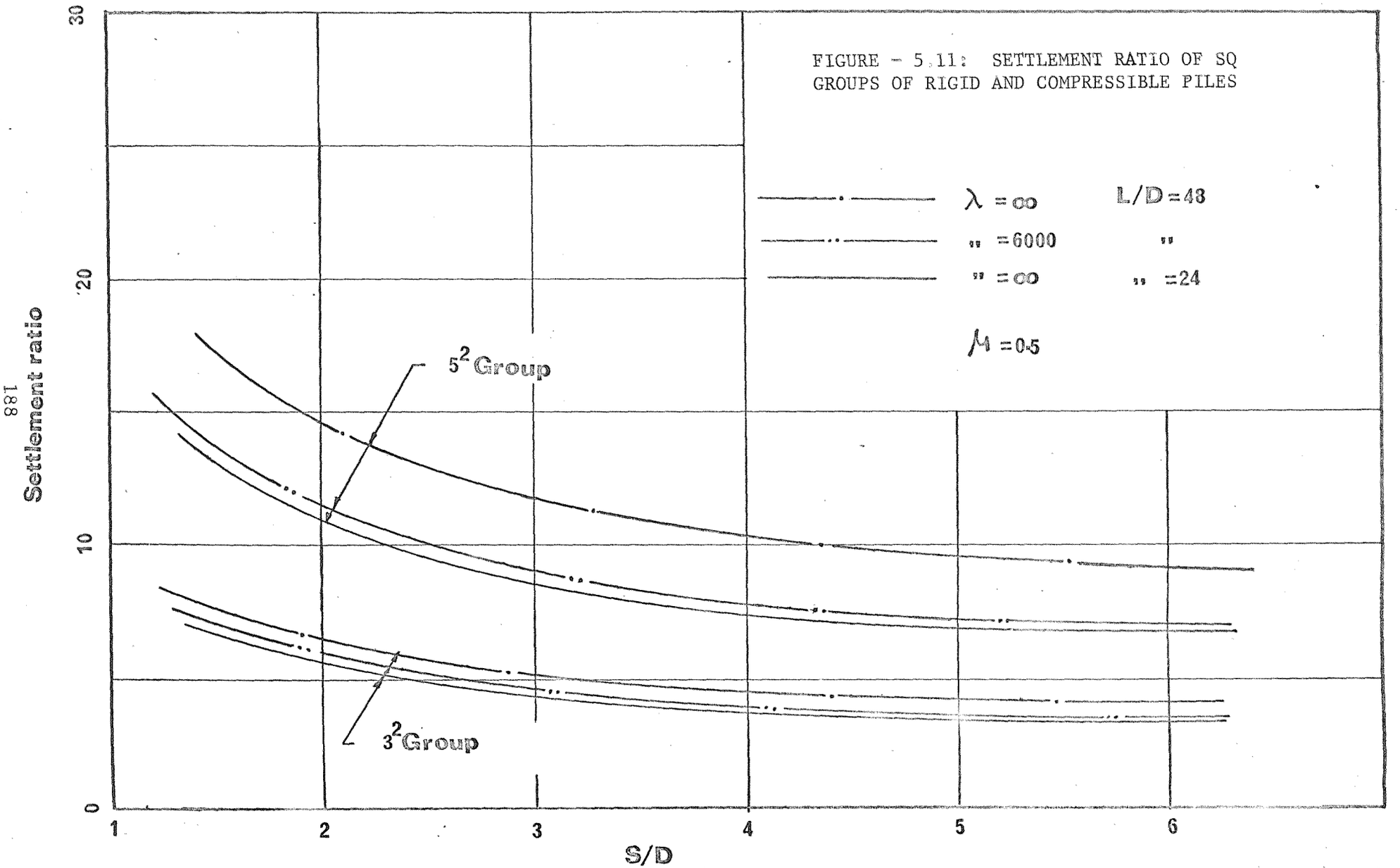

FIGURE - 5.11: SETTLEMENT RATIO OF SQ GROUPS OF RIGID AND COMPRESSIBLE PILES

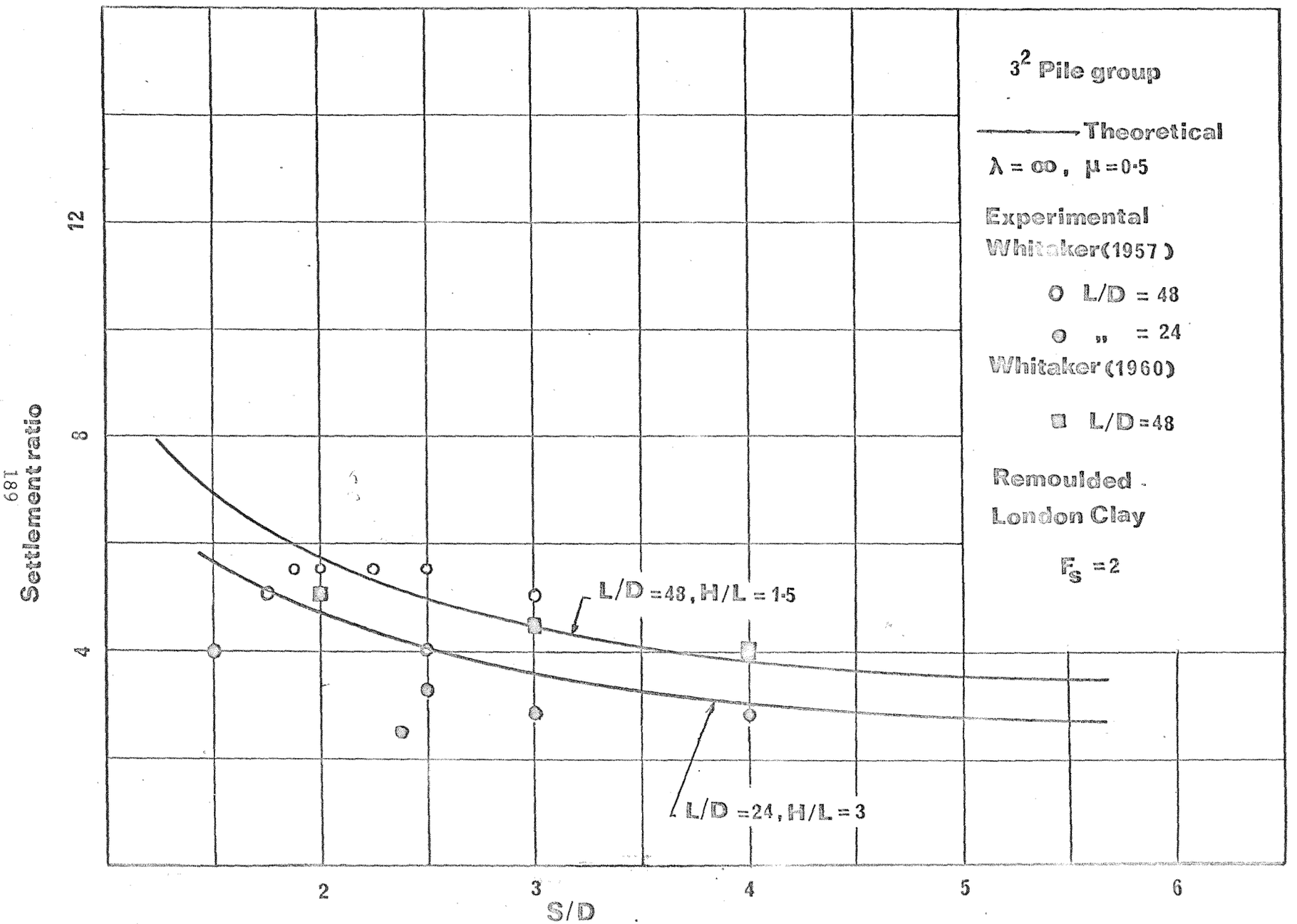

FIGURE - 5.12: COMPARISON WITH THE EXPERIMENTAL RESULTS FOR 3-SQ PILE GROUP (WHITAKER, 1957, 1960)

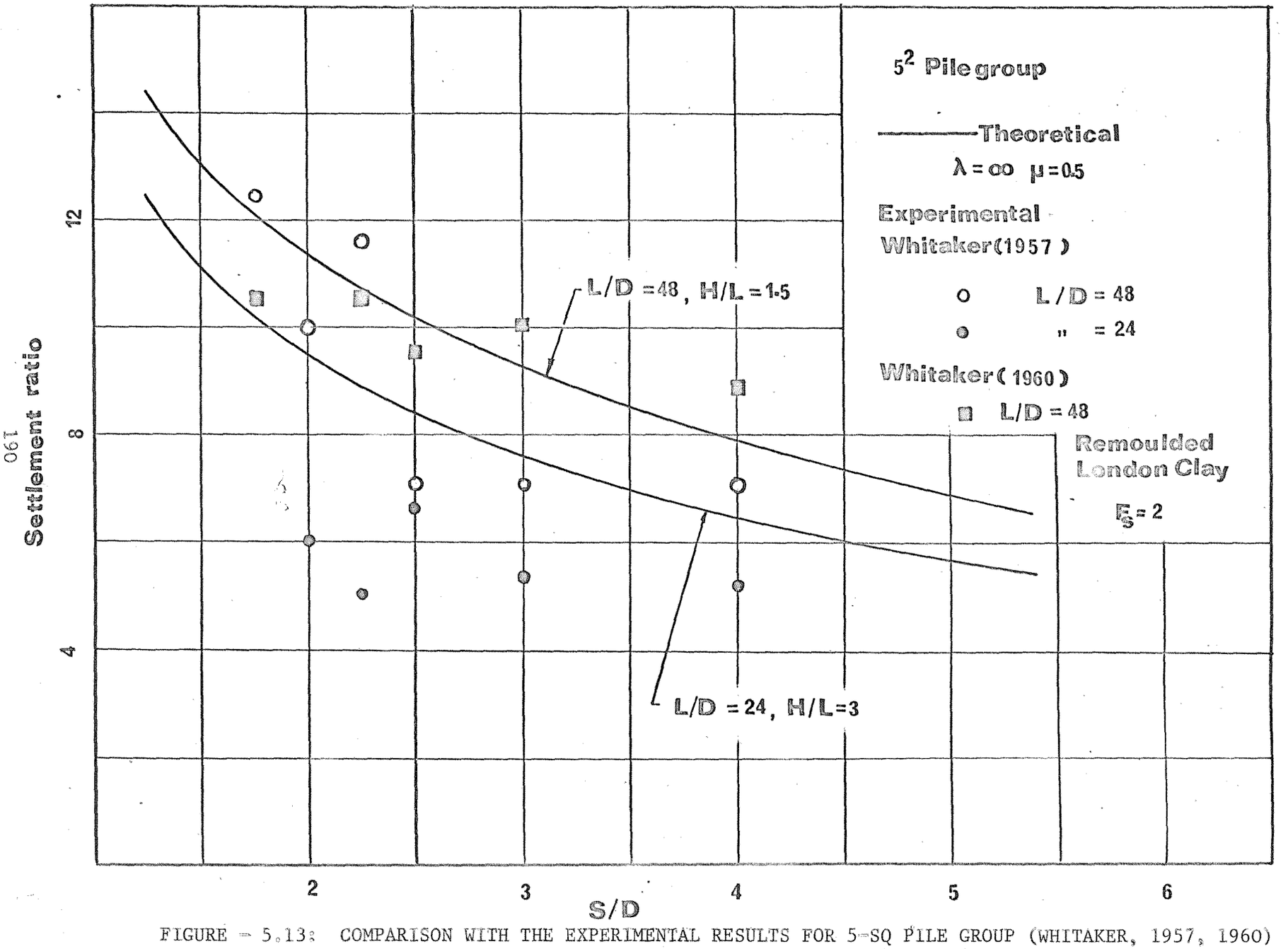

FIGURE - 5.13: COMPARISON WITH THE EXPERIMENTAL RESULTS FOR 5-SQ PILE GROUP (WHITAKER, 1957, 1960)

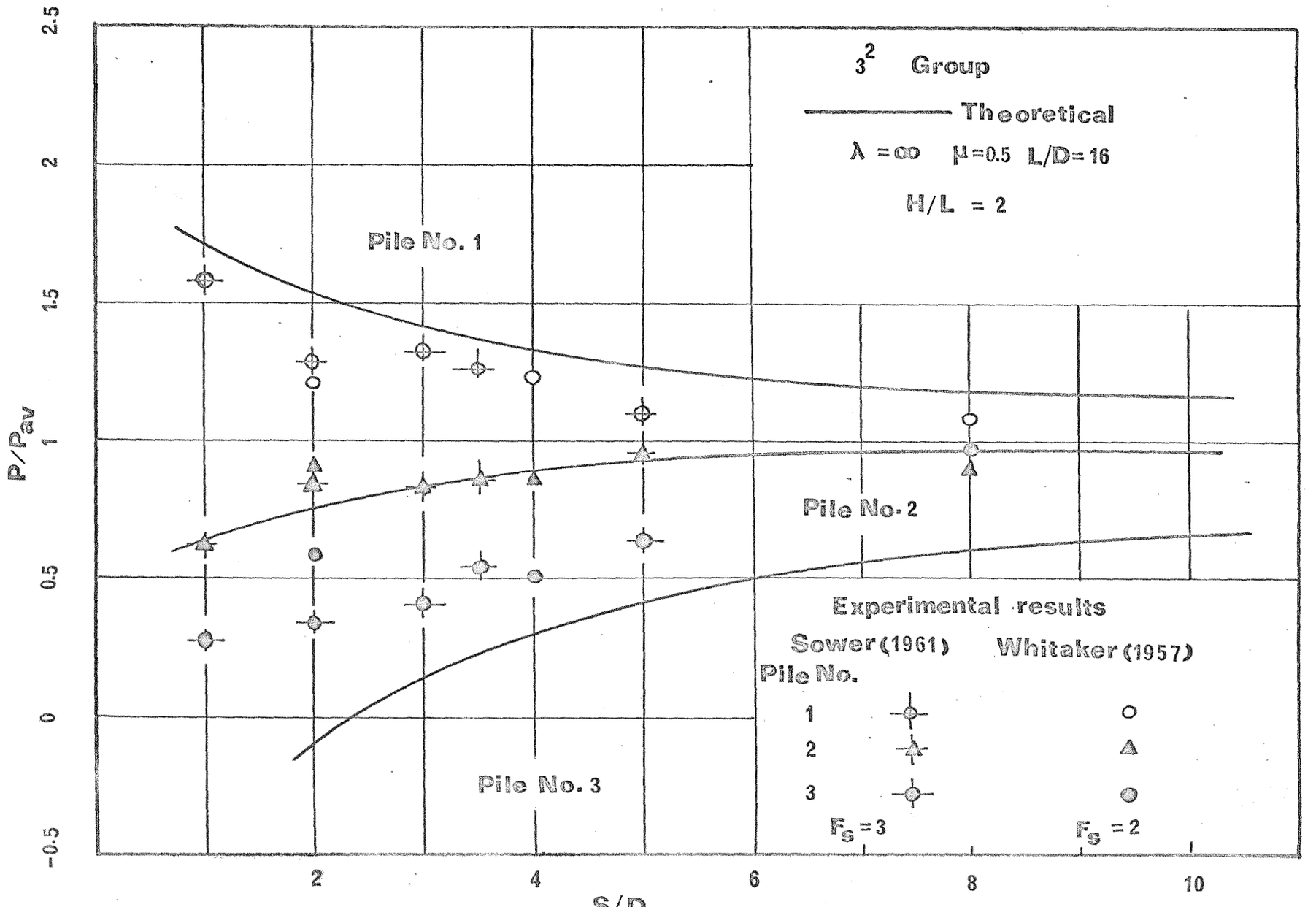

FIGURE - 5.14: COMPARISON WITH THE EXPERIMENTAL RESULTS FOR 3-SQ. PILE GROUPS (WHITAKER, 1957; SOWERS ET AL, 1961)

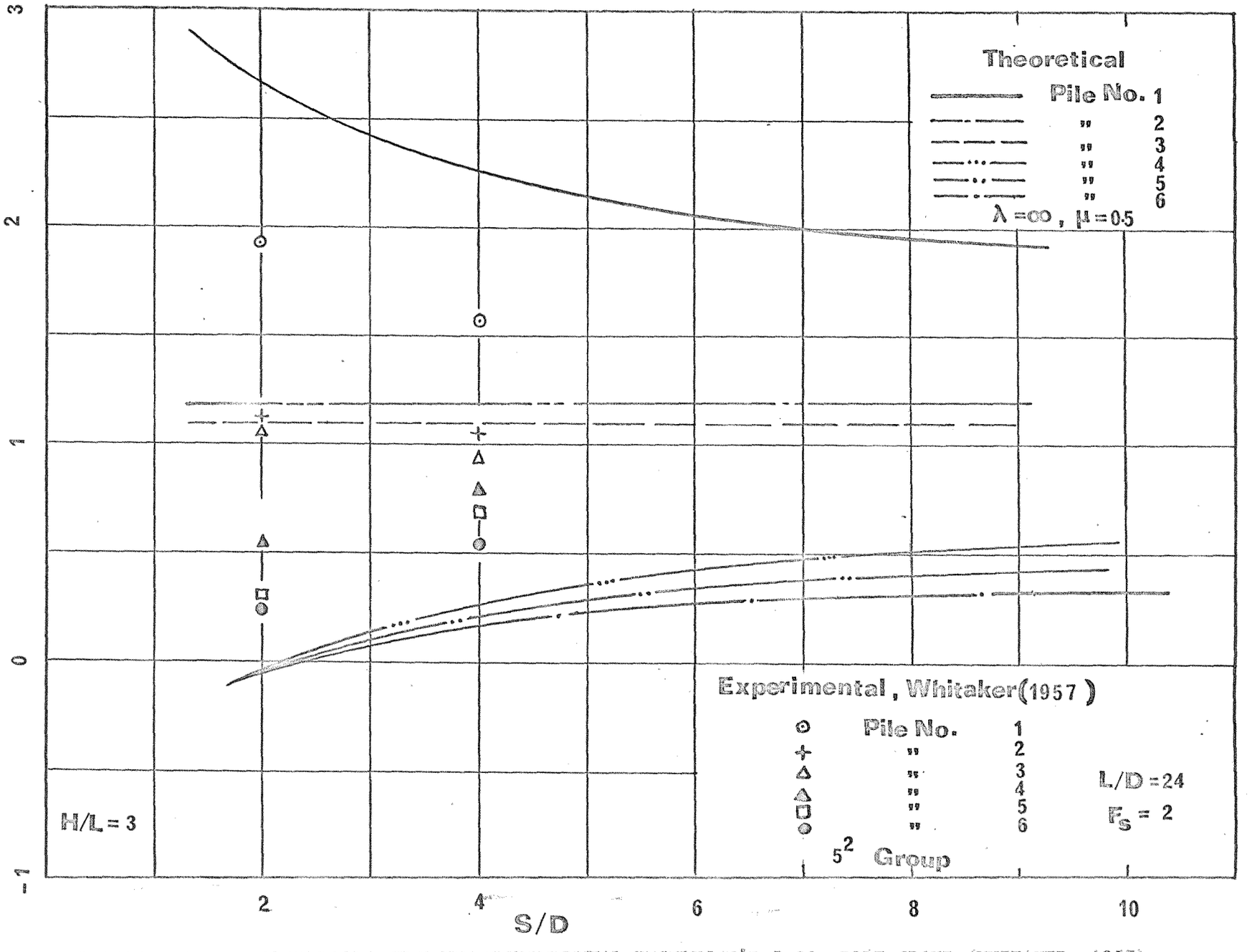

FIGURE - 5.15: COMPARISON WITH THE EXPERIMENTAL RESULTS FOR 5-SQ. PILE GROUP (WHITAKER, 1957)

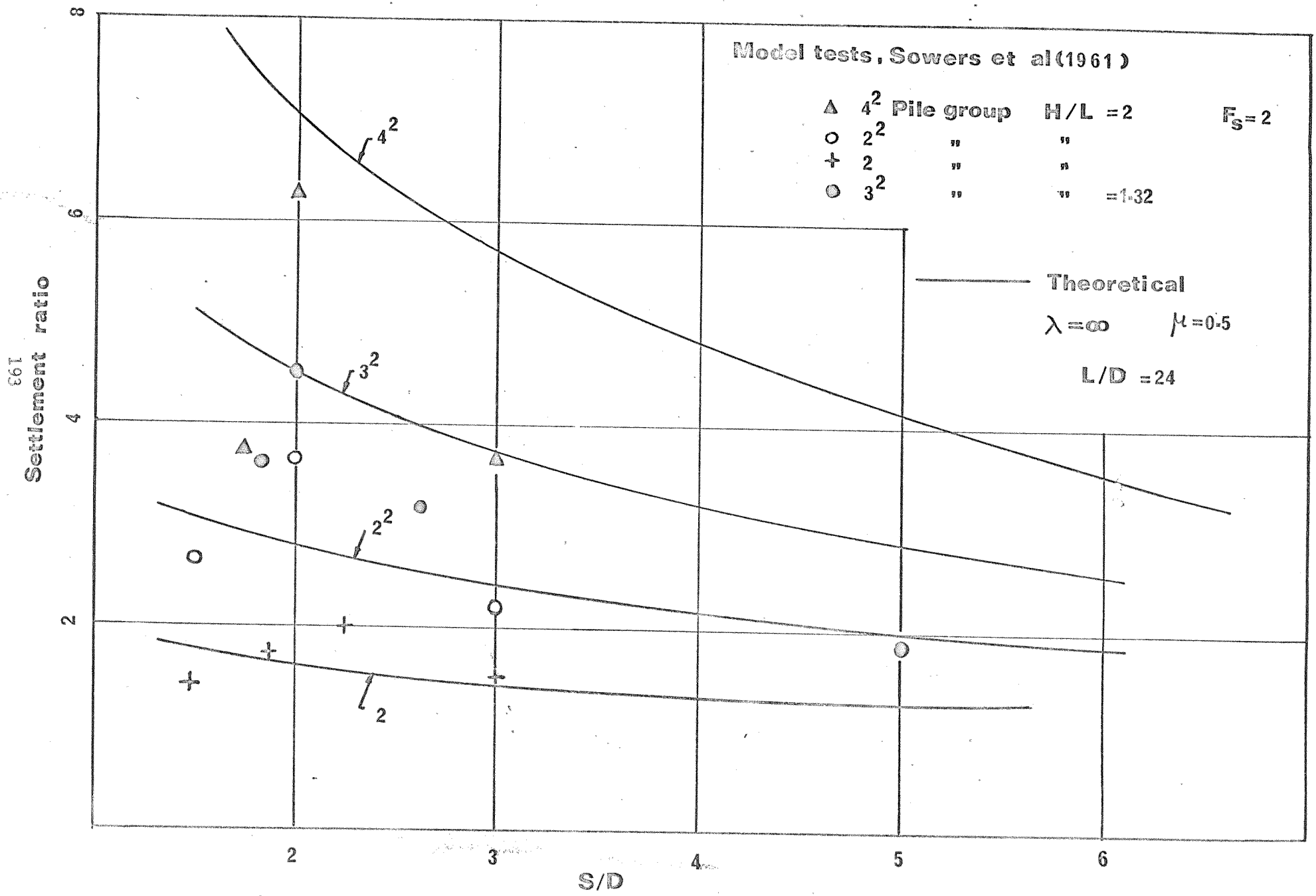

FIGURE - 5.16: COMPARISON WITH THE TEST RESULTS FROM SOWERS ET AL (1961)

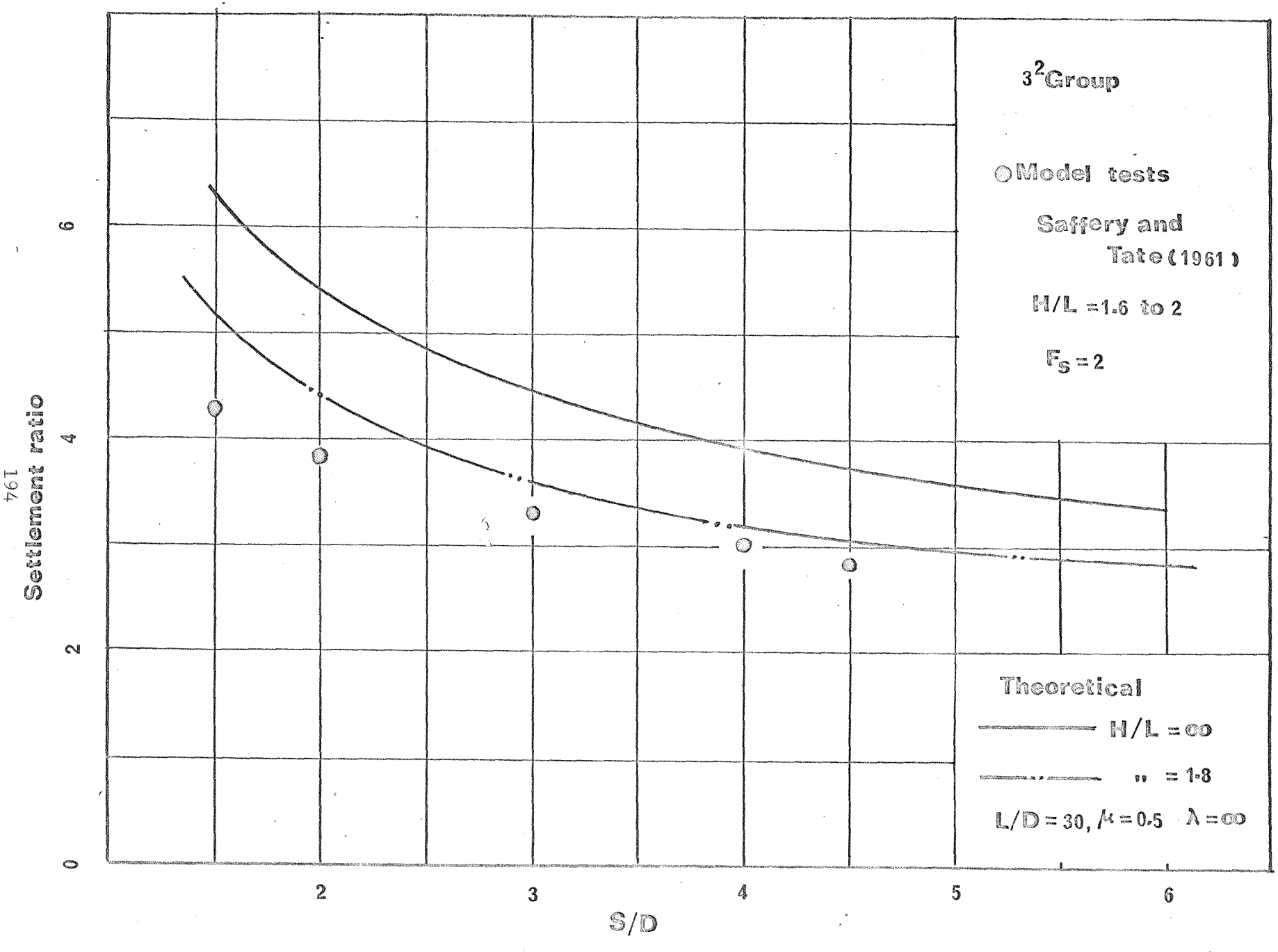

FIGURE – 5.17: COMPARISON WITH THE TEST RESULTS FOR 3-SQ. PILE GROUPS (SAFFERY AND TATE, 1961)

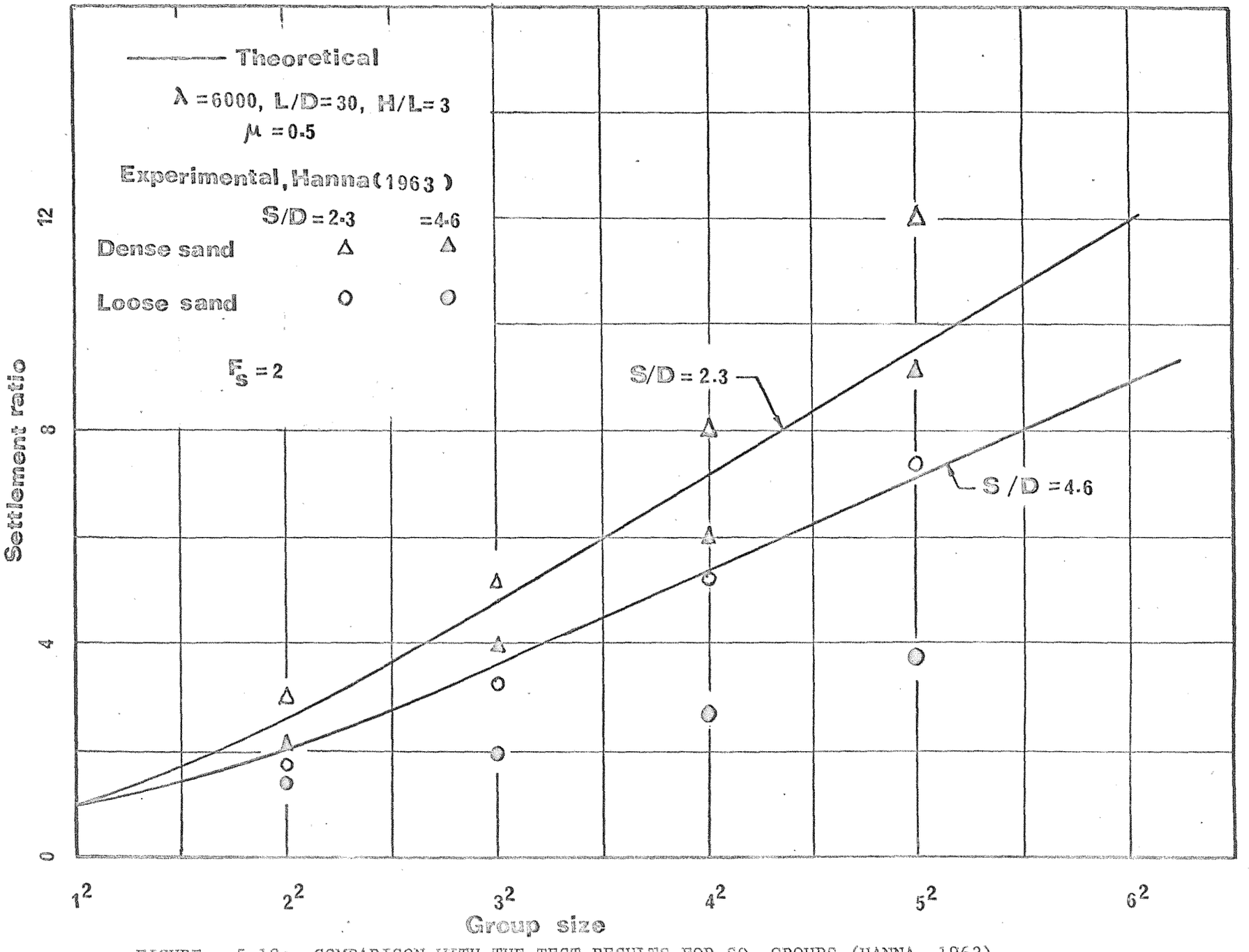

FIGURE - 5.18: COMPARISON WITH THE TEST RESULTS FOR SQ. GROUPS (HANNA, 1963)

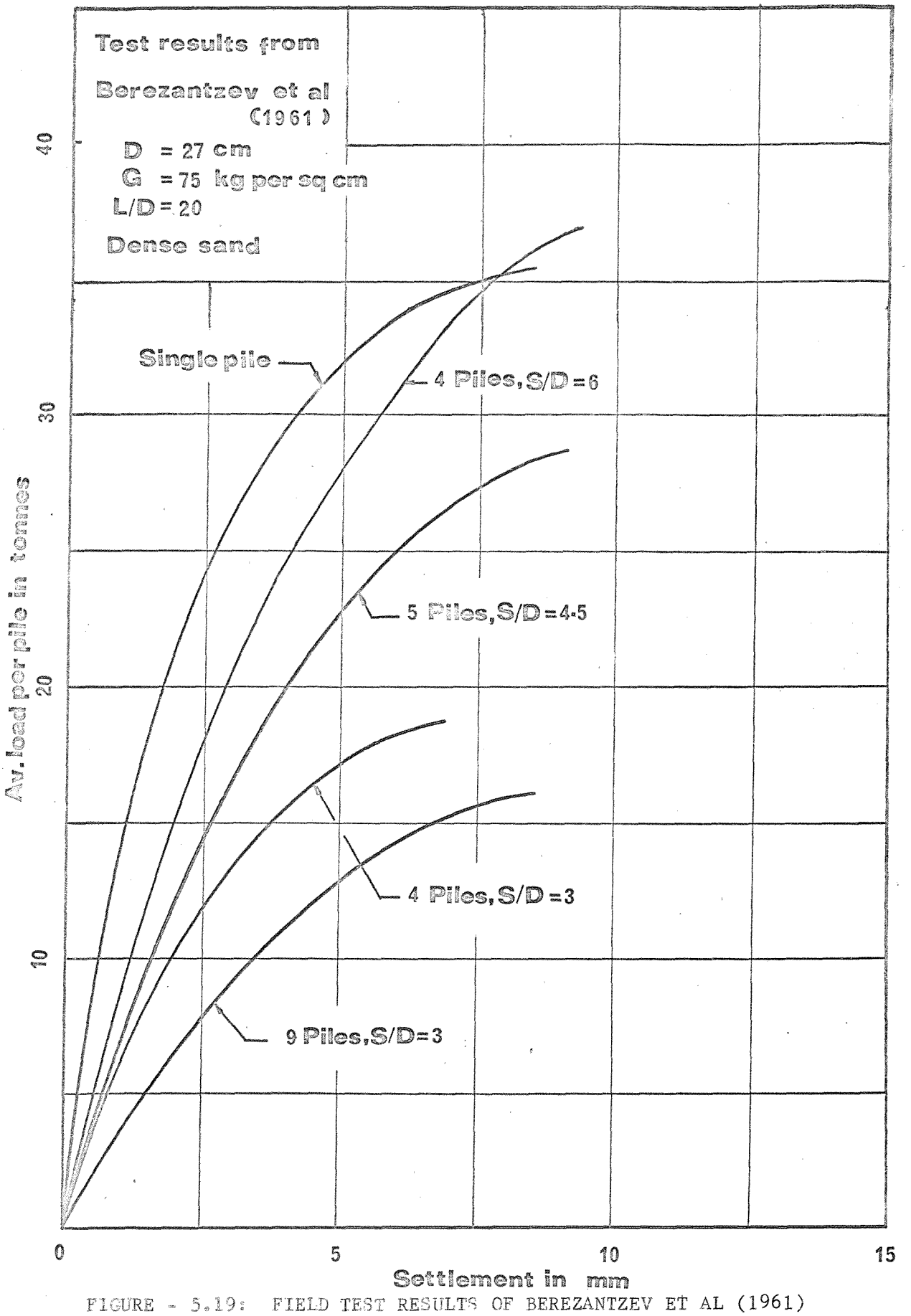

FIGURE - 5.19: FIELD TEST RESULTS OF BEREZANTZEV ET AL (1961)

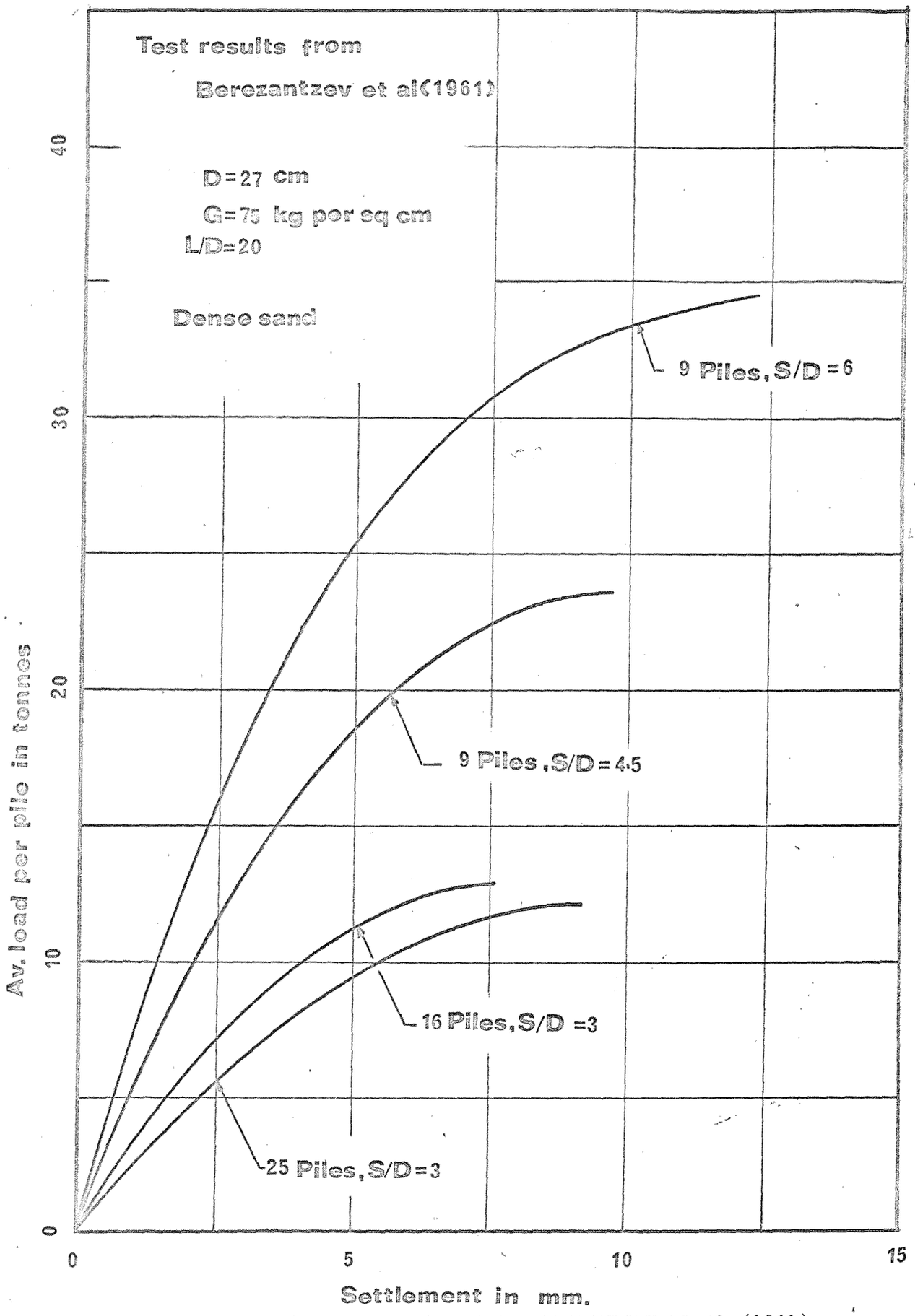

FIGURE - 5.20: FIELD TEST RESULTS FROM BEREZANTZEV ET AL (1961)

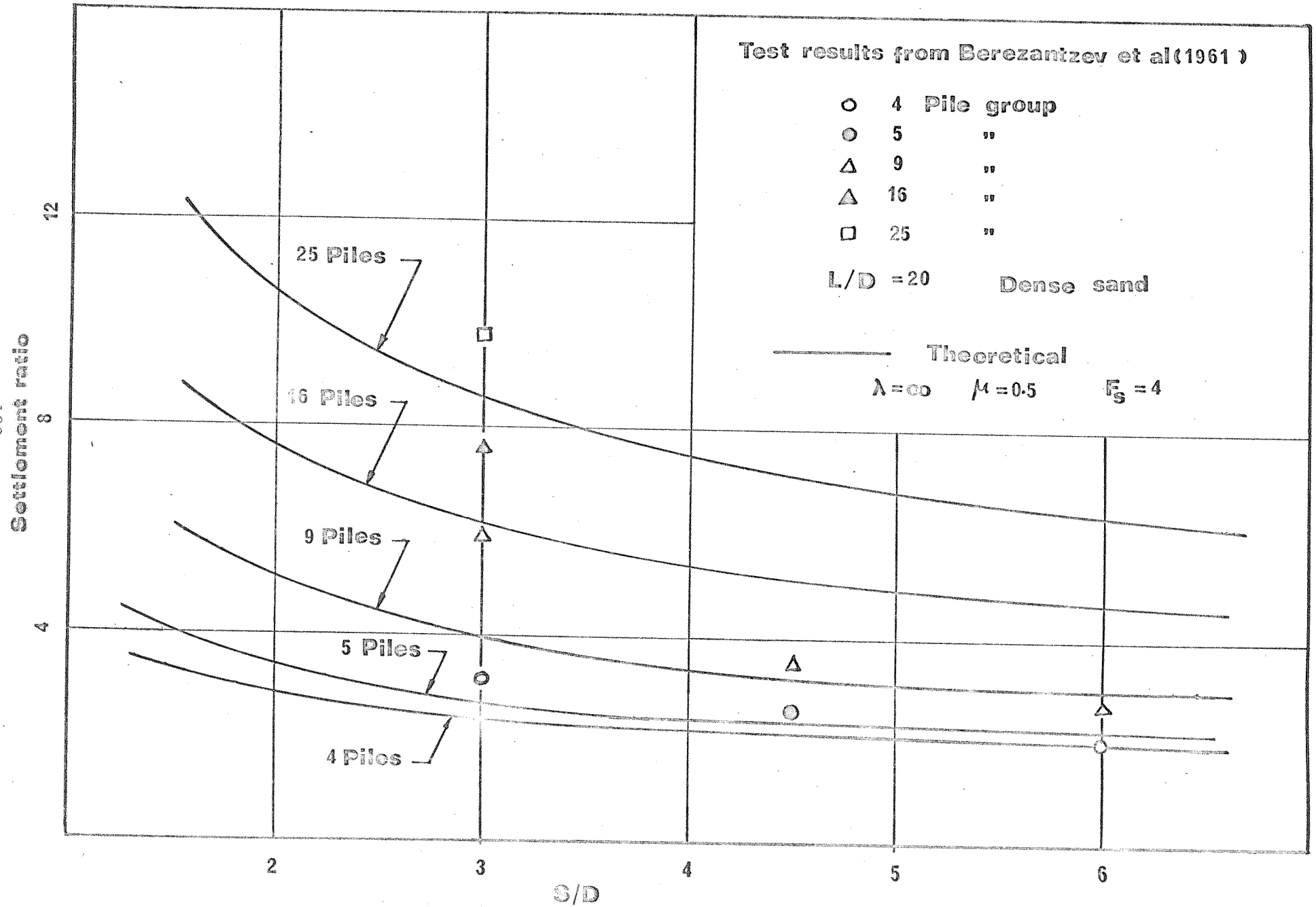

FIGURE - 5.21: COMPARISON WITH THE FIELD TEST RESULTS FROM BEREZANTZEV ET AL (1961)

Chapter 6

Analysis of pile groups with 'ground-contacting' pile cap

6.1 Summary

An elastic analysis of two problems concerning the interaction of an arbitrarily spaced group of piles and a smooth pile cap, of any shape, in contact with the ground surface viz.

(i) the load-displacement behaviour of the system,

(ii) the load distribution between the piles in the group,

are presented using the analysis for pile groups described in Chapter 5. The effect on the response of the system of pile length to diameter ratio, pile cap size and the compressibility ratio of the pile and the supporting medium has been investigated and specific results are presented graphically for a single pile with a square cap and typical pile groups in rectangular and square arrays.

6.2 General

Although the problem of the load displacement behaviour of a pile group - pile cap system is of considerable importance in foundation engineering the vast majority of available field and laboratory studies on piles have been concerned with single piles, or groups of free-standing piles. Theoretical analyses of pile and pile group behaviour have also avoided the interaction problem with the exception of a paper by Poulos (1968a) which considered a single rigid pile with a rigid circular cap resting on the ground.

The theoretical analysis presented in earlier chapters has shown encouraging correlation with the field and laboratory test results therefore in this chapter the foregoing analysis is extended to the complete "compressible pile group - rigid cap" system, of any geometry, where (i) the piles are assumed to be bonded to the supporting medium, which is assumed to be an ideally elastic half space, and (ii) the cap - medium interface is assumed to be smooth.

The effect of assumption (i) is discussed in Chapter 5 and that of the assumption (ii) in Chapter 3.

6.3 Development of the analysis

The details of the analytical method used have been described in Chapters 2, 3, 4 and 5, and only an outline of the essential steps is given below.

The following notation is used, Figure (6.1), C is the EFFECTIVE pile cap - medium interface area (i.e. the total cap area less that occupied by the group of N piles) and Q_c, P_s are load points and field points respectively on C. Similarly Q_s, P_s are load points and field points respectively on S, the TOTAL pile shaft plus base interface area for all N piles in the group. P(x,y,z) is a general field point in the medium.

The vertical displacement $w_1(P)$ of P due to a normal direct stress ϕ_c acting at Q_c, on an element dc of c can be written as

$$w_1(P) = \int_C \phi_c \, K(P,Q_c) \, dC \tag{6.1}$$

Similarly the vertical displacement $w_2(P)$ due to shaft-shear and direct normal stress over the base areas, ϕ_s at Q_s, on elements dS of the shaft and the base areas, included in S, can also be written as

$$w_2(P) = \int_S \phi_s . \, K(P,Q_s) \, dS \tag{6.2}$$

where $K(P,Q_c)$ and $K(P,Q_s)$ can be obtained from Mindlin's equations (Chapter, 2).

Hence the total vertical displacement w(P) of P due to the interface intensities ϕ_c and ϕ_s is obtained as:

$$w(P) = \int_C \phi_c \, K(P,Q_c) \, dC + \int_S \phi_s \, K(P,Q_s) \, dS \tag{6.3}$$

The integral representation satisfies the equations of equilibrium and compatibility everywhere in the half space (see Chapter 2) and also, because of the choice of singular solution, the following boundary conditions referred to the cartesian axes shown in Figure (6.1):

$$\begin{aligned} &\sigma_{zz} = \sigma_{xz} = \sigma_{yz} = 0, \text{ at } z = 0, \text{ outside C} \\ &\sigma_{xz} = \sigma_{yz} = 0, \text{ at } z = 0, \text{ inside C} \\ &\sigma_{xz} = \sigma_{yz} = 0, \text{ at } z = L, \text{ over the pile base area} \end{aligned} \tag{6.4}$$

Since the integral representation (6.3) exists, in the ordinary sense for the displacements at points on the surfaces S and C it can be equated directly to the displacement boundary condition of the problem. If we

now consider P to be at P_c on C we have from (6.3):

$$w(P_c) = \int_C \phi_c \, K(P_c,Q_c) \, dC + \int_S \phi_s \, K(P_c,Q_s) \, dS \qquad (6.5)$$

and when P is at P_s on S similarly,

$$w(P_s) = \int_C \phi_c \, K(P_s,Q_c) \, dC + \int_S \phi_s \, K(P_s,Q_s) \, dS \qquad (6.6)$$

Equations (6.5) and (6.6) have singularities in the kernels, K, when either points P_c and Q_c or P_s and Q_s coincide. Equations (6.5) and (6.6) do not take into account the horizontal displacement compatibility at the pile shaft - medium interfaces, however, it has been shown earlier (Chapter 4) that this approximation has a negligible effect on the load displacement behaviour of an axially loaded pile.

The above analysis is quite general and can be applied to pile groups of any geometry within a rigid cap of any shape when the vertical displacements at the interfaces are specified as follows:

$$w(P_c) = \text{constant} = 1 \text{ (say) on C}$$

$$\text{and either } w(P_s) = \text{constant} = 1 \text{ (say) on S, for a rigid pile} \qquad (6.7)$$

$$\text{or } w(P_s) = f(P_s) \text{ on S, for a compressible pile}$$

The function $f(P_s)$ allows for the pile compressibility and can be included in the analysis by the iterative procedure discussed in Chapter 4. Equations resulting from the substitution of (6.7) into (6.5) and (6.6) can be stated in a convenient matrix form by dividing, the pile-soil interfaces as in Chapter 5 and the EFFECTIVE cap-soil interface as in Chapter 3 into discrete elements thus (see equation 5.12):

$$\begin{Bmatrix} \{W^1\} \\ \cdot \\ \cdot \\ \cdot \\ \cdot \\ \{W^{NP}\} \\ \{W_c\} \end{Bmatrix} = \begin{bmatrix} [KSP]^{11} & \cdots & [KSP]^{1\,NP} & [KCP]^1 \\ \cdot & \cdot & \cdot & \cdot \\ \cdot & \cdot & \cdot & \cdot \\ \cdot & \cdot & \cdot & \cdot \\ \cdot & \cdot & \cdot & \cdot \\ [KSP]^{NP\,1} & \cdots & [KSP]^{NP\,NP} & [KCP]^{NP} \\ [KPC]^1 & \cdots & [KPC]^{NP} & [KCC] \end{bmatrix} \begin{Bmatrix} \{\phi^1\} \\ \circ \\ \circ \\ \circ \\ \circ \\ \{\phi^{NP}\} \\ \{\phi_c\} \end{Bmatrix} \qquad (6.8)$$

Where the quantities $\{W^1\}.....\{W^{NP}\}$, $\{\phi^1\}....\{\phi^{NP}\}$, $[KSP]^{11}.....[KSP]^{INP}$, $[KSP]^{NP1}.....[KSP]^{NP\,NP}$ etc. have been defined in Chapter 5.

$[KPC]^1....[KPC]^{NP}$ are matrices of coefficients identical to the matrices $[KPL]^1.....[KPL]^{NP}$ defined in Chapter 5.

$[KCP]^1.....[KCP]^{NP}$ are matrices identical to the matrices $[KLP]^1.....[KLP]^{NP}$, defined in Chapter 5.

$[KCC]$ is identical to $[KCC]$ defined in Chapter 3.

$\{\phi_c\}$ is the unknown direct normal stress at the cap-soil interface.

Equation (6.8) represents a set of linear equations that can be solved for the unknowns $\{\phi^1\}.....\{\phi^{NP}\}$ and $\{\phi_c\}$ for rigid and compressible pile groups.

6.4 Discussion of the computer programme and convergence of the solution

The computer programme developed for the analysis of the above problem is identical to that discussed in Chapter 5. The listing details are given in Banerjee (1969).

In the present analysis of the problems of pile cap - pile group systems with rectangular or square symmetry the integrals unvolving all the elements of the sub-matrices except those for $[KCC]$ have been evaluated by the use of numerical quadrature discussed in Chapter 5. The integrals involved in evaluating the coefficients of the sub-matrix $[KCC]$ have been discussed in Chapter 3.

For the solutions described in this chapter the pile shaft was

divided into 10 cylindrical segments and the pile base into 5 annular rings. The cap soil interface was divided into 144 elements which, because of the quadrantal symmetry, was reduced to 36 equations for the cap displacements. The number of equations representing the cap-soil interface were further reduced by ignoring the equations involving the displacements of the elements of pile cap area occupied by the pile cross-section.

A series of trial calculations were carried out for a 4-pile group ($L/D = 20$, $S/D = 2.5$, $\lambda = \infty$, $\mu = 0.5$) under a rigid square cap ($B/D = 5$). The calculated load obtained by using 10 equations for the shaft, 5 equations for the base and 32 equations for the cap was about 4½% lower than that obtained by the use of 5 equations for shaft, 3 for base and 8 equations for the cap and was about 3% higher than that obtained by the use of 15 equations for shaft 5 equations for base and 52 equations for the effective cap surface. Therefore, although there is some slight inaccuracy involved in the results presented in this chapter, by the use of 15 equations for each typical pile of the group and 32 equations for the cap, it was thought that these are justified by economics achieved in computer storage and run time.

6.5 Results of the analysis

The effects of length to diameter ratio, group size, pile compressibility ratio (λ), the distribution of the load between the cap and the individual piles in the group and the influence of the cap on the vertical stiffness of the group have been studied and typical results are presented graphically in Figures (6.2) to (6.10).

Figure (6.2) shows a comparison between the load-displacement behaviour of a single axially loaded pile with a square pile cap ($B = 2.5D$) and that of a similar single pile without a cap. The presence

of a pile cap is seen to produce only a small increase in the stiffness of the system (< 5%) for all but short piles (L/D < 20).

The distribution of the total load between the cap and pile is shown in Figure (6.3) for both rigid and a compressible pile. It is seen that, for $20 \leq L/D \leq 40$, the cap carried some 15% to 20% of the load although, from Figure (6.2), the effect of this load redistribution on the stiffness of the system is very small. These results are in general agreement with those calculated by Poulos (1968a) for a rigid pile with a circular cap resting on the ground surface. Similar information for a four-pile group appears in Figures (6.5) and (6.6) and here again, even though a rather higher proportion of the load is taken by the cap for a particular geometry used, the increase in the stiffness is negligible.

The effect of the pile spacings (S) and pile stiffness (λ) on the load-displacement behaviour of a capped 2-pile group is illustrated in Figure (6.4) from which a doubling of the pile spacing is seen to produce only a 5% to 10% increase in the system stiffness over the range of λ ($6000 \leq \lambda \leq \infty$). Figures (6.7) and (6.9) show the effect of varying S for capped group of 5 piles and 9 piles. Each doubling of S almost quadruples the cap area and in all cases, for $0 \leq L/D \leq 40$, each doubling increases the system stiffness by 25%.

Figures (6.8) and (6.10) illustrate how the load is shared between the different piles in capped 5 and 3^2 pile groups for various S and λ values. It is interesting to note here that although, for closely spaced piles ($S \approx 3D$), the effect of the caps on the load displacement behaviour is small they do radically effect the loads carried by the individual piles in the group (Compare with Figures, 5.5 and 5.8).

All the results for 2, 5 and 3^2 pile groups are summarised in Figure (6.11) where the effect of ground contacting caps and cap size on the system stiffness is given in terms of a settlement ratio (R_S =

the ratio of group settlement under a load of N x P to the single uncapped pile displacement under load P). The results of free-standing pile groups are also shown for comparison.

6.6 Conclusions

(i) An elastic analysis has been presented for the general compressible pile group problem including a rigid smooth 'ground contacting' cap.

(ii) The results of the analysis show,

(a) The load-displacement behaviour of pile groups with and without such caps are little different, the cap increasing the system stiffness by from 5% to 15% depending upon the group size and pile spacings.

(b) The presence of the cap does, however, change drastically the load carried by the different piles in the group.

(c) The proportion of the total group load taken by the caps of normal dimensions on piles with $20 \leq L/D \leq 40$ ranges from 20 to 60 percent depending upon the group size and pile spacing, being higher for the larger groups at larger spacings.

In applying the theoretical results and conclusions to practical field problems it should be borne in mind that the theoretical analyses are strictly applicable to homogeneous isotropic subsoil and do not take into account of effect of increase in stiffness of soil with depth, layering of the strata, effect of driving the piles etc. which affect the group behaviour. The trend of present analysis for the 3^2 pile group is in agreement with the experimental study due to Whitaker (1960), who found the settlement ratios of the capped group and uncapped group to be nearly equal.

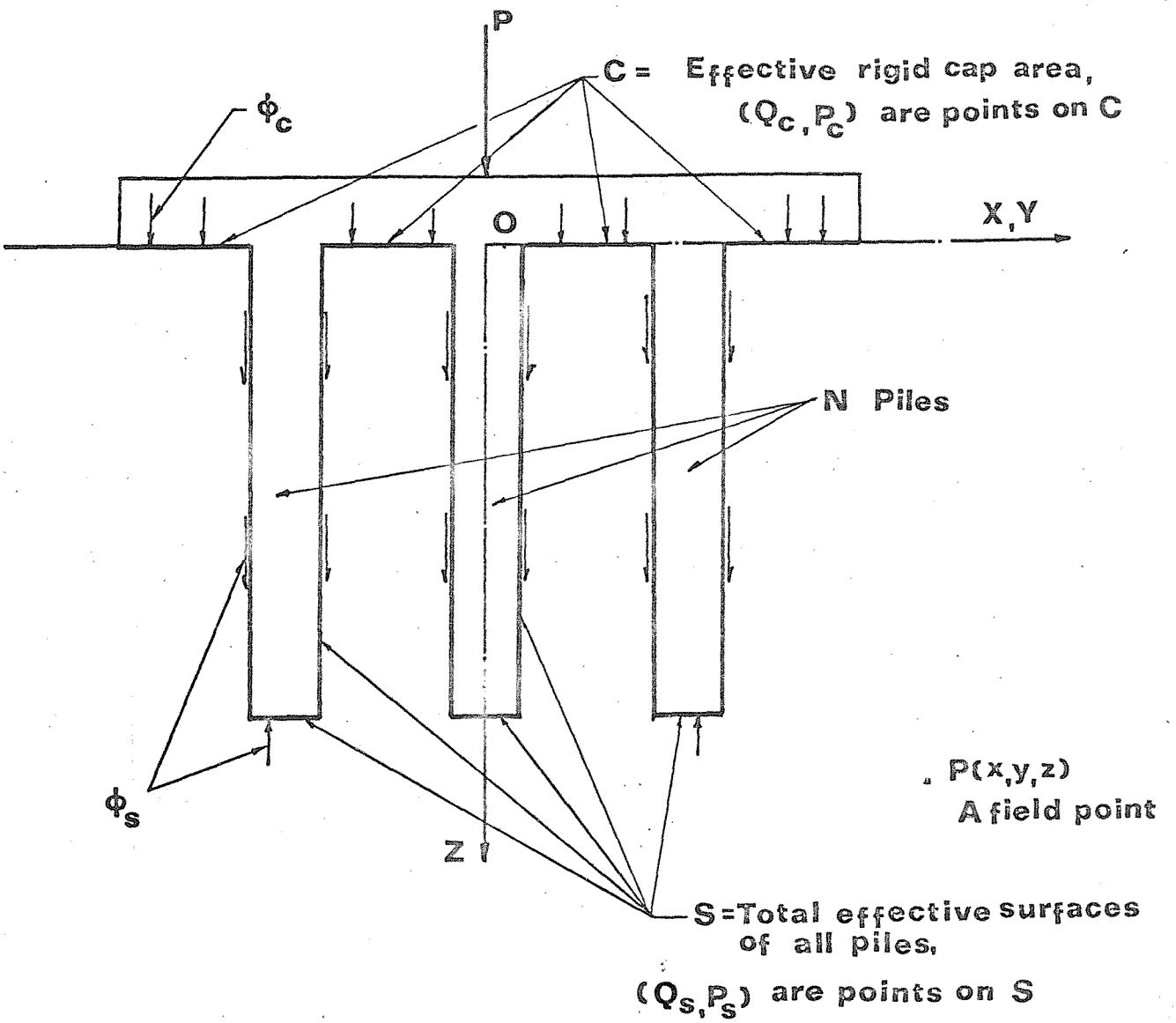

FIGURE - 6.1

GENERAL CAP GROUP SYSTEM

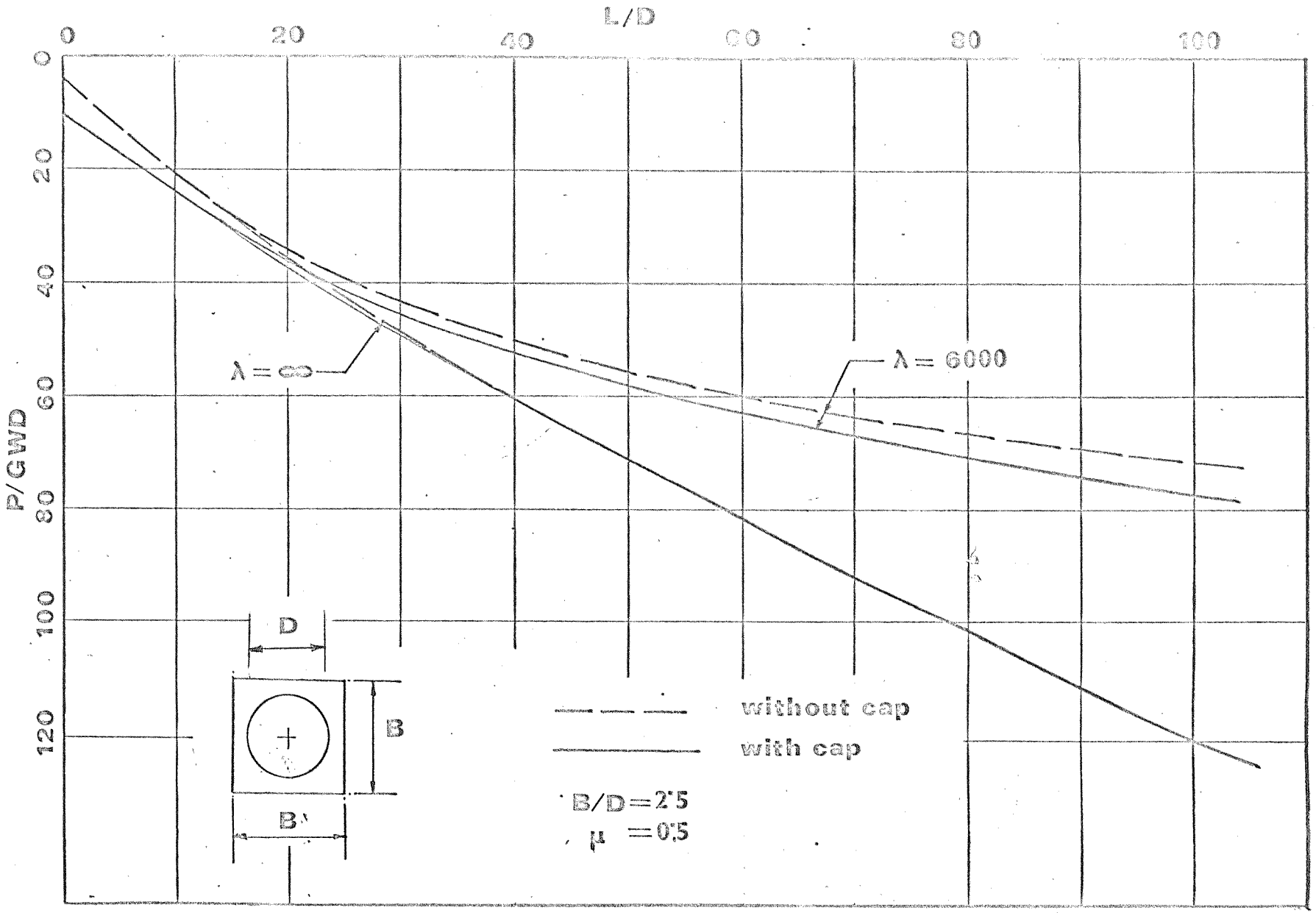

FIGURE - 6.2: LOAD-DISPLACEMENT RESPONSE OF CAPPED AND UNCAPPED PILES

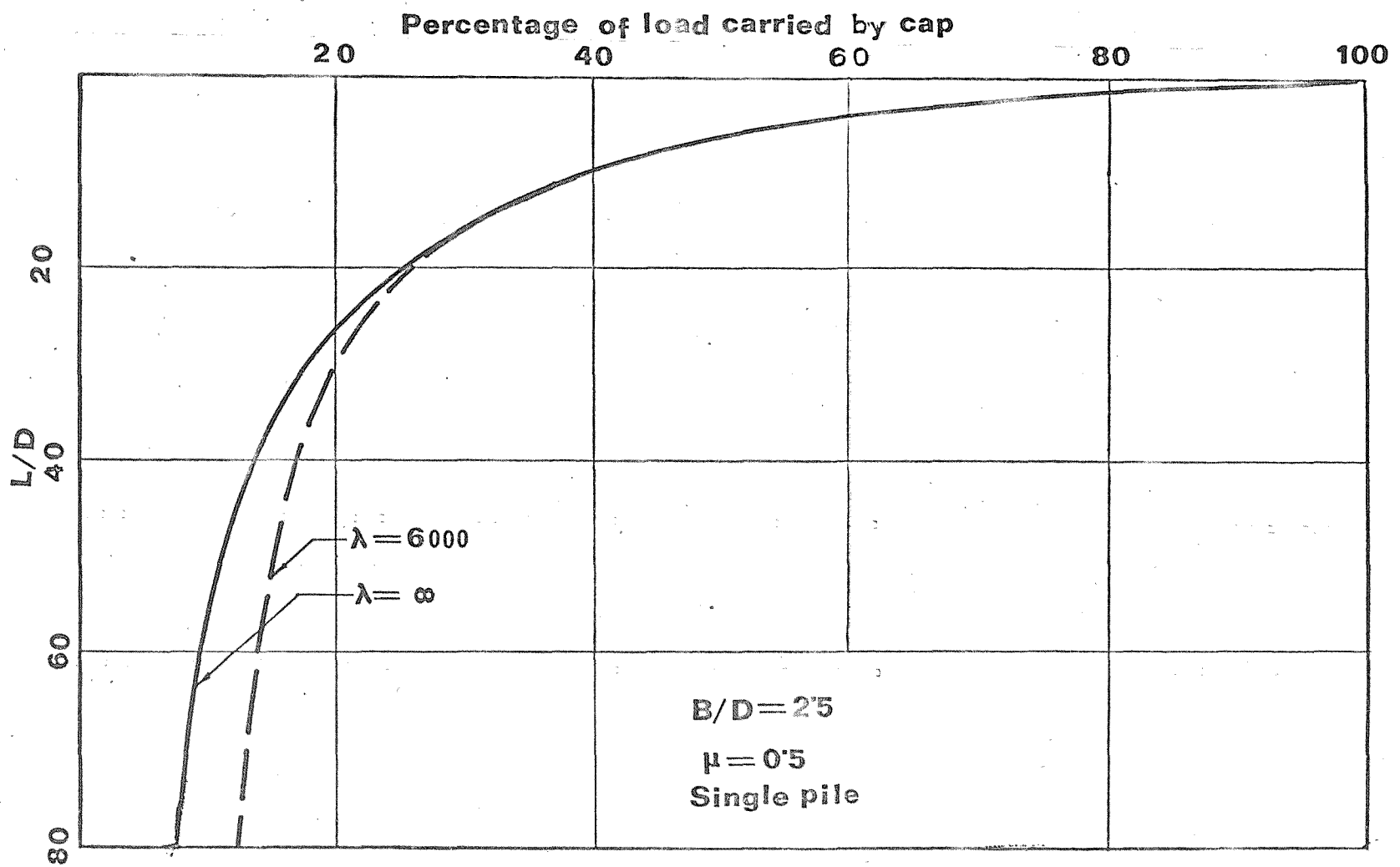

FIGURE - 6.3: DISTRIBUTION OF LOAD BETWEEN THE CAP AND THE PILE

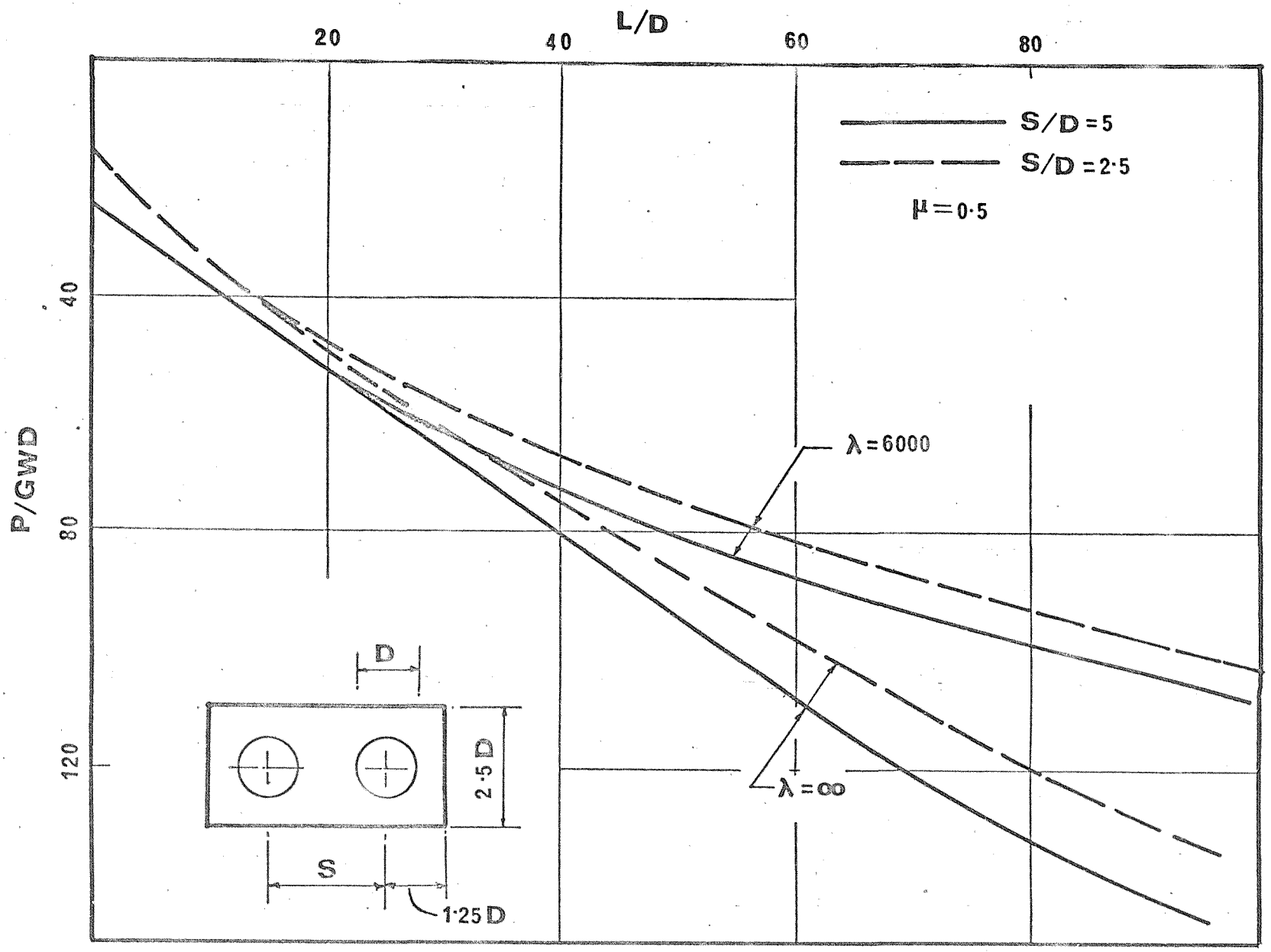

FIGURE - 6.4. LOAD-DISPLACEMENT RESPONSE OF TWO PILE GROUP WITH A RECTANGULAR CAP

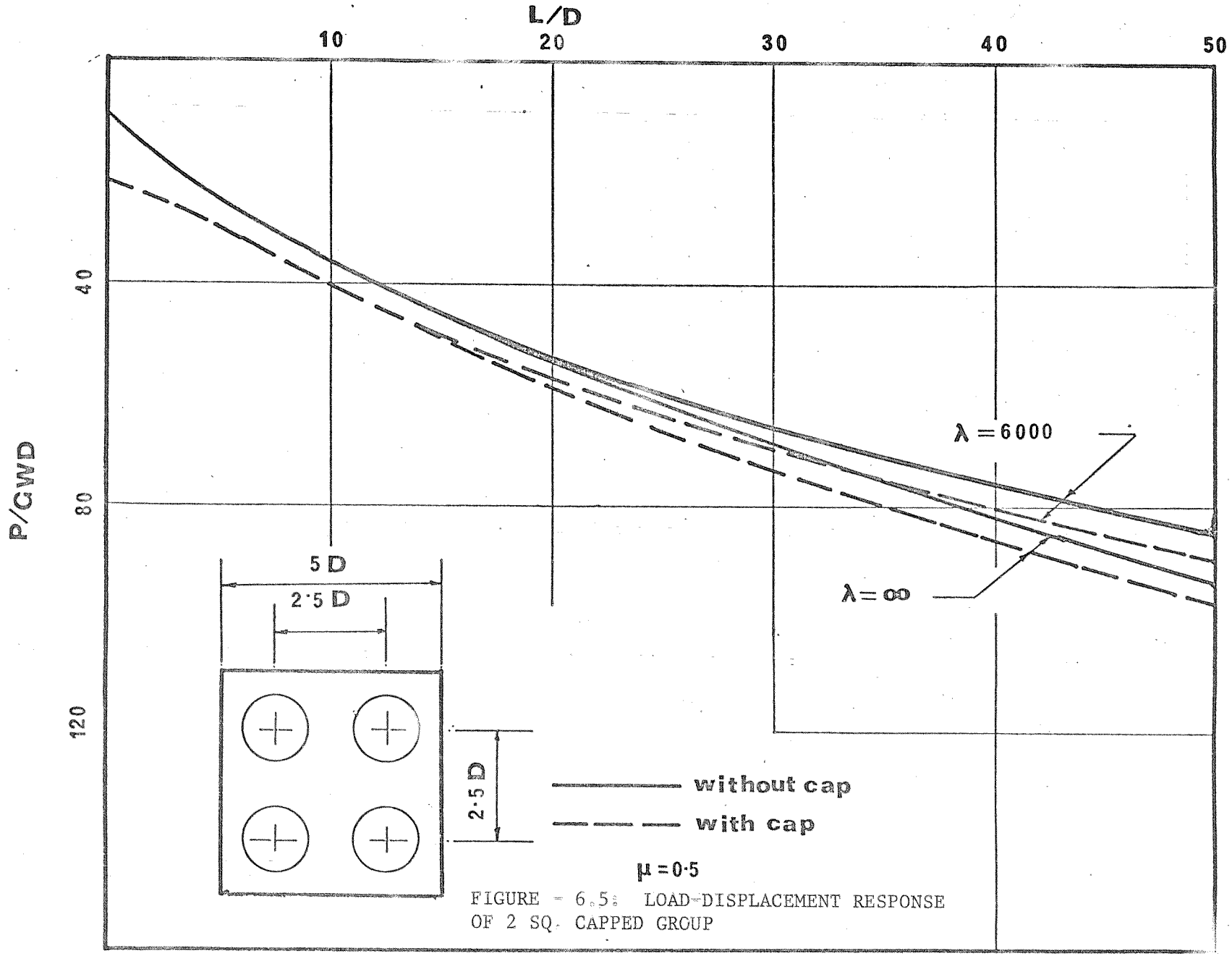

FIGURE - 6.5: LOAD-DISPLACEMENT RESPONSE OF 2 SQ. CAPPED GROUP

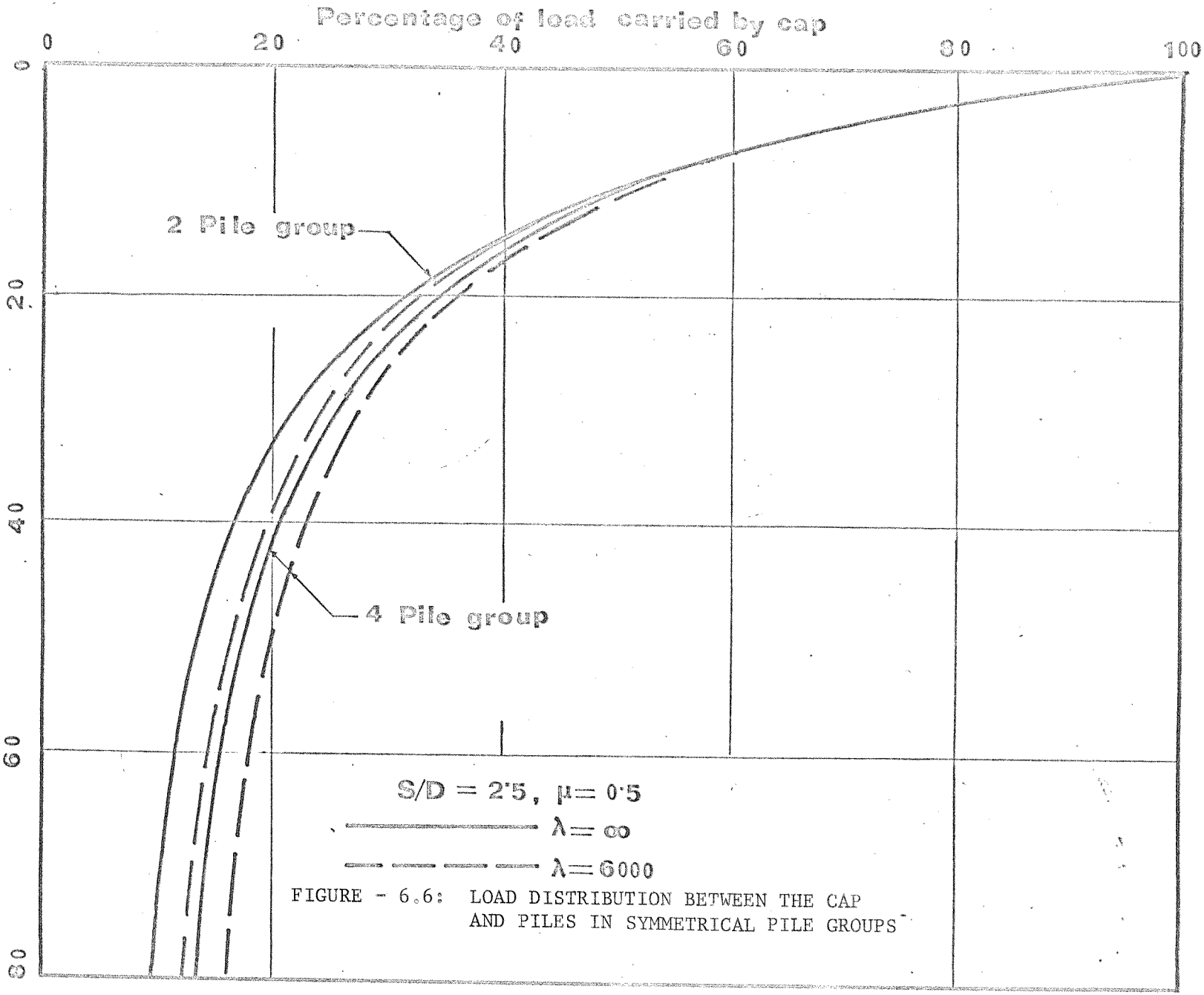

FIGURE - 6.6: LOAD DISTRIBUTION BETWEEN THE CAP AND PILES IN SYMMETRICAL PILE GROUPS

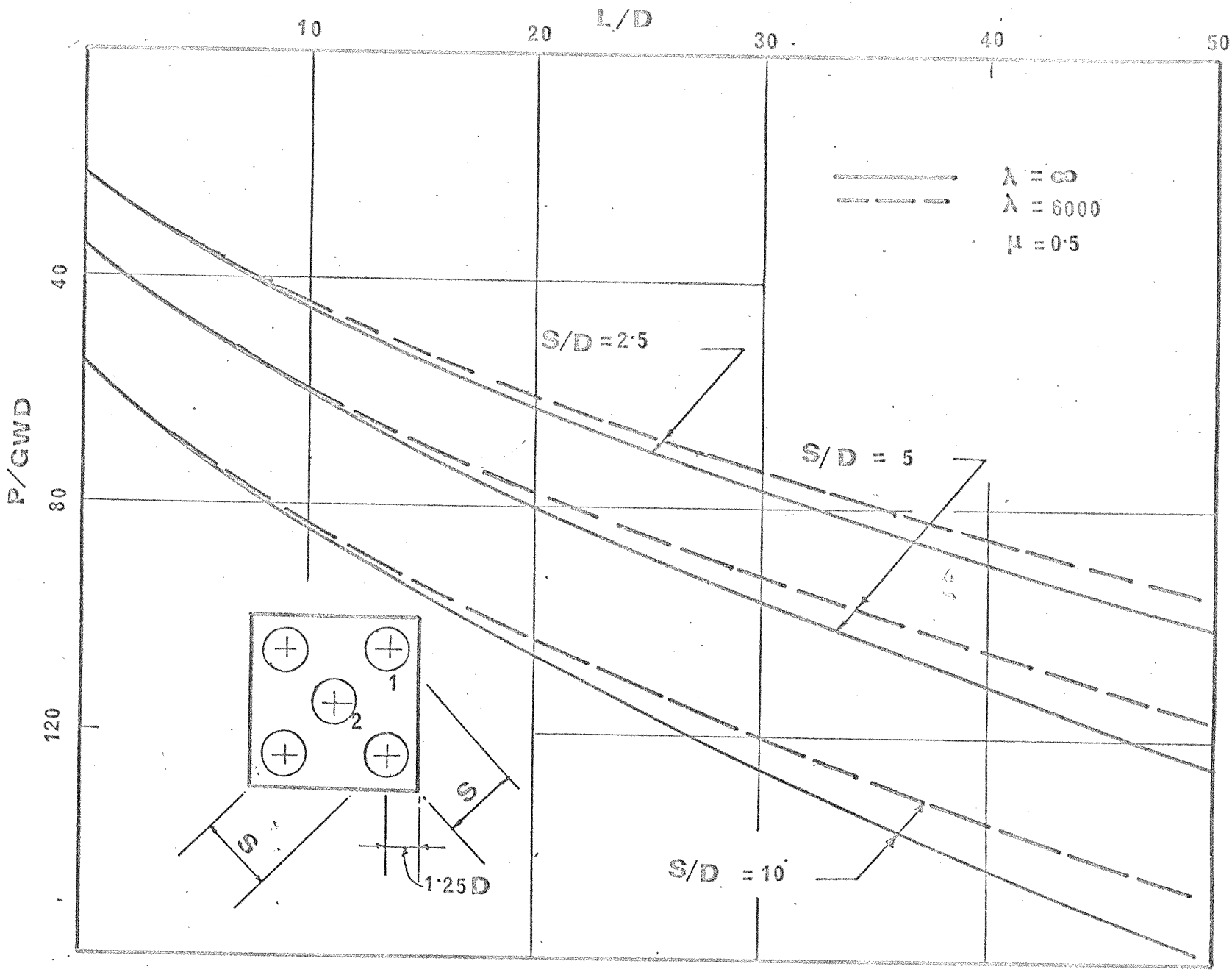

FIGURE - 6.7: LOAD-DISPLACEMENT RESPONSE OF CAPPED GROUP OF 5 PILES

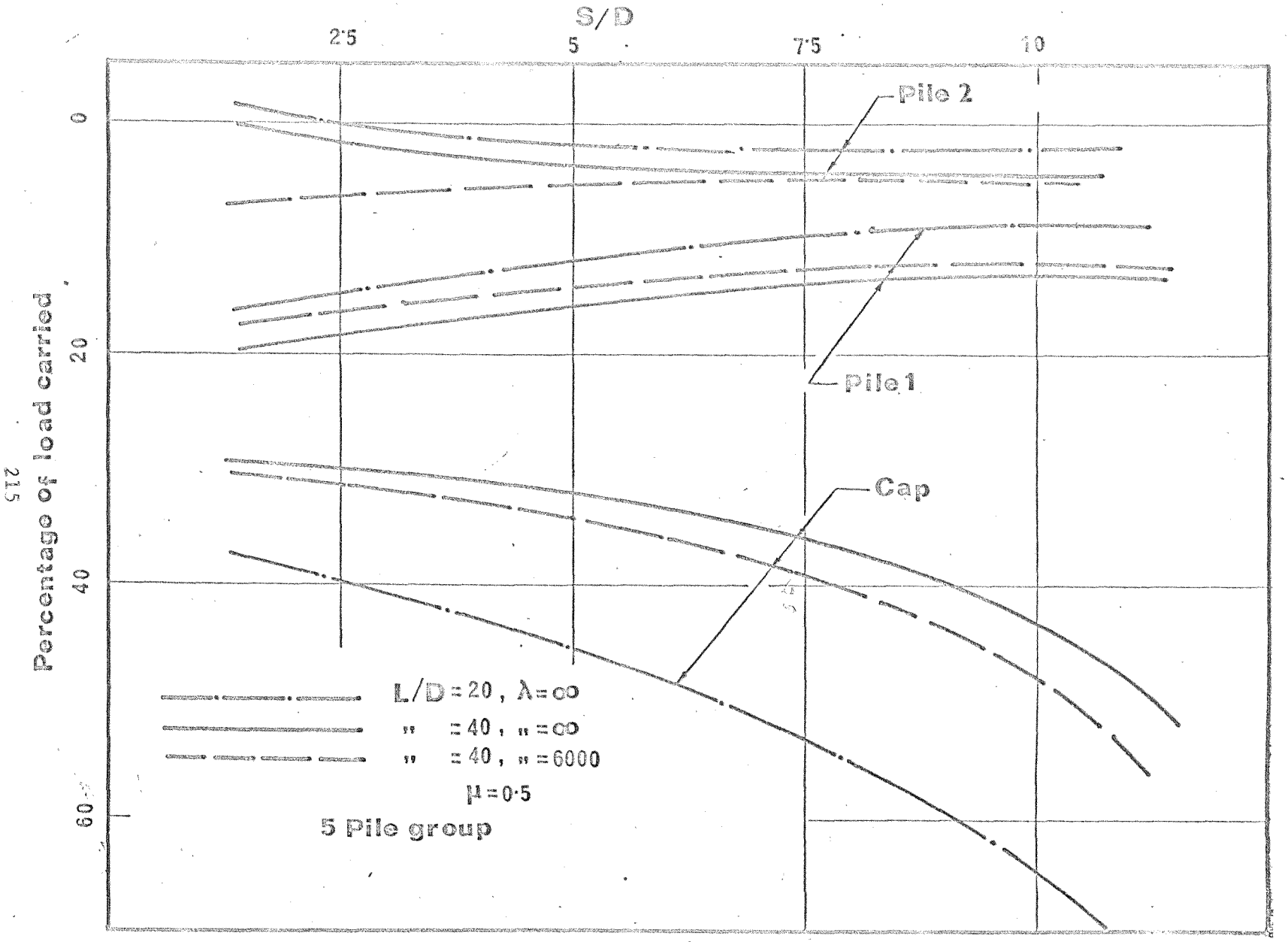

FIGURE - 6.8: DISTRIBUTION OF LOAD BETWEEN THE CAP AND INDIVIDUAL PILES IN A 5-PILE GROUP

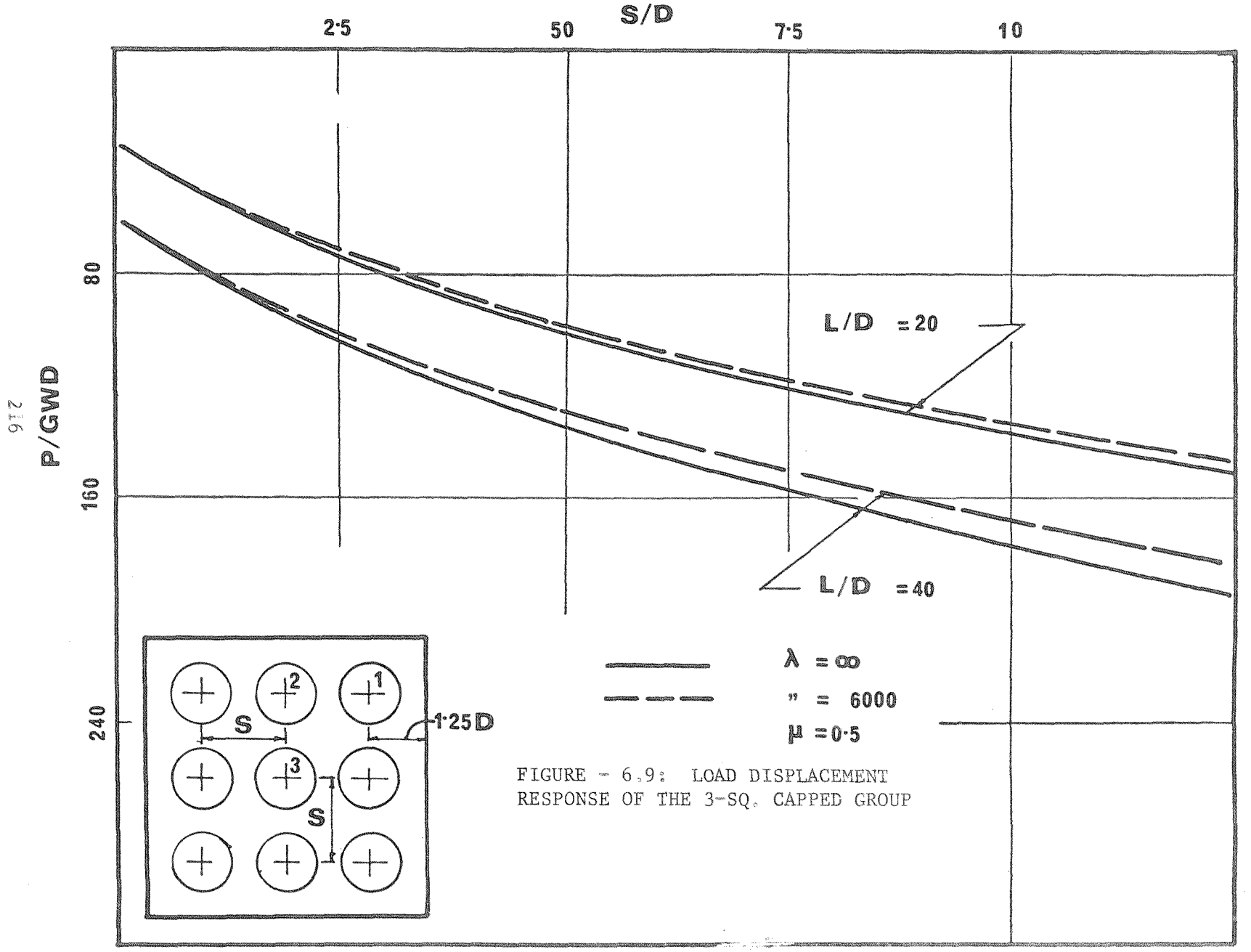

FIGURE - 6.9: LOAD DISPLACEMENT RESPONSE OF THE 3-SQ. CAPPED GROUP

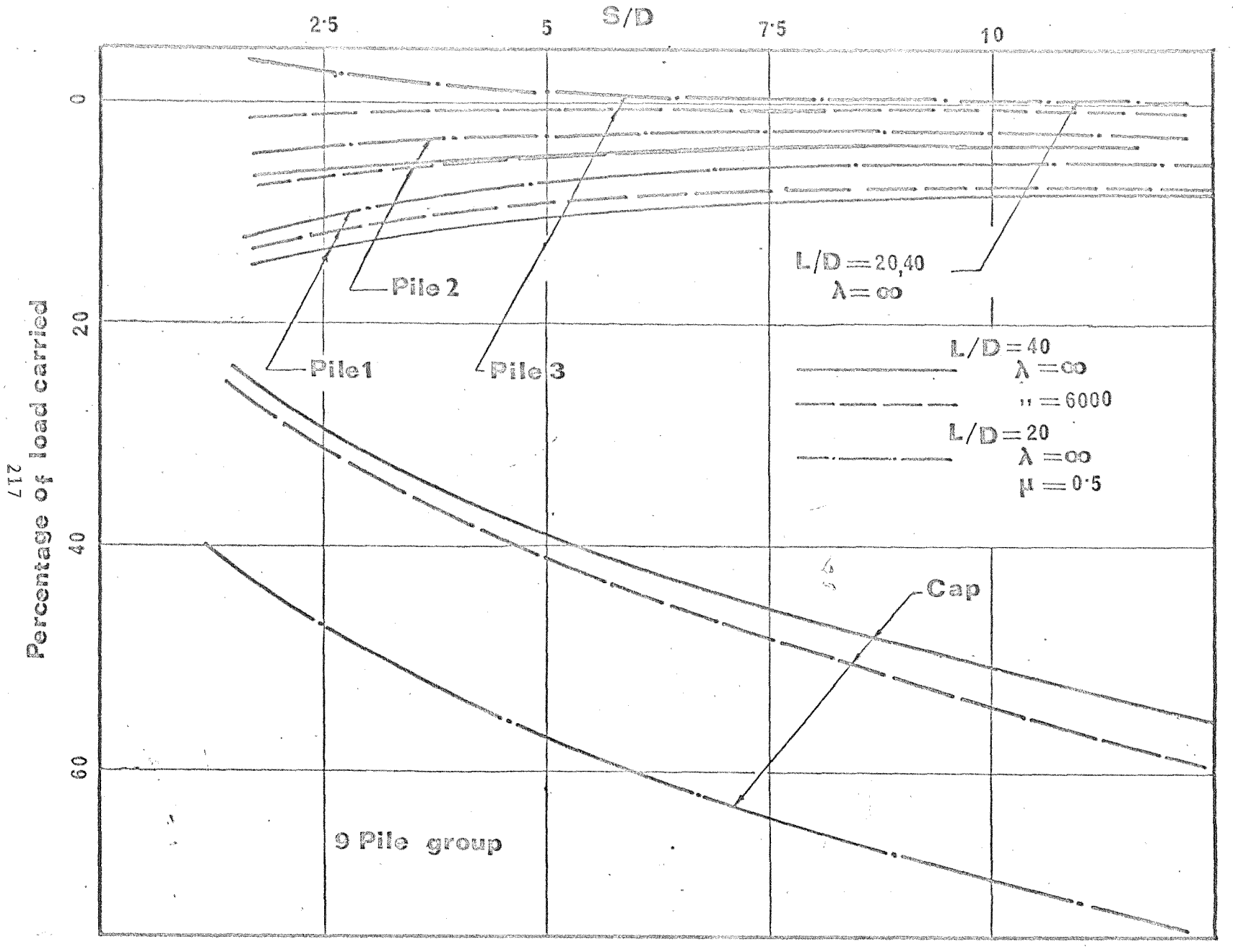

FIGURE - 6.10: DISTRIBUTION OF LOAD BETWEEN THE CAP AND INDIVIDUAL PILES IN A 3-SQ. PILE GROUP

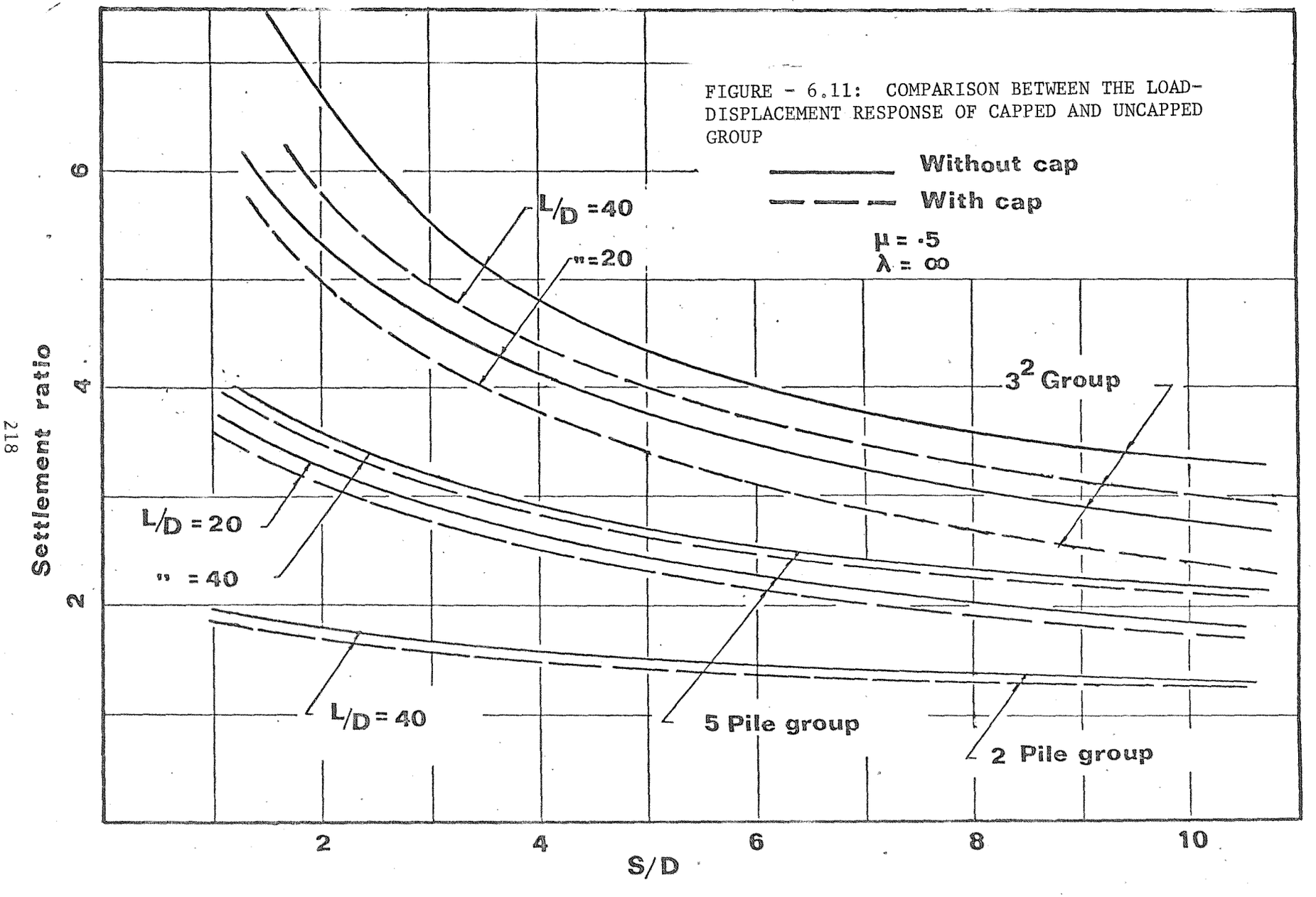

FIGURE - 6.11: COMPARISON BETWEEN THE LOAD-DISPLACEMENT RESPONSE OF CAPPED AND UNCAPPED GROUP

Chapter 7

The effect of induced pore water pressure on the ultimate bearing capacity of driven piles.

7.1 Summary

In this Chapter the effect of pore water pressure on the ultimate bearing capacity of driven piles is examined. The problem has been divided into two parts:

(i) Analysis of the stresses and pore water pressure developed due to pile driving assuming the soil to be an elastic ideally plastic porous skeleton saturated with an incompressible pore fluid.

(ii) Analysis of the dissipation of the pore water pressure and the changes of effective stresses around the pile assuming the soil skeleton to be elastic.

The ultimate bearing capacity of a driven pile in saturated clay in relation to the variation of the effective stresses along the pile shaft - soil interface is then investigated. The theoretical values of pore water pressure and ultimate bearing capacity are compared with published full scale field test data and reasonable agreement obtained.

7.2 General

The bearing capacity of a pile in clay increases with time after driving, partly due to the recovery of shear strength of the clay remoulded by pile driving and partly due to the dissipation of the induced pore water pressures. These phenomena have been recognised by many authors (Cummings et al, 1950; Seed and Reese, 1955; Yang, 1956; Lo and Stermac, 1963, 1965; Nishida, 1963; Airhart, 1967; Chandler, 1968), but no theoretical analysis based on reasonably realistic soil behaviour has yet been presented.

The analysis presented below makes the following assumptions:

(i) The soil is a homogeneous, isotropic, elastic-ideally plastic solid defined by elastic constants G and μ in the elastic range and by the generalised Von Mises yield criterion, octahedral shear stress = Constant, in the plastic region, with respect to the total stresses.

(ii) There is no volume change in the soil during pile driving.

(iii) The strain in the vertical direction is zero i.e. rotationally symmetric plane strain conditions prevail.

Assumption (i) is an idealisation of the stress-strain response of real soil, whereas (ii) will be true for any saturated normally consolidated clay deformed under undrained condition. In support of (iii) one may refer to the published results of Cummings et al (1950) and Lo and Stermac (1965) who measured respectively the moisture contents and pore water pressure at various radii and depths round the driven pile. Their observations established that:

(a) The ratio of the increase in pore water pressure to the effective mean pressure remains essentially constant with depth along the pile length and varies only in the radial direction (Lo and Stermac, 1965).

(b) There is a horizontal migration of pore water pressure initiated by pile driving but the change in moisture is uniform over the length of the pile and varies only with time (Cummings et al, 1950).

Thus the condition of plane strain is thought to be valid over the pile length except possibly near the ends.

A real pile is driven by a series of approximately instantaneous increases in penetration in which the soil at the tip of the pile is remoulded and pushed outwards. Thus if the pile is long, so that the end effects may be ignored, the mode of deformation of the soil around the pile is reasonably analogous to that of the expansion of a cylindrical cavity from zero radius to a finite radius.

The problem of elastic-plastic expansion of a long cylinder, and a sphere from a finite radius by radial stresses acting at their surfaces was obtained by Bishop, Hill and Mott (1945) assuming the material to be linearly elastic, in the elastic zone and rigid-plastic, obeying Von Mises yield criterion and Saint Venant's flow rule in the plastic zone. The solution they obtained showed a discontinuity of vertical stress at the elastic-plastic boundary. Although such a discontinuity of stress would not violate equilibrium, a later exact solution by Hill (1950) showed that the discontinuity, does not in fact occur if elastic strains are allowed for in the plastic zone (i.e. if an elastic-plastic material model is used. Hill obtained a solution of the problem of the expansion of a cylindrical cavity from zero radius to a finite radius by radial stresses acting at the surface of the cavity in a material obeying Prandtl-Reuss's flow rule in the plastic zone. Using Coulomb's yield criterion in lieu of Von Mises together with the same assumptions as Bishop et al (1945), Skempton Yassin and Gibson (1953) analysed the problem of the expansion of a spherical cavity within an infinite medium

which they applied to predict the ultimate end bearing capacity of a driven pile. Based on the same hypothesis Gibson (1963) analysed the expansion of a cylindrical cavity from a finite radius, in a granular medium, which he applied to problems associated with the 'Menard pressure-meter'.

A comprehensive numerical treatment of the problem of expansion of long cylindrical and spherical cavities from zero radius and from finite radius by radial pressure acting at their inner boundaries has been given by Ladani (1963). He obtained the shear strain at various radii from purely geometrical considerations and thence the stresses from experimental stress-strain curves.

An analytical solution of the problem of the expansion of a cylindrical cavity from zero radius to a finite radius by a system of radial and longitudinal shear stresses acting at its inner surface is given below, in which strains in the elastic zone are assumed to be infinitesimal but large strain theory is used in the plastic zone.

7.3 Expansion of a cylindrical cavity from zero radius to a finite radius

Referring to the cylindrical system of co-ordinates (r,θ,z) as shown in Figure (7.2), the equilibrium equation for an element (Figure 7.1) at a distance r from the oz axis can be written as:

$$\partial\sigma_{rr}/\partial r + \partial\sigma_{rz}/\partial z + (\sigma_{rr} - \sigma_{\theta\theta})/r = 0 \qquad (7.1)$$

$$\partial\sigma_{zz}/\partial z + \partial\sigma_{rz}/\partial z + \sigma_{rz}/r - \gamma = 0$$

where σ_{rr}, $\sigma_{\theta\theta}$ and σ_{zz} are the total normal stresses in r, θ and z direction respectively, σ_{rz} is the shear stress in rz plane and γ the bulk density of the material. The problem can be considered as:

(i) the expansion of an elastic cylinder, whose inner radius is r_o and outer radius ∞, by a system of stresses σ_o and τ_o, σ_o and

τ_o being the radial and shear stresses acting at the inner boundary,

(ii) the expansion of a fully plastic cylinder from zero radius to a finite radius by a system of stresses σ_i and τ_i at the inner boundary and σ_o, τ_o acting at the outer boundary (Figure 7.2).

Now for a long pile an element of soil of thickness dz at a depth z sufficient far from the ground surface will deform identically with the elements above and below it (this will be referred to approximately as a plane strain condition, here after). It is therefore quite reasonable for an element at a depth sufficiently far from the ground surface to assume (using a sign convention of compression positive):

$$\partial\sigma_{zz}/\ z = \gamma \text{ and } \partial\sigma_{rz}/\partial z = 0$$

Hence the equilibrium equations can be written as:

$$\begin{aligned} \partial\sigma_{rr}/\partial r + \tfrac{1}{r}(\sigma_{rr} - \sigma_{\theta\theta}) &= 0 \\ \partial\sigma_{rz}/\partial r + \sigma_{rz}/r &= 0 \end{aligned} \qquad (7.2)$$

and the problem is reduced to the solution of an elastic problem with the equilibrium equations given above, a plastic problem within the boundary governed by the yield criterion, incompressibility and the above equilibrium equations again and the compatibility of the stresses and displacements at the elastic-plastic boundary.

Solution for the stresses in the elastic domain

The equation of incompressibility combined with the condition of plane strain can be written as:

$$\varepsilon_{rr} + \varepsilon_{\theta\theta} = 0$$

where ε_{rr} and $\varepsilon_{\theta\theta}$ are the radial and circumferential strains respectively. For large displacements we have

$$\varepsilon_{rr} = (\partial u/\partial r)/(1 + \partial u/\partial r),\ \varepsilon_{\theta\theta} = u/(u+r)$$

Substituting these into the equation for incompressibility we get:

$$\partial/\partial r\ (u^2 + r\ u) = 0$$

which can be integrated to give:

$$u^2 + r\ u = C_1 \qquad (7.3)$$

where C_1 is a constant of integration. In the elastic zone, which we may expect to be at some distance from the pile, u^2 will be negligible in comparison with r u. Thus for $r \geq r_o$ we can write equation (7.3) as:

$$r\ u = C_1$$

Substituting the boundary condition for $u = u_o$ at $r = r_o$, where u_o is the radial displacement of the elastic-plastic boundary, we have:

$$u = u_o\ r_o/r$$

Hence $\varepsilon_{rr} = -u_o\ r_o/r^2$ and $\varepsilon_{\theta\theta} = u_o\ r_o/r^2$. By applying Hooke's law for incompressible material we get:

$$\sigma_{rr} = -2G.\ u_o\ r_o/r^2 \text{ and } \sigma_{\theta\theta} = 2G.\ u_o\ r_o/r^2.$$

Substituting these into the first equilibrium equation (7.2) we obtain:

$$\partial\sigma_{rr}/\partial r - 4G.\ u_o\ r_o/r^3 = 0$$

Integrating we get

$$\sigma_{rr} = C_2 - 2G.\ u_o\ r_o/r^2 \qquad (7.4)$$

where C_2 is a constant of integration. Substituting the boundary conditions:

$r = r_o$, $\sigma_{rr} = \sigma_o$

$r = \infty$, $\sigma_{rr} = K_o\gamma z = \gamma z$ (since $K_o = 1$ for incompressible material)

we obtain $u_o = (\gamma z - \sigma_o)\ r_o/2G$ and $C_2 = \gamma z$ (7.5)

Substituting (7.5) in (7.4) and the result obtained thereof if substituted into the first equilibrium equation we obtain:

$$\sigma_{rr} = \gamma z + (r_o/r)^2 . (\sigma_o - \gamma z) \tag{7.6.1}$$

$$\sigma_{\theta\theta} = \gamma z - (r_o/r)^2 (\sigma_o - \gamma z) \tag{7.6.2}$$

From the plane strain and incompressibility condition:

$$\sigma_{zz} = (\sigma_{rr} + \sigma_{\theta\theta})/2 = \gamma z \tag{7.6.3}$$

Now using the second equilibrium equation we obtain

$$\sigma_{rz} = C_3/r \tag{7.6.4}$$

where C_3 is a constant of integration which can be obtained by applying the boundary condition at $r = r_o$, $\sigma_{rz} = \tau_o$, therefore:

$$\sigma_{rz} = \tau_o . (r_o/r) \tag{7.6.5}$$

Equations (7.6.1) to (7.6.5) give the solution for the stresses in the elastic domain provided the unknown quantities r_o, σ_o and τ_o are known from the solution of the plastic region in the inner $r < r_o$ region.

Due to the symmetric expansion of the cavity the elastic-plastic boundary will also be a cylindrical surface. At this surface the soil will be in a state of incipient yielding. Thus, if we assume that the yield criterion of Von Mises modified for plane strain condition is valid, we have

$$(\sigma_{rr} - \sigma_{\theta\theta})^2 + 4 \sigma_{rz}^2 = 4C_u^2 \tag{7.7}$$

where C_u is the undrained cohesion of the soil. Substituting the values of the stresses obtained from equations (7.6.1) to (7.6.4) at $r = r_o$ into (7.7) we obtain:

$$(\sigma_o - \gamma z)^2 + \tau_o^2 = C_u^2 \qquad (7.8)$$

Solution in the plastic domain

The equilibrium equations are valid in this domain and hence equation (7.6.4) is also valid. Substituting the boundary condition $\sigma_{rz} = m\, C_u$ at $r = a$ (where m denotes the fraction of C_u mobilised at the pile-soil interface) in (7.6.4) we have

$$\sigma_{rz} = m.C_u\,(a/r) \qquad (7.9)$$

At $r = r_o$ we have $\tau_o = \sigma_{rz} = m\, C_u\,(a/r_o)$ which if we substitute in (7.8), we obtain

$$(\sigma_o - \gamma z) = C_u \left[1 - (ma/r_o)^2\right]^{\frac{1}{2}}. \qquad (7.10)$$

Again from the failure criterion we have:

$$(\sigma_{rr} - \sigma_{\theta\theta}) = 2\, C_u \left[1 - (ma/r)^2\right]^{\frac{1}{2}}. \qquad (7.11)$$

Equation (7.11) is valid throughout the plastic domain, hence, substituting (7.11) in the first equilibrium equation and integrating we get

$$\sigma_{rr} = 2\, C_u \left[1 - (ma/r)^2\right]^{\frac{1}{2}} - 2\, C_u \log \left[r + (r^2 - m^2a^2)^{\frac{1}{2}}\right] + C_3 \qquad (7.12)$$

The constant of integration C_3, can be obtained, by substituting the boundary condition at $r = r_o$; $\sigma_{rr} = \sigma_o$, where σ_o is given by equation (7.10):

$$\therefore \quad C_3 = \gamma z - C_u \left[1 - (ma/r_o)^2\right]^{\frac{1}{2}} + 2C_u \log \left[r_o + (r_o^2 - m^2a^2)^{\frac{1}{2}}\right] \qquad (7.13)$$

Equations (7.9) to (7.13) provide the radial, circumferential and shear stresses in the plastic domain. The vertical stress is given by the condition of incompressibility and plane strain, i.e. $\sigma_{zz} = (\sigma_{rr} + \sigma_{\theta\theta})/2$. The only problem left now is to determine the radius (r_o) of the elastic

plastic boundary.

Substituting the boundary condition at r = a; u = a in equation (7.3) we obtain

$$u^2 + r\,u = 2a^2$$

Hence the displacement at $r = r_o$ is given by $u_o^2 + r_o\,u_o = 2a^2$. If we assume again that the distance $r_o >> u_o$ so that u_o^2 is negligible in comparison with $r_o\,u_o$ we obtain

$$u_o = 2a^2/r_o \tag{7.14}$$

Hence from equations (7.5), (7.10) and (7.14) we obtain:

$$(r_o/a)^2 = 4(G/C_u)/\left[1 - (ma/r_o)^2\right]^{\frac{1}{2}} \tag{7.15}$$

Equation (7.15) can be solved to obtain (r_o/a) and hence the stresses in the elastic and plastic domains can be calculated from:

(i) for $r_o \leq r \leq \infty$

$$\sigma_{rr} = \gamma z + 4G.a^2/r^2,$$

$$\sigma_{\theta\theta} = \gamma z - 4G.a^2/r^2, \tag{7.16}$$

$$\sigma_{zz} = \gamma z, \quad \sigma_{rz} = m.C_u.a/r$$

(ii) for $a \leq r \leq r_o$

$$\sigma_{rr} = 2C_u\left[1 - (ma/r)^2\right]^{\frac{1}{2}} + 2C_u \log\left[\{r_o + (r_o^2 - m^2a^2)^{\frac{1}{2}}\}\right.$$
$$\left./\{r+(r^2-m^2a^2)^{\frac{1}{2}}\}\right] + \gamma z - C_u\left[1 - (ma/r_o)^2\right]^{\frac{1}{2}}.$$

$$\sigma_{\theta\theta} = 2C_u \log\left[\{r_o + (r_o^2 - m^2a^2)^{\frac{1}{2}}\}/\{r + (r^2-m^2a^2)^{\frac{1}{2}}\}\right]$$
$$+ \gamma z - C_u\left[1 - (ma/r_o)^2\right]^{\frac{1}{2}} \tag{7.17}$$

$$\sigma_{zz} = C_u\left[1 - (ma/r)^2\right]^{\frac{1}{2}} + 2C_u \log\left[\{r_o + (r_o^2-m^2a^2)^{\frac{1}{2}}\}\right.$$
$$\left./\{r + (r^2-m^2a^2)^{\frac{1}{2}}\}\right] + \gamma z - C_u\left[1 - (ma/r_o)^2\right]^{\frac{1}{2}}$$

$$\sigma_{rz} = (a/r).\ m.C_u.$$

G in the above equations may be approximated as $\beta\ C_u$ where β is a constant depending upon the type of clay and the stress history. Skempton and Henkel (1957) quoted a typical value of about 46 for saturated London Clay. For fully saturated normally consolidated clay the value of G (the tangent shear modulus) is reported (Mayerhof, 1951) from 30 C_u to 130 C_u. Figure 7.3 shows a typical distribution of the ratios of increase in σ_{rr}, $\sigma_{\theta\theta}$ σ_{zz} and σ_{rz} to the undrained cohesion C_u plotted against various (r/a) for $\beta = 36$ and $m = 1$. This figure suggests that for a saturated clay very high total stresses and hence pore water pressures may exist around a driven pile.

7.4 The pore water pressure induced around a driven pile

The foregoing analysis may be modified to obtain useful information about the distribution of pore water pressure around a driven pile. If we consider the foregoing idealised material is a two phase continuum i.e. an ideally elastic perfectly plastic skeleton saturated with incompressible fluid then all spherical components of stress will be carried by the fluid as pore pressure and deviatoric stresses only will be carried, with zero volume change, by the skeleton as effective stresses. Thus the stresses calculated in equation (7.16) and (7.17) are in fact the total stresses.

Pore water pressures in a water saturated elastic skeleton

If the pore water pressure is U and ΔU, $\Delta\sigma_{rr}$, $\Delta\sigma_{\theta\theta}$ and $\Delta\sigma_{zz}$ are the increases in U, σ_{rr}, $\sigma_{\theta\theta}$, σ_{zz} due to pile driving, we have the pore water pressure increase is given by

$$\Delta U = (\Delta\sigma_{rr} + \Delta\sigma_{\theta\theta} + \Delta\sigma_{zz})/3 \qquad (7.17.1)$$

Substituting equations (7.16) and (7.17) in (7.17.1) we obtain; the pore water pressure increase in the elastic zone as:

$$\Delta U = 0 \tag{7.18}$$

and in the plastic zone:

$$\Delta U/C_u = (\Delta\sigma_{rr} + \Delta\sigma_{\theta\theta} + \Delta\sigma_{zz})/3C_u$$

$$= \left[1 - (ma/r)^2\right]^{\frac{1}{2}} - \left[1 - (ma/r_o)^2\right]^{\frac{1}{2}}$$

$$+ 2 \log \left[\{r_o + (r_o - m^2a^2)^{\frac{1}{2}}\}/\{r + (r^2 - m^2a^2)^{\frac{1}{2}}\}\right] \tag{7.19}$$

where r_o is given by equation (7.15). Typical calculations for r_o within the range of quoted values of β show that the value of r_o lies between 10 to 24 pile radii. Thus the analysis suggests that beyond a radius of 10 a to 24 a pore water pressures would not increase due to pile driving. Field observations (Bjerrum, 1961; Lo and Stermac, 1963, 1965; Koizumi and Ito, 1967) show that pore water pressure increases even up to 40 times the radius of the pile which confirm as one would expect that the simple elastic-plastic model used is not powerful enough to fully represent realistic soil behaviour. However, we can modify the analysis as follows to make a semi-empirical allowance for the fact that real soil skeleton do exhibit volume change under shear stress changes.

Pore water pressure using Henkel's generalised pore pressure equation

The excess pore water pressure induced by total stress changes in any element of soil under a three dimensional stress system may be predicted by the equation (Henkel, 1960)

$$\Delta U = B(\Delta\sigma_{mean} + \alpha_1 \cdot \Delta\tau_{oct}) \tag{7.20}$$

where

B and α_1 are generalised pore water pressure parameters,

$\Delta\sigma_{mean}$ is the change in the spherical component of stress tensor and is equal to $(\Delta\sigma_{rr} + \Delta\sigma_{\theta\theta} + \Delta\sigma_{zz})/3$.

$\Delta\tau_{oct}$ is the change in the octahedral shear stress =

$$1/3.\Delta\left[(\sigma_{rr}-\sigma_{\theta\theta})^2 + (\sigma_{\theta\theta}-\sigma_{zz})^2 + (\sigma_{zz}-\sigma_{rr})^2 + 6\sigma_{rz}^2\right]^{\frac{1}{2}}.$$

This equation is a generalisation, due to Henkel of Skempton's empirical pore pressure equation. Since B = 1 for saturated clay, equation (7.20) can be written as:

$$\Delta U = \Delta\sigma_{mean} + \alpha_1 \Delta\tau_{oct} \qquad (7.21)$$

where $\alpha_1 = (3A-1)/\sqrt{2}$, A being Skempton's pore pressure coefficient for "triaxial" stress increment (Skempton, 1954). If we apply the incompressibility and plane strain condition of $\sigma_{zz} = (\sigma_{rr} + \sigma_{\theta\theta})/2$ we can write equation (7.21) as:

$$\Delta U = (\Delta\sigma_{rr} + \Delta\sigma_{\theta\theta})/2 + \Delta\left[(3/2)(\sigma_{rr}-\sigma_{\theta\theta})^2 + 6\sigma_{rz}^2\right]^{\frac{1}{2}}. (\alpha_1/3) \qquad (7.22)$$

From equations (7.16), (7.17) and (7.22) and replacing G by $\beta.C_u$ we obtain:

(i) for $r_o \leq r \leq \infty$

$$\Delta U/C_u = (\alpha_1/3)\left[96\beta^2(a/r)^4 + 6(ma/r)^2\right]^{\frac{1}{2}} \qquad (7.23)$$

(ii) for $a \leq r \leq r_o$

$$\Delta U/C_u = \left[1-(ma/r)^2\right]^{\frac{1}{2}} + 2\log\left[\{r_o+(r_o^2-m^2a^2)^{\frac{1}{2}}\}/\{r+(r^2-m^2a^2)^{\frac{1}{2}}\}\right] - \left[1-(ma/r_o)^2\right]^{\frac{1}{2}} + 0.81\,\alpha_1 \qquad (7.24)$$

Equations (7.23) and (7.24) predict the pore water pressure increase throughout the whole body once r_o has been obtained from equation (7.15). It should be noted that + sign of Δu would indicate pore water pressure

increase and a - sign would indicate pore water pressure decrease because of the compression positive sign convention adopted for this Chapter.

Figure (7.4) shows the distribution of excess pore water pressures around a pile driven in normally consolidated clay ($A \approx 1$), a water saturated elastic-plastic skeleton ($A = 1/3$), an overconsolidated clay ($A = 0$) and a highly overconsolidated clay ($A = -1/3$) for typical values of $\beta = 36$ and $m = 1$. It can be seen that pore water pressures of 4 to 6.5 times the undrained cohesion may exist at the pile shaft face. Also for highly overconsolidated clay the theoretical excess pore water pressure may be negative beyond 7 times the pile radius.

Comparison with field data and discussion

Bjerrum et al (1961) have given comprehensive results of pore water pressure measurements around driven piles. The measurements were made in connection with the construction of a bridge abutment in Southern Norway in a clay described as homogeneous, saturated and normally consolidated with an average cohesion (C_u) of 2.5 T/m^2 between depths of 5 to 15 metres below ground level. The increase in pore water pressures were measured at depths of 7.5 metres and 10 metres during driving. The 20 cm sq. piles were made by welding 20 cm x 20 cm angles together. For the purpose of comparing these field results with the theoretical results obtained from equations (7.23) and (7.24) the pile has been assumed to be of equivalent circular cross-section of 11.3 cm radius. The value of α_1 has been calculated by assuming $A \approx 1$ for normally consolidated clay and the roughness coefficient m is chosen to be unity. If we assume that equation (7.23) is applicable beyond say a distance $(r/a) = 20$ away from the pile, then the mean insitu measured values of (ΔU) can be substituted in this equation to obtain $\beta = 30$. With this value of β the ratio of $|\Delta U/C_u|_{(r/a)}$ to $|\Delta U/C_u|_{(r/a)=10}$ was computed from (7.23) and

(7.24) for various values of (r/a). The theoretical results show (Figure, 7.5) that there is a very close agreement with the measured values. It was apparently not possible to obtain any reliable field measurements of excess pore water pressure in the region close to the driven pile because of the general ground disturbance due to pile driving.

Theoretical results for $(\Delta U/C_u)$ for normally consolidated clay ($A \approx 1$) for $m = 1$ and $\beta = 20$, 40 and 60 are compared with the various field results (Lo and Stermac, 1965; Koizumi and Ito, 1967) in Figure (7.6). Lo and Stermac measured the excess pore water pressures at Wallaceburg, due to driving of 3.5 inches diameter cylindrical pile in a normally consolidated silty clay. The field results agree closely with the theoretical results for $\beta \approx 30$ except near the pile shaft surface. The deviation from the theoretical results may well have been increased by:

(i) Errors in the obtained excess pore water pressures near the pile shaft surface due to disturbances caused by the dynamic pile driving.

(ii) The drain rate in silty clay being such that the undrained conditions do not apply accurately and consequently volume changes may have occurred.

More recently Koizumi and Ito (1967) have published measurements of excess pore water pressures due to driving two 30 cm dia x 5.55 metres long piles into a normally consolidated layers of slightly organic silty clay containing shells. The undrained cohesion of the clay was 0.25 Kg/cm^2 at 1.5 metres depth increasing up to 0.4 Kg/cm^2 at the toe of the pile. Earth pressure cells and pore water pressure cells were incorporated along the face of the piles which were pushed in at a rate of 10 cm/minute using a Winch system to minimise the disturbances. The increase in the total normal radial stress on the pile face was found to be nearly

equal to the increase in the pore water pressure which is in agreement with the present analysis. The ratio of $[\Delta U/C_u]$ at the pile face was found to be within 5.25 to 6.75 between the depths of 1.5 and 5.5 metres which again agrees with the theoretical values at the pile shaft face (Figure, 7.6).

Further measurements of the pore pressure increase due to driving model H-piles into slightly overconsolidated Varved clay were reported by Lo and Stermac (1963). Present analysis is only relevant to piles with circular cross-section and therefore these results can not be compared with the theoretical ones.

7.5 Dissipation of the pore water pressure around a driven pile

After the pile is driven rapidly into a uniform stratum the increase in the total stresses and pore water pressures can be computed from equations (7.16), (7.17), (7.23) and (7.24) based on the estimates of the undrained parameters G, C_u and experimentally determined α_1 values. The excess pore water pressure will decay with time giving rise to time dependent total stresses and effective stresses around the pile. This process of consolidation around a long pile may be analysed after making the following assumptions:

(i) The soil is assumed to be an elastic skeleton defined by shear modulus G' and bulk modulus K' saturated with an incompressible pore fluid.

(ii) A plane strain axially symmetric situation prevails ($\varepsilon_{zz} = 0$), hence the stresses, displacements and pore water pressures are only dependent on the radial distance from the centre of the pile and time.

The process of consolidation around a driven pile may then be examined

as follows.

In the solution of consolidation problems, very often a linear differential equation deduced by Terzaghi is used:

$$C_v \nabla^2 U = \partial U/\partial t \qquad (7.25)$$

where $C_v = (K_h/\gamma_w)\ (K' + 4/3\ G')$, K_h = hydraulic permeability, K' and G' are the bulk modulus and shear modulus respectively with respect to the effective stresses, γ_w is the unit weight of the pore water, U is the excess pore water pressure, t is the time and ∇^2 is the Laplace operator, which in radially symmetric coordinate system is given by $\{\partial^2/\partial r^2 + (1/r)\partial/\partial r\}$.

Equation (7.25) is developed by assuming that there is a linear relationship between the quantity of water expelled and the change in excess pore water pressure and that is only valid in the case of one dimensional loading and drainage under the condition of zero lateral strain (Oedometer case). Therefore it cannot be applied directly to the solution of the present problem and we shall make use of the general three dimensional theory proposed by Biot (1941).

The true process of three-dimensional consolidation for cylindrical bodies can be described by two equations (de Leeuw, 1965) formulated on the basis of Biot's theory (Biot, 1941). The first being the storage equation for an incompressible pore fluid:

$$-(K_h/\gamma_w)\ \nabla^2 U = \partial e/\partial t \qquad (7.26)$$

where e is the volumetric strain. The second equation is the deformation equation which can be deduced by writing the equilibrium equation in the radial direction (r) in terms of the displacement as:

$$G'\ \nabla^2 u - G'\ u/r^2 + (K' + 1/3\ G')\ \partial e/\partial r = -\partial U/\partial r \qquad (7.27)$$

Differentiating both sides of equation (7.27) and dividing both sides of equation (7.27) and adding the results we obtain:

$$-(K' + 4/3\ G')\ \nabla^2 e = \nabla^2 U \tag{7.28}$$

Equation (7.26) and (7.28) are fundamental equations to be solved for our problem. We can integrate (7.28) to give:

$$-(K' + 4/3\ G')\ e(r,t) = U(r,t) + g(r,t) \tag{7.29}$$

where, $$\nabla^2\ g(r,t) = 0 \tag{7.30}$$

Thus the function g(r,t) causes divergence from the linear relationship between e and U postulated by Terzaghi in his consolidation theory. Substituting (7.29) in (7.26) we obtain:

$$C_v \nabla^2 U = \partial U/\partial t + \partial g/\partial t \tag{7.31}$$

Equations (7.29) to (7.31) are the necessary equations for determining the three unknown quantities e, U, g(r,t). Eliminating U between (7.27) and (7.29) we get:

$$G'\ (\nabla^2 u - u/r^2 - \partial e/\partial r) = \partial g/\partial r\ ,$$

$$\text{or}\quad \partial g/\partial r = 0,\quad \text{or}\ g = f(t)$$

But since for the present problem U = 0, e = 0, at r = ∞, we must have g = 0 for the equation (7.29) to be valid. Thus as a special case, for the solution of the present problem equation (7.31) does degenerate into Terzaghi's equation.

Solution for the variation of the pore water pressure and stresses with time

Equations (7.29) to (7.31) will be solved for the following boundary conditions in terms of displacement and pore water pressure:

(i) permeable pile

$$
\begin{aligned}
&U = f(r), \quad a \leq r \leq \infty \ , \ t = 0 \ ; \\
&U = 0 \quad , \quad r = a \quad\ \ , \ t > 0 \ ; \\
&U = 0 \quad , \quad r = \infty \quad\ \ , \ t \geq 0 \\
&u = 0 \quad , \quad r = a, \infty \ , \ t \geq 0
\end{aligned}
\tag{7.32}
$$

where u here denotes further radial displacement (infinitesimal) caused by the dissipation of pore water pressure.

and (ii) for impermeable pile

$$
\begin{aligned}
&U = f(r), \quad a \leq r \leq \infty \ , \ t = 0 \\
&\partial U/\partial r = 0, \quad\ \ r = a \ , \ t > 0 \\
&U = 0 \quad , \quad\ \ r = \infty \ , \ t \geq 0 \\
&u = 0 \quad , \quad\ \ r = a, \infty, \ t \geq 0
\end{aligned}
\tag{7.33}
$$

The function f(r) in the above is given by equations (7.23) and (7.24). These solutions are useful from a practical standpoint since estimates are often needed of the time required for the pore water pressure dissipation process to be essentially complete (i.e. approximate time required for the pile to essentially attain its maximum ultimate bearing capacity). Analytical solution of the system of equations listed above is out of question hence we now proceed to solve them numerically.

It is convenient to express equation (7.31) with $\partial g/\partial t = 0$, in nondimensional form by substituting $R = (r/a)$ and $T = (C_v.t/a^2)$. Thus we have:

$$
\partial U/\partial T = \partial^2 U/\partial R^2 + (1/R)\ \partial U/\partial R \tag{7.34}
$$

Expressing equation (7.34) in finite difference form over a finite radius we have (Scott, 1963):

$$
\begin{aligned}
U_{i,T+\Delta T} - U_{i,T} = [\Delta T/(2.\Delta R^2)]\ \Big[&\{(1+\Delta R/2R_i)U_{i-1} \\
&+ (1 - \Delta R/2R_i)\ U_{i+1} - 2U_i\}_T + \{(1+\Delta R/2R_i)U_{i-1} \\
&+ (1-\Delta R/2R_i)\ U_{i+1} - 2U_i\}_{T+\Delta T}\Big]
\end{aligned}
$$

For all the nodal points in R direction we may write the above in matrix notation as

$$\{U_{T+\Delta T}\} - \{U_T\} = (\Delta T/2.\Delta R^2)\ (\lceil D \rceil \{U_T\} + \lceil D \rceil \{U_{T+\Delta T}\}) \qquad (7.35)$$

where

$\{U_{T+\Delta T}\}$ and $\{U_T\}$ are the values of the pore water pressure at time $T+\Delta T$ and T respectively,

ΔT and ΔR are the steps of integration in T and R direction,

$\lceil D \rceil$ is the matrix of finite difference coefficients.

Equation (7.35) in which the values of $\{U_T\}$ are known (starting with $T = 0$), gives a set of simultaneous equations in the unknowns $\{U_{T+\Delta T}\}$ for chosen intervals of integration ΔR and ΔT. There is no restriction on ΔT and ΔR, other than the second difference must be a reasonable approximation to the actual second derivatives. In general, small time steps must be chosen for a greater change of the excess pore water pressure. In order to incorporate the boundary condition for an impermeable pile a fictitious node at $R = 0$ is needed (Scott, 1963).

Thus having obtained $\{U_{T+\Delta T}\}$ from a prescribed $\{U_T\}$ the change in the pore water pressure between the time T and $T+\Delta T$ may be obtained from:

$$\{DU\}_{T+\Delta T} = \{U_{T+\Delta T}\} - \{U_T\} \qquad (7.36)$$

This change in pore water pressure would cause a further change in e and hence u which may be related by equation (7.29) as:

$$\{DU\}_{T+\Delta T} = \lceil E \rceil \{u\}_{T+\Delta T} \qquad (7.37)$$

where $\{u\}_{T+\Delta T}$ is the change in radial displacements at the nodal points,

$\lceil E \rceil$ is the matrix of finite difference coefficients for $(K' + 4/3\ G')\ (\partial u/\partial r + u/r)/3$.

Solution of equation (7.37) gives the changes in the radial displacements at all the nodal points if the boundary conditions for the radial displacement u = 0 at r = a and u = 0 at r = (a large enough distance from the pile), are incorporated. Having obtained this the changes in the radial stress at a time T+ΔT can be obtained from:

$$\{D\sigma'_{rr}\}_{T+\Delta T} = [DR]\ \{u\}_{T+\Delta T} \qquad (7.38)$$

where

$\{D\sigma'_{rr}\}_{T+\Delta T}$ is the change in the effective radial stress around the pile during the time interval T, T+ΔT,

$[DR]$ is the matrix for finite difference coefficients for the expression $(K' + 4/3\ G')(\partial u/\partial r) + (K' - 2/3\ G')\ (u/r)$.

Now, the effective radial stress at time T = 0 can be obtained from equations (7.16), (7.17) and (7.19) (or equations (7.23) and (7.24)) as:

$$\{\sigma'_{rr}\}_{T=0} = \{\sigma_{rr}\}_{T=0} - \{U\}_{T=0} \qquad (7.39)$$

where $\{\sigma'_{rr}\}_{T=0}$ are the effective radial stresses at T = 0,

$\{\sigma_{rr}\}_{T=0}$ are the total radial stresses at T = 0 obtained from equations (7.16) and (7.17),

$\{U\}_{T=0}$ are the pore water pressures at T = 0 obtained from equation (7.19) or equations (7.23) and (7.24), at the nodal points.

The effective radial stresses at T = ΔT, 2ΔT, 3ΔT .... etc may be obtained by adding to $\{\sigma_{rr}'\}_{T=0}$ successively the values of $\{D\sigma_{rr}'\}_{T+\Delta T}$ calculated from equation (7.38). Thus the ultimate bearing capacity (P_u) of a long driven pile at any time after driving may be calculated from:

$$P_u = \sigma_{rr}'.\ \tan\delta.\ A_s \qquad (7.40)$$

where

σ_{rr}' is the effective radial stress at the shaft face,

δ is the coefficient of friction between the pile shaft and the soil medium,

A_s is the area of the shaft surface.

Description of the computer programme and results

The computer programme and the associated procedures developed for the above analyses are described below. The listing of the programme is given in Banerjee (1969).

'Procedures' Print array, Mult, Inp, Crout 2, Solve have been discussed in Chapters 3, 4 and 5.

Solcar : This procedure solves a banded system of symultaneous equation (7.41) by Gaussian elimination. The original matrices $[A]$ and $\{C\}$ are destroyed and the results $\{B\}$ are stored in $\{C\}$.

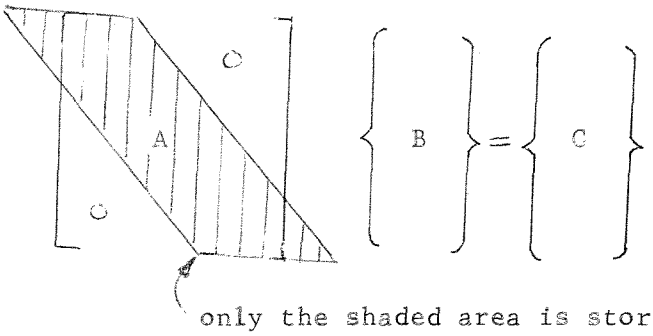

(7.41)

The main body of the programme essentially performs the following operations.

(i) Read data.

(ii) Check the time step.

(iii) Calculate the coefficients of the matrices $[D]$, $[E]$ and $[DR]$ by using finite difference approximations, and incorporate the boundary conditions given by equations (7.32) and (7.33).

(iv) Calculate $\{U\}_{T=0}$ at the nodal points from equations (7.18) and (7.19).

(v) Multiply $[D]$ and $\{U\}_{T=0}$ using the procedure 'Mult' and convert equation (7.35) into the form given by equation (7.41).

(vi) Compute $\{U\}_{T+\Delta T}$ by using 'Solcar'.

(vii) Calculate $\{DU\}_{T+\Delta T}$ via equation (7.36) and obtain $\{u\}_{T+\Delta T}$ by using 'Solcar'.

(viii) Multiply $[DR]$ and $\{u\}_{T+\Delta T}$ to obtain $\{D\sigma_{rr}'\}_{T+\Delta T}$

(ix) Obtain $\{\sigma_{rr}'\}$ and P_u via equations (7.39) and (7.40).

(x) Make $\{U\}_{T=0} = \{U\}_{T+\Delta T}$ and repeat the computational steps (v) to (x) until $\{U\}_{T+\Delta T}$ is less than a specified minimum i.e. until the pore water pressure dissipation process is essentially complete.

The numerical analysis involves the selection of a large enough radial distance in order to include the boundary conditions at infinity. The solutions described in the present work have been worked out by assuming this distance to be 15 times the radius of the pile. The ratio $M = T/(\Delta R)^2$ was found to have a considerable influence on the number of time steps required for the consolidation process to be essentially complete. From a series of trial computations it was observed that a range of $0.1 \leqslant M \leqslant 0.2$ was satisfactory. The accuracy of finite difference approximation would of course depend on smaller ΔR, particularly near the pile surface. The results described below have been calculated by using $\Delta R = 1/6$ i.e. $\Delta r = (1/6)a$, with the time step ΔT calculated to satisfy the condition $M = 0.15$.

Figures (7.7) and (7.8) shows the pore water pressures at time steps of 0, 1, 2, 4 and 8 for permeable and impermeable piles respectively. The pore water pressures at $(r/a) > 1.5$ are almost identical for both

piles. It is also interesting to note that for $(r/a) > 9$ the pore water pressures at $T > 0$ are higher than those at $T = 0$. The effect of the values of G' and K' on the corresponding effective radial stress at the pile face have been demonstrated in Figures (7.9) and (7.10). For a comparatively wide range of the values of the elastic modulii the variations in the stresses appear to be small.

Comparison with field data

Several authors (Seed and Reese, 1955; Yang, 1956; Airhart, 1967) have described full scale load tests on driven piles and observed from 6 to 10 fold increase in the ultimate bearing capacity with time with respect to that observed immediately after driving. The theoretical solution contains a number of parameters such as K_h, G', K', β, C_u etc., and hence to obtain any meaningful direct comparison with field results detailed information of these relevant parameters is necessary. Unfortunately it is not possible to obtain the value of these parameters from the test results described by the above mentioned authors.

Figure (7.11), which is reproduced from Soderberg (1962), shows the various observations of time dependent ultimate bearing capacity. These results have been expressed in a non-dimensional form in Figure (7.12) which shows the percentage increase in ultimate bearing capacity plotted against (T/T_{50}), where T is the time after driving and T_{50} is the time required to attain 50% of the maximum ultimate bearing capacity. Thus, by expressing the results in nondimensional form the effects of all but G' and K' have been eliminated. It is interesting to note that all the field results calculated from Figure (7.11) are quite close to each other and also the ultimate bearing capacity at $T \approx 0$ is about 15% of the maximum bearing capacity. The theoretical results for the ultimate bearing capacity corresponding to case (1) of Figure (7.10) have been plotted in Figure (7.12) by assuming the ultimate bearing capacity at $T = 0$ to be

15% of the maximum ultimate bearing capacity. This non-dimensional curve of the time dependent ultimate bearing capacity is found to be insensitive to variations in G' and K' within the quoted range in Figure (7.10). The agreement between the nondimensional theoretical and experimental results of Figure (7.12) is quite close to suggest that the time dependent bearing capacity of a driven pile can be predicted by extrapolating the results obtained from the load tests on piles at an early stage of the consolidation process.

7.6 Conclusions

A theoretical approach to understanding and predicting the increase in the pore water pressures and its effects on the ultimate bearing capacity of driven pile is developed. The conclusions of this study are summarised below:

(i) The increase in pore water pressure at the pile face may be up to 6.5 times the undrained cohesion of the soil.

(ii) For a pile driven into normally consolidated clay there may be no increase in effective stresses at the pile face immediately after driving.

(iii) The distribution of the pore water pressure due to pile driving is determined by three major parameters A, β and C_u, of which the evaluation of β appears to be difficult. However, it was found that β has a relatively small influence on the results, hence an approximately estimated value of β would give reasonably accurate results.

(iv) The ultimate bearing capacity of a driven pile may increase to 6 to 10 times of its value immediately after driving.

(v) The theoretical results have been compared with field test data with reasonable agreement.

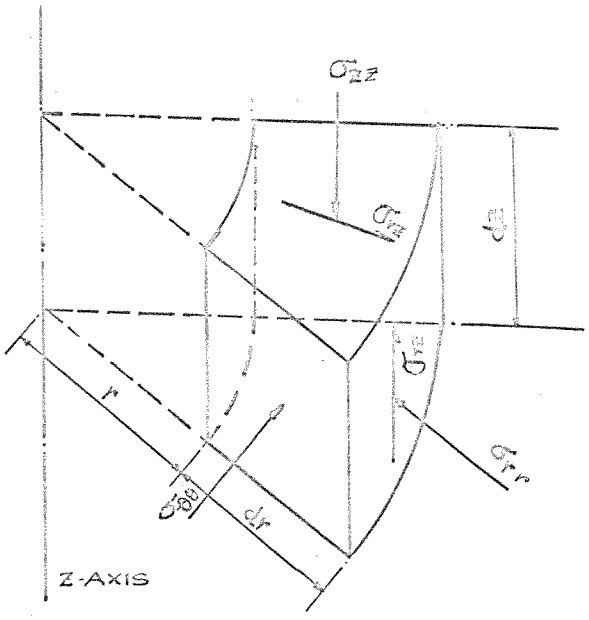

STRESSES ON AN ELEMENT

FIGURE – 7.1

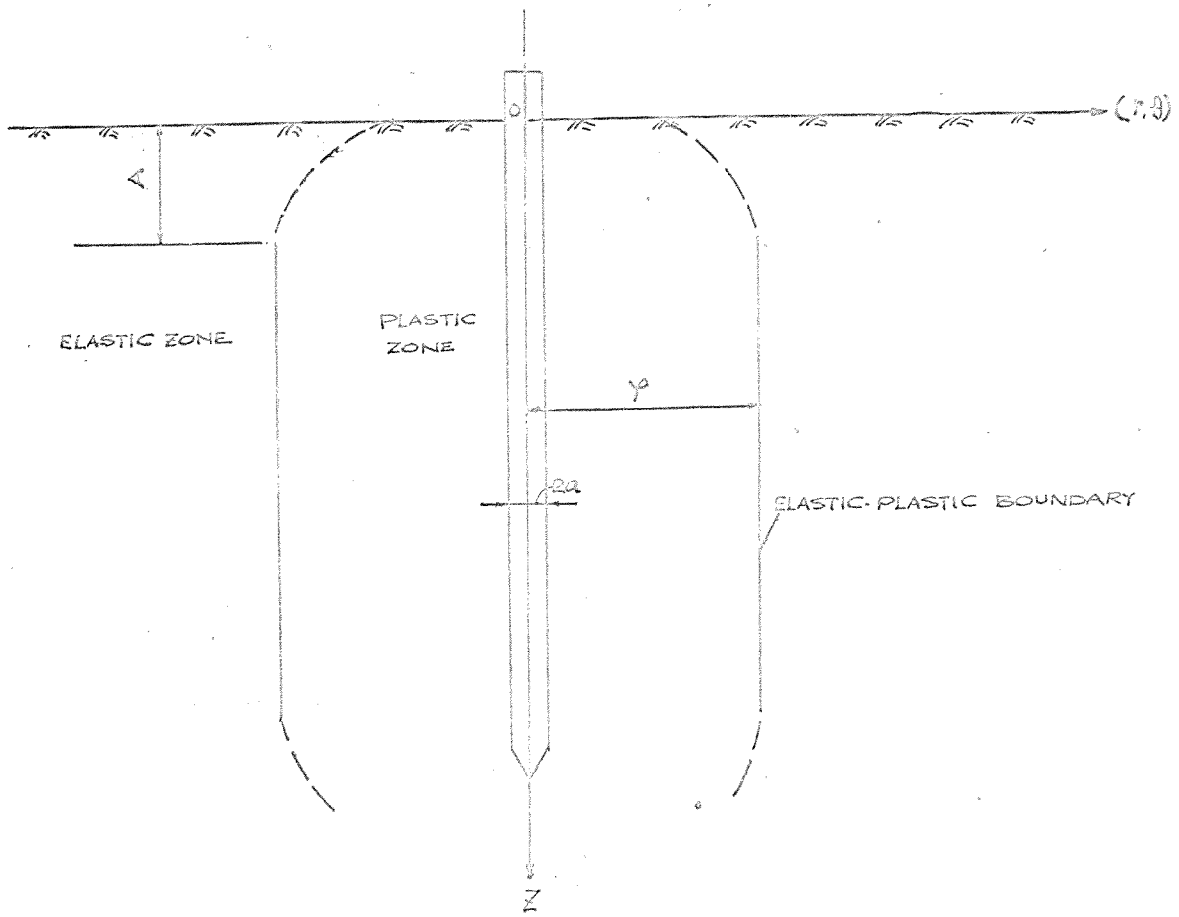

PROBABLE CONDITION AROUND A DRIVEN PILE.

FIGURE – 7.2

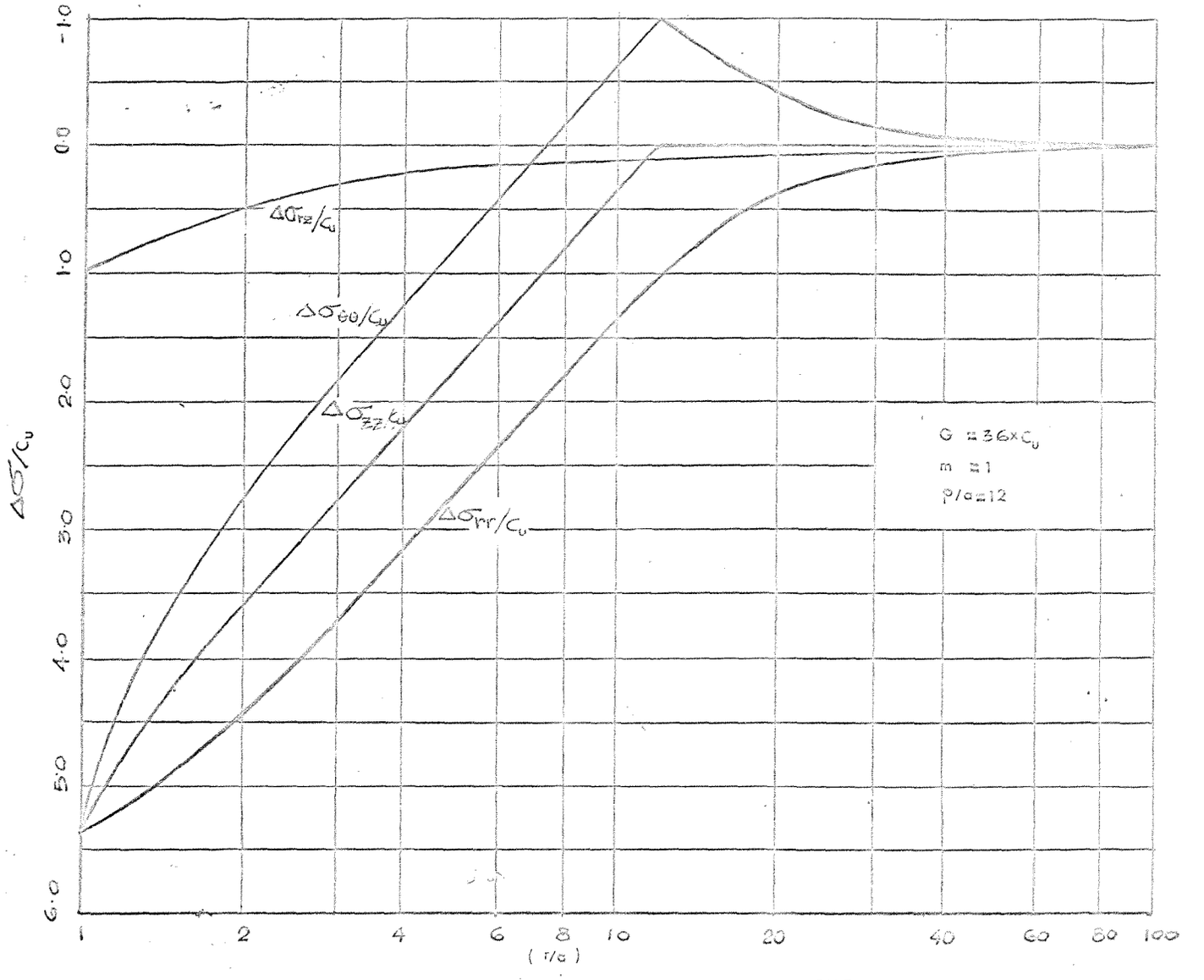

CHANGE IN THE STRESSES DUE TO A DRIVEN PILE

FIGURE - 7.3

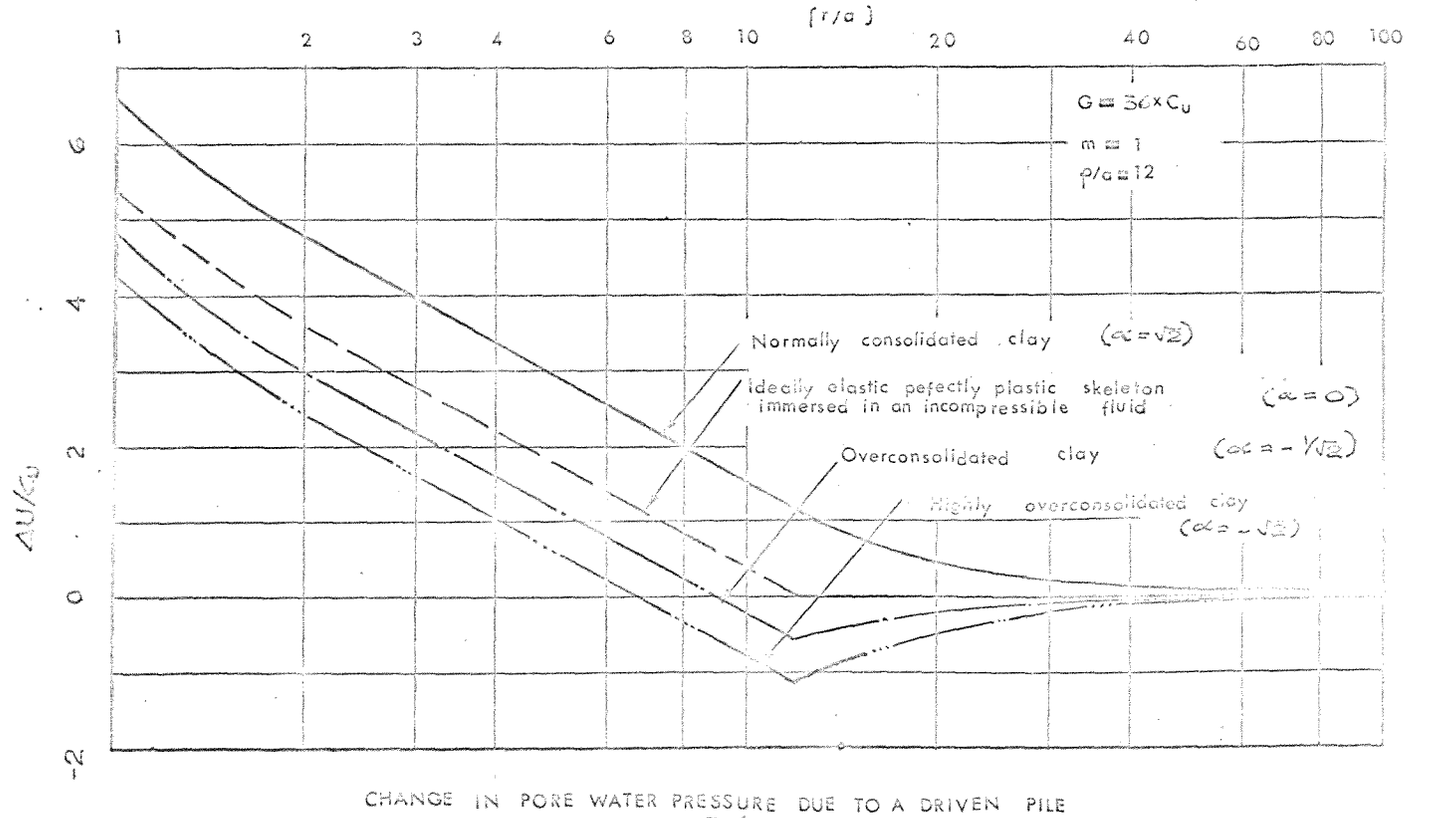

CHANGE IN PORE WATER PRESSURE DUE TO A DRIVEN PILE

FIGURE - 7.4

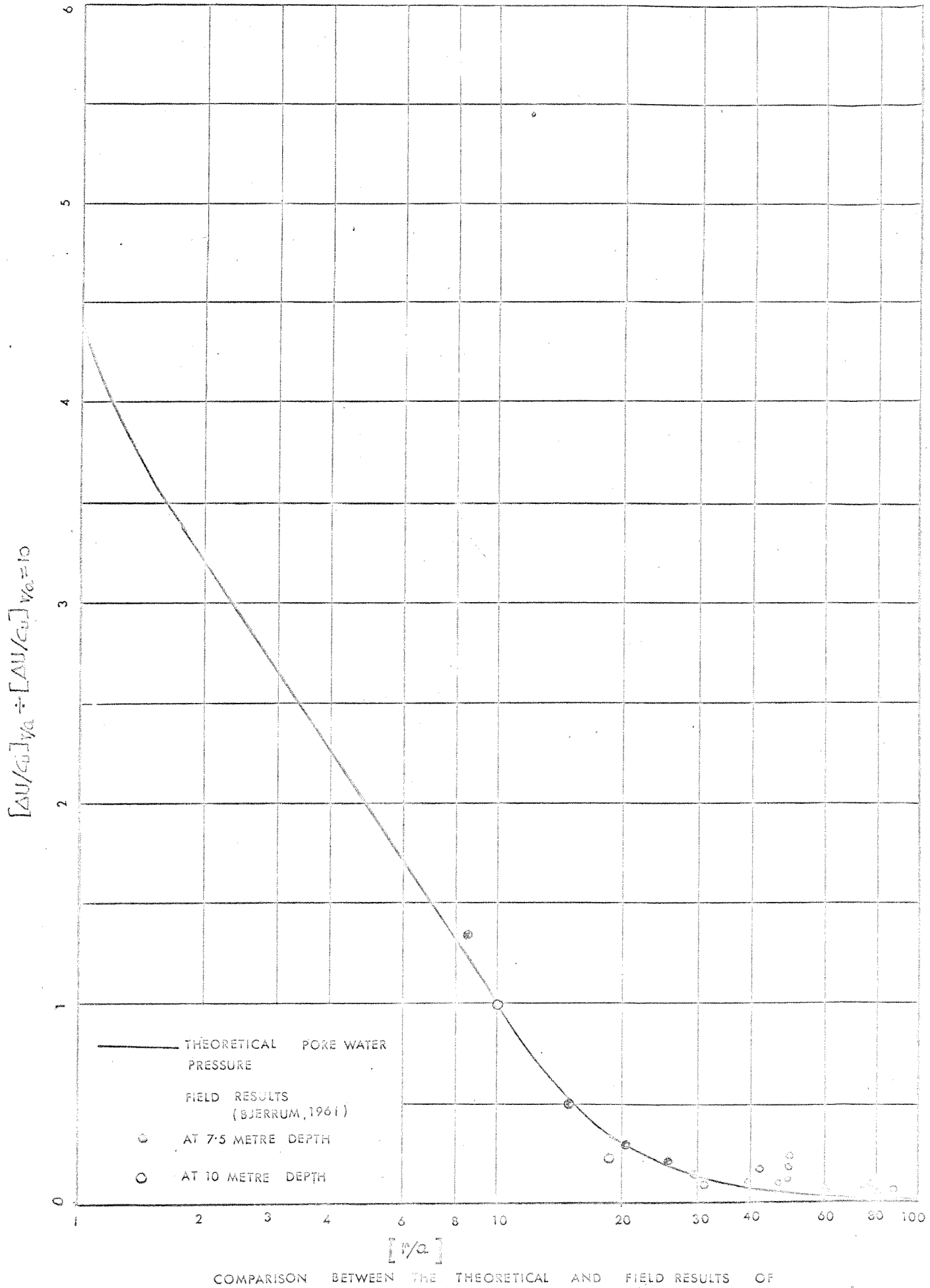

COMPARISON BETWEEN THE THEORETICAL AND FIELD RESULTS OF PORE WATER PRESSURE AROUND A DRIVEN PILE

FIGURE – 7.5

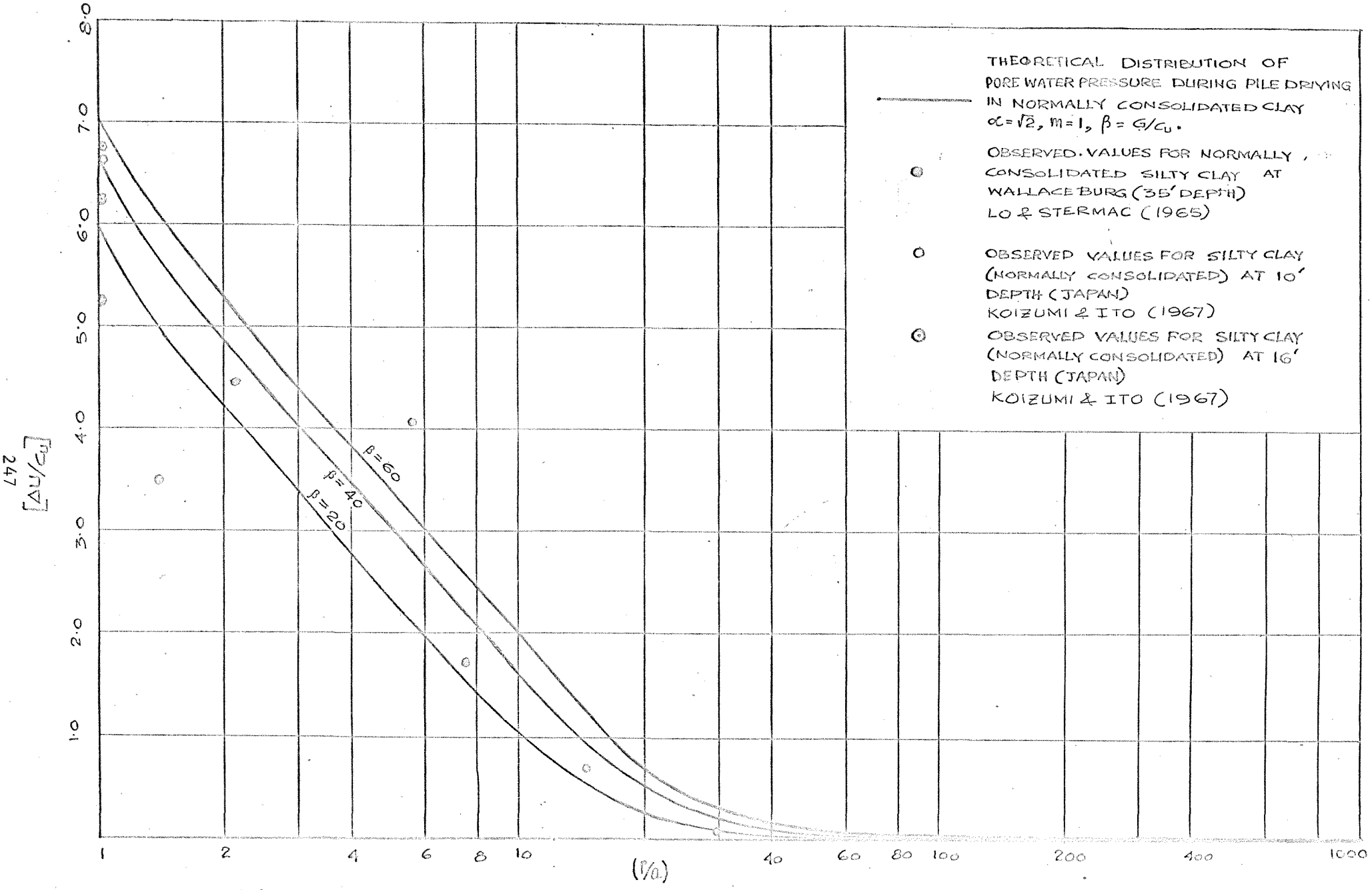

FIGURE 7.6 : COMPARISON BETWEEN THE THEORETICAL PORE WATER PRESSURE AND FIELD OBSERVATIONS

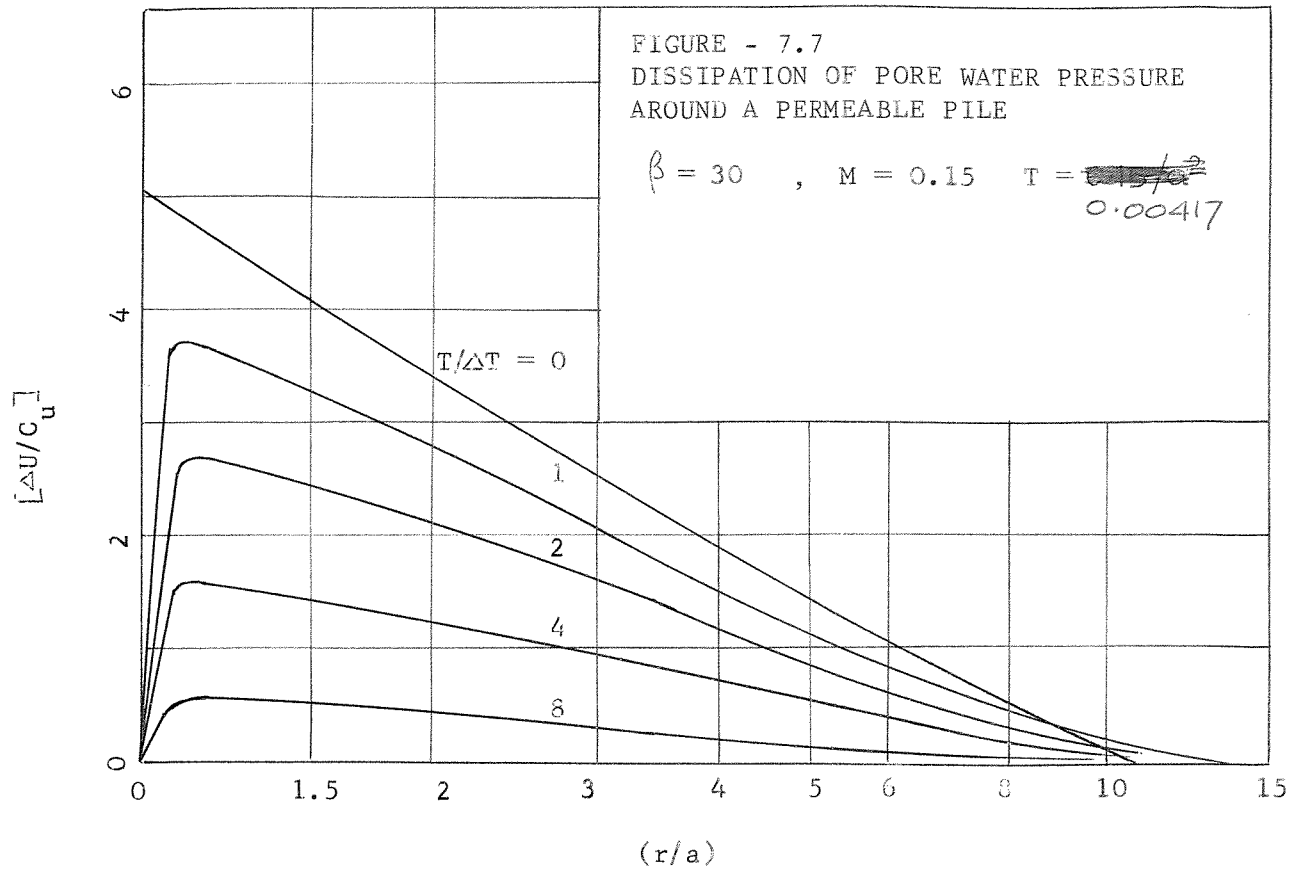
FIGURE - 7.7
DISSIPATION OF PORE WATER PRESSURE
AROUND A PERMEABLE PILE
β = 30 , M = 0.15 T = 0.00417
T/ΔT = 0
1
2
4
8
[ΔU/C_u]
(r/a)
0
1.5
2
3
4
5
6
8
10
15

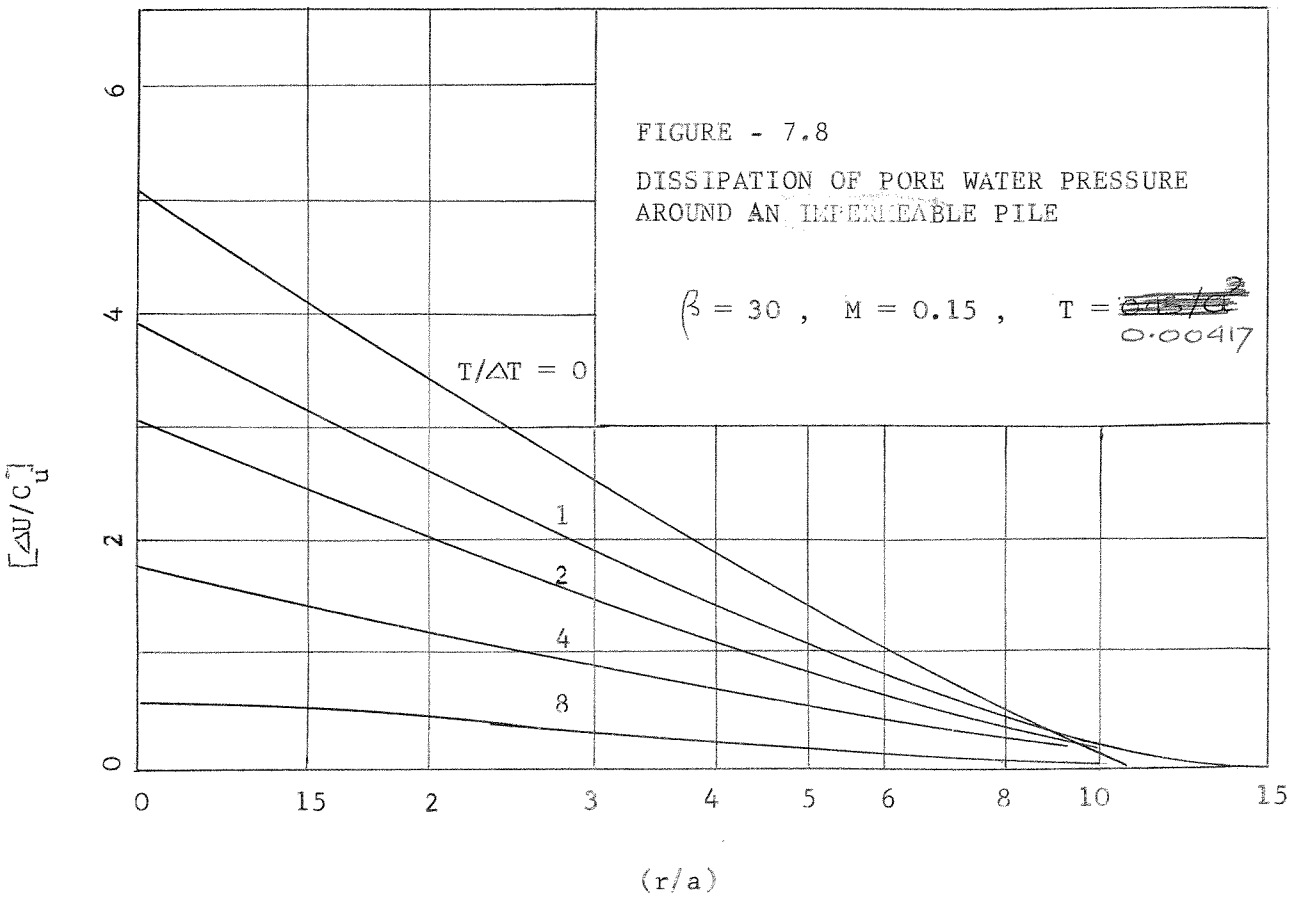
FIGURE - 7.8
DISSIPATION OF PORE WATER PRESSURE
AROUND AN IMPERMEABLE PILE
β = 30 , M = 0.15 , T = 0.00417
T/ΔT = 0
1
2
4
8
[ΔU/C_u]
(r/a)
0
15
2
3
4
5
6
8
10
15

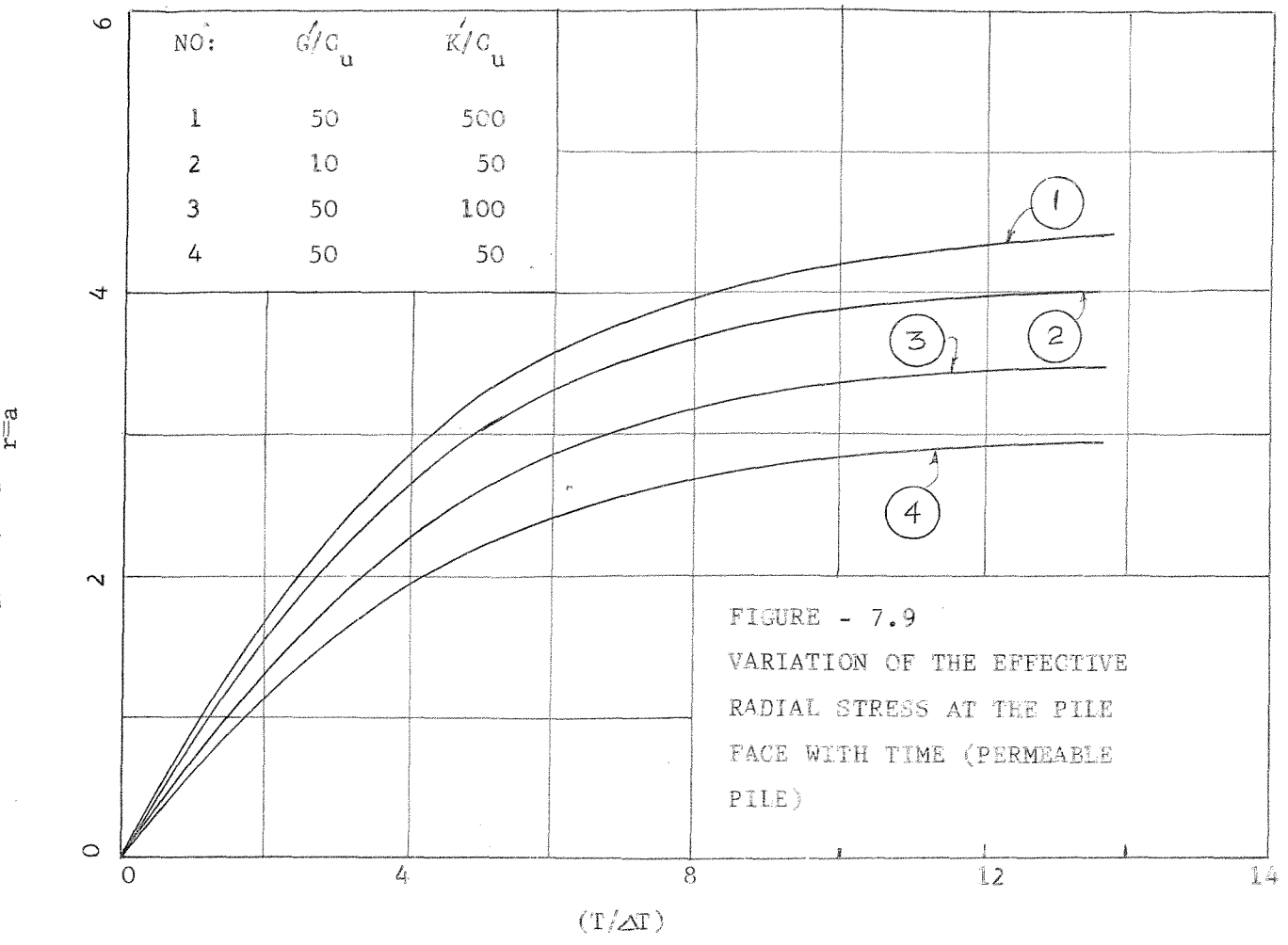

FIGURE - 7.9
VARIATION OF THE EFFECTIVE RADIAL STRESS AT THE PILE FACE WITH TIME (PERMEABLE PILE)

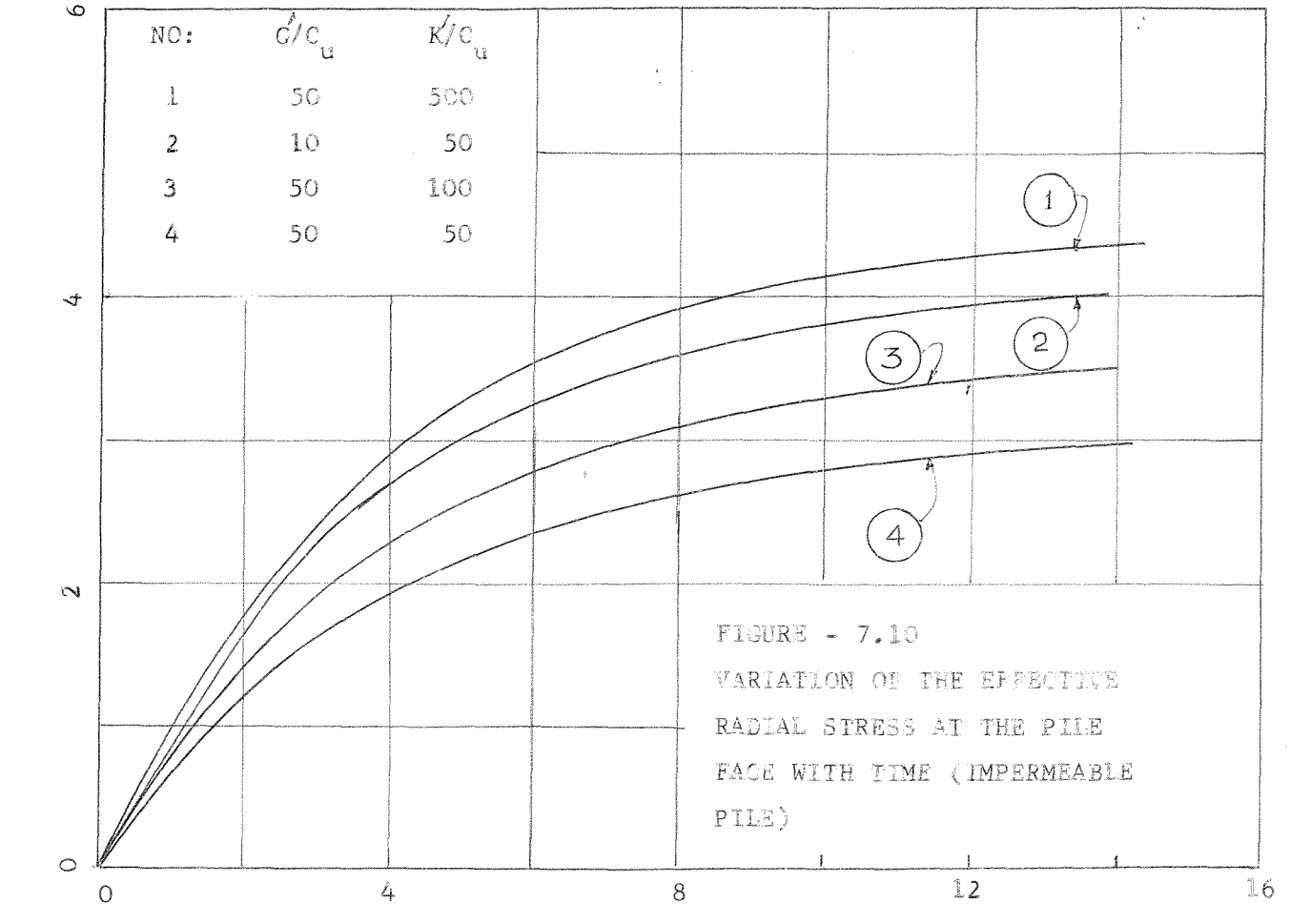

FIGURE - 7.10
VARIATION OF THE EFFECTIVE RADIAL STRESS AT THE PILE FACE WITH TIME (IMPERMEABLE PILE)

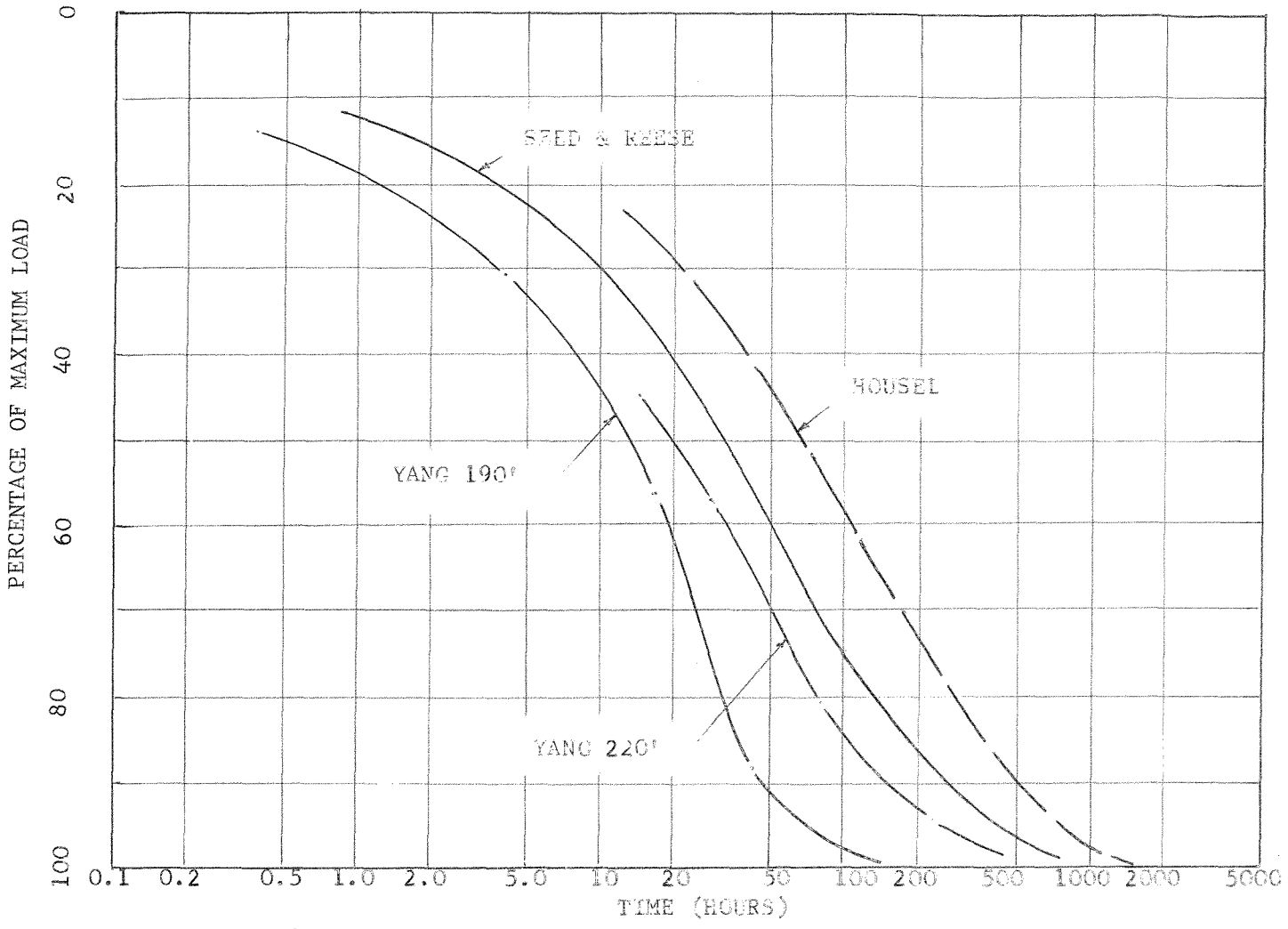

FIGURE - 7.11: FIELD RESULTS OF ULTIMATE BEARING CAPACITY OF DRIVEN PILES (FROM SODERBERG, 1962)

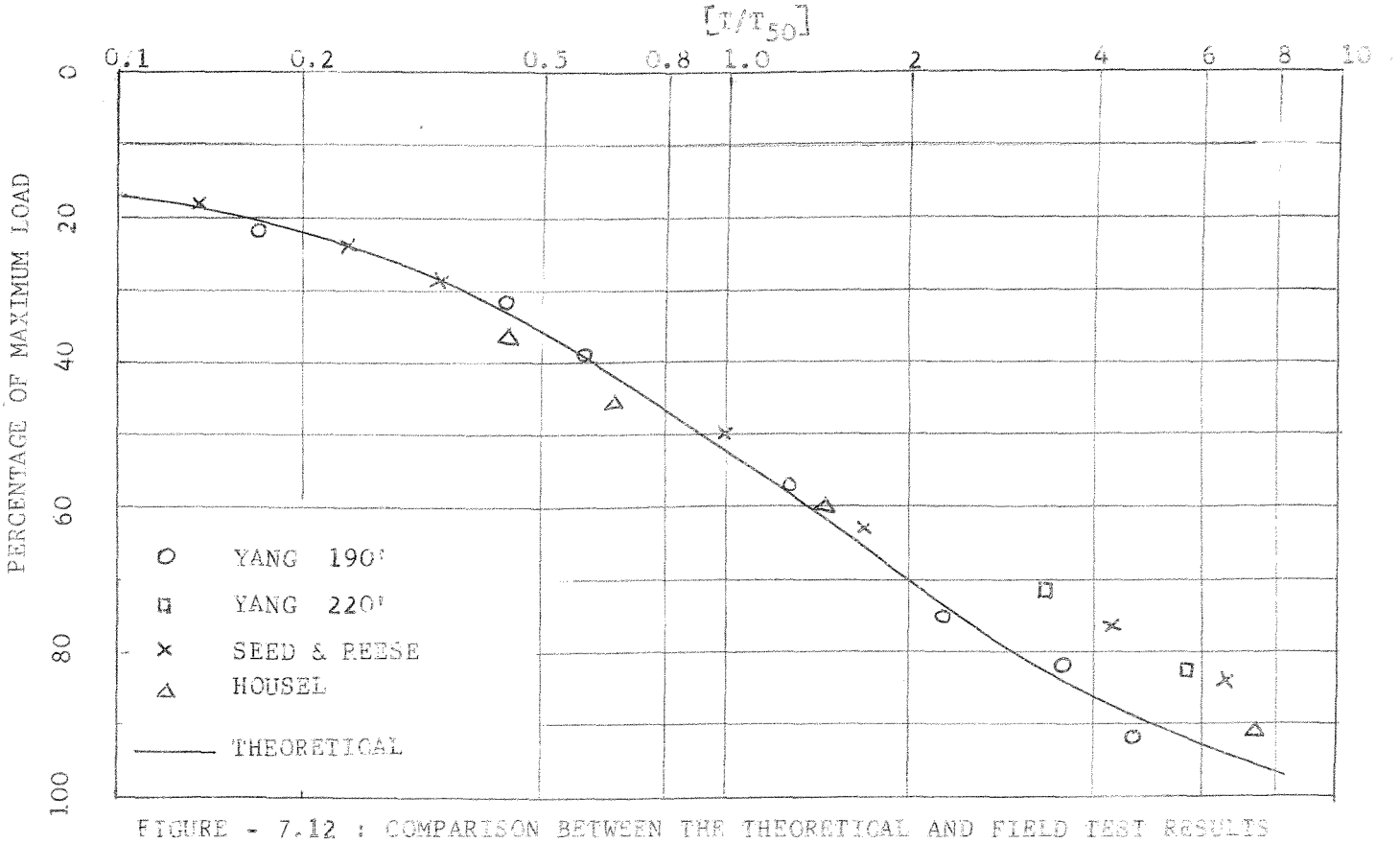

FIGURE - 7.12 : COMPARISON BETWEEN THE THEORETICAL AND FIELD TEST RESULTS

Chapter 8

Application of electro-osmosis to the driving of probes and blades in soils

8.1 Summary

In this Chapter the effects of electro-osmosis on the penetration resistance of blades and probes in clay is studied. A high speed, and a slow speed pile driving rig which have been developed to study the penetration resistance of probes and blades for a wide range of speeds of penetration is described. A series of tests was performed in which the speeds of penetration, the polarity of the electrodes and the voltage gradient across the electrodes was varied. The results of these tests are discussed. An analysis of probe soil interaction as affected by electro-osmosis is outlined.

8.2 Introduction

The phenomenon of electro-osmosis was discovered by 'Reuss' over 160 years ago. He observed that when a direct current was applied to a rigid, porous diaphragm which is submerged in water the pore water moves from the anode towards the cathode. Later Helmholtz (1879)* supplied the necessary mathematical support which was modified by Gouy (1910)* and others (Freundlich, 1926; Manegold and Solf, 1931)* but the quantitative results remained substantially unchanged (Casagrande, 1949).

8.2.1 Electro-osmotic flow

The currently accepted hypothesis of the mechanics of electro-osmotic flow through a single rigid capillary is based on the "diffuse double layer theory." The faces of clay minerals have a net residual negative charge which is balanced by the attraction of the exchangeable positive ions from the surrounding porewater. These positive ions in porewater orient themselves around the soil particle. The force of attraction between the particle and the exchangeable ions varies with the relative concentration of ions, and the temperature and the type of pore fluid. If an external potential difference is applied, it is observed that the soil particle and a thin layer of strongly attracted cations and water molecules will move (if they are free to move) with the negatively charged particle toward the anode. The diffuse system of counterions (which has a net positive charge) and the water associated with it, will move toward the cathode. Such a system is referred to as "The Diffuse Double Layer", the soil particle and the strongly adsorbed cations and the water molecules being one layer and the diffuse swarm of counterions constituting the other layer.

---

* Reported by Casagrande (1949).

A simplified diagrammatic representation of the water movement in a capillary is given in Figure (8.1), which shows the approximate velocity distribution over the cross section. Here d_1 indicates the thickness of that part of the double layer which is rigidly attached to the boundary wall, d_2 the thickness of that part of the double layer which can move, and d_3 the diameter of the inner free liquid.

The quantity of liquid moved in unit time through a capillary under the influence of a potential difference E has been obtained by Freundlich (1926) from the modified Helmholtz equation as:

$$Q_{e_1} = \frac{Dr^2 \xi E}{4\eta \ell} \qquad (8.1)$$

where r = radius of the capillary,

D = Dielectric constant of the fluid,

ξ = the electro-kinetic potential difference between that part of the double layer in the liquid which is bound to the wall, and the part which is free to move (termed zeta potential by Helmholtz),

η = coefficient of viscosity of liquid,

ℓ = length of the capillary.

Now if we consider a prism of saturated soil with a cross-sectional area A in contact with the electrodes and length ℓ equation (8.1) becomes:

$$Q_e = \frac{Dq\xi}{4\eta} \cdot \frac{E}{\ell} \cdot A \qquad (8.2)$$

where q is related to the porosity and to the cross-section of the pore space through which the water moves.

Equation (8.2) can alternatively be written as:

$$Q_e = K_e \cdot i_e \cdot A \qquad (8.3)$$

where $K_e = \frac{Dq\xi}{4\eta}$, and assumed to be a constant for a given soil and may be described as the "electro-osmotic permeability" of the soil and i_e is the electrical potential gradient. It is very interesting to note that equation (8.3) is very similar in form to Darcy's equation for hydraulic flow through a prism of soil:

$$Q_h = K_h \cdot i_h \cdot A \qquad (8.4)$$

where i_h is the hydraulic gradient, A the cross-sectional area, and K_h the hydraulic permeability of the soil.

There are however some fundamental differences between hydraulic and electro-osmotic flows. The electro-osmotic permeability K_e depends mainly on the pore area and is less dependent on the size and the shape of individual pores whereas K_h is strongly influenced by the shape and sizes of the pores. This has been shown analytically by Esrig and Majtenyi (1966) and experimentally by Casagrande (1949) and others (Piakowski, 1957; Lomize et al 1957). The distribution of the velocity of electro-osmotic flow and that of hydraulic flow across the cross-section of a single capillary are also different. This is shown in Figures (8.1) and (8.2).

8.2.2 The forces acting on soil particles and pore water during electro-osmosis

When an external electric potential is applied to a saturated soil mass, which has a network of electrical double layers at the soil-water interfaces, two equal and opposite systems of electrical forces are created simultaneously. One system of the electrical forces acting upon the negatively charged adsorbed layer tends to move the soil particle toward the anode and the other system, which acts on the positively charged movable layer, tends to move the pore water toward

the cathode. Due to the relative motion between the water and the soil, resisting forces are developed which are proportional to the relative velocity. In a rigid soil skeleton, the pore water flow reaches the steady state "instantaneously". If a saturated rigid soil mass is subjected to a combined hydraulic and electro-osmotic gradient, the seepage flow caused by the hydraulic gradient can be superimposed on the electro-osmotic flow. Assuming that they can be superimposed linearly, it can be shown (Wang and Vey, 1953) that at the steady state flow condition the resultant force on the soil particle due to the combined hydraulic and electro-osmotic action is equal to the resultant hydraulic seepage force.

The relation between the resultant hydraulic gradient under combined hydraulic and electro-osmotic action and the applied electric potential was established by Wang and Vey (1953) by making the following assumptions:

(1) The soil is perfectly saturated.

(2) The hydraulic flow obeys Darcy's Law (i.e. $V_{hx} = - K_{hx} \frac{\partial H}{\partial x}$ etc).

(3) The electric current obeys a similar law (i.e. $V_{ex} = - K_{ex} \frac{\partial E}{\partial x}$ etc).

(4) The electric current obeys Ohm's Law (i.e. $I_x = - \frac{1}{\rho_x} \frac{\partial E}{\partial x}$ etc).

(5) Both the pore water flow and the electric current flow obey the law of continuity.

Now within the system, at any position (x, y, z) the velocity of flow can be expressed as

$$\{V\} = - [K_h] \{\nabla\} H - [K_e] \{\nabla\} E \qquad (8.5)$$

where,

$$\{V\} = \begin{Bmatrix} V_x \\ V_y \\ V_z \end{Bmatrix}, \{\nabla\} = \begin{Bmatrix} \partial/\partial x \\ \partial/\partial y \\ \partial/\partial z \end{Bmatrix},$$

V_x, V_y, V_z being the velocities of the pore water in X, Y and Z directions respectively; and X, Y and Z axes are the principal axes of K_h and K_e,

$$[K_h] = \begin{bmatrix} K_{hx} & 0 & 0 \\ 0 & K_{hy} & 0 \\ 0 & 0 & K_{hz} \end{bmatrix} \text{ and } [K_e] = \begin{bmatrix} K_{ex} & 0 & 0 \\ 0 & K_{ey} & 0 \\ 0 & 0 & K_{ez} \end{bmatrix} ;$$

K_{hx}, K_{hy}, K_{hz} being the hydraulic permeabilities and K_{ex}, K_{ey} and K_{ez} are the electro-osmotic permeabilities in the X, Y and Z directions, respectively.

The law of continuity of hydraulic flow gives:

$$\{\nabla\}^* \{V\} = 0 \tag{8.6}$$

where $\{\nabla\}^*$ denotes the transpose of $\{\nabla\}$.

For the electric current Ohm's Law can be written as:

$$\{I\} = -[1/\rho]\{\nabla\}E$$

$$= -[C]\{\nabla\}E \tag{8.7}$$

where

$$\{I\} = \begin{Bmatrix} I_x \\ I_y \\ I_z \end{Bmatrix}, \quad [C] = [1/\rho] = \begin{bmatrix} 1/\rho_x & 0 & 0 \\ 0 & 1/\rho_y & 0 \\ 0 & 0 & 1/\rho_z \end{bmatrix},$$

if X, Y and Z are the principal axes of ρ,

I_x, I_y and I_z are the currents in the X, Y and Z directions respectively,

ρ_x, ρ_y and ρ_z are the resistivities in the X, Y and Z directions respectively.

The law of continuity of electric current flow gives

$$\{\nabla\}^{*}\{I\} = 0 \tag{8.8}$$

The above equations (8.5) to (8.8) of combined flow contain eight unknowns: the three velocity components (V_x, V_y, V_z), the three components of electric currents density (I_x, I_y, I_z), one resultant hydraulic potential or pore water head (H), and the applied electric potential (E). The other nine physical quantities, permeabilities and resistivities must be determined experimentally.

8.2.3 Solution of steady state electro-osmotic flow problems

Equations (8.5) to (8.8) are for a rigid soil skeleton and can only be applied to solve electro-osmotic flow problems where there is no volume change during electro-osmosis.

Then from equations (8.5) and (8.6) we have

$$-\{\nabla\}^{*}[K_h]\{\nabla\}H - \{\nabla\}^{*}[K_e]\{\nabla\}E = 0 \tag{8.9}$$

and combining equations (8.7) and (8.8) we have

$$\{\nabla\}\,[C]\{\nabla\}E = 0 \tag{8.10}$$

Equations (8.9) and (8.10) are Laplace equations of quasi-harmonic form, and thereby enable the well-developed theory of seepage to be extended the solution of corresponding electro-osmotic flow problems.

The function H determined from equations (8.9) and (8.10) is defined by the physical conditions of the problem. It appears that equations (8.9) and (8.10) enable us to reduce a steady state electro-osmotic seepage problem to the determination of a function, which is defined at the boundary of given problem and is quasi-harmonic (or harmonic) within the region. Solutions of some steady state seepage problems under electro-osmosis are given by Butterfield and Banerjee (1967) using a

finite difference technique.

8.2.4 Electro-osmotic consolidation of soil.

The electro-osmotic flow problem becomes much more involved when during the process of electro-osmosis the soil volume changes noticeably. This occurs in the electro-osmotic consolidation of soil. Electro-osmotic movements of water in soil are essentially of two types:

(i) Where the electro-osmotic forces transport water from a source (A) say, to a sink (B) (i.e. a free flowing electro-osmotic cell). The soil skeleton behaves as a capillary system on which the resultant stresses are very small (see Art.8.2.2) and there is therefore zero change in the soil moisture during the process.

(ii) Where the flow is restricted either by impermeable boundaries or by what is essentially the same thing, the source beyond the anode being the pore water in a fine grained soil mass. In this case there are very high resultant stresses set up in the soil skeleton.

In both these cases the resultant stresses cause consolidation of the soil skeleton as explained below. In (i) the consolidation is negligible whereas in (ii) it will be considerable. However the time taken to fully consolidate a large body of soil (i.e. produce appreciable changes in moisture content) is long enough to preclude major short term modifications of moisture content being achieved by electro-osmosis (or any other consolidating process).

Much research has been carried out (Casagrande, 1952; Schaad and Haefeli, 1947; Evans and Lewis, 1965; Preece, 1947; Vey, 1949) to try and interpret the basic mechanics of the electro-osmotic consolidation process but no completely successful theory has yet been produced.

The two following simple cases illustrate the consolidation of a soil sample under hydraulic and electrical potential gradients.

Case 1. Referring to Figure (8.3.1), the tank on the right hand side is filled to level YY 'aa' is sealed and the sample pore pressures therefore correspond to the YY level. If 'aa' is now opened flow starts and eventually, as the sample consolidates under the seepage forces, the piezometric level becomes xy (Figure, 8.3.2). In this steady state the increase in effective stresses $\delta\sigma$ is given by the ordinate δu in this figure and the soil skeleton is compressed against the end 'aa'. The consolidation process is therefore that of the dissipation of the triangular (XYY) excess pore pressure distribution with two free draining boundaries 'aa' and 'bb'. Now by the addition of a suitable electrical potential E across a-b, (Figure, 8.3.3), the steady state hydraulic flow can be cancelled. This will in no way alter the consolidation process since, in a free flowing electro-osmotic cell no net seepage forces are produced (see Art. 8.2.2).

Case 2. If however the end 'aa' always remains sealed there are no hydraulic seepage forces and the piezometric level remains at YY until E is applied. With 'aa' as the anode (Figure, 8.3.3) drainage can now only occur through 'bb' but the eventual steady state situation is again exactly as in Case 1. If 'aa' is rigid the net result of the compressive effective stresses in the soil skeleton is a displacement of the solids away from the cathode at 'bb', no final change in the soil state at 'bb' and considerable hardening at 'aa'.

During the process of consolidation, soil properties like resistivity, hydraulic permeability etc. change considerably. However, the observations by Wang and Vey (1953) suggest that a relationship exists between all electrical and mechanical properties of soil. Thus it is possible to try and postulate a comprehensive model to explain these changes in

mechanical and electrical properties of soil under electro-osmosis.

8.2.5 Electro-osmotic activity of soils

In general the velocity of pore water in soils under electro-osmosis depends upon the electric potential (E), the hydraulic potential (H), the salt concentration of pore water (C'), the water content of soil mass (M) and the temperature (t).

$$\{v\} = -[K_e]\{\nabla\}E - [K_h]\{\nabla\}H + [K_c]\{\nabla\}C' - [K_w]\{\nabla\}M - [K_t]\{\nabla\}t \qquad (8.11)$$

where K_c, K_w and K_t are properties of the soil mass and K_e and K_h are as defined previously. As a first approximation assuming no change in temperature, and ignoring C', the gradient M ultimately gives rise to a seepage field that superimposes on the external filtration field (Netoushil, 1953). Thus equation (8.11) reduces to

$$\{v\} = -[K_h]\{\nabla\}H - [K_e]\{\nabla\}E$$

$$= -[K_h]\left(\{\nabla\}H + [K_h]^{-1}[K_e]\{\nabla\}E\right)$$

$$\text{or } \{v\} = -[K_h]\{\nabla\}(H + H_e) \qquad (8.12)$$

Where $\{\nabla\}H_e = [K_h]^{-1}[K_e]\{\nabla\}E$ is a hydraulic gradient equivalent to the electrical potential gradient causing the electro-osmotic flow.

Experimental investigations of the electro-osmotic flow of water carried out by several research workers Casagrande, 1949, 1952; Lomize et al 1957) have shown that electro-osmotic permeability K_e can be considerably greater than the hydraulic permeability, depending on the colloidal content of the soil. It has already been mentioned that K_e varies very little with grain size, soil grading, shape of pores

etc. For most soils ranging from fine sand to heavy clays (e.g. London Clay) the value of K_e is about 5×10^{-5} cm/sec. (Casagrande, 1949, 1952). On the other hand K_h ranges typically from 3×10^{-3} cm/sec for dense fine sand to 7×10^{-9} cm/sec for London Clay. Thus the ratio of K_e/K_h for any soil is of major importance in practical applications of electro-osmosis in foundation engineering and earthworks. If K_e/K_h is less than 1 there is no advantage of electro-osmotic dewatering etc., over pumping. But if K_e/K_h is large then $H_e >> H$ for small E values hence electro-osmotic "dewatering" is very much better than any other method. Several practical applications of electro-osmosis in foundation and earthworks have been described by Casagrande (1952, 1962), Lomize et al (1957), Soderman and Milligan (1961).

Equations (8.5), (8.9) and (8.12) are based on the assumption that the electrical and hydro-mechanical forces are acting independently; whereas from the basic analysis of the physical process of electro-osmosis it is evident that the impressed electrical field must change the seepage properties of the soil. For the clayey soils investigated by Lomize et al (1957) the value of K_h under electro-osmosis was found to have increased by 8 to 15 times, the more hydrophilic the soil and the larger its density the greater the increase. This has been attributed to alteration of the shape or tortuosity of the capillaries under an impressed electrical field - an assumption that has been questioned (Esrig and Majteyni, 1966).

8.3 Reduction of apparent adhesion between soil and metal objects by electro-osmosis

Saturated clay soils adhere to metal objects as a result of two phenomenon, adhesion and negative porewater pressure or suction. The adhesive forces are intermolecular and they develop essentially on a direct contact with clay particles. If a very small gap is formed

between the object and the clay particles the adhesive forces become negligible. It has been shown by Peleg (1960) and Potyondy (1961) that a very thin layer of moisture between metal objects and clay reduces the adhesion considerably. Though the basic idea of adhesion between the metal implements and clay soils seems very simple, the magnitude, however, depends upon the cleanliness, humidity, oxide or other films, surface finish, velocity of sliding, contact pressure, grain size, direction of grain orientation, vibratory, static or dynamic loading, etc. Thus the problem is one of extreme complexity.

The forces due to negative pore water pressure play a very important part in the bonding forces between metal objects and soil. With atmospheric pressure p_o and absolute pore water pressure p, the bonding force per unit area due to suction is $(p_o - p)$. If the wetted area is A^1 (Figure 8.4) and the total area is A and $A^1/A = \alpha$ (say), then the equivalent total force per unit area due to this on the total area A is $\alpha(p_o - p)$.

Now if the surface tension is T, and the radii of curvature of the two menisci R_x, R_y, the suction pressure inside the water neck is given by

$$(p_o - p) = \frac{T}{R_x} + \frac{T}{R_y} \qquad (8.13)$$

Thus as the moisture content increases, R_x, R_y increase and therefore the suction pressure decreases, and, as the moisture content decreases R_x, R_y decrease and therefore the suction pressure increases. The ratio α is dependent on moisture content and contact pressure. It increases with the increase in moisture content and contact pressure. Thus it would appear that the total normal stress on A_s will have a maximum at some intermediate moisture content. An addition of water to the metal soil interface or complete drying of metal-soil interface will destroy

the suction and consequently detach the metal object from the soil.

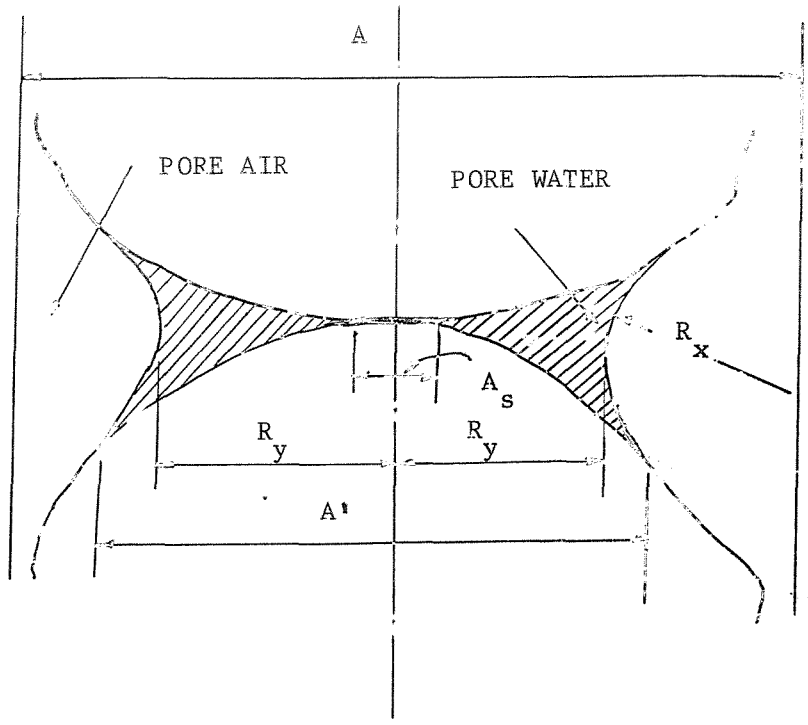

FIGURE - 8.4
SURFACE TENSION NEAR THE CONTACT
BETWEEN TWO PARTICLES

The suction contributes to the ultimate shear stress (τ_s) at the metal-soil interface. This contribution can be expressed as

$$\tau_s = \alpha(p_o - p) \tan\delta = \left(\frac{T}{R_x} + \frac{T}{R_y}\right) \tan\delta . \alpha \qquad (8.14)$$

where δ is the soil metal coefficient of friction.

It has been mentioned previously that when an electrical potential is applied across two electrodes driven into soil, two equal and opposite system of body forces are developed. One system acts in the porewater, pulling towards the cathode, the other system acts on the continuous solid phase and pulls towards the anode. Thus immediate compressive total stresses set up in the soil skeleton are reacting against the anode, which is held in equilibrium by a suction in the porefluid. Since the

soil does not behave exactly as an ideal water saturated elastic skeleton there will be an immediate reduction of the radial stress already existing around a driven probe. Thus a reduction in total radial stress will reduce the driving resistance of the probe.

During the application of electro-osmosis to a driven cathode probe a very thin film of moisture appears at the cathode, almost instantaneously with the switching on of the electric potential which helps to reduce the adhesion. Thus it is possible to reduce the apparent adhesion between a metal object and soil by electro-osmosis. Several research workers (Fountain and Payne, 1954; Zaslavasky and Ravina, 1965) have done experiments to investigate the effects of applying an electric potential to the adhesion existing between metal objects and soil but so far only a partial explanation of the phenomenon has been obtained.

The magnitude of the body forces set up during the application of an electrical potential to a driven cathode probe would depend on the applied potential 'E' and the ratio of electro-osmotic to hydraulic permeability. But this possible theoretical value will not be attained in a practical application because of inadequate sealing of the cathode and also near the anode the formation of gases (O_2) may prevent suction values exceeding one atmosphere. The suction of course may be greater in a completely saturated clay but in any case it is limited to the P_F value at the natural moisture content of the soil.

8.4 Electro-osmosis in the driving of probes and blades

Reltov and Novikov (1938) first suggested the use of electro-osmosis for facilitating the driving of piles into soil. Begemann (1953) published the results of laboratory studies and experiments on driving four reinforced concrete piles covered with strips of mild steel, using electro-osmosis. However his investigation did not include the effect

of various physucal and physiochemical factors on the effectiveness of driving piles and without this knowledge it is impossible to obtain the optimum benefit from electro-osmotic effects. Nikolaev (1962) investigated the influence of minerology, grain size distribution, moisture and porosity, area of electrodes on the sinking of a cathode pile. His work, however, does not include the effect of rate of penetration or the penetration resistance of a pile driven with or without electro-osmotic assistance.

On the basis of the preliminary investigation carried out by several research workers (Begemann, 1953; Nikolaev, 1962) and more recently by Butterfield and Banerjee (1967), it can be concluded that application of a negative electric potential to a probe reduces the skin friction by an amount up to about 70% depending on the applied voltage gradient and the probe geometry.

For a very short time application of electro-osmosis, such as in the sinking of probes in soils, the reduction in penetration resistance achieved is only temporary. Rapid restoration of the probe-soil gripping forces takes place almost immediately after switching off the applied potential. On this basis the electro-osmotic method of speeding up steel probe-driving operations may have some commercial application.

Apart from the beneficial results that can be achieved by driving probes and blades by electro-osmosis it should be borne in mind that application of a voltage gradient of high magnitude for a long time might lead to a very severe cracking of the ground surrounding the probe, which may be an unfavourable side effect.

The scope of the present work is to indicate the influence of voltage gradient and the speed of driving on penetration resitance of model probes in clay soils.

The application of an electric potential to the probe soil system gives rise to several complex physico-chemical phenomena most of which are not fully understood. Therefore in lieu of trying to evaluate the effects of these complex physico-chemical phenomena the present study was directed towards obtaining experimental relationships between penetration resistance, speed of penetration and voltage gradient.

8.4.1 Effect of electro-osmosis on penetrating probes and blades

During sinking of a cathodic probe with an applied D.C. potential a number of phenomena may occur which facilitate the driving operation:

(1) Bubbles of hydrogen form on the surface of the cathode as a result of electrolysis of water, these bubbles flow between the probe and the soil and therefore decrease the adhesion between the probe and soil during the time of sinking.

(2) In plastic clays the formation of a thin film of water on the surface of the cathode probe as a consequence of electro-osmosis is observed almost immediately the current is switched on. This film also reduces the adhesion between the probe and the soil.

(3) Due to continuous accumulation of moisture around the cathode the soil may even "wet up" to the liquid limit over a long period (Casagrande, 1952). This however takes a considerable time and can be ruled out completely for the short times involved in the application of electro-osmosis in the driving of probes.

(4) Due to development of body forces (mentioned in the Art. 8.2.2) the existing radial pressure around a driven pile decreases and thus contributes to the decrease in penetration resistance. The radial compressive stresses set up in the soil by a driven probe is thus reduced by an amount proportional to the voltage gradient and the "electro-osmotic activity" of the soil.

In the short term application of electro-osmosis to pile driving, the phenomena described in (2) and (4) appear to be the most significant, while in the long term application of electro-osmosis to such problems as the stabilisation of soil the effect of (3) and also many other complex physico-chemical phenomena are of relevance (Casagrande, 1962).

It has already been mentioned in Chapter 7 that very high porewater pressures develop when a pile is driven in clayey soil. Dissipation of this porewater pressure is primarily responsible for the increase of load carrying capacity of driven piles with time. The total time which a driven pile may take to reach its maximum load carrying capacity may in some cases take many months (Seed and Reese, 1955). It is possible to use electro-osmosis to dissipate the excess porewater pressure existing around the pile. The pile in this case will be made anodic and the cathode will be at some distance away from the pile. The corresponding time required for the pile to reach its maximum bearing capacity could thus be reduced considerably. In this case electro-osmosis is merely being used to accelerate an existing consolidation process.

8.4.2 Variation of electric potential during the application of electro-osmosis for a given probe electrode configuration

The rate of moisture movement in soil and the magnitude of the stresses set up in the soil skeleton are dependent on the magnitude and variation of the applied electric potential gradients. This it is necessary to investigate the distribution of the electric potential for a given probe electrode geometry.

In applications such as in plane problems (blade-plate electrode system) and in rotationally symmetric problems (co-axial probe-electrode system) the voltage gradient could be simply calculated. But it is generally difficult to provide a co-axial probe-electrode system for a

rotationally symmetric application of electro-osmosis. Hence an array of electrodes arranged around a central electrode (Figure, (8.5) has been used. The potential field for such a probe-electrode configuration can be obtained simply from an electric analogue. The analogue solution shown in Figure (8.5), shows that the actual voltage gradient at the pile face is about 4 times the average voltage gradient, the average voltage gradient being defined as the applied voltage divided by the radius R.

8.5 Apparatus for slow speed tests

8.5.1 Rotationally symmetric case:

Details of the model pile

The pile shaft consisted of a 3/4" diameter mild steel tubing of 3/32" wall thickness. The pile shaft was made in three sections, cut to their appropriate lengths and faced up in the lathe. Two shaft plugs were them machined to size. These had a central flange of 3/4" diameter with threaded connections each end. The function of these shaft plugs was to connect the two end pieces to the main pile shaft. The end pieces were designed to accommodate the load cells. An oval hole was cut just below the top plug in the side of the shaft for emerging wires from the bottom load cell. Four 3/32" diameter holes were also drilled radially in the bottom shaft plug, in the longitudinal direction, to take the wires from the bottom load cell up through the pile shaft. The outside surface of the pile shaft was cleaned after the assembly to get rid of the rust on the pile surface.

Details of Load cells

Two load cells were used. The one used on the top was to give a measurement of the total load acting on the pile during driving, whereas the bottom load cell was to give a measurement of end load at every

stage of driving. Thus it was possible to measure the shaft and end loads continuously during driving.

The core of the top load cell consisted of a solid cylinder of 7/16" diameter araldite. The base of this core was located in the centre of the top plug. Load was transmitted to the core by means of a spherical bearing resting on a mild steel cap glued to the top of the araldite core. Two foil strain gauges of 1/2" length were attached longitudinally to the core serving as active. Two similar gauges were attached circumferentially, acting as dummies. The cell was cased within the top 3/4" dia. tubing screwed to the top shaft plug. A P.V.C. bush was positioned between the casing and the load cell cap. The wires coming out of the top load cells were passed through two holes drilled in the cell casing. The details of the top load cell are given in Figure (8.6.1).

The bottom load cell was primarily a thin cylinder made out of a solid 3/4" dia. araldite core. The wall thickness of the cylinder was 1/16". It had 1/4" long and 1/2" dia. extension to the top end so that it can be pushed inside the pile. Two active strain gauges were attached longitudinally and two dummy strain gauges were attached circumferentially to the inside surface of the cylinder. The connecting wires to the strain gauges were taken through the 3/32" diameter holes in the bottom plug into the pile shaft and then out through the openings in the pile shaft at the top of the pile. The extensions of the araldite cell was then glued and pushed into the pile. The cell was then finally closed by a 3/4" diameter and 1/8" thick araldite disc glued to the bottom end. The bottom load cell was thus made perfectly watertight. The details of the bottom load cell can be seen in Figure (8.6.2).

Preparation of the sample

The clay bed was contained in a circular concrete cylinder of 4'6"

in diameter and 3'6" in depth. The bed was prepared from remoulded London Clay mixed in a large mixer and layered and compacted by hand in 3" layers. The surface of the sample was kept covered with wet sack and polythene sheets.

The driving rig

Basically the driving rig was the same as the one used by Johnston (1968). It constituted a network of steel girders from which the driving head was suspended. Four main girders extended from the ground to a height of about 8'0", each one being bolted to the concrete container at two points. Two joining girders were welded across each of the two pair of main vertical girders, so as to be parallel with each other. These two joining girders were fitted with trolleys capable of movement along the line of their supporting girders. From each trolley was suspended a 2" diameter threaded bar of length 3'0" and suspended from these was yet another girder. This supported the driving platform, which consisted of an inverted U section girder running along the suspended girder on another pair of trolleys. The driving platform itself supported and housed the electric driving motor, the system of driving shafts and chain sprockets and bearing plate.

By incorporating two pairs of trolleys in the rig, motion of the driving platform could be achieved in two perpendicular directions. Thus it could be moved horizontally to any required position over the clay bed. Furthermore the vertical adjustment could be made by using the 2" diameter threaded bars. These were supported above the upper set of trolleys by two large nuts welded to the steel threads. Thus by turning these nuts and so also the steel bars the girder supporting the driving platform could be raised or lowered, by its running up and down steel threads.

A triaxial machine motor and gearbox was used to drive the probes. The upper and lower axle was connected by chain and wheel system. To the lower axle was fitted a worm and wheel mechanism. The rotational motion of the wheel was transferred to 1½" diameter and 24" long threaded shaft by screw-nut mechanism. The assembly was thus capable of driving in 18" without any interruption.

The bearing plate was connected to the main driving shaft using a ball connector as found in standard triaxial testing machine for the attachment of a proving ring. On the underside of the plate, countersunk bores were made to locate the spherical bearings of the model pile and electrodes. These electrodes were made on a 3.04" radius around that for the model pile and at 120^{o} intervals. They were held together by a triangular wooden block made up of three pieces, with a one inch diameter hole at the centre. The purpose of this assembly was to keep the probes and the pile at a constant distance apart at every stage of driving.

The rate of driving for the apparatus was found to be 0.36" per minute by measuring the vertical movement by an ordinary dial gauge. A forward/reverse switch was placed in the electric motor circuit to enable motions of the shaft both up and down. It was possible to drive the rig manually by loosening the bottom sprocket restraining screw.

Other features of instrumentation

The wires from the top and bottom load cells are connected to four arm bridge of a Baldwin strain indicator through a Huggenberger junction box. The signals from the load cells were thus recorded directly in terms of micro-inch per inch against a particular setting of a gauge factor for the fail strain gauges.

The source of electric potential applied across the pile and the

probes was a 30 volt rectifier and the voltage applied could be varied from 0 to 30 volt D.C.

The load cells were calibrated in a heavy duty triaxial testing machine. This incorporated a central cross beam to support the centre of the model pile and to line it up vertically. The model pile passed through a bush at the centre of this beam and rested on a piece of rubber sheet resting on the base supporting plate. The load was measured by a proving ring in the usual manner. The bush was well greased to avoid possible error due to friction.

8.6 Dynamic driving rig:

Basic features of the apparatus

It was essentially a shaft carrying a sheet pile blade or a cylindrical probe at its lower end, sliding vertically within two linear bearings mounted on the structural frame. The top end of the shaft was held by an electromagnet hanging freely from a cantilever bracket. The cantilever bracket was fitted with a dial gauge which recorded deflection of the cantilever arm at a particular point. The cantilever bracket with the dial gauge was then used to read load held by the electromagnet. A 9" x 5" x 4" box was accommodated on the top of the pile connecting the shaft so that weight of the shaft, pile and the moving components could be increased, if necessary by putting some lead shots in the box. A displacement-time measuring device was fitted to the shaft and the displacement plot was recorded in a U.V. recorder. The box provided for lead shot was also used as housing for an accelerometer. The output from the accelerometer was recorded in the U.V. recorder. The whole frame was mounted on a rigid platform. The platform was on four levelling screws to make the base, and hence the structural frame,

vertical so that the vertical shaft could fall freely under gravity when released by the electromagnet. A set of buffer springs were placed on the both sides of the shaft. These springs were mounted on a horizontal channel that was also a structural member of the frame. A secondary horizontal beam channel fitted with rubber cushions was supported on the springs. A cylindrical welded stop was fitted to the 3/4" diameter shaft. The function of the welded stop, the spring and the horizontal beam channel assembly was to bring the shaft to rest after the required penetration of the probe is reached. The basic features of the apparatus can be seen in Plate 1.

Theory behind the design of the apparatus

Let the mass of the shaft, box and the blade m fall through a height h under gravity and then penetrate the soil sample. Then at any position of the blade inside the soil mass we have, by considering the dynamic equilibrium and applying the d'Alembert's principle,

$$m \cdot \frac{d^2x}{dt^2} + P = mg$$

where x is the distance (measured from the surface of the soil), t is the time and P is the penetration resistance offered by soil.

Assuming that P can be represented by a series polynomial

$$P = A + Bx + Cx^2 + \ldots\ldots$$

For simplicity we assume that P can be represented by

$$P = A + Bx$$

Then we have,

$$\frac{d^2x}{dt^2} + (B/_m)x + (g - A/_m) \qquad (8.15)$$

The solution of equation (8.15) under the boundary condition at t = o,

of $x = o$, $\frac{dx}{dt} = u_o$ where u_o is the velocity of blade at the surface of the soil, is

$$x = \frac{u_o}{\sqrt{B/_m}} \text{Sin } (\sqrt{B/_m})t - \frac{(g - A/_m)}{(B/_m)} \cdot \text{Cos } (\sqrt{B/_m})t + \frac{(g - A/_m)}{(B/_m)} \qquad (8.16)$$

Therefore the velocity V_t and acceleration f_t at any time t are given by:

$$V_t = u_o \text{ Cos } (\sqrt{B/_m})t + \frac{(g - A/_m)}{\sqrt{B/_m}} \cdot \text{Sin } (\sqrt{B/_m})t \qquad (8.17)$$

$$f_t = (g - A/_m) \text{ Cos } (\sqrt{B/_m})t - u_o (\sqrt{B/_m}) \text{ Sin } (\sqrt{B/_m})t \qquad (8.18)$$

In the equations (8.16) to (8.18) A and B are soil-blade parameters and are directly related to the dimensions of the blade and the cohesian of the soil.

The following points are worth noticing in connection with the above equations of velocity and acceleration:

(i) The hypothetical periodic time = $2\pi\sqrt{m/_B}$

(ii) The condition for constant rate of penetration demands $f_t = o$, i.e:

$$\tan (\sqrt{B/_m})t = \frac{g - A/_m}{u_o(\sqrt{B/_m})} \qquad (8.19)$$

Equation (8.19) provides the value of 'm' necessary to keep the velocity approximately constant over a small penetration.

Accelerometer assembly

The accelerometer used was the 'Vibrometer' type 5A/SA; ±5g range, 133 c/s resonant frequency with resistance strain gauge sensing element.

It was mounted on a $1\frac{1}{2}$" x 2" x $\frac{7}{8}$" thick perspex piece with a 1 cm^2 hole at the middle. It was split into two parts so that the accelerometer could be placed in 1 cm^2 hole horizontally at the centre of the driving shaft. The accelerometer was placed in the 1 cm^2 hole and the two pieces were then bolted together by two brass screws. Thus the accelerometer was firmly gripped by the perspex piece. The perspex piece was then fitted in a special housing provided within the 9" x 5" x 4" box at the bottom of the 3/4" diameter driving shaft. Care was taken to ensure that the centre of the mounting perspex piece and hence the centre of the accelerometer coincided with the centre line of the driving shaft. The three wire leads from the accelerometer and two 100 Ω resistors were made to form a Wheatstone bridge. The terminals of the bridge were taken out of the housing block through a $\frac{1}{8}$" diameter hole in the housing block. The specification details of the accelerometer used are given below:

Nominal value	= ±5g
Maximum load	= ±50g
Sensitivity	= 19.97 mv/v at 5g
(Resistance strain gauges as the sensing element)	
Excitation	= 3 to 8 volt D.C.
Natural frequency	= 133 c/s
Impedance	= 2 x 113 Ω

The two diagonal terminals of the bridge were connected to a $7\frac{1}{2}$ volt D.C. source while the other two terminals (output terminals) were connected to a 450 c/s galvanometer of an ultraviolet recorder with a 250 Ω damping resistance in parallel. It was possible to increase or decrease the deflection of the galvanometer by varying the resistances incorporated in the bridge so that the width of the

trace on the ultraviolet light sensitive recording paper can be measured with sufficient accuracy. The circuit diagram for the accelerometer is shown in Figure (8.7.1).

Photoelectric diode assembly

The photoelectric diode assembly was used to record the velocity of penetration of the pile at every stage of penetration. It essentially consists of three parts,

(1) The light source:

The purpose of the light bulb was to project light onto the eye of the photodiode the resistance of which varies with the light intensity falling on the eye. The light source used, was an ordinary 25 watt bulb connected to a 12 volt D.C. source. The bulb was painted black on all sides except the one facing the screen.

(2) The photodiode:

This was excited by a 6 volt D.C. source through an 1 MΩ resistance in series with it. The rating of the diode used was 1.67 MΩ for 1 ft. candle of light intensity. As the light intensity on the cell is increased so its resistance falls and the potential drop across it decreases.

Thus if x ft. candle is the light intensity falling on the eye of the photocell for the given configuration the voltage drop across the photocell is given by $\left[\frac{6 \times 10^{-6}}{1 + 1.67/x}\right] \times \frac{1.67}{x}$ volts, provided the photocell behaves linearly with respect to the light intensity. The nonlinearity, however, would not offset the purpose for which it was used. The voltage drop was measured by a 1000 c/s galvanometer which was damped critically by a 250Ω resistance across it. The trace of the galvanometer was recorded on ultraviolet recording paper. The light source and the photoelectric cell were mounted on the extended arms of an

adjustable magnetic clamp. The magnetic clamp itself was held fixed with the structural frame. The circuit diagram for the photocell assembly is given in Figure (8.7.2).

(3) The screen:

The purpose of the screen was to allow light to fall on the eye of the photocell at some preset intervals. A brass plate with 1 mm wide slits at 5 mm centre to centre was used. It was held fixed with the moving shaft and held vertically between the light source and the eye of the photocell which consists of the fixed part of the photoelectric assembly. Sufficient care was taken so that the gap between the moving and the fixed part of the photoelectric assembly was a minimum for the brass plate to pass clear of the photocell and the lamp.

The details of the photoelectric assembly can be seen in Plate 2.

The ultraviolet recorder

The recorder used was S.E. 2000 type and was capable of recording in 25 channels of which only four were used. It has a series of mirror galvanometers such that a beam of ultraviolet light from an ultraviolet lamp falls on the mirror and is reflected onto the light sensitive linograph direct print paper. Thus any small deflection of the galvanometer is automatically recorded as a deflection of the light trace across the recording paper.

Timer Circuit

This was an ordinary pulse generator which could generate step pulses at chosen time intervals. The function of the pulse recorded on the Ultra Violet Recorder was to check on the paper speed. As most of the penetration tests were highspeed ones it was not possible to depend on the rated paper speeds of the U.V. Recorder. The numerical analysis was carried out on a time base obtained from the pulses

generated at 10 milliseconds intervals. The circuit diagram for the timer circuit can be seen in Figure (8.7.3).

Event marking Device

This was used to obtain a marking on the recorded results at the instant when the pile is exactly touching the surface of the soil specimen. This was attained by using one terminal of a 1½ volt dry battery connected to the surface of soil sample while the other was connected to the pile through a 100 c/s galvanometer through a 400 KΩ resistance in series. The galvanometer was suitably damped by having a 250Ω resistance connected in parallel with it. As the pile touched the surface the electric circuit was complete and accordingly an instantaneous deflection of the galvanometer trace was obtained on the linograph paper. The circuit diagram for the event marks can be seen in Figure (8.7.4).

The electromagnet and the Triggering device

The electromagnet was designed to carry a maximum load of 70 lbs. The current necessary was supplied from a 12 volt heavy duty car battery. The electromagnet and the triggering switch for the paper drive of the ultraviolet recorder were connected to a special biased switch which could be switched momentarily on and off. Thus it was possible to control the electromagnet and the paper drive motor of the U.V. Recorder simultaneously.

Preparation of the sample

Samples of London Clay were mixed at a preset moisture content in a large mixer until the sample appeared to be homogeneous. It was then compacted in 3" layers in 2'0" long 1'3" wide and 9" deep containers by a 5 lb. hammer with 60 blows per layer, for a free drop of 12". The samples were kept covered with wet sacking and polythene sheets to prevent any loss of moisture.

8.7 Experimental investigation

8.7.1 Slow speed driving of model pile

Calibration of the Load Cells

The calibration of the model pile was carried out using a triaxial testing machine. The pile was loaded and unloaded at least 25 times to bed down the load cells. The pile was then loaded up to 150 lbs in increments of 10 lbs. The loads were measured by a 200 lbs, proving ring. The strain readings were measured in a Baldwin strain indicator using the four arm bridge. These tests were continued until the strain readings followed a regular and consistent pattern. A calibration chart (Figure 8.8) was then plotted of microstrain against load on the pile taking the mean of four test runs.

Slow Speed Driving of the probe with and without an applied electric potential

A series of penetration tests were performed without any applied D.C. potential. The loading frame with the pile held in position was lowered manually until the bottom of the pile touched the surface of soil. The pile was made perfectly vertical with the help of a spirit level. The loading plate was adjusted by releasing an adjusting screw provided at the bottom of the driving shaft. The loading plate was made absolutely horizontal and then the adjusting screw was tightened. Care was taken to ensure that the driving unit and the driving shaft were held rigid against any side sway. The driving shaft and the pile was thus held absolutely vertical with the bottom of the pile touching the ground surface and the top of the pile touching the countersink in the loading plate through a spherical ball bearing.

The initial readings of both load cells were taken by a Baldwin strain indicator. The drive motor was switched on and the readings

were taken at one minute intervals until a penetration of 16" was reached. The drive motor was switched off and then switched on to the reverse direction until the loading plate went back to its original position. The pile was then pulled out of the clay bed and thoroughly cleaned to have the same surface texture as before.

In driving the pile with an applied electric potential essentially the same operation was followed, except that three electrodes were arranged at 120 degree intervals around the model pile. These electrodes were held rigidly tight with the loading plate by screws through perspex adapters to prevent short circuiting. A triangular wooden block made in three pieces, having 1" diameter hold at the middle was used to prevent these electrodes going outwards with the pile held at the centre. The object of providing the 1" diameter hole at the centre was however to prevent any loss of load transfer due to friction between the block and the pile shaft. The steady D.C. source used for applying a steady D.C. potential was a rectifier plugged in 220 volts 50 c/s A.C. mains.

After the penetration tests samples from the compacted clay bed from different depths were taken by $1\frac{1}{2}$" sampling tubes. The moisture content and undrained triaxial shear strength of the samples were also determined.

Results

The shaft load was calculated by deducting the end load from the total load measured by the top load cell at different depths of penetration. Figure (8.9.1) to (8.9.5) show the shaft loads and the end loads of various depths for a range of applied D.C. potentials. (0 to ±0.4 volts/cm). Each point on these figures represents the mean of three tests. The moisture content and the undrained cohesion values of the samples are shown plotted against depth in Figure (8.10).

The decrease or increase in shaft adhesion due to an applied negative or positive D.C. potential respectively was defined as a nondimensional quantity given by $(P-P_E)/P$. Where, P = the penetration resistance of the probe without any applied D.C. potential and P_E = the penetration resistance of the probe with an applied D.C. potential.

Figure (8.11) shows the values of $(P-P_E)/P$ plotted against the average voltage gradient (E/R) in volts/cm, where E is the voltage applied between the pile and the electrodes and R is the radial distance between the centre of the probe to the centre of the electrodes. Since R was essentially constant for all the tests Figure (8.11) is virtually a plot of $(P-P_E)/P$ against 'E' to a different scale. It should be noted here that the results are interpreted in terms of the average (E/R) only for the purpose of possible field applications. The actual voltage gradient at the pile face for a given probe-electrode configuration would depend on the diameter of the electrodes and the radius 'R'. For the geometrical configuration such as the one used for all the tests the actual voltage gradient at the pile face 4 x E/R average.

The relationship between the current through the system for a penetration of 14" and the average (E/R) is shown in Figure (8.12). Contrary to the general expectation the relationship between the applied voltage gradient and the current was found to be non-linear.

Conclusions

It was found that application of an electric potential to a cathode probe reduces the shaft resistance considerably, whereas there is virtually no reduction in end load (see also Johnston, 1968). A reduction up to 85% in the shaft resistance could be achieved by an application of an average potential gradient of 0.4 volt/cm at a rate of penetration 0.36" per minute. The increase in the shaft resistance by making

the pile anodic was, however, found to be limited to 45% at an average voltage gradient of 0.4 volt/cm for the same rate of penetration. Thus if the total shaft resistances can be expressed (conventionally) as

$$P = \pi DL\ \alpha_o\ \overline{C_u}$$

$$P_e = \pi DL\ \alpha_E\ \overline{C_u}$$

where D and L are diameter and length of shaft respectively and $\overline{C_u}$ is the average undrained cohesion over the pile length, which can be assumed to remain virtually unaltered, for the short time application of an electric potential, α_o and α_E the nondimensional factors which are dependent on the change of interaction forces at the pile soil interface.

If now $\overline{C_u}$ can be taken as 4.00 psi (Figure, 8.10) over the whole length of the shaft. We obtain,

$$\text{average}\quad \alpha_o = \frac{P}{\pi DL\ \overline{C_u}} = 0.50.$$

Similarly average

$$\alpha_E\left\{\text{for } (E/R)_{av} = -0.4\ V/Cm\right\} = \frac{P_E}{\pi DL\ \overline{C_u}} = 0.08,$$

and average

$$\alpha_E\left\{\text{for } (E/R)_{av} = +0.4\ V/Cm\right\} = \frac{P_E}{\pi DL\ \overline{C_u}} = 0.76.$$

It is however conceivable that α_E for an application of a D.C. negative potential cannot be less than 0 and for an application of a D.C. positive potential cannot be greater than 1 provided that the duration of application is small enough not to change the value of $\overline{C_u}$. This is

reflected very well in Figure (8.11), which shows quite clearly that the increase in reduction or the increase in penetration resistance is almost linear with average (E/R) up to 0.2 volt/cm., beyond which the rate of decrease or increase is progressively less. Thus it would appear that the most economic average voltage gradient perhaps lies around 0.2 volts/cm.

The relationship between the applied voltage and current was found to be nonlinear (Figure 8.12). This nonlinearity was thought to be due to:

(i) The relationship between the voltage and current for any soil is not strictly linear, i.e. linear ohms law cannot strictly be applied to soils.

(ii) The clay bed was not 100% saturated, consequently there has been an almost instantaneous movement of the fluid phase resulting from the body forces on the fluid phase as soon as the potential was applied. This would result in change in almost immediate change in moisture content and consequently in resistivity. The change in resistivity would thus increase with increase in applied potential. Hence the deviation from linearity was found to be greater for higher voltage gradients. For a fully saturated soil there cannot be any change in resistivity due to moisture migration for short time applications of electric potential.

8.7.2 High speed driving of sheet pile blades

Calibration of the load measuring device

A cantilever bracket was used for measuring the weight of the driving shaft. The details can be seen in Plate (3). Lead shots of known weight were placed in the container on the rod with a spherical head at the top (Plate, 3). The deflection of the bracket at a given load was measured by a dial gauge. Figure (8.13) shows

the reading of the dial gauge plotted against the load applied to the bracket. The bracket was loaded several times and the readings of the dial gauge for a given load were remarkably consistent.

Driving of sheet pile blades with and without electro-osmosis

A series of high speed penetration tests were performed over a range of speeds from 2 to 6.8 ft/sec. The rate of penetration was varied by varying the height of fall. Coarse adjustment for height was done by raising the sample while the finer adjustment was done by turning the female adopter provided at the bottom of the cantilever bracket. The height of drop, that is the height between the trimmed and levelled top surface of the sample and the bottom edge of the blade, was measured.

All the electrical appliances were switched on. The frequency of timer signal and the speed of the ultraviolet recorder was selected so that a convenient spread of time scale plot could be attained. The photo-electric cell lighting was adjusted until a reasonable well defined trace was obtained on the ultraviolet recorder paper. The accelerometer trace and the base line trace (i.e. a reference line) were adjusted by turning the galvanometers so that both traces coincide at a point when the accelerometer is at rest. The event marking device was laid and the galvanometer was adjusted to give a sharp trace on the ultraviolet light sensitive paper.

A series of vane tests were done on the sample by a portable laboratory vane which was calibrated before hand with triaxial test results. Thus the vane tests results were directly transferred to equivalent underained triaxial values of shear strength.

From the measured values of cohesion a rough estimate of the penetration resistance of the pile was made, and thus a required

value of the weight of the moving components to attain constant velocity of penetration over a required range was obtained. The weight was adjusted by adding or reducing the amount of lead shot in the box provided at the top of the pile. The exact weight of the shaft, pile etc. and its moving components was measured from the dial gauge fitted to the cantilever bracket.

The triggering switch was pressed and the electromagnet thus automatically released the shaft which fell under gravity and penetrated the soil sample until brought to rest against the buffer device. The recorded paper trace out of the ultraviolet recorder was exposed to room lighting.

A series of driving tests were performed with an applied electric potential. The test procedure was essentially similar to the one described above except that two steel plates buried 2" inside the soil sample were used as anodes and the pile was made the cathode. The steel plates were buried parallel to each other and the pile was allowed to come down along a line equidistant from them. The necessary D.C. potential was supplied by a rectifier connected to a 220 volt 50 c/s A.C. mains.

Recording of data

The recording of all high speed penetration tests were done on linograph ultraviolet light sensitive paper. The paper was exposed to room lighting for a few minutes after recording and then as soon as the galvanometer traces became prominent it was stabilised by spraying linograph stabilising lacquer over the relevant part of the paper trace. A copy of typical paper trace can be seen in Figure (8.14).

8.7.2 Results of high speed driving of piles

Numerical Calculations

The basic analytical theory behind the design and performance of

the dynamic driving rig has been outlined previously. This section therefore outlines the scheme of numerical calculations used to obtain the penetration resistance (P), the velocity at any instant V_t and the distance penetrated (S) from the ultraviolet paper traces of velocity and acceleration.

Now let us start with the basic differential equation for acceleration $\ddot{X}$ of the pile at any instant 't' inside the soil mass at a depth X measured from the surface of the soil

$$m\ddot{X} + P = mg \tag{8.20}$$

where P = Penetration resistance offered by soil for penetration from ground level to the depth X

mg = Weight of the pile, shaft and all its moving components.

The equation (8.20) can be written as

$$R = m(g - \ddot{X}) \tag{8.21}$$

The right hand side of the (8.21) can be obtained from the recorded paper trace as shown in Figure (8.14).

The rest of the procedure of numerical calculations can better be described in the following steps:-

(i) From the measured height of fall calculate the initial velocity u_o by $u_o = \sqrt{2gh}$ where h = height of fall.

(ii) From the trace of the event marking device locate the exact position of the time-scale where the probe just touched the surface of the soil.

(iii) Having obtained the starting point the rest of the trace of the accelerometer, i.e. from the start up to the point where the velocity trace vanishes or the accelerometer

records the impact of the buffer springs whichever happens earlier, is divided in suitable numbers of divisions (Figure 8.14). This is to allow for the pile coming to rest before hitting the buffer due to the resistance offered by the soil alone.

(iv) The change in velocity at an instant t, ΔV_t is obtained from

$$\Delta V_t = \frac{1}{2} (\ddot{X}_t + \ddot{X}_{t+\Delta t}) \cdot \Delta t$$

where $\ddot{X}_t$ = acceleration at time 't' measured from the origin O (Figure (8.14).

$\ddot{X}_{t+\Delta t}$ = acceleration at time $(t+\Delta t)$.

Δt = time interval.

(v) Having obtained ΔV_t, $V_{t+\Delta t}$ can be obtained and hence the average velocity within the specified time interval $(t, t+\Delta t)$ can be obtained from

$$V_{av} = \frac{1}{2} (V_t + V_{t+\Delta t})$$

(vi) The distance traversed during the specified time interval can be obtained from

$$\Delta S_t = V_{av} \cdot \Delta t$$

(vii) Finally $S_{t+\Delta t}$ can be obtained from

$$S_{(t+\Delta t)} = S_t + \Delta S_t$$

where $S_{(t+\Delta t)}$ denotes the distance traversed in time $(t+\Delta t)$.
The computational steps (i) to (vii) can be performed very easily in tabulated form.

Presentation of the results

The results of high speed penetration tests of blades are given

in Figures (8.15.1) to (8.15.12). Each point on the graph shows the mean of four tests. The difference of the other results were within ±4% of the mean.

Figure (8.16) shows the ratio of P_D/P_S plotted against the average velocity over a 2" penetration (where P_D = mean dynamic penetration resistance and P_S = static penetration resistance for a 2" penetration of the blade). The static penetration resistance has been defined as the ultimate load which a stationary blade or probe, which has been pushed into soil by 2", can take without failure.

Figure (8.17) shows the ratio of P_E/P_D plotted against the average velocity of penetration over 2", P_E being the dynamic penetration resistance offered by the soil under an electric potential for a penetration of 2". The ratio P_E/P_D has been shown plotted for various values of voltage gradient.

8.8 Conclusions

The dynamic penetration resistance was found to be higher than the static penetration resistance. The ratio of P_D/P_S was found to vary from 2 to 2.75 when the velocity ranges from 2 ft/sec to 7 ft/sec, Figure (8.16). It would thus appear that the rate of increase in the ratio of P_D/P_S would be very rapid within the range of 0 to 2 ft/sec. It was not possible to investigate the dynamic penetration resistance within this range because of difficulty to keep the velocity of penetration approximately constant over this range.

The ratio P_E/P_D was found to be 0.75 to 0.98 depending on the voltage gradient when the velocity ranges from 2 ft/sec. to 6.5 ft/sec., (Figure, 8.17). The line representing the mean experimental results for 1 ft/sec has been projected back to the ordinate to show the probable curve linking the static test results of earlier investigation (Butterfield and Banerjee, 1967) for blades for the corresponding range of samples. It would appear from the dynamic test results that application of an electric potential does not reduce the penetration resistance to any significant amount. Hence it cannot be recommended for a continuous high speed earth cutting to which the project was directly related.

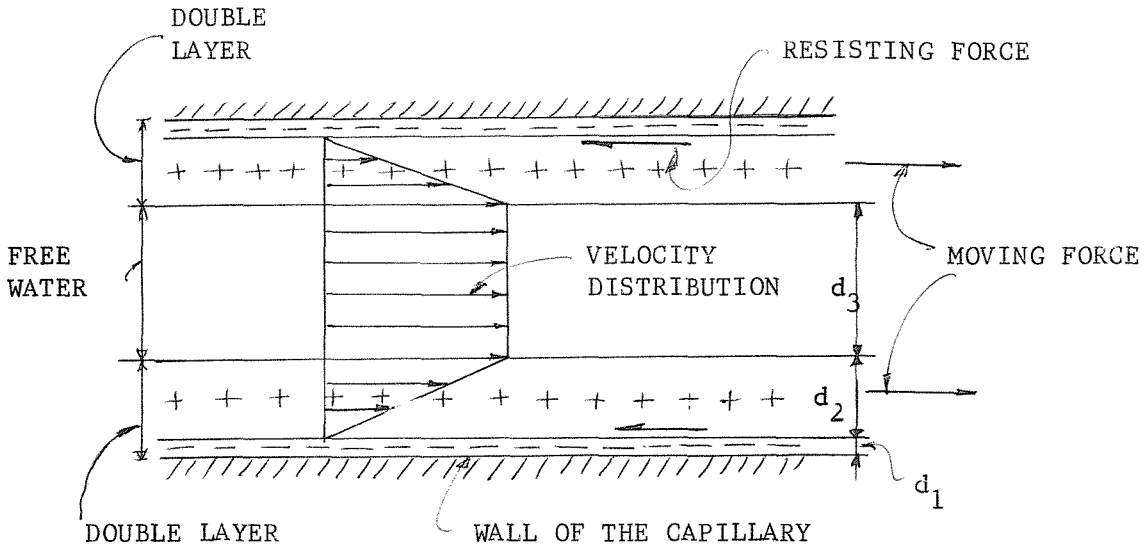

FIGURE 8.1: ELECTRO-OSMOTIC FLOW THROUGH A CAPILLARY

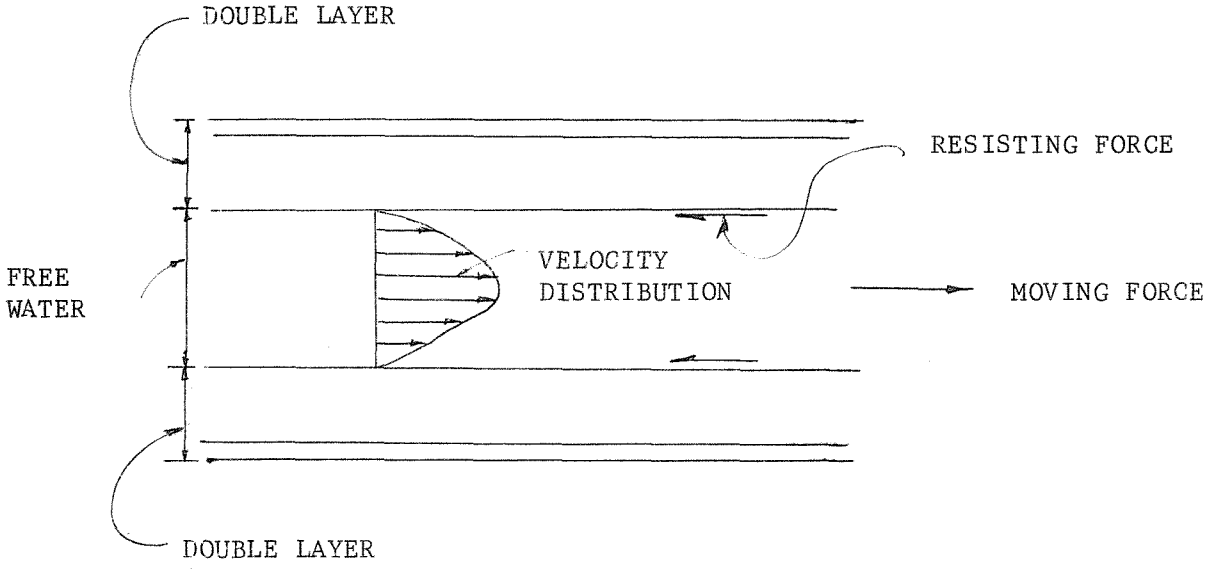

FIGURE 8.2: HYDRAULIC FLOW THROUGH A CAPILLARY

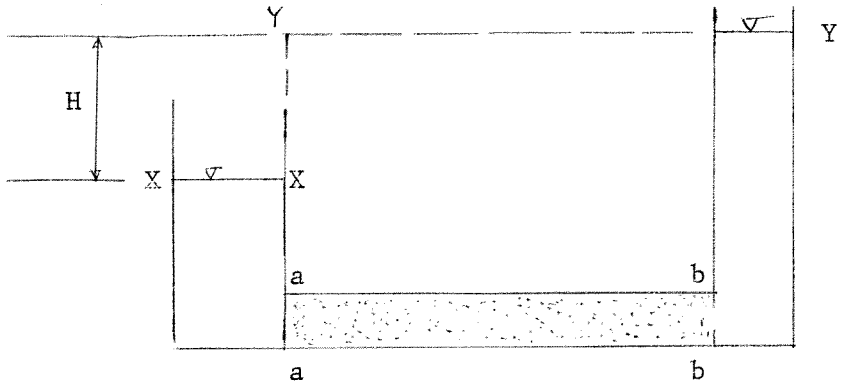

FIGURE 8.3.1

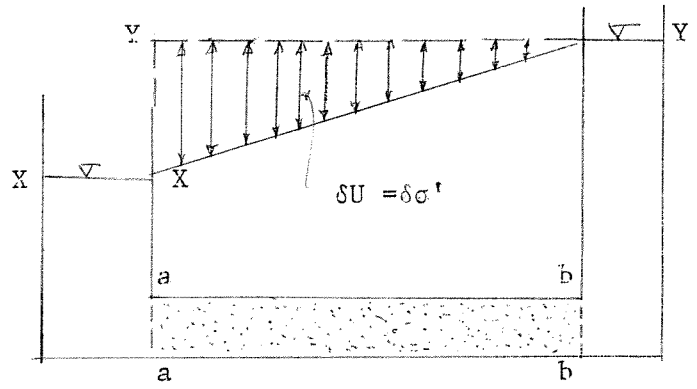

FIGURE 8.3.2

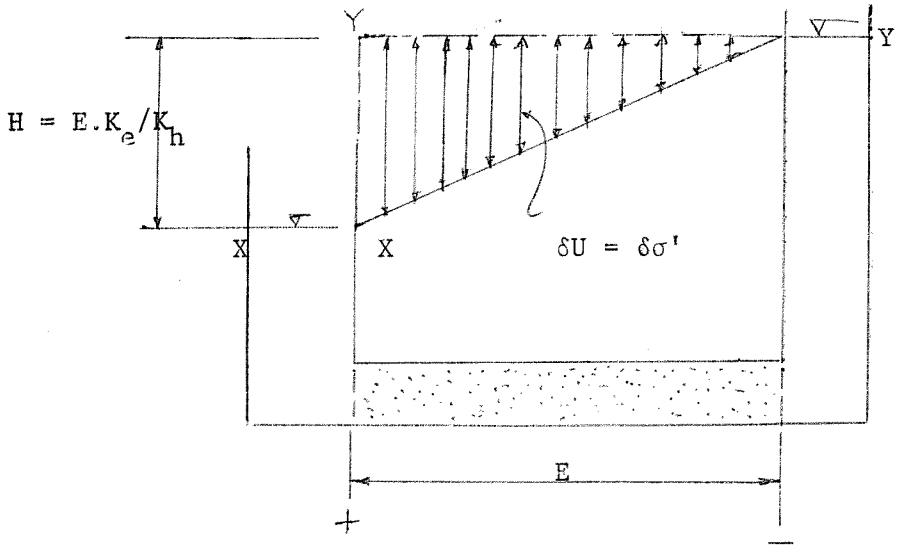

FIGURE 8.3.3

FIGURE - 8.3: ELECTRO-OSMOTIC CONSOLIDATION PROCESS

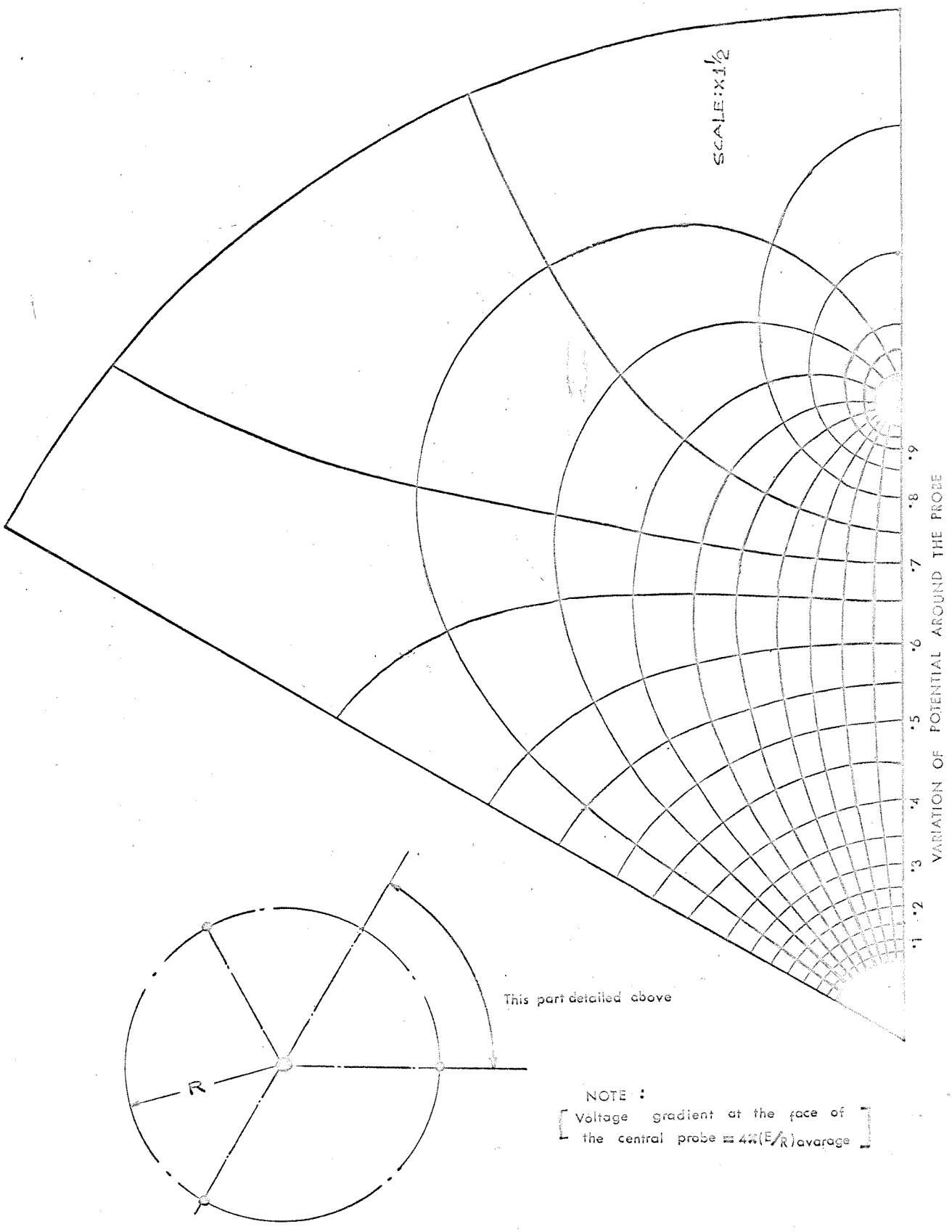

PLAN OF PROBE ELECTRODE CONFIGURATION

FIGURE- 8.5

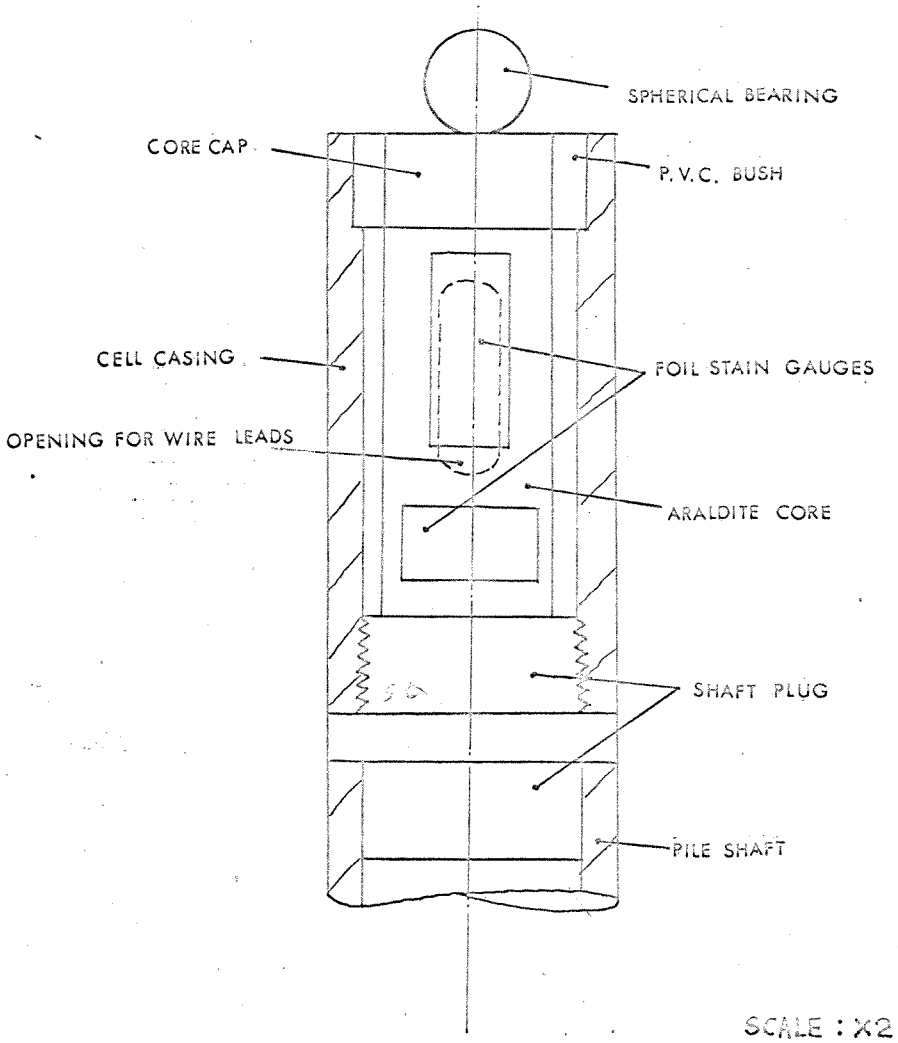

DETAILS OF TOP LOAD CELL

FIGURE- 8.6.1

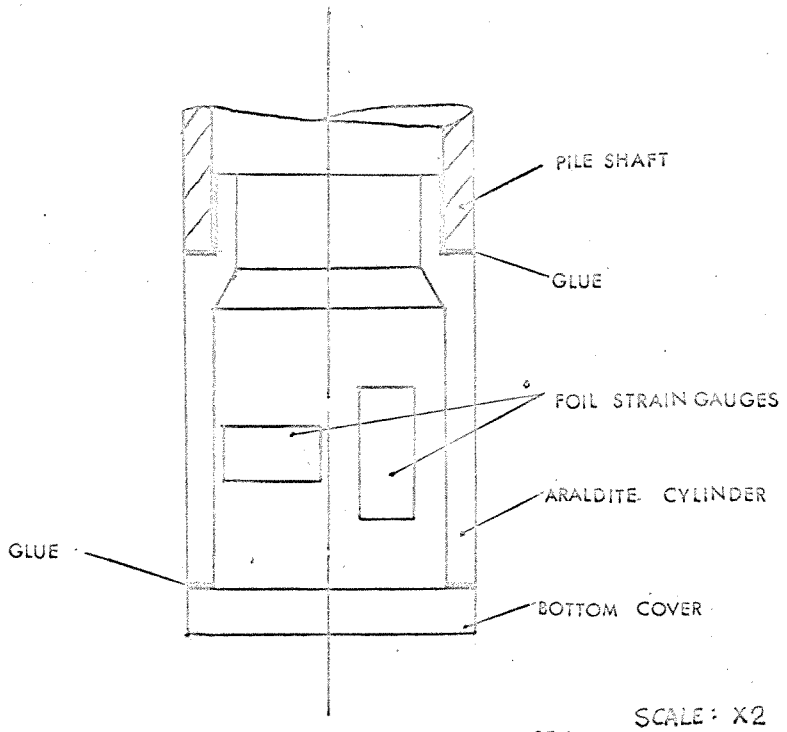

DETAILS OF BOTTOM LOAD CELL

FIGURE- 8.6.2

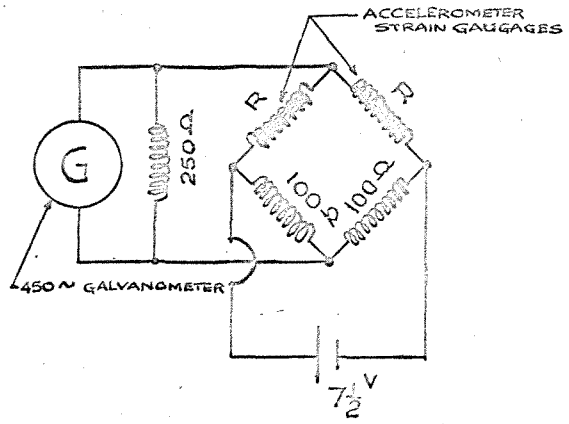

CIRCUIT DIAGRAM FOR THE ACCELEROMETER

FIGURE- 8.7.1

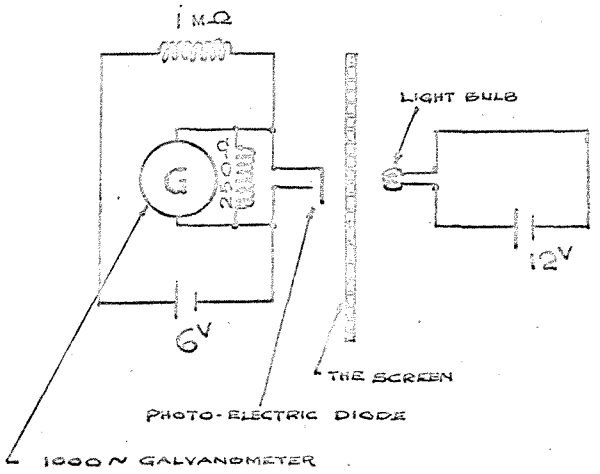

CIRCUIT DIAGRAM FOR THE PHOTO ELECTRIC CELL ASSEMBLY.

FIGURE- 8.7.2

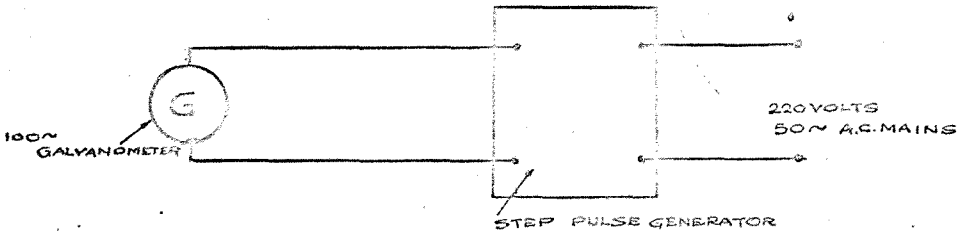

CIRCUIT DIAGRAM FOR THE TIMER DEVICE

FIGURE- 8.7.3

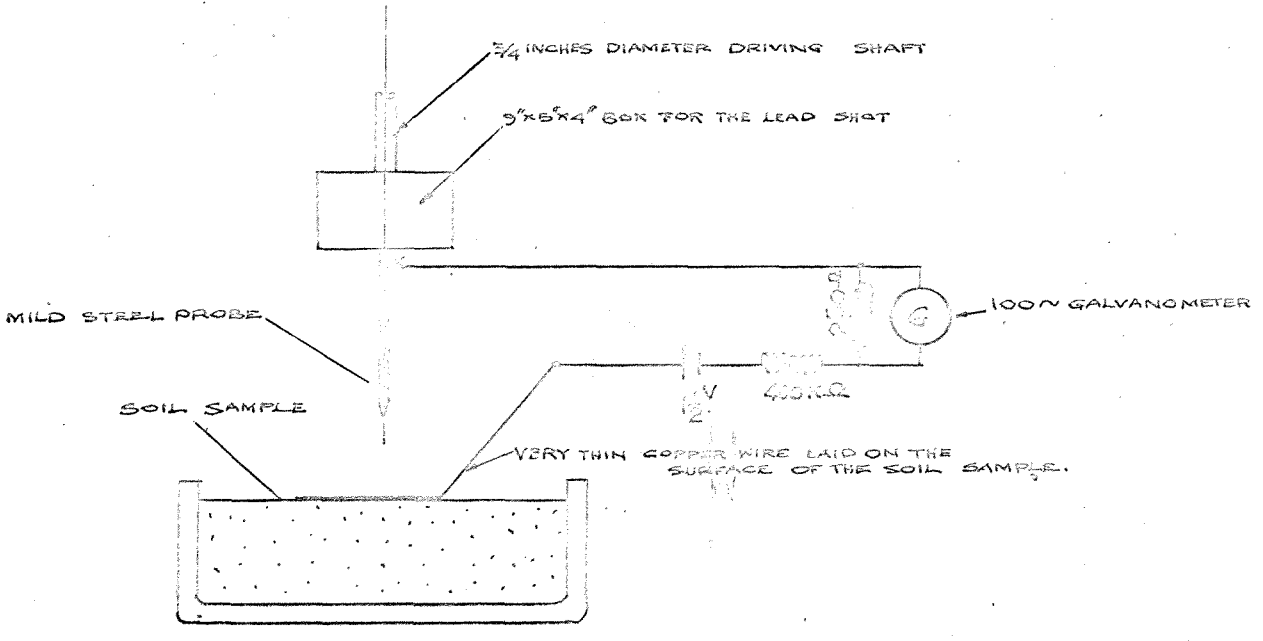

CIRCUIT DIAGRAM FOR THE EVENT MARKER.

FIGURE- 8.7.4

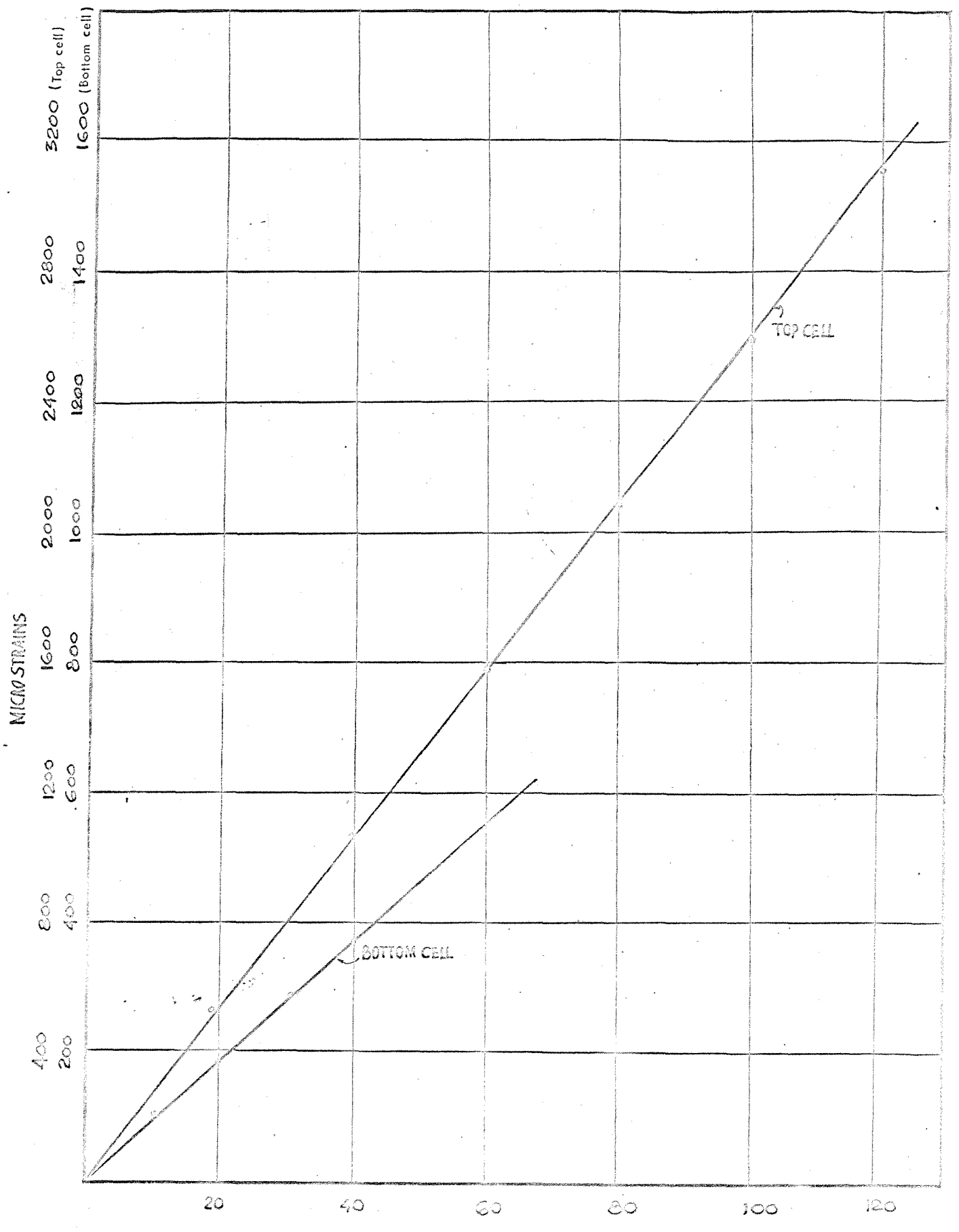

CALIBRATION CURVES FOR LOAD CELLS

FIGURE - 8.8

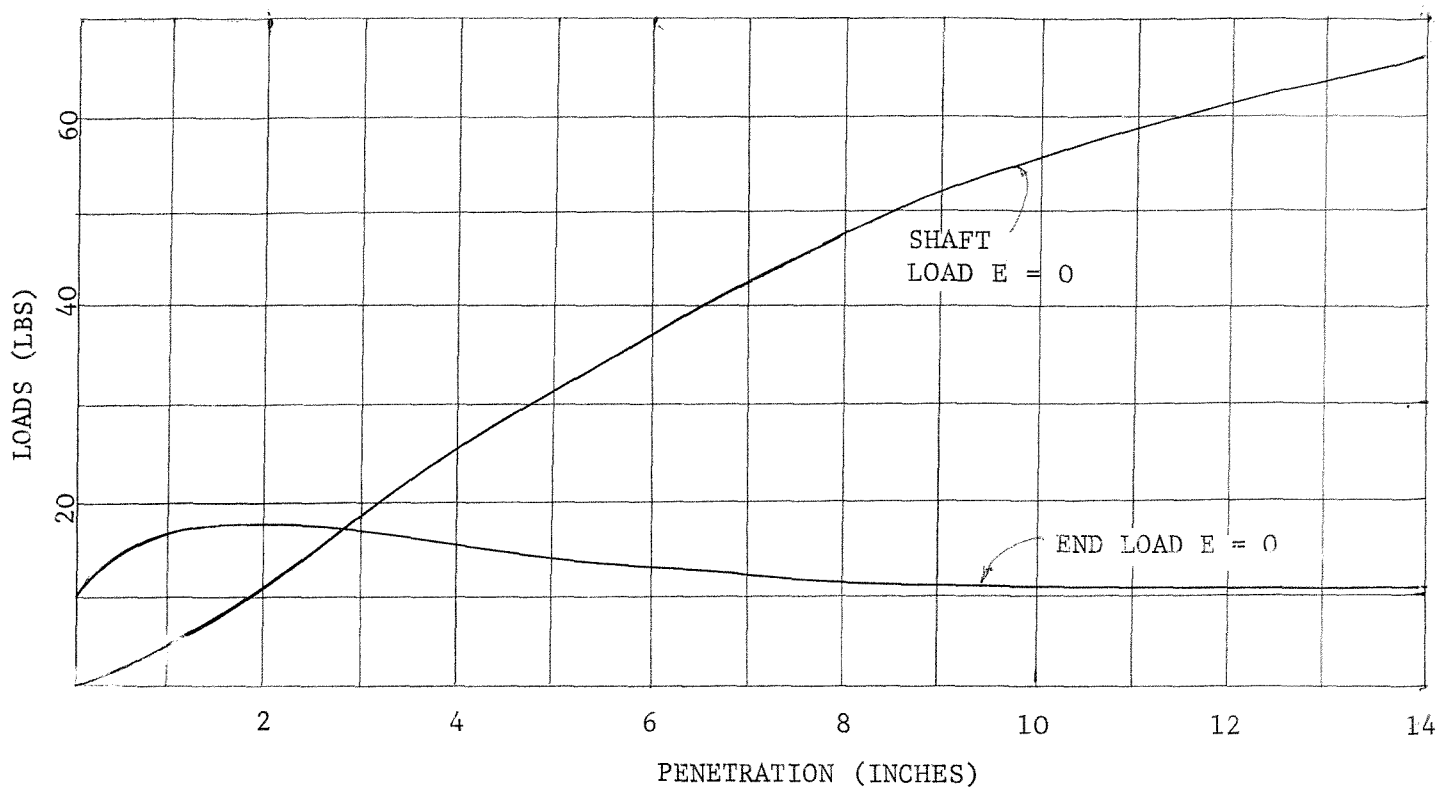

FIGURE - 8.9.1

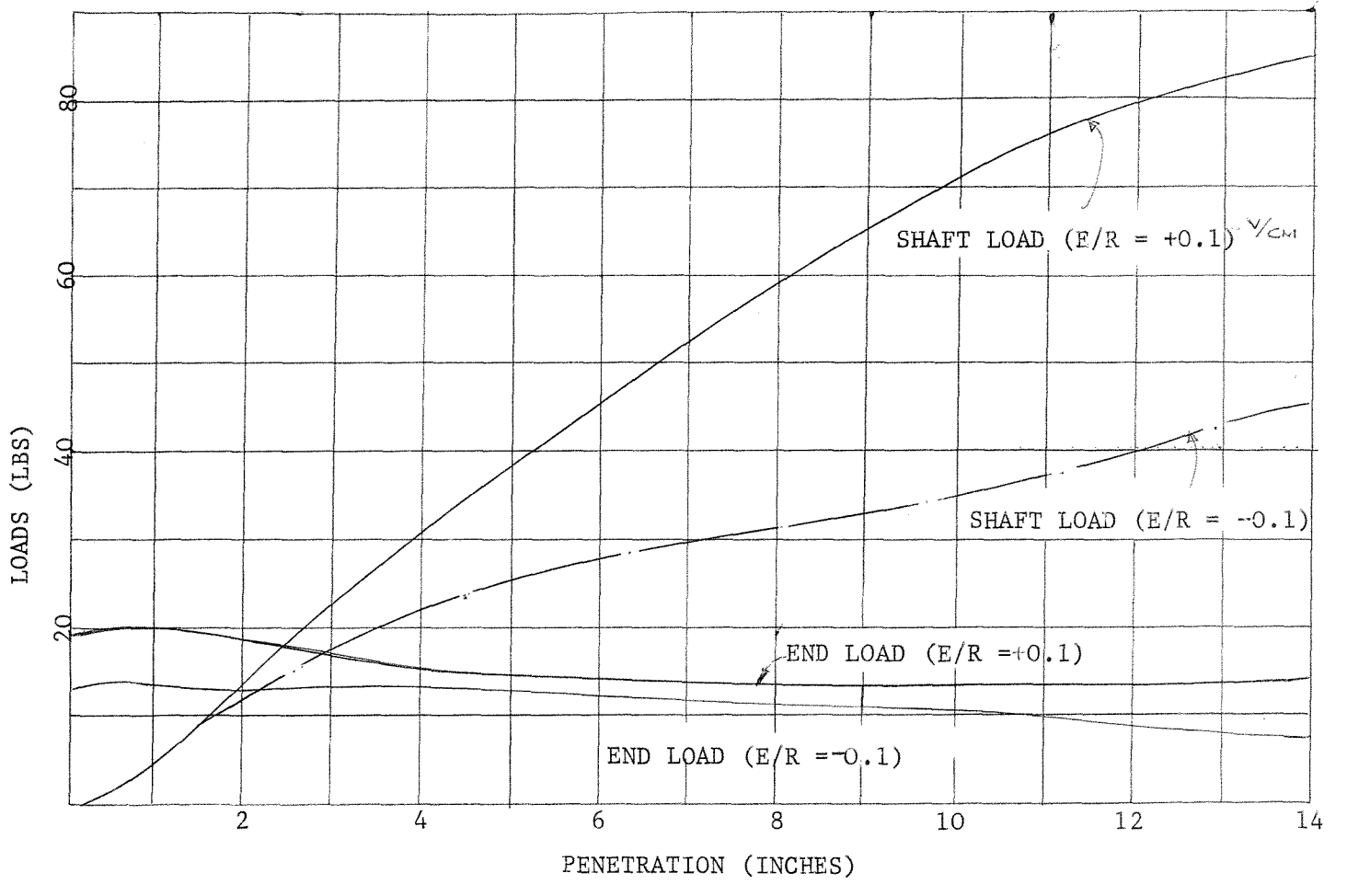

FIGURE 8.9.2

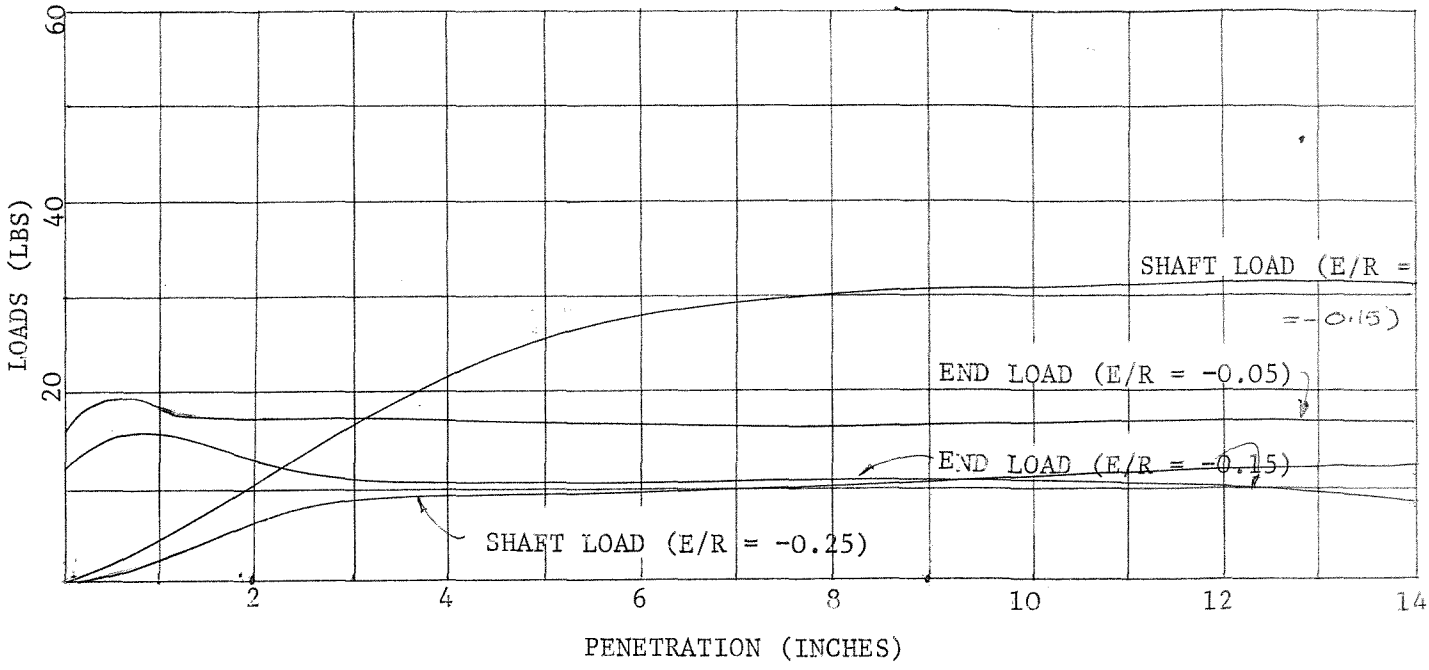

FIGURE - 8.9.3

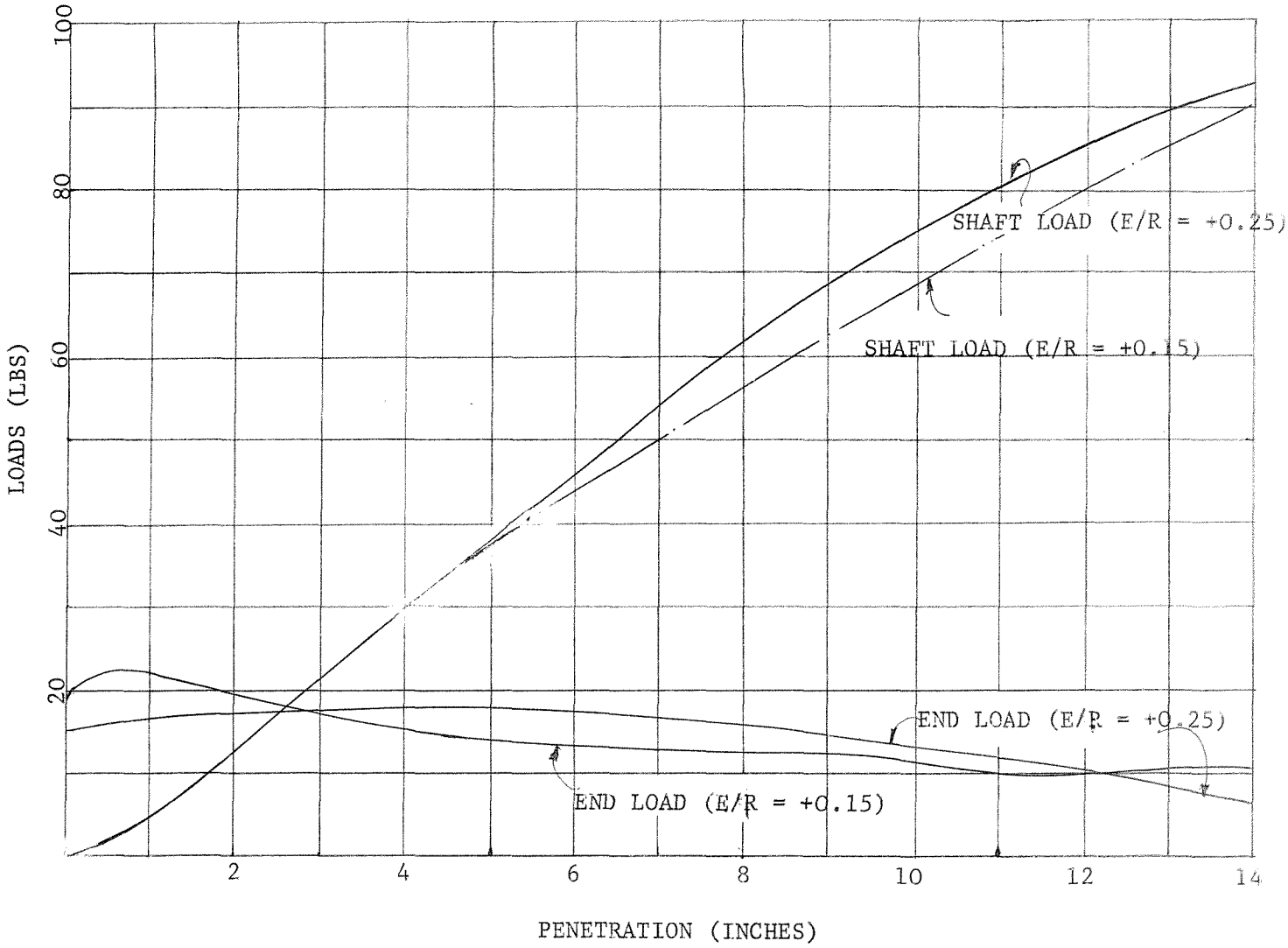

FIGURE - 8.9.4

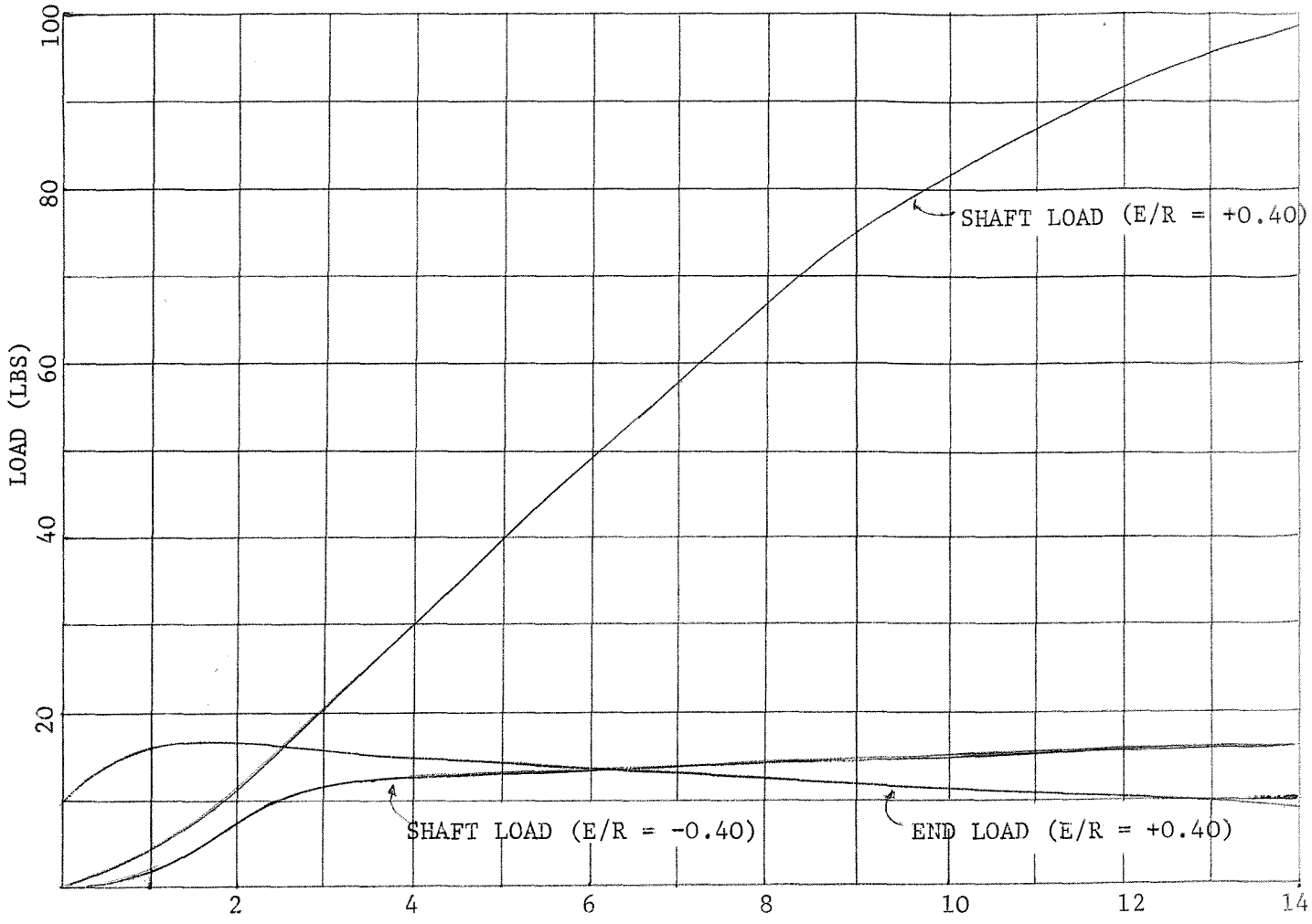

FIGURE - 8.9.5

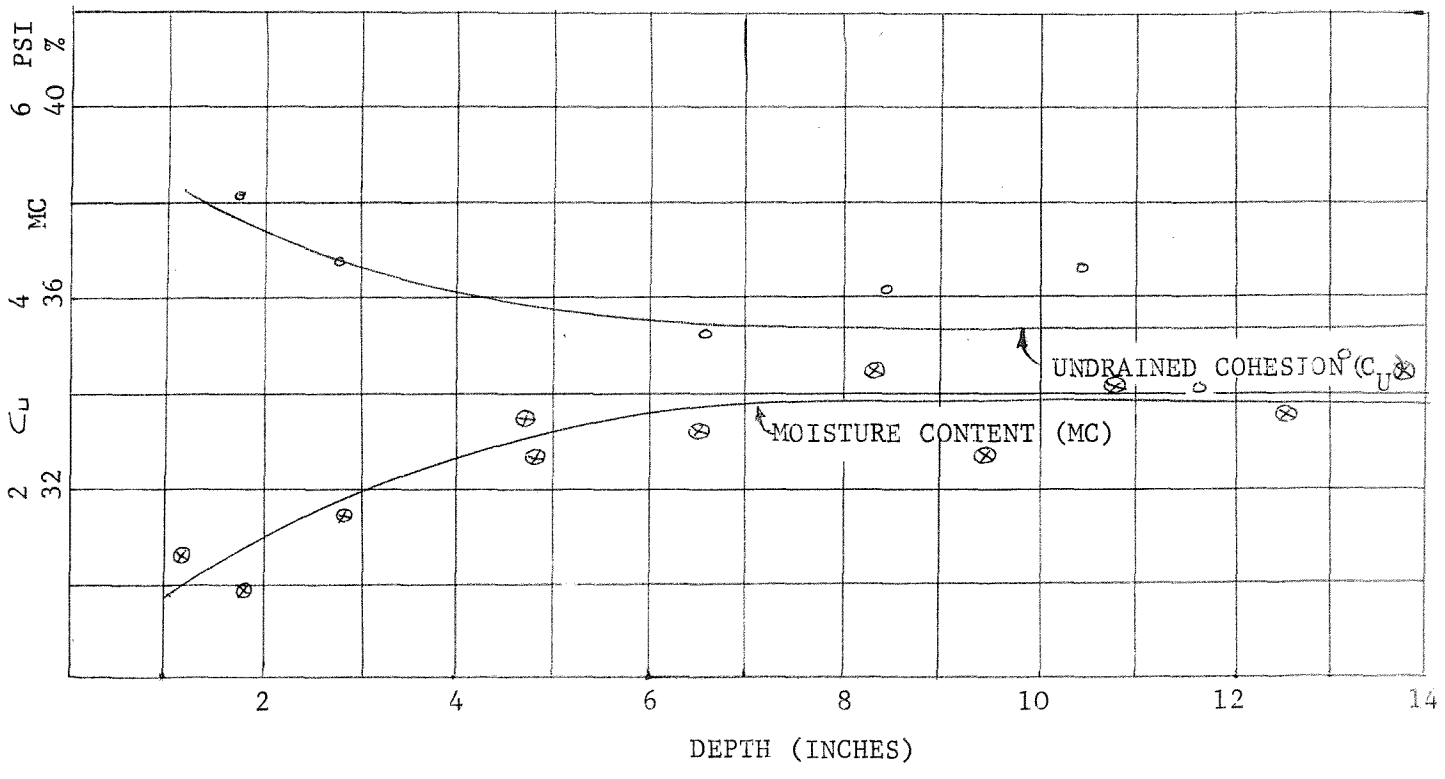

FIGURE - 8.10: UNDRAINED COHESION AND MOISTURE CONTENT VS DEPTH

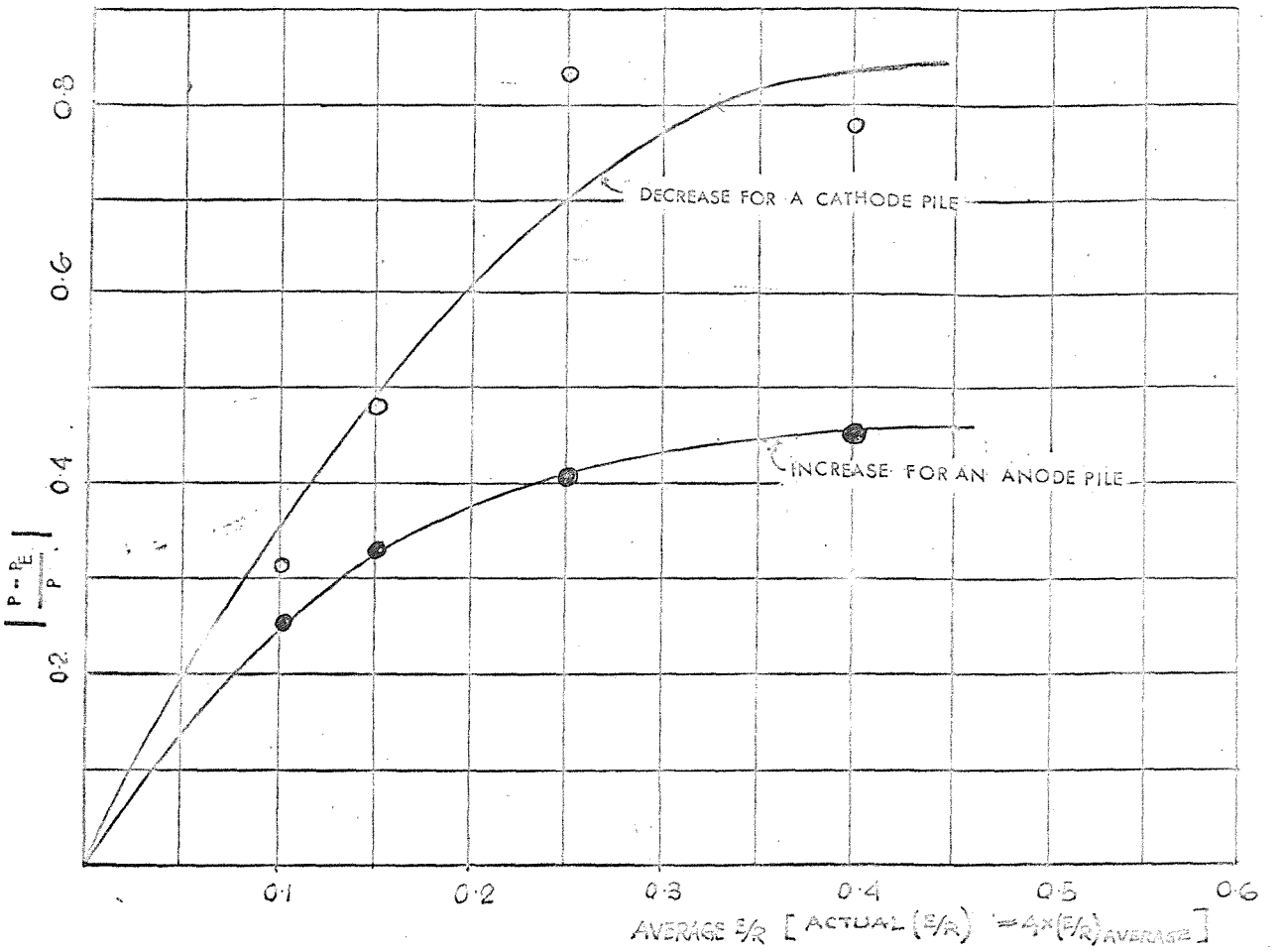

FIGURE- 8.11

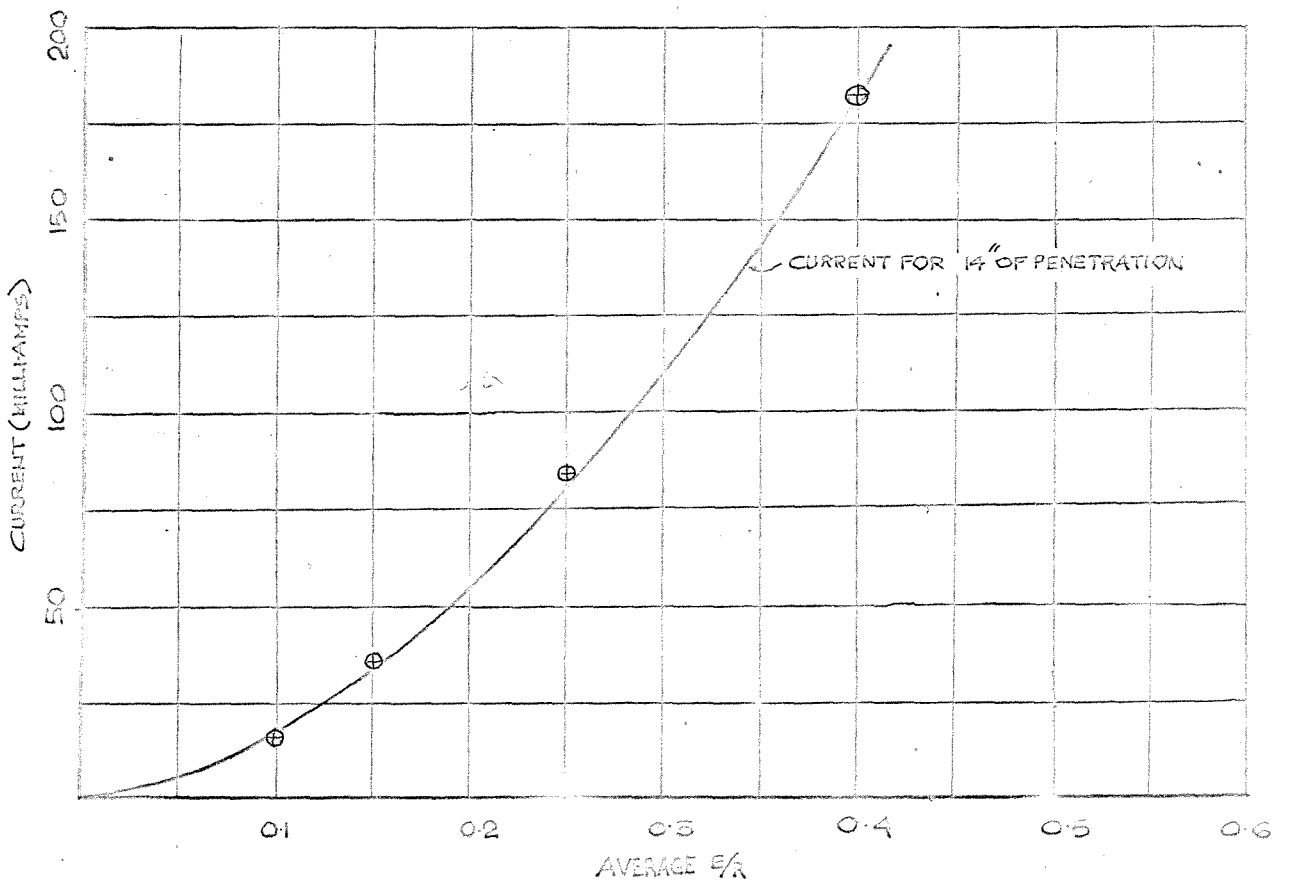

FIGURE - 8.12

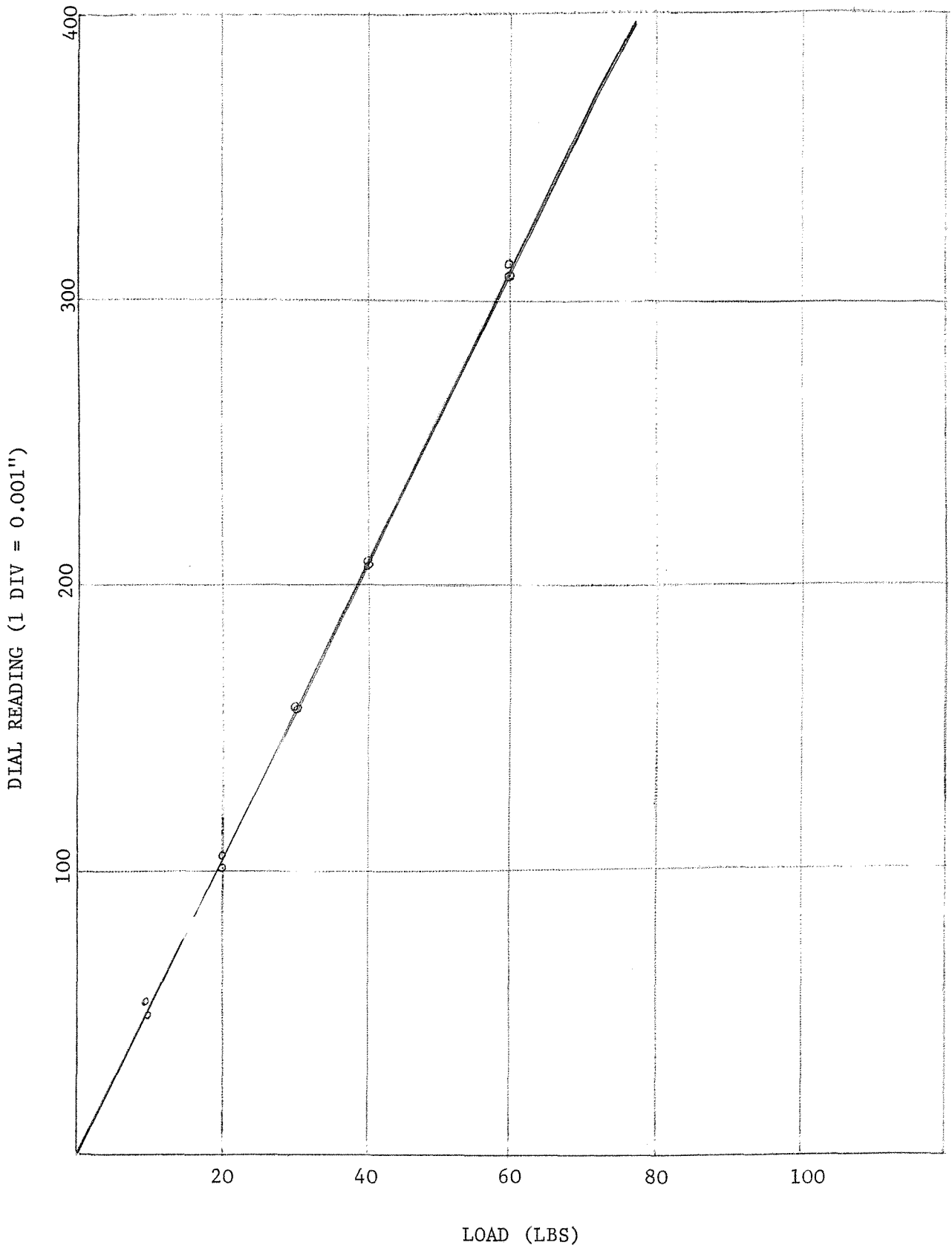

FIGURE - 8.13. CALIBRATION CURVES FOR THE CANTILEVER BRACKET

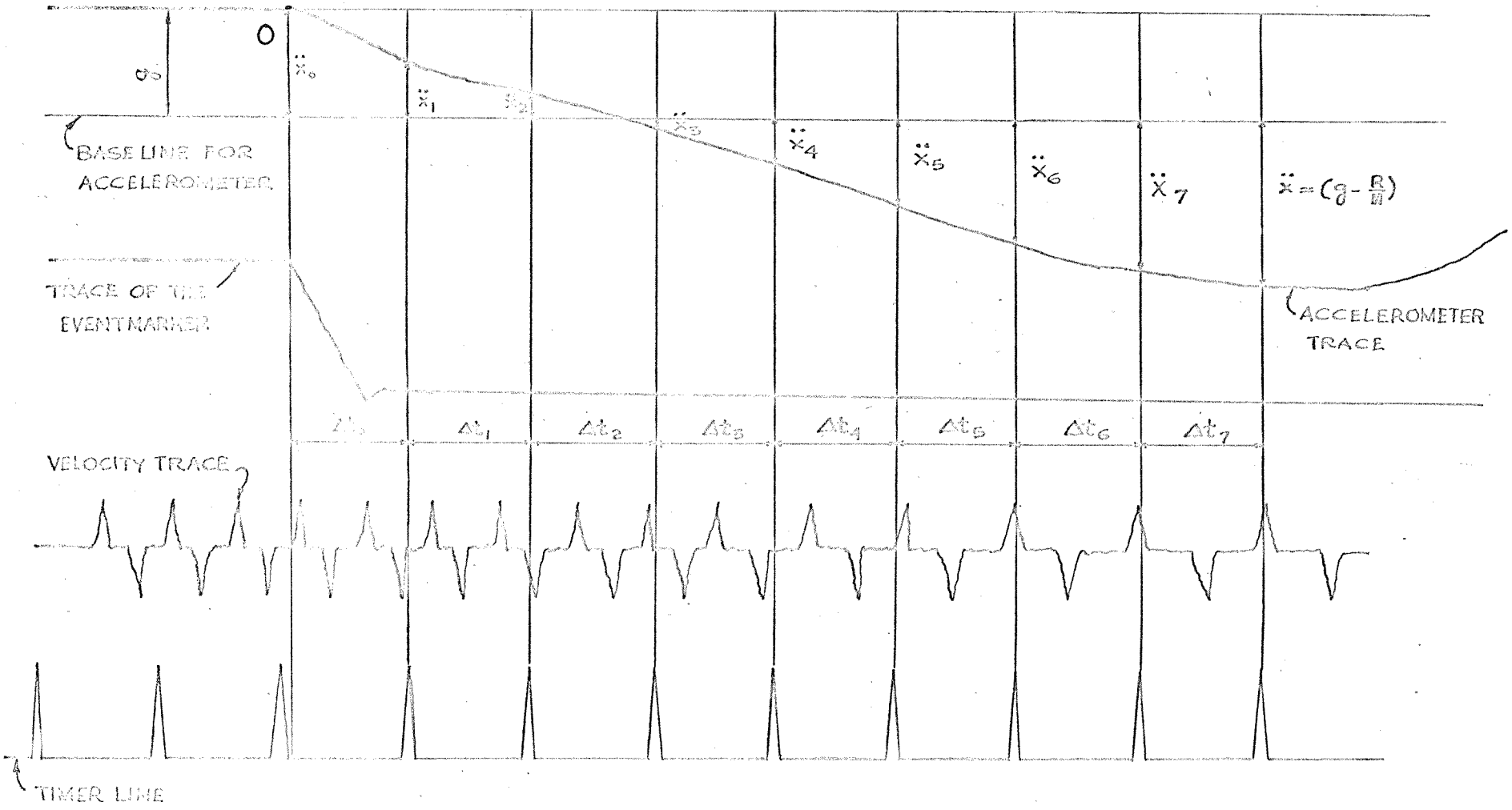

A TYPICAL PAPER TRACE FROM U.V RECORDER

FIGURE- 8.14

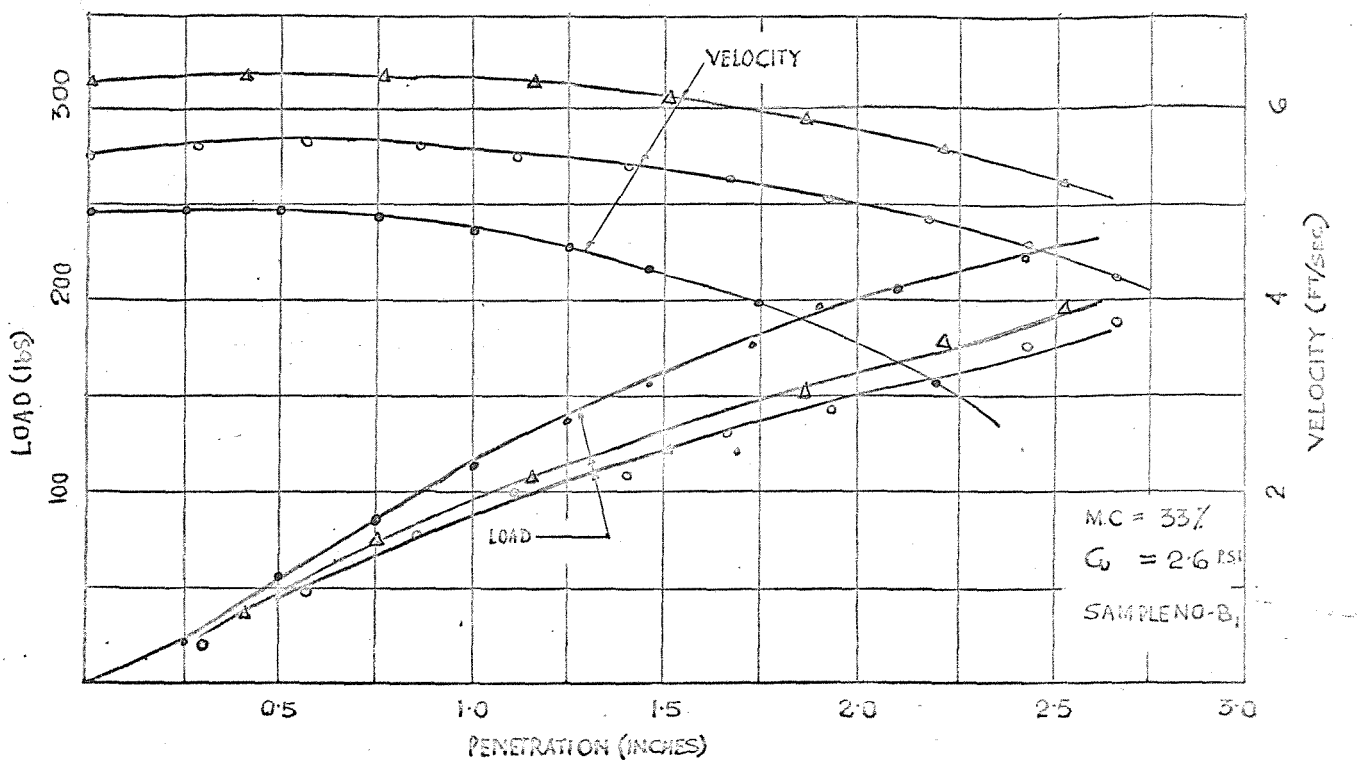

FIGURE- 8.15.1

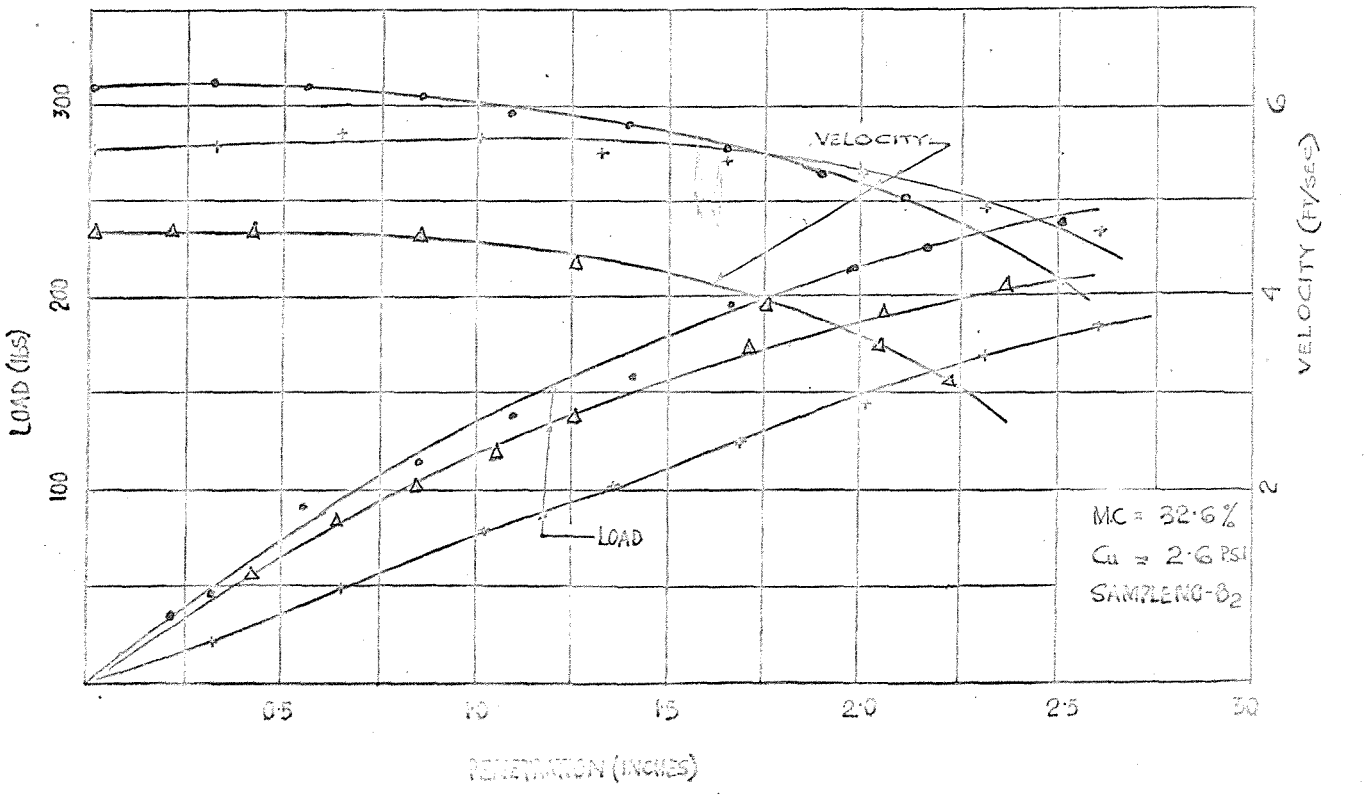

FIGURE - 8.15.2

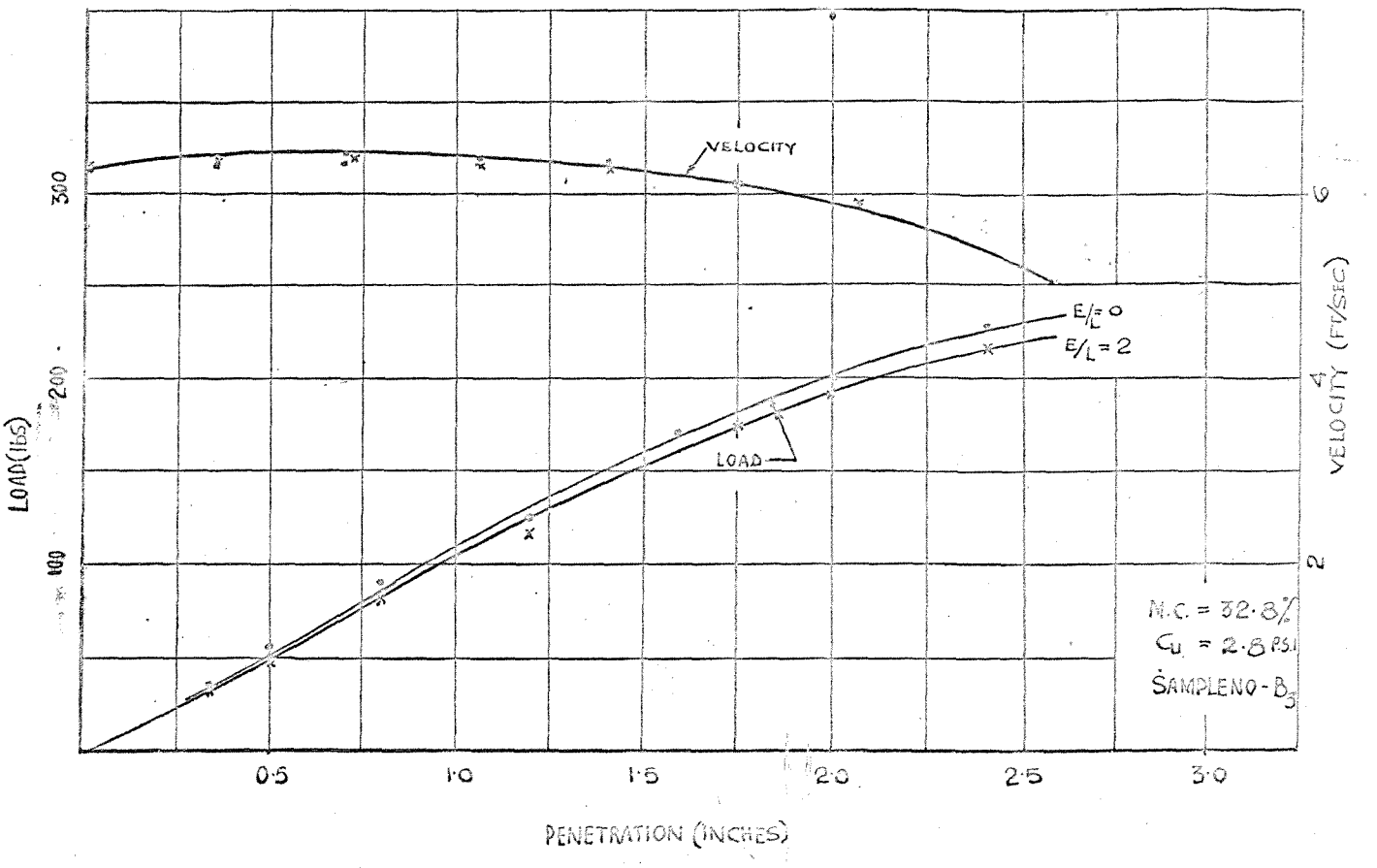

FIGURE- 8.15.3

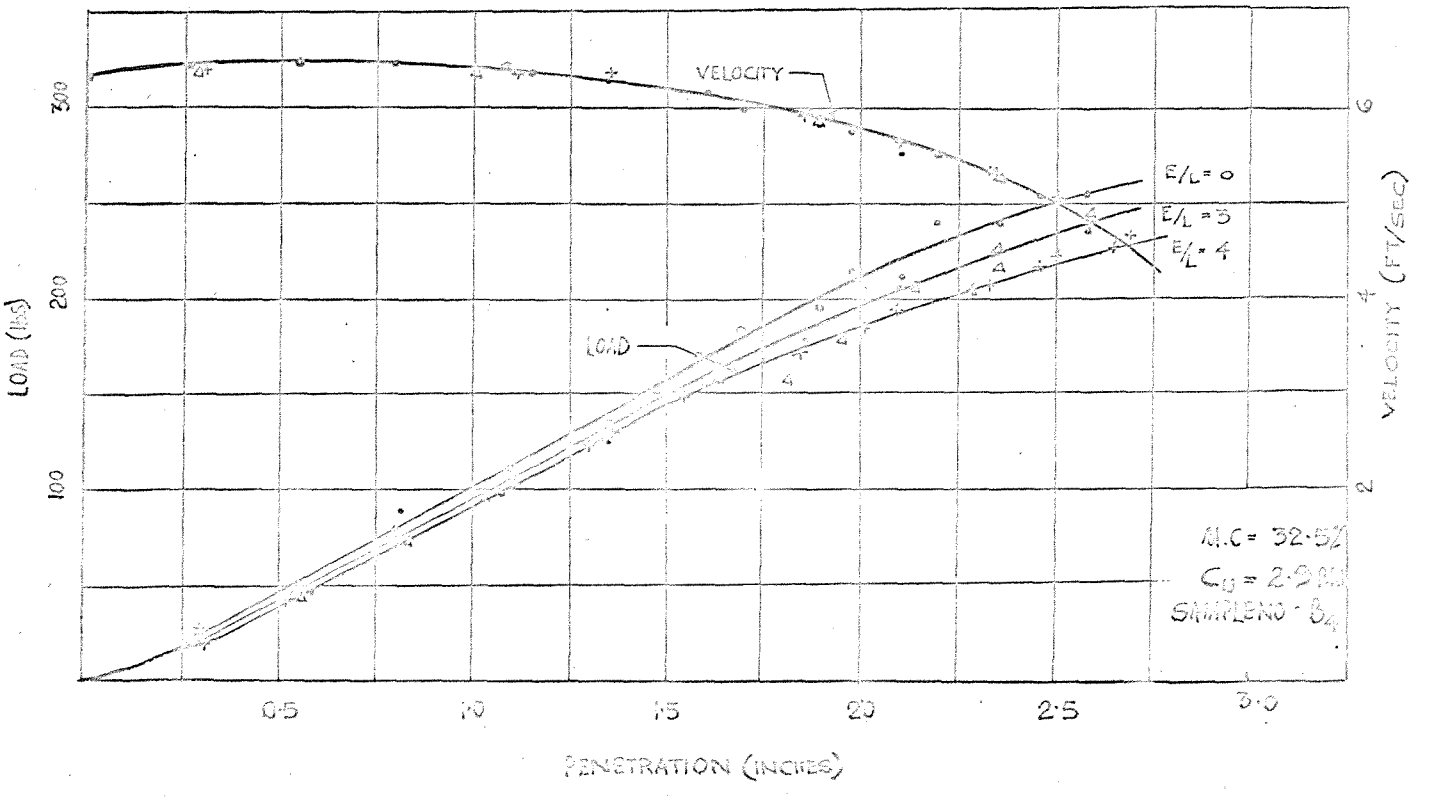

FIGURE- 8.15.4

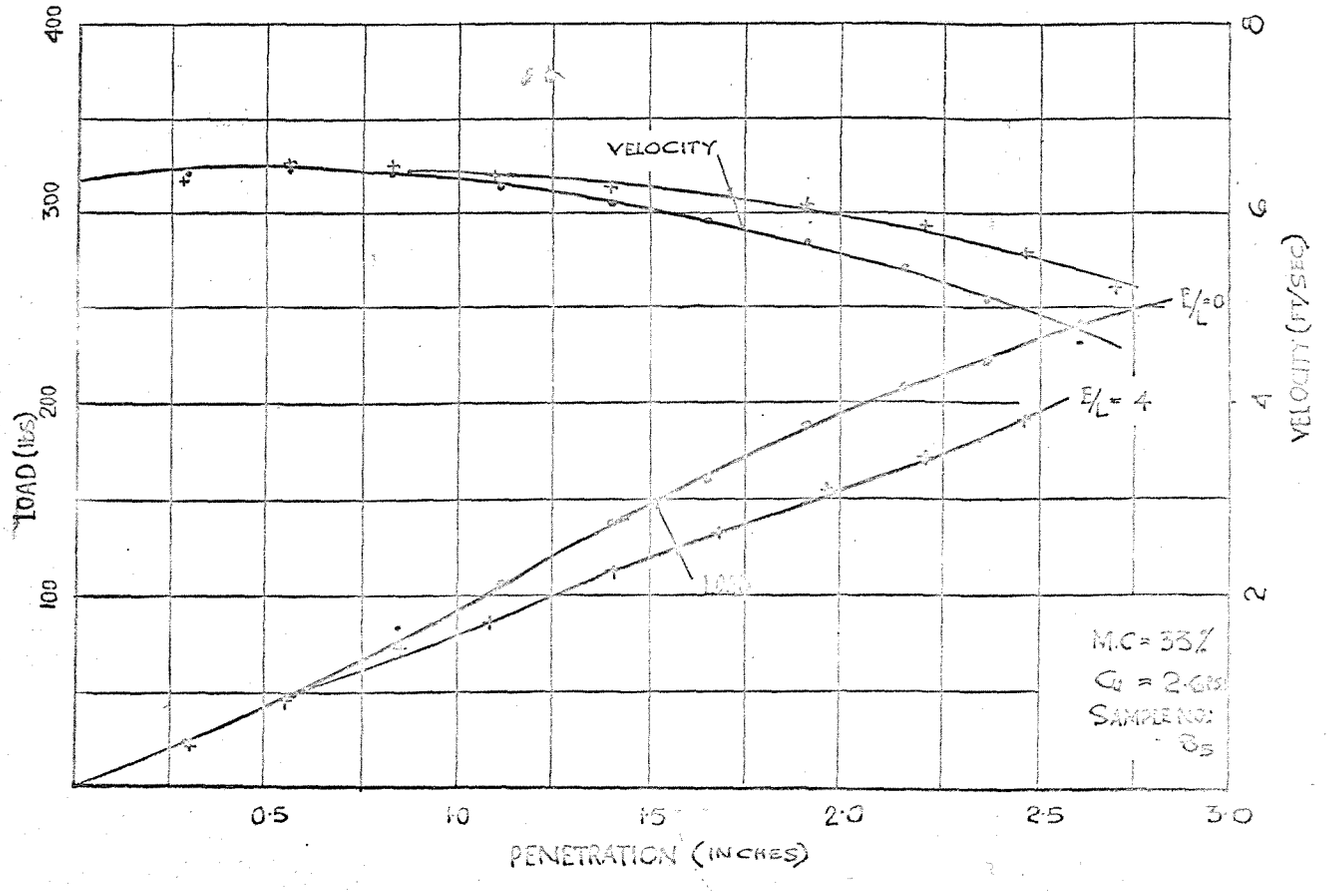

FIGURE - 8.15.5

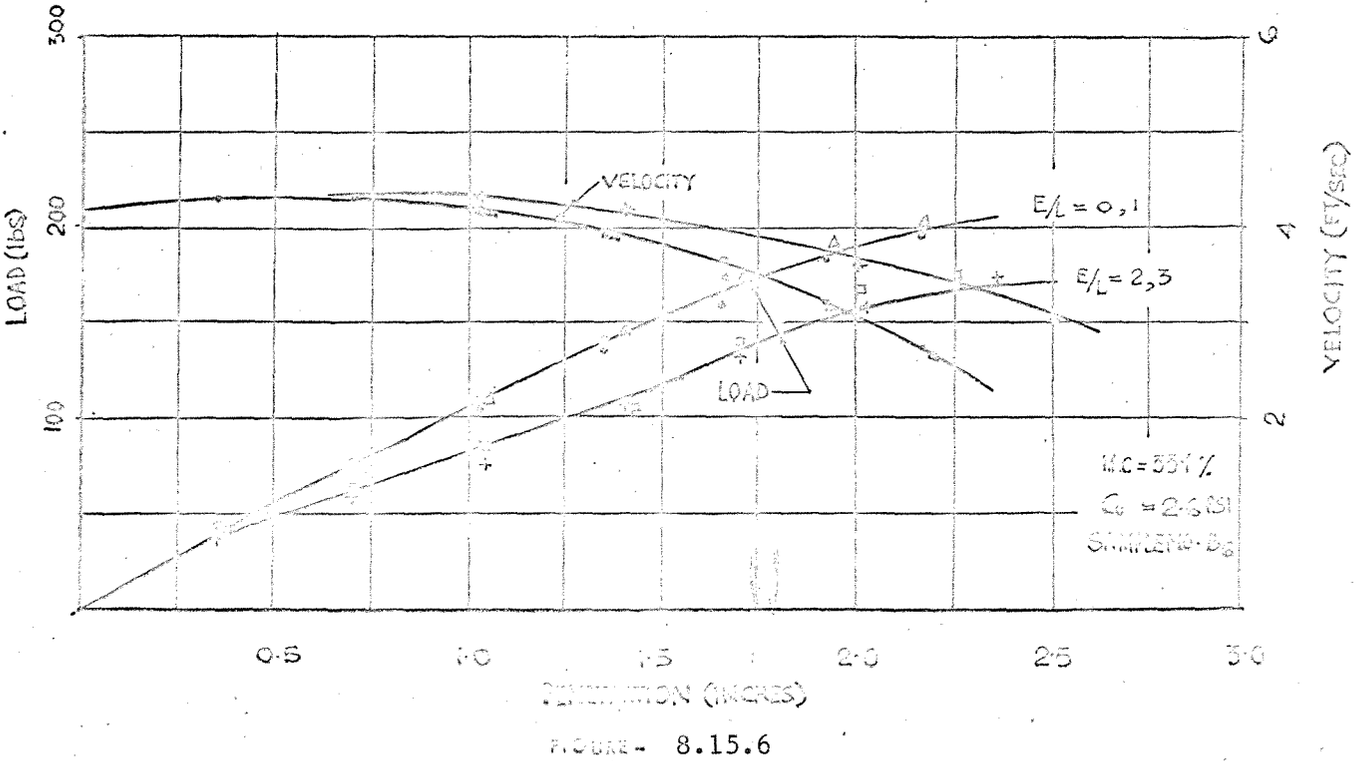

FIGURE - 8.15.6

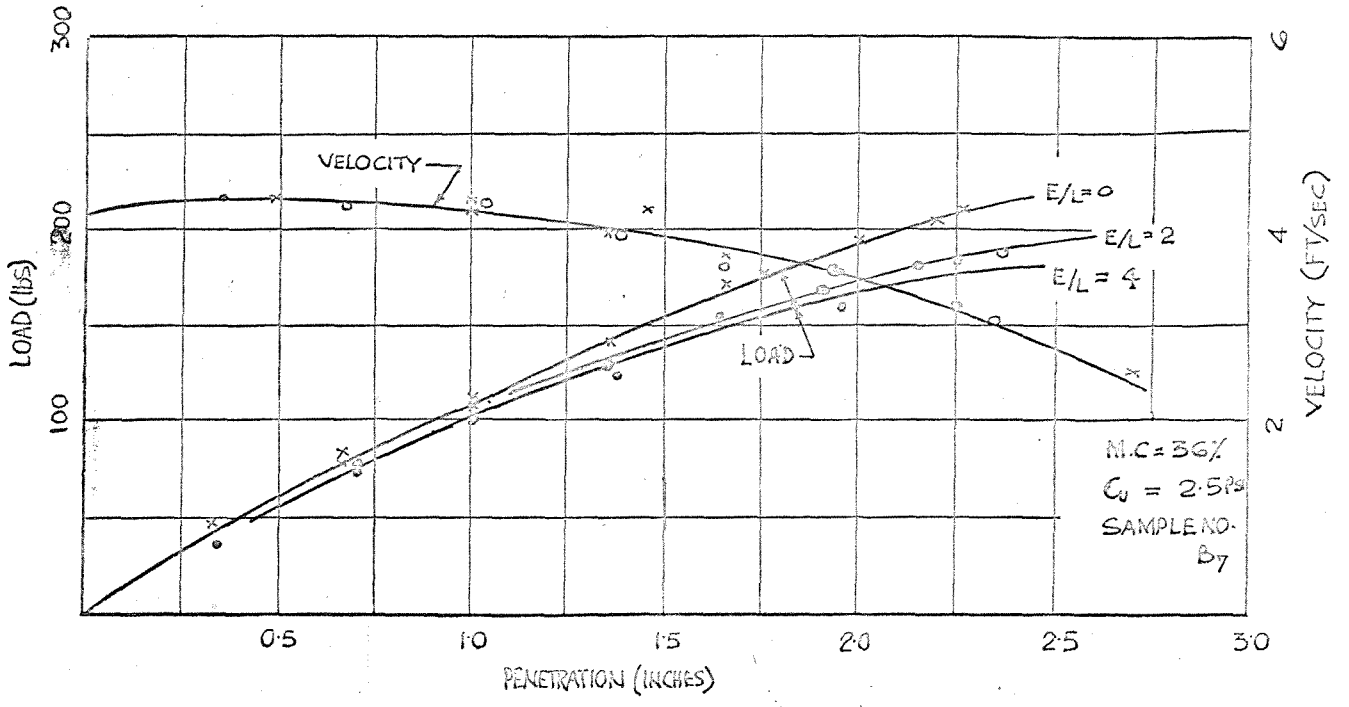

FIGURE – 8.15.7

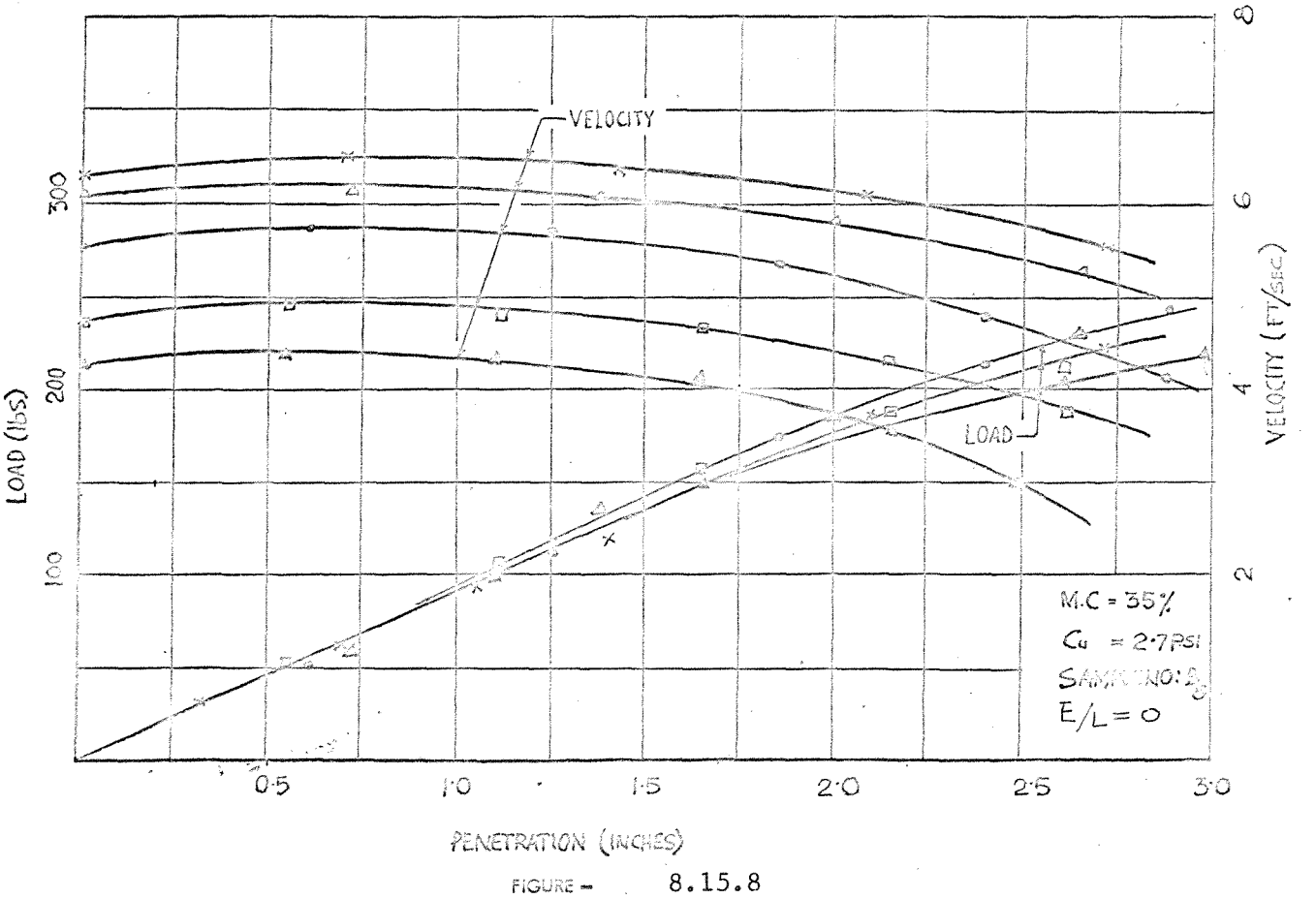

FIGURE – 8.15.8

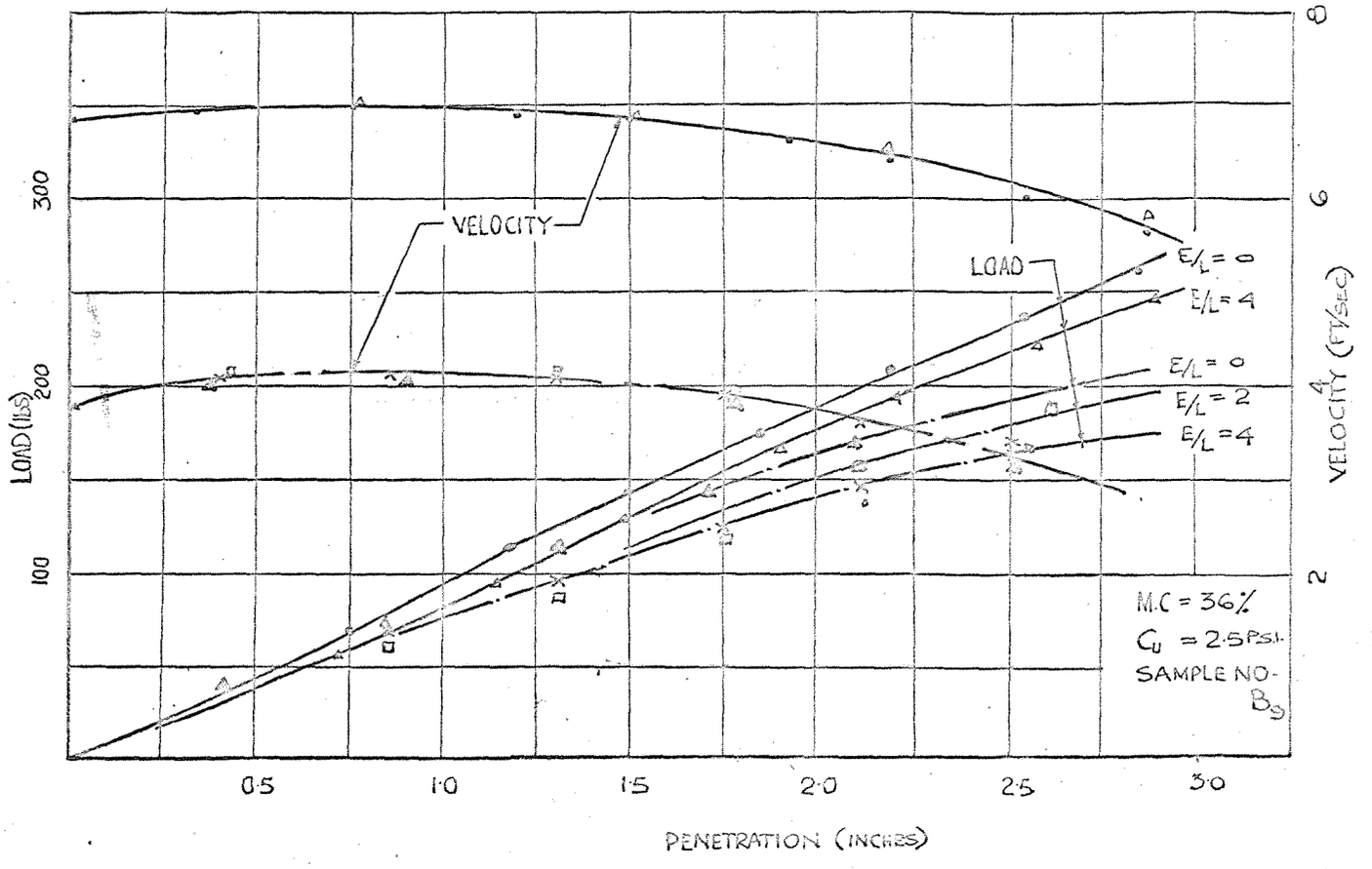

FIGURE – 8.15.9

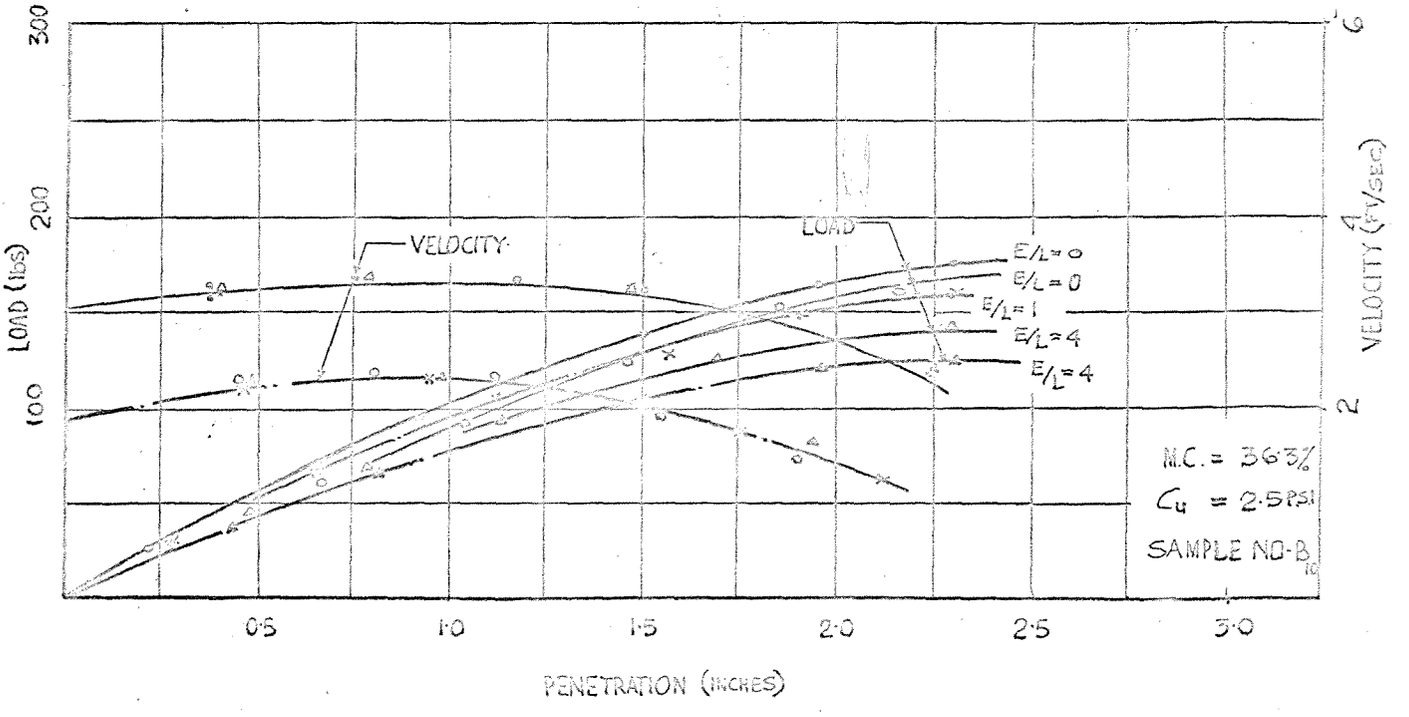

FIGURE – 8.15.10

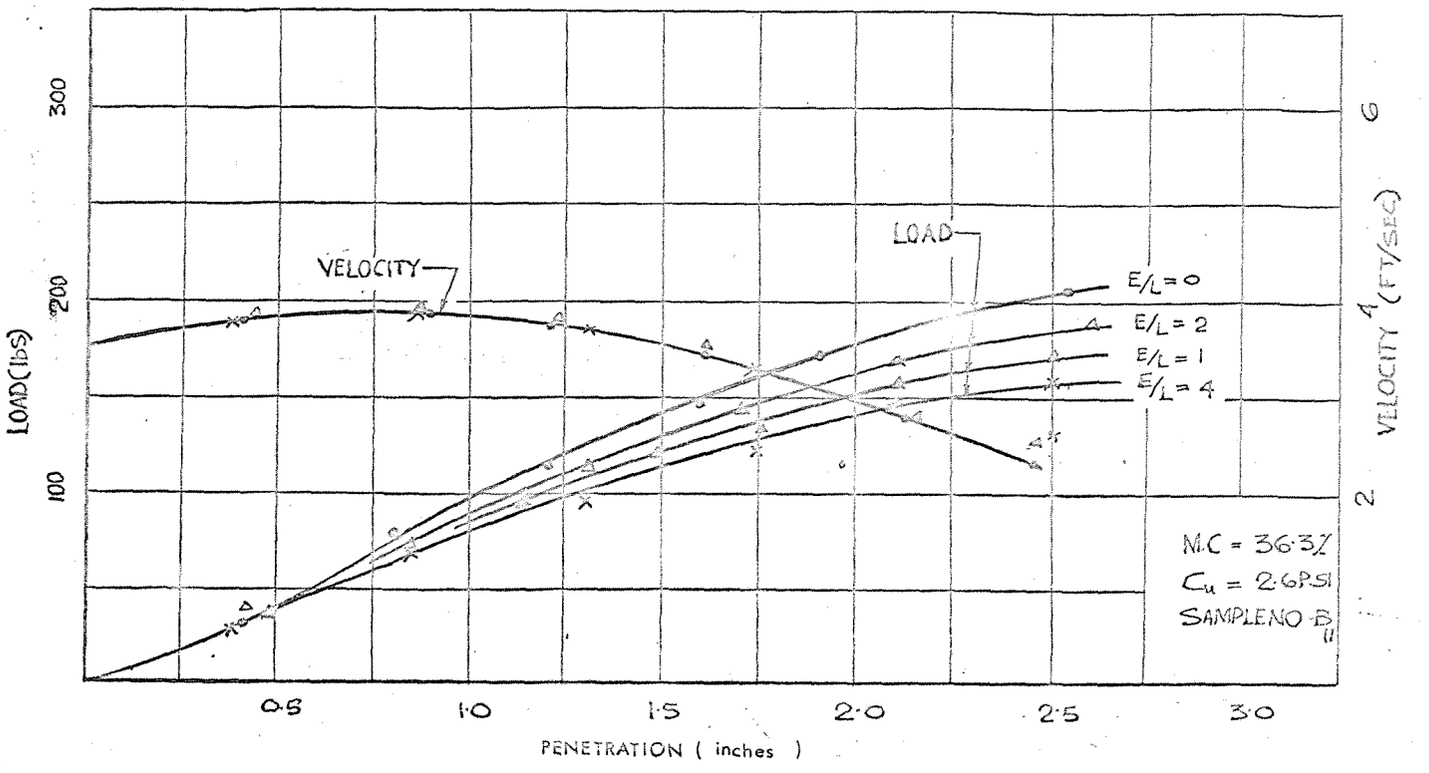

FIGURE- 8.15.11

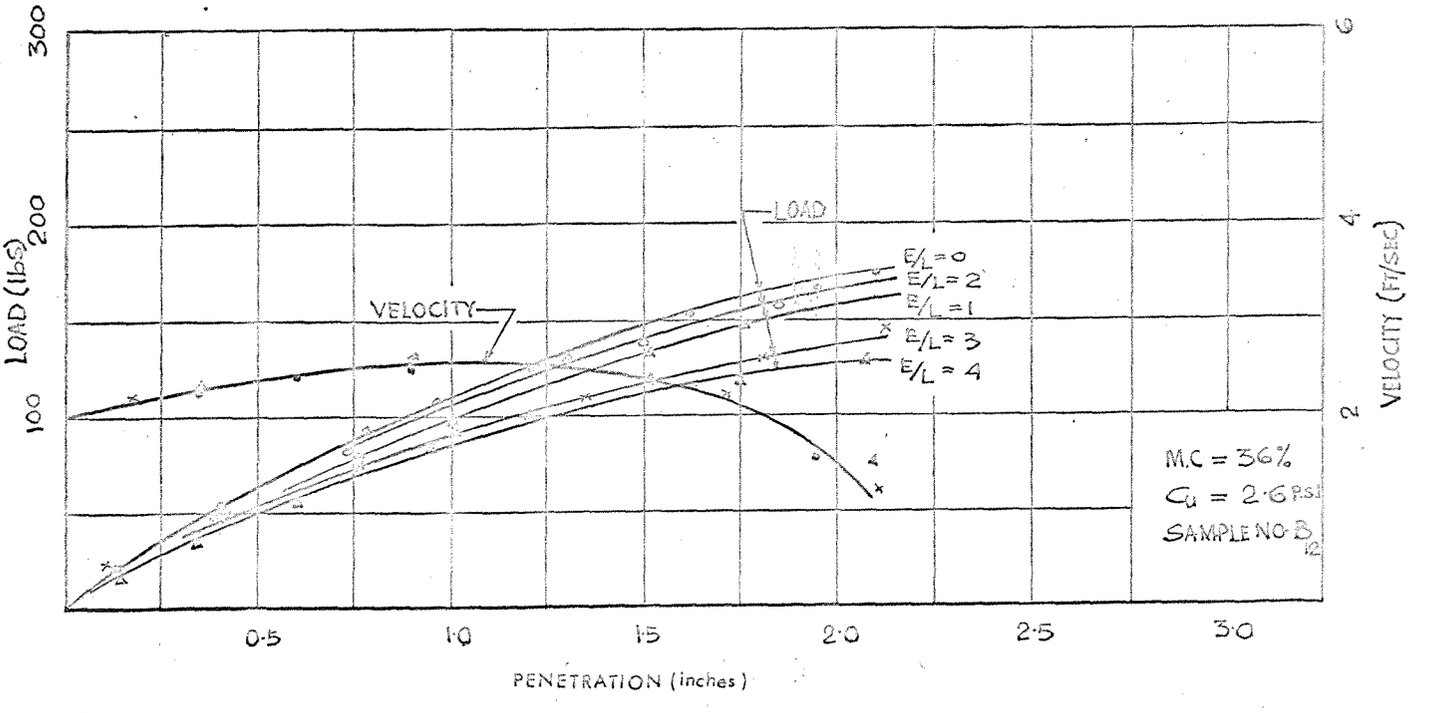

FIGURE- 8.15.12

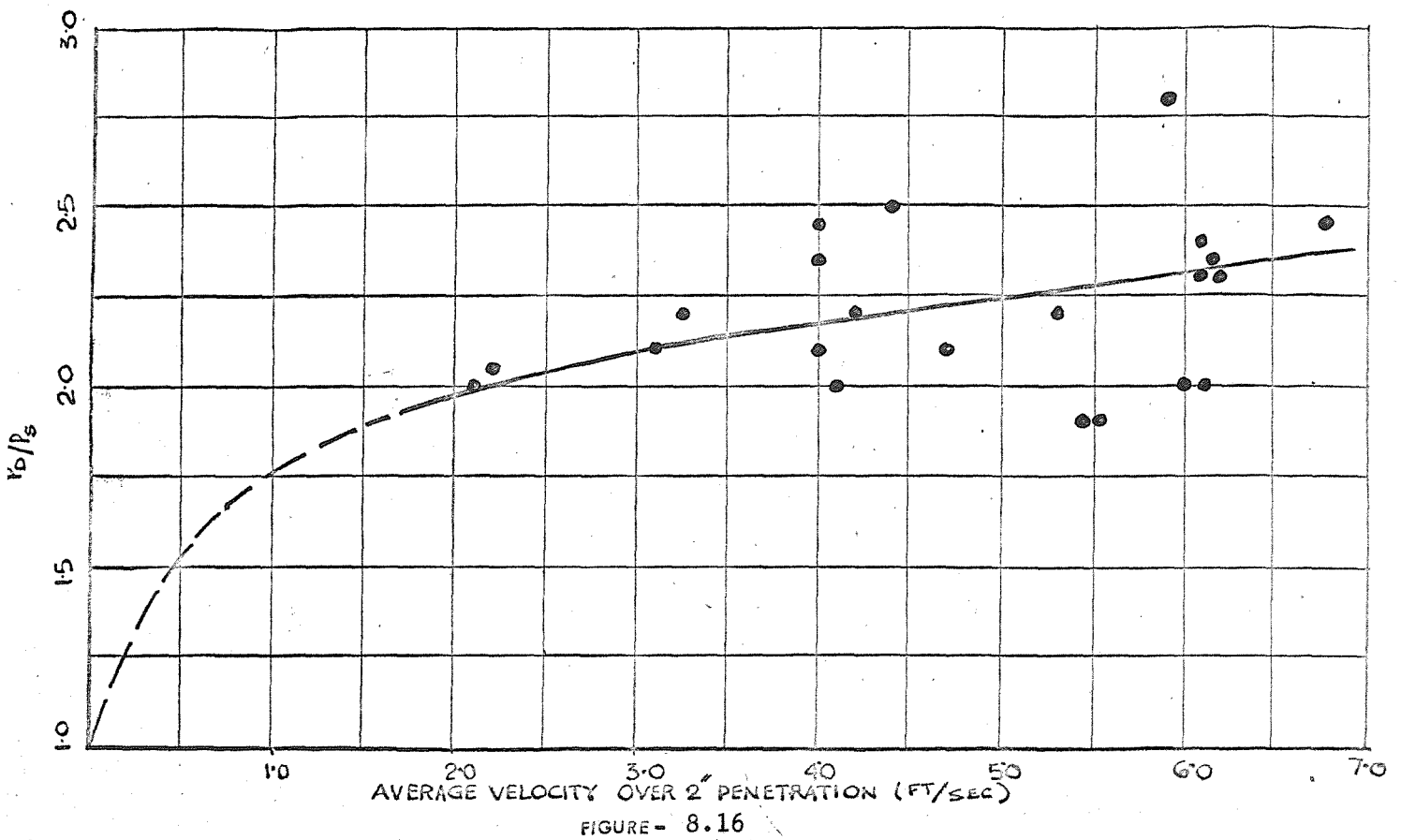

FIGURE - 8.16

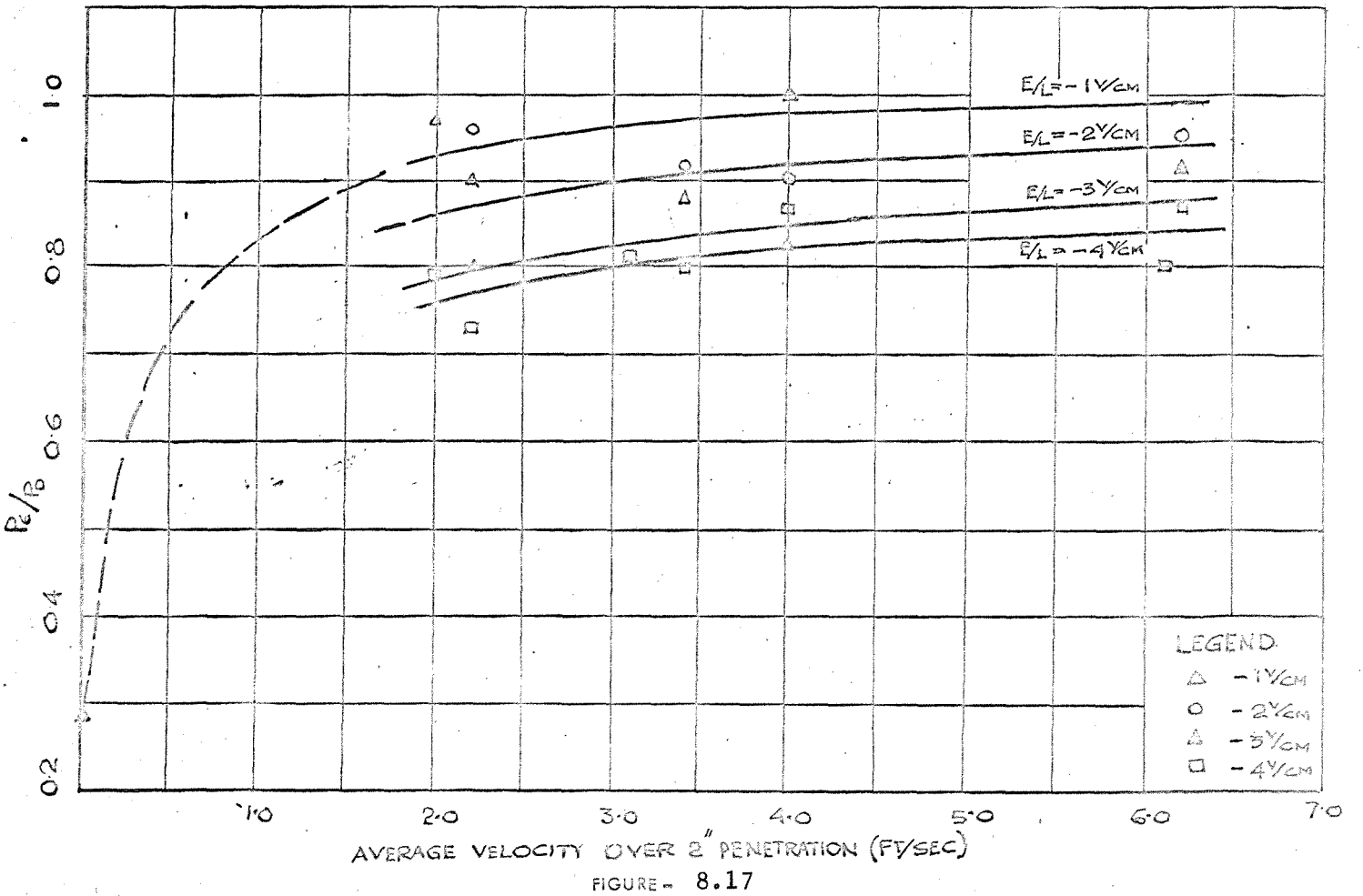

FIGURE - 8.17

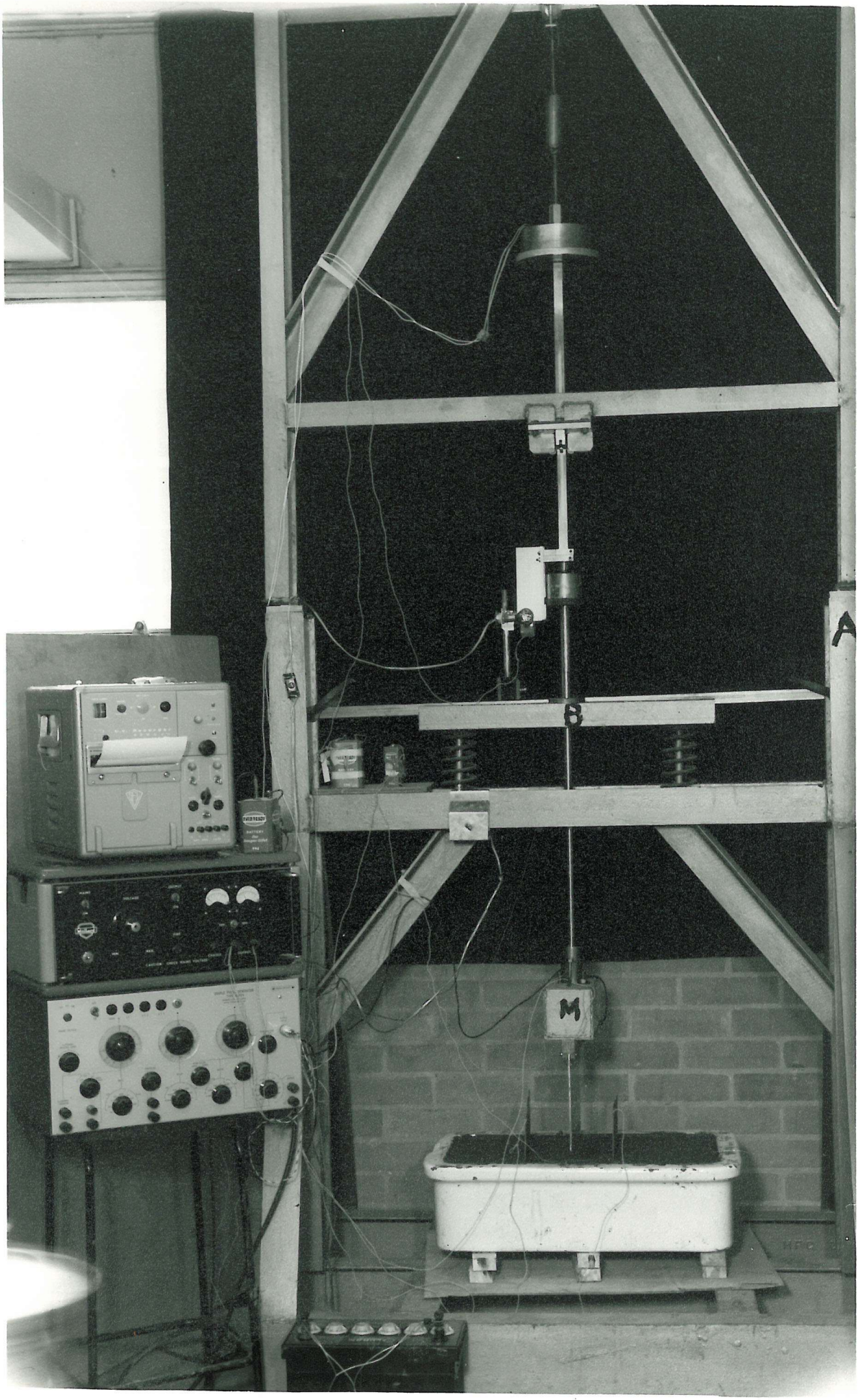

PLATE - 1

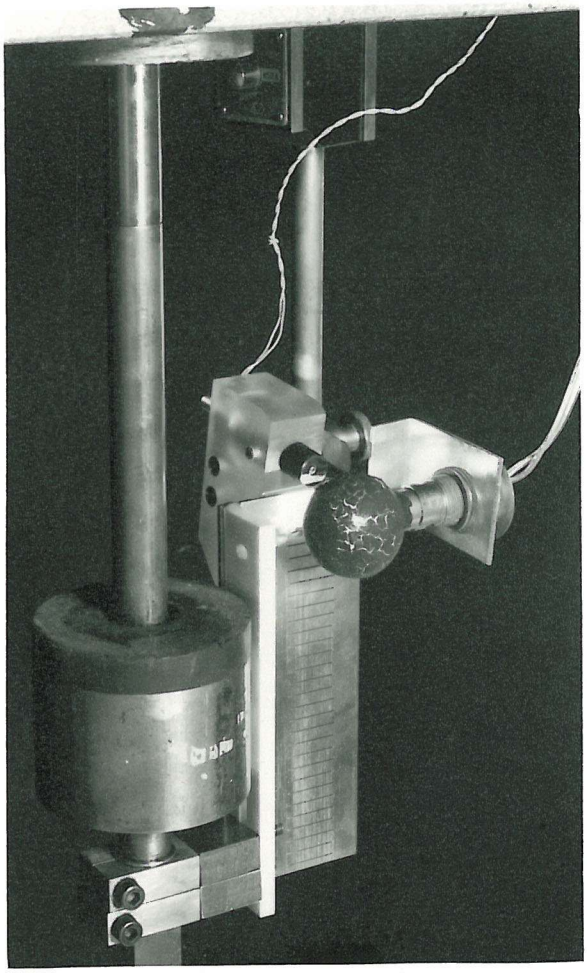

PLATE-2

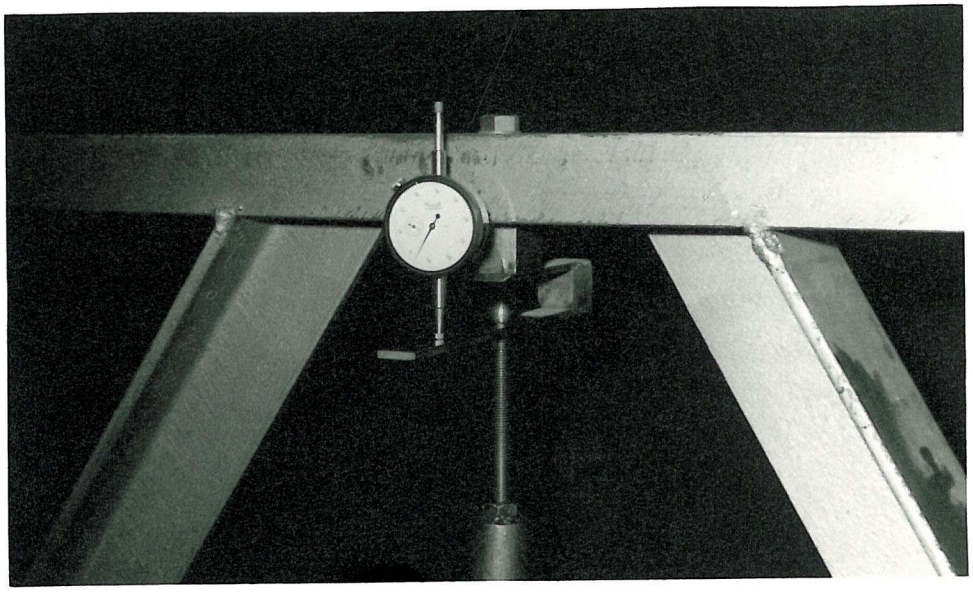

PLATE-3

CHAPTER 9

Final Conclusions and recommendations for further work.

The final discussions and conclusions of the results of the present investigation are presented below. The conclusions drawn from the present analysis of the load-displacement behaviour of piles and deep foundations are discussed with special reference to their applicability to practical situations. Recommendations are made for the direction of future work which should aim at systematic relaxation of the basic assumptions made herein and experimental verifications of the results of the various analyses.

The algorithm, using Mindlin's equations, in an integral equation method which has been developed for the elastic analysis of piles, pile groups and deep footings appears to be ideally suited for such problems as it automatically takes into account a half space with an unloaded boundary. The number of equations to be solved for such problems is much smaller in this method than the number necessary for similar problem by other numerical methods (such as the finite element method) because in the present method the surface is to be discretised whereas in the other methods the whole domain has to be discretised. Most of the computational time involved in the analysis is spent in forming the coefficients of the resulting system of linear algebraic equations. Hence the method is most suitable for high speed digital computers with relatively low storage capacity. The accuracy of the solution depends on the accuracy with which the integrals are replaced by the quadrature formulae. It was found that the most satisfactory numerical quadrature is the one which allows an accurate representation of the kernel function rather than the variation of the unknown intensity over the surface of the given domain. The principle of superposition used in the formulation of the integral equations restricts the application of the method to problems involving linear constitutive laws for the materials involved. The present analysis is only applicable to bodies enclosed within a smooth surface and hence produces good results away from the edges and corners and not so good near them (see Figure, 3.6). The method could

be extended to deal with piecewise homogeneous domain which is composed of a number of homogeneous domains. For such problems the fictitious intensities (i.e. the arbitrary functions) may be distributed over the surfaces of each homogeneous domain and a set of integral equations may then be derived to satisfy the boundary conditions and the compatibilities of the surfaces of the domains in contact with each other.

Application of the method to the solution of the problems related to piles, pile groups and buried rigid discs produced a number of interesting results which are in general agreement with practice. Although over-simplified constitutive laws for soils have been assumed, the comparison between the theoretical predictions with appropriate pseudo-elastic parameters and the field and laboratory test data, revealed encouraging correlations.

The load displacement characteristics of buried rigid discs have been analysed in Chapter 3. It was observed that the depth of burial, shape of the disc and depth of elastic layer strongly influence the settlement of the disc. Hence the conventional method of calculating the settlement of the buried rigid footings by the use of Boussinesq's solution (matching the contact areas) may produce results in error by up to 100%. The solutions presented are strictly applicable to bonded discs where tensile stresses can exist on the top surface of the disc. Whereas the stress distribution for an unbonded disc will be different from that for a bonded disc it is thought that the stiffness of both systems will not be radically different. The bonded solution will generally be applicable to deep footings when the weight of the soil above the footing level produce a net compressive stress on the top surface of the disc. It would be of interest to analyse the problem of an unbonded rigid disc where the displacement of the bottom surface of the disc is specified and the

vertical stress on the top surface is zero. For this mixed boundary value problem the fictitious intensities could be distributed over the surfaces of two discs indefinitely close to each other. The simultaneous system of integral equations may then be derived by satisfying the displacement boundary conditions of the bottom disc and stress boundary conditions of the top disc.

The problems of piles, pile groups and pile group-cap systems have been analysed in Chapters 4, 5 and 6. It was found the load-displacement response of such foundations are strongly influenced by the ratios of thickness of the layer to pile length, length to diameter, spacing to diameter, and compressibility of the pile to that of the soil. The reduction of settlement under a given load achieved by under-reaming is restricted to piles with length to diameter ratios of less than 20 and base to shaft diameter ratios of less than 3. These restrictions are in agreement with current practice. The settlement ratios of free-standing pile groups are found to be dependent on the width, breadth of the group, length to diameter ratio and thickness of the elastic layer and are almost independent of the number of piles in a group. Hence for free-standing pile groups it appears to be more economical to use fewer piles at larger spacings than to use many piles at close spacings. The settlement ratio of a group of 25 piles at spacings of 3 diameters may be as high as 15, which emphasises the importance of accurate evaluation of settlement for group design. Whereas the presence of a rigid cap bearing on the ground surface has little effect on the overall load-displacement response of the pile groups, it does change drastically the load carried by different piles in the group. The theoretical results have been compared with available laboratory model and full scale field test data. This comparison for axially loaded piles revaled that the

load-displacement relationships are in general agreement up to working loads of $P/P_u \sim 0.4$ and also that the behaviour of an under-reamed piles is predictable from the load test results on plain piles. Comparison between the theoretical and experimental results for free-standing pile group showed that the theoretical method is capable of predicting the settlement of groups of any geometry using an elastic parameter G obtained from the field test results on an isolated single pile, provided the values of Poisson's ratio is assumed. Poisson's ratio has a negligible influence on the settlement ratio. In the present analysis the settlement ratio has been defined as the ratio of the settlement of a group to the settlement of a single pile, where the average load per pile in the group is the same as that on the single pile. Unfortunately many previous investigators have used a different and much less satisfactory definition of the settlement ratio which gives rise to considerable confusion in interpreting their results and rather limits their utility for either checking the present analysis or logical general extrapolation to other field situations. The present analysis is of course strictly applicable only to homogeneous and isotropic sub-soil and does not take into account any soil stratification, changes in the soil properties caused by pile driving, the order of driving pile etc. which are all known to influence the pile group behaviour. Therefore a systematic experimental research programme is still needed to evaluate the importance of these variables.

The increase in stresses and pore water pressures developed due to driving a cylindrical pile into a saturated clay and its effect on the ultimate bearing capacity of a driven pile is examined in Chapter 7. An equation for predicting the pore water pressure increase around a driven pile is developed and compared with available full scale test

data with reasonable agreement. It was found that the increase in the pore water pressure at the pile-soil interface may amount to 5 to 6.5 times the undrained cohesion of the soil. This information may be very relevant to the analysis of the stability of foundations alongside the site in which the piles are being driven. The time dependent bearing capacity of driven piles with reference to the variation of the pore water pressures and effective stresses at the pile-soil interface is then examined. The analysis predicts the ultimate bearing capacity of a driven pile may increase with time from 6 to 10 times its value immediately after driving. Since the load tests on piles are inevitably carried out at an early stage when the process of consolidation is not essentially complete, these results may be helpful in predicting an extrapolated ultimate bearing capacity at the end of the consolidation process. The theoretical analysis is, however, based on a number of over-simplified assumptions, such as, that of plane strain, elastic-ideally plastic soil media etc. Therefore again a solution relaxing these assumptions with experimental support is required.

A topic which though not directly related to the general framework of the present investigation which may however be useful in connection with piled foundations is discussed in Chapter 8. A series of slow speed and high speed probe driving tests was carried out into saturated clay assisted by applied D.C. potentials. It was found that for cathodic probes application of an average voltage gradient of about 0.2 volts/cm can reduce the driving resistance by as much as 50% for slow speed driving (0.36"/minute) but when the speed of driving is increased beyond 2 ft/sec the reduction in penetration resistance achieved by this process is negligible. More detailed investigation of the slow speed and time dependent effects is currently being carried out but the phenomenon

appears to have no application towards improvement in continuous high speed pile driving operation.

REFERENCES

Airhart, T.P., (1967) "The response of a pile-soil system in a cohesive soil as a function of the excess pore water pressure and the engineering properties of the soil", Ph.D. thesis, Texas A and M University.

Allen, D.N. de G., (1955) "Relaxation methods", Mcgraw Hill, New York.

Baker, C.T.H., Fox, L., Mayer, D.F., Wright, K. (1966) "Numerical solution of Fredhlom's integral equation of first kind", Computer Journal, Vol. 7, p. 141.

Banerjee, P.K., (1969) "Computer programmes for the analysis of piled foundations", Report C.E/6/69, Southampton University.

Banerjee, P.K., and Butterfield, R., (1968) "Effect of an applied D.C. potential on the penetration resistance of model probes and blades in soils", Report C.E/18/68, Southampton University.

Begemann, H.K.S., (1953) "The effect of D.C. potential on the adhesion of clay to metal", Proc. third int. conf. S.M.F.E., Vol. 1, p. 57.

Berezantzev, V.G., Kristoforov, V.S., and Golubkov, V.N., (1961) "Load-bearing capacity and deformation of pile foundations", Proc. fifth int. conf. S.M.F.E., Vol. 2. p.11.

Bishop, R.F., Hill, R., and Mott, N.F., (1945) "The theory of indentation and hardness test", Proc. phys. Soc., Vol. 57, p.147.

Biot, M.A., (1935) "Effect of certain discontinuities on the pressure distribution in a loaded soil", Physics, vol. 6, p. 367.

" (1941) "General theory of three-dimensional consolidation", Jour. applied physics, vol. 12, p.155.

Bjerrum, L., Johannessen, I., (1961) "Pore pressure resulting from driving piles in soft clay", Pore pressure and suction in soil, Butterworth, London, p.108.

Boussinesq, J., (1885) "Application of potentials to the study of the equilibrium and movements in elastic soils" (in French), Gauthier-Villard, Paris.

Broms, B., (1966) "Methods of calculating the bearing capacity of pile - a summary", Sols Soils, No. 18-19, p.21.

Burland, J.B., Dunican, P., and Butler, J. (1966) "The behaviour and design of large diameter bored piles in stiff clay", Proc. Symp. Large bored piles, London, p.51.

Burmister, D.M., (1956) "Stress and displacement characteristics of a two layer rigid base soil system; Influence diagrams and practical applications", Proc. H.R.B., Vol. 35, p.773.

Butterfield, R., and Andrawes, K.Z., (1968) "Wedge penetration into soils", Report C.E/23/68. Southampton University.

Butterfield, R., and Banerjee, P.K., (1967) "Application of electro-osmosis to soils", Report C.E/24/67, Southampton University.

" (1969a) "A rigid disc embedded in elastic half space", Sent to A.S.C.E. (Engg. Mech. Divn.) for publication.

" (1969b) "An elastic analysis of piles and pile groups", Sent to A.S.C.E. (Soil Mech. Divn.) for publication.

" (1969c) "A note on the problem of a pile reinforced half space", To be published in Geotechnique.

Casagrande, L., (1949) "Electro-osmosis in soils", Geotechnique, Vol. 1, No. 3, p.159.

" (1952) "Electro-osmotic stabilisation of soils", Jour. Boston Soc. of Civil Engineers, January, p.285.

" (1962) "La Electro-osmosis y Fenomenos conexos" (in Spanish), Publicacion Numero 54, Del Instituto De Ingneeria, Universidad National Autonoma de Mexico.

Chellis, R.D., (1951) "Pile foundations", McGraw-Hill, New York.

Chandler, R.J., (1968) "The shaft friction of piles in cohesive soil in terms of effective stress", Civil Engineering and Public Works Review, January, p.48.

Cheung, Y.K., and Zienkiewicz, O.C., (1965) "Plates and tests on elastic foundations - an application of Finite Element Method", Int. Jour. Solids and Structures, Vol. 1, p. 451.

Clough, R.W., (1960) "The finite element in plane stress analysis", Proc. second A.S.C.E. Conf. on electronic computation, Pittsburg, Pa.

Cooke, R.W., and Whitaker, T., (1961) "Experiments with model piles with enlarged bases", Geotechnique, Vol. 11, No. 2, p.1.

Coyle, H.M., and Reese, L.C., (1966) "Load transfer for axially loaded pile in clay", Jour. A.S.C.E., S.M.2, p.1.

Cummings, A.E., (1940) "Dynamic pile driving formulas", Contribution to soil mechanics (1925-1940), Boston Society of Civil Engineers, Mass, p.392.

Cummings, A.E., Kerhoff, G.O., Peck, R.B. (1950) "Effect of driving piles into soft clay". Trans. A.S.C.E., Vol. 115, p.275.

D'appolonia, E., and Romualdi, J.P., (1963) "Load transfer in end bearing steel H-pile", Proc. A.S.C.E. 89, S.M.2, P.1.

D'appolonia, E., and Hribar, J.A., (1963) "Load transfer in a step-taper pile", Proc. A.S.C.E, S.M.6, p.57.

de Beer, E.E., (1963) "The scale effect in transposition of the results of deep sounding tests on the ultimate bearing capacity of piles and caisson foundations", Geotechnique, Vol. 13. No. 1, p.39.

de leeuw, E.H., (1965) "The theory of three-dimensional consolidation applied to cylindrical bodies", Proc. 6th Int. Conf. S.M.F.E., Vol. 1, p.287.

Deresiewicz, H., (1959) "The half space under pressure distributed over an elliptical portion of its plane boundary", Proc. A.S.M.E., Appl. Mech. Div., Paper No. 59-A-17.

Doroskhevich, N.M., and Bartolomey, A.A., (1965) "Discussion on pile foundations", Proc. 6th Int. Conf. S.M.F.E., Vol. 3, p.484.

Esrig, M.I., and Majtenyi, S., (1966) "A new equation for electro-osmotic flow and its implications for porous media", Highway research record, No. 11, H.R.B. publication 1331, March, p.31.

Evans, H.E., and Lewis, R.W., (1965) "Theoretical treatment of the electro-osmotic consolidation of soils", Civil Engineering and Public Works Review, Oct. p.1495.

Fleming, W.G.K., (1958) "The bearing capacity of pile groups", Ph.D. thesis, Queens University, Belfast.

Feda, J., (1963) "Skin friction of piles due to dilatancy", Proc. Int. Conf. S.M.F.E., Budapest, Sept. p.243.

Freundlich, M., (1926) "Colloidal and Capillory Chemistry", Translated by H. Stafford Hatfield, Menthuen and Co. London, p.239.

Fountain, E.R., and Payne, P.C.J., (1954) "Cause of non scouring in soil working implements", Trans. 5th Int. Conf. of Soil Science, Vol. 2, p.35.

Golder, H.Q., and Leonard, M.W.,	(1954)	"Some tests on bored piles in London Clay", Geotechnique, Vol. 4, No. 1, p.32.
Gibson, R.E.,	(1950)	"Discussion to a paper by G. Wilson", "The bearing capacity of a screw pile and screwcrete cylinder", (Jour. I.C.E., 34, 4, 1950), Jour. I.C.E., 34, p.382 (Suppl).
"	(1963)	"In-situ measurement of soil properties by pressuremetre", Civil Engineering and Public Works Review, May, p.615.
Gouy, M.,	(1910)	"Jour. de Physics et Le Radium", Vol. 4, No. 9, p.957.
Hanna, T.H.,	(1963)	"Model studies of foundation groups in sand", Geotechnique, Vol. 13, p.192.
Harr, M.E.,	(1966)	"Foundation of theoretical Soil Mech", McGraw-Hill, New York.
Helmholtz, V.H.,	(1879)	"Studien uber electrische", Annalen der physik und Chemie, Grenzschichten, Neue Floge Band, 7, No. 7, Wiedemann 7, p.337.
Henkel, D.J.,	(1960)	"The shear strength of saturated remoulded clays", Research Conf. on shear strength of cohesive soils, Boulder, Colorado Springs, p.551.
Hill, R.,	(1950)	"Mathematical theory of plasticity", Oxford University Press.
Johnston, I.W.,	(1968)	"The effect of electro-osmosis on the penetration resistance of a model pile in clay", Part II, Project report, Southampton University.
Kezdi, A.,	(1957)	"Bearing capacity of piles and pile groups", Proc. 4th Int. Conf. S.M.F.E., Vol. 2, p.46.
"	(1960)	"Bemerkungen Zur Frage der Tragfaehigueit von Pfahlgruppen", Proc. I.A.B.S.E., Stockholm.
Kishida, H., and Meyerhof, G.G.,	(1965)	"Bearing capacity of pile groups under eccentric loads in sand", Proc. 6th Int. Conf. S.M.F.E., Vol. 2, p.270.
Koizumi, Y., and Ito, K.,	(1967)	"Field tests with regard to pile driving and bearing capacity of piles foundations", Soils and Foundations (Japan), Vol. 7, No. 3, p.31.
Konder, R.L.,	(1962)	"Friction pile groups in cohesive soil", Jour. A.S.C.E., S.M.3, p.117.
Kupradze, V.D.,	(1964)	"Dynamic problems in elasticity", Progress in Solid Mechanics, Vol. 3, Ed. Sneddon, I.N. and Hill, R., North Holland.

Ladani, B., (1963) "Expansion of a cavity in a saturated medium", Jour. A.S.C.E., S.M.3, p.127.

Lee, I.K., (1963) "Elastic settlement of footing with rough interface", Proc. 4th Aust.-N.Z. Conf. S.M.F.E., Adelaide, p.225.

Lo, K.Y., and Stermac, A.G., (1963) "Correspondence", Geotechnique, Vol. 13, No. 3, p.163.

" (1965) "Induced pore pressure during pile driving operations", Proc. 6th Int. Conf. S.M.F.E., Vol. 2, p.285.

Lomize, G.M., Netoushil, A.V., and Rzhanitzin, B.A., "Electro-osmotic processes in clayey soils and dewatering during excavations", Proc. 4th Int. Conf. S.M.F.E., Vol. 1, p.61.

Love, A.E.H., (1929) "The stress produced in a semi-infinite solid by pressure on a part of boundary", Phil. Trans. Roy. Soc., London (A), Vol. 228, p.377.

" (1953) "A treatise on mathematical theory of elasticity", Dover.

Mackey, R.D., and Khafagy, A.A., (1968) "Vertical pressure distribution resulting from a flexible distributed load applied in the interior of a semi-infinite elastic medium", Civil Engg. and Public Works review, Feb. p.163.

Manegold, S., and Solf, H., (1937) "Uber Kappilarsysteme", Kolloidzeitschrift, Vol. 15.

Massonnet, C., (1965) "Numerical use of integral procedures", Stress analysis. Zienkiewicz, O.C. and Holister, G.S., John Wiley.

Mattes, N.S., (1969) "Correspondence", Geotechnique, Vol. 19, No. 1, p.157.

Mattes, N.S., and Poulos, H.G., (1969a) "Settlement of single compressible pile", Proc. A.S.C.E., S.M.1, p.189.

" (1969b) "An analysis of end bearing piles", Geotechnique, Vol. 19, No. 2.

Melan, E., (1932) "A line load in the interior of a semi-infinite solid", Zeits. f. angew. Math. Und. Mech, Vol.12, p.343.

Meyerhof. G.G., (1951) "Bearing capacity of foundations", Geotechnique, Vol. 2, No. 4, p. 300.

" (1959) "Compaction of sand and bearing capacity of piles", Jour. A.S.C.E., S.M.6, p.1.

Meyerhof, G.G., (1960) "The design of Franki piles with special reference to pile groups in sand", Proc. I.A.B.S.E., Stockholm, p.105.

Meyerhof, G.G., and Murdock, L.J., (1953) "An investigation of the bearing capacity of some bored and driven piles in London Clay", Geotechnique, Vol. 3, No. 7, p.267.

Mikhlin, S.G., (1957) "Integral equations", Pergamon Press.

" (1964) "Variational methods in mathematical Physics", Pergamon Press.

" (1965) "Multidimensional singular integral equations", Pergamon Press.

Mindlin, R.D., (1936) "Force at a point in the interior of a semi-infinite solid", Physics, May, p.195.

Muskhelishvili, N.I., (1953) "Some basic problems of mathematical theory of elasticity", E.P. Noordhoff Limited, Groningen, Nederland.

Nair, K., (1963) "A theoretical investigation of the load-displacement characteristics of a single pile", Ph.D. thesis, Ohio State University.

Netoushil, A.V., (1953) "Computations and investigation on models of electrical seepage in anisotropic media", (in Russian), Trans. Moscow Power Inst. Vol. 14, p.211.

Newmark, N.M., (1935) "Simplified computation of vertical pressure in elastic foundations", Circular No. 24, Engg. expt. St., University of Illinois, Urbana.

Nikolaev, B.A., (1963) "Pile driving by electro-osmosis". Translated from original Russian work by Consultant Bureau, New York.

Nishida, Y., (1960) "Bibliography of Pile foundations", The Yawata Iron and Steel Co. Ltd., Tokyo.

" (1961) "Determination of stresses around a compaction pile", Proc. 5th Int. Conf. S.M.F.E., Vol. 2, p.123.

" (1963) "Pore pressure in clay induced by pile friction", Proc. 2nd Pan. Am. Conf. S.M.F.E, Vol. 1, p.217.

" (1964) "Estimation of bearing capacity of piles in cohesionless soil", Trans. Japanese Soc. of C.E., p.49.

Oliveira, E.R.A., (1968) "Plane stress analysis by a general integral method", Jour. A.S.C.E., Engg. Mech. Divn., February, p.79.

Orrje, O., and Broms, B., (1967) "Effects of pile driving on soil properties", Proc. A.S.C.E., S.M.5, p.59.

Peck, R.B., Hanson, W.E., and Thornburn, T.H., (1953) "Foundation engineering", Wiley, New York.

Peleg, M., (1960) "Study of road friction observations", Report 1960, Technion, Faculty of Civil Engg. Haifa, Israel.

Piakowski, A., (1957) "Investigation on electro-osmotic flow in relation to different characteristics", Proc. 4th Int. Conf. S.M.F.E., Vol. 1, p.89.

Potyondy, J.G., (1961) "Skin friction between various soils and construction materials", Geotechnique, Vol. 11, No. 4, p.339.

Poulos, H.G., (1968a) "The influence of a rigid cap on the settlement behaviour of an axially loaded pile", Trans. Inst. C.E. (Australia), Vol. C.E.10, No. 2, p.206.

" (1968b) "The behaviour of a rigid circular plate resting on a finite elastic Layer", Trans. Inst. C.E. (Australia), Vol. C.E.10, No. 2, p.213.

" (1968c) "Analysis of the settlement of pile group", Geotechnique, Vol. 18, No. 4, p.449.

Poulos, H.G., and Davis, E.H., (1968) "The settlement behaviour of single axially loaded incompressible piles and piers", Geotechnique, Vol. 18, No. 3, p.351.

Preece, E.F., (1947) "Geotechnics and geotechnical research", Proc. H.R.B., 27th Annual meeting, p.385.

Reltov, B.F., and Novikov, A.V., (1938) "The use of electro-osmosis as a means of countering the effects of adhesive viscous soils on the working surface of construction machinery", Computations for thematic work (in Russian), Lib. of Scientific research, Inst. of Hydraulic Engg., U.S.S.R.

Robinsky, E.I., and Morrison, C.F., (1964) "Sand displacement and compaction around model friction piles", Canadian Geotechnique Journal, Vol. 1, No. 2, March, p.81.

Sadowski, M., (1928) "Two-dimensional problem in elastic theory", (in German), Z. angew, Math. und. Mech., Vol. 8, p.107.

Saffery, M.R., and Tate, A.P.K., (1961) "Model tests on pile group in a clay soil with particular reference to the behaviour of the group when it is loaded eccentrically", Proc. 5th Int. Conf. S.M.F.E., Vol. 2. p.129.

Salas, J.A.J., (1965) "Discussion", Division 4, Proc. 6th Int. Conf. S.M.F.E., Vol. 3, p.489.

Salas, J.A.J., and Belzunce, J.A., (1965) "Resolution theoretique de la distribution des forces dans les pieux", Proc. 6th Int. Conf. S.M.F.E., Vol. 2, p.309.

Schaad, W., and Haefeli, R., (1947) "Electrokinetische erscheinungen und ihre anwendung in der bodenmechanik", Schweiz. Pauzeitung, Vol. 65, p.16.

Schiff, S., (1961) "Discussion on pile foundations", Proc. 5th Int. Conf. S.M.F.E., Vol. 3. p.277.

Schiffman, R.L., and Aggarwala, B.D., (1961) "Stresses and displacements produced in semi-infinite elastic solid by a rigid elliptical footing", Proc. 5th Int. Conf. S.M.F.E., Vol. 1, p.795.

Scott, R.F., (1963) "Principles of soil mechanics", Addison Wesley, Mass.

Seed, H.B., and Reese, L.C., (1955) "The action of soft clay along friction piles", Proc. A.S.C.E., Vol. 81, Paper No. 842, p.43.

Skempton, A.W., (1951) "The bearing capacity of clays", Proc. Building Research Congress, Vol. 1, p.181.

" (1953) "Discussion: Piles and Pile foundations, Settlement of pile foundations", Proc. 3rd. Int. Conf. S.M.F.E., Vol. 3, p.172.

" (1954) "Pore pressure parameters A and B", Geotechnique, Vol. 4, p.143.

" (1959) "Cast-in-situ bored piles in London Clay", Geotechnique, Vol. 9 p. 153.

" (1966) "Summing up", Proc. Symp. on large bored piles, London, Butterworth.

Skempton, A.W., and Henkel, D.J., (1957) "Tests on London Clay from deep boring at Paddington, Victoria, Southbank", Proc. 4th Int. Conf. S.M.F.E., Vol. 1, p.100.

Skempton, A.W., Yassin, A.A., Gibson, R.E., (1953) "Theorie de la force portante des pieux dans le sable", Ann. de Inst. Tech. du batiment et des Travaux Publics, No. 63-64, p.285.

Smirnov, V.I., (1964) "A course in higher mathematics", Vol. 4, Pergamon Press.

Soderberg, L.O., (1962) "Consolidation theory applied to pile time effects", Geotechnique, Vol. 12, No. 3, p.217.

Soderman, L.G., and Milligan, V., (1961) "Capacity of friction piles in Varved Clay increased by electro-osmosis", Proc. 5th Int. Conf. S.M.F.E., Vol. 2, p.143.

Solkolovski, V.V., (1950) "Theory of Plasticity", 2nd Ed, Gostekhizdat.

Sowers, G.F., Martin, C.B., Wilson, L.L., (1961) "The bearing capacity of friction pile groups in homogeneous clay from model studies", Proc. 5th Int. Conf. S.M.F.E., Vol. 2, p.155.

Steinbrenner, W., (1934) "Tafeln Zur Setzungsberechnung", Strasse, Vol. 1, p.121.

Terzaghi, K., (1943) "Theoretical soil mechanics", John Wiley, New York.

Terzaghi, K., and Peck, R.B., (1948) "Soil mechanics in engineering practice", John Wiley, New York.

Thurman, A.G., (1964) "Computed Load capacity and movement of friction and end bearing piles in uniform and stratified soils", Ph.D. thesis, Carnegie Inst. of Tech., U.S.A.

Thurman, A.G., and D'appolonia, E., (1965) "Computed friction and end bearing piles embedded in uniform and stratified soils", Proc. 6th Conf. S.M.F.E., Vol. 2, p.323.

Tomlinson, M.J., (1957) "The adhesion of piles driven in clay soils", Proc. 4th Int. Conf. S.M.F.E., Vol. 2, p.66.

Turnbul, W.J., Maxwell, A., Ahlvin, R.G., (1961) "Stresses and deflection in homogeneous soil masses", Proc. 5th Int. Conf. S.M.F.E., Vol. 2, p.337.

Turner, M.J, Clough, R.W., et al (1956) "Stiffness and deflection analysis of complex structures", Jour. Aero. Science, Vol. 23, p.805.

Vey, E., (1949) "The mechanics of soil consolidation by electro-osmosis", Proc. 29th annual meeting, H.R.B, p.579.

Wang, J.W., and Vey, E., (1953) "Stresses in a saturated soilmass during electro-osmosis". Proc. 3rd Int. Conf. S.M.F.E., Vol. 1, p.75.

Watson, J.O., (1968) "An integral representation of the displacement of an elastic body", Report C.E/18/1968, Southampton University.

Westergaard, H.M., (1938) "A problem of elasticity", S. Timoshenko Sixtieth Aniversary volume, p.268, Macmillan, New York.

Whitaker, T., (1957) "Experiment with model piles in groups", Geotechnique, Vol. 7, p. 147.

Whitaker, T., (1960) "Some experiments on model piled foundations", Syp. Pile foundations, Proc. I.A.B.S.E., Stockholm, p.124.

Whitaker, T., and Cooke, R.W., (1966) "An investigation of shaft and base resistance of large bored piles in London Clay", Proc. Syp. Large Bored Piles, Butterworth, London.

Yang, N.C., (1956) "Redriving characteristics of piles", Proc. A.S.C.E., Vol. 82, S.M.3., p.17.

Zaslavsky, D., and Ravaina, I., (1965) "A review and study of some electro-kinetic phenomena", Symp. on moisture equilibria and moisture changes in soils, Australia.

Zienkiewicz, O.C., (1967) "Finite element method in structural and continuum mechanics", McGraw-Hill, New York.

APPENDIX 1

LIST OF INTEGRALS

$$(KSS)_{ij} = 2\int_{(j-1)G_1}^{jG_1}\int_{o}^{\pi} a.\ KW_1(c,r_1,z)\ d\theta\ dc\ ,$$

$$r_1 = \left[2a^2-2.a^2.\mathrm{Cos}\ \theta_\varepsilon\right]^{\frac{1}{2}}\ ;$$

$$(KRS)_{ij} = 2\int_{(j-1)G_1}^{jG_1}\int_{o}^{\pi} a.\ KW_3(c,r,z)\ d\theta\ dc,$$

$$r = a\ ;$$

$$(KBS)_{ij} = 2\int_{(j-1)G_2}^{jG_2}\int_{o}^{\pi} \varepsilon.\ KW_2(L,r_2,z)\ d\theta\ d\varepsilon\ ,$$

$$r_2 = \left[a^2+\varepsilon^2-2.a.\epsilon.\mathrm{Cos}\ \theta_\varepsilon\right]^{\frac{1}{2}}\ ;$$

$$(KSU)_{ij} = 2\int_{(j-1)G_1}^{jG_1}\int_{o}^{\pi} a.\ KU_1(c,r_1,z)\ d\theta\ dc,$$

$$r_1 = \left[2.a^2-2.a^2.\mathrm{Cos}\ \theta_\varepsilon\right]^{\frac{1}{2}}\ ;$$

$$(KRU)_{ij} = \int_{(j-1)G_1}^{jG_1}\int_{o}^{2\pi} a.\ KU_3(c,r,z)\ d\theta\ dc,\ r = a\ ;$$

$$(KBU)_{ij} = 2\int_{(j-1)G_2}^{jG_2}\int_{o}^{\pi} \varepsilon.\ KU_2(L,r_2,z)\ d\theta\ d\varepsilon,$$

$$r_2 = \left[a^2+\varepsilon^2-2.a.\varepsilon.\mathrm{Cos}\ \theta_\varepsilon\right]^{\frac{1}{2}}\ ;$$

where

$$z = (i - \frac{1}{2}) \cdot G_1 \quad .$$

$$(KSB)_{ij} = 2 \int_{(j-1)G_1}^{jG_1} \int_{o}^{\pi} a \cdot KW_1(c, r_1, z)\, d\theta\, dc,$$

$$r_1 = \left[r^2 + a^2 - 2 \cdot a \cdot r \cdot \text{Cos}\ \theta_\varepsilon\right]^{\frac{1}{2}} ;$$

$$(KRB)_{ij} = 2 \int_{(j-1)G_1}^{jG_1} \int_{o}^{\pi} a \cdot KW_3(c, r_1, z)\, d\theta\, dc,$$

$$r_1 = \left[r^2 + a^2 - 2 \cdot a \cdot r \cdot \text{Cos}\ \theta_\varepsilon\right]^{\frac{1}{2}} ;$$

$$(KBB)_{ij} = 2 \int_{(j-1)G_2}^{jG_1} \int_{o}^{\pi} \varepsilon \cdot KW_2(L, r_2, z)\, d\theta\, d\varepsilon,$$

$$r_2 = \left[r^2 + \varepsilon^2 - 2 \cdot r \cdot \varepsilon \cdot \text{Cos}\ \theta_\varepsilon\right]^{\frac{1}{2}} ;$$

where

$$r = (i - \frac{1}{2}) \cdot G_2 \ ; \quad z = L \cdot$$

$$(KLS)_{ij} = 2 \int_{(j-1)G_3}^{jG_3} \int_{o}^{\pi} \varepsilon \cdot KW_4(H, r_2, z)\, d\theta\, d\varepsilon$$

$$r_2 = \left[a^2 + \varepsilon^2 - 2\varepsilon a \cdot \text{Cos}\ \theta_\varepsilon\right]^{\frac{1}{2}} ;$$

where

$$z = (i - \frac{1}{2}) \cdot G_1$$

$$(KLB)_{ij} = 2 \int_{(j-1)G_3}^{jG_3} \int_{o}^{\pi} \varepsilon \cdot KW_4(H, r_2, L)\, d\theta\, d\varepsilon$$

$$r_2 = \left[r^2+\varepsilon^2-2r\varepsilon \text{ Cos } \theta_\varepsilon\right]^{\frac{1}{2}}$$

where

$$r = (1 - \tfrac{1}{2})G_2. \quad z = L.$$

$$(KSL)_{ij} = 2\int_{(j-1)G_1}^{jG_1} \int_{o}^{\pi} a.\ KW_1(c,r_1,H)\ d\theta\ dc$$

$$r_1 = \left[r^2+a^2-2ar \text{ Cos } \theta_\varepsilon\right]^{\frac{1}{2}}$$

$$(KBL)_{ij} = 2\int_{(j-1)G_2}^{jG_2} \int_{o}^{2\pi} \varepsilon.\ KW_2(L,r_2,H)\ d\theta\ d\varepsilon$$

$$r_2 = \left[r^2+\varepsilon^2-2r\varepsilon \text{ Cos } \theta_\varepsilon\right]^{\frac{1}{2}}$$

$$(KLL)_{ij} = 2\int_{(j-1)G_3}^{jG_3} \int_{o}^{2\pi} \varepsilon.\ KW_4(H,r_2,z)\ d\theta\ d\varepsilon$$

$$r_2 = \left[r^2+\varepsilon^2-2r\varepsilon \text{ Cos } \theta_\varepsilon\right]^{\frac{1}{2}}$$

where

$$r = (i - \tfrac{1}{2})G_3, \quad z = H.$$